*A*rthritis & *R*heumatology

An Official Journal of the American College of Rheumatology
www.arthritisrheum.org and wileyonlinelibrary.com

VOLUME 70   JULY 2018   NO. 7

Cover image: The figure on the cover (from Basu et al, page 1002) illustrates a brain functional magnetic resonance imaging representation of the default mode network and the insula. Rheumatoid arthritis patients with the highest levels of fibromyalgianess evidenced functional hyperconnectivity between this brain network and region.

In this **Issue**

Highlights from this issue of *A&R* | **By Lara C. Pullen, PhD**

Periodontally Healthy Patients with Rheumatoid Arthritis Have Dysbiotic Microbial Communities

Earlier research has shown that gram-negative anaerobes play an important role in the initiation of periodontitis

p. 1008 and possibly even the pathogenesis of rheumatoid arthritis (RA). Researchers have also identified an association between RA and a dysbiotic oral microbiome; however, the results are confounded by the presence of extensive periodontitis in these individuals.

In this issue, Lopez-Oliva et al (p. 1008) report on their investigation of the role of RA in modulating the periodontal microbiome. The investigators' study compared periodontally healthy individuals with RA and without RA. They found that the oral microbiome in patients with RA is enriched for inflammophilic and citrulline-producing organisms.

Specifically, when the researchers compared the subgingival microbiomes of patients with RA and controls, they found that 41.9% of the communities differed in abundance and 19% differed in membership. Controls tended to have sparse and predominantly congeneric co-occurrence networks. In contrast, patients with RA had a highly connected grid that contained a large intergeneric hub anchored by known periodontal pathogens. When the investigators performed predictive metagenomic analysis, they found that arachidonic acid and ester lipid metabolism pathways appeared to at least partially explain the robustness of the clustering.

When the team looked specifically at a periodontally healthy cohort, they found that *Porphyromonas gingivalis* and *Aggregatibacter actinomycetemcomitans* occurred at similar levels in patients with RA and controls. In contrast, Cryptobacterium curtum, an organism that can produce large amounts of citrulline, was a robust discriminant of the microbiome in individuals with RA. This finding led the authors to propose that these organisms may play a role in the production of autoantigenic citrullinated peptides in RA.
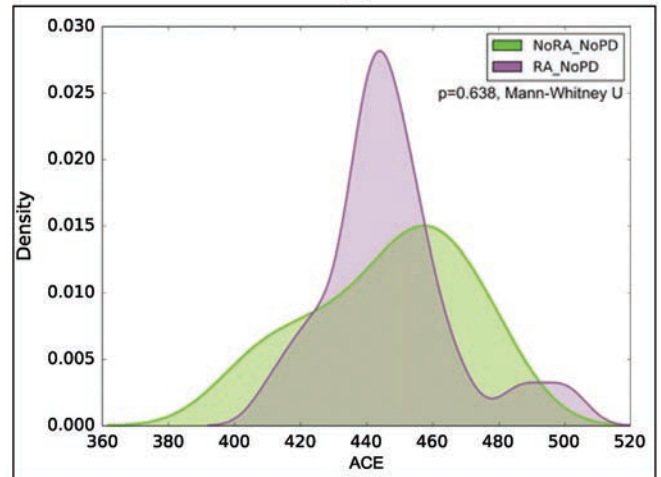
Figure 1. Differences in α- and β-diversity metrics between periodontally healthy subjects with RA (RA_NoPD) and periodontally healthy subjects without RA (NoRA_NoPD). Kernel plots of α-diversity (abundance-based coverage estimator [ACE]). The peak indicates the median value for each group. The x-axis indicates the data range.

Even Healthy Individuals Have Sacroiliitis

In this issue, de Winter et al (p. 1042) describe the results of their comparison of magnetic resonance images (MRIs) of the sacroiliac (SI) joints of healthy subjects and individuals with known mechan-

p. 1042 ical strain acting on the SI joints to those with axial spondyloarthritis (SpA) and patients with chronic back pain. The researchers found, using the Assessment of Spondyloarthritis international Society (ASAS) definition, that a substantial proportion (23.4%) of healthy individuals without current or past back pain had a magnetic resonance image (MRI) showing the presence of sacroiliitis—considered by trained readers to be highly suggestive of axial SpA.

Not surprisingly, 91.5% of patients with axial SpA had an MRI that was positive for sacroiliitis, and only 6.4% of patients with chronic back pain had an MRI positive for sacroiliitis. A more detailed analysis revealed that 12.5% of the runners and 57.1% of women with postpartum back pain had a positive MRI. When the investigators used a Spondyloarthritis Research Consortium of Canada (SPARCC) index cutoff of ≥2 for positivity, they found that 25.5% of healthy volunteers, 97.9% of positive axial SpA patients, 10.6% of controls with chronic back pain, 16.7% of runners, and 57.1% of women with postpartum back pain had positive MRIs.

When the researchers looked specifically at deep bone marrow edema (BME) lesions, they found them almost exclusively in patients with axial SpA. That said, 1 woman of 7 (14.3%) with postpartum back pain had deep BME lesions. The findings are consistent with results from a previous study in which 25% of healthy participants had BME lesions on MRIs of the SI joint.

Patients with AAV Can Be Classified by Cytokine Profile

In this issue, Berti et al (p. 1114) report the results of an exploratory analysis of patients with severe antineutrophil cytoplasmic antibody (ANCA)–associated vasculitis (AAV). They found that patients with proteinase 3 ANCA (PR3-ANCA) have distinct cytokine profiles when compared to patients with myeloperoxidase ANCA (MPO-ANCA). Similarly, patients with granulomatosis with polyangiitis (GPA) have cytokine profiles that are distinct from those in patients with microscopic polyangiitis (MPA).

Specifically, the levels of 9 circulating cytokines or immunoregulators were significantly higher in PR3-ANCA when compared to MPO-ANCA: interleukin-6 (IL-6),

granulocyte–macrophage colony-stimulating factor (GM-CSF), IL-15, IL-18, CXCL8/IL-8, CCL-17/thymus and activation-regulated chemokine (TARC), IL-18 binding protein (IL-18 BP), soluble IL-2 receptor α (sIL-2Rα), and nerve growth factor β (NGFβ). In contrast, 4 mediators were higher in MPO-ANCA than in PR3-ANCA: sIL6R, soluble tumor necrosis factor receptor type II (sTNFRII), neutrophil gelatinase-associated lipocalin (NGAL), and soluble intercellular adhesion molecule 1 (sICAM-1). Patients with GPA had higher levels of IL-6, GM-CSF, IL-15, IL-18, sIL-2Rα, and NGFβ than patients with MPA. In contrast, patients with MPA had higher levels of osteopontin, sTNFRII, and NGAL. In almost all cases, the difference between PR3-ANCA and

MPO-ANCA was larger than the difference between GPA and MPA.

When the investigators performed a multivariate analysis, they found that 8 circulating mediators distinguished patients with AAV better when grouped by ANCA than when grouped by clinical diagnosis: IL-15, IL-8, IL-18 BP, NGFβ, sICAM-1, TARC, osteopontin, and kidney injury molecule 1. Thus, the differences in the circulating immune mediators were more strongly associated with ANCA specificity than with clinical diagnosis. The results suggest that heterogeneity in the AAV subtypes extends beyond clinical phenotypes. In other words, certain combinations of pathways might be more important for PR3-ANCA than GPA, MPA, and MPO-ANCA.

Clinical Evolution in Patients with New-Onset Inflammatory Back Pain

Physicians diagnose inflammatory back pain (IBP) when patients report symptoms of morning stiffness and pain that changes with activity or rest. Since IBP can be an early

manifestation of spondyloarthritis (SpA), health care providers tend to use the presence of IBP as a factor when diagnosing SpA. Although rheumatologists know that some patients experience resolution of their IBP, the prognosis of patients with incident IBP is unknown.

In this issue, Wang et al (p. 1049) report the results of their investigation into the long-term outcomes in patients with IBP from a population-based cohort. They found that new-onset IBP resolves in most patients and progresses to SpA in only a minority of patients. The fact that IBP tends to resolve may underlie the difference between the prevalence of IBP (3–6%) and the prevalence of SpA (0.4–1.3%).

The investigators evaluated 5,304 patients with back pain and identified 124 patients with new-onset IBP. Patients were followed up for a median of 13.2 years, at which point IBP had progressed to SpA in 39 of the patients. Most patients (58) had resolution of IBP, and 15 patients developed a non-SpA diagnosis. The researchers calculated that, at 10 years, the probability of

Figure 1. Progression from IBP to SpA, a non-SpA diagnosis, or resolution of back pain (resolved) beginning at the time of fulfillment of IBP criteria. Area graph shows the proportion of each outcome, including SpA, a non-SpA diagnosis, resolution of back pain, or persistent IBP or unknown status (persist/unk) over time. The n values are the number of patients at risk at each time point.

having SpA was 30% and the probability of resolution of IBP was 43%. They identified uveitis, male sex, and family history of SpA as the most important predictors for progression to SpA. These results suggest that the symptom complex described by IBP may often reflect a self-limiting process.

Clinical **Connections**

Inflammation Intensity–Dependent Expression of Osteoinductive Wnt Proteins Is Critical for Ectopic New Bone Formation in Ankylosing Spondylitis

CORRESPONDENCE
Hiu Liu, MD, PhD: liuhui58@mail.sysu.edu.cn
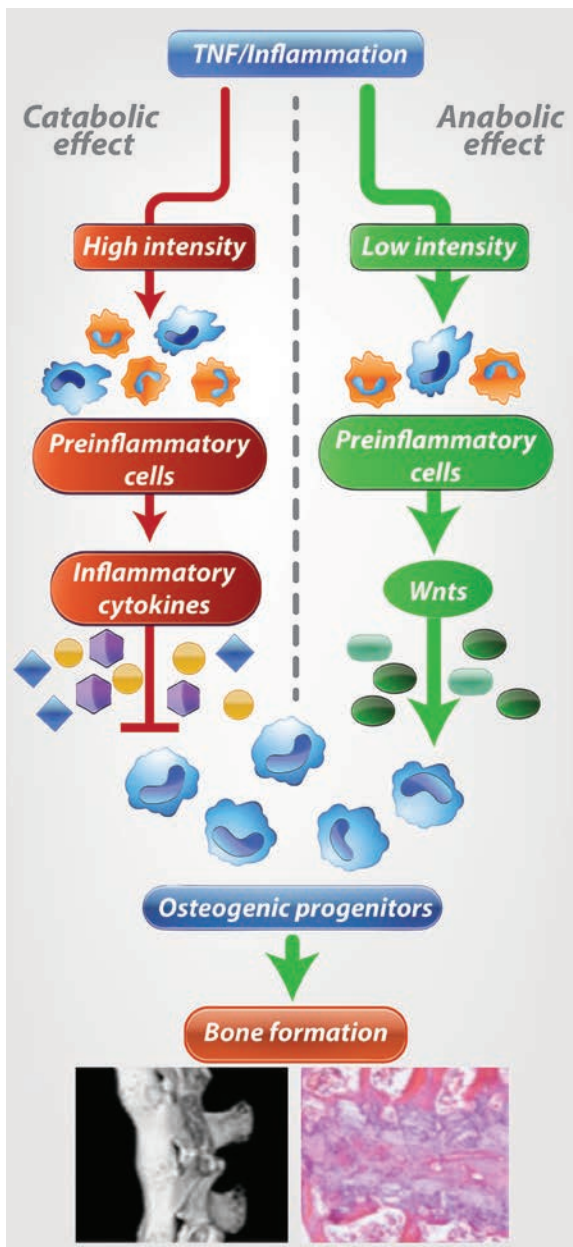
SUMMARY

Ectopic bone formation resulting in spinal fusion is a hallmark feature of disease in ankylosing spondylitis (AS). The relationship between inflammation and bone formation in AS is still an enigma. Since bone formation requires critical osteogenic molecules and pathways, inflammation-induced activation of osteogenic signaling pathways is a logical link between inflammation and new bone formation. Results of a study by Li et al suggest that Wnt proteins act as a molecular bridge between inflammation and bone formation. The authors established an in vitro cell culture system mimicking the inflammatory microenvironment of the bone-forming site and found that only secreted products from monocytes stimulated with low-dose tumor necrosis factor (TNF), but not high-dose TNF, induced persistent Wnt expression and new bone formation. Furthermore, both the canonical Wnt/β-catenin and noncanonical Wnt/protein kinase Cδ (PKCδ) signaling pathways were required for new bone formation. The association between Wnt proteins and new bone formation was confirmed in two distinct mouse models of AS; inhibiting either canonical or noncanonical Wnt signaling pathways suppressed ectopic bone formation and spinal kyphosis. These findings indicate that the osteogenic molecules induced by proinflammatory cytokines link inflammation and new bone formation and moreover, that inflammation intensity is a bone formation switch.

KEY POINTS

- Constitutive low-intensity inflammation stimulation can induce new bone formation.

- Inflammation-induced osteogenic signaling pathways link inflammation and bone formation.

- Both canonical Wnt/β-catenin and noncanonical Wnt/PKCδ signaling pathways are required for new bone formation in mouse models of AS.

Lupus Regulator Peptide P140 Represses B Cell Differentiation by Reducing HLA Class II Molecule Overexpression

CORRESPONDENCE
Sylviane Muller, PhD: sylviane.muller@unistra.fr
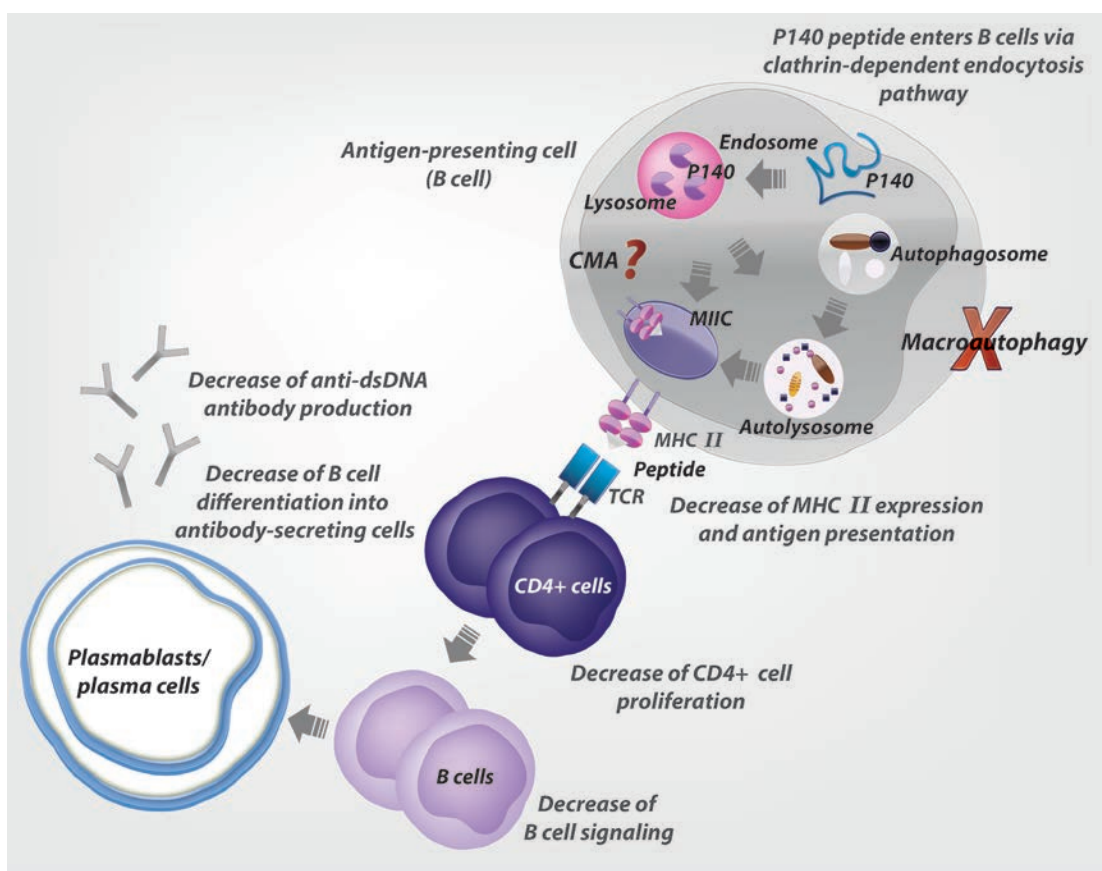
KEY POINTS

- P140 decreases the overexpression of MHC molecules occurring in antigen-presenting B cells in lupus.

- This effect hampers the process leading to presentation of self peptides to autoreactive T cells.

- As a downstream consequence, the activation of autoreactive B cells and their differentiation into autoantibody-secreting cells is repressed.

SUMMARY

Current treatments for systemic lupus erythematosus focus on downstream effector responses and do not target disease pathogenesis, which remains largely unknown. The action of the immunoregulatory peptide P140, which is under evaluation in clinical trials, was investigated in human cells by Wilhelm and colleagues. They found that P140 has no direct effect on B cell receptor signaling in memory, naive, mature, transitional, or B1 cells, suggesting that it does not alter B cell survival and maturation in these B cell subsets. However, it strongly reduces the overexpression of major histocompatibility complex (MHC) class II molecules on lupus B cells acting as antigen-presenting cells. P140 down-regulates differentiation of B cells into plasma cells and decreases IgG secretion. It reaches B cell lysosomes using a clathrin coat–dependent endocytosis portal. In late lysosomal vesicles, it likely hampers peptide–MHC molecule loading by down-regulating excessive autophagy processes, which ultimately down-regulates pathogenic autoantibody production.

*A*rthritis & *R*heumatology

An Official Journal of the American College of Rheumatology
www.arthritisrheum.org and wileyonlinelibrary.com

EDITORIAL

Functional Connectivity: Dissecting the Relationship Between the Brain and "Pain Centralization" in Rheumatoid Arthritis

Yvonne C. Lee (iD),[1] Vitaly Napadow,[2] and Marco L. Loggia[2]

Pain is a frequent and disabling symptom experienced by individuals with inflammatory arthritis. More than 50% of patients with inflammatory arthritis report visual analog scale (VAS) pain scores $\geq 30/100$ mm despite treatment with disease-modifying antirheumatic drugs (DMARDs) (1). Patients often equate pain with peripheral inflammation, as evidenced by studies demonstrating that pain is the primary factor influencing patient global assessment of disease activity (2). However, recent clinical studies suggest that rheumatoid arthritis (RA) patients may exhibit signs of central sensitization, which may be why treating peripheral inflammation does not always translate into effective pain relief (3). However, the only study to directly examine the predictive effect of temporal summation, a measure of central sensitization, did not reveal a significant association between temporal summation and DMARD response (4). Thus, the extent to which RA patients

demonstrate neural mechanisms consistent with central sensitization is still unclear.

Advances in neuroimaging have enabled the assessment of functional connectivity between brain regions, allowing researchers to better understand the neural mechanisms underlying spontaneous clinical pain states. Functional brain connectivity assesses synchronization in activity displayed by two or more brain regions when they are "communicating" (e.g., when one region is exchanging information with the other). The connectivity between the insular cortex and a network of brain regions collectively known as the default mode network (DMN) (a group of interconnected brain regions including the medial prefrontal cortex, posterior cingulate cortex, precuneus, inferior parietal lobule, hippocampal formation, and lateral temporal cortex [5]) has attracted particular attention in recent years. In healthy subjects, anterior and middle insula activity typically shows no correlation (or, sometimes, weak negative correlation) with DMN regions. However, in patients with chronic pain disorders, insula subregions can become functionally connected with the DMN.

Following the original observation by our group in fibromyalgia (FM) patients (6), an elevation of connectivity between the insula and the DMN (or to a specific core DMN region, such as the medial prefrontal cortex) has been documented in several pain conditions, including noninflammatory and inflammatory chronic low back pain (7–9), osteoarthritis (8), and migraine (10). Intriguingly, the strength of DMN–insula connectivity was positively correlated with clinical pain severity in many studies (6–8), although investigators in at least one study reported negative correlations in the context of an acute migraine attack (10). In addition, DMN–insula connectivity was found to be reduced

[1]Yvonne C. Lee, MD, MMSc: Northwestern University Feinberg School of Medicine, Chicago, Illinois; [2]Vitaly Napadow, PhD, Marco L. Loggia, PhD: Massachusetts General Hospital, Harvard Medical School, Charlestown, Massachusetts.

after successful pharmacologic (11) and nonpharmacologic (12) treatment, therefore raising the possibility that this feature may one day be considered an imaging biomarker of pain perception.

The study reported by Basu et al in this issue of *Arthritis & Rheumatology* tested the hypothesis that RA patients demonstrate neuronal hallmarks of pain centralization similar to those observed in FM (13). To this end, they enrolled 54 RA patients who met the 2010 American College of Rheumatology (ACR)/European League Against Rheumatism classification criteria (14) and who had experienced clinically significant fatigue during the past 3 months. The subjects underwent functional magnetic resonance imaging (fMRI), and an independent component analysis assessed functional connectivity between 4 networks of interest, including the DMN, and the rest of the brain. Subjects also completed the 2011 ACR FM survey, a measure of "fibromyalgianess" (FMness), which is thought to represent the clinical manifestations of pain centralization (15). In the study by Basu et al, the average score on the 2011 ACR FM survey was 13.2 (the cutoff for the ACR modified preliminary criteria for FM diagnosis is 13), which is compatible with previous studies suggesting that a significant number of RA patients demonstrate comorbid FM. Of note, the ACR FM survey score was significantly positively associated with DMN–insula functional connectivity.

With these results in a population of RA patients, Basu et al reinforce the generalizability of DMN–insula connectivity as a potential marker across etiologically heterogeneous pain conditions. However, the distinction between this study and studies of other conditions is that there was no correlation between DMN–insula connectivity and spontaneous clinical pain severity, assessed at the time of the scan. By showing that DMN–insula connectivity was more associated with FMness than with current pain severity, this study suggests another interpretation about the potential functional significance of this marker—that it is not a marker of "pain intensity" per se, but rather a marker of "pain centralization." It may be that previous studies demonstrated an association with clinical pain severity because pain intensity is more closely associated with measures of pain centralization (e.g., FMness) in functional pain disorders than in RA, which is known to have a significant peripheral component (e.g., peripheral joint inflammation). Of note, however, an fMRI study of patients with ankylosing spondylitis, a systemic rheumatic disease characterized by inflammatory back pain, did show associations between back pain severity and DMN connectivity with the salience network (of

which the insula is a prominent component) (9). Thus, future studies are needed to better understand the relationship between DMN–insula activity and pain severity in systemic inflammatory conditions. In particular, we recommend that studies include different measures of pain (e.g., pain severity, FMness, pain interference, pain catastrophizing, etc.) to better define the nature of observed associations.

Strengths of the study by Basu et al include the assessment of multiple relevant clinical characteristics, including age, sex, amitriptyline use, inflammatory disease activity measures (e.g., C-reactive protein [CRP] level and the Disease Activity Score in 28 joints [16]), and levels of pain, fatigue, sleep disturbance, and depression. By including age, sex, CRP level, and amitriptyline use in the linear regression models, Basu et al were able to take into account the roles of these variables as possible confounders of the association between network–whole brain connectivity and FMness. Ultimately, adjusting for these variables did not change the magnitude of the association, which reassures that the observed associations are not an artifact of confounding due to relationships between the covariates, network–whole brain connectivity, and FMness. The assessment of pain, fatigue, sleep disturbance, and depression also enabled analyses examining correlations between these variables and DMN–insula connectivity. These analyses were post hoc and should therefore be considered exploratory. Nevertheless, these results provide clues to the underlying cause of the association between DMN–insula connectivity and FMness, suggesting that this association may reflect a distinct phenotype associated with pain centralization.

Another strength of the study is the large sample size. With a study sample of 54 RA patients, this is the largest fMRI study to assess functional connectivity in individuals with RA. A sufficient sample size is required for stable and reproducible results and to enable correction for multiple testing, which is inherent in neuroimaging studies. Each fMRI image volume can comprise hundreds of thousands of voxels, or volume elements, each of which is used for separate statistical testing (17). Fortunately, neuroimagers take advantage of the fact that "genuine brain activity" tends to cluster in regions usually spanning many adjacent voxels (as opposed to random noise, which can lead to spurious small clusters in a "salt and pepper" pattern) (18). In the study by Basu et al, per commonly adopted procedure, the statistical significance of each cluster was determined based on the size of the cluster and a family-wise error cluster corrected P value of less than 0.05, thereby accounting for multiple comparisons.

Despite these strengths, the study had some limitations. Perhaps the most important was the absence of a control group, which limits whether we can truly conclude that DMN–insula connectivity is significantly altered in RA patients. Another potential limitation is that the data used to perform functional connectivity analyses were collected while the participants were engaged in a cognitive task (the Paced Auditory Serial Addition Test) rather than at rest. While computing connectivity metrics during a task is not uncommon (19), this feature may limit our ability to directly compare the results from Basu et al's study with those from previous studies evaluating the role of the DMN in chronic pain, as in most or all of those studies connectivity analyses were performed using unconstrained resting-state data.

As the authors note, another primary limitation is generalizability. Inclusion criteria required that participants have a score of >3 on the Chalder Fatigue Binary Scale (20), restricting the study sample to individuals with clinically meaningful levels of fatigue. Few studies have used the Chalder Fatigue Scale to assess fatigue in RA, and even fewer have reported on the binary scoring system (21). Thus, it is difficult to ascertain what a score of >3 means in the context of RA patients, and it would be informative to know the proportion of interested participants who were screened out because of this criterion. Future studies are needed to determine if the relationship between DMN–insula connectivity and FMness holds among individuals with lower levels of fatigue.

Finally, as with all fMRI studies, this study is limited in that it cannot provide direct information on the neurophysiologic processes underlying the observed neuroimaging signals. The investigators utilized a standard fMRI technique using an endogenous contrast mechanism called blood oxygen level–dependent (BOLD) imaging. BOLD fMRI takes advantage of neurovascular coupling in response to brain activity and serves as a proxy for neural activity. However, within each neuroimaging voxel, hundreds of thousands to millions of neurons exist, and the dynamic interrelationships between these neurons are complex. Thus, basing the interpretation of fMRI signal on neural activity, or "connectivity" as was used by Basu et al, requires several assumptions, the validity of which may differ from study to study (22).

Despite these limitations, fMRI can provide novel insights into the central nervous system (CNS) pathways involved in the expression of difficult-to-quantify symptoms, such as pain and fatigue, in RA. This study extends findings demonstrated in many previous studies of noninflammatory pain conditions to RA, a systemic inflammatory condition. Specifically,

the study provides evidence highlighting DMN–insula connectivity as one of the most reliable imaging markers of chronic pain reported in the literature thus far.

For rheumatologists, the implications of this observation are broad. First, by identifying associations between aberrant brain functional connectivity and phenotypic characteristics (primarily FMness and secondarily fatigue and sleep disturbance), this study underscores the importance of considering CNS factors, in addition to peripheral joint inflammation, when evaluating symptoms experienced by our RA patients. Second, by showing that despite associations between DMN–insula connectivity and FMness, DMN–insula connectivity was not associated with pain severity, this study highlights the importance of carefully considering the types of pain measures included in studies. FMness includes assessments of widespread pain (e.g., pain distribution) and somatic symptoms, while the pain VAS only assesses pain intensity. Although they are related, these concepts are inherently different. Third, by providing evidence of a neurobiologic underpinning for FMness in RA, this study points toward the potential role of treatment strategies previously shown to modulate DMN–insula connectivity (e.g., acupuncture, γ-aminobutyric acid analogs) in individuals with RA and high levels of FM symptoms (23).

In summary, the study by Basu et al is an important step toward understanding the role of the brain in modulating pain in patients with systemic inflammatory conditions. Future investigations of these findings are needed to examine their generalizability (e.g., in studies including RA patients with lower levels of fatigue, studies of newly diagnosed and hence drug-naive RA patients, etc.) and reproducibility (e.g., in observational longitudinal studies), as well as the responsiveness of these neuroimaging markers to interventions (e.g., in clinical trials of DMARDs and/or analgesic medications). As more neuroimaging studies are performed and reported, rheumatologists should become familiar with the strengths and limitations of these types of studies. Characterizing the complex interrelationships between the brain, peripheral nervous system, and immune pathways (both peripheral and central) holds promise for the development of safe and effective pain management strategies, which are sorely needed to improve quality of life for our patients with systemic inflammatory conditions.

AUTHOR CONTRIBUTIONS

REFERENCES

1. Rifbjerg-Madsen S, Christensen AW, Christensen R, Hetland ML, Bliddal H, Kristensen LE, et al. Pain and pain mechanisms in patients with inflammatory arthritis: a Danish nationwide cross-sectional DANBIO registry survey. PLoS One 2017;12: e0180014.

2. Ferreira RJ, Dougados M, Kirwan JR, Duarte C, de Wit M, Soubrier M, et al. Drivers of patient global assessment in patients with rheumatoid arthritis who are close to remission: an analysis of 1588 patients. Rheumatology (Oxford) 2017;56:1573–8.

3. Lee YC, Lu B, Edwards RR, Wasan AD, Nassikas NJ, Clauw DJ, et al. The role of sleep problems in central pain processing in rheumatoid arthritis. Arthritis Rheum 2013;65:59–68.

4. Christensen AW, Rifbjerg-Madsen S, Christensen R, Dreyer L, Boesen M, Ellegaard K, et al. Ultrasound Doppler but not temporal summation of pain predicts DAS28 response in rheumatoid arthritis: a prospective cohort study. Rheumatology (Oxford) 2016;55:1091–8.

5. Buckner RL, Andrews-Hanna JR, Schacter DL. The brain's default network: anatomy, function, and relevance to disease. Ann N Y Acad Sci 2008;1124:1–38.

6. Napadow V, LaCount L, Park K, As-Sanie S, Clauw DJ, Harris RE. Intrinsic brain connectivity in fibromyalgia is associated with chronic pain intensity. Arthritis Rheum 2010;62:2545–55.

7. Loggia ML, Kim J, Gollub RL, Vangel MG, Kirsch I, Kong J, et al. Default mode network connectivity encodes clinical pain: an arterial spin labeling study. Pain 2013;154:24–33.

8. Baliki MN, Mansour AR, Baria AT, Apkarian AV. Functional reorganization of the default mode network across chronic pain conditions. PLoS One 2014;9:e106133.

9. Hemington KS, Wu Q, Kucyi A, Inman RD, Davis KD. Abnormal cross-network functional connectivity in chronic pain and its association with clinical symptoms. Brain Struct Funct 2016;221:4203–19.

10. Coppola G, Di Renzo A, Tinelli E, Di Lorenzo C, Scapeccia M, Parisi V, et al. Resting state connectivity between default mode network and insula encodes acute migraine headache. Cephalalgia 2017:333102417715230.

11. Harris RE, Napadow V, Huggins JP, Pauer L, Kim J, Hampson J, et al. Pregabalin rectifies aberrant brain chemistry, connectivity, and functional response in chronic pain patients. Anesthesiology 2013;119:1453–64.

12. Napadow V, Kim J, Clauw DJ, Harris RE. Decreased intrinsic brain connectivity is associated with reduced clinical pain in fibromyalgia. Arthritis Rheum 2012;64:2398–403.

13. Basu N, Kaplan CM, Ichesco E, Larkin T, Harris RE, Murray A, et al. Neurobiologic features of fibromyalgia are also present among rheumatoid arthritis patients. Arthritis Rheumatol 2018; 70:1000–7.

14. Aletaha D, Neogi T, Silman AJ, Funovits J, Felson DT, Bingham CO III, et al. 2010 rheumatoid arthritis classification criteria: an American College of Rheumatology/European League Against Rheumatism collaborative initiative. Arthritis Rheum 2010;62: 2569–81.

15. Wolfe F, Clauw DJ, Fitzcharles MA, Goldenberg DL, Häuser W, Katz RS, et al. Fibromyalgia criteria and severity scales for clinical and epidemiological studies: a modification of the ACR preliminary diagnostic criteria for fibromyalgia. J Rheumatol 2011; 38:1113–22.

16. Prevoo ML, van 't Hof MA, Kuper HH, van Leeuwen MA, van de Putte LB, van Riel PL. Modified disease activity scores that include twenty-eight–joint counts: development and validation in a prospective longitudinal study of patients with rheumatoid arthritis. Arthritis Rheum 1995;38:44–8.

17. Lindquist MA. The statistical analysis of fMRI data. Stat Sci 2008;23:439–64.

18. Woo CW, Krishnan A, Wager TD. Cluster-extent based thresholding in fMRI analyses: pitfalls and recommendations. Neuroimage 2014;91:412–9.

19. Beaty RE, Kenett YN, Christensen AP, Rosenberg MD, Benedek M, Chen Q, et al. Robust prediction of individual creative ability from brain functional connectivity. Proc Natl Acad Sci U S A 2018;115:1087–92.

20. Chalder T, Berelowitz G, Pawlikowska T, Watts L, Wessely S, Wright D, et al. Development of a fatigue scale. J Psychosom Res 1993;37:147–53.

21. Hewlett S, Dures E, Almeida C. Measures of fatigue: Bristol Rheumatoid Arthritis Fatigue Multi-Dimensional Questionnaire (BRAF MDQ), Bristol Rheumatoid Arthritis Fatigue Numerical Rating Scales (BRAF NRS) for severity, effect, and coping, Chalder Fatigue Questionnaire (CFQ), Checklist Individual Strength (CIS20R and CIS8R), Fatigue Severity Scale (FSS), Functional Assessment Chronic Illness Therapy (Fatigue) (FACIT-F), Multi-Dimensional Assessment of Fatigue (MAF), Multi-Dimensional Fatigue Inventory (MFI), Pediatric Quality Of Life (PedsQL) Multi-Dimensional Fatigue Scale, Profile of Fatigue (ProF), Short Form 36 Vitality Subscale (SF-36 VT), and Visual Analog Scales (VAS). Arthritis Care Res (Hoboken) 2011;63 Suppl 11:S263–86.

22. Logothetis NK. What we can do and what we cannot do with fMRI. Nature 2008;453:869–78.

23. Napadow V, Harris RE. What has functional connectivity and chemical neuroimaging in fibromyalgia taught us about the mechanisms and management of 'centralized' pain? Arthritis Res Ther 2014;16:425.

EDITORIAL

Inflammatory Back Pain and Axial Spondyloarthritis: Lessons for Clinical Practice and Epidemiologic Research

Maureen Dubreuil [iD][1] and Joachim Sieper[2]

The delay between symptom onset and diagnosis in axial spondyloarthritis (SpA) remains unacceptably long, recently estimated to still be >6 years (1). Accumulating data demonstrate that early treatment with tumor necrosis factor inhibitors reduces both disease activity and radiographic progression in ankylosing spondylitis, the prototypical form of axial SpA (2,3). To encourage timely and correct diagnosis and enable early treatment, strategies to better identify patients with axial SpA have been studied in several populations (4). Many of these strategies relied on the presence of inflammatory back pain (IBP) as a criterion for referral to a rheumatologist, and IBP is one of the parameters used for classification of axial SpA (5). However, the specificity of IBP for an SpA diagnosis is limited, which makes it challenging to distinguish SpA from other causes of back pain, given that back pain is highly prevalent.

The term "inflammatory" back pain suggests that a patient's back pain is caused by inflammation. However, the definition of IBP is neither sensitive nor specific for SpA, meaning that not all SpA patients have IBP *and* that a substantial number of patients with other back pain diagnoses report the presence of IBP. IBP is generally considered present in people whose chronic back pain began insidiously at a young age, is associated with morning stiffness, and improves with movement but not with rest (6). However, a precise definition for this decades-old concept remains elusive despite attempts to refine it (7). For example, although IBP criteria specify

insidious onset of the pain and improvement with exercise, some SpA patients may report the opposite pattern —that heavy exertion worsens pain acutely, particularly during flares. Similarly, SpA patients who experience stiffness much of the day may not recognize "morning stiffness" as outlined in IBP criteria (7). The published specificity of IBP for an SpA diagnosis ranges from 72% to 92%, and subsequent attempts to revise IBP criteria resulted only in similar specificities (8,9).

Nonetheless, IBP is a relevant clinical parameter as a screening and diagnostic tool for axial SpA because back pain is so common. Indeed, the larger landscape of back pain is staggering: in the US, 19.4% of adults have chronic back pain. However, only ~5% of people with chronic back pain have SpA (10). Thus, the pretest probability for a patient with chronic back pain to have SpA is 5%. For example, if IBP is assumed to have a sensitivity of 75% and a specificity of 76% for SpA (resulting in a positive likelihood ratio of 3.1), the presence of IBP in a patient with chronic back pain increases the posttest probability of SpA only to 14% (11). Thus, although the symptom of IBP is an important parameter in the evaluation of people with chronic back pain, the value of IBP lies within the context of other clinical, laboratory, and imaging parameters.

Referral strategies have been developed with the aim of increasing the likelihood that patients who are referred from primary care to the specialist do have axial SpA. These referral strategies are necessary to avoid overwhelming the constrained resources that exist within the US (or any) health care system. When IBP was used as one of several screening parameters, ~33–46% of referred patients were ultimately diagnosed as having axial SpA by a rheumatologist in different studies (4). Thus, IBP seems to be suitable as a referral parameter for identifying axial SpA patients in primary care. If these criteria were incorporated as part of a more restrictive referral strategy, it would mean that more axial SpA patients would fail to be referred, and the opportunity to prevent morbidity among those patients would thereby be lost.

In this issue of *Arthritis & Rheumatology*, Wang and colleagues describe the clinical course in 124 patients with

new-onset IBP in the Rochester Epidemiology Project (REP), finding that 30% of IBP patients ultimately received a diagnosis of SpA (12). This study adds to the limited literature on IBP in the US, and by its observational nature, provides insight into how care for patients with back pain is truly provided in the real world, outside of specialized referral centers and structured research protocols.

The study by Wang et al importantly highlights lost opportunities in the community care of patients with back pain, and specifically those with axial SpA. First, Wang and colleagues report that only 2.3% of patients with back pain were found to have IBP. In contrast, estimates from the US National Health and Nutrition Examination Survey (NHANES), in which subjects were systematically queried about IBP features, suggest that nearly a quarter of adults with chronic back pain have IBP (13). Thus, the findings of Wang et al suggest that front-line providers either did not document IBP features in the electronic medical record (EMR) in a way that researchers could access or, more likely, that providers did not systematically ask patients with chronic back pain about IBP features (4,14). The challenge of defining and eliciting the presence of IBP may explain the low prevalence of IBP in this study. Rheumatologists, who are familiar with the nuanced features and descriptions of IBP, may capture its presence as part of a detailed history; however, the same nuance may not be appreciated by generalists in a referral intervention study, or in generalists' notes, as assessed in the study by Wang et al. A standardized assessment of patients with chronic back pain is likely to pick up more IBP cases as compared to the varied assessments performed during routine clinical care by general practitioners (25–31% of patients with chronic back pain had IBP in the NHANES, versus 2.3% in the study by Wang et al) (12,13).

A second lost opportunity is reflected in the low proportion of patients who were evaluated by a rheumatologist—only 23%. Similarly, only 21% of IBP patients underwent HLA–B27 testing, and a limited number of patients had pelvic radiographs or magnetic resonance imaging. Both HLA–B27 testing and pelvic radiography would be standard management of IBP under the care of a rheumatologist. One line of thinking may be that some patients did not need to be evaluated by a rheumatologist because their symptoms were mild or transient. However, it is likely that since the majority of IBP patients were not evaluated further, at least some patients with SpA were incorrectly diagnosed and undertreated, with resulting functional losses and other morbidity. Therefore, these findings highlight the need for primary care providers to better understand the importance of IBP as a screening tool for SpA and the value of early diagnosis and treatment in SpA.

Overall, despite the limited detection of IBP and low referral rate, the finding by Wang et al that 30% of IBP patients received a diagnosis of SpA is fairly consistent with the results of studies on referral strategies. Taken together, the study by Wang et al and existing literature clearly demonstrate that IBP is a syndrome that is common to diseases beyond SpA.

Beyond clinical practice, there is also the need to identify subjects with axial SpA in large data sets to allow epidemiologic research. Many studies of the epidemiology of extraarticular manifestations, comorbidities, or the comparative effectiveness of treatments in SpA would be prohibitively lengthy or expensive to perform prospectively. Thus, an accurate algorithm to predict axial SpA is also needed for research.

Accurately identifying SpA in observational studies also has challenges. The study by Wang et al demonstrates some of the challenges of using large EMR or claims data sets to address important research questions. First, although the authors began with >5,000 eligible subjects with back pain, the pool was reduced to 124 subjects with IBP, a number that is insufficient to provide precise estimates for many clinically important outcomes. Second, the process by which the larger pool was reduced (i.e., by which IBP patients were selected) was chart review, which is labor intensive and prone to human error and fatigue. Despite these challenges, large data sets like the REP have an important place in SpA research. These data sets are likely the only way in which we can learn about rare but severe disease manifestations or comorbidities in the near future. The large samples from such data sets are also necessary to detect small but common treatment effects, which are important on a population level (e.g., reductions in cardiovascular events or mortality).

In order to fully harness the potential of EMR data bases such as REP, more sophisticated programming tools are necessary to accurately predict and detect disease, and to more finely phenotype SpA subjects. Some predictive methods, including algorithms that incorporate diagnostic codes, and natural language processing, have been used in other diseases but rarely applied in SpA. SpA, with a myriad of potential manifestations, represents an ideal family of diseases for the application of some of these advanced methods *because* the disease heterogeneity makes statistical methods such as stratification or adjustment implausible. As computing power continues to become more accessible, these methods may become more common.

Furthermore, the study by Wang et al highlights the limitations of existing EMR infrastructure, particularly in the US. In the current system, potential subject populations are segmented into EMRs on the basis of

geography or insurer, rendering study samples fairly small and thereby limiting the precision of outcome estimates. Indeed, other observational studies based on EMR or administrative data from the US have suffered similar limitations, and many useful epidemiologic studies are performed in countries with single-EMR health care systems or other nationwide databases.

From the study by Wang et al and preexisting literature on IBP as a referral strategy or as a parameter for identification of axial SpA, several lessons have been learned. First, awareness of axial SpA must be increased among general practitioners and others who provide care to patients with back pain, in order to effectively channel those who have a moderate or high probability of SpA into care by a rheumatologist. While IBP may form the basis for referral strategies, IBP alone is neither necessary nor sufficient to diagnose axial SpA; rather, an IBP assessment must be part of a comprehensive evaluation that includes HLA–B27 testing and sacroiliac joint imaging. Strategies for identifying axial SpA must have high sensitivity, so that the vast majority of persons with axial SpA are evaluated by a rheumatologist. Simultaneously, these strategies must incorporate caution not to overburden rheumatologists with the care of patients with noninflammatory pain, who would be better suited in the care of other providers. Finally, epidemiologic research in SpA is likely to require large EMR databases and the use of advanced programming methods to accurately find and phenotype SpA cases. Taken together, the results of the study by Wang et al and of earlier trials of IBP as a referral or classification parameter clearly indicate that the majority of patients with symptoms of IBP do not have or develop axial SpA. Nonetheless, IBP is a relevant clinical tool as part of the assessment for axial SpA.

AUTHOR CONTRIBUTIONS

Drs. Dubreuil and Sieper drafted the article, revised it critically for important intellectual content, and approved the final version to be published.

REFERENCES

1. Jovaní V, Blasco-Blasco M, Ruiz-Cantero MT, Pascual E. Understanding how the diagnostic delay of spondyloarthritis differs between women and men: a systematic review and metaanalysis. J Rheumatol 2017;44:174–83.
2. Haroon N, Inman RD, Learch TJ, Weisman MH, Lee M, Rahbar MH, et al. The impact of tumor necrosis factor α inhibitors on radiographic progression in ankylosing spondylitis. Arthritis Rheum 2013;65:2645–54.
3. Rudwaleit M, Listing J, Brandt J, Braun J, Sieper J. Prediction of a major clinical response (BASDAI 50) to tumour necrosis factor α blockers in ankylosing spondylitis. Ann Rheum Dis 2004;63:665–70.
4. Danve A, Deodhar A. Screening and referral for axial spondyloarthritis: need of the hour. Clin Rheumatol 2015;34:987–93.
5. Rudwaleit M, van der Heijde D, Landewé R, Listing J, Akkoc N, Brandt J, et al. The development of Assessment of Spondylo-Arthritis international Society classification criteria for axial spondyloarthritis (part II): validation and final selection. Ann Rheum Dis 2009;68:777–83.
6. Burgos-Vargas R, Braun J. Inflammatory back pain. Rheum Dis Clin North Am 2012;38:487–99.
7. Weisman MH. Inflammatory back pain: the United States perspective. Rheum Dis Clin North Am 2012;38:501–12.
8. Rudwaleit M, Metter A, Listing J, Sieper J, Braun J. Inflammatory back pain in ankylosing spondylitis: a reassessment of the clinical history for application as classification and diagnostic criteria. Arthritis Rheum 2006;54:569–78.
9. Sieper J, van der Heijde D, Landewé R, Brandt J, Burgos-Vagas R, Collantes-Estevez E, et al. New criteria for inflammatory back pain in patients with chronic back pain: a real patient exercise by experts from the Assessment of SpondyloArthritis international Society (ASAS). Ann Rheum Dis 2009;68:784–8.
10. Reveille JD, Witter JP, Weisman MH. Prevalence of axial spondylarthritis in the United States: estimates from a cross-sectional survey. Arthritis Care Res (Hoboken) 2012;64:905–10.
11. Rudwaleit M, van der Heijde D, Khan MA, Braun J, Sieper J. How to diagnose axial spondyloarthritis early. Ann Rheum Dis 2004;63:535–43.
12. Wang R, Crowson CS, Wright K, Ward MM. Clinical evolution in patients with new-onset inflammatory back pain: a population-based cohort study. Arthritis Rheumatol 2018;70:1049–55.
13. Weisman MH, Witter JP, Reveille JD. The prevalence of inflammatory back pain: population-based estimates from the US National Health and Nutrition Examination Survey, 2009–10. Ann Rheum Dis 2013;72:369–73.
14. Van Onna M, Gorter S, van Meerendonk A, van Tubergen A. General practitioners' perceptions of their ability to identify and refer patients with suspected axial spondyloarthritis: a qualitative study. J Rheumatol 2014;41:897–901.

REVIEW

Synovial Cell Metabolism and Chronic Inflammation in Rheumatoid Arthritis

Jane Falconer,[1] Anne N. Murphy,[2] Stephen P. Young,[1] Andrew R. Clark,[3] Stefano Tiziani,[4] Monica Guma,[2] and Christopher D. Buckley[5,6]

Metabolomic studies of body fluids show that immune-mediated inflammatory diseases such as rheumatoid arthritis (RA) are associated with metabolic disruption. This is likely to reflect the increased bioenergetic and biosynthetic demands of sustained inflammation and changes in nutrient and oxygen availability in damaged tissue. The synovial membrane lining layer is the principal site of inflammation in RA. Here, the resident cells are fibroblast-like synoviocytes (FLS) and synovial tissue macrophages, which are transformed toward overproduction of enzymes that degrade cartilage and bone and cytokines that promote immune cell infiltration. Recent studies have shown metabolic changes in both FLS and macrophages from RA patients, and these may be therapeutically targetable. However, because the origins and subset-specific functions of synoviocytes are poorly understood, and the signaling modules that control metabolic deviation in RA synovial cells are yet to be explored, significant additional research is needed to translate these findings to clinical application. Furthermore, in many inflamed tissues, different cell types can forge metabolic collaborations through solute carriers in their membranes to meet a high demand for energy or biomolecules. Such relationships are likely to exist in the synovium and have not been studied. Finally, it is not yet known whether metabolic change is a consequence of disease or whether primary changes to cellular metabolism might underlie or contribute to the pathogenesis of early-stage disease. In this review article, we collate what is known about metabolism in synovial tissue cells and highlight future directions of research in this area.

Introduction

Rheumatoid arthritis (RA) is a systemic chronic inflammatory disease that principally manifests in the articular joints. Recent research has yielded biologic therapies and small molecules to target signaling pathways and pathogenic components involved in inflammation and immunity, but in spite of these reasonably successful treatments, very few RA patients are able to achieve and remain in a state of drug-free disease remission. Innovative strategies are needed to obtain new insights into mechanisms that underlie disease pathogenesis and to identify potential new treatments.

In fields such as oncology, the concept of undermining or reprogramming metabolism to improve patient outcomes is established, and we and other investigators believe that using similar strategies in immune-mediated inflammatory diseases has great potential (1,2). For 3 decades, researchers have hypothesized an intermediate role for metabolic alterations and local hypoxia in RA pathology (3,4). Indeed, RA and related immune-mediated inflammatory diseases are associated with systemically measurable metabolic disruption. This is likely to reflect the increased bioenergetic and biosynthetic demand placed on immune and stromal cells in a persistently activated state. We now

have the tools to better understand and translate past observations and to explore our hypothesis that metabolic deviation in synovial cells has a role in early pathogenesis rather than being a consequence of tissue damage.

Qualitative changes to cellular metabolism are indeed essential to support physiologic and pathologic responses seen in the RA synovium, and we describe these changes below. RA-associated characteristics include proliferation, migration, and invasion, which are hallmarks of activated fibroblast-like synoviocyte (FLS) behavior, and also proinflammatory mediator production, which is characteristic of activated synovial tissue macrophages (5–7). The phenotypic transformation of FLS from a quiescent cell to an aggressive, metabolically active cell, the activation of synovial tissue macrophages, and the increasingly hypoxic and nutrient-deprived microenvironment that develops in the RA joint are characteristics that closely resemble those seen in solid tumors.

Immunometabolism research has recently expanded after lessons were gleaned from the more advanced cancer literature, and this has led to the identification of potential new drug targets for immune-mediated pathologies (1,8). Limitation of metabolic substrate availability, modulation of signaling pathways that control metabolism, and targeting of channels through which metabolic intermediates are shared are exciting new strategies for treatment. Because there is now widespread acceptance that the future of RA treatment may lie in targeting synovial tissue and in particular the stromal cell microenvironment, it is logical to apply new therapies targeting metabolism in the synovium (9,10). In this review article, we describe our current knowledge of synovial metabolism and the therapeutic opportunities this field might present. We focus on FLS and synovial tissue macrophages, which together form a destructive frontier (pannus), the aberrant behavior of which is underpinned by pathologic metabolic changes.

A systemic metabolic phenotype in RA

Metabolic perturbations have long been associated with RA, and the hallmark "calor" (heat) observed in the rheumatoid joint is widely considered to be a consequence of metabolic activity. Daily whole-body resting energy expenditure is 8% higher in patients with RA than in healthy individuals, which suggests that these metabolic changes are significant and systemic (11). RA patients have an increased susceptibility to cardiovascular comorbidity and metabolic syndrome during the progression of their disease that is associated with disruption of lipid and glucose metabolism (12). Furthermore, the catabolic condition "cachexia" occurs in patients with RA, with

muscle atrophy and increase in body fat associated with systemically elevated levels of proinflammatory cytokines such as tumor necrosis factor (TNF), interleukin-1β (IL-1β), leukocyte inhibitory factor, interferon-γ (IFNγ), and IL-6 (13).

Untargeted metabolomic studies of body fluids are helping to characterize the observed systemic symptoms and changes alluded to above. These involve analysis of small molecules (<3 kd) usually using 1-dimensional nuclear magnetic resonance spectroscopy, or mass spectrometry coupled to gas or liquid phase separation techniques, technologies that our group recently compared and evaluated (14). This approach has highlighted urinary metabolite signatures that can identify the 6 most prevalent immune-mediated inflammatory diseases (15) and a serum metabolite signature that is correlated with the C-reactive protein (CRP) level and links metabolism with underlying inflammatory mechanisms (16). Serum (17) and synovial fluid (SF) (18,19) metabolomic profiles have also demonstrated the potential to distinguish RA from psoriatic arthritis and other diseases (14). Furthermore, our data and that of other investigators show that patient responses to biologic agents including etanercept and rituximab can be predicted from urine, serum, and plasma metabolic profiles, highlighting the power of metabolomics in stratifying patients and directing RA treatment (20–22).

Because immune and stromal cells within the inflamed joints are known to produce inflammatory cytokines, it is likely that they are contributing to the global metabolic phenotype in RA. However, information elucidating the metabolic profiles of individual cell types involved in chronicity or resolution of inflammation has been sparse. Such information will be important to link disease-associated metabolites to pathogenic processes and to gain a full understanding of RA pathogenesis.

The rheumatoid synovium

Although RA is a systemic disease, the major manifestations are joint pain and loss of function. The normal diarthrodial joint is lined with a thin soft tissue membrane, the synovium, that comprises a sublining and a thin intimal lining layer and produces and encapsulates a lubricating hyaluronic acid–rich fluid (23). Resident to the tissue are 2 heterogeneous and inadequately characterized cell types: 1) synovial tissue macrophages, a mixed population of embryonically seeded cells and cells that have differentiated from circulating monocytes (24,25) and 2) FLS (mesenchyme-derived cells) that, compared with fibroblasts in other anatomic locations, are characterized by the expression of UDP-glucose 6-dehydrogenase, an enzyme that is required for the synthesis of hyaluronic acid and

complement decay-accelerating factor (also known as CD55) (26). Collaborative networks such as the National Institutes of Health Accelerating Medicines Partnership are facilitating the effective digestion of tissue to obtain pure populations of FLS and synovial tissue macrophages. This, combined with a growing profile of soluble and surface markers and revolutions in fate-mapping and single-cell analysis techniques, is improving our ability to study and understand the functions of these important cells (27,28).

The hallmark of RA is a macroscopically visible change in the synovial lining layer that becomes inflamed, hyperplastic, and invasive of local cartilage and bone (29).

This is driven by a complex interaction between chronically activated and epigenetically transformed synoviocytes and infiltrating cells of the innate and adaptive immune systems (5,30). Both FLS and synovial tissue macrophages contribute to synovial inflammation by producing mediators that recruit and activate immune cells. Importantly, through production of cytokines such as TNF and granulocyte–macrophage colony-stimulating factor, FLS and synovial tissue macrophages also contribute to one another's chronic activation and survival. These cytokines act on FLS and synovial tissue macrophages in a paracrine manner, helping to drive disease chronicity (30). However, it is the FLS in the intimal lining that form
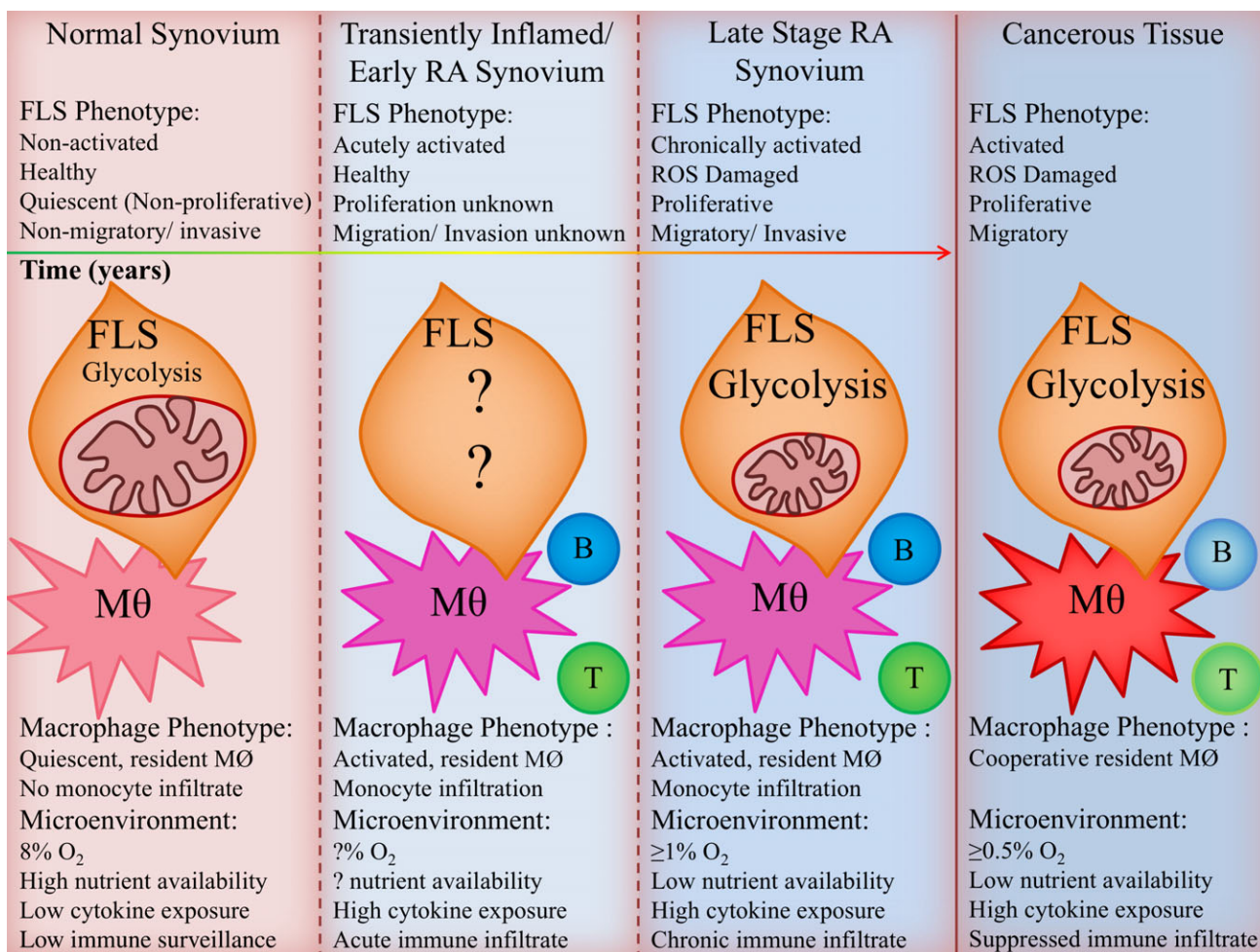
Figure 1. Similarities between rheumatoid arthritis (RA) synovium and the solid tumor microenvironment. In both tissues, fibroblasts and macrophages reside in close proximity and within an oxygen- and nutrient-deprived, cytokine-rich environment. Here they sustain mitochondrial damage and take on a chronically activated phenotype supported by increased glycolytic metabolism. In RA, the fibroblasts themselves are proliferative, invasive, and migratory; in cancer, fibroblasts support proliferation, invasion, and metastasis of tumor cells. Adaptive immune cell–fibroblast interactions are different in the tumor microenvironment versus the RA microenvironment. Activated T cells (green) and B cells (blue) are present in the RA synovium but are suppressed in the tumor microenvironment. Little is known about fibroblast or macrophage metabolism in early RA and the metabolic changes that take place during the transition from health to disease. FLS = fibroblast-like synoviocyte; Mθ = macrophage; ROS = reactive oxygen species.

the aggressive pannus and are the major effectors of tissue damage through production of extracellular matrix–degrading enzymes such as matrix metalloproteinases and cathepsins (30).

Although the joint exists at an oxygen tension as low as 8% even in health, the microenvironment in RA is characterized by severe hypoxia at oxygen tensions that fall to <1% (31). Nutrient availability is also low, because immune cells and activated synoviocytes consume available resources at a rate that exceeds their delivery. Synovial angiogenesis, which is mediated by factors released by both FLS and synovial tissue macrophages and enhances the ingress of leukocytes into the synovial tissue, is insufficient, and the aggressive front formed by the hyperplastic synovial lining increases the distance between blood vessels and synoviocytes (32,33). RA FLS are transformed from a quiescent state to an aggressive, invasive phenotype, and they persist despite enrichment of apoptosis-inducing factors such as oxygen radicals, nitric oxide, and cytokines supplied by activated synovial tissue macrophages. As such, the synovium bears resemblance to tumor tissue, and cells are likely to be subject to elevated bioenergetic and biosynthetic demands similar to those seen in cancer. This comparison is summarized in Figure 1.

It is likely that adaptation of mitochondria and cytoplasmic metabolic pathways is needed to meet the requirements of chronic inflammation in RA. Indeed, in the few studies that profiled the metabolome of FLS, profound metabolic differences were identified in end-stage RA compared with osteoarthritis, and many of these are described below (34,35). Our unpublished data showed a correlation between systemic inflammation (as measured by the CRP level) and the metabolic profile of FLS from patients with very early RA. However, there are few studies comparing FLS from patients with early RA with FLS from healthy subjects or assessing changes during the transformation to a chronically activated phenotype in early disease. Consequently, we are currently unable to determine whether metabolic adaptation of fibroblasts is a normal response to chronic inflammation or whether primary changes to cellular metabolism might themselves underlie or contribute to disease pathogenesis. There also are few studies of synovial tissue macrophages, and most of what is known about RA macrophage metabolism is based on animal models or studies of cells differentiated in vitro from SF or peripheral blood monocytes (36). Because macrophages in healthy synovium are thought to be largely yolk sac–derived, and cues leading to monocyte differentiation in tissue are poorly defined, there is a pressing need for better characterization of synovial macrophage subsets and their metabolism (37).

The dynamic metabolic response in health

The function of the metabolic machinery within a cell is to provide the energy and biomolecules necessary to perform resting and activated functions while managing the production of potentially damaging by-products such as lactate and reactive oxygen species (ROS). Recent studies of immune cells have identified important roles for metabolism in supporting and even directing cell differentiation and fate. These studies have characterized the extent of metabolic plasticity required for cellular responses to stimulation (8). Six main pathways are involved in these functions (see Figure 2). Of these, oxidative phosphorylation (comprising the tricarboxylic acid [TCA] cycle and the mitochondrial electron transport chain) and fatty acid oxidation are oxygen dependent and take place in the mitochondria while utilizing substrates taken up from the cytoplasm. Glycolysis, the pentose phosphate pathway, amino acid metabolism, and fatty acid synthesis are oxygen independent and largely take place in the cytoplasm. However, fatty acid and amino acid intermediates are also shared with mitochondrial processes, and use of the pentose phosphate pathway to maintain redox balance requires oxygen (8).

Normal physiologic metabolism and metabolic responses to inflammatory events are poorly studied in tissue-resident populations such as fibroblasts and embryonically seeded macrophages (25). This is largely due to the practicality of disentwining cells from the extracellular matrix, a challenge that researchers are making great efforts to address (38). Indeed, there has been limited progress since the stromal cell metabolism field was thoroughly reviewed in 2014 (39). One study defined what is known about resting healthy fibroblast metabolism, showing that foreskin-derived cells are predominantly glycolytic and dependent on the pentose phosphate pathway even during quiescence (40). These pathways lead to biomolecule synthesis and support the anabolic processes associated with extracellular matrix production and this is likely to also apply to FLS, which maintain SF and produce it in excess in RA.

Reversible regulation in the balance of cytoplasmic and mitochondrial metabolism is crucial for all cells to respond and adapt to changing microenvironments. Metabolic change is orchestrated by signaling pathways responding to nutrient energy and oxygen levels as well as growth factor, pattern recognition, and cytokine receptors. The pathways involved have been reviewed previously (41,42) and are summarized in Figure 2. These include the master regulators mechanistic target of rapamycin (mTOR) pathway and 5′-adenosine monophosphate–activated protein kinase (AMPK) pathway, which work in opposition to one another. The mTOR network is a nutrient-sensing system.
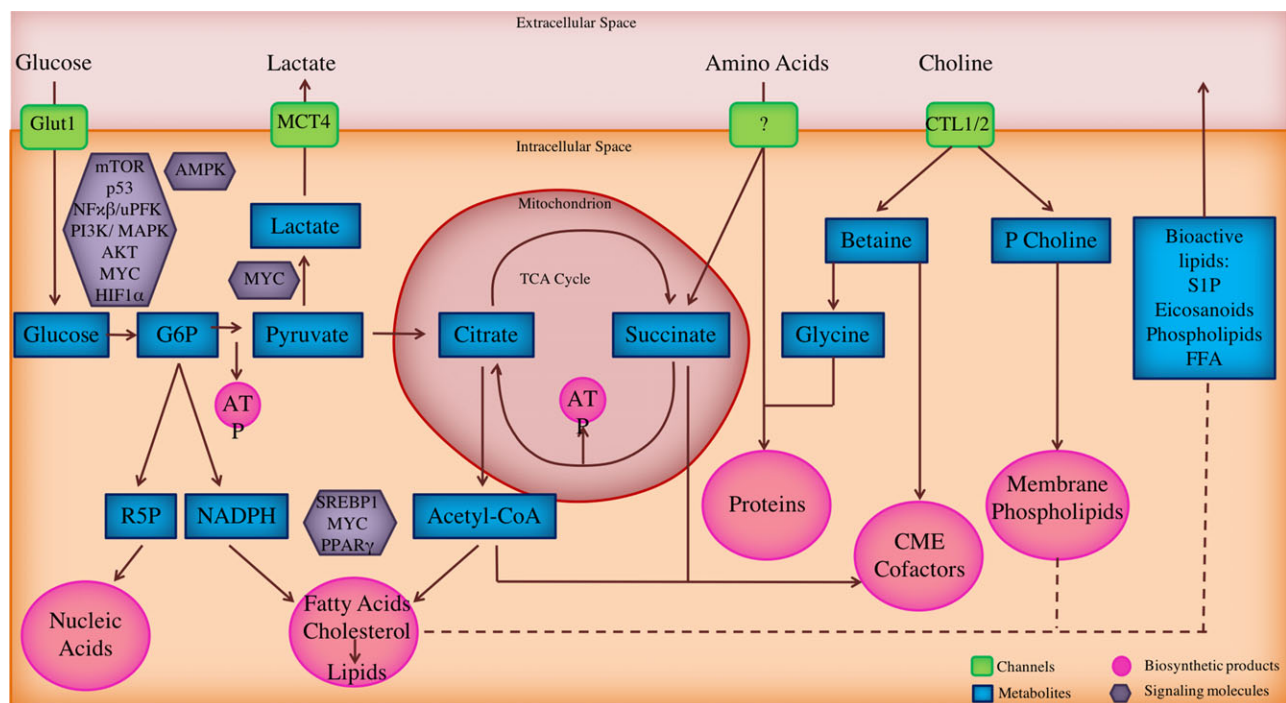
Figure 2. Major pathways important in synoviocyte metabolism. Fibroblast-like synoviocytes (FLS) and monocyte-derived macrophages are heavily reliant on glucose metabolism and regulate glucose transporter member 1 (GLUT-1) in response to inflammatory and stress stimuli. This fuels ATP production under conditions of high energy demand. Glucose is used in the pentose phosphate pathway to synthesize building blocks for nucleic acids and to generate NADPH to control redox status and support lipid synthesis. Alternatively, glucose is metabolized via glycolysis to pyruvate, which either is transported into the mitochondria to contribute to tricarboxylic acid (TCA) cycle flux or is converted to lactate in the cytoplasm and removed from the cell via monocarboxylate transporter 4 (MCT4). TCA cycle flux contributes to ATP production via oxidative and substrate-level phosphorylation. When matrix citrate levels rise, citrate is transported to the cytoplasm and yields acetyl-coenzyme A (acetyl-CoA), the starting material for synthesis of fatty acid (FA), cholesterol, and lipids. Some such lipids are exported from the cell as bioactive metabolites such as sphingosine 1 phosphate (S1P), free FA (FFA), phospholipids, and eicosanoids. Acetyl-CoA as well as succinate generated from the TCA cycle can be used in the production of chromatin-modifying enzymes (CMEs) and cofactors. Choline is taken up via choline transporter-like proteins 1 and 2 (CTL1/2) and is an important substrate in FLS biology. Choline can be converted to betaine, which is used in the production of CMEs and cofactors or converted to glycine for use in protein synthesis. Alternatively, choline is phosphorylated to phosphocholine and utilized in membrane phospholipid and bioactive lipid synthesis. A number of signaling molecules that control the described metabolic pathways have been identified but have been explored sparsely in FLS. mTOR = mechanistic target of rapamycin; AMPK = 5′-adenosine monophosphate–activated protein kinase; p53 = cellular tumor antigen p53; uPFK = ubiquitous phosphofructokinase 2; PI3K = phosphatidylinositol 3-kinase; P choline = phosphorylated choline; Myc = Myc proto-oncogene protein; HIF-1α = hypoxia-inducible factor 1α; G6P = glucose-6-phosphate; R5P = ribose-5-phosphate; SREBP = sterol regulatory element binding protein; PPARγ = peroxisome proliferator-activated receptor γ.

Mechanistic target of rapamycin complex 1 (mTORC-1) or mTORC-2 complex formation downstream of the phosphatidylinositol 3-kinase (PI3K) pathway or the MAPK pathway induces activation of Akt and transcription factors hypoxia-inducible factor 1α (HIF-1α) and Myc, which in turn activate glycolytic pathway genes up-regulating aerobic glycolysis. Sterol regulatory element binding proteins and peroxisome proliferator–activated receptor γ (PPARγ) acting downstream of mTORC-1 also activate genes that up-regulate fatty acid synthesis.

Other pathways have also been shown to activate glycolysis in an HIF-1α–independent manner, including the NF-κB pathway involving ubiquitous phosphofructokinase

2. AMPK is an energy-sensing system that often is considered to be a metabolic checkpoint, because it can inhibit glycolysis, control cell proliferation, and promote mitochondrial biogenesis when activated under conditions of energetic stress (43,44). Downstream nuclear respiratory factor 1 (NRF-1), NRF-2, and PPARγ coactivator 1α (PGC-1α), as well as sirtuin 1– or STAT-6–activated PGC-1β, induce mitochondrial biogenesis and fusion (discussed below), induce protective antioxidant enzymes, and promote oxidative metabolism. The mTOR pathway has also been shown to be important in polarization of macrophages to proinflammatory (M1) or pro-resolving (M2) phenotypes and in activation of both macrophage subtypes, and this has

Table 1. Definitions of terms used in the context of this review*

Term	Definition
Aerobic glycolysis	The metabolic pathway that utilizes glucose to generate ATP in the presence of oxygen. End products of this process are pyruvate, which can be imported into mitochondria for use in the TCA cycle, or lactate, which is expelled from the cell as waste.
Anabolism	The enzymatic synthesis of molecules from smaller components.
Anaplerosis	The replenishment of metabolic intermediates into the TCA cycle as substrates for biosynthesis and the generation of ATP.
Bioenergetics	The study of energy production by cells. Often associated with use of a Seahorse analyzer to assess glycolysis and oxidative phosphorylation rates in real time.
Catabolism	The enzymatic degradation of molecules into smaller products.
Cataplerosis	The removal of TCA cycle intermediates for use in biosynthesis or to prevent buildup within mitochondria.
Electron transport chain	A set of complexes of the inner mitochondrial membrane that shuttle electrons from NADH and $FADH_2$ to oxygen. The redox reactions of the chain produce an electrochemical gradient of protons across the membrane, which drives synthesis of ATP by oxidative phosphorylation.
Hypoxia	Oxygen deficiency in tissue, such that oxygen tension is lower than that under healthy physiologic conditions. Normal oxygen levels differ between tissues, and therefore the level at which a tissue is considered to be hypoxic is variable. The arthritic joint has an oxygen tension of 8% in health and <3% in RA.
Imaging mass spectrometry	A mass spectrometry–based technique that allows the spatial distribution of the metabolome to be visualized in a tissue section. This offers insights into where pathogenic metabolic changes are taking place in tissues and has not yet been applied to the synovium.
Immunometabolism	The research field that investigates metabolism in the context of immunity and inflammation. Because stromal cells are crucial to both induction and resolution of these processes, we consider the study of their metabolic processes to be embedded in this field.
Metabolic coupling	The transfer of metabolites between cells in a manner that benefits the biosynthetic and bioenergetic requirements of the recipient cell.
Metabolic flux analysis	Also known as "stable isotope metabolic tracer analysis," this is a ^{13}C isotope–tracing methodology involving incubation of cells with a stable isotope, quantitation of metabolite labeling using mass spectrometry or NMR spectroscopy, and computational fitting of the data to a model, allowing estimates of pathway-specific flux.
Metabolic memory	Imprinting of a metabolic phenotype on a cell by cues within its microenvironment, such that the phenotype is maintained after the cues are removed or the cells are removed from the tissue.
Metabolome	All substrates, intermediates, and products of metabolism associated with a given system or compartment. These may be intracellular or extracellular.
Metabolomics	Used synonymously with the term "metabolic profiling," this is the identification and measurement of all or a targeted set of metabolites within a body fluid, cell population, or tissue, conducted by NMR spectroscopy or mass spectrometry.
Mitochondrial biogenesis	The generation of greater mitochondrial mass to increase the capacity for mitochondrial function and ATP production within a cell; this process is important to health but has not been investigated in RA.
Mitochondrial dynamics	The balance and transition between mitochondrial fusion and fission, movement, and degradation. These processes are important to health but have not been investigated in RA.
Mitochondrial fission	The division of mitochondrial networks into individual punctate organelles, principally controlled by outer membrane proteins DRP1 and FIS1.
Mitochondrial fusion	The formation of tubular mitochondrial networks through Mfn-1-, Mfn-2, and Opa-1–mediated joining of individual organelle membranes. This process is associated with increased ATP production and protection of mitochondrial DNA from reactive oxygen species.
Mitophagy	Mitochondrial-selective autophagy. The selective degradation of defective mitochondria without the release of inflammatory mitochondria-associated DAMPs.
Oxidative phosphorylation	Generation of ATP by mitochondrial ATP synthase and driven by the electrochemical gradient of protons generated by the electron transport chain.
Pentose phosphate pathway	The pathway that oxidizes glucose to generate NADPH for the maintenance of the cellular redox balance and 5 carbon sugars utilized in anabolic processes such as nucleic acid synthesis.
Positron emission tomography	Use of a radioactive tracer isotope incorporated into a metabolic substrate to visualize metabolizing cells in a whole organism. Commonly, labeled glucose is used to identify tumors but also is useful for highlighting sites of inflammation such as the rheumatoid joint.
Reverse Warburg effect	The production of high-energy metabolic intermediates by one cell to anaplerotically feed ATP production by a neighboring cell. This effect is currently characterized only in epithelial tumors where cancer-associated fibroblasts feed lactate and other metabolites to tumor cells through channels such as monocarboxylate transporters.
TCA	The TCA cycle is a series of chemical reactions that take place in the mitochondrial matrix, generating ATP by substrate-level phosphorylation and NADH and $FADH_2$ by oxidation of fuel molecules. NADH and $FADH_2$ are further oxidized by the electron transport chain.
Warburg effect	Pathologic increase in glycolysis associated with reduced oxidative phosphorylation despite the presence of oxygen. The term describes a cellular bioenergetic phenotype classically associated with tumor cells but currently also associated with activated immune cells.

* TCA = tricarboxylic acid; RA = rheumatoid arthritis; NMR = nuclear magnetic resonance; DRP1 = dynamin-related protein 1; FIS1 = mitochondrial fission 1; Mfn-1 = mitofusin 1; Opa-1= optic atrophy 1; DAMPs = damage-associated molecular patterns.

been thoroughly reviewed (45). AMPK activation in macrophages is associated with suppression of IL-6 production, antiinflammatory M2 macrophage differentiation from SF monocytes, and suppressed inflammation in K/BxN mouse serum–induced arthritis (46,47). The signaling pathways that instruct stromal cell behavior are less well defined. Activation of mTOR has been linked to invasive properties in FLS from arthritic rats (48). Furthermore, mice deficient in NRF-2, which acts downstream of AMPK, showed more severe cartilage injuries and more oxidative damage in a murine model of arthritis (49). However, no link between metabolism and cell signaling has been identified in human FLS or synovial tissue macrophages, and it is unknown whether signaling pathways controlling the metabolic phenotype are dysregulated in RA.

Mitochondrial responses in the RA synovium

Under normoxic conditions, mitochondrial oxidative phosphorylation is the most efficient source of ATP (50). In addition, mitochondria integrate various metabolic pathways and through this process produce intermediates needed for the synthesis of lipids, steroid hormones, and heme. Other more specialized mitochondrial functions include maintenance of Ca^{2+} homeostasis, regulation of apoptosis, and production of the physiologic levels of ROS that act as signaling molecules (50). Importantly, mitochondria have mechanisms to respond spatially and temporally to heterogeneous nutrient and oxygen concentrations, increased ATP demands, and increased stress signals, including oxidative stress, for continued support of cellular functions and survival. These mechanisms include overexpression of antioxidant enzymes and remodeling of respiratory complex subunits, changes in substrate usage (using glutamine, pyruvate, fatty acids, and ketone bodies), or switching toward increased glycolysis when energy demand outpaces oxygen delivery (50).

Changes in mitochondrial biogenesis, mitochondrial-selective autophagy (mitophagy), and the equilibrium between mitochondrial fusion and fission are also critical to maintain normal mitochondrial and cellular function (Table 1 and Figure 3). Mitochondrial biogenesis is induced through the signaling pathways described above, not only in association with cell division but also in response to oxidative stimuli and increased energy requirements. The flux between fusion and fission of mitochondria in response to stress is also crucial to maintaining the metabolic capacity of the mitochondria as well as protecting genetic stability. Mitophagy plays a pivotal role in the maintenance of mitochondrial homeostasis, by regulating the size and quality of the mitochondrial population. In addition, mitophagy eliminates damaged mitochondria under diverse stress conditions, which is critical because mitochondrial DNA (mtDNA) is a damage-associated molecular pattern molecule that contributes to systemic inflammatory responses (51). Modulation of mitochondrial dynamics, biogenesis, and mitophagy can be deleterious and associated with aging in mouse models and multiple serious human diseases, highlighting the importance of these processes in cell phenotype and function (51,52). Furthermore, mitochondrial surveillance and quality control mechanisms including mitochondrial biogenesis and mitophagy decline with age, causing progressive deterioration of mitochondrial function. This may have a role in diseases such as RA and suggests that targeting mitochondrial processes could be beneficial for restoring cell function (53).

Surprisingly little is known about mitochondrial function and dynamics in FLS or synovial tissue macrophages. However, a growing body of literature describes mitochondrial metabolism downstream of glycolytic glucose consumption and its role in differentiation and activation of proinflammatory and pro-resolving monocyte-derived macrophage subtypes. These model systems might inform synovial tissue research. For example, stimulation of macrophages with lipopolysaccharide and IFNγ (so-called M1-polarizing conditions) produces proinflammatory cells that may resemble those that populate the RA synovium. This leads to inhibition of the TCA cycle and the mitochondrial oxidative phosphorylation pathway to which it is coupled, and results in up-regulation of glucose transporter 1 (GLUT-1) to facilitate efficient uptake of glucose.

Glucose is consumed through up-regulated aerobic glycolysis, resulting in production of lactate, which must be extruded from the cell to prevent damaging lactic acidosis (54). Production of reactive oxygen is increased, partly as a consequence of reversed electron transport by mitochondria, and certain intermediates of the TCA cycle (notably, succinate) accumulate. This promotes expression of the proinflammatory cytokine IL-1β by inhibiting prolyl hydroxylases and activating the transcription factor HIF-1α. Succinate has also been linked to changes in methylation of DNA and associated histone proteins to alter gene expression (55). Furthermore, isocitrate is diverted from the Krebs cycle and metabolized to itaconic acid, which is another, more recently identified TCA cycle inhibitor (56). RA synovial macrophages express HIF-1α, consistent with a switch to glycolytic metabolism, but efforts are required to characterize mitochondrial metabolism and dynamics in resident and infiltrating synovial tissue macrophages (57).

In several studies, mitochondria were observed in FLS from patients with late-stage RA. Reductions in
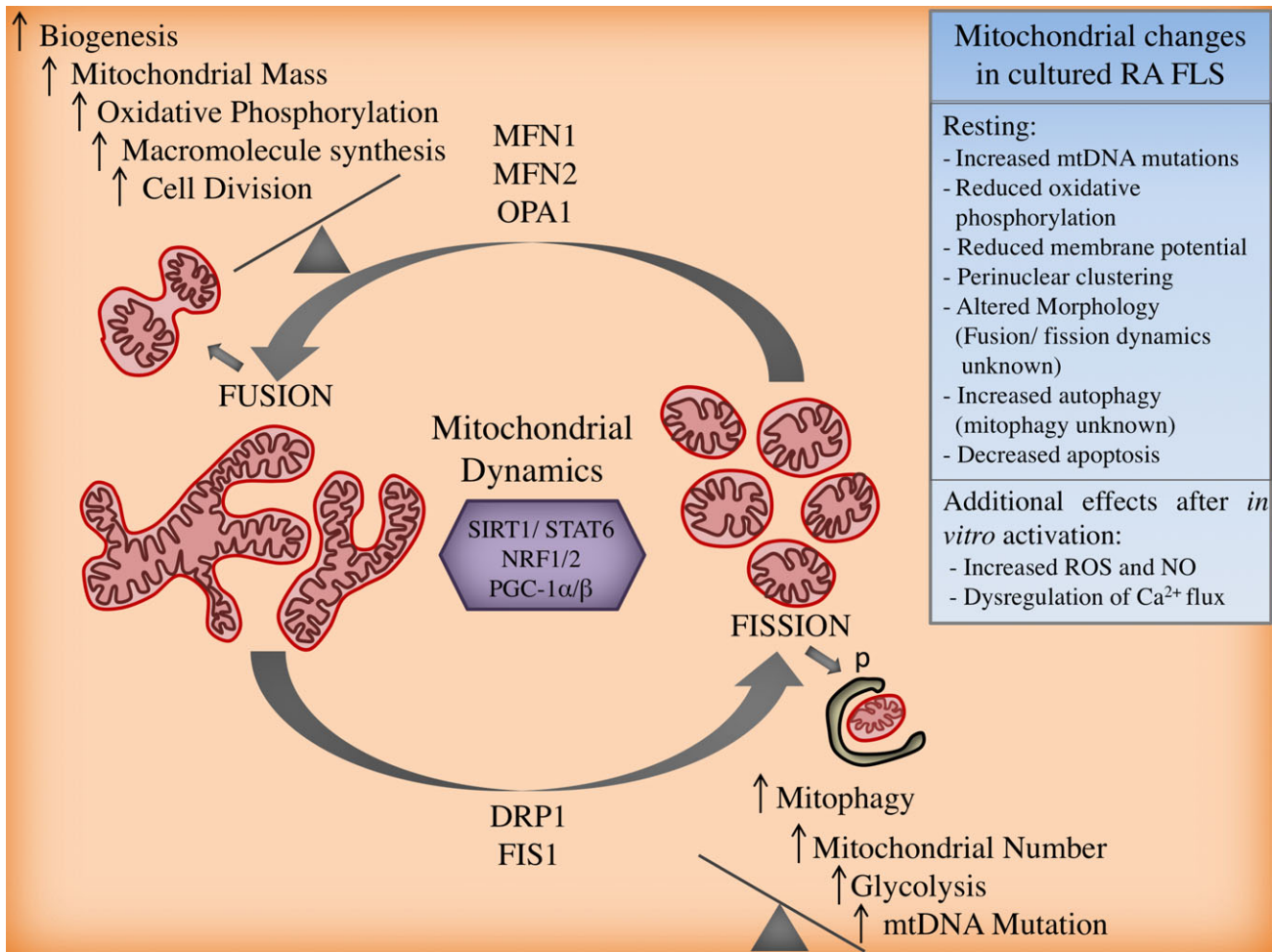
Figure 3. Mitochondrial fusion and fission cycle. Mitochondrial morphology changes dynamically in response to stress and changing energy demand. This occurs under the control of signaling molecules including sirtuin 1 (SIRT-1), STAT-6, nuclear respiratory factors 1 and 2 (Nrf-1/2), and peroxisome proliferator-activated receptor γ (PPARγ) coactivators 1α and β (PGC-1α/β). Mitochondria fuse to make tubular networks under the control of mitofusins 1 and 2 (Mfn-1) and optic atrophy 1 (Opa-1), a mechanism that is thought to increase ATP production by oxidative phosphorylation, protect mitochondrial DNA (mtDNA) from damage in the presence of elevated levels of reactive oxygen species (ROS), and lead to mitochondrial biogenesis and increased mitochondrial mass. Mitochondrial fission occurs under the control of dynamin-related protein 1 (DRP1) and mitochondrial fission 1 (FIS1) and produces increased numbers of punctate mitochondria. Fission usually corresponds with reduced oxidative phosphorylation and increased aerobic glycolysis and can predispose to mitochondrial-selective autophagy (mitophagy) to regulate mitochondrial mass or remove damaged organelles. **Inset,** Mitochondrial changes in rheumatoid arthritis (RA) fibroblast-like synoviocytes (FLS), in a resting state and after stimulation with proinflammatory cytokines, suggesting possible changes in mitochondrial dynamics that have not yet been investigated. NO = nitric oxide.

respiration and membrane potential (58) and changes to mitochondrial morphology (50) have been observed in unstimulated cells when compared with OA FLS. Further changes suggestive of mitochondrial dysfunction such as perinuclear clustering of mitochondria, abnormally dark cristae, and autophagosome formation have been associated with lower basal mitochondrial membrane potential as well as lower basal, maximum, and ATP-linked mitochondrial respiratory rates (58). In a complementary study in which RA FLS were compared with OA FLS, our group recently showed that RA FLS had a higher ratio of glycolytic rate to respiratory rate, implying a shift toward reliance on glycolysis to meet the energy demand of the cells (60).

Changes in mitochondrial metabolism can be induced in FLS by cytokines and growth factors, including IL-17, TNF, and platelet-derived growth factor (PDGF), which are associated with RA and related inflammatory conditions (58,61). The reported consequences, although incompletely understood, include

reduced ATP production by oxidative phosphorylation, production of excessive reactive oxygen and nitrogen species, dysregulation of Ca^{2+}, opening of the permeability transition pore, and initiation of cell death in vitro.

Significant increases in mtDNA mutation frequency have been demonstrated in inflamed synovial tissue and were positively correlated with macroscopic synovitis, vascularity, and SF levels of TNF and IFNγ (62). Another study showed that exposure of RA synovial tissue to 1% oxygen in vivo induced mtDNA mutations, suggesting that the inflamed and hypoxic joint microenvironment may be eliciting the mitochondrial changes observed in RA FLS and likely to be occurring in synovial tissue macrophages (31). Hypoxia also altered the bioenergetics of cultured FLS by promoting a switch to glycolysis while attenuating mitochondrial respiration and ATP synthesis. This supported abnormal angiogenesis, cellular invasion, and pannus formation (59). Additional in vitro studies indicated an increased number of mtDNA mutations and ROS levels in RA FLS compared with OA FLS (63), correlating with elevated matrix metalloproteinase expression and an invasive phenotype in RA (61,64).

The findings described above suggest that there are mitochondrial changes in FLS from patients with late-stage RA that are maintained in in vitro culture, yet we lack understanding regarding which changes are a normal response to meet metabolic demands of inflammation, which might play a role in driving the pathology of chronic disease and which are the result of damage and an increasingly hypoxic environment. In fact, resistance to induction of programmed cell death (apoptosis) by apoptotic signals abundant in the inflamed joint is a prominent characteristic of the RA synovium (65) and sustains the synovial hyperplasia that characterizes the rheumatoid pannus. This would suggest that mitochondrial responses induced by hypoxia and inflammation in synoviocytes are able to repurpose the mitochondrion as a biosynthetic hub similar to that in tumor cells (66) and with conserved mechanisms for limiting oxidative stress and supporting effector functions and proliferation (5). Finally, although information regarding mitophagy in the synovium is lacking, it has been suggested that TNF significantly induces mitophagy and mitochondrial antigen presentation in mouse macrophages, with implications for RA (67).

Several studies have shown altered autophagy in RA FLS, which could also contribute to synovial hyperplasia. RA FLS show an increase in genes involved in autophagy such as beclin 1 and light chain 3, which are inversely correlated with their apoptosis rate (68,69). In addition, RA FLS under endoplasmic reticulum stress may increase autophagy while becoming resistant to apoptotic death (70). Further studies are needed to understand the tangled relationship between metabolism, apoptosis, and autophagy in synoviocytes and to identify whether restoring normal metabolism and mitochondrial function might have therapeutic potential in RA.

Glucose metabolism in the RA synovium

Glucose and other metabolites such as glutamine, fatty acids, and ketone bodies can be metabolized through the TCA cycle in metabolically active tissue, but a shift away from oxidative phosphorylation toward aerobic glycolysis often occurs in response to cellular activation and in inflamed tissues (71). This supports various biosynthetic pathways and, consequently, the metabolic requirements for proliferation and cytokine production. Accelerated glucose metabolism is a hallmark of proliferative and activated cells (72) and can be observed with clinical imaging. Several studies have used fluoro-2-deoxyglucose (FDG), which is taken up by glycolytic cells to form FDG phosphate and can be shown by positron emission tomography (PET) to accumulate in swollen joints (73). Indeed, glycolytic inhibition by 3-bromopyruvate (BrPa) administered in a serum transfer animal model significantly decreased arthritis severity, highlighting the importance of glucose metabolism in fueling pathologic processes and making it a promising target for therapeutic intervention in RA (60). However, as discussed in a recent review by Weyand and Goronzy comparing macrophages and T cells, cells can coexist in the same microenvironment and utilize metabolites differently (74). This highlights the need to dissect glucose utilization in different synoviocytes, because any successful treatment will necessarily be cell type specific.

Metabolic profiling of synovial tissue has revealed that FLS consistently show altered basal glucose metabolism in RA (34,35,75), and we and other investigators have observed that stimuli such as PDGF and TNF increase in vitro glucose metabolism by both glycolysis and mitochondrial respiration (60). Furthermore, the glucose channel GLUT-1 is up-regulated in response to hypoxia and cytokines and is correlated with phenotypic perturbations in RA FLS (59,60). Glucose deprivation or glycolytic inhibitors such as 2-deoxy-D-glucose, BrPa (60), and 3-(3-Pyridinyl)-1-(4-pyridinyl)-2-propen-1-one (59) have been shown to impair cytokine secretion, proliferation, migration, and invasion in RA FLS. Although glucose metabolism is enhanced in activated macrophages, no data for synovial tissue macrophages are currently available.

Diversion of glucose metabolism away from glycolysis and toward the pentose phosphate pathway is important to support a biosynthetic role of some cells. A role for this pathway in RA was highlighted by a study of T cells, which showed impaired glycolytic flux due to elevated

pentose shunt activity and up-regulation of phosphofructokinase (76). In light of RA synoviocyte mitochondrial responses and the elevated ROS production described above, increased flux of glucose through the pentose phosphate pathway might also be expected in these cells to produce cytoplasmic NADPH and drive the reducing power of ROS detoxification enzyme systems in both the cytoplasm and the mitochondrial compartments. Indeed, a global increase in glucose metabolism (via both the pentose phosphate pathway and glycolysis) was observed in total synoviocytes (4), and recent metabolite profiling of FLS (77) showed that both metabolites associated with glycolysis and the pentose phosphate pathway were significantly increased in RA compared with OA, together with other metabolites that belonged to the amine, fatty acid, phosphate, and organic acid classes. Although this hints at the importance of the pentose phosphate pathway, its role, and the importance of NADPH production and other antioxidant mechanisms such as the up-regulation of the glutathione oxidation pathway have not yet been dissected in FLS and resident synovial tissue macrophages populations, and such research might yield new opportunities for therapeutic intervention in RA.

Functions have emerged for glucose metabolites, metabolic enzymes, and TCA cycle intermediates, which are secondary to their canonical roles in metabolic pathways. For instance, succinate stabilizes the transcription factor HIF-1α in activated macrophages and also rat synovial fibroblasts, promoting glycolysis (55,78). Succinate and other metabolites including α-ketoglutarate, fumarate, and acetyl-coenzyme A might be expected to accumulate in macrophages and FLS under hypoxic conditions and are involved in eliciting important epigenetic changes, with the potential for driving chronic inflammation remaining unexplored (55,78). In addition, essential glycolytic enzymes have been reported to translocate to the nucleus or mitochondria, where they function independently of their canonical metabolic roles in the regulation of cytokines and antiapoptotic responses (79,80). For example, pyruvate kinase muscle enzyme M2 (PKM2) also stabilizes HIF-1α, promoting inflammatory M1-type macrophage differentiation. Use of a small-molecule modulator of PKM2 to prevent nuclear translocation has potential for driving a shift toward an M2 phenotype and restoration of tolerance in diseases such as RA.

The hexokinase enzymes are also important regulators of metabolism. Hexokinase type I is known to drive cleavage and activation of pro–IL-1β in macrophages via the NLRP3 inflammasome and the downstream activation of caspase 1 (81), although this has not been studied in synovial tissue macrophages.

Hexokinase type II also binds to the mitochondrial membrane via its interaction with the outer membrane porin protein (also termed the voltage-dependent anion channel), and this interaction inhibits the release of intermembrane proapoptotic proteins, thereby protecting cells against apoptosis. Importantly, the expression of hexokinase type II is increased in RA FLS compared with OA FLS, and this might provide an important link between metabolism and apoptosis resistance in the RA synovium (60).

Lipid metabolism in the RA synovium

Lipids are known to be important for fueling adaptive immunity and in the resolution of inflammation. However, their role in these processes is complex and our understanding incomplete (8,82). A few studies have shown lipid changes in RA FLS, although this has not been studied in synovial tissue macrophages. Metabolomic profiling has shown a perturbation of lipid metabolism in RA FLS versus OA FLS (34), and recent studies have identified important roles for molecules that interact with lipids such as choline, an important component of membrane phospholipids that may be limiting in proliferating cells such as RA FLS. PET scanning with ^{11}C-choline, which is already in clinical use to identify prostate cancer metastasis, showed increased uptake in inflamed arthritic joints (83), and choline is present at elevated levels in RA FLS and synovium (34,75). It is of interest that choline transporter-like protein 1 (CTL1) (high affinity) and CTL2 (low affinity) are also highly expressed in RA FLS, and the functional inhibition of choline transporters promoted apoptotic FLS death (84).

Our group previously reported a possible therapeutic benefit in targeting choline kinase, the enzyme that catalyzes the first step in the cytidine diphosphate/choline pathway and that is essential for phosphatidylcholine biosynthesis. Inhibition of choline kinase suppressed migration and enhanced apoptosis in cultured RA FLS and significantly "decreased arthritis in pretreatment protocols as well as in established disease" (35). In addition, phospholipase enzymes specifically cleave phosphatidylcholine, producing phosphatidic acid and choline. Agonist-induced phospholipase D activation results in phosphatidic acid synthesis, which is thought to be involved in a variety of rapid cellular responses such as cytokine secretion (85). In RA FLS and RA synovial biopsy explants, phospholipase D isoform–specific inhibitors significantly reduced constitutive secretion of IL-6 and IL-8, further highlighting the importance of phospholipid metabolism in inflammation (86). Another study showed that activated FLS from

patients with inflammatory arthritis and animal models of inflammatory arthritis express significant quantities of autotaxin, which catalyzes the conversion of lysophosphatidylcholines (LPCs) to lysophosphatidic acid (LPA). Notably, high levels of LPC and low phosphatidylcholine: LPC ratios in plasma were shown to represent a reliable measure of inflammation (87). TNF-induced autotaxin expression in FLS and LPA, in turn, induced an activated FLS phenotype in synergy with TNF (88,89). Conditional genetic ablation of autoxin in mesenchymal cells, including FLS, resulted in disease attenuation in animal models of arthritis (90).

Metabolic coupling of cells in the RA synovium

The problem with many of the studies described above is that they tend to treat FLS and synovial tissue macrophages as if they exist in isolation. However, metabolism is not a private function, and metabolites produced by one cell can have profound effects on the biology of another. As described above, metabolites such as succinate, citrate, and isocitrate accumulate in inflammatory macrophages and control metabolism in a feedback loop. It is possible that such metabolites derived from synovial tissue macrophages might have a role in influencing the metabolism and function of proximal FLS, but this has not yet been investigated. Indeed, metabolite exchange between stromal and parenchymal cells is an essential function common to numerous metabolically active tissues including muscle, nerve, kidney, liver, and testicle.

Solute carriers including the monocarboxylate transporters (MCTs) are used as a means of physiologic metabolic coupling between different cell types, as extensively reviewed (91). Here, macrophage-like cells
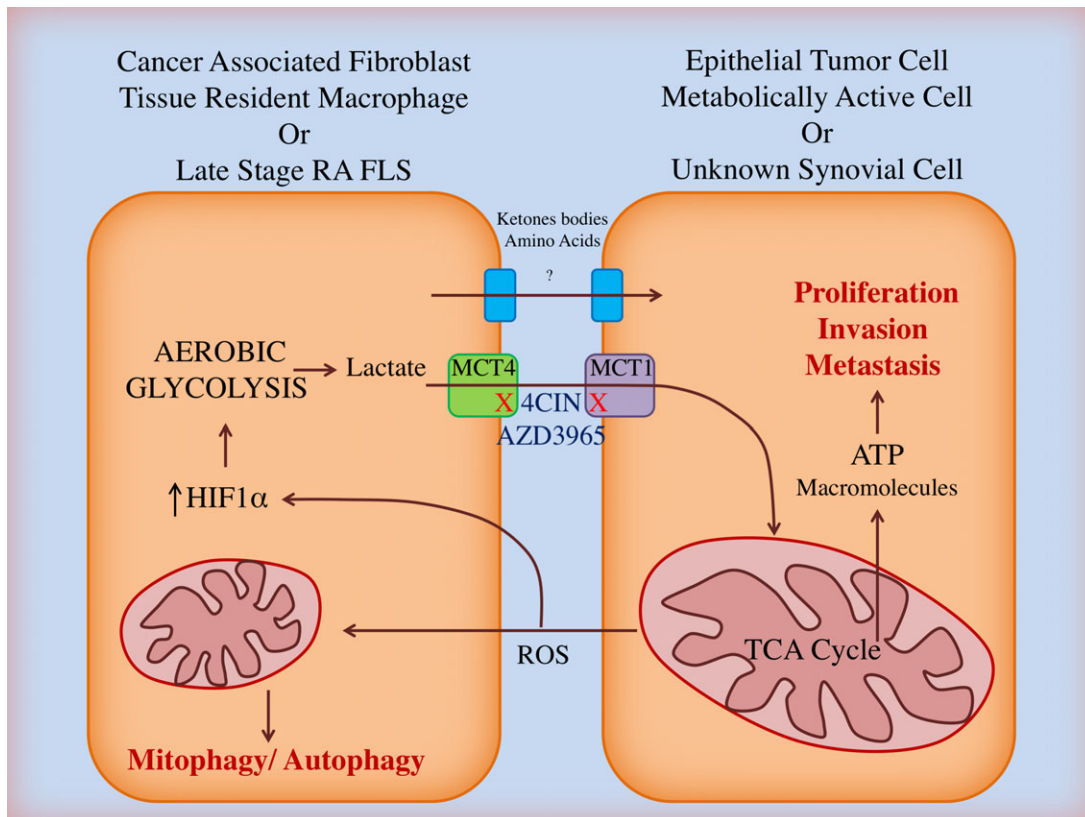
Figure 4. The reverse Warburg effect in cancer and rheumatoid arthritis (RA). In epithelial tumors, the reactive oxygen species (ROS) produced by metabolically active cancer cells cause mitochondria-selective autophagy (mitophagy) and activate HIF-1α in local cancer-associated fibroblasts (CAFs). As a result, the CAFs up-regulate aerobic glycolysis, producing copious lactate that is expelled from the cell via MCT4 and taken up by the cancer cell via MCT1. Lactate, pyruvate, and other metabolic intermediates such as amino acids and ketone bodies can feed the mitochondrial TCA cycle in cancer cells or local endothelium to increase ATP and biomolecule synthesis and drive pathogenic proliferation, invasion, and metastasis. MCT1 and MCT4 can be blocked in vitro using the small-molecule inhibitor α-cyano-4-hydroxycinnamic acid (4CIN) and in vivo using AZD3965, which is in early-phase clinical trials for treatment of small cell lung cancer. In RA, it is known that mitochondrial damage, HIF-1α activation, and up-regulation of MCT4 can be induced by the pathogenic microenvironment in fibroblast-like synoviocytes (FLS) from patients with late-stage disease, but the metabolic relationships between these cells and other cells within the joint have yet to be elucidated. See Figure 2 for other definitions.

commonly provide high-energy metabolic intermediates such as lactate and pyruvate to bioenergetically demanding partner cells, where they can anaplerotically fuel the TCA cycle. A similar mechanism has been identified in epithelial cancers in which both Warburg and so-called "reverse Warburg" metabolism have been demonstrated and highlighted as therapeutic targets (92). The Warburg effect describes up-regulation of aerobic glycolysis in the tumor cell itself and in the presence of ample oxygen.

The reverse Warburg effect describes a situation in which cancer-associated fibroblasts provide lactate, ketone bodies, and amino acids passed through MCTs to fuel tumor cell proliferative behavior (93), as well as local angiogenesis associated with metastasis (94). Due to commonalities in cell behavior and microenvironment, one could hypothesize that similar symbiotic relationships might exist in the synovium to fuel immune cell effector function and FLS pathogenic behavior (Figure 4). Fujii et al previously showed that FLS from patients with late-stage RA have elevated levels of MCT4 compared with OA FLS, and that small interfering RNA knockdown of MCT4 reduced arthritis severity in the murine collagen-induced arthritis model, linking their findings to apoptosis resistance and synovial acidification (95).

Expulsion via MCT4 is likely to be a necessary mechanism to protect cells against the damaging effects of lactate accumulation. However, whether the lactate can be taken up and utilized by other cells is unknown. It is very likely that the role of MCTs and the sharing of metabolites between cells will differ during the course of RA as a reflection of mitochondrial health and changes to the joint microenvironment. Consequently, it will be important to study metabolic coupling in normal tissue and during the acute phase of disease to determine whether such relationships exist and if so, to exploit their therapeutic potential; such an approach is showing promise in cancer (96).

Expanding knowledge of fibroblast metabolism

Studies of metabolism in cultured synovial cells have been important for understanding RA biology. Such studies have illustrated a "metabolic memory" that is epigenetically imprinted upon cells in an inflammatory microenvironment and is lasting in in vitro culture. Metabolomic analysis continues to be a useful strategy for providing a metabolic snapshot of the status of such cells and to hint toward pathways worthy of further study. Use of technologies such as Seahorse analysis to observe bioenergetic responses, small-molecule metabolic inhibitors, and animal models have also played a role in expanding our understanding of the field. However, for capturing the dynamic processes that regulate cellular metabolism,

stable isotope metabolic tracer analysis is a powerful technique that has not yet been applied to synoviocytes (97). This technique provides a comprehensive biologic overview, allowing simulation and reconstruction of metabolism, and can provide insight at the compartment level (e.g., mitochondria versus cytoplasm, depending on the tracer) (98). The increased concentration of a metabolite can be associated with either the up-regulation of the enzyme responsible for synthesis or the down-regulation of the one consuming it, and metabolic tracer analysis allows these processes to be deconvoluted where traditional metabolomics is less informative (99,100). Several heavy isotopes are available and include ^{2}H, ^{15}N, and ^{18}O, but the most commonly used is ^{13}C. The most common isotopically labeled tracers are ^{13}C-labeled glucose and ^{13}C-labeled glutamine, because these metabolites are the main energy sources in many mammalian systems (101). The recent development of approaches to apply tandem mass spectrometry (MS) to isotope tracing has offered the opportunity to determine positional labeling based on mass fragmentation (102).

As alluded to above, studying metabolic relationships of synoviocytes after treatment (103) and between FLS and synovial tissue macrophages within the RA synovium is an important future direction. Stable isotope analysis in concert with small-molecule inhibitors will allow us to trace metabolite exchange between cells in culture. There is also a pressing need for conditional knockout animals to observe the importance of metabolite channels, transporters, and enzymes in inflammatory diseases as an area of great therapeutic potential. Finally, better histologic markers are improving our understanding of FLS subsets, resident and infiltrating synovial tissue macrophages, and the tissue organization of these cells. Imaging MS can provide a metabolomic snapshot on a per-pixel basis and may reveal spatially distinct metabolic signatures and important metabolic heterogeneity within the synovial environment (104).

Metabolic pathways as therapeutic targets in RA

Metabolic rewiring of immune cells has been viewed as a promising source of novel drug targets (8,14,105), but resetting metabolism in tissues central to RA pathogenesis offers additional opportunities for disease modulation and restoration of homeostasis in RA. In fact, rheumatologists already use the antimetabolites methotrexate and leflunomide for the treatment of patients with inflammatory arthritis. Both drugs inhibit reproduction of rapidly dividing cells such as lymphocytes but have also been shown to inhibit FLS functions (106,107). Of interest is the observation that sulfasalazine, which was initially developed as an

antiinflammatory drug to treat RA, was subsequently shown to inhibit xCT, a cystine–glutamate exchange transporter (108).

Targeted approaches to metabolic inhibition are required to inhibit aggressive behavior in pathologic cell types and leave those that aid resolution intact. Potentiation or restoration of protective mechanisms such as mitochondrial fusion and biogenesis and mechanisms that promote resolution of inflammation may also be favorable. Indeed, small molecules such as Mdivi-1 that potentiate mitochondrial fusion have already shown potential in animal models of sepsis and may have further-reaching applications (109). In addition, metformin is used for the clinical management of type II diabetes and has shown promise in mouse models of arthritis (110). Although the effects of metformin on FLS are unknown, it is thought to act on immune cells both by inhibiting complex I of the mitochondrial electron transport chain and through effects on the signaling molecule AMPK. Use of other AMPK activators that will control cell proliferation and promote mitochondrial biogenesis might be another approach (43,44).

The signaling molecule PI3K regulates glycolysis upstream of mTOR, and inhibitors of this molecule are in early-stage clinical trials for cancer and show potential in RA (111). Furthermore, blockers of key glycolytic enzymes including phosphofructokinase/fructose-2,6-bisphosphatase 3 are showing promise for working in synergy with other inhibitors that target the angiogenic factor vascular endothelial growth factor (112). Inhibiting glycolytic intermediates including succinate or lactate production could be of interest if proven to fuel synovial cell activation. Use of a small-molecule modulator of PKM2 to prevent nuclear translocation also has potential for driving a shift toward an M2 phenotype and restoration of tolerance in diseases such as RA. In FLS, HK2 release from the mitochondrial membrane could potentially trigger FLS apoptosis. However, a better understanding of the signaling pathways that dictate the metabolic phenotype of immune and stromal cells in RA is required to capitalize on this area.

Blockers of the MCTs that are central to metabolic coupling have been used in as yet unpublished first-in-man trials for epithelial cancers, and the effects of their knockdown in experimental arthritis suggest that they offer potential in RA (95). Other solute carrier transporters, including GLUT-1, amino acids, or choline, are potential therapeutic targets that are yet to be explored in arthritis. Furthermore, better stratification of patients through prognostic metabolomic analysis (16) and techniques such as PET scanning with ^{11}C-choline (83) may improve treatment of patients who are nonresponders to

existing therapies. Overall, whether targeting metabolism truly presents an option to increase the drug armamentarium in rheumatic diseases remains to be determined.

Conclusions

Systemic metabolism, immunometabolism, and stromal cell metabolism are altered in RA, and a growing body of literature in this field offer novel biomarkers for patient stratification and avenues for treatment. However, we are far from having an exhaustive understanding of the pathways that discern the normal or pathogenic phenotypes of synovium-resident cells in order to capitalize on these therapeutic opportunities. It will be important to better understand mitochondrial metabolism and dynamics, which are sparsely studied in the synovium, with a view to harnessing fusion and biogenesis pathways to restore mitochondrial health and tip the balance away from aerobic glycolysis in RA. Future directions toward use of cells sorted directly from synovial tissue and phenotyping with single-cell transcriptomic analysis promise to improve our understanding of FLS and synovial tissue macrophage biology, and there is a need for metabolic profiling of these cells prior to de-differentiation associated with cell culture.

Growing evidence suggests that multiple fibroblast and macrophage subsets are present in the inflamed synovium, and their characterization will aid in directing new treatment aimed at those with a pathogenic and not a protective phenotype. Furthermore, the metabolic interactions between FLS, synovial tissue macrophages, and infiltrating immune cells have not been explored, and lessons from cancer biology suggest that this will provide further opportunities for therapeutic intervention. There is a pressing need for techniques such as stable isotope–based metabolic tracer analysis to track these interactions. Finally, there is a strategic window of opportunity such that RA patients receiving disease-modifying treatments within 3 months of symptom development show a much improved prognosis when compared with patients treated after this time point (113). To date, all studies of FLS metabolism have been conducted in cells derived from the joints of patients with late-stage disease after arthroplasty, and studies of macrophages have used cells differentiated from monocytes in vitro.

As we begin to understand that transient metabolic responses in acute inflammation may differ significantly from metabolic adaptation to damage in chronic inflammation, characterization of cells from healthy tissue and from the earliest stages of human disease is needed to inform appropriate future therapeutic strategies, with the ultimate goal of drug-free remission or cure of RA.

AUTHOR CONTRIBUTIONS

All authors were involved in drafting the article or revising it critically for important intellectual content, and all authors approved the final version to be published.

REFERENCES

1. Bettencourt IA, Powell JD. Targeting metabolism as a novel therapeutic approach to autoimmunity, inflammation, and transplantation. J Immunol 2017;198:999–1005.
2. Patel CH, Powell JD. Targeting T cell metabolism to regulate T cell activation, differentiation and function in disease. Curr Opin Immunol 2017;46:82–8.
3. Ahlqvist J. A hypothesis on the pathogenesis of rheumatoid and other non-specific synovitides. IV A. The possible intermediate role of local hypoxia and metabolic alterations. Med Hypotheses 1984;13:257–302.
4. Henderson B, Bitensky L, Chayen J. Glycolytic activity in human synovial lining cells in rheumatoid arthritis. Ann Rheum Dis 1979;38:63–7.
5. Bottini N, Firestein GS. Duality of fibroblast-like synoviocytes in RA: passive responders and imprinted aggressors. Nat Rev Rheumatol 2013;9:24–33.
6. Bustamante MF, Garcia-Carbonell R, Whisenant KD, Guma M. Fibroblast-like synoviocyte metabolism in the pathogenesis of rheumatoid arthritis. Arthritis Res Ther 2017;19:110.
7. Naylor AJ, Filer A, Buckley CD. The role of stromal cells in the persistence of chronic inflammation. Clin Exp Immunol 2013;171:30–5.
8. O'Neill LA, Kishton RJ, Rathmell J. A guide to immunometabolism for immunologists. Nat Rev Immunol 2016;16:553–65.
9. Patel R, Filer A, Barone F, Buckley CD. Stroma: fertile soil for inflammation. Best Pract Res Clin Rheumatol 2014;28:565–76.
10. Juarez M, Filer A, Buckley CD. Fibroblasts as therapeutic targets in rheumatoid arthritis and cancer. Swiss Med Wkly 2012;142:w13529.
11. Metsios GS, Stavropoulos-Kalinoglou A, Nevill AM, Douglas KM, Koutedakis Y, Kitas GD. Cigarette smoking significantly increases basal metabolic rate in patients with rheumatoid arthritis. Ann Rheum Dis 2008;67:70–3.
12. Cojocaru M, Cojocaru IM, Silosi I, Vrabie CD. Metabolic syndrome in rheumatoid arthritis. Mædica 2012;7:148–52.
13. Cederholm T, Wretlind B, Hellstrom K, Andersson B, Engstrom L, Brismar K, et al. Enhanced generation of interleukins 1 β and 6 may contribute to the cachexia of chronic disease. Am J Clin Nutr 1997;65:876–82.
14. Guma M, Tiziani S, Firestein GS. Metabolomics in rheumatic diseases: desperately seeking biomarkers. Nat Rev Rheumatol 2016;12:269–81.
15. Alonso A, Julià A, Vinaixa M, Domènech E, Fernández-Nebro A, Cañete JD, et al. Urine metabolome profiling of immune-mediated inflammatory diseases. BMC Med 2016;14:133.
16. Young SP, Kapoor SR, Viant MR, Byrne JJ, Filer A, Buckley CD, et al. The impact of inflammation on metabolomic profiles in patients with arthritis. Arthritis Rheum 2013;65:2015–23.
17. Madsen RK, Lundstedt T, Gabrielsson J, Sennbro CJ, Alenius GM, Moritz T, et al. Diagnostic properties of metabolic perturbations in rheumatoid arthritis. Arthritis Res Ther 2011;13:R19.
18. Hugle T, Kovacs H, Heijnen IA, Daikeler T, Baisch U, Hicks JM, et al. Synovial fluid metabolomics in different forms of arthritis assessed by nuclear magnetic resonance spectroscopy. Clin Exp Rheumatol 2012;30:240–5.
19. Kim S, Hwang J, Xuan J, Jung YH, Cha HS, Kim KH. Global metabolite profiling of synovial fluid for the specific diagnosis of rheumatoid arthritis from other inflammatory arthritis. PLoS One 2014;9:e97501.
20. Cuppen BV, Fu J, van Wietmarschen HA, Harms AC, Koval S, Marijnissen AC, et al. Exploring the inflammatory metabolomic profile to predict response to TNF-α inhibitors in rheumatoid arthritis. PLoS One 2016;11:e0163087.
21. Sweeney SR, Kavanaugh A, Lodi A, Wang B, Boyle D, Tiziani S, et al. Metabolomic profiling predicts outcome of rituximab therapy in rheumatoid arthritis. RMD Open 2016;2:e000289.
22. Tatar Z, Migne C, Petera M, Gaudin P, Lequerre T, Marotte H, et al. Variations in the metabolome in response to disease activity of rheumatoid arthritis. BMC Musculoskelet Disord 2016;17:353.
23. Smith MD. The normal synovium. Open Rheumatol J 2011;5: 100–6.
24. Misharin AV, Cuda CM, Saber R, Turner JD, Gierut AK, Haines GK III, et al. Nonclassical Ly6C(-) monocytes drive the development of inflammatory arthritis in mice. Cell Rep 2014;9: 591–604.
25. Udalova IA, Mantovani A, Feldmann M. Macrophage heterogeneity in the context of rheumatoid arthritis. Nat Rev Rheumatol 2016;12:472–85.
26. Bottini N, Firestein GS. Duality of fibroblast-like synoviocytes in RA: passive responders and imprinted aggressors. Nat Rev Rheumatol 2013;9:24–33.
27. Croft AP, Naylor AJ, Marshall JL, Hardie DL, Zimmermann B, Turner J, et al. Rheumatoid synovial fibroblasts differentiate into distinct subsets in the presence of cytokines and cartilage. Arthritis Res Ther 2016;18:270.
28. Mizoguchi F, Slowikowski K, Chang SK, Rao DA, Nguyen H, Noss EH, et al. Identification of synovial fibroblast subsets that define pathology in rheumatoid arthritis [abstract]. Arthritis Rheumatol 2015;67 Suppl 10. URL: http://acrabstracts.org/abstract/identification-of-synovial-fibroblast-subsets-that-define-pathology-in-rheumatoid-arthritis/.
29. Firestein GS. Evolving concepts of rheumatoid arthritis. Nature 2003;423:356–61.
30. Bartok B, Firestein GS. Fibroblast-like synoviocytes: key effector cells in rheumatoid arthritis. Immunol Rev 2010;233:233–55.
31. Biniecka M, Fox E, Gao W, Ng CT, Veale DJ, Fearon U, et al. Hypoxia induces mitochondrial mutagenesis and dysfunction in inflammatory arthritis. Arthritis Rheum 2011;63:2172–82.
32. Gaber T, Dziurla R, Tripmacher R, Burmester GR, Buttgereit F. Hypoxia inducible factor (HIF) in rheumatology: low O2! See what HIF can do! Ann Rheum Dis 2005;64:971–80.
33. Szekanecz Z, Besenyei T, Paragh G, Koch AE. Angiogenesis in rheumatoid arthritis. Autoimmunity 2009;42:563–73.
34. Ahn JK, Kim S, Hwang J, Kim J, Kim KH, Cha HS. GC/TOF-MS-based metabolomic profiling in cultured fibroblast-like synoviocytes from rheumatoid arthritis. Joint Bone Spine 2016;83: 707–13.
35. Guma M, Sanchez-Lopez E, Lodi A, Garcia-Carbonell R, Tiziani S, Karin M, et al. Choline kinase inhibition in rheumatoid arthritis. Ann Rheum Dis 2015;74:1399–407.
36. Kurowska-Stolarska M, Alivernini S. Synovial tissue macrophages: friend or foe? RMD Open 2017;3:e000627.
37. Weyand CM, Zeisbrich M, Goronzy JJ. Metabolic signatures of T-cells and macrophages in rheumatoid arthritis. Curr Opin Immunol 2017;46:112–20.
38. Nayar S, Campos J, Steinthal N, Barone F. Tissue digestion for stromal cell and leukocyte isolation. Methods Mol Biol 2017;1591:225–34.
39. Ghesquiere B, Wong BW, Kuchnio A, Carmeliet P. Metabolism of stromal and immune cells in health and disease. Nature 2014; 511:167–76.
40. Lemons JM, Feng XJ, Bennett BD, Legesse-Miller A, Johnson EL, Raitman I, et al. Quiescent fibroblasts exhibit high metabolic activity. PLoS Biol 2010;8:e1000514.
41. O'Neill LA, Hardie DG. Metabolism of inflammation limited by AMPK and pseudo-starvation. Nature 2013;493:346–55.

42. Weichhart T, Hengstschlager M, Linke M. Regulation of innate immune cell function by mTOR. Nat Rev Immunol 2015;15:599–614.

43. Yuan HX, Xiong Y, Guan KL. Nutrient sensing, metabolism, and cell growth control. Mol Cell 2013;49:379–87.

44. Vincent EE, Coelho PP, Blagih J, Griss T, Viollet B, Jones RG. Differential effects of AMPK agonists on cell growth and metabolism. Oncogene 2015;34:3627–39.

45. Covarrubias AJ, Aksoylar HI, Horng T. Control of macrophage metabolism and activation by mTOR and Akt signaling. Semin Immunol 2015;27:286–96.

46. Guma M, Wang Y, Viollet B, Liu-Bryan R. AMPK activation by A-769662 controls IL-6 expression in inflammatory arthritis. PLoS One 2015;10:e0140452.

47. Park SY, Lee SW, Lee SY, Hong KW, Bae SS, Kim K, et al. SIRT1/adenosine monophosphate-activated protein kinase α signaling enhances macrophage polarization to an anti-inflammatory phenotype in rheumatoid arthritis. Front Immunol 2017;8:1135.

48. Wruck CJ, Fragoulis A, Gurzynski A, Brandenburg LO, Kan YW, Chan K, et al. Role of oxidative stress in rheumatoid arthritis: insights from the Nrf2-knockout mice. Ann Rheum Dis 2011;70:844–50.

49. Jornayvaz FR, Shulman GI. Regulation of mitochondrial biogenesis. Essays Biochem 2010;47:69–84.

50. Osellame LD, Blacker TS, Duchen MR. Cellular and molecular mechanisms of mitochondrial function. Best Pract Res Clin Endocrinol Metab 2012;26:711–23.

51. Krysko DV, Agostinis P, Krysko O, Garg AD, Bachert C, Lambrecht BN, et al. Emerging role of damage-associated molecular patterns derived from mitochondria in inflammation. Trends Immunol 2011;32:157–64.

52. Wai T, Langer T. Mitochondrial dynamics and metabolic regulation. Trends Endocrinol Metab 2016;27:105–17.

53. Seo AY, Joseph AM, Dutta D, Hwang JC, Aris JP, Leeuwenburgh C. New insights into the role of mitochondria in aging: mitochondrial dynamics and more. J Cell Sci 2010;123:2533–42.

54. Corcoran SE, O'Neill LA. HIF1α and metabolic reprogramming in inflammation. J Clin Invest 2016;126:3699–707.

55. Mills E, O'Neill LA. Succinate: a metabolic signal in inflammation. Trends Cell Biol 2014;24:313–20.

56. Lampropoulou V, Sergushichev A, Bambouskova M, Nair S, Vincent EE, Loginicheva E, et al. Itaconate links inhibition of succinate dehydrogenase with macrophage metabolic remodeling and regulation of inflammation. Cell Metab 2016;24:158–66.

57. Hollander AP, Corke KP, Freemont AJ, Lewis CE. Expression of hypoxia-inducible factor 1α by macrophages in the rheumatoid synovium: implications for targeting of therapeutic genes to the inflamed joint. Arthritis Rheum 2001;44:1540–4.

58. Kim EK, Kwon JE, Lee SY, Lee EJ, Kim DS, Moon SJ, et al. IL-17-mediated mitochondrial dysfunction impairs apoptosis in rheumatoid arthritis synovial fibroblasts through activation of autophagy. Cell Death Dis 2017;8:e2565.

59. Biniecka M, Canavan M, McGarry T, Gao W, McCormick J, Cregan S, et al. Dysregulated bioenergetics: a key regulator of joint inflammation. Ann Rheum Dis 2016;75:2192–200.

60. Garcia-Carbonell R, Divakaruni AS, Lodi A, Vicente-Suarez I, Saha A, Cheroutre H, et al. Critical role of glucose metabolism in rheumatoid arthritis fibroblast-like synoviocytes. Arthritis Rheumatol 2016;68:1614–26.

61. Fearon U, Canavan M, Biniecka M, Veale DJ. Hypoxia, mitochondrial dysfunction and synovial invasiveness in rheumatoid arthritis. Nat Rev Rheumatol 2016;12:385–97.

62. Ng CT, Biniecka M, Kennedy A, McCormick J, FitzGerald O, Bresnihan B, et al. Synovial tissue hypoxia and inflammation in vivo. Ann Rheum Dis 2010;69:1389–95.

63. Da Sylva TR, Connor A, Mburu Y, Keystone E, Wu GE. Somatic mutations in the mitochondria of rheumatoid arthritis synoviocytes. Arthritis Res Ther 2005;7:R844–51.

64. Harty LC, Biniecka M, O'Sullivan J, Fox E, Mulhall K, Veale DJ, et al. Mitochondrial mutagenesis correlates with the local inflammatory environment in arthritis. Ann Rheum Dis 2012;71:582–8.

65. Pope RM. Apoptosis as a therapeutic tool in rheumatoid arthritis. Nat Rev Immunol 2002;2:527.

66. Mayers JR, Vander Heiden MG. Famine versus feast: understanding the metabolism of tumors in vivo. Trends Biochem Sci 2015;40:130–40.

67. Bell C, English L, Boulais J, Chemali M, Caron-Lizotte O, Desjardins M, et al. Quantitative proteomics reveals the induction of mitophagy in tumor necrosis factor-α-activated (TNFα) macrophages. Mol Cell Proteomics 2013;12:2394–407.

68. Xu K, Xu P, Yao JF, Zhang YG, Hou WK, Lu SM. Reduced apoptosis correlates with enhanced autophagy in synovial tissues of rheumatoid arthritis. Inflamm Res 2013;62:229–37.

69. Zhang J, Song X, Cao W, Lu J, Wang X, Wang G, et al. Autophagy and mitochondrial dysfunction in adjuvant-arthritis rats treatment with resveratrol. Sci Rep 2016;6:32928.

70. Shin YJ, Han SH, Kim DS, Lee GH, Yoo WH, Kang YM, et al. Autophagy induction and CHOP under-expression promotes survival of fibroblasts from rheumatoid arthritis patients under endoplasmic reticulum stress. Arthritis Res Ther 2010;12:R19.

71. Vander Heiden MG, Cantley LC, Thompson CB. Understanding the Warburg effect: the metabolic requirements of cell proliferation. Science 2009;324:1029–33.

72. Gatenby RA, Gillies RJ. Why do cancers have high aerobic glycolysis? Nat Rev Cancer 2004;4:891–9.

73. Kubota K, Ito K, Morooka M, Mitsumoto T, Kurihara K, Yamashita H, et al. Whole-body FDG-PET/CT on rheumatoid arthritis of large joints. Ann Nucl Med 2009;23:783–91.

74. Weyand CM, Goronzy JJ. Immunometabolism in early and late stages of rheumatoid arthritis. Nat Rev Rheumatol 2017;13:291–301.

75. Volchenkov R, Dung Cao M, Elgstoen KB, Goll GL, Eikvar K, Bjorneboe O, et al. Metabolic profiling of synovial tissue shows altered glucose and choline metabolism in rheumatoid arthritis samples. Scand J Rheumatol 2016:1–2.

76. Yang Z, Fujii H, Mohan SV, Goronzy JJ, Weyand CM. Phosphofructokinase deficiency impairs ATP generation, autophagy, and redox balance in rheumatoid arthritis T cells. J Exp Med 2013;210:2119–34.

77. Ahn JK, Kim S, Hwang J, Kim J, Kim KH, Cha HS. GC/TOF-MS-based metabolomic profiling in cultured fibroblast-like synoviocytes from rheumatoid arthritis. Joint Bone Spine 2016;83:707–13.

78. Li Y, Zheng JY, Liu JQ, Yang J, Liu Y, Wang C, et al. Succinate/NLRP3 inflammasome induces synovial fibroblast activation: therapeutical effects of clematichinenoside AR on arthritis. Front Immunol 2016;7:532.

79. Chang CH, Curtis JD, Maggi LB Jr, Faubert B, Villarino AV, O'Sullivan D, et al. Posttranscriptional control of T cell effector function by aerobic glycolysis. Cell 2013;153:1239–51.

80. Yu X, Li S. Non-metabolic functions of glycolytic enzymes in tumorigenesis. Oncogene 2016;36:2629–36.

81. Moon JS, Hisata S, Park MA, DeNicola GM, Ryter SW, Nakahira K, et al. mTORC1-induced HK1-dependent glycolysis regulates NLRP3 inflammasome activation. Cell Rep 2015;12:102–15.

82. Nomura M, Liu J, Rovira II, Gonzalez-Hurtado E, Lee J, Wolfgang MJ, et al. Fatty acid oxidation in macrophage polarization. Nat Immunol 2016;17:216–7.

83. Roivainen A, Parkkola R, Yli-Kerttula T, Lehikoinen P, Viljanen T, Möttönen T, et al. Use of positron emission tomography with methyl-^{11}C-choline and 2-^{18}F-fluoro-2-deoxy-D-glucose in comparison with magnetic resonance imaging for the assessment of inflammatory proliferation of synovium. Arthritis Rheum 2003;48:3077–84.

84. Seki M, Kawai Y, Ishii C, Yamanaka T, Odawara M, Inazu M. Functional analysis of choline transporters in rheumatoid arthritis synovial fibroblasts. Mod Rheumatol 2017;27:995–1003.

85. Lim HK, Choi YA, Park W, Lee T, Ryu SH, Kim SY, et al. Phosphatidic acid regulates systemic inflammatory responses by modulating the Akt-mammalian target of rapamycin-p70 S6 kinase 1 pathway. J Biol Chem 2003;278:45117–27.

86. Friday SC, Fox DA. Phospholipase D enzymes facilitate IL-17- and TNFα-induced expression of proinflammatory genes in rheumatoid arthritis synovial fibroblasts (RASF). Immunol Lett 2016;174:9–18.

87. Fuchs B, Schiller J, Wagner U, Hantzschel H, Arnold K. The phosphatidylcholine/lysophosphatidylcholine ratio in human plasma is an indicator of the severity of rheumatoid arthritis: investigations by 31P NMR and MALDI-TOF MS. Clin Biochem 2005;38:925–33.

88. Bourgoin SG, Zhao C. Autotaxin and lysophospholipids in rheumatoid arthritis. Curr Opin Investig Drugs 2010;11:515–26.

89. Miyabe Y, Miyabe C, Iwai Y, Yokoyama W, Sekine C, Sugimoto K, et al. Activation of fibroblast-like synoviocytes derived from rheumatoid arthritis via lysophosphatidic acid-lysophosphatidic acid receptor 1 cascade. Arthritis Res Ther 2014;16:461.

90. Nikitopoulou I, Oikonomou N, Karouzakis E, Sevastou I, Nikolaidou-Katsaridou N, Zhao Z, et al. Autotaxin expression from synovial fibroblasts is essential for the pathogenesis of modeled arthritis. J Exp Med 2012;209:925–33.

91. Halestrap AP. Monocarboxylic acid transport. Compr Physiol 2013;3:1611–43.

92. Pavlides S, Whitaker-Menezes D, Castello-Cros R, Flomenberg N, Witkiewicz AK, Frank PG, et al. The reverse Warburg effect: aerobic glycolysis in cancer associated fibroblasts and the tumor stroma. Cell Cycle 2009;8:3984–4001.

93. Pavlides S, Vera I, Gandara R, Sneddon S, Pestell RG, Mercier I, et al. Warburg meets autophagy: cancer-associated fibroblasts accelerate tumor growth and metastasis via oxidative stress, mitophagy, and aerobic glycolysis. Antioxid Redox Signal 2012;16:1264–84.

94. Vegran F, Boidot R, Michiels C, Sonveaux P, Feron O. Lactate influx through the endothelial cell monocarboxylate transporter MCT1 supports an NF-κB/IL-8 pathway that drives tumor angiogenesis. Cancer Res 2011;71:2550–60.

95. Fujii W, Kawahito Y, Nagahara H, Kukida Y, Seno T, Yamamoto A, et al. Monocarboxylate transporter 4, associated with the acidification of synovial fluid, is a novel therapeutic target for inflammatory arthritis. Arthritis Rheumatol 2015;67:2888–96.

96. Sanita P, Capulli M, Teti A, Galatioto GP, Vicentini C, Chiarugi P, et al. Tumor-stroma metabolic relationship based on lactate shuttle can sustain prostate cancer progression. BMC Cancer 2014;14:154.

97. Metallo CM. Metabolic analysis using stable isotopes. Metallo CM, editor. Waltham (MA): Elsevier Academic Press; 2015.

98. Zamboni N. 13 C metabolic flux analysis in complex systems. Curr Opin Biotechnol 2011;22:103–8.

99. Birkemeyer C, Luedemann A, Wagner C, Erban A, Kopka J. Metabolome analysis: the potential of in vivo labeling with stable isotopes for metabolite profiling. Trends Biotechnol 2005; 23:28–33.

100. Rodrigues TB, Serrao EM, Kennedy BW, Hu DE, Kettunen MI, Brindle KM. Magnetic resonance imaging of tumor glycolysis using hyperpolarized ^{13}C-labeled glucose. Nat Med 2014;20:93–7.

101. Schug ZT, Peck B, Jones DT, Zhang Q, Grosskurth S, Alam IS, et al. Acetyl-CoA synthetase 2 promotes acetate utilization and maintains cancer cell growth under metabolic stress. Cancer Cell 2015;27:57–71.

102. Choi J, Grossbach MT, Antoniewicz MR. Measuring complete isotopomer distribution of aspartate using gas chromatography/tandem mass spectrometry. Anal Chem 2012;84:4628–32.

103. Ahn JK, Kim S, Hwang J, Kim J, Lee YS, Koh EM, et al. Metabolomic elucidation of the effects of curcumin on fibroblast-like synoviocytes in rheumatoid arthritis. PLoS One 2015;10:e0145539.

104. Rocha B, Ruiz-Romero C, Blanco FJ. Mass spectrometry imaging: a novel technology in rheumatology. Nat Rev Rheumatol 2017;13:52–63.

105. Galluzzi L, Kepp O, Vander Heiden MG, Kroemer G. Metabolic targets for cancer therapy. Nat Rev Drug Discov 2013;12:829–46.

106. Lories RJ, Derese I, De Bari C, Luyten FP. In vitro growth rate of fibroblast-like synovial cells is reduced by methotrexate treatment. Ann Rheum Dis 2003;62:568–71.

107. Vergne-Salle P, Leger DY, Bertin P, Treves R, Beneytout JL, Liagre B. Effects of the active metabolite of leflunomide, A77 1726, on cytokine release and the MAPK signalling pathway in human rheumatoid arthritis synoviocytes. Cytokine 2005;31:335–48.

108. Timmerman LA, Holton T, Yuneva M, Louie RJ, Padro M, Daemen A, et al. Glutamine sensitivity analysis identifies the xCT antiporter as a common triple-negative breast tumor therapeutic target. Cancer Cell 2013;24:450–65.

109. Buck MD, O'Sullivan D, Klein Geltink RI, Curtis JD, Chang CH, Sanin DE, et al. Mitochondrial dynamics controls T cell fate through metabolic programming. Cell 2016;166:63–76.

110. Son HJ, Lee J. Metformin attenuates experimental autoimmune arthritis through reciprocal regulation of Th17/Treg balance and osteoclastogenesis. Mediators Inflamm 2014;2014:973986.

111. Massacesi C, Di Tomaso E, Urban P, Germa C, Quadt C, Trandafir L, et al. PI3K inhibitors as new cancer therapeutics: implications for clinical trial design. Onco Targets Ther 2016;9:203–10.

112. Schoors S, De Bock K, Cantelmo AR, Georgiadou M, Ghesquiere B, Cauwenberghs S, et al. Partial and transient reduction of glycolysis by PFKFB3 blockade reduces pathological angiogenesis. Cell Metab 2014;19:37–48.

113. Raza K, Filer A. The therapeutic window of opportunity in rheumatoid arthritis: does it ever close? Ann Rheum Dis 2015; 74:793–4.

Neurobiologic Features of Fibromyalgia Are Also Present Among Rheumatoid Arthritis Patients

Neil Basu,[1] Chelsea M. Kaplan,[2] Eric Ichesco,[2] Tony Larkin,[2] Richard E. Harris,[2] Alison Murray,[1] Gordon Waiter,[1] and Daniel J. Clauw[2]

Objective. **Many patients with rheumatoid arthritis (RA) report pain despite excellent control of inflammation with immunotherapies. Variable degrees of coexisting fibromyalgia (FM) may explain this disparity. FM has been characterized by aberrant brain functional connectivity, especially between the default mode network (DMN) and insula. We undertook this study to test the hypothesis that RA patients with the highest 2011 American College of Rheumatology FM survey criteria scores—a continuous measure of the degree of FM also known as "fibromyalgianess" (FMness)—would demonstrate functional connectivity abnormalities similar to those in FM.**

Methods. **RA patients underwent an 11-minute functional connectivity magnetic resonance imaging (MRI) brain scan and a clinical evaluation which included a measure of FMness. Brain networks were isolated from functional connectivity MRI data. Individual patient network-to–whole brain connectivity analyses were then conducted, followed by group-level regression, which correlated the connectivity of each network with FMness. Results were significant on the cluster level with a family-wise error (FWE) rate *P* value less than 0.05 derived from an uncorrected voxel-level *P* value less than 0.001.**

Results. **A total of 54 patients participated (mean age 54.9 years, 75.9% women, mean FMness score 13.2 [range 1–29]). From the whole brain analyses, a single significant positive correlation between DMN connectivity to the left mid/posterior insula and FMness (r = 0.58, FWE-corrected *P* = 0.001) was demonstrated.**

Conclusion. **RA patients who have increased levels of FMness appear to share neurobiologic features consistently observed in FM patients. This study is the first to provide neuroimaging evidence that RA is a mixed pain state, with many patients' symptoms being related to the central nervous system rather than to classic inflammatory mechanisms.**

Rheumatoid arthritis (RA) is an archetypal chronic inflammatory disorder which is principally characterized by peripheral joint pain, stiffness, and swelling. Recently, management of RA has been revolutionized by the early and aggressive application of antiinflammatory therapies. These advances have led to tremendous average improvements in objective outcomes and even disability, but as many as 50% of patients continue to report clinically significant levels of pain despite excellent control of their peripheral inflammation (1,2).

This disconnect between improvements in inflammation and improvements in pain suggests that there is a likely contribution of pain mechanisms that are in addition to and distinct from peripheral inflammation. Central sensitization—a consequence of dysfunctional central nervous system (CNS) pain processing which defines the primary chronic pain syndrome of fibromyalgia (FM)—may represent one such mechanism (3). This possibility is supported by clinical epidemiologic research which has revealed evidence of coexisting FM in 13–25% of RA patients (4). This compares to a prevalence of 1–5% in the general population (5). An additional 7–15% of RA patients have hallmark features of FM (which include somatic symptoms such as fatigue as well as chronic pain) without meeting the American College of Rheumatology (ACR) 1990 classification criteria (4,6). Wolfe and colleagues derived a

continuous scale from the ACR FM survey criteria (7) and found that it predicted pain and disability in RA even among patients who did not fully satisfy the FM criteria. The term fibromyalgianess (FMness) was subsequently introduced to reflect this wide phenotypic range (8).

Very few studies have examined whether the prevalent FMness phenotype in RA is underpinned by the same central sensitization pathways as demonstrated in "primary" FM. If this is true, it would greatly enhance the argument for "primary" FM therapeutic approaches (which are quite distinct from current peripherally directed antiinflammatory RA therapies) to benefit RA patients who have clinical features of FMness.

Advanced neuroimaging techniques have been crucial in delineating the neurobiologic features of central sensitization in "primary" FM, but these have not previously been applied to concomitant FM in RA. Recent studies have used functional connectivity magnetic resonance imaging (MRI), an adaptation of functional MRI data that examines temporal correlations in the MRI signal across various brain networks and regions. These connections are thought to be important for the maintenance of synaptic connectivity, and as such they modulate the efficiency and extent of neuronal transmission in the brain.

Among FM patients, the dorsal attention, sensorimotor, and salience brain networks have been implicated in having increased connectivity to pronociceptive brain areas and decreased connectivity to antinociceptive brain areas (9–11). However, currently the most convincing and reproducible functional connectivity MRI evidence relates to the association between the default mode network (DMN) and the insular cortex, which are otherwise implicated in self-referential mental activity (12) and multimodal sensory processing (13), respectively. This specific connection is cross-sectionally associated with FM and pain intensity (14) and longitudinally associated with change of FM pain following both efficacious pharmacologic (pregabalin) and nonpharmacologic (acupuncture) treatments (15,16). The robustness of this finding is further corroborated by magnetoencephalography (a more direct measure of brain connectivity) (17–19). These same patterns have been noted in other conditions known to be accompanied by central sensitization, such as irritable bowel syndrome and low back pain (18,19). Taken together, these data indicate that functional connectivity —and specifically DMN–insular cortex hyperconnectivity —may be a key biologic marker of both the presence and the severity of FM-related pain and central sensitization.

As yet, no studies have investigated whether functional connectivity MRI features of FM are observed in RA patients with co-occurring FM. Specifically, we hypothesized that RA patients reporting the highest levels of FMness would demonstrate functional connectivity MRI features of FM.

PATIENTS AND METHODS

Patients. A total of 335 RA patients were approached through a UK regional rheumatology service. Of those, 193 indicated interest in the study. Participants were considered eligible if they met the 2010 ACR/European League Against Rheumatism classification criteria (20) and had a clinically significant level of fatigue for at least 3 months (defined as a score of >3 on the Chalder Fatigue Binary Scale) (21). Exclusion criteria were contraindications to MRI and left-handedness. A total of 73 patients fulfilled these criteria, and ultimately 54 RA patients completed the study.

All consenting participants underwent a clinical evaluation. This included a measure of FMness using the ACR FM survey criteria, which combine a measure of widespread pain (number of painful sites [0–19]) with a symptom severity scale (e.g., fatigue, subjective cognitive problems, headache, poor mood; scores range from 0 to 12) (7). In addition, their levels of systemic inflammation (C-reactive protein [CRP] level), disease activity (Disease Activity Score in 28 joints [DAS28]) (22), current overall fatigue and pain severity (numerical rating scales of 0–10), sleep disturbance (Jenkins' sleep problems scale [23]), and depression (Hospital Anxiety and Depression Scale [24]) were recorded. Participants then underwent a functional MRI (fMRI) brain scan.

Ethical approval. Ethical approval for the study was obtained from the North of Scotland Research Ethics Committee. All participants provided written informed consent according to the Declaration of Helsinki.

Data acquisition. Each participant underwent an 11-minute functional scan while completing the Paced Auditory Serial Addition Test (PASAT), a validated measure of cognitive function (auditory processing, calculation, working memory, attention) that has been previously used in an fMRI context (25). The PASAT was given in a block design with three 3-minute "on" periods interspersed with four 30-second rest periods. The functional images were acquired by an Achieva 3T X-series MR system (Philips Medical Systems) with an 8-channel phased-array head coil using a T2-weighted gradient-echo single-shot echo-planar imaging pulse sequence with the following parameters: repetition time (TR) 3,000 msec, echo time (TE) 30 msec, flip angle 90°, in-plane SENSE acceleration 2, 128 × 128–pixel matrix size with 30 slices, field of view (FOV) 240 mm, voxel dimensions 1.88 mm × 1.88 mm × 5 mm, and 226 volumes. The first 4 volumes were discarded to avoid equilibration effects. A high-resolution T1-weighted fast-field echo 3-dimensional structural scan was collected for normalization (TR 8.2 msec, TE 3.8 msec, inversion recovery time 1,018 msec, flip angle 8°, FOV 240 mm, 240 × 240–pixel matrix size with 160 slices, and voxel dimensions 0.94 mm × 0.94 mm × 1 mm).

Preprocessing. All data were checked for motion > than 3.76 mm and 5° rotation and visually inspected for artifacts. No participants were excluded for these reasons. Functional connectivity MRI data were preprocessed using SPM8 (Wellcome Department of Cognitive Neurology, London, UK) running on MatLab R2014a (MathWorks), as previously described (25). Briefly, the functional images were realigned, and the structural image was

Table 1. Clinical characteristics of the patients*

RA disease activity†	3.62 ± 1.30
CRP, mg/liter	7.78 ± 8.54
Current fatigue‡	4.59 ± 2.19
Depression§	6.89 ± 3.92
Sleep disturbance¶	15.67 ± 5.46
Current overall pain‡	3.81 ± 2.38

* Values are the mean ± SD. RA = rheumatoid arthritis; CRP = C-reactive protein.
† Disease Activity Score in 28 joints.
‡ On a numerical rating scale of 0–10.
§ Hospital Anxiety and Depression Scale.
¶ Jenkins' sleep problems scale.

coregistered to mean functional image and then segmented. The structural and functional scans were normalized to the standard statistical parametric mapping Montreal Neurological Institute template gray prior probability map via the individuals' segmented gray matter image. Functional scans were smoothed with an 8-mm full width at half maximum Gaussian kernel.

Independent component analysis (ICA). We performed group ICA using a Group ICA of fMRI Toolbox to create group-specific network masks (26). Component estimates were validated using ICASSO software (27) over 20 iterations to ensure the accuracy and reliability of results. Subject-specific spatial maps and time courses were generated using a GICA3 back-reconstruction method. The networks of interest were the DMN, dorsal attention, sensorimotor, and salience brain networks. These components were verified by spatial correlation between the component maps and previously identified templates

(28). Spatial masks of the mean component map for each network were created using a MarsBaR Toolbox (http://matthew.dynevor. org/research/abstracts/marsbar/marsbar.pdf) for seed-based connectivity analyses.

Network-to–whole brain connectivity analysis. The preprocessed functional data were entered into a Functional Connectivity Toolbox (CONN; Cognitive and Affective Neuroscience Laboratory, Massachusetts Institute of Technology, Cambridge [www.nitrc.org/projects/conn]) version 15 in SPM8 (29). A nuisance regression using a CompCor method (30) was performed with 6 subject-specific motion parameters, the signal from white matter and cerebrospinal fluid, and their first-order derivatives included as confounders. A band pass filter (0.01–0.1 Hz) was applied to remove linear drifts and high-frequency noise in the data. The mean component maps generated from ICA were used as seeds. Beta maps for each individual representing connectivity between the network of interest and the rest of the brain were generated. The task beta maps were then passed onto second-level group analyses in SPM8. Using a multiple regression model, we assessed the association between network–whole brain connectivity and FMness with age and sex originally included as covariates of no interest, followed by additional corrections for the putative confounders of CRP level and amitriptyline use. The resulting maps were thresholded at an uncorrected voxelwise $P < 0.001$, and significance was set at $P < 0.05$ family-wise error (FWE) cluster corrected for multiple comparisons. The average Fisher-transformed r values of significant clusters were extracted from the first-level beta maps for each subject using MarsBaR. These values were brought into Stata version 12.1
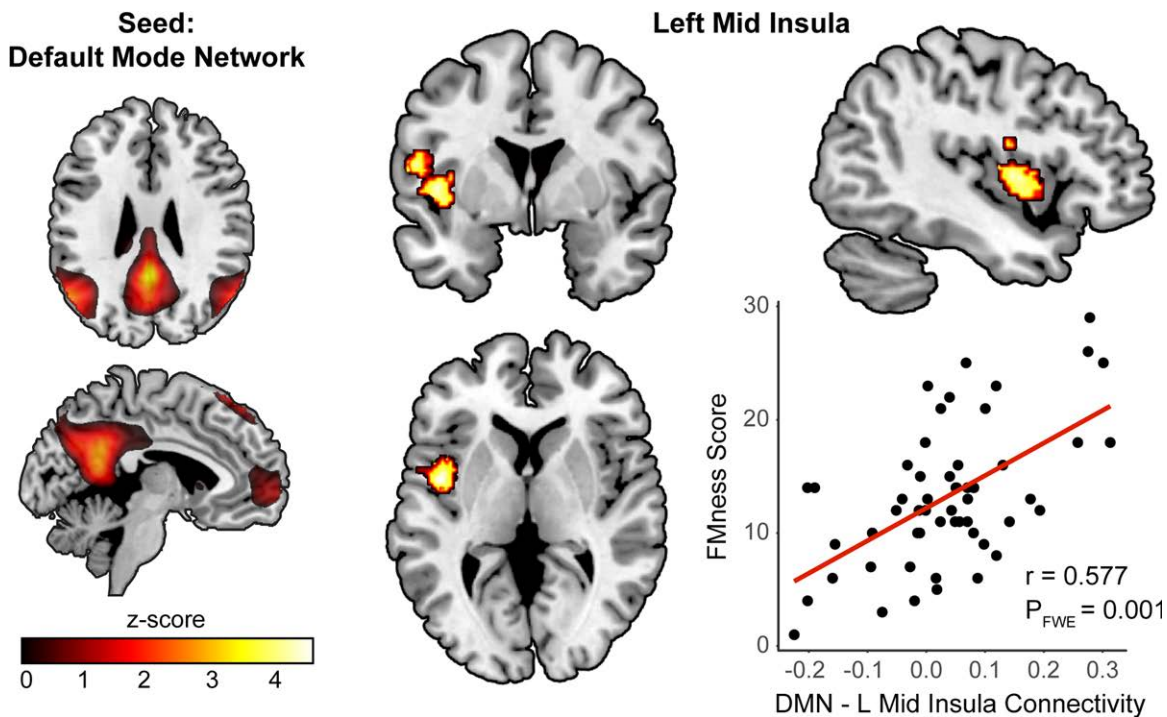
Figure 1. Increased brain connectivity between the default mode network (DMN) and left mid/posterior insula in rheumatoid arthritis patients is associated with fibromyalgianess (FMness). Scatterplots show positive correlations for interindividual differences in brain connectivity (Fisher-transformed r values) with the total FMness score. FWE = family-wise error.

(StataCorp) to enable sensitivity analyses and test post hoc correlations analyses with disease and symptom measures.

RESULTS

Clinical characteristics. A total of 54 patients completed the study. Their mean ± SD age was 54.9 ± 11.41 years, 41 were women, and their mean ± SD disease duration was 11.49 ± 8.64 years. Their mean ± SD FMness score was 13.20 ± 6.21 (range 1–29), and 5 were receiving pharmacologic treatment for FM (all low-dose amitriptyline). Other characteristics of the patients are displayed in Table 1. Correlations of FMness scores with these characteristics are shown in Supplementary Table 1, available on the *Arthritis & Rheumatology* web site at http://onlinelibrary.wiley.com/doi/10.1002/art.40451/abstract.

DMN–insula functional connectivity is associated with FMness in RA. There was a significant positive correlation between DMN connectivity to the left mid/posterior insula and the FMness score (r = 0.572, FWE-corrected $P = 0.001$) in RA patients. The association remained significant after controlling for age and sex (r = 0.577, FWE-corrected $P = 0.001$) (Figure 1). Furthermore, analyses correcting for the putative confounding factors of inflammation (CRP level) and amitriptyline use did not alter this observation (r = 0.568, FWE-corrected $P = 0.001$ and r = 0.556, FWE-corrected $P = 0.009$, respectively). No significant correlations with any of the other networks of interest were identified. Furthermore, a sensitivity analysis of only those patients (n = 27) who did not fulfill the ACR preliminary criteria for FM (31) (total score <13) again yielded a

highly significant correlation of DMN–insula connectivity with the FMness score (r = 0.51, $P = 0.006$).

We then examined correlations with phenotypic features (Table 2). First, the individual components of the FMness score were examined, the widespread pain index and the symptom severity scale, in order to determine whether the DMN–insula connectivity relationship was directed by one or both components. Both the widespread pain index (r = 0.50, $P = 0.0001$) and the symptom severity scale (r = 0.41, $P = 0.002$) were significantly associated, indicating important contributions from both. This was further corroborated by significant associations with chronic fatigue ($P = 0.002$) and sleep disturbance ($P = 0.02$), although interestingly, there was no association between DMN–insula connectivity and pain reported at the time of the scan ($P = 0.52$). We next explored correlations between the identified functional connection and RA disease features. Overall disease activity (the DAS28) was significantly correlated ($P = 0.002$), although CRP level was not ($P = 0.19$).

DISCUSSION

To our knowledge, this study is the first to provide objective neuroimaging evidence that RA is a mixed pain state displaying characteristics of central sensitization. RA patients who reported high levels of FMness demonstrated significantly higher functional connectivity between the DMN and insula—a recognized neurobiologic feature of "primary" FM. Furthermore, the ACR FM survey appears to be a strong surrogate for this neurobiologic marker of central sensitization and could be a useful future tool to support clinicians' evaluation of pain and inform subsequent management.

Our group and others have previously identified significant alterations in DMN–insula connectivity in FM. The insula is a highly connected region of the brain with multiple functional features that routinely involve the integration and conversion of physiologic inputs into higher-level outputs (32). Numerous studies have implicated the insula's involvement in different disorders and dimensions of pain, including FM (33). Its purported role as a key relay station in pain processing has been supported by direct electric stimulation studies of the region, which have effected painful sensations in some patients (34). The DMN comprises synchronously functioning regions—including the posterior cingulate cortex, medial prefrontal cortex, and lateral parietal lobes—that are commonly associated with activities of introspection and are also found to be disrupted in chronic pain (35). It is not known whether this network is a modulator of pain (potentially via descending inhibitory pathways [36]) and/

Table 2. Disease and symptom correlations with default mode network–insula connectivity*

Phenotypic feature	Correlation†	P
FM widespread pain index	0.50	0.0001
FM symptom severity scale	0.41	0.002
Disease duration	0.03	0.83
RA disease activity‡	0.41	0.002
Swollen joint count	0.25	0.07
Tender joint count	0.32	0.02
CRP	0.18	0.19
Current overall pain§	0.09	0.52
Current fatigue§	0.26	0.06
Chronic fatigue¶	0.40	0.002
Depression#	0.10	0.46
Sleep disturbance**	0.31	0.02

* FM = fibromyalgia; RA = rheumatoid arthritis.
† All are Pearson's correlation coefficient (r) except for C-reactive protein (CRP), for which Spearman's rho was used due to distribution.
‡ Disease Activity Score in 28 joints.
§ On a numerical rating scale of 0–10.
¶ Chalder Fatigue Binary Scale.
# Hospital Anxiety and Depression Scale.
** Jenkins' sleep problems scale.

or related somatic features or whether it is exclusively a consequence of chronic pain exposure (35). Given these possible complementary roles in pain processing, it is plausible to speculate that the DMN and the insula may be functionally connected in FM (14–17).

In the current study, we expanded on these findings by identifying a significant alteration of the very same functional connection in relation to phenotypic features of FM coexisting in another chronic pain disorder (with a distinct primary pathophysiology relating to inflammation). The presence of this connection despite the apparent absence of an association with significant concurrent peripheral inflammation or overall levels of pain further supports the apparent specificity of the DMN–insula connection as a marker of a distinct pain subtype. It is, however, interesting to consider the significant correlation with the DAS28, which appears to be principally driven by tender joint counts and not swollen joint counts. This is consistent with studies that have demonstrated worse DAS28 scores in patients with both RA and FM, which in turn leads to more frequent use of biologic therapies (37,38). That said, we cannot discount the possibility that inflammation may have some role in driving central sensitization.

Although no other study has applied neuroimaging to characterize FM in a coexisting disorder, dysfunctional DMN–insula functional connectivity has been observed in irritable bowel syndrome (18), chronic back pain (19), and migraine (39), all of which are pain conditions in which central sensitization has been implicated (40). Interestingly, these conditions are also associated with somatic symptoms (41,42), which is consistent with our post hoc analysis indicating that the DMN–insula functional connection relates not only to pain but also to symptoms such as fatigue and cognitive dysfunction (as measured by the Symptom Severity Index [7]). One notable discrepancy with previous non-RA studies is the absence of a correlation with current pain severity (which we have further confirmed with a voxelwise search of the insula). We speculate that patients with RA have more ongoing nociceptive input due to inflammation compared to other studied clinical populations in which central sensitization contributes more to current pain. A final point is that this connection remains significant even among those RA patients who do not fulfill ACR criteria for FM, providing further evidence that FM is a continuous construct rather than a discrete construct.

Our findings indicate that centralized pain pathways coexist with more established peripheral inflammation–driven pathways in RA. This is corroborated by quantitative sensory testing studies that suggest the existence of dysfunctional CNS pain pathways in RA by consistently showing hyperalgesia and allodynia (43). Specifically, lower pain–pressure thresholds have been measured across both diseased joints and nonjoint sites in RA patients with concomitant FM than in RA patients without concomitant FM (44).

Our study builds on the few functional neuroimaging studies that have been conducted in RA. Although previous studies have been small and limited to provoking acute experimental pain at the site of joints (rather than sites without disease), they have provided evidence supporting a role of mixed CNS mechanisms in RA-related pain. Using positron emission tomography, Jones and Derbyshire originally reported differential cortical responses to acute pain between 6 RA patients and a population of patients with chronic pain who had depression and dysfunctional coping. They subsequently speculated that the CNS mechanisms of inflammatory pain were distinct from those of other types of pain (45). More recently, Rech and colleagues conducted evoked pain fMRI in 10 RA patients before and after anti–tumor necrosis factor therapy, and they observed differences in brain activation between responders and nonresponders (46). This again implies the possible existence of different neural signatures for different types of pain, since responders are more likely than nonresponders to have pain originating from inflammation.

The present study is strengthened by its large sample size (54 patients). To our knowledge, ours is the largest neuroimaging investigation of any inflammatory rheumatic disease, thus reducing the risk of the false-positive results that are endemic in neuroscience. The robustness of these results is further enhanced by our conservative analytic methodology. Despite our using a data-driven global scan approach, only the key DMN–insula functional connection was identified. Furthermore, these data were acquired using a scanner in a center that has not previously contributed to the literature, which shows the importance of this connection. Finally, replication of this specific pattern of coactivation in the context of a task (rather than with patients in a resting state, as with previous studies) not only strengthens validity but also enhances existing views that functional connectivity MRI largely reflects intrinsic communication networks that are unrelated to conscious activities (47).

Certain limitations to this study should also be considered. First, although the study population included a demographically representative cohort of RA patients with a mixture of disease activity states, there was a bias toward selecting patients with significant levels of fatigue. However, this sample enrichment enabled greater power to detect the mechanistic associations inherent in the research question. It also cannot be assumed that these findings may generalize to other rheumatic conditions, and the intriguing possibility that they may so generalize should be the subject of future experiments.

Second, due to the cross-sectional design, no assumption can be made regarding whether DMN–insula functional connectivity has a causal role in FMness. However, these data do reinforce previous studies that propose this connection, at least as a biologic marker of the FM construct, and so they are adequate to address our primary research question.

Third, although this is the largest study of its kind, the sample size cannot allow us to confidently exclude the existence of other relevant network-to-region connections (which most likely exist), and the study still lacks sufficient power to fully and independently correct for the multiple putative confounding variables that are implicated in FM. That said, our results remained significant following individual adjustments for age and sex. The latter is of particular interest because previous studies of functional connectivity in "primary" FM have included female subjects almost exclusively. Since numerous sex differences in FM biology have been reported (48), the generalizability observed here serves to further enhance the usefulness of the DMN–insula marker.

We have shown that central sensitization is not confined to individuals with "primary" FM and coexists in patients with the biologically distinct disorder of RA. Such evidence for shared mechanisms could inform future clinical decision-making. It is challenging for physicians to distinguish different pain states in patients, particularly those with a preexisting chronic pain disorder. This is especially true since the centralized pain state of FMness is not only common but also artificially inflates routinely used measures of peripherally based inflammatory pain states (e.g., the DAS28) (8) that are pivotal in guiding clinicians' prescriptions of antiinflammatory treatment. As a consequence, inappropriate prescribing of antiinflammatory therapies for pain that is actually not inflammatory in origin is likely common and is probably a principal reason why many RA patients continue to report pain following antiinflammatory therapy despite apparent resolution of inflammation (1). RA patients who report significant pain and who have evidence of high levels of functional connectivity between the insula and DMN are more likely to benefit from centrally acting therapies which are effective for FM, instead of or in addition to antiinflammatory therapies. These currently include both pharmacologic agents (e.g., neuroleptics) and nonpharmacologic agents (e.g., cognitive-behavioral therapy) (49).

Unfortunately, limited access, expense, and specialized analysis requirements will likely prohibit implementation of functional connectivity MRI in routine practice; however, this technology may not be essential given the demonstrated relationship with the ACR FM survey score. Instead, application of this measure as a point-of-care tool may enable clinicians to quantify the contribution of central sensitization to their patients' pain and subsequently inform management choices. Future refinements and abbreviations of this tool will hasten translation. Moreover, since coexisting FM is a common issue among many diseases (musculoskeletal and beyond) (50–54), such a tool may be generically applicable, and therefore testing across the spectrum of chronic pain disorders may finally move the pain field into the era of personalized medicine.

AUTHOR CONTRIBUTIONS

All authors were involved in drafting the article or revising it critically for important intellectual content, and all authors approved the final version to be published. Dr. Basu had full access to all of the data in the study and takes responsibility for the integrity of the data and the accuracy of the data analysis.
Study conception and design. Basu, Kaplan, Ichesco, Larkin, Harris, Murray, Waiter, Clauw.
Acquisition of data. Basu, Murray, Waiter.
Analysis and interpretation of data. Basu, Kaplan, Ichesco, Larkin, Harris, Murray, Waiter, Clauw.

REFERENCES

1. McWilliams DF, Walsh DA. Factors predicting pain and early discontinuation of tumour necrosis factor-α-inhibitors in people with rheumatoid arthritis: results from the British Society for Rheumatology Biologics Register. BMC Musculoskelet Disord 2016;17:337.
2. Wolfe F, Michaud K. Assessment of pain in rheumatoid arthritis: minimal clinically significant difference, predictors, and the effect of anti-tumor necrosis factor therapy. J Rheumatol 2007;34:1674–83.
3. Clauw DJ. Fibromyalgia: a clinical review. JAMA 2014;311:1547–55.
4. Lee YC. Effect and treatment of chronic pain in inflammatory arthritis. Curr Rheumatol Rep 2013;15:300.
5. Jones GT, Atzeni F, Beasley M, Fluss E, Sarzi-Puttini P, Macfarlane GJ. The prevalence of fibromyalgia in the general population: a comparison of the American College of Rheumatology 1990, 2010, and modified 2010 classification criteria. Arthritis Rheumatol 2015;67:568–75.
6. Wolfe F, Smythe HA, Yunus MB, Bennett RM, Bombardier C, Goldenberg DL, et al. The American College of Rheumatology 1990 criteria for the classification of fibromyalgia: report of the Multicenter Criteria Committee. Arthritis Rheum 1990;33:160–72.
7. Wolfe F, Clauw DJ, Fitzcharles MA, Goldenberg DL, Häuser W, Katz RS, et al. Fibromyalgia criteria and severity scales for

clinical and epidemiological studies: a modification of the ACR preliminary diagnostic criteria for fibromyalgia. J Rheumatol 2011; 38:1113–22.

8. Wolfe F, Michaud K, Busch RE, Katz RS, Rasker JJ, Shahouri SH, et al. Polysymptomatic distress in patients with rheumatoid arthritis: understanding disproportionate response and its spectrum. Arthritis Care Res (Hoboken) 2014;66:1465–71.

9. Ichesco E, Schmidt-Wilcke T, Bhavsar R, Clauw DJ, Peltier SJ, Kim J, et al. Altered resting state connectivity of the insular cortex in individuals with fibromyalgia. J Pain 2014;15:815–26e1.

10. Bushnell MC, Ceko M, Low LA. Cognitive and emotional control of pain and its disruption in chronic pain. Nat Rev Neurosci 2013;14:502–11.

11. Flodin P, Martinsen S, Lofgren M, Bileviciute-Ljungar I, Kosek E, Fransson P. Fibromyalgia is associated with decreased connectivity between pain- and sensorimotor brain areas. Brain Connect 2014;4:587–94.

12. Gusnard DA, Akbudak E, Shulman GL, Raichle ME. Medial prefrontal cortex and self-referential mental activity: relation to a default mode of brain function. Proc Natl Acad Sci U S A 2001; 98:4259–64.

13. Craig AD. How do you feel? Interoception: the sense of the physiological condition of the body. Nat Rev Neurosci 2002;3:655–66.

14. Napadow V, LaCount L, Park K, As-Sanie S, Clauw DJ, Harris RE. Intrinsic brain connectivity in fibromyalgia is associated with chronic pain intensity. Arthritis Rheum 2010;62:2545–55.

15. Harris RE, Napadow V, Huggins JP, Pauer L, Kim J, Hampson J, et al. Pregabalin rectifies aberrant brain chemistry, connectivity, and functional response in chronic pain patients. Anesthesiology 2013;119:1453–64.

16. Napadow V, Kim J, Clauw DJ, Harris RE. Decreased intrinsic brain connectivity is associated with reduced clinical pain in fibromyalgia. Arthritis Rheum 2012;64:2398–403.

17. Hsiao FJ, Wang SJ, Lin YY, Fuh JL, Ko YC, Wang PN, et al. Altered insula-default mode network connectivity in fibromyalgia: a resting-state magnetoencephalographic study. J Headache Pain 2017;18:89.

18. Letzen JE, Craggs JG, Perlstein WM, Price DD, Robinson ME. Functional connectivity of the default mode network and its association with pain networks in irritable bowel patients assessed via lidocaine treatment. J Pain 2013;14:1077–87.

19. Loggia ML, Kim J, Gollub RL, Vangel MG, Kirsch I, Kong J, et al. Default mode network connectivity encodes clinical pain: an arterial spin labeling study. Pain 2013;154:24–33.

20. Aletaha D, Neogi T, Silman AJ, Funovits J, Felson DT, Bingham CO III, et al. 2010 rheumatoid arthritis classification criteria: an American College of Rheumatology/European League Against Rheumatism collaborative initiative. Arthritis Rheum 2010;62: 2569–81.

21. Chalder T, Berelowitz G, Pawlikowska T, Watts L, Wessely S, Wright D, et al. Development of a fatigue scale. J Psychosom Res 1993;37:147–53.

22. Prevoo ML, van't Hof MA, Kuper HH, van Leeuwen MA, van de Putte LB, van Riel PL. Modified disease activity scores that include twenty-eight–joint counts: development and validation in a prospective longitudinal study of patients with rheumatoid arthritis. Arthritis Rheum 1995;38:44–8.

23. Jenkins CD, Stanton BA, Niemcryk SJ, Rose RM. A scale for the estimation of sleep problems in clinical research. J Clin Epidemiol 1988;41:313–21.

24. Zigmond AS, Snaith RP. The hospital anxiety and depression scale. Acta Psychiatr Scand 1983;67:361–70.

25. Basu N, Murray AD, Jones GT, Reid DM, Macfarlane GJ, Waiter GD. Neural correlates of fatigue in granulomatosis with polyangiitis: a functional magnetic resonance imaging study. Rheumatology (Oxford) 2014;53:2080–7.

26. Calhoun VD, Adali T, Pekar JJ. A method for comparing group fMRI data using independent component analysis: application to

27. Himberg J, Hyvarinen A, Esposito F. Validating the independent components of neuroimaging time series via clustering and visualization. Neuroimage 2004;22:1214–22.

28. Beckmann CF, DeLuca M, Devlin JT, Smith SM. Investigations into resting-state connectivity using independent component analysis. Philos Trans R Soc Lond B Biol Sci 2005;360:1001–13.

29. Whitfield-Gabrieli S, Nieto-Castanon A. Conn: a functional connectivity toolbox for correlated and anticorrelated brain networks. Brain Connect 2012;2:125–41.

30. Behzadi Y, Restom K, Liau J, Liu TT. A component based noise correction method (CompCor) for BOLD and perfusion based fMRI. Neuroimage 2007;37:90–101.

31. Wolfe F, Clauw DJ, FitzCharles MA, Goldenberg DL, Katz RS, Mease P, et al. The American College of Rheumatology preliminary diagnostic criteria for fibromyalgia and measurement of symptom severity. Arthritis Care Res (Hoboken) 2010;62:600–10.

32. Borsook D, Veggeberg R, Erpelding N, Borra R, Linnman C, Burstein R, et al. The insula: a "hub of activity" in migraine. Neuroscientist 2016;22:632–52.

33. Coppieters I, Meeus M, Kregel J, Caeyenberghs K, De Pauw R, Goubert D, et al. Relations between brain alterations and clinical pain measures in chronic musculoskeletal pain: a systematic review. J Pain 2016;17:949–62.

34. Mazzola L, Isnard J, Peyron R, Guenot M, Mauguiere F. Somatotopic organization of pain responses to direct electrical stimulation of the human insular cortex. Pain 2009;146:99–104.

35. Baliki MN, Geha PY, Apkarian AV, Chialvo DR. Beyond feeling: chronic pain hurts the brain, disrupting the default-mode network dynamics. J Neurosci 2008;28:1398–403.

36. Kucyi A, Salomons TV, Davis KD. Mind wandering away from pain dynamically engages antinociceptive and default mode brain networks. Proc Natl Acad Sci U S A 2013;110:18692–7.

37. Ranzolin A, Brenol JC, Bredemeier M, Guarienti J, Rizzatti M, Feldman D, et al. Association of concomitant fibromyalgia with worse disease activity score in 28 joints, health assessment questionnaire, and short form 36 scores in patients with rheumatoid arthritis. Arthritis Rheum 2009;61:794–800.

38. Lage-Hansen PR, Chrysidis S, Lage-Hansen M, Hougaard A, Ejstrup L, Amris K. Concomitant fibromyalgia in rheumatoid arthritis is associated with the more frequent use of biological therapy: a cross-sectional study. Scand J Rheumatol 2016;45: 45–8.

39. Coppola G, Di Renzo A, Tinelli E, Di Lorenzo C, Scapeccia M, Parisi V, et al. Resting state connectivity between default mode network and insula encodes acute migraine headache. Cephalalgia 2017:333102417715230.

40. Woolf CJ. Central sensitization: implications for the diagnosis and treatment of pain. Pain 2011;152:S2–15.

41. Grassini S, Nordin S. Comorbidity in migraine with functional somatic syndromes, psychiatric disorders and inflammatory diseases: a matter of central sensitization? Behav Med 2017;43: 91–9.

42. Hartvigsen J, Natvig B, Ferreira M. Is it all about a pain in the back? Best Pract Res Clin Rheumatol 2013;27:613–23.

43. Meeus M, Vervisch S, De Clerck LS, Moorkens G, Hans G, Nijs J. Central sensitization in patients with rheumatoid arthritis: a systematic literature review. Semin Arthritis Rheum 2012;41: 556–67.

44. Lee YC, Chibnik LB, Lu B, Wasan AD, Edwards RR, Fossel AH, et al. The relationship between disease activity, sleep, psychiatric distress and pain sensitivity in rheumatoid arthritis: a cross-sectional study. Arthritis Res Ther 2009;11:R160.

45. Jones AK, Derbyshire SW. Reduced cortical responses to noxious heat in patients with rheumatoid arthritis. Ann Rheum Dis 1997;56:601–7.

46. Rech J, Hess A, Finzel S, Kreitz S, Sergeeva M, Englbrecht M, et al. Association of brain functional magnetic resonance activity

visual, motor and visuomotor tasks. Magn Reson Imaging 2004;22:1181–91.

with response to tumor necrosis factor inhibition in rheumatoid arthritis. Arthritis Rheum 2013;65:325–33.

47. Cole MW, Bassett DS, Power JD, Braver TS, Petersen SE. Intrinsic and task-evoked network architectures of the human brain. Neuron 2014;83:238–51.

48. Fillingim RB, King CD, Ribeiro-Dasilva MC, Rahim-Williams B, Riley JL III. Sex, gender, and pain: a review of recent clinical and experimental findings. J Pain 2009;10:447–85.

49. Macfarlane GJ, Kronisch C, Dean LE, Atzeni F, Häuser W, Fluß E, et al. EULAR revised recommendations for the management of fibromyalgia. Ann Rheum Dis 2017;76:318–28.

50. Hajj-Ali RA, Wilke WS, Calabrese LH, Hoffman GS, Liu X, Bena J, et al. Pilot study to assess the frequency of fibromyalgia, depression, and sleep disorders in patients with granulomatosis with polyangiitis (Wegener's). Arthritis Care Res (Hoboken) 2011;63:827–33.

51. Torrente-Segarra V, Salman-Monte TC, Rúa-Figueroa I, Pérez-Vicente S, López-Longo FJ, Galindo-Izquierdo M, et al. Fibromyalgia prevalence and related factors in a large registry of patients with systemic lupus erythematosus. Clin Exp Rheumatol 2016;34:S40–7.

52. Choi BY, Oh HJ, Lee YJ, Song YW. Prevalence and clinical impact of fibromyalgia in patients with primary Sjogren's syndrome. Clin Exp Rheumatol 2016;34:S9–13.

53. Macfarlane GJ, Barnish MS, Pathan E, Martin KR, Haywood KL, Siebert S, et al. Co-occurrence and characteristics of patients with axial spondyloarthritis who meet criteria for fibromyalgia: results from a UK national register. Arthritis Rheumatol 2017;69:2144–50.

54. Sinaii N, Cleary SD, Ballweg ML, Nieman LK, Stratton P. High rates of autoimmune and endocrine disorders, fibromyalgia, chronic fatigue syndrome and atopic diseases among women with endometriosis: a survey analysis. Hum Reprod 2002;17:2715–24.

Dysbiotic Subgingival Microbial Communities in Periodontally Healthy Patients With Rheumatoid Arthritis

Isabel Lopez-Oliva,[1] Akshay D. Paropkari,[2] Shweta Saraswat,[2] Stefan Serban,[1] Zehra Yonel,[1] Praveen Sharma,[1] Paola de Pablo,[3] Karim Raza,[3] Andrew Filer,[4] Iain Chapple,[1] Thomas Dietrich,[1] Melissa M. Grant,[1] and Purnima S. Kumar[2]

Objective. Studies that demonstrate an association between rheumatoid arthritis (RA) and dysbiotic oral microbiomes are often confounded by the presence of extensive periodontitis in these individuals. This study was undertaken to investigate the role of RA in modulating the periodontal microbiome by comparing periodontally healthy individuals with RA to those without RA.

Methods. Subgingival plaque was collected from periodontally healthy individuals (22 with RA and 19 without RA), and the 16S gene was sequenced on an Illumina MiSeq platform. Bacterial biodiversity and co-occurrence patterns were examined using the QIIME and PhyloToAST pipelines.

Results. The subgingival microbiomes differed significantly between patients with RA and controls based on both community membership and the abundance of lineages, with 41.9% of the community differing in abundance and 19% in membership. In contrast to the sparse and predominantly congeneric co-occurrence networks seen in controls, RA patients revealed a highly connected grid containing a large intergeneric hub anchored by known periodontal pathogens. Predictive metagenomic analysis (PICRUSt) demonstrated that arachidonic acid and ester lipid metabolism pathways might partly explain the robustness of this clustering. As expected from a periodontally healthy cohort, *Porphyromonas gingivalis* and *Aggregatibacter actinomycetemcomitans* were not significantly different between groups; however, *Cryptobacterium curtum*, another organism capable of producing large amounts of citrulline, emerged as a robust discriminant of the microbiome in individuals with RA.

Conclusion. Our data demonstrate that the oral microbiome in RA is enriched for inflammophilic and citrulline-producing organisms, which may play a role in the production of autoantigenic citrullinated peptides in RA.

Rheumatoid arthritis (RA) has been associated with periodontal disease, a bacterially initiated chronic inflammation that leads to the destruction of tooth-supporting tissue (1). Although periodontal disease and RA share similar inflammatory pathways as well as genetic and environmental risk factors, these are insufficient to explain this connection (1).

While the cause of RA remains unknown, it has been hypothesized that oral microbiota (2,3), in particular the periodontal pathogens *Porphyromonas gingivalis* and *Aggregatibacter actinomycetemcomitans*, may play a critical role in its pathogenesis (4,5).

Studies using next-generation sequencing methods have demonstrated that the oral microbiome is altered in RA (6,7). However, the majority of those studies included individuals with moderate to severe periodontitis (7) or individuals whose periodontal health status was not established (6). Periodontitis by itself is a significant modifier of the oral microbiome (8), making it difficult to dissect the relative contributions of periodontitis and RA to microbial dysbiosis.

Given the potential role oral bacteria may play in the pathogenesis of RA, we set out to characterize the periodontal microbiome in periodontally healthy individuals with and those without RA, using next-generation sequencing.

PATIENTS AND METHODS

The study sample included patients with RA and non-RA controls. All participants were periodontally healthy. Subgingival plaque samples were collected and analyzed using 16S ribosomal DNA sequencing. Further details are given in the Supplementary Methods, available on the *Arthritis & Rheumatology* web site at http://onlinelibrary.wiley.com/doi/10.1002/art.40485/abstract. The sequences are deposited in the Sequence Read Archive of NCBI (project number: PRJNA391575).

RESULTS

We examined 22 patients with RA and 19 non-RA controls. There was a statistically significant but clinically inconsequential difference between groups in periodontal measures, in particular probing pocket depth and clinical attachment loss (gingival recession plus probing pocket depth) (Table 1). Principal Coordinates Analysis of both unweighted and weighted UniFrac distances demonstrated significant clustering of the microbiomes based on RA status ($P = 0.001$ by Adonis test) (Figure 1A), indicating that these groups differed both with regard to the presence or absence of lineages (community membership), and with regard to the relative abundances of lineages within communities (community structure) (Figure 1B).

Since patients with RA differed from controls in both community membership and community structure, we identified species-level operational taxonomic units (OTUs) that contributed to this difference using an increasingly granular top-down approach. Patients with RA had greater abundances of both gram-positive and gram-negative obligate anaerobes, while facultative anaerobes (especially gram-negative ones) were identified in greater abundance in non-RA controls ($P < 0.05$ by Wilcoxon signed rank test) (Figure 1C).

We then used DESeq2 (9) to identify differentially abundant OTUs with P values less than 0.05 after adjusting for multiple testing, and Fisher's exact test to examine

Table 1. Clinical and demographic characteristics of the periodontally healthy subjects with RA and those without RA*

	RA (n = 22)	Non-RA (n = 19)
Age in years, mean (IQR)	60 (54.1–63.4)	36 (32.9–41.6)†
Sex, % male	23	32
Ethnicity, %		
White	95	89
Asian	5	11
Smoking history, %		
Never	62	90
Former	29	5
Current	9	5
Alcohol consumption, %		
Never	11	14
1–4 times/month	73	45
1–4 times/week	16	41
Clinical periodontal characteristics, mean (IQR)		
PPD, mm	2.3 (2.2–2.4)	1.6 (1.5–1.7)†
Number of sites with PPD >4 mm	1.2 (0–2)	0.9 (0–3)
Number of sites with bleeding on probing	6 (0–19)	4 (1–16)
Gingival recession, mm	0.28 (0.01–0.26)	0.13 (0.04–0.2)†
Measures of RA severity, mean (IQR)		
ESR	8 (8.7–21.7)	–
Patient's global assessment of disease activity (VAS)	41 (31.7–58.5)	–
DAS28	3.4 (2.7–3.9)	–

* RA = rheumatoid arthritis; IQR = interquartile range; PPD = probing pocket depth; ESR = erythrocyte sedimentation rate; VAS = visual analog scale; DAS28 = Disease Activity Score in 28 joints.
† $P < 0.05$ by Mann-Whitney test.

the frequency of detection. We identified 558 OTUs from 3,963,291 classifiable sequences (mean 107,115 sequences per sample, range 69,626–182,993). Rarefaction curves demonstrated that all samples approached saturation or had plateaued. Two hundred twenty-nine OTUs (41.9% of the community) differed significantly in structure and 105 OTUs (19%) differed significantly in membership between groups (Figure 1D and Supplementary Table 1, available on the *Arthritis & Rheumatology* web site at http://onlinelibrary.wiley.com/doi/10.1002/art.40485/abstract). Certain species were significantly more abundant in patients with RA, including those belonging to the genera *Actinomyces* (odds ratios [ORs] varying from 4 to 9 for each species within the genus), *Cryptobacterium* (OR 36), *Dialister* (OR 4), *Desulfovibrio* (OR 26), *Fretibacterium* (ORs 9–12), *Leptotrichia* (ORs 7–26), *Prevotella* (ORs 0.04–6), *Selenomonas* (ORs 0–7), *Treponema* (ORs 0–7), and *Veillonellaceae [G1]* (ORs 0–6).

In contrast, several species belonging to the genera *Aggregatibacter*, *Gemella*, *Granulicatella*, *Haemophilus*, *Neisseria*, and *Streptococci* not only demonstrated lower abundances but were also less frequently detected in RA.
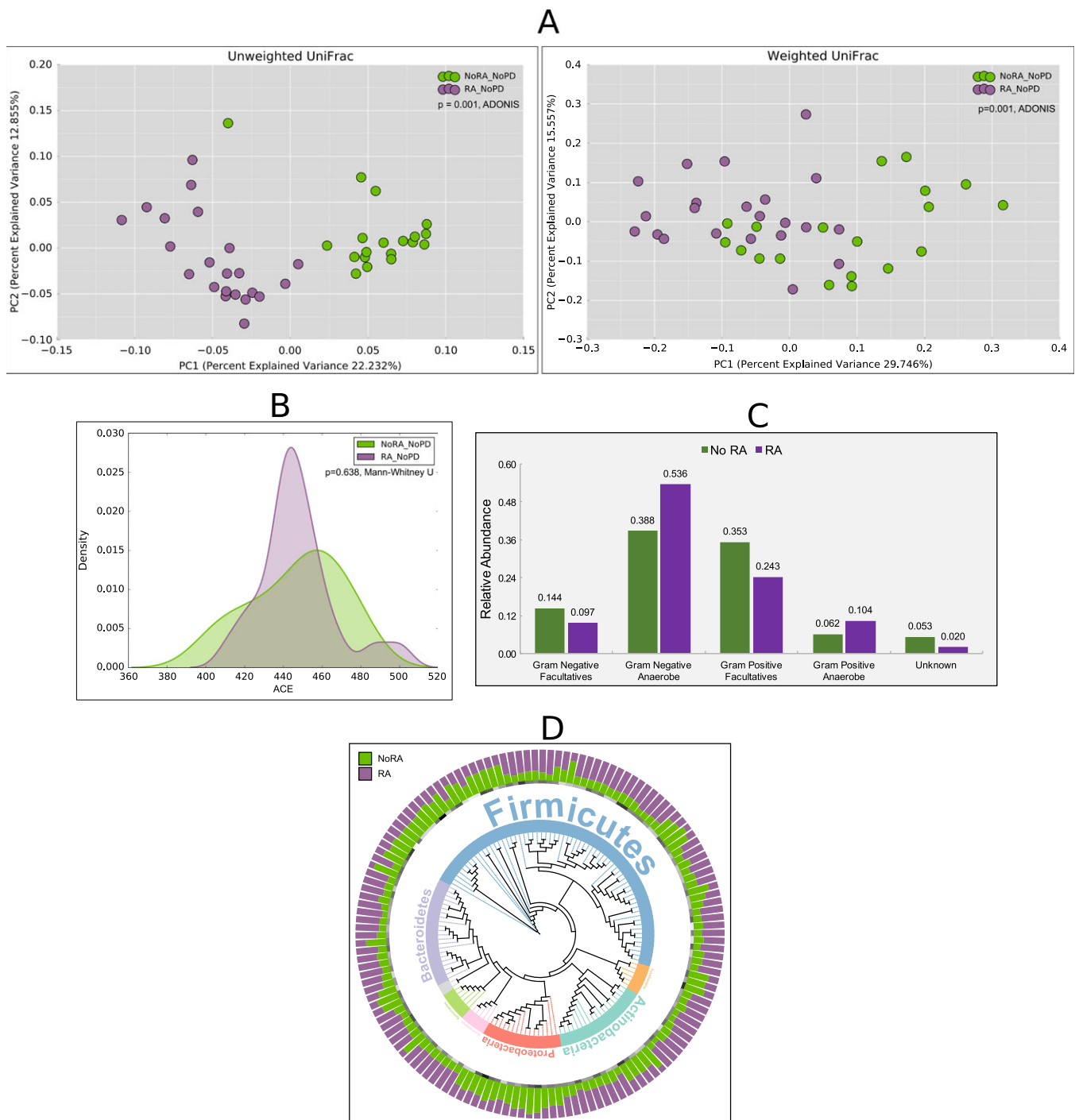
Figure 1. Differences in α- and β-diversity metrics between periodontally healthy subjects with rheumatoid arthritis (RA) (RA_NoPD) and periodontally healthy subjects without RA (NoRA_NoPD). **A**, Principal Coordinates Analysis plots of unweighted and weighted UniFrac distances. **B**, Kernel plots of α-diversity (abundance-based coverage estimator [ACE]). The peak indicates the median value for each group. The x-axis indicates the data range. PC1 = principal coordinate 1. **C**, Distribution of species by Gram staining and oxygen requirement characteristics. **D**, Phylogenetic tree representing normalized mean relative abundance (stacked bar chart), core species (circles represent species present in ≥80% of samples in a group), and phylum-level taxonomic annotation (colored strips and text) for significantly different and differentially abundant species-level operational taxonomic units (tree leaves). Data for **D** are presented in Supplementary Table 1, available on the *Arthritis & Rheumatology* web site at http://onlinelibrary.wiley.com/doi/10.1002/art.40485/abstract.
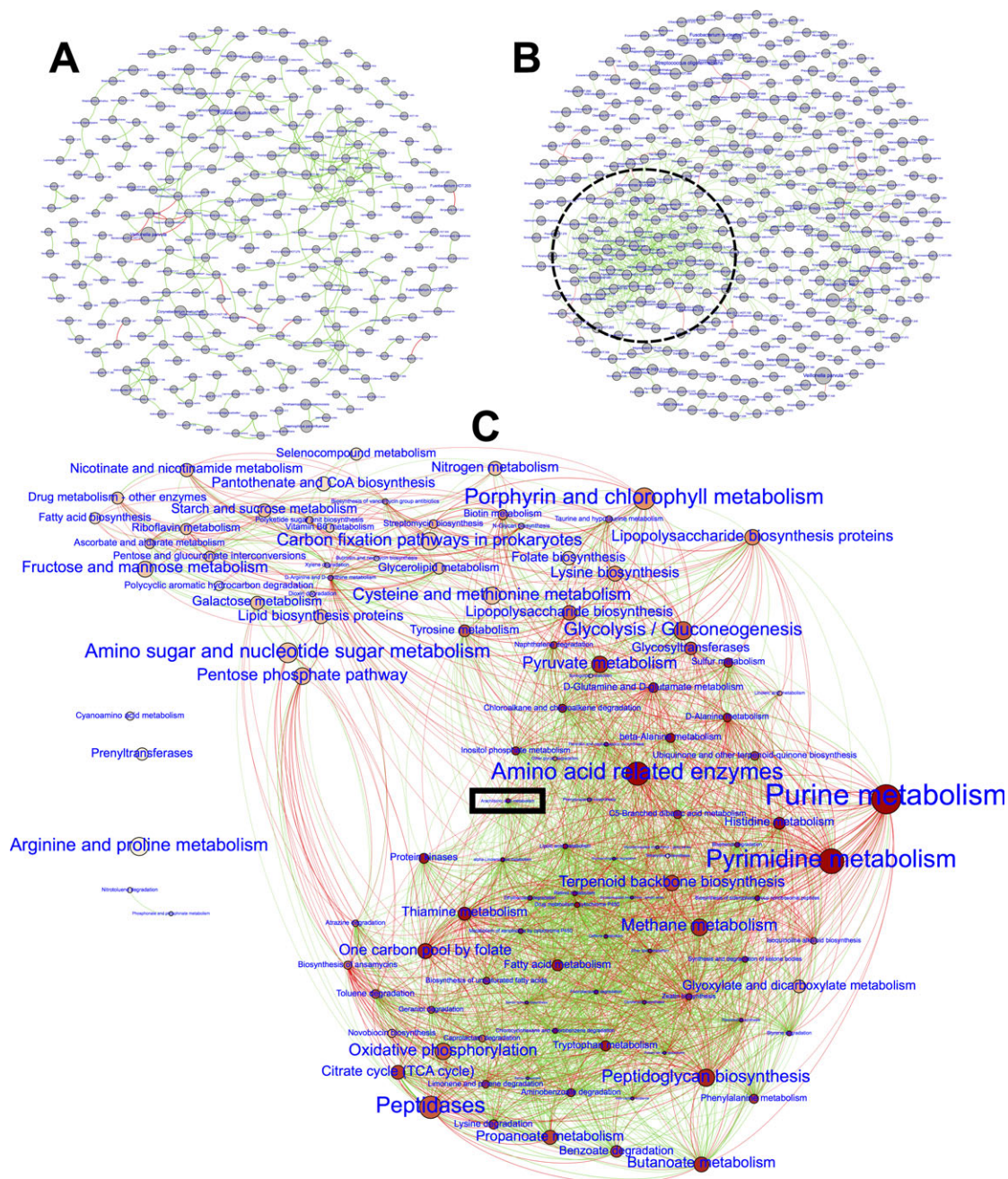
Figure 2. **A** and **B**, Co-occurrence networks in periodontally healthy subjects without rheumatoid arthritis (RA) (**A**) and periodontally healthy subjects with RA (**B**). **C**, Metabolic pathways shared by the bacterial hub in the circled area in **B**. Each network graph contains nodes (circles) and edges (connections representing Spearman's rho). Nodes represent species-level operational taxonomic units in **A** and **B** and genes encoding for metabolic functions in **C**. The size of the nodes indicates relative abundance. Edges represent significant and robust Spearman's correlations (ρ ≥ 0.75, *P* < 0.05). Green edges indicate positive correlations, and red edges indicate negative correlations. Data for **C** are presented in Supplementary Table 2, available on the *Arthritis & Rheumatology* web site at http://onlinelibrary.wiley.com/doi/10.1002/art.40485/abstract. Color figure can be viewed in the online issue, which is available at http://onlinelibrary.wiley.com/doi/10.1002/art.40485/abstract.

These significantly abundant species accounted for a median of 28% (range 12–82%) of each individual's microbiome in patients with RA, indicating that these differences are not attributable to the rare biosphere.

Since the subgingival microbiome is known to be significantly heterogeneous among individuals (10), we used the core microbiome (suite of species identified in ≥80% of subjects) to compare stable associations between

groups. Three hundred twenty-six OTUs were identified in the core microbiome of all study participants and 364 were identified in patients with RA. Structure was significantly different in 27.7% of the community (101 OTUs), and membership was significantly different in 10.9% (40 OTUs), with 38 species unique to the RA core microbiome (Figure 1D). Importantly, 157 of the 229 species identified above belonged to the core microbiome.

Sparse, congeneric networks were observed in non-RA controls (Figure 2). In contrast, the network topology of individuals with RA revealed a highly connected grid with a robust intergeneric hub. Of the 157 core species, 83 were incorporated in this hub, further reinforcing our observation that in patients with RA, the environment imposes a selection drive. Importantly, known pathogenic species belonging to *Treponema*, *Selenomonas*, *Filifactor*, *Campylobacter*, and *Fretibacterium* were tightly interwoven into this hub, and 12 gram-negative species were identified as network anchors. Interestingly, species traditionally associated with RA, for example, *P gingivalis* and *A actinomycetemcomitans*, were not part of the network cluster.

Since there is little literature-based information to provide insights into the biologic basis for this tight clustering, we combined predictive metagenomic analysis (PICRUSt) (11) with network graph theory and core microbiome analysis to explore if shared functionality could explain co-occurrence (Figure 2). Bacterial arachidonic acid and ether lipid metabolism genes exhibited the greatest betweenness centrality (reflecting the amount of control that these nodes exert over the interactions of other nodes in the network) (12), and the highest degree centrality (an indication that they are the central focal point of the structure).

DISCUSSION

Gram-negative anaerobes are known to play important roles in initiating periodontitis, and emerging evidence also implicates them in the pathogenesis of RA (6–13). Our results show that gram-negative anaerobes are significantly more abundant in patients with RA, even those who are periodontally healthy, consistent with a dysbiotic state. Such a status might indicate a preclinical phase of periodontitis. As expected in a periodontally healthy adult cohort, *P gingivalis* and *A actinomycetemcomitans* were neither dominant members of the microbiome nor significantly different between groups. Taken together with previous studies (13), our data imply that gram-negative bacteria other than *P gingivalis* and *A actinomycetemcomitans* may play a role in the initiation of RA, while evidence from the literature suggests that these two species may be critical to disease perpetuation.

Recent investigations have demonstrated that while substantial microbial heterogeneity exists among healthy individuals, a robust core microbiome is identifiable in individuals who smoke or are pregnant (14–16). The findings of the present study parallel these previous observations and support the ecological plaque hypothesis (17), suggesting that RA imposes a habitat filter on the subgingival environment, preferentially promoting the growth of certain organisms.

Traditional statistical methods assume bacterial presence and abundance to be independent variables, but in reality bacterial presence in a biofilm is driven by interdependent nutritional and metabolic interactions. Therefore, we combined network graph theory with DESeq and core microbiome analysis to examine co-occurrence patterns and identify important community members (network anchors). No network anchors were identifiable in controls (since betweenness centrality was homogeneous between species), indicating that this is an ecological niche in equilibrium. However, the tightly woven hub of anaerobes suggest that a small group of anaerobic bacteria play an important role in controlling the flow of resources in the RA-influenced microbiome, implying that even small changes in these anchors could affect community assembly in people with RA. These species may be potential targets for microbial disruption.

Arachidonic acid is essential for cell membrane integrity. It is metabolized to prostaglandin E_2 and other proinflammatory eicosanoids that are implicated in the development of RA. The ability to metabolize arachidonic acid into proinflammatory eicosanoids is an emergent property of opportunistic pathogens (18). Arachidonic acid is also known to inhibit the growth and epithelial adhesion of beneficial species in the gut (19). Taken together, the data indicate that the subgingival microbiome is both influenced by, and influences, the inflammatory burden of RA.

One of the most intriguing findings was the identification of *Cryptobacterium curtum* as a predominant member of the RA-influenced periodontal microbiome. This gram-positive, asaccharolytic, anaerobic rod (which was previously misclassified as *Eubacterium saburreum*) degrades arginine through the arginine deiminase pathway and produces substantial amounts of citrulline, ornithine, and ammonia (20). We have previously identified this as a periodontal pathogen (21), and translocation from oral sources has been implicated in the etiology of distant infections such as pelvic abscesses, gynecologic infections, and wounds (22). More importantly, *C curtum* is enriched in the oral and gut microbiomes of early RA cases (6,23). Consistent with previous studies, we observed that this species was a member of the core microbiome in RA patients. Compared to non-RA controls,

this species demonstrated a 100-fold greater abundance in RA with 39-fold greater odds of detection. While this unusually high association does not necessarily suggest an etiopathogenic role for *C curtum*, this organism is certainly a candidate for further studies. In light of evidence that antibodies against citrullinated protein and peptides precede the clinical onset of RA by several years, have high specificity for RA at over 95% (24,25), and that we previously observed antibodies characteristic of RA, including citrullinated and noncitrullinated peptides of the RA autoantigens in individuals with periodontitis (3), the ability of *C curtum* to degrade arginine via the arginine deiminase pathway and to produce substantial amounts of citrulline is of particular interest. The presence of *C curtum* in the plaque may therefore be a contributing factor in the development of RA autoantigens and warrants further investigation.

In summary, our data suggest that RA plays a major role in shaping the oral microbiome. The microbiome in RA is enriched for proinflammatory organisms and those capable of producing substantial amounts of citrulline (proantigenic). An ability to metabolize arachidonic acid and ether lipids appears to be a shared function among the species observed in individuals with RA. Our findings lend further credence to a link between the oral microbiome and RA; however, longitudinal studies are needed to understand directionality and causality, and also to characterize potentially "driver species" that could serve as biomarkers of RA.

AUTHOR CONTRIBUTIONS

All authors were involved in drafting the article or revising it critically for important intellectual content, and all authors approved the final version to be published. Dr. Kumar had full access to all of the data in the study and takes responsibility for the integrity of the data and the accuracy of the data analysis.

Study conception and design. Lopez-Oliva, Paropkari, Chapple, Dietrich, Grant, Kumar.

Acquisition of data. Lopez-Oliva, Paropkari, Saraswat, Serban, Yonel, Sharma, de Pablo, Raza, Filer, Chapple, Dietrich, Grant, Kumar.

Analysis and interpretation of data. Lopez-Oliva, Paropkari, Saraswat, Serban, Yonel, Sharma, de Pablo, Raza, Filer, Chapple, Dietrich, Grant, Kumar.

REFERENCES

1. Kaur S, White S, Bartold M. Periodontal disease as a risk factor for rheumatoid arthritis: a systematic review. JBI Libr Syst Rev 2012;10 Suppl:1–12.
2. De Pablo P, Chapple IL, Buckley CD, Dietrich T. Periodontitis in systemic rheumatic diseases. Nat Rev Rheumatol 2009;5:218–24.
3. De Pablo P, Dietrich T, Chapple IL, Milward M, Chowdhury M, Charles PJ, et al. The autoantibody repertoire in periodontitis: a role in the induction of autoimmunity to citrullinated proteins in rheumatoid arthritis? Ann Rheum Dis 2014;73:580–6.
4. Wegner N, Wait R, Sroka A, Eick S, Nguyen KA, Lundberg K, et al. Peptidylarginine deiminase from Porphyromonas gingivalis citrullinates human fibrinogen and α-enolase: implications for autoimmunity in rheumatoid arthritis. Arthritis Rheum 2010;62:2662–72.
5. Konig MF, Abusleme L, Reinholdt J, Palmer RJ, Teles RP, Sampson K, et al. Aggregatibacter actinomycetemcomitans–induced hypercitrullination links periodontal infection to autoimmunity in rheumatoid arthritis. Sci Transl Med 2016;8:369ra176.
6. Zhang X, Zhang D, Jia H, Feng Q, Wang D, Liang D, et al. The oral and gut microbiomes are perturbed in rheumatoid arthritis and partly normalized after treatment. Nat Med 2015;21:895–905.
7. Scher JU, Ubeda C, Equinda M, Khanin R, Buischi Y, Viale A, et al. Periodontal disease and the oral microbiota in new-onset rheumatoid arthritis. Arthritis Rheum 2012;64:3083–94.
8. Griffen AL, Beall CJ, Campbell JH, Firestone ND, Kumar PS, Yang ZK, et al. Distinct and complex bacterial profiles in human periodontitis and health revealed by 16S pyrosequencing. ISME J 2012;6:1176–85.
9. Love MI, Huber W, Anders S. Moderated estimation of fold change and dispersion for RNA-seq data with DESeq2. Genome Biol 2014;15:550.
10. Paster BJ, Boches SK, Galvin JL, Ericson RE, Lau CN, Levanos VA, et al. Bacterial diversity in human subgingival plaque. J Bacteriol 2001;183:3770–83.
11. Langille MG, Zaneveld J, Caporaso JG, McDonald D, Knights D, Reyes JA, et al. Predictive functional profiling of microbial communities using 16S rRNA marker gene sequences. Nat Biotechnol 2013;31:814–21.
12. Yoon J, Blumer A, Lee K. An algorithm for modularity analysis of directed and weighted biological networks based on edge-betweenness centrality. Bioinformatics 2006;22:3106–8.
13. Mikuls TR, Payne JB, Yu F, Thiele GM, Reynolds RJ, Cannon GW, et al. Periodontitis and porphyromonas gingivalis in patients with rheumatoid arthritis. Arthritis Rheum 2014;66:1090–100.
14. Mason MR, Preshaw PM, Nagaraja HN, Dabdoub SM, Rahman A, Kumar PS. The subgingival microbiome of clinically healthy current and never smokers. ISME J 2015;9:268–72.
15. Paropkari AD, Leblebicioglu B, Christian LM, Kumar PS. Smoking, pregnancy and the subgingival microbiome. Sci Rep 2016;6:30388.
16. Jetté ME, Dill-McFarland KA, Hanshew AS, Suen G, Thibeault SL. The human laryngeal microbiome: effects of cigarette smoke and reflux. Sci Rep 2016;6:35882.
17. Marsh PD. Microbial ecology of dental plaque and its significance in health and disease. Adv Dent Res 1994;8:263–71.
18. Fourie R, Ells R, Swart CW, Sebolai OM, Albertyn J, Pohl CH. Candida albicans and Pseudomonas aeruginosa interaction, with focus on the role of eicosanoids. Front Physiol 2016;7:64.
19. Kankaanpaa P, Yang B, Kallio H, Isolauri E, Salminen S. Effects of polyunsaturated fatty acids in growth medium on lipid composition and on physicochemical surface properties of lactobacilli. Appl Environ Microbiol 2004;70:129–36.
20. Uematsu H, Sato N, Djais A, Hoshino E. Degradation of arginine by Slackia exigua ATCC 700122 and Cryptobacterium curtum ATCC 700683. Oral Microbiol Immunol 2006;21:381–84.
21. Kumar PS, Griffen AL, Barton JA, Paster BJ, Moeschberger ML, Leys EJ. New bacterial species associated with chronic periodontitis. J Dent Res 2003;5:338–44.
22. Brook I, Frazier EH. Significant recovery of nonsporulating anaerobic rods from clinical specimens. Clin Infect Dis 1993;16:476–80.
23. Vaahtovuo J, Munukka E, Korkeamaki M, Luukkainen R, Toivanen P. Fecal microbiota in early rheumatoid arthritis. J Rheumatol 2008;35:1500–5.
24. Schellekens GA, de Jong BA, van den Hoogen FH, van de Putte LB, van Venrooij WJ. Citrulline is an essential constituent of antigenic determinants recognized by rheumatoid arthritis-specific autoantibodies. J Clin Invest 1998;101:273–81.
25. Schellekens GA, Visser H, de Jong BA, van den Hoogen FH, Hazes JM, Breedveld FC, et al. The diagnostic properties of rheumatoid arthritis antibodies recognizing a cyclic citrullinated peptide. Arthritis Rheum 2000;43:155–63.

BRIEF REPORT

Attenuated Effectiveness of Tumor Necrosis Factor Inhibitors for Anti–Human T Lymphotropic Virus Type I Antibody–Positive Rheumatoid Arthritis

Takahisa Suzuki,[1] Shoichi Fukui,[2] Kunihiko Umekita,[3] Junya Miyamoto,[4] Masataka Umeda,[5] Ayako Nishino,[2] Akitomo Okada,[1] Tomohiro Koga,[2] Shin-ya Kawashiri,[2] Naoki Iwamoto,[2] Kunihiro Ichinose,[2] Mami Tamai,[2] Keita Fujikawa,[6] Toshiyuki Aramaki,[7] Akinari Mizokami,[6] Naoki Matsuoka,[8] Yukitaka Ueki,[7] Katsumi Eguchi,[7] Shuntaro Sato,[4] Toshihiko Hidaka,[9] Tomoki Origuchi,[2] Akihiko Okayama,[3] Atsushi Kawakami,[2] and Hideki Nakamura[2]

Objective. **To evaluate the effectiveness of tumor necrosis factor (TNF) inhibitors for the treatment of human T lymphotropic virus type I (HTLV-I)–positive patients with rheumatoid arthritis (RA) in an area endemic for HTLV-I infection.**

Methods. **We conducted an observational study of 585 RA patients in whom TNF inhibitors were newly introduced as a first biologic disease-modifying antirheumatic drug in an area in southwestern Japan that is endemic for HTLV-I infection.**

Results. **Fifty patients (8.5%) were anti–HTLV-I antibody–positive. The ages of the patients in this group were significantly higher at entry compared with the ages of patients who were anti–HTLV-I antibody–negative (n = 535). The median Disease Activity Score in 28 joints using the erythrocyte sedimentation rate (DAS28-ESR) was**

5.21. Among the total group of patients, 82% were anti–citrullinated protein antibody (ACPA)–positive. The persistence rate of TNF inhibitors at 24 weeks was 89%. The median DAS28-ESR was significantly decreased at 24 weeks in each group. The European League Against Rheumatism (EULAR) response rate was significantly better in the anti–HTLV-I antibody–negative patients (P = 0.0277). Multiple regression analysis demonstrated that anti–HTLV-I antibody status was significantly associated with the EULAR response rate and change in the DAS28-ESR and was prominent especially in the ACPA-negative subjects. No patients developed adult T cell leukemia/lymphoma (ATL) or HTLV-I–associated myelopathy (HAM) during the 24-week treatment period.

Conclusion. **The efficacy of TNF inhibitors may be attenuated in anti–HTLV-I antibody–positive patients with RA. ATL and HAM did not develop when TNF inhibitors were used for 24 weeks, but the long-term risk is not known.**

Tumor necrosis factor (TNF) has a major role in many inflammatory diseases, including rheumatoid arthritis (RA), ankylosing spondylitis (AS), and inflammatory bowel disease (IBD). The development of TNF inhibitors thus holds promise for new treatments targeting a specific cytokine; such an approach is distinct from the use of conventional nonspecific immunosuppressive agents. In fact, TNF inhibitors have already become promising treatments for RA (1), AS (2), and IBD (3).

Human T lymphotropic virus type I (HTLV-I) is associated with a number of diseases such as adult T cell leukemia/lymphoma (ATL), HTLV-I–associated myelopathy/tropical spastic paraparesis (HAM/TSP), and autoimmune diseases such as the arthropathies, Sjögren's syndrome, and uveitis (4). The HTLV-I virus infects primarily CD4+ T lymphocytes but also synovial fibroblasts and salivary gland

epithelial cells, and HTLV-I infection can modify the functions of these cells (4–6). In this context, a previous study by our group that was conducted in an area endemic for HTLV-I infection showed that HTLV-I–positive patients with RA are more resistant to TNF inhibitors compared with HTLV-I–negative RA patients (7).

One case of ATL was reported to have occurred 27 months after the initiation of adalimumab for the treatment of spondyloarthritis (8). Although TNF inhibitor treatment had no effect on proliferation of an HTLV-I–infected cell line in vitro (9), it has not been established whether TNF inhibitors affect the HTLV-I infection status, including the occurrence of ATL or HAM/TSP. In addition, the precise ability of TNF inhibitors to decrease disease activity under inflammatory conditions, such as in the presence of high levels of TNF or interleukin-6 (IL-6), also has not been determined in patients with HTLV-I infection. Since TNF inhibitors have become a first-line biologic disease-modifying antirheumatic drug (DMARD) treatment in clinical practice, it is crucial to determine their efficacy and safety in HTLV-I–positive RA patients, especially in areas endemic for HTLV-I infection.

In a previous study by our group (7), we compared the response to TNF inhibitors in 10 HTLV-I–positive RA patients with that in 20 HTLV-I–negative patients with RA (matched for age and sex), in a single area with a high prevalence of HTLV-I, Miyazaki Prefecture. We observed that the treatment outcomes were generally affected by several background elements, such as disease activity at the start of treatment and positivity for rheumatoid factor (RF) or anti–citrullinated protein antibodies (ACPAs). However, we were unable to evaluate the confounding factors due to the limited number of cases. In the current study, therefore, we attempted to resolve this problem by including all of the RA patients for whom TNF inhibitors were newly introduced as a first biologic DMARD during the study period and performed multivariable analyses to examine and confirm the genuine effects of HTLV-I on TNF inhibitor treatment of RA patients in multiple hospitals in the Nagasaki and Miyazaki Prefectures in Japan, which are known as areas endemic for HTLV-I infection.

PATIENTS AND METHODS

Study design. This was a retrospective cohort study in patients with RA with or without anti–HTLV-I antibodies who were treated with TNF inhibitors in Nagasaki Prefecture and Miyazaki Prefecture in Japan, which are known as areas endemic for HTLV-I infection (10).

Patients. We reviewed the cases of all RA patients in whom TNF inhibitors were newly introduced as a first biologic DMARD between June 2001 and June 2013 at hospitals in Nagasaki Prefecture and Miyazaki Prefecture. RA patients who were switched from a biologic DMARD to a TNF inhibitor were excluded. All patients fulfilled the American College of Rheumatology (ACR) 1987 revised criteria for the classification of RA (11) and/or the ACR/European League Against Rheumatism (EULAR) 2010 classification criteria for RA (12). All of the patients included in our previous study (7) were excluded. A final total of 585 patients with RA were included in the study.

This study was approved by the Institutional Review Board of Nagasaki University Hospital (NU120087), the Research Ethics Committee of the University of Miyazaki (no. 859), and the Research Ethics Committees of Isahaya General Hospital (approved July 7, 2012), Sasebo Chuo Hospital (no. 2016-23), Nagasaki Medical Hospital of Rheumatology (approved February 20, 2013), and Zenjinkai Shimin-no-Mori Hospital (approved August 20, 2012). Informed consent for the use of their data was obtained from some of the patients, and an opt-out strategy was chosen for the rest of the patients.

Data collection. Using the patients' medical records, we collected the demographic and clinical characteristics, laboratory data, treatments at entry, and therapeutic outcomes at 24 weeks.

Evaluations of the efficacy and safety of the TNF inhibitors. The clinical disease activity of RA in each patient was evaluated using the Disease Activity Score in 28 joints using the erythrocyte sedimentation rate (DAS28-ESR) (13) at baseline (0 weeks) and at 24 weeks after the initiation of the TNF inhibitor treatment. For evaluation of the patients' responses to the treatments, the EULAR response criteria (14) were used. These criteria classify individual patients as having no response, a moderate response, or a good response depending on the extent of change in the DAS28-ESR and the achieved level of the DAS28-ESR. The primary end point was the EULAR response at the 24-week time point. The secondary end point was the change in the patients' DAS28-ESR between entry and the 24-week time point. For assessment of the safety of TNF inhibitor treatment, we determined the occurrence of ATL or HAM/TSP at the 24-week time point of treatment.

Time points of anti–HTLV-I antibody assay. HTLV-I antibody was measured using one of the conventional methods, i.e., either chemiluminescence immunoassay (Architect HTLV; Abbott), enzyme-linked chemiluminescence assay (Lumipulse Presto HTLV kit; Fujirebio), or a particle agglutination test (Serodia-HTLV-I kit; Fujirebio). The time point of anti–HTLV-I antibody assay differed among patients, with some examined before, some examined during, and some examined after the start of TNF inhibitor treatment. However, the anti–HTLV-I antibody status had been checked in all patients by January 2014.

Statistical analysis. We compared the baseline characteristics of the anti–HTLV-I antibody–positive (n = 50) and anti–HTLV-I antibody–negative (n = 535) RA patients. Categorical variables were described as frequencies and quantitative variables as the median and interquartile range. The association between variables was assessed using Fisher's exact test for categorical variables and Wilcoxon's rank sum test for quantitative variables. The paired t-test was used to detect differences in change in the DAS28-ESR achieved by TNF inhibitors between the anti–HTLV-I antibody–positive patients and the anti–HTLV-I antibody–negative patients. We used the Cochran-Armitage test to compare the trend of EULAR responses between anti–HTLV-I antibody–positive patients and anti–HTLV-I antibody–negative patients.

We performed a multiple mixed-effects regression analysis with a random hospital-specific intercept to determine factors that contribute to the EULAR response. Here, we defined the EULAR responses as none, moderate, and good. We included variables that exhibited a significant difference between the anti–HTLV-I antibody–positive and anti–HTLV-I antibody–negative groups. We excluded the type of TNF inhibitor as a variable, because all types of TNF inhibitors are equally suggested as the first biologic DMARDs in the EULAR recommendations (15). In addition, we included clinically important variables in the model. Finally, we used age at entry, sex, anti–HTLV-I antibody positivity, ACPA status, concomitant use of methotrexate (MTX), concomitant use of prednisolone, the DAS28-ESR at entry, and the interaction term between anti–HTLV-I antibody positivity and ACPA status as fixed effects.

We analyzed change in the DAS28-ESR values from baseline to the 24-week time point, using a linear mixed-effects regression model with an unstructured residual covariance matrix for measurements within the hospital. Age at entry, sex, anti–HTLV-I antibody positivity, ACPA status, concomitant use of MTX, concomitant use of prednisolone, the DAS28-ESR at entry, and the interaction term between anti–HTLV-I antibody positivity and ACPA status were used as fixed effects. Subgroup analyses were performed to examine the effects of TNF inhibitors across ACPA status using the above multiple regressions (excluding ACPA status and interaction term), which were the complete case analyses. ACPA status was not available for 183 patients (31.3%).

Because complete case analyses can lead to a loss of power and biased results, we performed a multiple imputation analysis. To investigate variables associated with missing ACPA status, descriptive statistics and Fisher's exact test for categorical variables and Wilcoxon's rank sum test for quantitative variables were performed both in the cohort with missing ACPA status and in the cohort in which the ACPA status was not missing (see Supplementary Table 1, available on the *Arthritis & Rheumatology* web site at http://onlinelibrary.wiley.com/doi/10.1002/art.40461/abstract).

A logit model was used for imputation of ACPA status for age at entry, sex, hospital, disease duration, anti–HTLV-I antibody positivity, concomitant use of MTX, concomitant use of prednisolone, type of TNF inhibitor, persistence at 24 weeks, and EULAR response. Each of these variables in the logit model was consecutively selected as the dependent variable in the missing-data imputation of ACPA status and the variables considered to be related to the absence of data on ACPA status ($P < 0.1$). However, tender joint counts (28 joints assessed) at entry, ESR at entry, physician's global assessment at entry, Simplified Disease Activity Index (SDAI) (16) at entry, and Clinical Disease Activity Index (16) at entry were not included in the logit model, because these factors were strongly related to EULAR response and suspected of multicollinearity. We repeated the imputation 1,000 times, followed by application of Rubin's rule to combine the estimated parameters and standard errors.

All tests were 2-sided. P values less than 0.05 were considered significant. All statistical analyses were performed

Table 1. Demographic, clinical, and laboratory characteristics, treatments, and disease activity in the total patient group, anti–HTLV-I antibody–positive patients, and anti–HTLV-I antibody–negative patients at entry*

Variable	Total (n = 585)	Anti–HTLV-I antibody positive (n = 50)	Anti–HTLV-I antibody negative (n = 535)
Age, median (IQR) years	59 (51–68)	64 (57–73)	59 (50–68)†
Female, no. (%)	482 (82)	44 (88)	438 (82)
Disease duration, median (IQR) months	69 (21–155)	90 (22–175)	69 (21–148)
RF positive, no. (%) (no. of patients evaluated)	453 (79) (574)	38 (81) (47)	415 (79) (527)
ACPA positive, no. (%) (no. of patients evaluated)	331 (82) (402)	30 (73) (41)	301 (83) (361)
Concomitant MTX use, no. (%)	431 (74)	42 (84)	389 (73)
Concomitant MTX dosage, mg/week (IQR)	8.0 (6.0–8.0)	8.0 (6.0–8.0)	8.0 (6.0–8.0)
Concomitant pred. use, no. (%)	365 (62)	31 (62)	334 (62)
Concomitant pred. dosage, mg/day (IQR)	5.0 (3.0–7.5)	5.0 (3.0–7.5)	5.0 (3.0–7.5)
Tender joint count in 28 joints, median (IQR)	6 (3–12)	7 (3–12)	6 (3–12)
Swollen joint count in 28 joints, median (IQR)	4 (2–6)	4 (1–7)	4 (2–6)
ESR, median (IQR) mm/hour	45 (24–72)	36 (22–78)	46 (25–71)
CRP, median (IQR) mg/dl	1.00 (0.31–2.82)	0.99 (0.22–2.38)	1.00 (0.32–2.91)
Physician's global assessment score, median (IQR) (1–100-mm VAS)	40 (25–51)	42 (30–60)	40 (25–50)
Patient's global assessment score, median (IQR) (0–100-mm VAS)	50 (29–65)	50 (30–68)	50 (28–64)
DAS28-ESR, median (IQR)	5.21 (4.23–6.19)	5.23 (3.98–6.19)	5.21 (4.24–6.19)
SDAI score, median (IQR)	21.3 (13.7–31.4)	20.2 (13.3–34.2)	21.5 (13.7–31.4)
CDAI score, median (IQR)	20.0 (12.8–28.0)	18.0 (12.0–29.3)	20.0 (12.8–28.0)
Persistence rate at 24 weeks, %	89	82	90

* In the total group, 226 patients received infliximab (IFX), 251 etanercept (ETN), 88 adalimumab (ADA), 18 golimumab (GOL), and 2 certolizumab pegol (CZP). In the anti–human T lymphotropic virus type I (anti–HTLV-I) antibody–positive group, 17 patients received IFX, 20 ETN, 9 ADA, 2 GOL, and 2 CZP. In the anti–HTLV-I antibody–negative group, 209 patients received IFX, 231 ETN, 79 ADA, 16 GOL, and 0 CZP. IQR = interquartile range; RF = rheumatoid factor; ACPA = anti–citrullinated protein antibody; MTX = methotrexate; pred. = prednisolone; CRP = C-reactive protein; VAS = visual analog scale; DAS28-ESR = Disease Activity Score in 28 joints using the erythrocyte sedimentation rate; SDAI = Simplified Disease Activity Index; CDAI = Clinical Disease Activity Index.
† $P = 0.0024$ versus anti–HTLV-I antibody–positive.

using JMP Statistical Software version 11 and SAS version 9.4. GraphPad Prism version 7.0 was used to create the figure.

RESULTS

Patient characteristics. Table 1 shows the demographic and clinical characteristics of the total group of patients, anti–HTLV-I antibody–positive patients, and anti–HTLV-I antibody–negative patients. Fifty (8.5%) of the 585 patients were anti–HTLV-I antibody–positive. Patients in the anti–HTLV-I antibody–positive group were significantly older at entry compared with the 535 anti–HTLV-I antibody–negative patients (64 years versus 59 years; $P = 0.0024$). Eighty-two percent of the patients were female, and the median disease duration was 69 months. Eighty-two percent of the total group of patients (n = 402 analyzed) were ACPA-positive.

The median DAS28-ESR was 5.21, which indicated high disease activity. Infliximab, etanercept, adalimumab, golimumab, and certolizumab pegol were used as TNF inhibitors. There were no significant differences between the anti–HTLV-I antibody–positive and anti–HTLV-I antibody–negative groups in terms of the percentage of female patients, disease duration, RF positivity, ACPA positivity, frequency of MTX treatment, and frequency of prednisolone treatment at entry, or disease activity.

Overall efficacy and safety of the TNF inhibitors. The EULAR responses were significantly better in the HTLV-I–negative patients compared with the HTLV-I–positive patients ($P = 0.0277$) (Figure 1A). The mean DAS28-ESR values were significantly decreased from 5.03 (anti–HTLV-I antibody–positive group) and 5.19 (anti–HTLV-I antibody–negative group) at entry to 3.62 and 3.39 at 24 weeks, respectively (Figure 1B). The decrease in the DAS28-ESR was significantly greater in the HTLV-I–negative patients compared with the HTLV-I–positive patients ($P = 0.0378$) (Figure 1B). In the total group, the persistence rate of TNF inhibitors at 24 weeks was 89%, and the rate did not differ significantly between the 2 patient groups (Table 1). None of the patients developed ATL or HAM/TSP during the 24 weeks of TNF inhibitor treatment.

Factors associated with the achievement of good and moderate responses. Among the factors age at entry, sex, anti–HTLV-I antibody positivity, ACPA positivity, concomitant MTX use at entry, concomitant prednisolone use at entry, and DAS28-ESR at entry, those that were significantly associated with good and moderate EULAR responses by the multiple mixed-effects regression analysis were anti–HTLV-I antibody positivity and the DAS28-ESR at entry in the overall patient group (odds ratio 0.24 and 1.70, respectively [$P = 0.0407$ and $P < 0.0001$, respectively]) (Table 2).
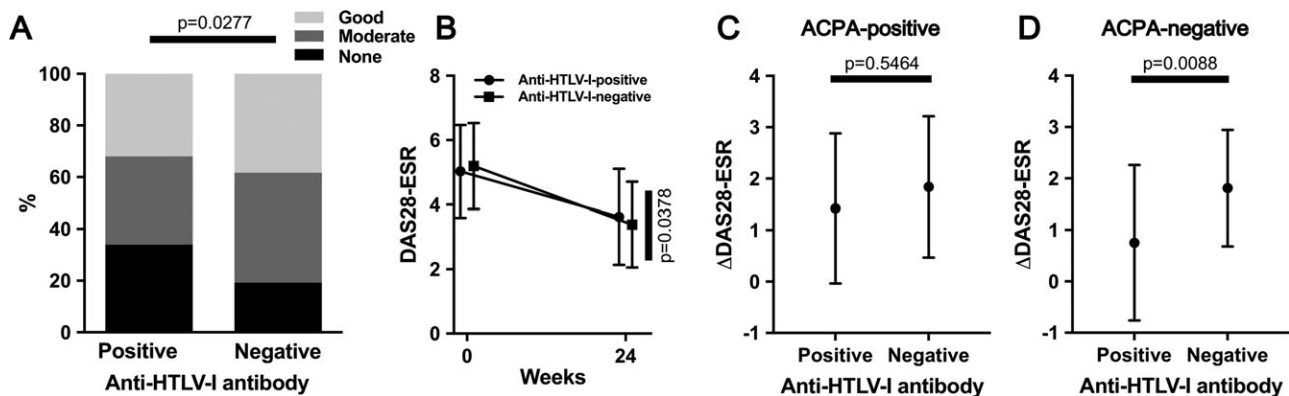
Figure 1. Efficacy and safety of tumor necrosis factor inhibitors. **A,** Among the anti–human T lymphotropic virus type I (anti–HTLV-I) antibody–positive patients, 32.0% had a good European League Against Rheumatism response, 34.0% had a moderate response, and 34.0% had no response. Among the anti–HTLV-I antibody–negative patients, 38.3% had a good response, 42.4% had a moderate response, and 19.3% had no response. Thus, the responses in the anti–HTLV-I antibody–negative patients were significantly better than those in the anti–HTLV-I antibody–positive patients ($P = 0.0277$). **B,** The Disease Activity Score in 28 joints using the erythrocyte sedimentation rate (DAS28-ESR) decreased significantly, from a mean ± SD of 5.03 ± 1.44 in anti–HTLV-I antibody–positive patients and 5.19 ± 1.33 in anti–HTLV-I antibody–negative patients at entry to 3.62 ± 1.49 and 3.39 ± 1.33, respectively, at 24 weeks. Anti–HTLV-I antibody–positive patients had a smaller change in the DAS28-ESR compared with anti–HTLV-I antibody–negative patients ($P = 0.0378$). **C,** Among the anti–citrullinated protein antibody (ACPA)–positive patients, there was no significant difference in change in the DAS28-ESR between the anti–HTLV-I antibody–positive patients and the anti–HTLV-I antibody–negative patients (mean ± SD 1.42 ± 1.46 and 1.84 ± 1.37, respectively [$P = 0.5464$]). **D,** Among the ACPA-negative patients, change in the DAS28-ESR was significantly greater in the anti–HTLV-I antibody–negative patients compared with the anti–HTLV-I antibody–positive patients (mean ± SD 1.81 ± 1.13 and 0.75 ± 1.51, respectively [$P = 0.0088$]). P values in **C** and **D** were calculated using linear mixed-effects regression analysis, including age at entry, sex, anti–HTLV-I antibody positivity, concomitant methotrexate use at entry, concomitant prednisolone use at entry, and DAS28-ESR at entry, as shown in Table 2.

Table 2. Multiple regression analysis of the EULAR response and change in the DAS28-ESR*

End point, variable	Total		ACPA positive		ACPA negative	
	OR or coefficient (95% CI)	P	OR or coefficient (95% CI)	P	OR or coefficient (95% CI)	P
EULAR response (none to moderate and good)						
Age at entry	0.99 (0.98, 1.01)	0.3279	0.99 (0.97, 1.01)	0.5014	0.99 (0.95, 1.04)	0.6601
Sex (response in men vs. response in women)	1.75 (0.95, 3.21)	0.0704	2.01 (0.90, 4.48)	0.0862	3.32 (0.53, 20.75)	0.1960
Anti–HTLV-I antibody positive	0.24 (0.06, 0.94)	0.0407	0.55 (0.23, 1.29)	0.1659	0.19 (0.04, 0.82)	0.0271
ACPA positive	0.82 (0.39, 1.70)	0.5908	–	–	–	–
Concomitant MTX use at entry	1.40 (0.85, 2.30)	0.1890	1.99 (1.04, 3.80)	0.0379	0.94 (0.26, 3.40)	0.9179
Concomitant pred. use at entry	0.88 (0.56, 1.37)	0.5593	0.98 (0.55, 1.73)	0.9367	0.82 (0.22, 3.06)	0.7612
DAS28-ESR at entry	1.70 (1.43, 2.02)	<0.0001	1.55 (1.26, 1.91)	<0.0001	1.44 (0.77, 2.67)	0.2467
Interaction term between anti–HTLV-I antibody positivity and ACPA positivity	3.03 (0.61, 15.05)	0.1748	–	–	–	–
Change in DAS28-ESR						
Age at entry	−0.0065 (−0.0134, 0.0005)	0.0674	−0.0064 (−0.0166, 0.0037)	0.2149	−0.0062 (−0.0254, 0.0130)	0.5236
Sex (change in men vs. change in women)	0.4103 (0.1724, 0.6482)	0.0007	0.4045 (0.0710, 0.7380)	0.0176	0.7511 (0.0379, 1.4642)	0.0393
Anti–HTLV-I antibody positive	−0.8613 (−1.5564, −0.1662)	0.0152	−0.1413 (−0.6018, 0.3192)	0.5464	−1.0448 (−1.8164, −0.2732)	0.0088
ACPA positive	−0.0608 (−0.3524, 0.2308)	0.6830	–	–	–	–
Concomitant MTX use at entry	0.1981 (−0.0185, 0.4146)	0.0730	0.4040 (0.0846, 0.7234)	0.0133	0.1773 (−0.4500, 0.8045)	0.5739
Concomitant pred. use at entry	−0.1915 (−0.3812, −0.0018)	0.0479	−0.2302 (−0.4999, 0.0395)	0.0941	−0.3227 (−0.9177, 0.2724)	0.2823
DAS28-ESR at entry	0.5169 (0.4474, 0.5864)	<0.0001	0.5153 (0.4196, 0.6110)	<0.0001	0.3042 (0.0186, 0.5899)	0.0372
Anti–HTLV-I antibody positive and ACPA positive	0.7670 (−0.0344, 1.5685)	0.607	–	–	–	–

* Values for the end point European League Against Rheumatism (EULAR) response are the odds ratio (OR) (95% confidence interval [95% CI]); values for the end point Disease Activity Score in 28 joints using the erythrocyte sedimentation rate (DAS28-ESR) at entry are the coefficient (95% CI). ACPA = anti–citrullinated protein antibody; anti–HTLV-I = anti–human T lymphotropic virus type I; MTX = methotrexate; pred. = prednisolone.

Evaluation of the effect of ACPA positivity. We divided the patients into 2 groups: ACPA-positive (anti–HTLV-I antibody–positive [n = 30] and anti–HTLV-I antibody–negative [n = 301]) and ACPA-negative (anti–HTLV-I antibody–positive [n = 11] and anti–HTLV-I antibody–negative [n = 60]). There was a significant association between anti–HTLV-I antibody positivity and moderate/good EULAR responses in the ACPA-negative patients (odds ratio 0.19, P = 0.0271) (Table 2) but not in the ACPA-positive patients. When the patients were divided into RF-positive and RF-negative groups, there was no significant difference in the EULAR response rates between the 2 groups (data not shown).

Factors associated with change in the DAS28-ESR. Among the factors age at entry, sex, anti–HTLV-I antibody positivity, ACPA positivity, concomitant MTX use at entry, concomitant prednisolone use at entry, and the DAS28-ESR at entry, those that were significantly associated with change in the DAS28-ESR, as determined by linear mixed-effects regression analysis, were sex (change in men compared with change in women), anti–HTLV-I antibody positivity, concomitant prednisolone use at entry, and the DAS28-ESR at entry in the overall patient group (coefficients 0.4103, –0.8613, –0.1915, and 0.5169, respectively [P = 0.0007, P = 0.0152, P = 0.0479, and P < 0.0001, respectively]) (Table 2).

The effects of differences in anti–HTLV-I antibody status in ACPA-positive patients and ACPA-negative patients were examined (Figures 1C and D), with exclusion of confounding effects between anti–HTLV-I antibody status and ACPA status. Within the ACPA-positive group, there was no significant difference in change in the DAS28-ESR between the HTLV-I–positive and HTLV-I–negative patients (Figure 1C), but in the ACPA-negative group, the HTLV-I–negative patients had a significantly greater change in the DAS28-ESR compared with the HTLV-I–positive patients (P = 0.0088) (Figure 1D) in the linear mixed regression analysis including age at entry, sex, anti–HTLV-I antibody positivity, concomitant MTX use at entry, concomitant prednisolone use at entry, and the DAS28-ESR at entry (Table 2).

Evaluation of calendar time effects. To evaluate the calendar time effect, we divided patients into 2 groups: those treated in 2001–2010 and those treated in 2011–2013, because publication of the 2010 RA classification criteria (12) was an epoch-making event for clinicians and dramatically changed the objective of TNF inhibitor treatment. There were many differences between patients treated in 2001–2010 and those treated in 2011–2013 (see Supplementary Table 2, available on the *Arthritis & Rheumatology* web site at http://onlinelibrary.wiley.com/doi/10.1002/art.40461/abstract). Multiple linear mixed-effects regression analysis

showed the same trends in terms of the effects of anti–HTLV-I antibody positivity on the EULAR response and change in the DAS28-ESR in both the 2001–2010 and 2011–2013 treatment groups, but these associations did not reach statistical significance, as they did in the overall patient group (see Supplementary Table 3).

DISCUSSION

The current study, which was conducted in an area endemic for HTLV-I infection, revealed independent variables at entry that can be used to predict the clinical efficacy of TNF inhibitors for treating RA patients. As reported previously, we observed that the DAS28 at entry and sex are associated with improvement in the DAS28. Söderlin et al demonstrated that a high DAS28 at entry indicates a better SDAI response to treatment in patients treated with their first anti-TNF drug (17), which is consistent with our findings in the current study. Regarding sex, a previous investigation indicated that female sex may be an independent predictor of being treatment-resistant for remission both in patients with early-stage RA and in those with established RA (18). Although the baseline characteristics as well as the treatment regimens in the current study were different from those in the above-mentioned reports, our current data are consistent with previous observations. In consideration of the above-described results, the overall baseline characteristics and the clinical responses of the study population in the current study may not be very different from those observed in the previous studies.

The most intriguing point of the current study is that we were able to compare the effects of TNF inhibitors between HTLV-I–positive and HTLV-I–negative patients. The difference in the effects of TNF inhibitors as related to HTLV-I is quite meaningful in light of the inflammation that might be caused by HTLV-I and the pathogenesis of arthritis. In particular, the attenuated effectiveness of TNF inhibitors suggests that HTLV-I infection may cause inflammation through cytokines, excluding TNF.

Some studies have shown a relationship between inflammation and HTLV-I infection. It was previously reported that HTLV-I–infected T cells induced the production of interferon-γ (IFNγ) (9,19) and IL-6 in addition to TNF (9). Besides infecting T cells, HTLV-I infects synovial fibroblasts (5) and CD68+ macrophages (20) and enhances the production of cytokines. Theses cytokines include TNF (5,20) and IL-1α (5). Clinically, patients with HAM/TSP have been reported to show high circulating levels of TNF- and IL-2–secreting HTLV-I–specific CD4+ T cells (21). Based on these reports, it appears that the proinflammatory status of HTLV-I–infected patients, particularly

characterized by the presence of IFNγ, IL-6, IL-1α, and IL-2, may attenuate the effectiveness of TNF inhibitors.

It is worth noting that another study by our group showed a high seroprevalence (20.4%) of anti–HTLV-I antibody in RA patients living in an area in Nagasaki Prefecture that is endemic for HTLV-I infection (22). Thus, a second possibility to consider is that HTLV-I infection itself might be directly involved in the pathologic process in RA. In that previous study (22), we observed no significant differences in clinical and laboratory findings, including RF status, between HTLV-I–positive and HTLV-I–negative RA patients, but we demonstrated for the first time, using subanalysis, that the resistance to TNF inhibitors among HTLV-I–positive RA patients was present in the ACPA-negative subgroup and not in the ACPA-positive subgroup.

It is generally accepted that the clinical response of ACPA-negative RA patients to TNF inhibitors is better than or equivalent to that of ACPA-positive RA patients (23) in areas where HTLV-I infection is not endemic. Consistent with the observations in our previous investigation (22), in the current study we observed no significant difference in the presence or absence of RF between HTLV-I–positive and HTLV-I–negative RA patients. A low response to TNF inhibitor treatment in ACPA-negative patients with HTLV-I antibodies is a new characteristic finding, although it is important to note that only a small number of ACPA-negative patients with anti–HTLV-I antibodies were included; specifically, 11 of our 71 ACPA-negative patients were positive for anti–HTLV-I antibodies.

Because there is some difference in genetic predisposition between ACPA-negative RA patients and ACPA-positive RA patients (24), the network of inflammatory cytokines might be different between these 2 groups. Because IL-6–driven CD4+ T cell activation via STAT-3 is reported to be a feature of ACPA-negative RA (25), foregoing IL-6 production by HTLV-I–infected cells in ACPA-negative RA patients may attenuate the effectiveness of TNF inhibitors in ACPA-negative patients with anti–HTLV-I antibody positivity.

The lifetime risks for the occurrence of ATL or HAM/TSP in HTLV-I–infected patients are estimated to be 2.5–5% or 0.3–2%, respectively (26). Although these risks are not very high, ATL and HAM/TSP are life-threatening diseases, and thus the development of ATL or HAM/TSP in HTLV-I–positive patients is a critical matter. There were no occurrences of ATL or HAM/TSP during the 24 weeks of TNF inhibitor treatment in the current study, which might serve as a short-term safety profile for TNF inhibitors in areas endemic for HTLV-I infections. A previous study analyzed the response to

treatment with TNF inhibitors and change in HTLV-I markers, such as proviral load and clonality of HTLV-I–infected cells, in 2 patients with RA and revealed no significant change in either of these patients (27).

Our study has some limitations. First, we could not evaluate the long-term outcomes for efficacy and safety. The efficacy of biologic DMARDs, including TNF inhibitors, may be attenuated over time (28), and the 24-week observational results of the current study may not precisely reflect the real efficacy of TNF inhibitors in HTLV-I–positive RA patients compared with HTLV-I–negative RA patients. In addition, proviral load is known to be a clinically useful marker in ATL (29) and HAM/TSP (30). However, due to the relatively low prevalence of ATL and HAM/TSP, long-term follow-up with more patient-years along with HTLV-I markers will also be needed to account for the risk of these diseases.

The efficacy of TNF inhibitors was attenuated when these agents were used to treat anti–HTLV-I antibody–positive patients, especially among the ACPA-negative patients. Although TNF inhibitors may not increase the risks of ATL and HAM/TSP, the long-term efficacy and safety of TNF inhibitors must be further examined.

AUTHOR CONTRIBUTIONS

REFERENCES

1. Bathon JM, Martin RW, Fleischmann RM, Tesser JR, Schiff MH, Keystone EC, et al. A comparison of etanercept and methotrexate in patients with early rheumatoid arthritis. N Engl J Med 2000;343:1586–93.
2. Gorman JD, Sack KE, Davis JC Jr. Treatment of ankylosing spondylitis by inhibition of tumor necrosis factor α. N Engl J Med 2002;346:1349–56.
3. Rutgeerts P, Sandborn WJ, Feagan BG, Reinisch W, Olson A, Johanns J, et al. Infliximab for induction and maintenance therapy for ulcerative colitis. N Engl J Med 2005;353:2462–76.
4. Quaresma JA, Yoshikawa GT, Koyama RV, Dias GA, Fujihara S, Fuzii HT. HTLV-1, immune response and autoimmunity. Viruses 2015;8.
5. Sakai M, Eguchi K, Terada K, Nakashima M, Yamashita I, Ida H, et al. Infection of human synovial cells by human T cell lymphotropic virus type I. Proliferation and granulocyte/macrophage colony-stimulating factor production by synovial cells. J Clin Invest 1993;92:1957–66.

6. Nakamura H, Takahashi Y, Yamamoto-Fukuda T, Horai Y, Nakashima Y, Arima K, et al. Direct infection of primary salivary gland epithelial cells by human T lymphotropic virus type I in patients with Sjögren's syndrome. Arthritis Rheumatol 2015;67: 1096–106.

7. Umekita K, Hidaka T, Miyauchi S, Ueno S, Kubo K, Takajo I, et al. Treatment with anti–tumor necrosis factor biologic agents in human T lymphotropic virus type I–positive patients with rheumatoid arthritis. Arthritis Care Res (Hoboken) 2014;66:788–92.

8. Bittencourt AL, Oliveira PD, Bittencourt VG, Carvalho EM, Farre L. Adult T-cell leukemia/lymphoma triggered by adalimumab. J Clin Virol 2013;58:494–6.

9. Fukui S, Nakamura H, Takahashi Y, Iwamoto N, Hasegawa H, Yanagihara K, et al. Tumor necrosis factor α inhibitors have no effect on a human T-lymphotropic virus type-I (HTLV-I)-infected cell line from patients with HTLV-I-associated myelopathy. BMC Immunol 2017;18:7.

10. Kaplan JE, Osame M, Kubota H, Igata A, Nishitani H, Maeda Y, et al. The risk of development of HTLV-I-associated myelopathy/tropical spastic paraparesis among persons infected with HTLV-I. J Acquir Immune Defic Syndr 1990;3:1096–101.

11. Arnett FC, Edworthy SM, Bloch DA, McShane DJ, Fries JF, Cooper NS, et al. The American Rheumatism Association 1987 revised criteria for the classification of rheumatoid arthritis. Arthritis Rheum 1988;31:315–24.

12. Aletaha D, Neogi T, Silman AJ, Funovits J, Felson DT, Bingham CO III, et al. 2010 rheumatoid arthritis classification criteria: an American College of Rheumatology/European League Against Rheumatism collaborative initiative. Arthritis Rheum 2010;62: 2569–81.

13. Prevoo ML, van 't Hof MA, Kuper HH, van Leeuwen MA, van de Putte LB, van Riel PL. Modified disease activity scores that include twenty-eight–joint counts: development and validation in a prospective longitudinal study of patients with rheumatoid arthritis. Arthritis Rheum 1995;38:44–8.

14. Fransen J, van Riel PL. The Disease Activity Score and the EULAR response criteria. Clin Exp Rheumatol 2005;23 Suppl 39:S93–9.

15. Smolen JS, Landewé R, Bijlsma J, Burmester G, Chatzidionysiou K, Dougados M, et al. EULAR recommendations for the management of rheumatoid arthritis with synthetic and biological disease-modifying antirheumatic drugs: 2016 update. Ann Rheum Dis 2017;76:960–77.

16. Aletaha D, Nell VP, Stamm T, Uffmann M, Pflugbeil S, Machold K, et al. Acute phase reactants add little to composite disease activity indices for rheumatoid arthritis: validation of a clinical activity score. Arthritis Res Ther 2005;7:R796–806.

17. Söderlin MK, Petersson IF, Geborek P. The effect of smoking on response and drug survival in rheumatoid arthritis patients treated with their first anti-TNF drug. Scand J Rheumatol 2012;41: 1–9.

18. Forslind K, Hafstrom I, Ahlmen M, Svensson B. Sex: a major predictor of remission in early rheumatoid arthritis? Ann Rheum Dis 2007;66:46–52.

19. Araya N, Sato T, Ando H, Tomaru U, Yoshida M, Coler-Reilly A, et al. HTLV-1 induces a Th1-like state in CD4+CCR4+ T cells. J Clin Invest 2014;124:3431–42.

20. Yin W, Hasunuma T, Kobata T, Sumida T, Nishioka K. Synovial hyperplasia in HTLV-I associated arthropathy is induced by tumor necrosis factor-α produced by HTLV-I infected CD68+ cells. J Rheumatol 2000;27:874–81.

21. Goon PK, Igakura T, Hanon E, Mosley AJ, Asquith B, Gould KG, et al. High circulating frequencies of tumor necrosis factor α- and interleukin-2-secreting human T-lymphotropic virus type 1 (HTLV-1)-specific CD4+ T cells in patients with HTLV-1-associated neurological disease. J Virol 2003;77:9716–22.

22. Eguchi K, Origuchi T, Takashima H, Iwata K, Katamine S, Nagataki S. High seroprevalence of anti–HTLV-I antibody in rheumatoid arthritis. Arthritis Rheum 1996;39:463–6.

23. Kiely PD. Biologic efficacy optimization: a step towards personalized medicine. Rheumatology (Oxford) 2016;55:780–8.

24. Terao C, Ohmura K, Ikari K, Kochi Y, Maruya E, Katayama M, et al. ACPA-negative RA consists of two genetically distinct subsets based on RF positivity in Japanese. PLoS One 2012;7:e40067.

25. Anderson AE, Pratt AG, Sedhom MA, Doran JP, Routledge C, Hargreaves B, et al. IL-6-driven STAT signalling in circulating CD4+ lymphocytes is a marker for early anticitrullinated peptide antibody-negative rheumatoid arthritis. Ann Rheum Dis 2016;75: 466–73.

26. Iwanaga M, Watanabe T, Utsunomiya A, Okayama A, Uchimaru K, Koh KR, et al. Human T-cell leukemia virus type I (HTLV-1) proviral load and disease progression in asymptomatic HTLV-1 carriers: a nationwide prospective study in Japan. Blood 2010; 116:1211–9.

27. Umekita K, Umeki K, Miyauchi S, Ueno S, Kubo K, Kusumoto N, et al. Use of anti-tumor necrosis factor biologics in the treatment of rheumatoid arthritis does not change human T-lymphotropic virus type 1 markers: a case series. Mod Rheumatol 2015;25:794–7.

28. Atzeni F, Sarzi-Puttini P, Gorla R, Marchesoni A, Caporali R. Switching rheumatoid arthritis treatments: an update. Autoimmun Rev 2011;10:397–403.

29. Yonekura K, Utsunomiya A, Seto M, Takatsuka Y, Takeuchi S, Tokunaga M, et al. Human T-lymphotropic virus type I proviral loads in patients with adult T-cell leukemia-lymphoma: comparison between cutaneous type and other subtypes. J Dermatol 2015;42:1143–8.

30. Matsuzaki T, Nakagawa M, Nagai M, Usuku K, Higuchi I, Arimura K, et al. HTLV-I proviral load correlates with progression of motor disability in HAM/TSP: analysis of 239 HAM/TSP patients including 64 patients followed up for 10 years. J Neurovirol 2001;7: 228–34.

Female Reproductive and Hormonal Factors and Incidence of Primary Total Knee Arthroplasty Due to Osteoarthritis

Sultana Monira Hussain [ID],[1] Yuanyuan Wang,[1] Graham G. Giles,[2] Stephen Graves,[3] Anita E. Wluka [ID],[1] and Flavia M. Cicuttini[1]

Objective. To examine the associations of female reproductive and hormonal factors with incidence of total knee arthroplasty (TKA) for osteoarthritis (OA), and to determine whether the associations differ according to overweight/obesity status.

Methods. This study included 22,289 women in the Melbourne Collaborative Cohort Study. Data on age at menarche, pregnancy, parity, years of menstruation, oral contraceptive (OC) use, menopausal status, and hormone replacement therapy (HRT) were collected in 1990–1994. Incidence of TKA during 2001–2013 was determined by linking cohort records to the Australian Orthopaedic Association National Joint Replacement Registry. All analyses were adjusted for age, body mass index (BMI) at midlife, change in BMI (from early reproductive age to midlife), country of birth, physical activity, smoking, and education level.

Results. Over the course of 12.7 years, 1,208 TKAs for OA were identified. Ever being pregnant was associated with increased risk of TKA (hazard ratio [HR] 1.32 [95% confidence interval (95% CI) 1.06–1.63]). Parity was positively associated with risk of TKA (*P* for trend = 0.003). OC users had increased risk of TKA compared with non-users (for OC use of <5 years, HR 1.25 [95% CI 1.08–1.45]; for OC use of ≥5 years, HR 1.17 [95% CI 1.00–1.37]). A 1-year increase in menstruation was associated with a 1% decrease in risk of TKA (HR 0.99 [95% CI 0.97–0.99]). These associations remained significant only in women of normal weight at early reproductive age. Current HRT users had increased risk of TKA compared with non-users (HR 1.37 [95% CI 1.14–1.64]); the association was significant only in non-obese women at midlife.

Conclusion. Reproductive and hormonal factors were associated with risk of knee OA. These associations remained significant in women of normal weight at early reproductive age and in non-obese women at midlife. Further work is needed to understand the complex effect of these factors on knee OA.

Knee osteoarthritis (OA) is a prevalent disabling disease with multifactorial etiology including age, obesity, physical activity, malalignment, and genetics (1). Women have a higher prevalence and incidence of knee OA than men after age 50 years (2), suggesting a role for hormonal factors in the pathogenesis of OA. A number of studies have examined the association of reproductive and hormonal factors with knee OA, but the results are inconclusive. Increasing parity has been reported as a risk factor for radiographic knee OA and total knee arthroplasty (TKA) for OA (3,4), while other studies have found no association of parity with radiographic knee OA or TKA due to OA (5,6). A large prospective cohort study found increased risk of TKA associated with low age at menarche (6), but this finding was contradicted by another large-scale cohort study showing no association (4). No associations have been reported of the use of oral contraceptives (OCs) with knee cartilage volume (5), radiographic knee OA

(7), or TKA (4,6). While hormone replacement therapy (HRT) has been shown to be a protective factor for knee cartilage (8) and to protect against radiographic knee OA (9,10), other studies have found no association of HRT with knee pain due to OA (11), with knee cartilage (12), or with TKA (6,13). One study showed increased risk of TKA in relation to HRT (4). These discrepant findings may be attributable to differences across studies in terms of evaluation criteria for OA (symptomatic, radiographic, or TKA), classification of exposures, study populations, and study designs.

A number of reproductive factors, such as menarche, parity, menopause, use of OCs, and HRT, are associated with obesity (14), a major risk factor for knee OA. For example, women gain weight and central body fat at the menopausal transition (15). Thus, it is important to examine whether the associations of reproductive and hormonal factors with knee OA are modified and/or confounded by obesity, as obesity may influence the hormonal status of an individual (16). This is of significant clinical and public health importance, given that there is no cure for knee OA and that we are faced with the global trend of increasing prevalence of knee OA and obesity.

Established cohorts, such as the Melbourne Collaborative Cohort Study (MCCS), provide an unprecedented opportunity to examine new hypotheses of OA pathogenesis involving sex steroid hormones, metabolic syndrome, index finger–to–ring finger length ratio, body weight trajectories, gene mutations, physical activity, ethnicity, and body adiposity. The MCCS was able to take advantage of this opportunity because of its community-based recruitment of participants (which was completely independent of musculoskeletal disease), the long follow-up period, and the richness of prospectively collected data (17). Using the MCCS data, we aimed to determine 1) whether reproductive factors (age at menarche, pregnancy, parity, duration of menstruation in years) and OC use increase the risk of TKA for OA, and whether the associations differ according to overweight status during early reproductive years (ages 18–21); and 2) whether menopause and HRT use increase the risk of TKA for OA, and whether the associations differ according to obesity status during midlife.

SUBJECTS AND METHODS

Study participants. The MCCS is a prospective cohort study of 41,514 participants (24,469 women) ages 27–75 years (99.3% were ages 40–69 years) recruited via the electoral roll, advertisements, and community announcements in local media in 1990–1994 (18). Southern European migrants to Australia were deliberately oversampled to extend the range of lifestyle exposures and to increase genetic variation. The purpose of the study was to investigate prospectively the role of diet and other lifestyle factors in causing common chronic diseases (17). The study protocol was approved by the Cancer Council Victoria Human Research Ethics Committee. Of the recruited participants, 4.8% were excluded because 1) they died or left Australia prior to January 1, 2001; 2) at the MCCS second follow-up visit, they had reported a primary joint replacement prior to January 1, 2001; or 3) their first recorded procedure was a revision joint replacement as recorded in the Australian Orthopaedic Association National Joint Replacement Registry (AOA NJRR). The current study examined data for 22,289 women.

Assessment of sociodemographic, comorbidity, and anthropometric data. At baseline, sociodemographic factors including date of birth, country of birth, smoking, physical activity during leisure time, education level, and physician-diagnosed hypertension and diabetes mellitus were collected by face-to-face interviews. Height and weight were measured according to written protocols based on standard procedures. Body mass index (BMI) was calculated. Since the mean ± SD age of participants at baseline was 54.6 ± 8.6 years, weight and BMI at study entry were termed as weight and BMI at midlife. Participants were asked what their weight had been between ages 18 and 21 years (early reproductive age). These data were previously reported (19,20). Change in BMI from early reproductive age to midlife was calculated.

Assessment of reproductive and hormonal factors. At baseline, information was collected on age at menarche, ever being pregnant, number of live births (parity), menopausal status, age at menopause, and having had a hysterectomy or ovariectomy. Each woman was asked if she had ever taken HRT or OCs and, if so, for how long and whether they were current or previous users. Years of menstruation was calculated for women who experienced a natural menopause by deducting the age at menarche from the age at menopause.

Incidence of TKA for OA. The AOA NJRR collects information on prostheses, patient demographics, and type of and reason for arthroplasty. Data are collected from both public and private hospitals and validated using a sequential multilevel matching process against State and Territory Health Department unit record data. Following the validation process and retrieval of unreported records, the Registry collects an almost complete set of data relating to arthroplasties (>99%) in Australia (21). This study examined the first knee arthroplasty with a contemporaneous diagnosis of OA, as recorded in the AOA NJRR. If one person had multiple arthroplasties, such as bilateral knee arthroplasties or both knee and hip arthroplasties, the first recorded procedure was considered the event. Matching of MCCS participants using first name, surname, date of birth, and sex to the AOA NJRR in order to identify those who had had an arthroplasty performed between January 1, 2001 and December 31, 2013 was done using the Freely Extensible Biomedical Record Linkage system. The linkage study was approved by the Human Research Ethics Committees of Cancer Council Victoria and Monash University. Knee OA was defined as the first recorded primary total joint arthroplasty that was a TKA for OA.

Statistical analysis. Cox proportional hazards regression models were used to estimate the hazard ratios (HRs) with 95% confidence intervals (95% CIs) for TKA associated with each individual reproductive and hormonal factor, with age as the time scale. BMI at midlife, change in BMI from early reproductive age to midlife, country of birth, physical activity, smoking,

and education level were included in all models. Additional adjustment was done for comorbidities (hypertension [yes/no], diabetes mellitus [yes/no]). Follow-up for TKA (i.e., calculation of person-time) began January 1, 2001 and ended at the date of the first TKA for OA or at the date of censoring. Subjects were censored at the date of the first TKA performed for indications other than OA, the date of death, the date of leaving Australia, or the end of follow-up (December 31, 2013), whichever came first. Association of HRT use, duration of HRT use, age at menopause, and years of menstruation with TKA were analyzed only in women who experienced natural menopause at baseline and did not undergo an ovariectomy. To examine whether the

relationship of reproductive factors and OCs with the risk of TKA for OA was modified by overweight status, stratified analysis was performed based on overweight status at early reproductive age (18–21 years). Similarly, stratified analysis was performed based on obesity status at midlife to examine the association of age at menopause, years of menstruation, and HRT with risk of TKA. All these analyses were repeated in the subgroup of women who attended follow-up during 2004–2007 (n = 15,828) with additional adjustment for change in BMI from midlife (1990–1994) to 2004–2007 follow-up.

Tests based on Schoenfeld residuals and graphical methods using Kaplan-Meier curves showed no evidence that

Table 1. Baseline characteristics of the study participants*

	Total knee replacement (n = 1,208)	No joint replacement (n = 21,081)	P
Age, mean $\pm$ SD years	57.6 $\pm$ 7.3	54.4 $\pm$ 8.6	<0.001
Body mass index at midlife, mean $\pm$ SD kg/m^2	29.7 $\pm$ 5.3	26.5 $\pm$ 4.8	<0.001
Overweight/obese at early reproductive age	191 (15.8)	2,483 (11.8)	<0.001
Obese at midlife	501 (41.5)	4,335 (20.6)	<0.001
Country of birth			<0.001
Australia/UK	979 (81.0)	16,179 (76.8)	
Italy/Greece	229 (19.0)	4,902 (23.2)	
Education			<0.001
Primary and some secondary	821 (68.5)	13,029 (62.4)	
Completed secondary and degree/diploma	378 (31.5)	7,866 (37.6)	
Vigorous physical activity			0.03
None	968 (80.1)	16,942 (80.4)	
1–2 times/week	153 (12.7)	2,513 (11.9)	
≥3 times/week	87 (7.2)	1,622 (7.7)	
Smoking			<0.001
Nonsmoker	886 (73.3)	14,549 (69.0)	
Ex-smoker	261 (21.6)	4,594 (21.8)	
Current smoker	61 (5.1)	1,935 (9.2)	
Diabetes mellitus	31 (2.6)	638 (3.0)	0.002
Hypertension	380 (31.5)	4,506 (21.4)	<0.001
Age at menarche, mean $\pm$ SD years	13.0 $\pm$ 1.7	13.1 $\pm$ 1.6	0.004
Ever pregnant	1,110 (91.9)	18,729 (88.9)	<0.001
Parity			<0.001
0	126 (10.5)	3,002 (14.2)	
1	85 (7.1)	1,815 (8.6)	
2	337 (27.9)	6,948 (33.0)	
3	335 (27.8)	5,411 (25.7)	
≥4	323 (26.8)	3,892 (18.5)	
Duration of oral contraceptive use			0.002
No use ever	526 (44.0)	8,516 (41.5)	
<5 years	357 (30.4)	5,921 (28.8)	
≥5 years	291 (24.8)	6,092 (29.7)	
Postmenopausal†	848 (76.9)	11,484 (58.3)	<0.001
Age at menopause, mean $\pm$ SD years†	49.3 $\pm$ 5.0	49.3 $\pm$ 4.9	0.18
Years of menstruation, mean $\pm$ SD†	36.3 $\pm$ 5.5	36.1 $\pm$ 5.1	0.04
HRT‡			<0.001
Never	600 (71.2)	8,280 (72.3)	
Past	85 (10.1)	1,293 (11.3)	
Current	158 (18.7)	1,884 (16.4)	
Duration of HRT‡			0.001
No use ever	600 (78.3)	8,280 (79.1)	
<1 year	108 (14.1)	1,513 (14.5)	
≥1 year	58 (7.6)	679 (6.5)	
Ovariectomy	149 (44.2)	1,938 (44.2)	0.94

* Except where indicated otherwise, values are the number (%).
† Only those having natural menopause (n = 12,332).
‡ Only those having natural menopause and hormone replacement therapy (HRT) data not missing (n = 12,300 for HRT, n = 11,238 for duration of HRT).

proportional hazards assumptions were violated. All statistical analyses were performed using Stata 13.0 SE (StataCorp).

RESULTS

Over a mean ± SD 12.7 ± 2.9 years of follow-up, we identified 1,208 women with incident TKA for OA. Descriptive statistics of the participants' characteristics are shown in Table 1. Women who received a TKA were older, had greater BMI at midlife and lower levels of education, were more likely to be overweight/obese during early reproductive life and obese at midlife, and were more likely to have been born in Australia/New Zealand than those who had had no joint replacement, while they were less likely to smoke. Those who had had a TKA were more likely to have been pregnant, to have higher parity, and to be postmenopausal; more of them were currently using HRT compared with those who had had no joint replacement.

Table 2 shows reproductive and hormonal factors according to overweight status during early reproductive years, and menopausal status and HRT-related factors according to obesity status at midlife. Women who were overweight/obese at early reproductive age had an earlier onset of menarche and shorter duration of OC use compared with women of normal weight. Women who were obese at midlife were more likely to be postmenopausal, less likely to be current HRT users, and had shorter duration of HRT use compared with non-obese women.

The associations of reproductive and hormonal factors with risk of TKA are presented in Table 3. After adjustment, ever being pregnant was associated with increased risk of TKA (HR 1.32 [95% CI 1.06–1.63]). There was a positive linear association of parity with the risk of TKA. Using nulliparous women as the reference, the adjusted HRs were 1.10 (95% CI 0.83–1.47), 1.18 (95% CI 0.95–1.46), 1.25 (95% CI 1.01–1.55), and 1.35 (95% CI 1.09–1.68) for parity 1, 2, 3, and ≥4, respectively (P for trend = 0.003). Women taking OCs had an increased risk of TKA compared with non-users. Using never users as the reference, the adjusted HRs were 1.25 (95% CI 1.08–1.45) for OC use of <5 years and 1.17 (95% CI 1.00–1.37) for OC use of ≥5 years. Years of menstruation was negatively associated with risk of TKA (HR 0.99

Table 2. Reproductive and hormonal factors at ages 18–21 years and at midlife according to overweight or obesity status*

	Normal weight or normal/overweight†	Overweight/obese or obese‡	P
Women at early reproductive age (ages 18–21 years; n = 22,289)			
Age at menarche, mean ± SD years	13.1 ± 1.6	12.9 ± 1.8	<0.001
Ever pregnant	17,494 (89.2)	2,345 (87.8)	0.03
Parity			0.47
0	2,722 (13.9)	406 (15.2)	
1	1,672 (8.5)	228 (8.6)	
2	6,427 (32.8)	858 (32.1)	
3	5,067 (25.8)	679 (25.5)	
≥4	3,718 (19.0)	497 (18.6)	
Duration of oral contraceptive use			<0.001
No use ever	7,576 (39.7)	1,466 (56.1)	
<5 years	5,653 (29.6)	625 (23.9)	
≥5 years	5,859 (30.7)	524 (20.0)	
Years of menstruation, mean ± SD§	34.2 ± 6.3	34.8 ± 6.1	0.05
Postmenopausal women (n = 12,332)			
Age at menopause, mean ± SD years§	49.3 ± 4.9	49.2 ± 5.0	0.04
Years of menstruation, mean ± SD§	35.1 ± 5.7	35.4 ± 5.6	0.07
HRT¶			<0.001
Never	6,406 (69.3)	2,474 (80.9)	
Past	1,111 (12.0)	267 (8.7)	
Current	1,725 (18.7)	317 (10.4)	
Duration of HRT¶			<0.001
No use ever	6,406 (76.5)	2,474 (86.4)	
<1 year	1,344 (16.1)	277 (9.7)	
≥1 year	624 (7.5)	113 (4.0)	

* Except where indicated otherwise, values are the number (%).
† Women who had been of normal weight at early reproductive age (n = 19,615) and postmenopausal women who were currently normal or overweight (n = 9,266).
‡ Women who had been overweight/obese at early reproductive age (n = 2,674) and postmenopausal women who were currently obese (n = 3,066).
§ Only those having natural menopause (n = 12,332).
¶ Only those having natural menopause and hormone replacement therapy (HRT) data not missing (n = 12,300 for HRT, n = 11,238 for duration of HRT).

Table 3. Associations between reproductive and hormonal factors and risk of total knee arthroplasty for osteoarthritis*

	Total population		Normal weight or normal/overweight†		Overweight/obese or obese‡	
	HR (95% CI)	P	HR (95% CI)	P	HR (95% CI)	P
Women at early reproductive age (ages 18–21 years; n = 22,289)						
Age at menarche, years	1.00 (0.97–1.04)	0.91	1.02 (0.98–1.06)	0.34	0.91 (0.82–1.00)	0.06
Ever pregnant (yes vs. no)	1.32 (1.06–1.63)	0.01	1.40 (1.10–1.78)	0.01	0.93 (0.57–1.53)	0.78
Parity categories						
0	1.00		1.00		1.00	
1	1.10 (0.83–1.47)	0.50	1.04 (0.76–1.42)	0.80	1.43 (0.71–2.87)	0.32
2	1.18 (0.95–1.46)	0.14	1.18 (0.93–1.49)	0.17	1.12 (0.64–1.96)	0.69
3	1.25 (1.01–1.55)	0.04	1.24 (0.98–1.57)	0.07	1.26 (0.73–2.20)	0.41
≥4	1.35 (1.09–1.68)	0.01	1.38 (1.09–1.74)	0.01	1.07 (0.61–1.90)	0.81
P for trend	0.003		0.002		0.91	
Duration of oral contraceptive use, categories						
No use ever	1.00		1.00		1.00	
<5 years	1.25 (1.08–1.45)	0.002	1.37 (1.17–1.60)	<0.001	0.72 (0.47–1.11)	0.13
≥5 years	1.17 (1.00–1.37)	0.05	1.25 (1.05–1.48)	0.01	0.85 (0.54–1.33)	0.49
Years of menstruation (n = 12,332)	0.99 (0.97–0.99)	0.01	0.98 (0.97–1.00)	0.01	0.99 (0.96–1.02)	0.61
Women at midlife (postmenopausal; n = 12,332)						
Age at menopause, years (n = 12,332)	0.99 (0.97–1.01)	0.42	1.00 (0.97–1.03)	0.99	0.98 (0.95–1.01)	0.18
Years of menstruation (n = 12,332)	0.99 (0.97–0.99)	0.01	0.98 (0.97–0.99)	0.03	0.99 (0.97–1.00)	0.10
HRT (n = 12,300)						
Never	1.00		1.00		1.00	
Past	0.99 (0.79–1.25)	0.94	0.86 (0.64–1.17)	0.34	1.20 (0.84–1.73)	0.31
Current	1.37 (1.14–1.64)	0.001	1.39 (1.12–1.74)	0.003	1.38 (0.99–1.92)	0.054
Duration of HRT (n = 11,238)						
No use ever	1.00		1.00		1.00	
<1 year	1.12 (0.91–1.39)	0.27	1.05 (0.80–1.36)	0.73	1.29 (0.91–1.84)	0.15
≥1 year	1.30 (0.99–1.72)	0.06	1.36 (0.99–1.89)	0.06	1.21 (0.71–2.05)	0.49
P for trend	0.03		0.06		0.19	

* Adjusted for body mass index at midlife, change in body mass index (early to midlife), country of birth, education level, vigorous physical activity, and smoking status. HR = hazard ratio; 95% CI = 95% confidence interval; HRT = hormone replacement therapy.
† Women who had been of normal weight at early reproductive age (n = 19,615) and postmenopausal women who were currently normal or overweight (n = 9,266).
‡ Women who had been overweight/obese at early reproductive age (n = 2,674) and postmenopausal women who were currently obese (n = 3,066).

[95% CI 0.97–0.99]). All of these associations remained significant in women of normal weight at early reproductive age, but they were not significant in women who were overweight/obese despite the lower rate of TKA in the normal weight group compared with the overweight/obese group (5.2% versus 7.1%). No association was observed of age at menarche with TKA.

Current HRT users had an increased risk of TKA compared with non-users (HR 1.37 [95% CI 1.14–1.64]). There was a linear association of increasing duration of HRT use with increased risk of TKA. Using never use of HRT as the reference, the adjusted HRs were 1.12 (95% CI 0.91–1.39) for HRT use of <1 year and HR 1.30 (95% CI 0.99–1.72) for HRT use of ≥1 year (P for trend = 0.03). All of the significant associations observed for the total population remained significant in those who were non-obese at midlife. There was a marginally significant association of HRT use with increased risk of TKA in the obese group (HR 1.38 [95% CI 0.99–1.92]). There was a trend toward a positive linear association of duration of HRT

use with risk of TKA in non-obese women (P for trend = 0.06). The rate of TKA was lower in women who were normal/overweight at midlife than in women who were obese at midlife (4.0% versus 10.4%). No association was observed of age at menopause with TKA. Additional adjustment for comorbidities did not change the results (data not shown). Furthermore, we performed subgroup analysis with additional adjustment for change in BMI from midlife (1990–1994) to 2004–2007 follow-up. The results were of a direction and magnitude similar to those of the total population as presented in Table 3 (see Supplementary Table 1, available on the *Arthritis & Rheumatology* web site at http://onlinelibrary.wiley.com/doi/10.1002/art.40483/abstract).

DISCUSSION

Ever being pregnant, increasing parity, taking OCs, current HRT use, and longer duration of HRT use were associated with increased risk of TKA for

OA, while prolonged years of menstruation was associated with reduced risk. In subgroup analyses, all the associations between reproductive factors and TKA remained significant for women of normal weight but not for overweight/obese women at early reproductive age. Similarly, current HRT use was associated with increased risk of TKA in non-obese women at midlife but not in obese women at midlife. No association was observed between age at menarche or age at menopause and TKA.

Consistent with 2 previous studies (3,4), we found that pregnancy and parity increased the risk of TKA. This may have been due to weight gain during pregnancy and postpartum weight retention (3,4), which are common (22). We found that women of normal weight gained more weight from early reproductive age to midlife compared with overweight/obese women. However, the association of pregnancy and parity with TKA was independent of BMI at midlife and independent of change in BMI from early reproductive age to midlife. In a subgroup analysis based on overweight status at early reproductive age (obesity is not common at this age), increased risk of TKA in relation to pregnancy and parity was seen in women of normal weight but not in overweight/obese women, despite a higher incidence of TKA in overweight/obese women. These findings suggest that the relationship of pregnancy and parity with TKA for OA is complex and may not simply be mediated through increased weight gain associated with pregnancy and parity.

While neither age at menarche nor age at menopause was associated with risk of TKA, increasing years of menstruation was associated with decreased risk of TKA for OA. This remained significant in women of normal weight in early reproductive life, but not in those who had been overweight/obese. There is no clear association between age at menarche and age at menopause, with studies showing direct association, inverse association, or no association (23). Years of menstruation is a marker of prolonged reproductive life and active ovarian function (23). Hormonal depletion at the end of the active reproductive period is linked to tissue damage and organ dysfunction (24) and to an increase in the risk of several diseases (25–27). The results of our study suggest a protective effect of prolonged reproductive life on decreased risk of TKA.

Use of OCs increased the risk of TKA for OA in women of normal weight at early reproductive age, and current HRT use increased the risk of TKA for OA in women who were not obese in midlife. The relationship between reproductive hormone supplementation and knee OA is complex. Although greater exposure to estrogen may promote OA changes by increasing cartilage damage

(28), it is unclear whether hormone supplementation increases circulating sex hormone to levels sufficient to affect joint structure significantly. Among healthy women, HRT users have more knee cartilage volume than non-users (8). The effect of exogenous hormones (OCs and HRT) on joint health can be determined by many factors, including age at starting OCs, time elapsed from onset of menopause to starting HRT, and duration of HRT use.

We found that current HRT users started using HRT at an older age than past users (mean ± SD 53.9 ± 7.0 years versus 50.3 ± 7.5 years; $P = 0.01$). As the average age at onset of menopause in developed countries is 51 years (29), these data suggest that past HRT users began HRT at menopausal transition, while current users began HRT ~3 years after menopause. It may be that, analogous to other diseases (30,31), starting HRT later in menopause is associated with increased risk of knee OA. Alternatively, the association between HRT use and TKA may be due to nonbiologic factors, with women taking HRT having more access to health services, including TKA. However, we adjusted for confounders for TKA, and Australians have universal coverage so they can readily access TKA (32,33). Paradoxically, exposure to OCs increased the risk of knee OA but prolonged years of menstruation decreased the risk. Along with estrogen, other sex hormones might play a role in protecting women from knee OA development and progression. Prolonged years of menstruation increases exposure not only to estrogen but also to other endogenous sex hormones. The use of OCs might change the circulatory levels of endogenous hormones unfavorably, thus affecting joint health adversely. Further work will be needed to clarify this and the differences in OA outcomes based on the type of OC.

We observed significant associations of reproductive factors and taking OCs with the risk of TKA in women of normal weight but not in women who were overweight/obese at early reproductive ages, and of current HRT use with TKA in normal/overweight women but not in obese women at midlife. The underlying mechanism might be explained by the association of reproductive factors with obesity (34), inflammation (35), and endothelial dysfunction (35,36). Overweight/obese women have already been exposed to increased mechanical loading and have inflammation and endothelial dysfunction, which are known risk factors for knee OA, due to excessive fat mass. This may mask any additional association of reproductive factors with TKA. If a person is obese, the excessive joint loading may be more likely to drive OA pathogenesis and progression. These findings suggest that the influence of reproductive and hormonal factors on the risk of TKA due to OA is complex and warrants further investigation.

Our results need to be considered within the study's limitations. We defined OA based on arthroplasty. Arthroplasty for OA may be influenced by factors such as access to health care, socioeconomic status, and patient preference, in addition to disease severity. This study was carried out in Australia where there is universal health coverage, so access to arthroplasty is available to all. Nevertheless, arthroplasty does reflect end-stage joint disease. We performed analysis with age as the time scale and adjusted for BMI at midlife, change in BMI (early to midlife), country of birth, education level, physical activity, smoking, and comorbidity. TKA was ascertained from the AOA NJRR. We did not have accurate arthroplasty data prior to 2001. This may have resulted in nondifferential misclassification of TKA.

Participants were asked at midlife (ages 40–69 years) to recall their weight at ages 18–21 years, which may have introduced bias by under-reporting of weight, especially by overweight and obese women (37). However, we observed higher incidence of TKA in overweight/obese women at early reproductive age. In this study we examined weight at midlife (1990–1994, baseline) and TKA between 2001 and 2013. In the subgroup of women (n = 15,828) with weight measured at the 2004–2007 follow-up, there was strong correlation between weight measured at 1990–1994 and weight measured at 2004–2007 (r = 0.90), supporting the notion that weight trajectories tend to remain stable in healthy adult women (38). We repeated all the analyses in this subgroup adjusting for change in BMI from midlife (1990–1994) to 2004–2007 follow-up, and we found that the direction and magnitude of the results were similar to those of the total population. However, we could not adjust for weight history of entire life since weight was not measured repeatedly throughout life including at the time of pregnancy.

The self-reported reproductive and hormonal data were collected at baseline when the women included were middle-aged. Any misclassification would most likely have been nondifferential, resulting in underestimation of the associations. Reproductive history and OC use would not have changed, but HRT use and its duration might have changed during the follow-up. As duration of HRT use was associated with increased risk of TKA, not updating the duration of HRT may have resulted in an underestimation of the association. Although we do not have data on types of OCs, the combined OCs were most commonly used at that time (39). It remains possible that residual confounding contributed to the association of hormonal factors with risk of TKA.

Ever being pregnant, increasing parity, OC use, current HRT use, and increasing duration of HRT use are risk factors for TKA due to OA, while prolonged years of menstruation decreases the risk. These findings add to the ongoing literature regarding the complex relationship of reproductive and hormonal factors with risk of knee OA. Given the huge burden of knee OA and associated TKA in women worldwide, further studies are needed to understand the complex association of reproductive factors with risk of knee OA, along with the role of obesity in this relationship.

AUTHOR CONTRIBUTIONS

All authors were involved in drafting the article or revising it critically for important intellectual content, and all authors approved the final version to be published. Dr. Wang had full access to all of the data in the study and takes responsibility for the integrity of the data and the accuracy of the data analysis.
Study conception and design. Hussain, Wang, Cicuttini.
Acquisition of data. Giles, Graves.
Analysis and interpretation of data. Hussain, Wang, Giles, Graves, Wluka, Cicuttini.

REFERENCES

1. Felson DT. Risk factors for osteoarthritis: understanding joint vulnerability. Clin Orthop Relat Res 2004;427 Suppl:S16–21.
2. Felson DT. Epidemiology of hip and knee osteoarthritis. Epidemiol Rev 1988;10:1–28.
3. Wise BL, Niu J, Zhang Y, Felson DT, Bradley LA, Segal N, et al. The association of parity with osteoarthritis and knee replacement in the multicenter osteoarthritis study. Osteoarthritis Cartilage 2013;21:1849–54.
4. Liu B, Balkwill A, Cooper C, Roddam A, Brown A, Beral V. Reproductive history, hormonal factors and the incidence of hip and knee replacement for osteoarthritis in middle-aged women. Ann Rheum Dis 2009;68:1165–70.
5. Wei S, Venn A, Ding C, Martel-Pelletier J, Pelletier JP, Abram F, et al. The associations between parity, other reproductive factors and cartilage in women aged 50–80 years. Osteoarthritis Cartilage 2011;19:1307–13.
6. Hellevik AI, Nordsletten L, Johnsen MB, Fenstad AM, Furnes O, Storheim K, et al. Age of menarche is associated with knee joint replacement due to primary osteoarthritis (The HUNT Study and the Norwegian Arthroplasty Register). Osteoarthritis Cartilage 2017;25:1654–62.
7. Sandmark H, Hogstedt C, Lewold S, Vingard E. Osteoarthrosis of the knee in men and women in association with overweight, smoking, and hormone therapy. Ann Rheum Dis 1999;58:151–5.

8. Wluka AE, Davis SR, Bailey M, Stuckey SL, Cicuttini FM. Users of oestrogen replacement therapy have more knee cartilage than non-users. Ann Rheum Dis 2001;60:332–6.

9. Spector TD, Nandra D, Hart DJ, Doyle DV. Is hormone replacement therapy protective for hand and knee osteoarthritis in women? The Chingford Study. Ann Rheum Dis 1997;56:432–4.

10. Hart DJ, Doyle DV, Spector TD. Incidence and risk factors for radiographic knee osteoarthritis in middle-aged women: the Chingford Study. Arthritis Rheum 1999;42:17–24.

11. Nevitt MC, Felson DT, Williams EN, Grady D, for the Heart and Estrogen/Progestin Replacement Study Research Group. The effect of estrogen plus progestin on knee symptoms and related disability in postmenopausal women: the Heart and Estrogen/Progestin Replacement Study, a randomized, double-blind, placebo-controlled trial. Arthritis Rheum 2001;44:811–8.

12. Zhang Y, McAlindon TE, Hannan MT, Chaisson CE, Klein R, Wilson PW, et al. Estrogen replacement therapy and worsening of radiographic knee osteoarthritis: the Framingham Study. Arthritis Rheum 1998;41:1867–73.

13. Cirillo DJ, Wallace RB, Wu L, Yood RA. Effect of hormone therapy on risk of hip and knee joint replacement in the Women's Health Initiative. Arthritis Rheum 2006;54:3194–204.

14. Newby PK, Dickman PW, Adami HO, Wolk A. Early anthropometric measures and reproductive factors as predictors of body mass index and obesity among older women. Int J Obes (Lond) 2005;29:1084–92.

15. Sutton-Tyrrell K, Zhao X, Santoro N, Lasley B, Sowers M, Johnston J, et al. Reproductive hormones and obesity: 9 years of observation from the Study of Women's Health Across the Nation. Am J Epidemiol 2010;171:1203–13.

16. Brown LM, Gent L, Davis K, Clegg DJ. Metabolic impact of sex hormones on obesity. Brain Res 2010;1350:77–85.

17. Milne RL, Fletcher AS, MacInnis RJ, Hodge AM, Hopkins AH, Bassett JK, et al. Cohort profile: the Melbourne Collaborative Cohort Study (Health 2020). Int J Epidemiol 2017;46:1757–1757i.

18. Giles GG, English DR. The Melbourne Collaborative Cohort Study. IARC Sci Publ 2002;156:69–70.

19. Wang Y, Wluka AE, Simpson JA, Giles GG, Graves SE, de Steiger RN, et al. Body weight at early and middle adulthood, weight gain and persistent overweight from early adulthood are predictors of the risk of total knee and hip replacement for osteoarthritis. Rheumatology (Oxford) 2013;52:1033–41.

20. Krishnan K, Bassett JK, Macinnis RJ, English DR, Hopper JL, McLean CA, et al. Associations between weight in early adulthood, change in weight and breast cancer risk in postmenopausal women. Cancer Epidemiol Biomarkers Prev 2013; 22:1409–16.

21. Australian Orthopaedic Association National Joint Replacement Registry. Annual report. Adelaide: AOA; 2016.

22. Mannan M, Doi SA, Mamun AA. Association between weight gain during pregnancy and postpartum weight retention and obesity: a bias-adjusted meta-analysis. Nutr Rev 2013;71:343–52.

23. Forman MR, Mangini LD, Thelus-Jean R, Hayward MD. Life-course origins of the ages at menarche and menopause. Adolesc Health Med Ther 2013;4:1–21.

24. Rocca WA, Shuster LT, Grossardt BR, Maraganore DM, Gostout BS, Geda YE, et al. Long-term effects of bilateral oophorectomy on brain aging: unanswered questions from the Mayo Clinic Cohort Study of Oophorectomy and Aging. Women's Health (Lond) 2009;5:39–48.

25. Cohen LS, Soares CN, Vitonis AF, Otto MW, Harlow BL. Risk for new onset of depression during the menopausal transition: the Harvard study of moods and cycles. Arch Gen Psychiatry 2006;63:385–90.

26. Bove R, Secor E, Chibnik LB, Barnes LL, Schneider JA, Bennett DA, et al. Age at surgical menopause influences cognitive decline and Alzheimer pathology in older women. Neurology 2014; 82:222–9.

27. Svejme O, Ahlborg HG, Nilsson JA, Karlsson MK. Low BMD is an independent predictor of fracture and early menopause of mortality in post-menopausal women: a 34-year prospective study. Maturitas 2013;74:341–5.

28. Felson DT, Nevitt MC. The effects of estrogen on osteoarthritis. Curr Opin Rheumatol 1998;10:269–72.

29. Muka T, Oliver-Williams C, Kunutsor S, Laven JS, Fauser BC, Chowdhury R, et al. Association of age at onset of menopause and time since onset of menopause with cardiovascular outcomes, intermediate vascular traits, and all-cause mortality: a systematic review and meta-analysis. JAMA Cardiol 2016;1:767–76.

30. Salpeter SR, Walsh JM, Greyber E, Salpeter EE. Coronary heart disease events associated with hormone therapy in younger and older women: a meta-analysis. J Gen Intern Med 2006;21:363–6.

31. Salpeter SR, Walsh JM, Greyber E, Ormiston TM, Salpeter EE. Mortality associated with hormone replacement therapy in younger and older women: a meta-analysis. J Gen Intern Med 2004;19:791–804.

32. Lohmander LS, Gerhardsson de Verdier M, Rollof J, Nilsson PM, Engström G. Incidence of severe knee and hip osteoarthritis in relation to different measures of body mass: a population-based prospective cohort study. Ann Rheum Dis 2009;68:490–6.

33. Hussain SM, Cicuttini FM, Bell RJ, Robinson PJ, Davis SR, Giles GG, et al. Incidence of total knee and hip replacement for osteoarthritis in relation to circulating sex steroid hormone concentrations in women. Arthritis Rheumatol 2014;66:2144–51.

34. Lovejoy JC. The influence of sex hormones on obesity across the female life span. J Womens Health 1998;7:1247–56.

35. Jabbour HN, Sales KJ, Catalano RD, Norman JE. Inflammatory pathways in female reproductive health and disease. Reproduction 2009;138:903–19.

36. Campesi I, Occhioni S, Tonolo G, Cherchi S, Basili S, Carru C, et al. Ageing/menopausal status in healthy women and ageing in healthy men differently affect cardiometabolic parameters. Int J Med Sci 2016;13:124–32.

37. Brunner Huber LR. Validity of self-reported height and weight in women of reproductive age. Matern Child Health J 2007;11:137–44.

38. Heo M, Faith MS, Pietrobelli A. Resistance to change of adulthood body mass index. Int J Obes 2002;26:1404.

39. Richters J, Grulich AE, de Visser RO, Smith AM, Rissel CE. Sex in Australia: contraceptive practices among a representative sample of women. Aust N Z J Public Health 2003;27:210–6.

Impaired Proteasomal Function in Human Osteoarthritic Chondrocytes Can Contribute to Decreased Levels of SOX9 and Aggrecan

Ramon L. Serrano,[1] Liang-Yu Chen,[1] Martin K. Lotz,[2] Ru Liu-Bryan,[1] and Robert Terkeltaub[1]

Objective. Osteoarthritis (OA) chondrocytes exhibit impairment of autophagy, one arm of the proteostasis network that coordinates proteome and organelle quality control and degradation. Deficient proteostasis impacts differentiation and viability, and inflammatory processes in aging and disease. The present study was undertaken to assess ubiquitin proteasome system proteasomal function in OA chondrocytes.

Methods. We evaluated human knee cartilage by immunohistochemistry, and assessed proteasomal function, levels of proteasomal core subunits and chaperones, and autophagy in cultured chondrocytes. Assays included Western blotting, quantitative reverse transcription–polymerase chain reaction, proteasomal protease activity assessment, and cell immunofluorescence analysis.

Results. Human knee OA cartilage exhibited polyubiquitin accumulation, with increased ubiquitin K48-linked polyubiquitinated proteins in situ, suggesting proteasomal impairment. Cultured OA chondrocytes demonstrated accumulation of K48 polyubiquitinated proteins, significantly reduced 20S proteasome core protease activity, and decreased levels of phosphorylated FOXO4 and proteasome 26S subunit, non-ATPase 11 (PSMD11), a FOXO4-inducible promoter of proteasomal activation. Levels of proteasome subunit β type 3 (PSMB3), PSMB5, PSMB6, and proteasome assembly chaperone 1 were not decreased in OA chondrocytes. In normal chondrocytes, PSMD11 small interfering RNA knockdown stimulated certain autophagy machinery elements, increased extracellular nitric oxide (NO) levels, and reduced chondrocytic master transcription factor SOX9 protein and messenger RNA (mRNA) and aggrecan (*AGC1*) mRNA. PSMD11 gain-of-function by transfection increased proteasomal function, increased levels of SOX9-induced *AGC1* mRNA, stimulated elements of the autophagic machinery, and inhibited extracellular levels of interleukin-1–induced NO and matrix metalloproteinase 13 in OA chondrocytes.

Conclusion. Deficient PSMD11, associated with reduced phosphorylated FOXO4, promotes impaired proteasomal function in OA chondrocytes, dysregulation of chondrocytic homeostasis, and decreased levels of *SOX9* mRNA, SOX9 protein, and *AGC1* mRNA. Chondrocyte proteasomal impairment may be a therapeutic target for OA.

Osteoarthritis (OA) is a highly prevalent disease of the whole joint, in which aging, biomechanical injury, inflammation, metabolism, and other processes converge to promote altered articular chondrocyte differentiation and function, and ultimate cartilage failure (1). Multiple hallmarks of tissue aging (2) are detected in OA articular chondrocytes (1). These include deficient activities of cell homeostasis signaling by FOXO transcription factor and AMP-activated protein kinase (AMPK) (3,4), mitochondrial dysfunction (5,6), and dysregulated proteostasis (5,7–11).

The proteostasis network, which includes the unfolded protein response (UPR), autophagy, and the ubiquitin–proteasome system (UPS), coordinates proteome synthesis and folding, and uses chaperones to direct proteins to loci for degradation (12–14). UPR activation alleviates stress from accumulation of damaged proteins in the endoplasmic reticulum lumen, but in some conditions, including experimental OA, dysregulated UPR activity can contribute to inflammation, tissue damage, and degeneration (14–16). Conversely, distinct UPR genes and responses appear decreased in OA chondrocytes (17).

The autophagic process primarily degrades proteins and organelles under hypoxic and low nutrition/energy states, thereby exerting quality control and generating cell

energy via recycling (5,7–11). Autophagy is constitutively active in normal articular chondrocytes, promoted by factors including FOXO, AMPK, and regulated in development and DNA damage response 1 (REDD-1) (18–20). Autophagy, AMPK activity, FOXO, and REDD-1 are decreased in aged and OA cartilage (3,4,19,20). Pharmacologic and transgenic inhibition of autophagy potentiates OA in mice (7,8), contrasting with the chondroprotective effects of autophagy up-regulation (7,10,11).

The UPS accounts for ~80–90% of cell protein breakdown in proteostasis, via preferential degradation, within proteasomes, of damaged polyubiquitinated proteins and many short-lived, regulatory cytosolic proteins (e.g., IκB, cyclins) (12,21). In the UPS, isopeptide bonds between ubiquitin and protein substrates are formed by ubiquitin-activating, ubiquitin-conjugating, and ubiquitin-protein ligases (E1, E2, and E3, respectively) (21). Other ubiquitin molecules are sequentially conjugated to 1 of 7 lysine residues of attached ubiquitin, most commonly at ubiquitin K48, which targets proteins for proteasomal degradation (21). Alternatively, mono- or polyubiquitination (e.g., via K63) affects protein function and trafficking and reduces pressure on the proteasome by stimulating substrate aggregation and removal by chaperone-mediated autophagy (21–25).

The 26S proteasome, composed of 33 distinct subunits, is a cytosolic, energy-requiring ATP-driven "latent proteolytic machine" regulated largely via substrate access, subunit expression, assembly, turnover, and function (12,21). Polyubiquitinated proteins bind a multi-unit 19S "regulatory cap." Substrates are partially unfolded, facilitated by deubiquitinating enzymes, to enter the barrel-shaped 20S proteolytic core (12,21). The 20S particle has 4 heptameric rings; the 2 outer ring α-subunits regulate substrate access to the proteolytic core, and 2 inner ring β-subunits exert chymotrypsin-, trypsin-, and caspase-like activities (21). The 19S cap ATPases stimulate proteolytic activity by opening the 20S "gate" for substrate access (21). Additional regulation is exerted by proteasome-dedicated chaperones and subunits, including proteasome assembly chaperone 1 (PSMG1) (26) and proteasome 26S subunit, non-ATPase 11 (PSMD11) (27–30). The UPS also networks extensively with autophagy (12,13), FOXOs, and AMPK (31,32).

Differing proteostasis demands, aging patterns, and stressors are linked with variances in UPS composition and activity between tissues, and with age (33). Robust UPS capacity in youth maintains proteome integrity and inhibits senescence (34). Aging facilitates UPS failure via accumulated misfolded proteins, and in some tissues, UPS collapse under stress predates aging (21). UPS failure promotes multiple hallmarks of aging (12,13,21,22,31), senescence and death in cells, disease in multiple tissues, and decreased organism longevity (21).

Prior studies using modulation of proteasomal function in OA have been limited to experimental rat and mouse knee OA in young, wild-type animals (35–38). Those investigations assessed nascent disease triggered by surgically induced knee instability or monosodium iodoacetate, and principally analyzed effects of potent, broad proteasomal protease pharmacologic inhibition using the peptide aldehyde MG132, with administration started prior to OA onset (35–38). MG132 treatment was chondroprotective, with the integrity of proteasomal function appearing to be permissive for OA development and early disease advancement; decreased proteasomal degradation of the NF-κB inhibitor IκB was implicated in these effects, by lessening inflammation and cartilage matrix catabolism (35–38). In the present study, we characterized proteasomal dysfunction in human chondrocytes from human donors with knee OA. The results elucidated previously unidentified potential pathophysiologic impacts of chondrocyte proteasomal impairment in established human OA, and a molecular mechanism for selective reversibility of some OA-promoting effects in diseased chondrocytes via improved proteasomal function.

MATERIALS AND METHODS

Reagents. Except as otherwise noted, all chemical reagents were from Sigma-Aldrich. Recombinant human interlukin-1β (IL-1β) was from Gemini Bio-Products. High-glucose Dulbecco's modified Eagle's medium (DMEM) with L-glutamine and penicillin/streptomycin solution was from Mediatech. The matrix metalloproteinase 13 (MMP-13) enzyme-linked immunosorbent assay kit was from ThermoFisher.

Human tissue samples and cell culture. All human subject studies were approved by the San Diego Veterans Administration and Scripps Research Institute Institutional Review Boards. Human knee chondrocytes were isolated from autopsy donors and were graded macroscopically, as previously described (6). We studied samples graded 0 (normal), I (cartilage with an intact surface), and IV (moderate-to-severe OA, with overt fibrillation). There was no preselection of donors or donor samples for any characteristic other than OA or non-OA. Chondrocytes were cultured in high-glucose DMEM with L-glutamine and 100 IU/ml penicillin/100 μg/ml streptomycin, supplemented with 10% fetal calf serum, at 37°C (6). Chondrocytes were studied at first passage or, where indicated, as primary cells.

Immunohistochemistry analysis. Paraffin-embedded human knee cartilage sections were incubated with primary antibody for 18 hours at 4°C. We used rabbit anti-K48–linked proteins (05-1307; EMD Millipore) and anti–total ubiquitin (sc-166553; Santa Cruz Biotechnology) antibodies. With horseradish peroxidase (HRP)–conjugated secondary antibodies we used a SuperPicture Polymer Detection Kit (Thermo Scientific), with diaminobenzidine substrate for colorimetric detection.

Transfection and expression plasmid construction. Human PSMD11 complementary DNA (cDNA) (pQTEV-PSMD11, ID 31333; Addgene) was amplified by polymerase chain reaction (PCR) and subcloned, with and without human influenza hemagglutinin (HA) tagging at the N-terminal, into pCDNA3.1+ plasmid vector between the *Xho* I and *Bam* HI sites, with verification by

sequencing. Primers are listed in Supplementary Table 1, available on the *Arthritis & Rheumatology* web site at http://onlinelibrary.wiley.com/doi/10.1002/art.40456/abstract. Human chondrocytes were cultured for 16–18 hours in 6-well plates and then transfected for 72 hours with PSMD11 using XtremeGENE HP DNA reagent according to the instructions of the manufacturer (Roche).

Western blotting. Sodium dodecyl sulfate–polyacrylamide gel electrophoresis of cultured chondrocyte lysates in Bis-Tris gels (Thermo Scientific) and Western blotting were performed as previously described (6). Primary antibodies to PSMG1 (#13378), PSMD11 (#14303), proteasome subunit β type 5 (PSMB5) (#12919), PSMB6 (#13267), caspase 3 (#9662), poly (ADP-ribose) polymerase (#9532), FOXO1 (#2880), FOXO3a (#12829), FOXO4 (#2499), phosphorylated FOXO1/FOXO3a (#9464), SOX9 (#82630), light chain 3A/B (LC3/A/B; #12741), p62 (#8025), and HA-tag (#3724) were from Cell Signaling Technology. Antibodies to phosphorylated FOXO4 (#47278) and to MMP-13 (#3533) were from Abcam and BioVision, respectively, and antibody to PSMB3 (#140458) was from Abcam. Secondary antibodies (1:5,000) were conjugated with HRP and detected with ECL reagent (Super Pico or Femto; Thermo Scientific), using either x-ray film or a Gel Doc system (Bio-Rad). Quantification of band intensity was performed with ImageStudioLite (Li-Cor), with intensity of bands calculated relative to the background from the same membrane.

Proteasome activity assay. Proteasome activity assays were performed to analyze chymotrypsin-like activity at the core proteasome particle, utilizing an AMC-tagged peptide substrate (Succ-LLVY-AMC) that releases free, highly fluorescent AMC in the presence of protease activity. Briefly, cells were lysed at 4°C in phosphate buffered saline (PBS) containing 0.5% Nonidet P40, followed by centrifugation (15,000 revolutions per minute, 4°C). After determination of protein levels, the supernatant was assayed for chymotrypsin-like activity using a proteasome activity kit (ab107921) according to the instructions of the manufacturer (Abcam). Aliquots of protein (10 μg), including samples and positive control from the manufacturer, were assayed in triplicate, with and without proteasome inhibitor MG132 (200 μ*M*) and incubated in the dark for 30 minutes at 37°C. Output at 350/440 nm (excitation/emission) was measured on a fluorometric microplate reader at time 1 (T1) and time 2 (T2; 25 minutes later). Relative fluorescence units (RFU) were determined as follows:

$$\Delta\text{RFU} = (\text{RFU}_{T2} - i\text{RFU}_{T2}) - (\text{RFU}_{T1} - i\text{RFU}_{T1}),$$

where iRFU represents wells containing proteasome inhibitor showing nonproteasome activity. Proteasome activity was calculated as

$$\text{Proteasome activity} = \left(\frac{B}{(T2 - T1) \times V}\right) \times D,$$

where B = amount of AMC in the sample well (pmoles), V = sample volume (μl) added to the reaction well, T1 = time (minutes) of the first reading (RFU$_{T1}$ and iRFU$_{T1}$), T2 = time (minutes) of the second reading (RFU$_{T2}$ and iRFU$_{T2}$), and D = sample dilution factor. Calibration curves were calculated for AMC concentration and purified 20S proteasome activity.

Quantitative reverse transcription–PCR (RT-PCR). RNA was extracted and isolated from cultured human chondrocytes utilizing an RNeasy Mini kit (Qiagen). RNA levels were quantified with a NanoDrop 1000 spectrophotometer (Thermo Scientific); samples with 260 nm/280 nm absorbance ratios of >2.0 were used for RT. Equal amounts of total RNA from each sample were subjected to RT-PCR using a Transcriptor High Fidelity cDNA Synthesis Kit (Roche), which includes anchored oligo(dT)$_{18}$ and random hexamer primers. Quantitative RT-PCR was performed using a 480 Light Cycler (Roche) and specific primer sets (Supplementary Table 1, http://onlinelibrary.wiley.com/doi/10.1002/art.40456/abstract). Levels of messenger RNA (mRNA) for genes of interest were calculated as fold change from control or as the ratio of the copy number of the gene of interest to the copy number of the total housekeeping gene *GAPDH*. For absolute quantification, a pGEM-T Easy vector system (Promega) was used to clone gene fragments (*GAPDH, AGC1, SOX9*, and *PSMD11*).

Immunofluorescence analysis. Human chondrocytes were cultured for 16–18 hours on 6-well plates containing round coverslips (12 mm; VWR) and then transfected for 72 hours (XtremeGENE siRNA Transfection Reagent; Roche) with PSMD11 small interfering RNA (siRNA) (On-Target, L-011367-01-0005; GE Dharmacon). Culture medium was removed from plates, and cells were fixed/permeabilized with cold methanol (−20°C) for 15 minutes. Serial washes were performed with PBS, followed by blocking with 1% bovine serum albumin in PBS for 2 hours at room temperature. Incubation with primary IgG was conducted overnight at 4°C with rabbit anti-LC3A/B, rabbit anti–lysosome-associated membrane protein 1 (ab24170; Abcam), or rabbit anti-p62/sequestosome 1 (88588; Cell Signaling Technology). Incubation with secondary antibodies was done for 2 hours at 22°C, using Alexa Fluor 488–conjugated goat anti-rabbit IgG (A11034; Thermo Fisher) or Alexa Fluor 555–conjugated goat anti-rabbit IgG (21429; Thermo Scientific). A BZ-X700 microscope (Keyence) was used for imaging.

Chromatin immunoprecipitation (ChIP) assay. We tested a defined, specific 48-bp sequence in the SOX9-binding enhancer region of the type II collagen α1 chain (*COL2A1*) for cartilage expression (39). We also assessed a defined, functional SOX9–hypoxia-inducible factor 1α complex binding site in the 5′-untranslated region (5′-UTR) of *AGC1* (40). To do so, we used primers corresponding to nucleotides 60–82 (forward) and 220–240 (reverse) in the *AGC1* −640 to −510 5′-UTR (GenBank accession no. AF031586). ChIP assay was performed according to the instructions of the manufacturer (Millipore), using protein A–agarose/salmon sperm DNA (50% slurry) to reduce nonspecific background, and immunoprecipitation with SOX9 antibody (ab3697; Abcam). Following elution of histone–DNA complexes and DNA recovery by phenol/chloroform extraction, DNA was resuspended in 10 μl TE buffer. PCR was conducted with 1 μl eluate, 2 μl of 20 μ*M* primers for *COL2A1* and *AGC1* (Supplementary Table 1, http://onlinelibrary.wiley.com/doi/10.1002/art.40456/abstract), 10 μl KAPA2G Fast ReadyMix PCR (Kapa Biosystems reagent from Sigma-Aldrich), and H$_2$O up to 20 μl reaction volume.

Statistical analysis. GraphPad Prism was used for statistical analysis. The significance of differences between mean values from unpaired samples was assessed by two-way analysis of variance with Bonferroni post hoc test or by unpaired *t*-test.

RESULTS

Increased levels of ubiquitinated protein substrates in human OA chondrocytes and OA cartilage in situ. We observed increased levels of ubiquitinated proteins in OA chondrocytes compared to normal chondrocytes, on Western

blots of cell lysates analyzed for total ubiquitin (Figure 1A) and K48-linked substrates (Figure 1B). Levels of both ubiquitin (Figure 2A) and K48-linked polyubiquitin (Figure 2B) were also increased in human knee OA cartilage compared to normal cartilage, as assessed by immunohistochemistry. In grade IV OA cartilage specimens, polyubiquitin staining was particularly intense in chondrocyte clusters (Figure 2B).

Decreased chondrocyte proteasome activity in OA. Proteasome activity was significantly decreased in cultured chondrocyte lysates from grade IV OA samples compared to samples from normal donors (Figure 3A). Western blot examination of 3 of the 7 20S proteasome core β-subunit constituents of the inner ring, where catalytic activity is localized, revealed no significant decrease in PSMB3, PSMB5, or PSMB6 levels in grade IV OA chondrocytes (Figure 3B). Hence, we assessed the critical proteasome regulatory subunits PSMG1 and PSMD11 (27,28), since PSMG1 facilitates 20S proteasome assembly by promoting grouping of the β-subunits into the heteroheptameric α ring (26) and PSMD11 stabilizes the interaction between the
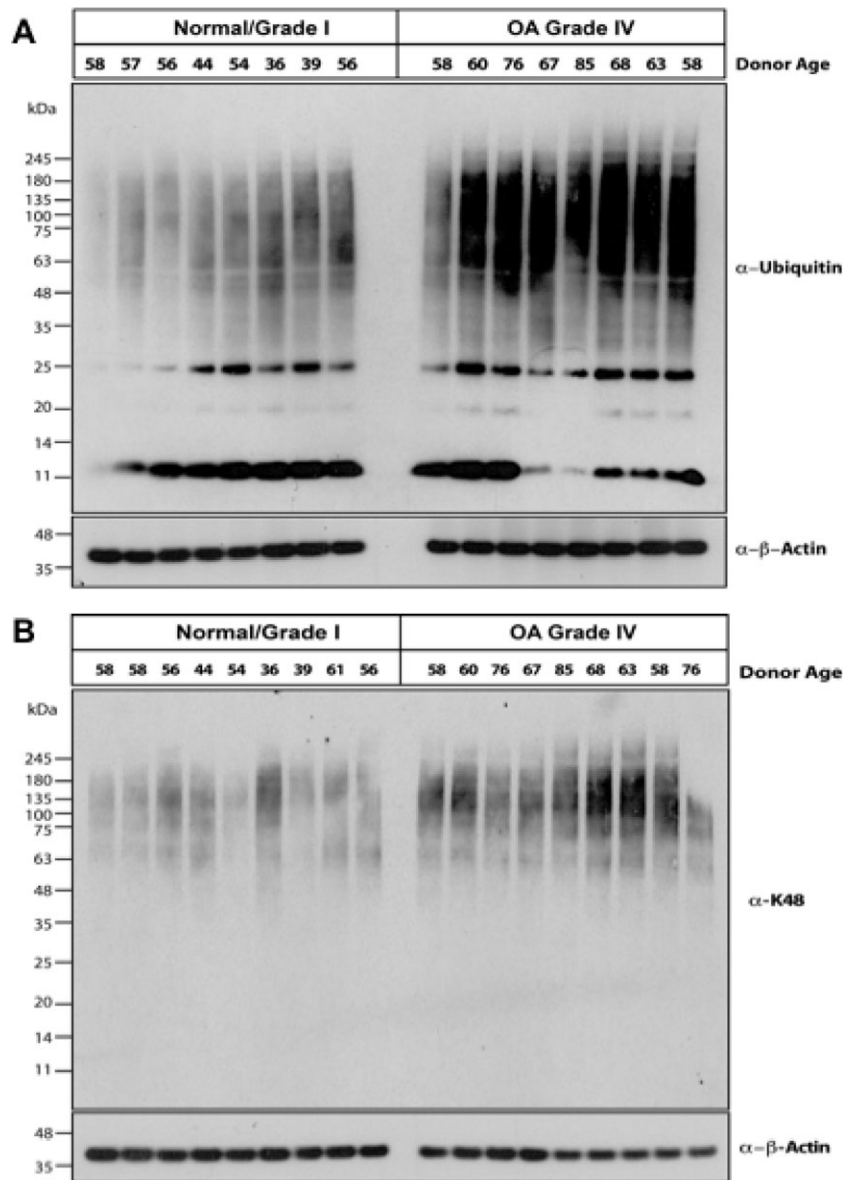
Figure 1. Increased levels of ubiquitin and polyubiquitinated substrates in human knee osteoarthritis (OA) chondrocytes. Equal aliquots (10 μg) of lysates from normal (grade 0/grade I) and grade IV OA human articular chondrocytes were used for sodium dodecyl sulfate–polyacrylamide gel electrophoresis/Western blot analysis, utilizing antibodies directed against ubiquitin (n = 8 per group) (**A**) and K48-linked ubiquitin (n = 9 per group) (**B**). Equal protein loading was confirmed by blotting for β-actin.
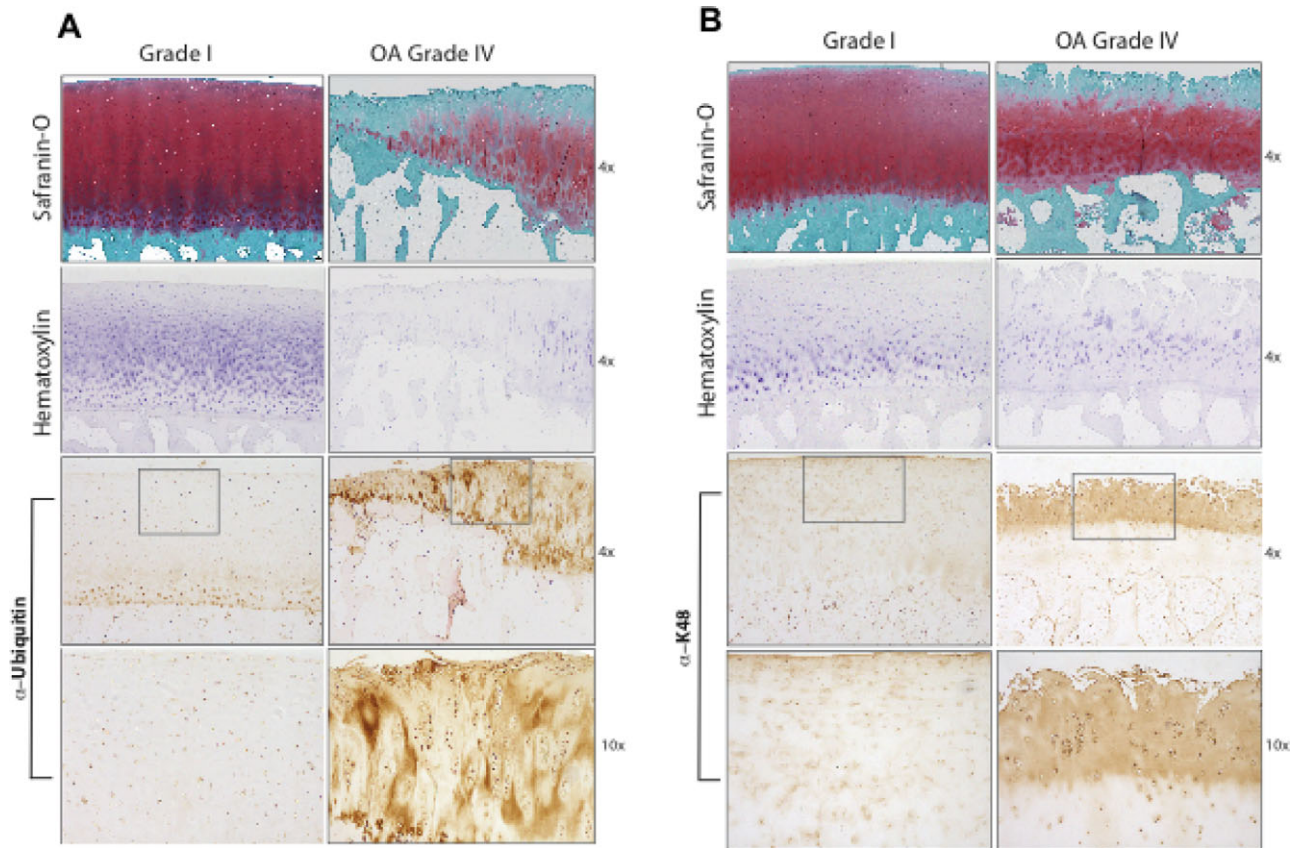
Figure 2. Increased levels of ubiquitin and polyubiquitinated substrates in human knee osteoarthritis (OA) cartilage in situ. Immunohistochemistry analysis of paraffin-embedded sections from normal (grade I) and grade IV OA human knee articular cartilage was performed using antibodies specific for ubiquitin (**A**) and K48-linked ubiquitin (**B**). For images showing Safranin O and hematoxylin staining, original magnification × 4. For immunohistochemistry images, original magnification × 4 or × 10 (panels at the bottom are higher-magnification views of the boxed areas in the panels immediately above). Results are representative of 12 normal donors and 12 OA donors.

19S and 20S subunits of the proteasome (27,28). PSMG1 levels were not significantly decreased in OA chondrocytes (Figure 3C). In contrast, however, OA chondrocytes exhibited decreased levels of PSDM11 protein (Figure 4A) and mRNA (Figure 4B). Levels of FOXO4, a transcription factor that stimulates *PSMD11* mRNA expression (28,31), were comparable in normal and OA chondrocytes. Phosphorylation of FOXOs is required for translocation to the nucleus and subsequent functionality (41), and we observed markedly reduced levels of p-FOXO4 in OA chondrocytes compared to normal chondrocytes (Figure 4C).

Decreased PSMD11 reduces levels of SOX9 and *AGC1* mRNA in chondrocytes. We first assessed, via transfection with PSMD11 siRNA, the functional implications of selective decrease of PSMD11 expression in normal chondrocytes. We validated induction of decreases in levels of PSMD11, associated with reduced proteasome activity and increased levels of K48 polyubiquitinated peptides (Supplementary Figures 1A and B, available on the

Arthritis & Rheumatology web site at http://onlinelibrary.wiley.com/doi/10.1002/art.40456/abstract), without significant changes in total and phosphorylated FOXO1, FOXO3a, and FOXO4 (Supplementary Figure 1C). Under these conditions, in normal chondrocytes, PSMD11 knockdown induced a >70% increase in extracellular NO levels in response to IL-1β (10 ng/ml), but there was no significant difference in MMP-13 protein levels (Figure 5A). *MMP3* and *MMP13* mRNA levels were not significantly affected by PSMD11 siRNA (results not shown). In contrast, PSMD11 siRNA knockdown reduced *SOX9* and *AGC1* mRNA levels (Figure 5B) and attenuated SOX9 protein in normal chondrocytes (Figure 5C). In normal chondrocytes, PSMD11 siRNA stimulated multiple elements of the autophagic machinery, specifically evidenced by LC3A/B-I to LC3A/B-II conversion and increased levels of the autophagy–UPS adaptor and LC3-binding protein p62 (13) (Figure 5C), with associated perinuclear colocalization of p62 and LC3A/B (Figure 5D).
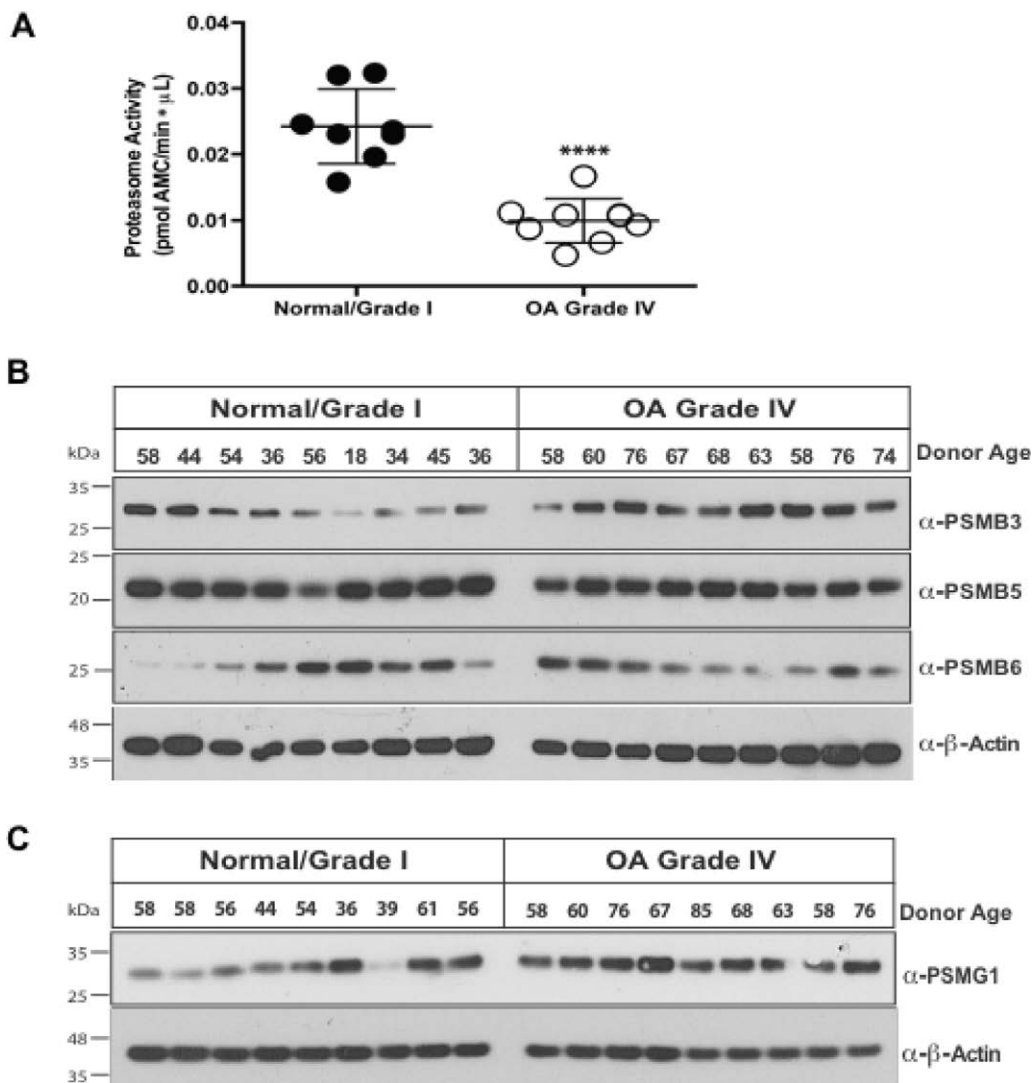
Figure 3. Proteasome activity is diminished in osteoarthritis (OA) chondrocytes, without significant decreases in levels of critical 20S inner ring β-subunits (proteasome subunit β type 3 [PSMB3], PSMB5, PSMB6) and proteasome assembly chaperone 1 (PSMG1). **A,** Lysates were collected from normal chondrocytes (n = 8) and grade IV OA chondrocytes (n = 8) in the absence of protease inhibitors, and protein aliquots (10 μg) were assayed for 20S proteasome function using Succ-LLVY-AMC substrate (37°C, excitation/emission 350 nm/440 nm). Replicate controls were assayed with proteasome inhibitor MG132 (200 μM). We observed a >50% decrease in proteasome protease activity in OA chondrocytes. Symbols represent individual donors; bars show the mean ± SEM. **** = $P < 0.0001$ by unpaired t-test. **B** and **C,** Aliquots (10 μg) of protein extracted from primary chondrocytes (n = 9 normal; n = 9 grade IV OA) were analyzed by Western blotting to determine levels of critical 20S proteasomal inner ring β-subunits, revealing that there was no significant variation between normal and grade IV OA samples (**B**) and that levels of PSMG1 were not appreciably decreased in OA chondrocytes compared to normal donor cells (**C**).

Effects of PSMD11 gain-of-function in human OA chondrocytes. Since levels of PSMD11 were decreased in grade IV OA chondrocytes, we induced selective PSMD11 gain-of-function by transfection in OA cells. To do so, we used an approach previously shown to be effective in stem cells (28). Transfecting HA-tagged PSMD11 cDNA, we achieved significant increases in proteasome activity and observed associated decreases in levels of K48

polyubiquitinated substrates in OA chondrocytes (Figures 6A and B), markedly lower levels of IL-1β–induced extracellular NO (Supplementary Figure 2A, on the *Arthritis & Rheumatology* web site at http://onlinelibrary.wiley.com/doi/10.1002/art.40456/abstract), decreased intracellular and extracellular MMP-13 (Supplementary Figures 2A and B), and increased SOX9 protein in 5 of 5 human OA chondrocyte donor samples tested (Figure 6C). Moreover,
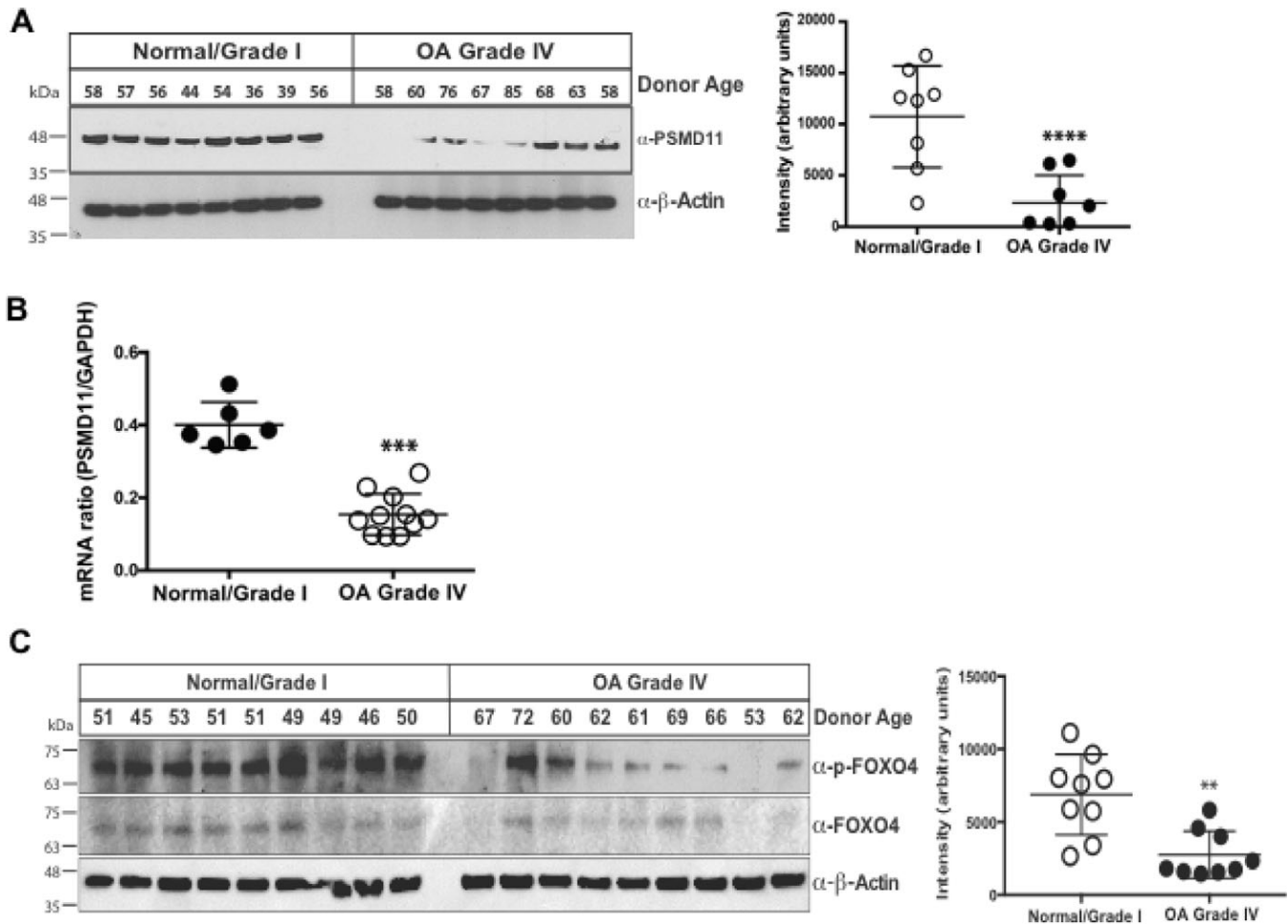
Figure 4. Reduced levels of proteasome 26S subunit, non-ATPase 11 (PSMD11) and phosphorylated FOXO4 in osteoarthritis (OA) chondrocytes. **A,** Western blotting of chondrocyte lysates, with densitometric analysis, revealed decreased PSMD11 levels in grade IV OA compared to normal donor cells. **B,** Analysis by reverse transcriptase–polymerase chain reaction demonstrated that *PSMD11* mRNA levels were significantly decreased in grade IV OA compared to normal chondrocytes. Western blotting with densitometric analysis also revealed decreased p-FOXO4 levels, but no consistent changes in levels of total FOXO4, in grade IV OA compared to normal donor chondrocytes. Symbols represent individual donors; bars show the mean ± SEM. ** = $P = 0.0013$; *** = $P = 0.0008$; **** = $P < 0.0001$, by unpaired *t*-test.

ChIP assays demonstrated that PSMD11 gain-of-function increased SOX9 binding to the *AGC1* 5′-UTR and *COL2A1* enhancer (Figure 6D). Under these conditions, PSMD11 gain-of-function stimulated multiple elements of the autophagic machinery, evidenced by changes in LC3A/B conversion and p62 (Supplementary Figure 3A, http://onlinelibrary.wiley.com/doi/10.1002/art.40456/abstract) and associated increases in perinuclear colocalization of p62 and LC3A/B in 5 of 5 OA chondrocyte donor samples tested (data not shown). Last, PSMD11 transfection induced increased SOX9 nuclear localization and levels of *SOX9*, *AGC1*, and *COL2A1* mRNA in OA chondrocytes (Supplementary Figures 3B and C).

DISCUSSION

In this study, we demonstrated that proteasomal function is impaired in human knee OA chondrocytes, and that integrity of proteasomal function plays a significant role in maintenance of differentiation of cultured chondrocytes. Our studies included analyses of intersections between proteasomal function and autophagy in normal and OA chondrocytes.

Selective induction of proteasomal dysfunction in normal donor chondrocytes, achieved using PSMD11 siRNA, stimulated multiple elements of the autophagic machinery, including p62 and p62 perinuclear colocalization with LC3. This finding may be due to an acute stress
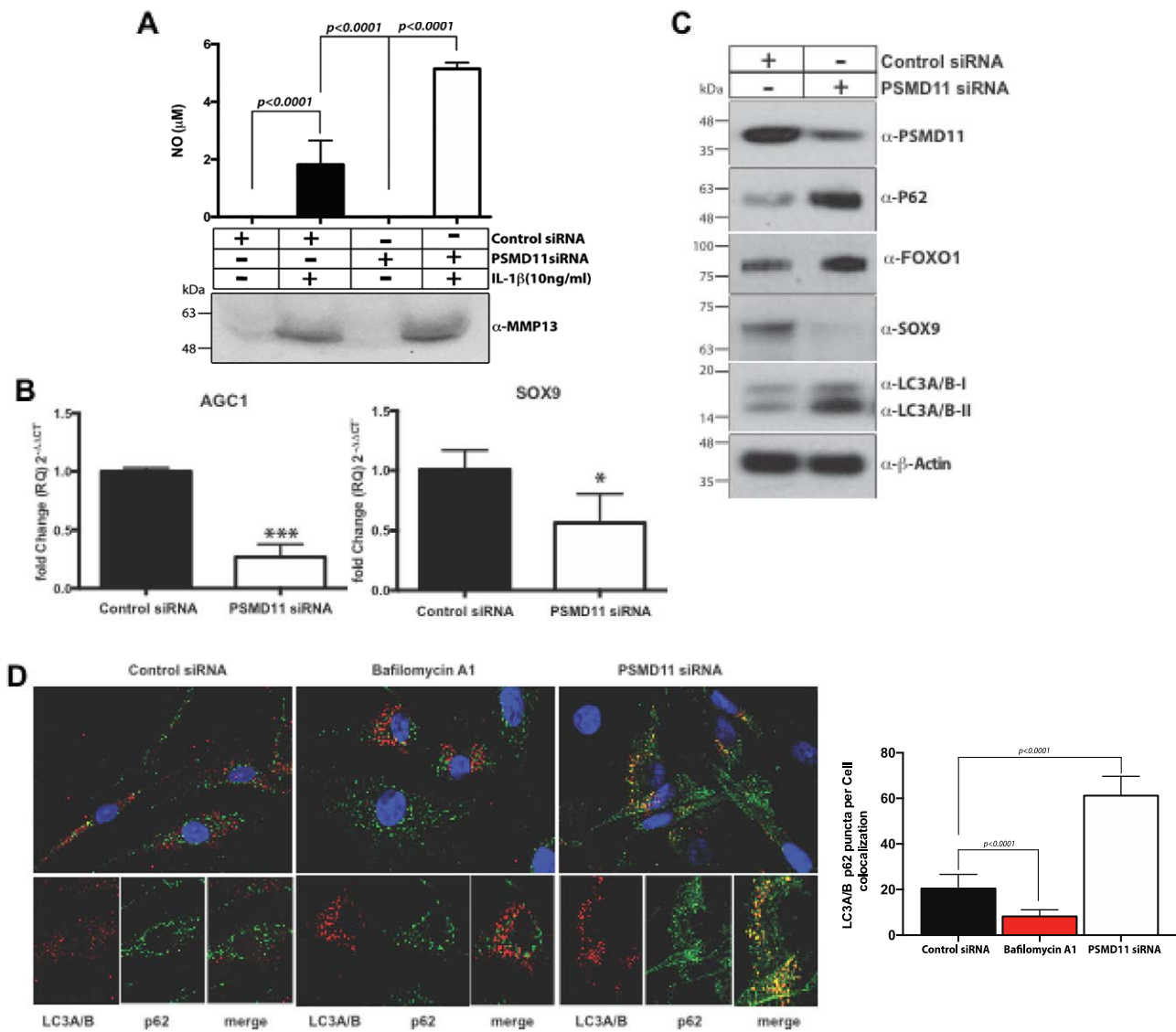
Figure 5. *PSMD11* small interfering RNA (siRNA) knockdown induces increased extracellular nitric oxide (NO) levels, decreased SOX9 levels, and diminished *AGC1* mRNA levels and stimulates elements of the autophagy process in normal chondrocytes. We studied the effects of *PSMD11* siRNA knockdown on extracellular NO and matrix metalloproteinase 13 (MMP-13) levels in response to interleukin-1β (IL-1β) treatment (10 ng/ml) in normal human knee chondrocytes (**A**). We also analyzed the effects of *PSMD11* siRNA on *AGC1* and *SOX9* mRNA (**B**), on SOX9, on autophagy-related light chain 3A/B-I (LC3A/B-I) to LC3A/B-II conversion, and on the autophagy–ubiquitin–proteasome system adaptor and LC3-binding protein p62 (**C**), and on perinuclear colocalization of p62 and LC3A/B-I to LC3A/B-II conversion in normal chondrocytes (**D**) (original magnification × 40), with 300 cells per treatment counted to quantify structures where LC3A/B and p62 colocalized. *P* values were determined by two-way analysis of variance (multiple comparison with Bonferroni post hoc test). In **A**, **B**, and **D**, bars show the mean ± SEM. * = *P* = 0.037; *** = *P* = 0.0004. RQ = relative quantity. Color figure can be viewed in the online issue, which is available at http://onlinelibrary.wiley.com/doi/10.1002/art.40456/abstract.

response to PSMD11 knockdown in healthy cells able to adaptively increase autophagy to support proteostasis. Gain of proteasomal function in OA donor chondrocytes, achieved selectively by PSMD11 transfection, induced increases in elements of the autophagic machinery. Distinct autophagic pathways (microautophagy, chaperone-mediated autophagy, and macroautophagy) effect degradation of

cytosolic proteins, using multiple enzymes and differing cargo delivery to lysosomes or vacuoles, and with ordered phases of each process (13). Full examination of cross-talk between the UPS and autophagy processes (13), and evaluation of ultimate autophagic protein degradation, were beyond the scope of this study. However, effectiveness of the autophagic process in OA chondrocytes is known to be
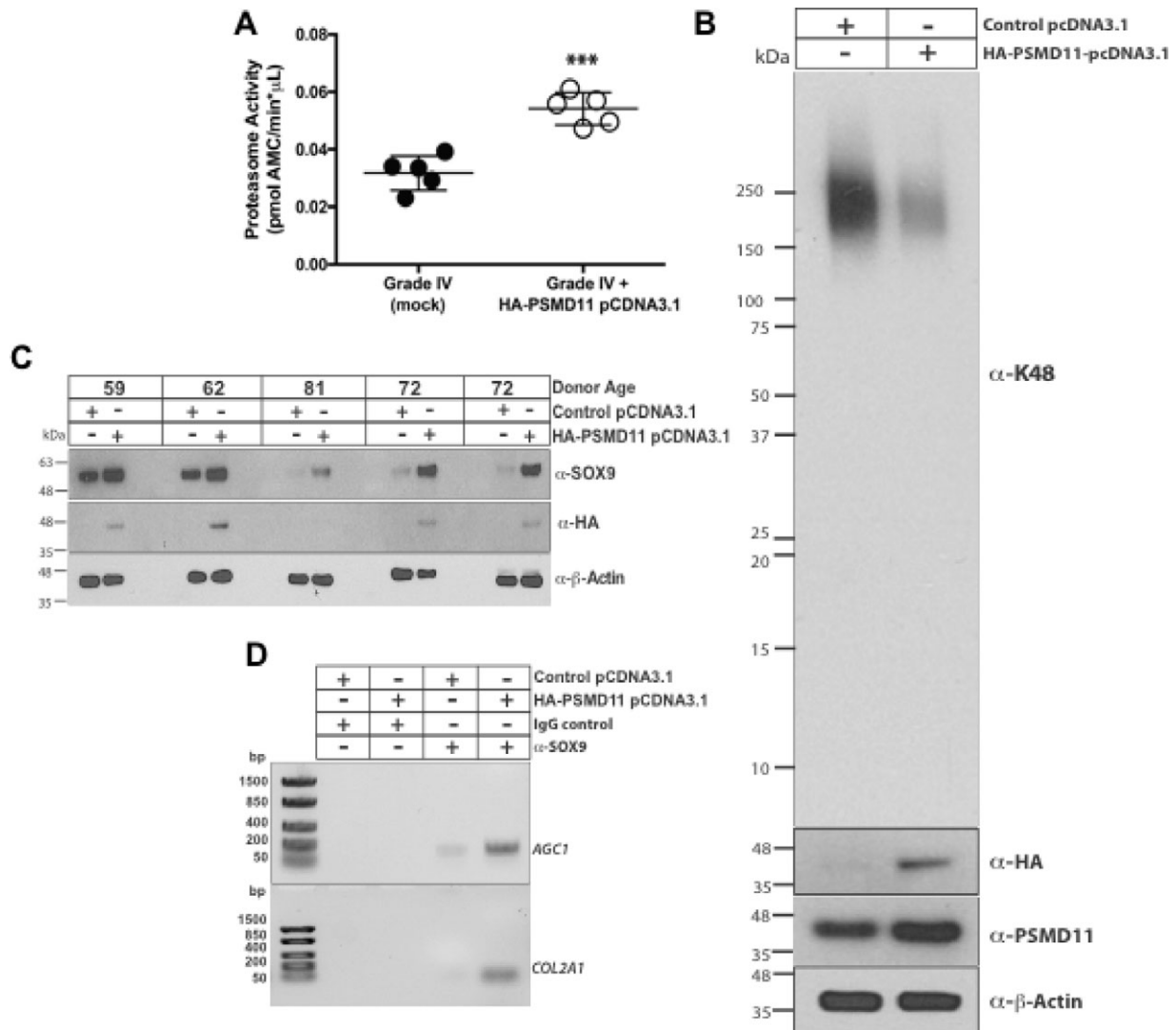
Figure 6. Effects of selective proteasome 26S subunit, non-ATPase 11 (PSMD11) gain-of-function in cultured human knee osteoarthritis (OA) chondrocytes. **A** and **B,** Transfecting grade IV OA chondrocytes, we assessed the effects of hemagglutinin (HA) tag-*PSMD11* plasmid, compared to control plasmid transfection, on proteasome activity (**A**) (n = 5 normal donors; n = 5 OA donors) and on accumulation of K48-polyubiquitinated proteins (**B**). In **A**, symbols represent individual donors; bars show the mean ± SEM. *** = $P = 0.0003$ by unpaired *t*-test. In **B**, representative results are shown. **C,** Effects of PSMD11 gain-of-function, by transfection in OA chondrocytes (n = 5 different donors), on SOX9 levels were assessed, and its ability to augment cellular HA was validated. **D,** By chromatin immunoprecipitation assay, we separately analyzed the effect of PSMD11 gain-of-function on nuclear SOX9 binding to the *AGC1* 5′-untranslated region and to *COL2A1* enhancer.

decreased once OA is well- established (3,4,19,20). As such, our results suggest that compromise of proteasomal function is likely more deleterious in aging and OA chondrocytes (12) by a compound proteostasis defect that includes autophagy impairment (7–11). The impact of proteasomal dysfunction in OA chondrocytes could potentially be amplified by decreased autophagic removal of damaged proteasomes (42).

Our study defined molecular mechanistic factors contributing to deficient proteasomal function in human knee OA chondrocytes, and associated accumulation of

K48 polyubiquitinated substrates. Specifically, we linked proteasomal dysfunction in OA chondrocytes to decreases in PSMD11 and the PSMD11 transcription inducer p-FOXO4, but not total FOXO4. PSMD11, a 19S proteasomal subunit, is required for assembly of a functional 20S proteasomal core (27,28,31). Essentially, 20S particles exist as free complexes, with constitutively latent proteolytic activity primed by 19S particle ATPases that also permit access of proteins to the 20S core (27,28). Two members of the FOXO family, FOXO1 and FOXO3, are decreased in aging and OA chondrocytes in vitro, and

articular cartilage in situ (3,19). Though FOXO1 and FOXO3 are far more abundant than FOXO4 in human articular chondrocytes, unlike FOXO4 they do not have a defined role in regulating proteasomal activity.

The observed decrease in PSMD11 in OA chondrocytes was at least partially selective, relative to other modulators of proteasome assembly and 20S proteasomal core protease activity. Specifically, 3 inner ring β-subunits and the 20S particle assembly chaperone PSMG1 were not decreased in OA compared to normal human knee chondrocytes. Another central finding was that selective PSMD11 gain-of-function by transfection improved proteasomal function in OA chondrocytes, evidenced by increased 20S chymotrypsin-like proteolytic activity and decreased K48 polyubiquitinated substrates. PSMD11 is regulated by factors other than FOXO4, including cAMP and protein kinase A (PKA) signaling, which transcriptionally support PSMD11 expression (30). However, cAMP and PKA signaling have mixed effects on matrix catabolism by articular chondrocytes that would theoretically limit their potential translational utility in increasing proteasomal function in OA chondrocytes.

Selective modulation of PSMD11, beyond effects on proteasomal function, had marked functional impact in normal and OA chondrocytes, with major effects on maintenance of SOX9 and chondrocytic differentiation. We identified affected responses to include levels of SOX9 protein and SOX9 nuclear translocation and binding to regions in the AGC1 5′-UTR and COL2A1 enhancer, and levels of AGC1 and COL2A1 mRNA expression. SOX9 is influenced by multiple signals, including those provided by a variety of growth factors, transcription factors, and epigenetic modifications (43). As such, the net contributions of PSMD11 and proteasomal function on SOX9, AGC1, and maintenance of articular chondrocytic differentiation, remain to be determined in both early and late OA.

PSMD11-selective modulation of proteasomal function significantly affected IL-1β–triggered extracellular NO levels in both normal and OA chondrocytes, and extracellular MMP-13 in OA chondrocytes. The NO findings carry significance partly due to the capacity of NO to exert both antianabolic and procatabolic effects on extracellular matrix homeostasis in cartilage, including suppression of proteoglycans and collagen synthesis (44). Additionally, excess NO promotes chondrocyte apoptosis (45,46). NO is generated and degraded by a variety of mechanisms in chondrocytes (46). Moreover, the UPS regulates NO metabolism by complex and paradoxical mechanisms, including regulation of inducible NO synthase (iNOS) expression by NF-κB, and of proteasomal degradation of iNOS (47,48). Hence, the mechanism of the observed capacity of proteasomal dysfunction to modulate extracellular NO in chondrocytes could be multifactorial.

Both UPS dysfunction and OA increase progressively with aging (1,2,21), and this study was not designed or powered to distinguish effects of aging from those of OA in chondrocytes. That question clearly will require further study. Another limitation is that our studies of protease activity in isolated proteasomes from cytosol, rather than whole cells, could have readily underestimated the extent of decreased proteasomal function in OA chondrocytes. In this context, substrate selection and gate opening are highly regulated processes that are highly dependent on ATP. OA chondrocytes have decreased ATP levels, largely due to mitochondrial dysfunction (6).

Our results support a model in which impaired chondrocyte proteasomal function in established OA renders cartilage damage more difficult to slow and potentially reverse. However, there could well be substantially less chondrocyte proteasomal impairment in earlier stages of OA, such as those previously studied (35–38). The chondrocyte UPS dysfunction studied here may reflect an advanced stage of disease, given that we focused on chondrocytes from donors with advanced (grade IV) OA. Further studies on UPS effects in chondrocytes from early OA cartilage would be of interest. In this regard, multiple pharmacologic proteasome protease inhibitors, including MG132, increase autophagy in normal cells (13,49). As such, our results suggest that chondroprotective effects of MG132 administration in young rodents with nascent experimental knee OA (35–38) may have been partly mediated by induction of increased autophagy in the normal chondrocytes of these young animals. Other in vivo chondroprotective mechanisms of pharmacologic proteasomal inhibition by MG132 in young animals could include suppression of articular inflammatory processes, cartilage matrix catabolism, and pain (35–38), partially via increased protein stability of the proteasomal degradation–regulated native NF-κB inhibitor IκB (37,38).

Proteasomal protease inhibitors such as MG132 are only one means to elucidate proteasome function in OA. Specifically, in a study of rodent knee instability–induced OA using mice transgenic for K48R-mutated ubiquitin to investigate focused interference with polyubiquitination, only marginal and focal chondroprotection was observed, albeit in a system with potentially problematic residual effects of endogenous normal ubiquitin (38). Ultimately, investigations into the impact of the phenotype of proteasomal dysfunction in OA chondrocytes would benefit most from replication of specific molecular mechanisms that cause impairment of proteasomal function. This is particularly the case because not only proteasomal core proteases,

but also deubiquitinases, impart and tune proteasomal functionality (13,21).

In conclusion, we have provided what is, to our knowledge, the first evidence of impaired proteasomal function in human OA chondrocytes. We mechanistically linked decreases in chondrocyte PSMD11 and p-FOXO4 to consequent decreases in SOX9, and in *AGC1* and *COL2A1* mRNA levels, along with increased extracellular NO in response to inflammatory stimulation. However, we note that UPS dysfunction promotes disease partly by effects on diverse processes, promoting mitochondrial dysfunction, oxidative stress, and altered insulin-like growth factor receptor, insulin receptor, phosphatidylinositol 3-kinase, and Akt signaling (12,13,21,22,31). Translationally, our results revealed that proteasomal gain-of-function, achieved in a highly selective manner by PSMD11 gain-of-function, stimulated elements of the autophagy process in both normal and advanced knee OA chondrocytes, and also increased SOX9, *AGC1* 5′-UTR, and *COL2A1* enhancer binding, and *AGC1* and *COL2A1* mRNA levels. There are emerging pharmacologic means to up-regulate 20S proteasomal activity, including by use of small molecules such as deubiquitinase inhibitors (50). The chondrocyte proteasome could provide a novel, pharmacologically targetable therapy in OA, which would potentially be more chondroprotective in well-established disease.

ACKNOWLEDGMENT

AUTHOR CONTRIBUTIONS

All authors were involved in drafting the article or revising it critically for important intellectual content, and all authors approved the final version to be published. Dr. Terkeltaub had full access to all of the data in the study and takes responsibility for the integrity of the data and the accuracy of the data analysis.
Study conception and design. Serrano, Liu-Bryan, Terkeltaub.
Acquisition of data. Serrano, Chen, Lotz.
Analysis and interpretation of data. Serrano, Chen, Lotz, Liu-Bryan, Terkeltaub.

REFERENCES

1. Loeser RF, Collins JA, Diekman BO. Ageing and the pathogenesis of osteoarthritis [review]. Nat Rev Rheumatol 2016;12:412–20.
2. López-Otín C, Blasco MA, Partridge L, Serrano M, Kroemer G. The hallmarks of aging [review]. Cell 2013;153:1194–217.
3. Akasaki Y, Hasegawa A, Saito M, Asahara H, Iwamoto Y, Lotz MK. Dysregulated FOXO transcription factors in articular cartilage in aging and osteoarthritis. Osteoarthritis Cartilage 2014;22:162–70.
4. Terkeltaub R, Yang B, Lotz M, Liu-Bryan R. Chondrocyte AMP-activated protein kinase activity suppresses matrix degradation responses to proinflammatory cytokines interleukin-1β and tumor necrosis factor α. Arthritis Rheum 2011;63:1928–37.
5. López de Figueroa P, Lotz MK, Blanco FJ, Caramés B. Autophagy activation and protection from mitochondrial dysfunction in human chondrocytes. Arthritis Rheumatol 2015;67:966–76.
6. Wang Y, Zhao X, Lotz M, Terkeltaub R, Liu-Bryan R. Mitochondrial biogenesis is impaired in osteoarthritis chondrocytes but reversible via peroxisome proliferator–activated receptor γ coactivator 1α. Arthritis Rheumatol 2015;67:2141–53.
7. Cheng NT, Guo A, Meng H. The protective role of autophagy in experimental osteoarthritis, and the therapeutic effects of Torin 1 on osteoarthritis by activating autophagy. BMC Musculoskelet Disord 2016;17:150.
8. Bouderlique T, Vuppalapati KK, Newton PT, Li L, Barenius B, Chagin AS. Targeted deletion of Atg5 in chondrocytes promotes age-related osteoarthritis. Ann Rheum Dis 2016;75:627–31.
9. Caramés B, Olmer M, Kiosses WB, Lotz MK. The relationship of autophagy defects to cartilage damage during joint aging in a mouse model. Arthritis Rheumatol 2015;67:1568–76.
10. Takayama K, Kawakami Y, Kobayashi M, Greco N, Cummins JH, Matsushita T, et al. Local intra-articular injection of rapamycin delays articular cartilage degeneration in a murine model of osteoarthritis. Arthritis Res Ther 2014;16:482.
11. Zhang Y, Vasheghani F, Li YH, Blati M, Simeone K, Fahmi H, et al. Cartilage-specific deletion of mTOR upregulates autophagy and protects mice from osteoarthritis. Ann Rheum Dis 2015;74:1432–40.
12. Vilchez D, Saez I, Dillin A. The role of protein clearance mechanisms in organismal ageing and age-related diseases [review]. Nat Commun 2014;5:5659.
13. Lilienbaum A. Relationship between the proteasomal system and autophagy [review]. Int J Biochem Mol Biol 2013;4:1–26.
14. Hotamisligil GS, Davis RJ. Cell signaling and stress responses [review]. Cold Spring Harb Perspect Biol 2016;8:a006072.
15. Husa M, Petursson F, Lotz M, Terkeltaub R, Liu-Bryan R. C/EBP homologous protein drives pro-catabolic responses in chondrocytes. Arthritis Res Ther 2013;15:R218.
16. Uehara Y, Hirose J, Yamabe S, Okamoto N, Okada T, Oyadomari S, et al. Endoplasmic reticulum stress-induced apoptosis contributes to articular cartilage degeneration via C/EBP homologous protein. Osteoarthritis Cartilage 2014;22:1007–17.
17. Li YH, Tardif G, Hum D, Kapoor M, Fahmi H, Pelletier JP, et al. The unfolded protein response genes in human osteoarthritic chondrocytes: PERK emerges as a potential therapeutic target. Arthritis Res Ther 2016;18:172.
18. Matsuzaki T, Alvarez-Garcia O, Mokuda S, Nagira K, Olmer M, Gamini R, et al. FoxO transcription factors modulate autophagy and proteoglycan 4 in cartilage homeostasis and osteoarthritis. Sci Transl Med 2018;10. pii: eaan0746.
19. Akasaki Y, Alvarez-Garcia O, Saito M, Caramés B, Iwamoto Y, Lotz MK. FoxO transcription factors support oxidative stress resistance in human chondrocytes. Arthritis Rheumatol 2014;66:3349–58.
20. Alvarez-Garcia O, Matsuzaki T, Olmer M, Plate L, Kelly JW, Lotz MK. Regulated in development and DNA damage response 1 deficiency impairs autophagy and mitochondrial biogenesis in articular cartilage and increases the severity of experimental osteoarthritis. Arthritis Rheumatol 2017;69:1418–28.
21. Labbadia J, Morimoto RI. The biology of proteostasis in aging and disease [review]. Annu Rev Biochem 2015;84:435–64.
22. Löw P. The role of ubiquitin-proteasome system in ageing. Gen Comp Endocrinol 2011;172:39–43.
23. Erpapazoglou Z, Walker O, Haguenauer-Tsapis R. Versatile roles of k63-linked ubiquitin chains in trafficking [review]. Cells 2014;3:1027–88.

24. Ferreira JV, Soares AR, Ramalho JS, Pereira P, Girao H. K63 linked ubiquitin chain formation is a signal for HIF1A degradation by chaperone-mediated autophagy. Sci Rep 2015;5:10210.

25. Nanduri P, Hao R, Fitzpatrick T, Yao TP. Chaperone-mediated 26S proteasome remodeling facilitates free K63 ubiquitin chain production and aggresome clearance. J Biol Chem 2015;290: 9455–64.

26. Sasaki K, Hamazaki J, Koike M, Hirano Y, Komatsu M, Uchiyama Y, et al. PAC1 gene knockout reveals an essential role of chaperone-mediated 20S proteasome biogenesis and latent 20S proteasomes in cellular homeostasis. Mol Cell Biol 2010;30:3864–74.

27. Pathare GR, Nagy I, Bohn S, Unverdorben P, Hubert A, Körner R, et al. The proteasomal subunit Rpn6 is a molecular clamp holding the core and regulatory subcomplexes together. Proc Natl Acad Sci U S A 2012;109:149–54.

28. Vilchez D, Boyer L, Morantte I, Lutz M, Merkwirth C, Joyce D, et al. Increased proteasome activity in human embryonic stem cells is regulated by PSMD11. Nature 2012;489:304–8.

29. Moreno D, Viana R, Sanz P. Two-hybrid analysis identifies PSMD11, a non-ATPase subunit of the proteasome, as a novel interaction partner of AMP-activated protein kinase. Int J Biochem Cell Biol 2009;41:2431–9.

30. Lokireddy S, Kukushkin NV, Goldberg AL. cAMP-induced phosphorylation of 26S proteasomes on Rpn6/PSMD11 enhances their activity and the degradation of misfolded proteins. Proc Natl Acad Sci U S A 2015;112:E7176–85.

31. Kevei É, Hoppe T. Ubiquitin sets the timer: impacts on aging and longevity [review]. Nat Struct Mol Biol 2014;21:290–2.

32. Ronnebaum SM, Patterson C, Schisler JC. UPS: metabolic and proteolytic homeostasis linked via AMPK and the ubiquitin proteasome system [review]. Mol Endocrinol 2014;28:1602–15.

33. Gidalevitz T, Prahlad V, Morimoto RI. The stress of protein misfolding: from single cells to multicellular organisms [review]. Cold Spring Harb Perspect Biol 2011;3:a009704.

34. Schröter F, Adjaye J. The proteasome complex and the maintenance of pluripotency: sustain the fate by mopping up? Stem Cell Res Ther 2014;5:24.

35. Ahmed AS, Li J, Erlandsson-Harris H, Stark A, Bakalkin G, Ahmed M. Suppression of pain and joint destruction by inhibition of the proteasome system in experimental osteoarthritis. Pain 2012;153:18–26.

36. Etienne S, Gaborit N, Henrionnet C, Pinzano A, Galois L, Netter P, et al. Local induction of heat shock protein 70 (Hsp70) by proteasome inhibition confers chondroprotection during surgically induced osteoarthritis in the rat knee. Biomed Mater Eng 2008; 18:253–60.

37. Ye J, Qing Z, Ma J, Wang Z. Effect of proteasome inhibitor on NF-κB and MMP-9 expression in synovial tissues of osteoarthritis rats. Int J Clin Exp Med 2017;10:402–9.

38. Radwan M, Wilkinson DJ, Hui W, Destrument AP, Charlton SH, Barter MJ, et al. Protection against murine osteoarthritis by inhibition of the 26S proteasome and lysine-48 linked ubiquitination. Ann Rheum Dis 2015;74:1580–7.

39. Lefebvre V, Huang W, Harley VR, Goodfellow PN, de Crombrugghe B. SOX9 is a potent activator of the chondrocyte-specific enhancer of the pro α1(II) collagen gene. Mol Cell Biol 1997;17:2336–46.

40. Duval E, Leclercq S, Elissalde JM, Demoor M, Galéra P, Boumédiene K. Hypoxia-inducible factor 1α inhibits the fibroblast-like markers type I and type III collagen during hypoxia-induced chondrocyte redifferentiation: hypoxia not only induces type II collagen and aggrecan, but it also inhibits type I and type III collagen in the hypoxia-inducible factor 1α-dependent redifferentiation of chondrocytes [published erratum appears in Arthritis Rheum 2014;66:1394]. Arthritis Rheum 2009;60:3038–48.

41. Van Der Heide LP, Hoekman MF, Smidt MP. The ins and outs of FoxO shuttling: mechanisms of FoxO translocation and transcriptional regulation [review]. Biochem J 2004;380:297–309.

42. Marshall RS, Li F, Gemperline DC, Book AJ, Vierstra RD. Autophagic degradation of the 26S proteasome is mediated by the dual ATG8/ubiquitin receptor RPN10 in arabidopsis. Mol Cell 2015;58:1053–66.

43. Liu CF, Samsa WE, Zhou G, Lefebvre V. Transcriptional control of chondrocyte specification and differentiation [review]. Semin Cell Dev Biol 2017;62:34–49.

44. Cao M, Stefanovic-Racic M, Georgescu HI, Miller LA, Evans CH. Generation of nitric oxide by lapine meniscal cells and its effect on matrix metabolism: stimulation of collagen production by arginine. J Orthop Res 1998;16:104–11.

45. Kühn K, Shikhman AR, Lotz M. Role of nitric oxide, reactive oxygen species, and p38 MAP kinase in the regulation of human chondrocyte apoptosis. J Cell Physiol 2003;197:379–87.

46. Lotz M. The role of nitric oxide in articular cartilage damage [review]. Rheum Dis Clin North Am 1999;25:269–82.

47. Qureshi AA, Tan X, Reis JC, Badr MZ, Papasian CJ, Morrison DC, et al. Suppression of nitric oxide induction and pro-inflammatory cytokines by novel proteasome inhibitors in various experimental models. Lipids Health Dis 2011;10:177.

48. Kolodziejski PJ, Musial A, Koo JS, Eissa NT. Ubiquitination of inducible nitric oxide synthase is required for its degradation. Proc Natl Acad Sci U S A 2002;99:12315–20.

49. Ding WX, Ni HM, Gao W, Yoshimori T, Stolz DB, Ron D, et al. Linking of autophagy to ubiquitin-proteasome system is important for the regulation of endoplasmic reticulum stress and cell viability. Am J Pathol 2007;171:513–24.

50. Chondrogianni N, Voutetakis K, Kapetanou M, Delitsikou V, Papaevgeniou N, Sakellari M, et al. Proteasome activation: an innovative promising approach for delaying aging and retarding age-related diseases [review]. Ageing Res Rev 2015;23:37–55.

Magnetic Resonance Imaging of the Sacroiliac Joints Indicating Sacroiliitis According to the Assessment of SpondyloArthritis international Society Definition in Healthy Individuals, Runners, and Women With Postpartum Back Pain

Janneke de Winter,[1] Manouk de Hooge,[2] Marleen van de Sande,[1] Henriëtte de Jong,[1]
Lonneke van Hoeven,[3] Anoek de Koning,[4] Inger Jorid Berg,[5] Roberta Ramonda,[6]
Dominique Baeten,[7] Désirée van der Heijde,[4] Angelique Weel,[3] and Robert Landewé[8]

***Objective*.** To compare magnetic resonance images (MRIs) of the sacroiliac (SI) joints of healthy subjects and individuals with known mechanical strain acting upon the SI joints to those of patients with axial spondyloarthritis (SpA) and patients with chronic back pain.

***Methods*.** Three readers who had received standardized training and were blinded with regard to study group randomly scored MRIs of the SI joints of 172 subjects, including 47 healthy individuals without current or past back pain, 47 axial SpA patients from the Spondyloarthritis Caught Early (SPACE) cohort (with a previous MRI confirmed positive for sacroiliitis), 47 controls with chronic back pain (irrespective of MRI results) from the SPACE cohort, 7 women with postpartum back pain, and 24 frequent runners. MRIs were scored according to the Assessment of SpondyloArthritis international Society (ASAS) definition and Spondyloarthritis Research Consortium of Canada (SPARCC) index.

***Results*.** Of the 47 healthy volunteers, 11 (23.4%) had an MRI positive for sacroiliitis, compared to 43 (91.5%) of 47 axial SpA patients and 3 (6.4%) of 47 patients with chronic back pain. Three (12.5%) of the 24 runners and 4 (57.1%) of the 7 women with postpartum back pain had a positive MRI. Using a SPARCC cutoff of ≥2 for positivity, 12 (25.5%) of 47 healthy volunteers, 46 (97.9%) of 47 positive axial SpA patients, 5 (10.6%) of 47 controls with chronic back pain, 4 (16.7%) of 24 runners, and 4 (57.1%) of 7 women with postpartum back pain had positive MRIs. Deep bone marrow edema (BME) lesions were not found in healthy volunteers, patients with chronic back pain, or runners, but were found in 42 (89.4%) of 47 positive axial SpA patients and in 1 (14.3%) of 7 women with postpartum back pain.

***Conclusion*.** A substantial proportion of healthy individuals without current or past back pain has an MRI positive for sacroiliitis according to the ASAS definition. Deep (extensive) BME lesions are almost exclusively found in axial SpA patients.

[1]Janneke de Winter, MD, Marleen van de Sande, MD, PhD, Henriëtte de Jong, MD: Amsterdam Rheumatology and Immunology Center, Academic Medical Center, University of Amsterdam, Amsterdam, The Netherlands; [2]Manouk de Hooge, PhD: Leiden University Medical Center, Leiden, The Netherlands, and Ghent University Hospital, Ghent, Belgium; [3]Lonneke van Hoeven, MD, PhD, Angelique Weel, MD, PhD: Maasstad Hospital, Rotterdam, The Netherlands; [4]Anoek de Koning, MD, Désirée van der Heijde, MD, PhD: Leiden University Medical Center, Leiden, The Netherlands; [5]Inger Jorid Berg, MD: Diakonhjemmet Hospital, Oslo, Norway; [6]Roberta Ramonda, MD, PhD: University of Padua, Padua, Italy; [7]Dominique Baeten, MD, PhD: Amsterdam Rheumatology and Immunology Center, Academic Medical Center, University of Amsterdam, Amsterdam, The Netherlands, and UCB, Brussels, Belgium; [8]Robert Landewé, MD, PhD: Amsterdam Rheumatology and Immunology Center, Academic Medical Center, University of Amsterdam, Amsterdam, The Netherlands and Zuyderland Medical Center, Heerlen, The Netherlands.

Drs. Weel and Landewé contributed equally to this work.

Address correspondence to Robert Landewé, MD, PhD, Department of Clinical Immunology and Rheumatology, Amsterdam Rheumatology and Immunology Center, Academic Medical Center/ University of Amsterdam, F4-105, PO Box 22660, Amsterdam 1100 DD, The Netherlands. E-mail: landewe@rlandewe.nl.

Submitted for publication September 15, 2017; accepted in revised form February 27, 2018.

Axial spondyloarthritis (SpA) is among the most prevalent forms of chronic inflammatory arthritis (1,2). In recent decades, magnetic resonance imaging (MRI) has been increasingly used to visualize inflammation in the sacroiliac (SI) joints. Inflammation on MRI facilitates the early identification of patients with axial SpA since it precedes structural damage on radiography (3,4). Of all patients with axial SpA, 20–42% have active sacroiliitis on MRI (5–8), but signs of presumed sacroiliitis may also occur in individuals without axial SpA. One study by Weber et al showed that of 59 healthy volunteers, up to

22% had signs of sacroiliitis on MRI (9). Arnbak and colleagues showed that of 1,020 unselected patients with chronic back pain, 21% had sacroiliitis on MRI according to the Assessment of SpondyloArthritis international Society (ASAS) definition (10). The specificity of MRI of the SI joints for SpA-specific sacroiliitis is not well known and physicians may rely too much on a positive finding (11).

In order to obtain insight into the prevalence and extent of SI joint inflammation in healthy individuals, and in those with known mechanical strain acting upon the SI joints, we compared MRIs of the SI joints in 1) healthy individuals without any signs of current or past back pain, 2) patients with classic axial SpA with a documented positive MRI of the SI joints after central reading, 3) patients with chronic back pain, 4) frequent runners, and 5) women with postpartum back pain.

The primary hypothesis was that the difference between axial SpA and non–axial SpA with regard to the presence of sacroiliitis on MRI was quantitative (extent) rather than qualitative (present versus absent).

PATIENTS AND METHODS

Selection of the study participants. The present study included participants from the Maasstad MRI project and the Spondyloarthritis Caught Early (SPACE) cohort. The Maasstad MRI project included healthy participants, frequent runners, and women with postpartum back pain (12). Healthy participants were employees of Maasstad Hospital and Erasmus University Medical Center (Rotterdam, The Netherlands). Male and female participants between 18 and 45 years of age were included. Runners who were running at least 5 km twice per week were recruited via an athletics club. Healthy participants and runners with any form of current or past acute or chronic back pain and those with contraindication to MRI were excluded. Women with postpartum back pain that presented ≤3 months after pregnancy were included in the Maasstad MRI project and additionally selected from the SPACE cohort.

We selected positive and negative controls from the SPACE cohort. The SPACE cohort is an ongoing, prospective, longitudinal, multicenter cohort that started in 2009 and has been described in detail elsewhere (13). In short, the SPACE cohort includes patients ages ≥16 years with chronic back pain (with a duration of ≥3 months but ≤2 years) with an onset before the age of 45 years. We used baseline data unless specified otherwise. Positive SPACE controls were defined as patients with axial SpA (who were diagnosed by a rheumatologist and fulfilled the ASAS criteria for axial SpA [3]) with an MRI of the SI joints that was previously scored as positive for sacroiliitis according to the ASAS definition by at least 2 of 3 central readers. Negative SPACE controls were defined as patients with chronic back pain (who were neither diagnosed as having axial SpA nor fulfilled the ASAS criteria for axial SpA), irrespective of their MRI findings. Healthy controls were matched with positive and negative SPACE controls for age and sex.

The local medical ethics committees of the participating sites approved the study, and all participants gave their written informed consent.

MRI. MRI was performed on 1.5T systems. At least 12 slices of coronal oblique T1-weighted turbo spin-echo and short tau inversion recovery sequences of the SI joints were acquired. The slice thickness was 4 mm.

Scoring. Three readers (JdW, MdH, and RL) who had received standardized training and were blinded with regard to subject group independently scored all MRIs in random order. The readers were instructed to quantify MRIs as positive or negative by judging for the presence or absence of bone marrow edema (BME) according to the ASAS definition that was recently updated by the ASAS MRI working group (14). As this definition describes, the focus was on scoring only lesions that were considered "highly suggestive of axial SpA" as positive. In addition, the readers quantified the extent of BME according to the Spondyloarthritis Research Consortium of Canada (SPARCC) scoring system (15). For SPARCC scoring, 6 consecutive coronal slices were selected and each SI joint was divided into 4 quadrants: the upper and lower ilium and upper and lower sacrum. Each quadrant was assigned a score of 1 for the presence of BME or 0 for the absence of BME. Each coronal slice per SI joint was also scored for the presence of "intense" lesions (high signal as bright as or brighter than that of veins or

Table 1. Characteristics of the healthy participants, patients with axial SpA with a previous MRI positive for sacroiliitis (positive controls), patients with chronic back pain (negative controls), runners, and women with postpartum back pain*

	Healthy participants (n = 47)	Patients with axial SpA (n = 47)	Controls with chronic back pain (n = 47)	Runners (n = 24)	Women with postpartum back pain (n = 7)
Men	21 (44.7)	21 (44.7)	21 (44.7)	12 (50.0)	0 (0)
Age, mean ± SD years	30.9 ± 6.5	31.5 ± 6.9	30.7 ± 6.5	34.3 ± 7.7	30.1 ± 7.2
Axial SpA diagnosis	0 (0)	47 (100)	0 (0)	0 (0)	0 (0)
HLA–B27 positive	NA	35 (74.5)	0 (0)	NA	NA
Duration of back pain, mean ± SD months	NA	13.4 ± 7.4	12.8 ± 7.8	NA	NA
Inflammatory back pain	NA	35 (74.5)	26 (55.3)	NA	NA
Alternating buttock pain	NA	40 (85.1)	20 (42.6)	NA	NA
ASAS axial SpA criteria	NA	47 (100)	NA	NA	NA
Modified New York criteria	NA	13 (29.5)	0 (0)	NA	NA

* Except where indicated otherwise, values are the number (%). SpA = spondyloarthritis; MRI = magnetic resonance imaging; NA = not applicable; ASAS = Assessment of SpondyloArthritis international Society.

intervertebral discs) or "deep" lesions (a homogeneous, unequivocal increase in signal extending ≥1 cm from the articular surface). The maximum SPARCC score for all 6 slices was 48 for BME, 12 for intensity, and 12 for depth, resulting in a maximum total score of 72 (15). To determine the distribution of BME anatomically in the SI joints, we used the SPARCC distribution of the 4 quadrants, divided into anterior and posterior slices. BME was considered to occur in a particular region if it was concordantly recorded at that region by at least 2 of the 3 readers.

In the analysis, an MRI was considered positive if at least 2 of 3 readers agreed it met the ASAS MRI working group criteria for defining sacroiliitis by MRI (14). SPARCC scores are presented as the mean total SPARCC scores from all 3 readers. We chose SPARCC score cutoff values of ≥2 and ≥5 to discriminate between low and high SPARCC scores.

Statistical analysis. Categorical data are presented as the number (percent), and continuous data are presented as the mean ± SD or as the median (interquartile range) as appropriate. The chi-square test and Mann-Whitney U test were used for comparing categorical and continuous data, respectively. Interreader agreement on positive/negative MRI

of the SI joints was investigated using Cohen's kappa coefficient and interpreted according to the standards of Landis and Koch (16). Interreader agreement on SPARCC scores was evaluated using intraclass correlation coefficients (ICCs). We performed all analyses in SPSS version 24.0.

RESULTS

Study participants. In total, we evaluated 141 MRIs of the SI joints of 47 healthy participants from the Maasstad MRI project, matched with 47 patients with axial SpA with MRIs positive for sacroiliitis and 47 controls with chronic back pain irrespective of MRI outcome from the SPACE cohort. We also included MRIs of the SI joints of 24 runners from the Maasstad MRI project and 7 women with postpartum back pain (4 from the Maasstad MRI project and 3 from the SPACE cohort). The baseline characteristics of the study population are shown in Table 1.
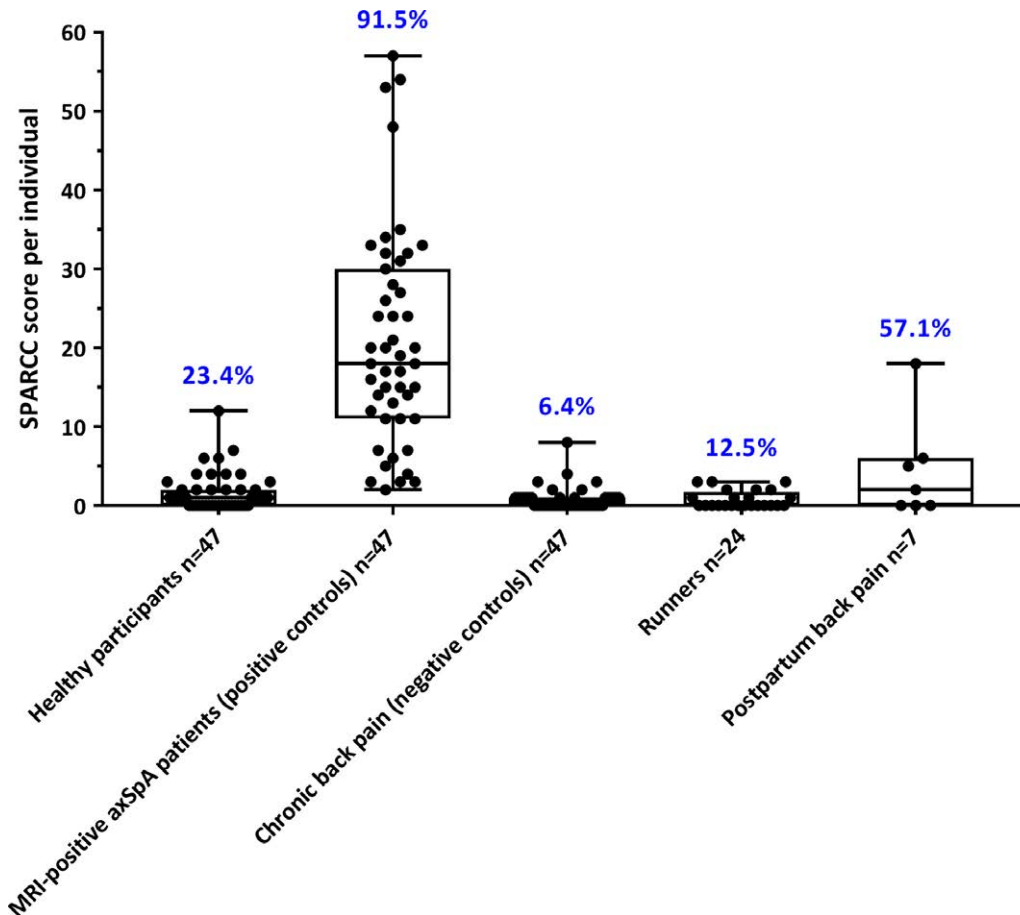
Figure 1. Sacroiliitis on magnetic resonance images (MRIs) of the sacroiliac joints in the study population. Data are shown as box plots. Each box represents the 25th to 75th percentiles. Lines inside the boxes represent the median. Lines outside the boxes represent the minimum and maximum values. Each circle represents a single subject. Values shown above the box plots are the percentage of subjects with an MRI indicating sacroiliitis according to the Assessment of SpondyloArthritis international Society definition. For positive controls and negative controls, "positive" and "negative" refer to the final diagnosis (axial spondyloarthritis [axSpA] or no axial SpA) after vigorous diagnostic evaluation, and not to the MRI result per se. SPARCC = Spondyloarthritis Research Consortium of Canada.

Table 2. Anatomic distribution of bone marrow edema in the SI joint quadrants on MRI*

	Upper ilium		Lower ilium		Upper sacrum		Lower sacrum	
	Anterior	Posterior	Anterior	Posterior	Anterior	Posterior	Anterior	Posterior
Positive MRI of the SI joints (n = 64)	44 (68.8)	34 (53.1)	48 (75.0)	53 (82.8)	39 (60.9)	37 (57.8)	37 (57.8)	43 (67.2)
Negative MRI of the SI joints (n = 108)	4 (3.7)	7 (6.5)	18 (16.7)	16 (14.8)	5 (4.6)	7 (6.5)	3 (2.8)	4 (3.7)
Healthy participants (n = 47)	2 (4.3)	2 (4.3)	10 (21.3)	18 (38.3)	4 (8.5)	2 (4.3)	3 (6.4)	6 (12.8)
Patients with axial SpA (n = 47)	39 (83.0)	34 (72.3)	41 (87.2)	41 (87.2)	33 (70.2)	36 (76.6)	33 (70.2)	35 (74.5)
Controls with chronic back pain (n = 47)	2 (4.3)	4 (8.5)	11 (23.4)	5 (10.6)	3 (6.4)	3 (6.4)	1 (2.1)	2 (4.3)
Runners (n = 24)	4 (16.7)	1 (4.2)	1 (4.2)	2 (8.3)	2 (8.3)	1 (4.2)	1 (4.2)	2 (8.3)
Women with postpartum back pain (n = 7)	1 (14.3)	0 (0)	3 (43.0)	3 (43.0)	2 (28.6)	2 (28.6)	2 (28.6)	2 (28.6)

* Magnetic resonance images (MRIs) that indicated sacroiliitis according to the Assessment of SpondyloArthritis international Society (ASAS) definition were considered positive. Those that did not meet the ASAS definition were considered negative. Values are the number (%). SI = sacroiliac; SpA = spondyloarthritis.

Scoring agreement. The 3 readers agreed moderately well on the absence or presence of BME (absolute agreement within the 3 reader pairs 75%, 76%, and 80%, respectively; Cohen's κ = 0.48, 0.50, and 0.59, respectively). Readers correlated far better on absolute SPARCC scores (ICCs of 0.82, 0.82, and 0.96, respectively).

Scoring results. *Scoring according to the ASAS definition.* Figure 1 shows the proportion of subjects with MRIs positive for sacroiliitis according to the ASAS definition in the different groups. Of the 47 healthy participants, 11 (23.4%) had a positive MRI. Of the 47 positive controls with axial SpA, 43 (91.5%) had a positive MRI, and of the 47 controls with chronic back pain, only 3 (6.4%) had a positive MRI. Of the 24 runners, 3 (12.5%) had a positive MRI, and of the 7 women with postpartum back pain, 4 (57.1%) had a positive MRI.

SPARCC scores. Figure 1 shows the individual and mean SPARCC scores for the different patient categories. The mean ± SD SPARCC score was 1.7 ± 2.4 for the 47 healthy participants, 20.9 ± 13.7 for the 47 positive axial SpA controls, and 0.8 ± 1.4 for the 47 non-SpA back pain controls. The mean ± SD SPARCC score was 0.8 ± 1.1 for the runners and 4.5 ± 6.3 for the 7 women with postpartum back pain.

At a SPARCC cutoff score of ≥2, 12 (25.5%) of the 47 healthy volunteers, 46 (97.9%) of the 47 positive axial SpA controls, 5 (10.6%) of the 47 non-SpA back pain controls, 4 (16.7%) of the 24 runners, and 4 (57.1%) of the 7 women with postpartum back pain were considered to have sacroiliitis on MRI. At a SPARCC cutoff score of ≥5, 4 (8.5%) of the 47 healthy volunteers, 41 (87.2%) of the 47 positive patients with axial SpA, 1 (2.1%) of the 47 patients with chronic back pain, 0 (0%) of the 24 runners, and 2 (28.6%) of the 7 women with postpartum back pain were considered to have sacroiliitis on MRI.

Deep lesions (a homogeneous, unequivocal increase in signal ≥1 cm from the articular surface) were almost exclusively found in positive controls with axial SpA (42 [89.4%] of the 47 had deep lesions). Such lesions

were not found in the healthy volunteers, controls with chronic back pain, or runners and were found in only 1 (14.3%) of the 7 women with postpartum back pain.

Anatomic location of BME. We compared the location of BME in MRIs considered positive for sacroiliitis to those considered negative for sacroiliitis (according to the ASAS definition) (Table 2). In positive MRIs, BME was found most frequently in the posterior lower ilium (in 53 [82.8%] of 64 MRIs). In negative MRIs, BME was found most frequently in the anterior lower ilium (in 18 [16.7%] of 108 MRIs). Overall, BME was most frequently found in the posterior lower ilium (in 69 [40.1%] of 172 MRIs), and least frequently found in the anterior lower sacrum (in 40 [23.3%] of 172 MRIs).

DISCUSSION

The results of our study suggest that 1) one-fourth of asymptomatic healthy individuals and more than half of women presenting with postpartum back pain who do not have axial SpA may have an MRI positive for sacroiliitis according to the ASAS definition, meaning that their MRI lesions are considered highly suggestive of axial SpA by trained readers, 2) frequent runners do not seem to have more lesions than healthy asymptomatic individuals, 3) high SPARCC scores (≥5) rarely occur in healthy individuals, patients with chronic back pain without axial SpA, or runners, 4) deep (extensive) lesions are highly specific for axial SpA–associated sacroiliitis, and 5) BME lesions in healthy participants are preferably but not exclusively located in the lower iliac bone.

Our finding of positive MRIs in healthy individuals is consistent with the findings of Weber and Maksymowych, who showed that 25% of healthy participants have BME lesions on MRIs of the SI joints (17). Our findings of positive MRIs in women with postpartum back pain are also consistent with a previous study showing that 60% of women with postpartum back pain have BME lesions on MRI of the SI joints (18). Differently than we

hypothesized, our data suggest that the proportion of runners with BME lesions on MRI of the SI joints is not higher than the proportion of healthy participants with BME lesions on MRI of the SI joints. However, little demographic or lifestyle data were collected, and our group of healthy participants might have included runners. Further research should correct for possible confounding factors such as body mass index and general health status.

In this study, BME lesions in MRIs scored positive for sacroiliitis and in the MRIs of healthy participants were most frequently found in the posterior lower ilium, which is consistent with data from Weber et al showing a similar preferential location in amateur and professional athletes (19). In patients with axial SpA, lesions occur throughout the SI joints. BME was seen in the anterior lower ilium in 16.7% of the MRIs in which lesions were not highly specific for SpA.

The percentage of patients with chronic back pain with BME lesions was lower than the percentage of healthy volunteers with BME lesions (6.4% versus 23.4%, respectively). This is an artifact caused by channeling patients with an MRI negative for sacroiliitis toward the (non–axial SpA) chronic back pain group, a rational diagnostic approach since a clinical diagnosis of axial SpA (or the exclusion thereof) relies on clinical signs and laboratory findings as well as imaging results (MRI). Similarly, the 91.5% positive MRI rate in the axial SpA group is the consequence of channeling. Prior MRI studies have been used to classify these patients as having axial SpA. As such, the low prevalence of MRI positivity found in the chronic back pain group—and the high prevalence found in the axial SpA group—adds to the credibility of our findings (internal validity).

One of the most important reasons to perform this study is that misclassification of MRIs of the SI joints as positive is a real threat, which may lead to a spuriously high number of patients being diagnosed as having axial SpA. Evidence of such a spurious mechanism has been reported by Arnbak et al (10) and Van Hoeven et al (20), showing that nearly 25% of patients with chronic back pain could be classified as having axial SpA when MRI of the SI joints was the leading factor in the diagnostic consideration. Since we and others have demonstrated that MRIs that are highly suggestive of axial SpA may be seen frequently in unaffected individuals, relying too much on a positive MRI finding will result in overdiagnosis, and consequently in overtreatment, of these patients who may have nonspecific chronic back pain rather than axial SpA.

The only means to avoid overdiagnosis of axial SpA as a diagnostician is to act based on thorough knowledge of the clinical syndrome of axial SpA and MRI abnormalities thereof, to ask for diagnostic MRI of the SI joints only in patients in whom there is a moderately high suspicion of axial SpA (e.g., based on clinical algorithms) (21), and to always consider alternative (more likely) diagnoses before making a diagnosis of axial SpA. A highly specific and sensitive gold standard for axial SpA is lacking (a positive MRI finding can definitely not serve as a gold standard) and the diagnosis of axial SpA relies on skillful pattern recognition rather than on diagnostic imaging. Obviously, the ASAS criteria for axial SpA are not meant to differentiate subjects with no back pain from patients with axial SpA in clinical practice. But the purpose of this study was not to validate the ASAS criteria; this study was undertaken to test the specificity of MRI of the SI joints (and not to test the diagnostic value of MRI of the SI joints). A sound starting point then is to compare 2 extreme groups. Therefore, in this study we included patients with chronic back pain who do not meet the ASAS classification criteria as a negative control group, and have contrasted them to patients with axial SpA formerly judged to have positive MRI findings who do meet the ASAS classification criteria as a positive control group.

Our finding that deep (extensive) lesions appeared almost exclusively in axial SpA controls has not been observed before and needs confirmation in another cohort of patients with axial SpA. This finding may help to create a stricter definition of a positive finding on MRI of the SI joints indicating axial SpA, so that overdiagnosis of axial SpA (and associated health care expenses) will be limited.

Our study has important strengths. The three readers who had received standardized training were completely blinded with regard to all of the clinical information and information regarding the hospital of recruitment during the scoring process. The study set was a deliberate mix of previously positive and previously negative control MRIs, derived from the SPACE cohort, in order to constrain bias by reader expectation. These controls were matched for sex and age. Most importantly, though, the experienced readers were instructed (and agreed) to only score according to ASAS guidelines, which indicates that only MRI findings that are highly suggestive of axial SpA should be considered positive, and MRIs of the SI joints with solitary white spots, which may count in the SPARCC scoring system, should be considered negative. The not more than moderate interreader agreement obtained among these experienced and trained readers testifies to the inherent difficulty of interpreting the ASAS definition that starts with "lesions highly suggestive of axial SpA." Since patients with axial SpA have far more extensive lesions than non-SpA patients or healthy individuals, and this extent is reflected by high SPARCC scores, interreader

agreements based on continuous SPARCC scores were far better. But this finding will not help to avoid misdiagnosis since a diagnosis is based on a binomial choice (positive or negative) rather than on a SPARCC score.

A final strength of this study is that it combined several groups of individuals with and individuals without symptoms in one setting. It allows us to speculate that runners may not show higher rates of MRI positivity than asymptomatic individuals, but that postpartum patients with back pain potentially do.

Our study also has limitations. First, the clinical and demographic information on healthy participants, runners, and women with postpartum back pain was rather limited. Individuals who we considered asymptomatic could still have had SpA-related symptoms that would have been revealed if more data had been obtained according to a study protocol (such as the SPACE protocol). It is unlikely that the 25% of MRIs that were classified as positive were related to undiagnosed or early axial SpA, since individuals with any sign of current or past back pain were excluded. Second, the groups of runners and women with postpartum back pain were rather small, due to reasons of convenience, and therefore conclusions should be drawn with caution. Third, this study focused exclusively on inflammatory lesions. To date, however, it is unclear if potential refining of SpA-specific inflammatory lesions or alternatively combining information on inflammation and structural changes may help in the diagnosis of axial SpA (14). Fourth, the arbitrary threshold of back pain starting within 3 months after delivery in the group of women with postpartum back pain was not supported by the literature. However, it was our aim to include only women in whom incident back pain was most likely related to delivery. Fifth, in this study, different MRI scanners were used, which in theory may violate the blinding of the readers and thus contribute to a biased result, but several MRI scanners were used across subgroups, and the same type of MRI scanner was used in different subgroups, so we conclude that such a form of expectation bias is highly unlikely.

Finally, readers agreed only moderately on the presence or absence of BME. Interreader agreement is dependent on several factors, including the quality of the images, the presence of a unique protocol, and the level of training of the readers. This study included patients and individuals from different sources, scanned with different machines, by different technicians, using slightly different protocols, as in common clinical practice. This level of variability has an impact on measurement error. While readers were trained in a standardized manner, the variability in the quality of the images likely resulted in kappa values that were slightly lower than values obtained in, for example, randomized controlled trials or cohort studies conducted under a protocol. Given these limitations and considering the high level of interreader agreement on SPARCC scores, the interreader agreement in this study is still very acceptable.

We conclude that a substantial proportion of healthy and asymptomatic individuals, runners, and women with postpartum back pain may have positive findings on MRI of the SI joints that are highly suggestive, but not reflective, of axial SpA. Patients with axial SpA have more extensive lesions (reflected by SPARCC scores ≥5 and the presence of deep lesions) than healthy, asymptomatic individuals.

ACKNOWLEDGMENTS

AUTHOR CONTRIBUTIONS

All authors were involved in drafting the article or revising it critically for important intellectual content, and all authors approved the final version to be published. Dr. de Winter had full access to all of the data in the study and takes responsibility for the integrity of the data and the accuracy of the data analysis.
Study conception and design. de Winter, van Hoeven, Baeten, van der Heijde, Weel, Landewé.
Acquisition of data. de Winter, de Hooge, de Jong, van Hoeven, de Koning, Berg, Ramonda, Baeten, van der Heijde, Weel.
Analysis and interpretation of data. de Winter, de Hooge, van de Sande, Baeten, van der Heijde, Landewé.

ADDITIONAL DISCLOSURES

REFERENCES

1. Reveille JD, Witter JP, Weisman MH. Prevalence of axial spondylarthritis in the United States: estimates from a cross-sectional survey. Arthritis Care Res (Hoboken) 2012;64:905–10.
2. Dougados M, Baeten D. Spondyloarthritis. Lancet 2011;377: 2127–37.
3. Rudwaleit M, van der Heijde D, Landewé R, Listing J, Akkoc N, Brandt J, et al. The development of Assessment of Spondylo-Arthritis international Society classification criteria for axial spondyloarthritis (part II): validation and final selection. Ann Rheum Dis 2009;68:777–83.
4. Dougados M, Sepriano A, Molto A, van Lunteren M, Ramiro S, de Hooge M, et al. Sacroiliac radiographic progression in recent onset axial spondyloarthritis: the 5-year data of the DESIR cohort. Ann Rheum Dis 2017;76:1823–8.
5. Ciurea A, Scherer A, Exer P, Bernhard JJ, Dudler J, Beyeler B, et al. Tumor necrosis factor α inhibition in radiographic and non-radiographic axial spondyloarthritis: results from a large observational cohort. Arthritis Rheum 2013;65:3096–106.
6. Blachier M, Canouï-Poitrine F, Dougados M, Lethuaut A, Fautrel B, Ferkal S, et al. Factors associated with radiographic lesions in early axial spondyloarthritis: results from the DESIR cohort. Rheumatology (Oxford) 2013;52:1686–93.

7. Heuft-Dorenbosch L, Weijers R, Landewé R, van der Linden S, van der Heijde D. Magnetic resonance imaging changes of sacroiliac joints in patients with recent-onset inflammatory back pain: inter-reader reliability and prevalence of abnormalities. Arthritis Res Ther 2006;8:R11.

8. Van den Berg R, Lenczner G, Thévenin F, Claudepierre P, Feydy A, Reijnierse M, et al. Classification of axial SpA based on positive imaging (radiographs and/or MRI of the sacroiliac joints) by local rheumatologists or radiologists versus central trained readers in the DESIR cohort. Ann Rheum Dis 2015;74:2016–21.

9. Weber U, Lambert RG, Østergaard M, Hodler J, Pedersen SJ, Maksymowych WP. The diagnostic utility of magnetic resonance imaging in spondylarthritis: an international multicenter evaluation of one hundred eighty-seven subjects. Arthritis Rheum 2010;62:3048–58.

10. Arnbak B, Grethe Jurik A, Hørslev-Petersen K, Hendricks O, Hermansen LT, Loft AG, et al. Associations between spondyloarthritis features and magnetic resonance imaging findings: a cross-sectional analysis of 1,020 patients with persistent low back pain. Arthritis Rheumatol 2016;68:892–900.

11. Deodhar A. Sacroiliac joint magnetic resonance imaging in the diagnosis of axial spondyloarthritis: "a tiny bit of white on two consecutive slices" may be objective, but not specific [editorial]. Arthritis Rheumatol 2016;68:775–8.

12. Van Hoeven L, Luime JJ, de Buck PD, Hazes JM, Weel AE. Bone marrow edema and structural lesions in the sacroiliac joint in a large cohort of patients with axial spondyloarthritis, chronic low back pain and healthy controls [abstract]. Arthritis Rheum 2013;65 Suppl:S1239.

13. Van den Berg R, de Hooge M, van Gaalen F, Reijnierse M, Huizinga T, van der Heijde D. Percentage of patients with spondyloarthritis in patients referred because of chronic back pain and performance of classification criteria: experience from the Spondyloarthritis Caught Early (SPACE) cohort. Rheumatology (Oxford) 2013;52:1492–9.

14. Lambert RG, Bakker PA, van der Heijde D, Weber U, Rudwaleit M, Hermann KG, et al. Defining active sacroiliitis on MRI for classification of axial spondyloarthritis: update by the ASAS MRI working group. Ann Rheum Dis 2016;75:1958–63.

15. Maksymowych WP, Inman RD, Salonen D, Dhillon SS, Krishnananthan R, Stone M, et al. Spondyloarthritis Research Consortium of Canada magnetic resonance imaging index for assessment of spinal inflammation in ankylosing spondylitis. Arthritis Rheum 2005;53:502–9.

16. Landis JR, Koch GG. The measurement of observer agreement for categorical data. Biometrics 1977;33:159–74.

17. Weber U, Maksymowych WP. Sensitivity and specificity of magnetic resonance imaging for axial spondyloarthritis. Am J Med Sci 2011;341:272–7.

18. Eshed I, Miloh-Raz H, Dulitzki M, Lidar Z, Aharoni D, Liberman B, et al. Peripartum changes of the sacroiliac joints on MRI: increasing mechanical load correlating with signs of edema and inflammation kindling spondyloarthropathy in the genetically prone. Clin Rheumatol 2015;34:1419–26.

19. Weber U, Jurik AG, Zejden A, Larsen E, Jørgensen SH, Rufibach K, et al. Bone marrow oedema in sacroiliac joints of young athletes shows most frequently in the posterior inferior ilium. Ann Rheum Dis 2017;76 Suppl 2:101.

20. Van Hoeven L, Luime J, Han H, Vergouwe Y, Weel A. Identifying axial spondyloarthritis in Dutch primary care patients, ages 20–45 years, with chronic low back pain. Arthritis Care Res (Hoboken) 2014;66:446–53.

21. Van den Berg R, de Hooge M, Rudwaleit M, Sieper J, van Gaalen F, Reijnierse M, et al. ASAS modification of the Berlin algorithm for diagnosing axial spondyloarthritis: results from the SPondyloArthritis Caught Early (SPACE)-cohort and from the Assessment of SpondyloArthritis international Society (ASAS)-cohort. Ann Rheum Dis 2013;72:1646–53.

Clinical Evolution in Patients With New-Onset Inflammatory Back Pain

A Population-Based Cohort Study

Runsheng Wang,[1] Cynthia S. Crowson,[2] Kerry Wright,[2] and Michael M. Ward[3]

Objective. Inflammatory back pain (IBP) is often an early manifestation of spondyloarthritis (SpA), but the prognosis of patients with incident IBP is unknown. This study was undertaken to investigate long-term outcomes in patients with IBP, and predictors of progression to SpA, in a population-based cohort.

Methods. We conducted a retrospective, longitudinal study using the Rochester Epidemiology Project, a longstanding population-based cohort of residents of Olmsted County, MN. Patients ages 16–35 years with clinical visits for back pain from 1999 to 2003 were identified, and we screened these patients for the presence of new-onset IBP and performed medical record reviews to collect data on clinical, laboratory, and imaging features of SpA. Outcomes in these patients were followed up until July 2016. We used survival analysis for competing risks to examine progression to either SpA, a non-SpA diagnosis, or resolution of back pain. Recursive partitioning was used to identify predictors of progression to SpA.

Results. Among 5,304 patients with back pain, we identified 124 patients with new-onset IBP. After a median follow-up of 13.2 years, IBP had progressed to SpA in 39 patients, 15 patients developed a non-SpA diagnosis, and 58 patients had resolution of IBP. At 10 years, the probability of having SpA was 30%, while the probability of resolution of IBP was 43%. The most important predictors for progression to SpA were uveitis, male sex, and family history of SpA.

Conclusion. In a minority of patients, new-onset IBP progresses to SpA, while IBP resolves in many. That IBP often resolves may explain the difference between the prevalence of IBP (3–6%) and the prevalence of SpA (0.4–1.3%).

[1]Runsheng Wang, MD, MHS: Columbia University College of Physicians and Surgeons, New York, New York, and National Institute of Arthritis and Musculoskeletal and Skin Diseases, NIH, Bethesda, Maryland; [2]Cynthia S. Crowson, PhD, Kerry Wright, MBBS: Mayo Clinic, Rochester, Minnesota; [3]Michael M. Ward, MD, MPH: National Institute of Arthritis and Musculoskeletal and Skin Diseases, NIH, Bethesda, Maryland.

Address correspondence to Runsheng Wang, MD, MHS, Columbia University College of Physicians and Surgeons, P & S Building, Suite 3450, 630 West 168th Street, New York, NY 10032. E-mail: rw2646@cumc.columbia.edu.

Inflammatory back pain (IBP) is a form of chronic low back pain, typically with gradual onset in young adulthood, characterized by improvement with exercise and worsening with inactivity, and associated with morning stiffness. IBP is commonly considered a sine qua non of spondyloarthritis (SpA), and its presence is considered an indication to refer patients to appropriate specialists for further evaluation (1). It is an important component of the modified New York criteria for ankylosing spondylitis (AS) (2), as well as the recent Assessment of Spondylo-Arthritis international Society (ASAS) classification criteria for axial SpA (3).

The importance of distinguishing IBP from other more common forms of low back pain is evidenced by attempts to codify the unique features of this symptom. The Calin, Berlin, and ASAS criteria for IBP have specificities for a diagnosis of SpA that range from 72% to 91.7% (4–8). With such high specificity, it has been assumed that most patients with IBP either have, or will later develop, SpA.

The prevalence of IBP among adults ages 20–69 years in the US is 5.0–6.0%, based on data from the

2009–2010 National Health and Nutrition Examination Survey (NHANES) (9). In contrast, the prevalence of SpA is estimated to range from 0.4% to 1.3% (10,11). This gap between the prevalence of IBP (the symptom) and the prevalence of SpA (the disease) is unexplained. It could mean that IBP features are common components of back pain due to many different disorders, and that the IBP criteria are less specific when applied to the general population. Alternatively, it could indicate that a substantial number of patients with IBP have inflammatory symptoms that do not evolve to AS or SpA. Although several reports have described the clinical evolution in patients with possible AS or undifferentiated SpA, no studies have specifically examined long-term outcomes in patients with IBP who do not necessarily have other SpA features (12–14).

To address these questions, study of an inception cohort of patients with IBP with a long follow-up is needed, given that it may take up to 10 years from symptom onset to diagnosis of SpA (15). In addition, the study should include patients who present to primary care as well as many diverse specialties, given that many types of providers care for patients with back pain. Therefore, we conducted a retrospective longitudinal study of a population-based cohort from the Rochester Epidemiology Project (REP). Our goal was to determine long-term clinical outcomes in patients with new-onset IBP, and specifically to determine the proportion in whom IBP progressed to a clinical diagnosis of SpA. Finding that IBP progressed to SpA in a large proportion of patients would support the notion that IBP and SpA are tightly linked processes. Alternatively, finding that IBP progressed to conditions other than SpA in many patients would suggest limited specificity of IBP symptoms for a diagnosis of SpA. Finding that IBP resolved in many patients would indicate that IBP can be a self-limited problem. We also sought to identify whether there were subgroups of patients who, based on demographic or clinical characteristics, were more likely to experience progression to SpA.

PATIENTS AND METHODS

Data source and patient inclusion. The REP is a medical record–linkage system with longitudinal medical data on the complete population of Olmsted County, MN (108,095 persons in 2000), with a 98% participation rate in 2000 (16). Medical records from all subspecialties are included, which is particularly important in a retrospective study of IBP. Diagnoses and symptoms present at each visit are extensively coded using both International Classification of Diseases, Ninth Revision (ICD-9) and Hospital International Classification of Diseases Adaptation (HICDA) codes. This study was approved by the institutional review boards of the Mayo Clinic and Olmsted Medical Center, Rochester, MN.

We included Olmsted County residents who had newly identified IBP at an age of 16–35 years between January 1, 1999 and December 31, 2003. These years were chosen because electronic medical records (EMRs) were adopted in 1999, and to allow for at least 12 years of follow-up. Our operational definition of IBP was fulfillment of any 1 of the 3 IBP criteria sets (Calin, Berlin, or ASAS) based on medical record review, or notation of the presence of IBP by a treating rheumatologist (even if the patient did not fulfill any of the 3 criteria sets) (4–6).

Case ascertainment and data collection. We used 3 steps to identify patients with new-onset IBP: 1) electronic searches of medical records for relevant diagnosis and procedure codes, 2) screening of EMRs of potentially eligible back pain visits for implicit diagnosis of IBP, and 3) detailed chart review of those who screened positive for IBP on implicit review to apply explicit IBP criteria. Data are available upon request from the corresponding author.

Specifically, we started with a search for patients ages 16–35 years with a diagnosis of back pain in 2000–2003, using ICD-9 codes and HICDA codes for back pain. A complete list of codes is available upon request from the corresponding author. We excluded patients who had a back pain visit and a diagnosis code for external causes of injury and poisoning (E-code) on the same day, patients who had a back pain visit and a code for pregnancy on the same day, and patients with diagnosis codes for sciatica (ICD-9 724.3) or lumbosacral neuritis (ICD-9 724.4) and a procedure code for laminectomy/discectomy within 1 year of either of these diagnoses. These exclusions were based on preliminary chart reviews that showed that these patients had very low likelihoods of having IBP. Additionally, in preliminary work, the yield of cases of incident IBP was much lower among patients older than 35 years, so we set this as the maximum age at onset for this study.

The initial search identified 5,304 patients who had a medical visit for back pain (not necessarily new-onset back pain) in 2000–2003, at age 16–35. Two rheumatologists (RW and MMW) reviewed the medical records for these back pain visits, and each patient was classified as having "no IBP," "possible IBP," or "definite IBP" based on the reviewers' impression of back pain descriptions. Charts of all patients with "possible IBP" or "definite IBP" were reviewed and confirmed by both reviewers. To ensure the specificity of our cohort, a third rheumatologist (KW) who was not involved in the initial screening also reviewed the records of patients who had been classified as having "possible IBP" and "definite IBP" to confirm or refute the presence of IBP. One investigator (RW) undertook a detailed chart review of the records of patients who had "possible IBP" or "definite IBP."

To identify incident cases, we then identified those who had no back pain visits before January 1, 1999, and who fulfilled our operational definition of IBP, as the inception cohort of patients with IBP. The date that the patient first fulfilled the IBP definition was defined as the IBP incidence date. We also collected demographic information, data on SpA-related clinical features, clinical diagnosis, and laboratory results, including the presence or absence of markers of inflammation and HLA–B27 status, through follow-up until the end of data collection on July 31, 2016. Clinical SpA features included a history of uveitis, peripheral arthritis, psoriasis, dactylitis, enthesitis, inflammatory bowel disease, or reactive arthritis, good response to nonsteroidal antiinflammatory drugs, and family history of SpA, as recorded in the medical records. Clinical features that were

not described or documented in the medical records were considered absent. HLA–B27 was not tested in all patients, and was categorized as positive, negative, or unknown.

The primary outcome was the development of SpA, including either AS according to the modified New York criteria or a clinical diagnosis of SpA, psoriatic arthritis, inflammatory bowel disease–associated arthritis, or reactive arthritis by the treating rheumatologist. Given that all patients satisfied the clinical criterion for IBP, AS was defined as the presence of bilateral grade 2 or unilateral grade 3 or 4 sacroiliitis based on a review of all available pelvis, hip, lumbar spine, and abdominal radiographs by one reader (MMW) (2). Diagnoses other than SpA that explained the patient's back pain symptoms, such as degenerative spine conditions and fibromyalgia, were recorded as well.

For patients who developed SpA, the outcome date was defined as the date of a clinical diagnosis of SpA or the date of the first radiographs that showed sacroiliitis, whichever occurred first. For patients diagnosed as having non-SpA conditions, the outcome date was the date of non-SpA diagnosis. Patients who received no specific diagnosis for their back pain during follow-up were categorized into 1 of 2 outcome groups: 1) those who continued to report back pain on visits within 1 year of their last recorded medical visit were defined as having persistent IBP without a diagnosis of SpA, and 2) those whose back pain was recorded as resolved at a medical visit and did not later recur, or whose last medical visit on which back pain was reported was >1 year prior to their last recorded medical visit, were defined as having IBP resolved. For those whose back pain resolved, the outcome date was the date of the visit documenting the resolution of back pain; when this was not recorded, the midpoint between the date of the last medical visit with back pain and the

date of the last medical visit was used. The remaining patients, whose IBP was persistent without a specific diagnosis throughout follow-up, were censored at their last medical visit. If a patient had both SpA and a non-SpA diagnosis, we designated SpA as the outcome, regardless of whether the non-SpA diagnosis preceded the SpA diagnosis.

Statistical analysis. Descriptive statistics were used to summarize the data. Aalen-Johansen methods, a multistate generalization of cumulative incidence with adjustment for competing risks, were used to examine the progression to 3 outcomes: SpA, a specific non-SpA diagnosis, or resolution of IBP (17).

We performed 2 sensitivity analyses. The first sensitivity analysis included patients who were considered to have "possible IBP" or "definite IBP" by all 3 reviewers and fulfilled the explicit IBP definition. The second sensitivity analysis used the date of onset of back pain, rather than the date of fulfillment of IBP criteria, as the start date for the analysis. In some patients, the reported onset of back pain was months, or occasionally years, earlier than the time when IBP was documented in the medical records, and the time of onset of back pain may reflect the true start of IBP.

We used recursive partitioning methods and Cox proportional hazards models with a time-to-event outcome to identify predictors of progression to SpA. Recursive partitioning identifies predictors that best segregate subgroups with different prognoses. Through its hierarchical tree structure, the method also identifies interactions between predictors that are prognostically influential. Demographic features, clinical SpA features, inflammatory markers, and HLA–B27 status were used as potential predictors in these analyses. Tenfold cross-validation was used to prune the tree by applying a 1 minus standard error

Table 1. Demographic and clinical features of the 124 patients with IBP*

	Main analysis (n = 124)	Sensitivity analysis 1 (n = 113)†
Age at inclusion, mean ± SD years	27.8 ± 5.0	28.0 ± 4.8
Age at onset of back pain, mean ± SD years	25.0 ± 5.5	25.0 ± 5.4
Duration of follow-up, median (IQR) years	13.2 (8.9–14.6)	13.3 (9.2–14.6)
Male	82 (66)	76 (67)
Uveitis	13 (10)	13 (12)
Dactylitis	5 (4)	5 (4)
Enthesitis	18 (15)	17 (15)
Arthritis	8 (6)	8 (7)
IBD	4 (3)	4 (4)
Psoriasis	8 (6)	8 (7)
Reactive arthritis	1 (1)	1 (1)
Family history of SpA	17 (14)	17 (15)
HLA–B27		
Positive	20 (16)	20 (18)
Negative	19 (15)	19 (17)
Not tested	85 (69)	74 (66)
History of smoking	46 (37)	42 (37)
Good response to NSAIDs	51 (41)	49 (43)
Elevated markers of inflammation	16 (13)	16 (14)
Rheumatologist visit	29 (23)	29 (26)
Loss to follow-up, no.	5	5
Number of follow-up radiographs, median (range)	2 (1–6)	2 (1–6)

* Except where indicated otherwise, values are the number (%). IQR = interquartile range; IBD = inflammatory bowel disease; SpA = spondyloarthritis; NSAIDs = nonsteroidal antiinflammatory drugs.

† Included patients who were considered as having "possible inflammatory back pain (IBP)" or "definite IBP" by all 3 reviewers and fulfilled the explicit IBP definition.

rule to the complexity parameter to avoid overfitting. Analyses were performed using R version 3.2.3 (R Foundation for Statistical Computing).
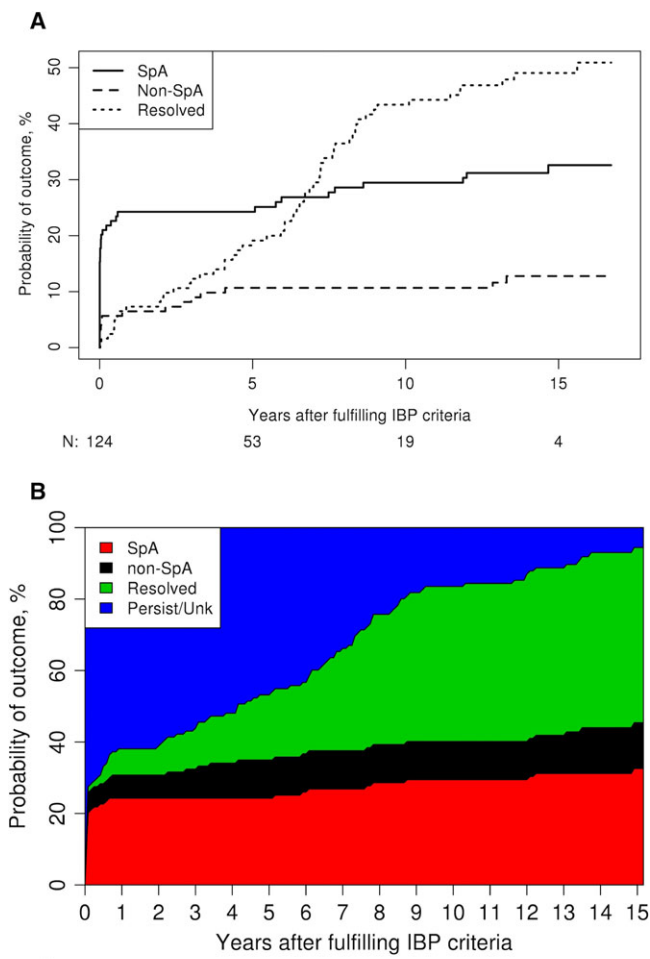
RESULTS

Study cohort. Of 5,304 Olmsted County residents who had clinical visits for back pain at ages 16–35 years, 172 patients had "possible IBP" or "definite IBP" on implicit review (data are available upon request from the corresponding author). After detailed medical record review, 124 patients with new-onset IBP were identified (2.3% of all patients with visits for new back pain) (Table 1). There were 82 men and 42 women in the

Figure 1. Progression from inflammatory back pain (IBP) to spondyloarthritis (SpA), a non-SpA diagnosis, or resolution of back pain (resolved) beginning at the time of fulfillment of IBP criteria. **A,** Cumulative incidence curves for the progression to each outcome. **B,** Area graph showing the proportion of each outcome, including SpA, a non-SpA diagnosis, resolution of back pain, or persistent IBP or unknown status (persist/unk), over time. The n values are the number of patients at risk at each time point.

cohort. The mean ± SD age at inclusion was 27.8 ± 5.0 years. The mean ± SD age at onset of back pain was 25.0 ± 5.5 years. Ninety-two percent of the cohort fulfilled the Calin criteria, 28% fulfilled the Berlin criteria, and 48% fulfilled the ASAS criteria for IBP. Twenty-nine patients (23%) were evaluated at least once by a rheumatologist. In fourteen patients (11%), IBP was explicitly documented by the treating rheumatologist, and 1 of these patients did not fulfill any of the IBP criteria sets. The median duration of follow-up of the cohort was 13.2 years (interquartile range 8.9–14.6 years). The median number of follow-up pelvis or spine radiographs was 2 (range 1–6).

Progression to SpA. At the end of the follow-up period, IBP had progressed to SpA in 39 patients, including 33 patients with AS based on radiographic sacroiliitis and 6 with SpA based on clinical diagnosis by the treating rheumatologist. In 15 patients IBP evolved to non-SpA conditions, including degenerative disc conditions in 9, fibromyalgia in 3, mechanical back pain in 2, and systemic lupus erythematosus in 1 patient. In 58 patients IBP resolved during the follow-up period. Five patients were censored because of loss to follow-up.

The cumulative probabilities that IBP had evolved to SpA at 5, 10, and 15 years were 24% (95% confidence interval [95% CI] 16–31), 30% (95% CI 21–37), and 33% (95% CI 24–42), respectively (Figures 1A and B). The cumulative probabilities that IBP had evolved to a specific non-SpA diagnosis at 5, 10, and 15 years were 11% (95% CI 5–16), 11% (95% CI 5–16), and 13% (95% CI 6–19), respectively. The cumulative probabilities that symptoms of IBP had resolved at 5, 10, and 15 years were 19% (95% CI 12–26), 43% (95% CI 34–52), and 49% (95% CI 39–57), respectively. Of note, within the first year of inclusion, the probability of evolving to SpA was 24% (95% CI 16–31%), and the probability of evolving to a non-SpA diagnosis was 6% (95% CI 2–11%). Results were similar in the sensitivity analysis that included patients who were classified as having IBP by all 3 reviewers (data are available upon request from the corresponding author). In the sensitivity analysis in which follow-up started at the time of back pain onset, the cumulative probabilities that IBP had evolved to SpA at 5, 10, and 15 years were 20% (95% CI 12–26), 27% (95% CI 19–35), and 31% (95% CI 22–38), respectively (Figures 2A and B). The cumulative probabilities that IBP had evolved to a specific non-SpA diagnosis at 5, 10, and 15 years were 7% (95% CI 2–11), 11% (95% CI 5–16), and 12% (95% CI 6–17), respectively. The cumulative probabilities that IBP had resolved at 5, 10, and 15 years were 15% (95% CI 8–21), 36% (95% CI 27–44), and 43% (95% CI 33–51), respectively.

Predictors of progression to SpA. Recursive partitioning identified a history of uveitis, male sex, and family
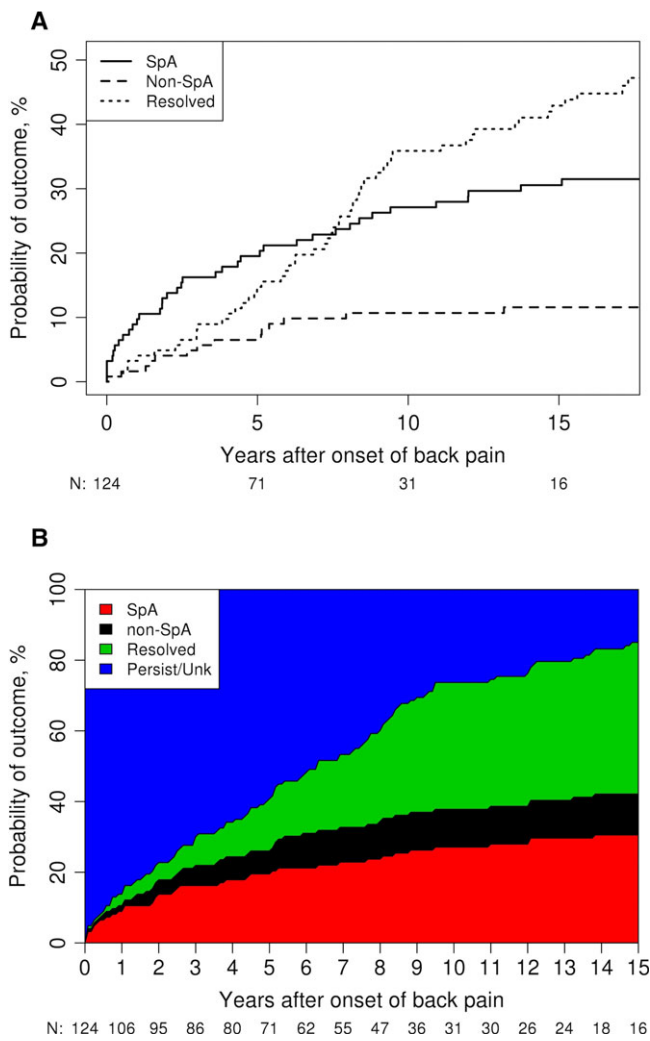
Figure 2. Progression from inflammatory back pain (IBP) to spondyloarthritis (SpA), a non-SpA diagnosis, or resolution of back pain (resolved) beginning at the time of onset of back pain. **A,** Cumulative incidence curves for the progression to each outcome. **B,** Area graph showing the proportion of each outcome, including SpA, a non-SpA diagnosis, resolution of back pain, or persistent IBP or unknown status (persist/unk), over time. The n values are the number of patients at risk at each time point.

history of SpA as the most important predictors of developing SpA (Figure 3). Patients with a history of uveitis had a 5-fold higher risk of developing SpA compared to those without a history of uveitis (hazard ratio [HR] 5.0 [95% CI 2.5–10.2]). Among those without a history of uveitis, men had a 2.7-fold higher risk of SpA compared to women (HR 2.7 [95% CI 1.0–7.1]). Among men with no personal history of uveitis, a family history of SpA increased the risk of developing SpA by 3.2-fold compared to men without a family history of SpA (HR 3.2 [95% CI 1.3–8.1]). Among men with no personal history of uveitis or family history of

SpA, those who were tested for HLA–B27 had a 3-fold higher risk of progression to SpA compared to those who were not tested (HR 3.1 [95% CI 1.2–8.1]).

The absolute risk of having developed SpA 5 years after the onset of IBP ranged from 69% for those with a history of uveitis to 8% for women with no history of uveitis. Risks in other subgroups were intermediate. Other clinical features, such as peripheral arthritis, enthesitis, dactylitis, and inflammatory bowel disease, were not identified as prognostically important.

DISCUSSION

Despite the widespread use of IBP in the diagnosis of SpA, little is known about long-term outcomes in patients with IBP. In this population-based study, we found that IBP progressed to SpA in fewer than one-third of the patients during a follow-up period of >13 years. IBP symptoms resolved in almost one-half of the patients. In our cohort, a history of uveitis was the most important predictor of whether a patient was likely to experience progression to SpA.

The finding that IBP resolved without progression in a large proportion of patients suggests that the symptom complex described by IBP may often reflect a self-limited process. This could represent inflammation that is either not intense enough or not sustained enough to result in established SpA. In this way, IBP should be considered analogous to arthralgia, which may not always be associated with objective arthritis. It could also suggest that IBP is associated with a broader differential diagnosis than solely SpA. In many patients, IBP persisted for several years before resolving, suggesting that inflammation was not always transient.

Alternatively, patients without a true inflammatory cause of back pain may have also reported symptoms of IBP, in part because the language describing morning stiffness and changes with activity or rest can be imprecise (18). Clinicians and patients may interpret and discuss these concepts differently. These patients may have gone on to either be diagnosed with a specific non-SpA disease or have their back pain resolve. Some misclassification could occur due to the limited specificity of the construct or the words used to describe IBP.

Several surveys have been conducted to describe the prevalence of IBP in general populations. In a study conducted in the UK, 20% of patients with back pain fulfilled the Calin criteria for IBP; among them, only 5% had radiographic sacroiliitis (19). In another UK population-based survey, the prevalence of IBP in patients who presented to their primary care provider with back pain ranged from 7.7% to 15.4%, depending on the criteria
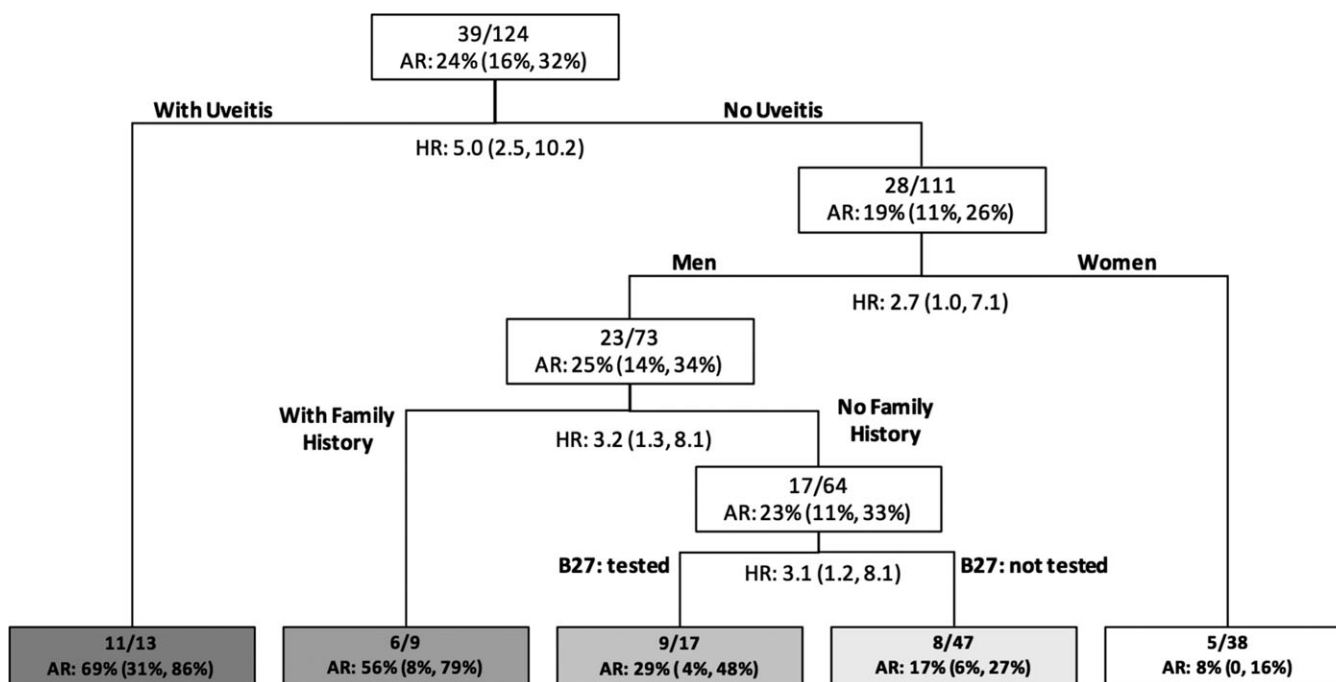
Figure 3. Recursive partitioning model for progression of inflammatory back pain (IBP) to spondyloarthritis (SpA), developed using all predictors. The variable on the top of the tree, history of uveitis, resulted in the best separation of the risk for developing SpA. The hazard ratio (HR) for progression to SpA was 5.0 for the group with a history of uveitis compared to the group without a history of uveitis. These subgroups were then repeatedly split, based on the presence or absence of other clinical features, until the final groups that were most homogeneous for their risk of progression to SpA were obtained. Values are the number of patients in whom IBP progressed to SpA/total number of patients in the group. Values for absolute risk (AR) are the 5-year absolute risk (95% confidence interval [95% CI]).

used (20). The prevalence of IBP in Mexico was estimated at 3.0% (21). In the 2009–2010 NHANES, the prevalence of IBP ranged from 5.0% to 6.0%, depending on the criteria used (9), while the estimated prevalence of SpA in the US is 1.0% (10). Our finding that in the majority of patients IBP does not progress to SpA explains this gap between the prevalence of IBP and that of SpA.

Uveitis was the most important predictor of the development of SpA in this cohort, a finding consistent with the results of a previous study (8). Up to 50% of patients with AS have at least 1 episode of uveitis during the course of their disease (22). Genetic studies of AS and uveitis have shown shared associations with HLA–B27, as well as *IL23R*, *ERAP1*, and the intergenic locus *2p15* (23). In addition, sex and family history also played a role in predicting progression to SpA in patients with IBP. These findings are consistent with the notion that the risk of developing SpA is largely genetically determined. The results also indicate that not all SpA-associated features are equally predictive of progression, and weighting of different features may be useful for this purpose.

In our main analysis, there was a steep increase in SpA at the time patients met the IBP criteria. It is likely that patients had some IBP symptoms for years, and at the time of their initial visit, both IBP and a diagnosis of SpA were identified simultaneously. Because of the design of this study, in which patients were assessed only when they presented for a medical visit rather than at pre-specified time intervals, this analysis may have misspecified the true onset of IBP. We addressed this issue in a sensitivity analysis that used the onset of back pain as time 0, which showed a more gradual progression to SpA.

This study had several limitations due to its retrospective nature. We emphasized specificity in the patients who were included, and likely omitted some cases in which the treating physician failed to recognize or document the presence of IBP features. Misclassification of these patients may have occurred because the patients had less typical or prominent IBP symptoms, and may have been even less likely to experience progression to SpA than patients with typical or prominent IBP symptoms. Patient follow-up was based on clinical need, so those with milder symptoms may not have been reevaluated as frequently. This could have resulted in an underestimation of the progression to SpA. In addition, over time, patients may accommodate to their back pain symptoms, and it may not have remained an active issue during clinical encounters. This could lead to an overestimation

of resolution. In the analysis of predictors of progression, we considered any undocumented clinical feature as not present, which could lead to an underrecognition of some risk factors. Only 31% of patients were tested for HLA–B27, and diagnostic suspicion bias likely contributed to the prognostic importance of the results related to HLA testing. If HLA testing had been done universally, the predictors of progression might have been different. We did not find peripheral arthritis, enthesitis, dactylitis, or inflammatory bowel disease to be prognostically important; however, the sample size in our study may not be large enough to examine these conditions. Medication history was not included in our analysis. These limitations are balanced by the strengths of the study, which is the first population-based study of outcomes in patients with IBP. We also had the advantage of accessing complete medical records over an extended time, which allowed tracking of clinical outcomes.

Our findings indicate that while IBP can be a precursor of SpA, the presence of IBP does not predestine patients to develop SpA. IBP is more accurately considered a symptom complex of a specific type of arthralgia that may or may not be associated with SpA and may be self-limited. Therefore, caution should be taken to not overinterpret the implications of IBP for diagnosis, and to seek objective findings and other aspects of the medical history when counseling patients regarding their prognosis for progression to SpA.

AUTHOR CONTRIBUTIONS

All authors were involved in drafting the article or revising it critically for important intellectual content, and all authors approved the final version to be published. Dr. Wang had full access to all of the data in the study and takes responsibility for the integrity of the data and the accuracy of the data analysis.
Study conception and design. Wang, Ward.
Acquisition of data. Wang, Wright, Ward.
Analysis and interpretation of data. Wang, Crowson, Ward.

REFERENCES

1. Brandt HC, Spiller I, Song I, Vahldiek JL, Rudwaleit M, Sieper J. Performance of referral recommendations in patients with chronic back pain and suspected axial spondyloarthritis. Ann Rheum Dis 2007;66:1479–84.
2. Van der Linden S, Valkenburg HA, Cats A. Evaluation of diagnostic criteria for ankylosing spondylitis: a proposal for modification of the New York criteria. Arthritis Rheum 1984;27:361–8.
3. Rudwaleit M, Landewe R, van der Heijde D, Listing J, Brandt J, Braun J, et al. The development of Assessment of SpondyloArthritis international Society classification criteria for axial spondyloarthritis (part I): classification of paper patients by expert opinion including uncertainty appraisal. Ann Rheum Dis 2009;68:770–6.
4. Calin A, Porta J, Fries JF, Schurman DJ. Clinical history as a screening test for ankylosing spondylitis. JAMA 1977;237:2613–4.
5. Rudwaleit M, Metter A, Listing J, Sieper J, Braun J. Inflammatory back pain in ankylosing spondylitis: a reassessment of the clinical history for application as classification and diagnostic criteria. Arthritis Rheum 2006;54:569–78.
6. Sieper J, van der Heijde D, Landewe R, Brandt J, Burgos-Vagas R, Collantes-Estevez E, et al. New criteria for inflammatory back pain in patients with chronic back pain: a real patient exercise by experts from the Assessment of SpondyloArthritis international Society (ASAS). Ann Rheum Dis 2009;68:784–8.
7. Solmaz D, Akar S, Soysal O, Akkoc Y, Can G, Gerdan V, et al. Performance of different criteria sets for inflammatory back pain in patients with axial spondyloarthritis with and without radiographic sacroiliitis. Clin Rheumatol 2014;33:1475–9.
8. Braun A, Saracbasi E, Grifka J, Schnitker J, Braun J. Identifying patients with axial spondyloarthritis in primary care: how useful are items indicative of inflammatory back pain? Ann Rheum Dis 2011;70:1782–7.
9. Weisman MH, Witter JP, Reveille JD. The prevalence of inflammatory back pain: population-based estimates from the US National Health and Nutrition Examination Survey, 2009–10. Ann Rheum Dis 2013;72:369–73.
10. Helmick CG, Felson DT, Lawrence RC, Gabriel S, Hirsch R, Kwoh CK, et al. Estimates of the prevalence of arthritis and other rheumatic conditions in the United States: Part I. Arthritis Rheum 2008;58:15–25.
11. Reveille JD. Epidemiology of spondyloarthritis in North America. Am J Med Sci 2011;341:284–6.
12. Mau W, Zeidler H, Mau R, Majewski A, Freyschmidt J, Stangel W, et al. Clinical features and prognosis of patients with possible ankylosing spondylitis: results of a 10-year followup. J Rheumatol 1988;15:1109–14.
13. Huerta-Sil G, Casasola-Vargas JC, Londoño JD, Rivas-Ruíz R, Chávez J, Pacheco-Tena C, et al. Low grade radiographic sacroiliitis as prognostic factor in patients with undifferentiated spondyloarthritis fulfilling diagnostic criteria for ankylosing spondylitis throughout follow up. Ann Rheum Dis 2006;65:642–6.
14. Sampaio-Barros PD, Bortoluzzo AB, Conde RA, Costallat LT, Samara AM, Bertolo MB. Undifferentiated spondyloarthritis: a longterm followup. J Rheumatol 2010;37:1195–9.
15. Feldtkeller E, Khan MA, van der Heijde D, van der Linden S, Braun J. Age at disease onset and diagnosis delay in HLA-B27 negative vs. positive patients with ankylosing spondylitis. Rheumatol Int 2003;23:61–6.
16. St Sauver JL, Grossardt BR, Yawn BP, Melton LJ III, Pankratz JJ, Brue SM, et al. Data resource profile: the Rochester Epidemiology Project (REP) medical records-linkage system. Int J Epidemiol 2012;41:1614–24.
17. Putter H, Fiocco M, Geskus RB. Tutorial in biostatistics: competing risks and multi-state models. Stat Med 2007;26:2389–430.
18. Lineker S, Badley E, Charles C, Hart L, Streiner D. Defining morning stiffness in rheumatoid arthritis. J Rheumatol 1999;26:1052–7.
19. Calin A, Kaye B, Sternberg M, Antell B, Chan M. The prevalence and nature of back pain in an industrial complex: a questionnaire and radiographic and HLA analysis. Spine 1980;5:201–5.
20. Hamilton L, Macgregor A, Warmington V, Pinch E, Gaffney K. The prevalence of inflammatory back pain in a UK primary care population. Rheumatology (Oxford) 2014;53:161–4.
21. Peláez-Ballestas I, Flores-Camacho R, Rodriguez-Amado J, Sanin LH, Valerio JE, Navarro-Zarza E, et al. Prevalence of back pain in the community: a COPCORD-based study in the Mexican population. J Rheumatol Suppl 2011;86:26–30.
22. Rosenbaum JT. Uveitis in spondyloarthritis including psoriatic arthritis, ankylosing spondylitis, and inflammatory bowel disease. Clin Rheumatol 2015;34:999–1002.
23. Robinson PC, Claushuis TA, Cortes A, Martin TM, Evans DM, Leo P, et al. Genetic dissection of acute anterior uveitis reveals similarities and differences in associations observed with ankylosing spondylitis. Arthritis Rheumatol 2015;67:140–51.

Inflammation Intensity–Dependent Expression of Osteoinductive Wnt Proteins Is Critical for Ectopic New Bone Formation in Ankylosing Spondylitis

Xiang Li,[1] Jianru Wang,[2] Zhongping Zhan,[1] Sibei Li,[3] Zhaomin Zheng,[2] Taiping Wang,[4] Kuibo Zhang,[5] Hehai Pan,[1] Zemin Li,[1] Nu Zhang,[1] and Hui Liu[2]

Objective. To investigate the molecular mechanism underlying inflammation-related ectopic new bone formation in ankylosing spondylitis (AS).

Methods. Spinal tissues and sera were collected from patients with AS and healthy volunteers and examined for the expression of Wnt proteins. An in vitro cell culture system mimicking the local inflammatory microenvironment of bone-forming sites was established to study the relationship between inflammation and Wnt expression, the regulatory mechanism of inflammation-induced Wnt expression, and the role of Wnt signaling in new bone formation. Modified collagen-induced arthritis (CIA) and proteoglycan-induced spondylitis (PGIS) animal models were used to confirm the key findings in vivo.

Results. The levels of osteoinductive Wnt proteins were increased in sera and spinal ligament tissues from patients with AS. Constitutive low-intensity tumor necrosis factor (TNF) stimulation, but not short-term or high-intensity TNF stimulation, induced persistent expression of osteoinductive Wnt proteins and subsequent bone formation through NF-κB (p65) and JNK/activator protein 1 (c-Jun) signaling pathways. Furthermore, inhibition of either the Wnt/β-catenin or Wnt/protein kinase Cδ (PKCδ) pathway significantly suppressed new bone formation. The increased expression of Wnt proteins was confirmed in both the modified CIA and PGIS models. A kyphotic and ankylosing phenotype of the spine was seen during long-term observation in the modified CIA model. Inhibition of either the Wnt/β-catenin or Wnt/PKCδ signaling pathway significantly reduced the incidence and severity of this phenotype.

Conclusion. Inflammation intensity–dependent expression of osteoinductive Wnt proteins is a key link between inflammation and ectopic new bone formation in AS. Activation of both the canonical Wnt/β-catenin and noncanonical Wnt/PKCδ pathways is required for inflammation-induced new bone formation.

Ankylosing spondylitis (AS) is the most common form of spondyloarthritis (SpA). In addition to inflammatory back pain and damage to bone and joint structures, the characteristic ectopic formation of new bone and fusion of spinal segments in the axial skeleton are key contributors to the AS disease burden (1,2). Although an increasing number of breakthrough findings on AS etiology and symptom-controlling therapy have been published, the mechanism underlying new bone formation has not been equally emphasized or investigated. Consequently, targeted and effective treatments that prevent ankylosis progression have not yet been developed (1).

An understanding of the elusive relationship between chronic inflammation and bone formation is critical to develop a treatment strategy for aberrant new bone formation. Magnetic resonance imaging has been used extensively to analyze their correlation. Vertebral

syndesmophytes are more likely to develop from inflammatory lesions, supporting the notion of a sequential destructive–constructive relationship between inflammation and bone formation. However, the majority of vertebral syndesmophytes develop at sites with no evidence of previous inflammation, suggesting a certain degree of independence (3–7). Contradictory findings have also been reported regarding the outcomes of anti–tumor necrosis factor (anti-TNF) therapy. Most clinical and animal studies have indicated that TNF inhibitor treatment is effective for controlling inflammation-related symptoms but does not prevent the progression of structural changes (7–13). In contrast, recent long-term studies conducted over 5–8 years have indicated that anti-TNF therapy might decrease the progression of new bone formation (14). Nonsteroidal antiinflammatory drugs (NSAIDs) have also been shown to reduce the progression of ankylosis and to counteract the effect of inflammation on disease progression (15,16).

Since bone formation requires critical osteogenic molecules and pathways, inflammation/stress-induced activation of osteogenic signaling pathways is considered a logical link between inflammation and new bone formation (17–21). BMP, Wnt, and hedgehog signaling pathways have previously been investigated and shown to be involved in spinal fusion in patients with AS (17,19). These pathways are activated by either inflammation or mechanical stress (20).

A link between the Wnt signaling pathway and AS was first reported by Diarra et al, who found that Dkk-1, an inhibitor of the canonical Wnt/β-catenin pathway, was expressed at a lower level in patients with AS than in controls and patients with rheumatoid arthritis (RA) (22). In a later study by Appel et al, the expression of another Wnt/β-catenin pathway inhibitor, sclerostin, was demonstrated to be decreased in patients with AS, and this molecule was found to be linked to radiographic progression in AS (23). Since then, accumulating evidence has shown that a low level or dysfunction of Dkk-1 or sclerostin plays a role in new bone formation by enhancing the activity of the canonical Wnt pathway (23–26). However, whether Wnt proteins are overexpressed and correlate with the pathogenesis of this disease has not been determined. Wnt proteins participate in complex pathways that are involved in numerous molecular events. It is well known that the β-catenin–dependent canonical Wnt signaling pathway plays a critical role in osteogenesis. Among the noncanonical pathways, the Wnt/retinoic acid receptor–related orphan nuclear receptor 2, Wnt/p38 MAPK, and Wnt/protein kinase Cδ (PKCδ) pathways have also been shown to be important for bone formation in a β-catenin–independent manner (27–29). However, whether and how

these pathways are involved in ectopic new bone formation in AS remain to be clarified.

In this study, we explored the bridging role of Wnt in the correlation between inflammation and new bone formation in patients with AS. The results of the present study might shed more light on the enigma of inflammation-related new bone formation in AS and facilitate the improvement of therapeutic strategies for slowing ankylosis progression.

MATERIALS AND METHODS

Human tissue. The Medical Ethics Committee of the First Affiliated Hospital of Sun Yat-sen University approved the procedures performed in this study. Seventy-three patients and 35 healthy volunteers were consecutively enrolled at 2 hospitals between September 2013 and December 2015. Written informed consent was obtained from all subjects. Patients with AS fulfilled the modified New York criteria (30). Patient demographic and clinical data are presented in Supplementary Table 1, available on the *Arthritis & Rheumatology* web site at http://onlinelibrary.wiley.com/doi/10.1002/art.40468/abstract. Patients with early-stage AS (a disease duration of <3 years with no significant spinal deformity or ankylosis) were divided into 2 groups according to the absence or presence of syndesmophytes. One group of patients had no vertebral syndesmophytes (modified Stoke Ankylosing Spondylitis Spine Score [mSASSS] <2 in all segments) (31), and the other group presented with ≥1 vertebral syndesmophyte or bony bridging (mSASSS ≥2 in at least 1 segment). By comparison, patients who underwent correction surgeries for fixed and deformed spine were considered to have late-stage AS. (see Supplementary Methods, available on the *Arthritis & Rheumatology* web site at http://onlinelibrary.wiley.com/doi/10.1002/art.40468/abstract). Thirty-nine samples of ligamentum flavum, supraspinous ligament, interspinous ligament (Supplementary Figure 1, available on the *Arthritis & Rheumatology* web site at http://onlinelibrary.wiley.com/doi/10.1002/art.40468/abstract), and bone marrow blood were obtained during spinal surgery, which was performed by senior surgeons, and 108 peripheral venous blood samples were collected from outpatient clinical services.

Cell culture. A preosteoblast cell line, MC3T3-E1 subclone 14, and a monocyte cell line, RAW 264.7, were purchased from ATCC. Rat osteoblasts, human bone marrow stem cells, and human monocytes were isolated, identified, and cultured as previously described (32–36). Additional details are provided in the Supplementary Methods.

To induce osteogenesis, different progenitor cells were plated in a 6-well plate at a density of 2×10^5 cells/well and cultured for 24 hours. The cells were then switched to osteogenic medium consisting of α-minimum essential medium supplemented with 10% fetal bovine serum (FBS), 50 μg/ml L-ascorbic acid, 0.1 μM dexamethasone, and 10 mM β-glycerophosphate to induce osteogenesis. The medium was changed every 3–4 days (37).

RAW 264.7 cells were treated with different doses of TNF for different periods of time to generate conditioned medium or with phosphate buffered saline to generate control conditioned medium. Every 2 days medium was collected and replaced with fresh medium. The collected conditioned medium was concentrated (20:1) by centrifugation at 5,000*g* and 4°C for

30 minutes using a Centricon protein concentrator (Millipore). The concentrated conditioned medium was diluted into fresh medium supplemented with 10% FBS (1:10) and used to induce osteogenesis (2 ml per well of a 6-well plate at a density of 2×10^5/well). The conditioned medium used to induce osteogenesis was generated from RAW 264.7 cells that had been treated with TNF for 14 days.

Real-time quantitative reverse transcription–polymerase chain reaction (qRT-PCR). Total RNA was extracted from cells using TRIzol reagent (Invitrogen), and qRT-PCR was performed to analyze gene expression at the messenger RNA (mRNA) level as previously described (37) (see Supplementary Methods and Supplementary Table 2, available on the *Arthritis & Rheumatology* web site at http://onlinelibrary. wiley.com/doi/10.1002/art.40468/abstract).

Western blot analysis. Cells were lysed in radioimmunoprecipitation assay buffer, total proteins were extracted, and protein concentrations were determined using a bicinchoninic acid assay. Western blotting was performed as previously described (37) (see Supplementary Methods for details).
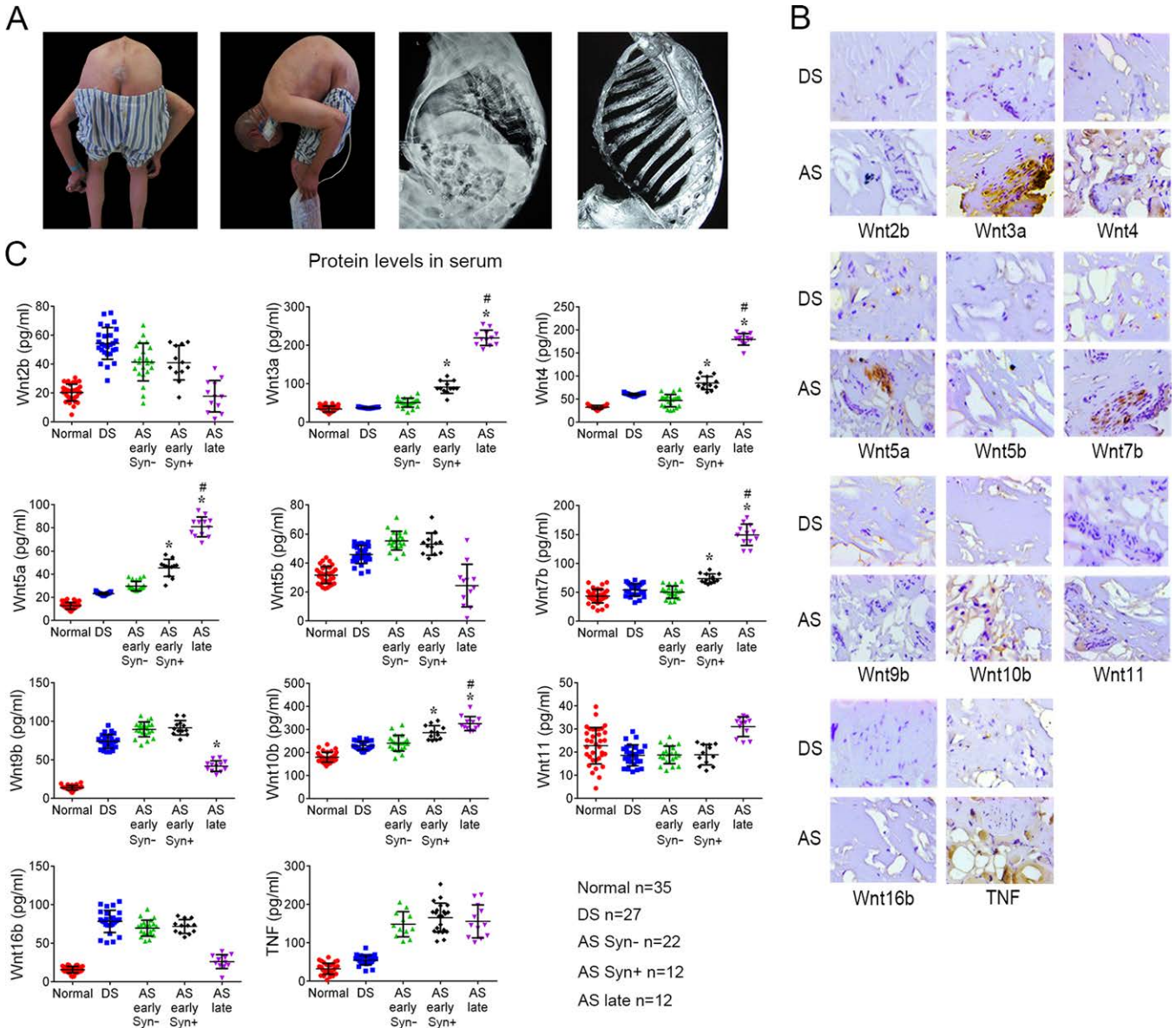
Figure 1. Increased expression of Wnt proteins in spinal tissue and sera from patients with ankylosing spondylitis (AS). **A**, Clinical, radiographic, and computed tomography images of a patient with severe AS. **B**, Immunohistochemical staining of Wnt proteins and tumor necrosis factor (TNF) in spinal tissue from patients with AS or degenerative spine diseases (DS). **C**, Enzyme-linked immunosorbent assay analyses of serum Wnt proteins and TNF levels in patients with AS, patients with degenerative spine diseases, and healthy controls. Bars show the mean ± SD of triplicate experiments. * = $P < 0.05$ versus healthy controls, patients with degenerative spine diseases, and patients with AS without syndesmophytes (Syn–); # = $P < 0.05$ versus patients with AS with syndesmophytes (Syn+).

Enzyme-linked immunosorbent assay (ELISA). Cells were stimulated with different concentrations of TNF for different durations. Briefly, the protein levels of Wnts, Dkk-1, and TNF in cell culture supernatants and sera were determined using an ELISA kit according to the recommendations of the manufacturer (HuaMei). The sensitivity of ELISA for all proteins was 10 pg/ml.

Luciferase reporter assay. RAW 264.7 cells were plated at a density of 1×10^4 cells/cm^2 and transfected with a mixture of luciferase reporter plasmids (Promega), according to the manufacturer's instructions. Luciferase activity was measured with a Luciferase assay kit (Promega). The data were normalized to *Renilla* luciferase activity, and relative luciferase units were calculated as the ratio of firefly luciferase activity to *Renilla* luciferase activity.

Chromatin immunoprecipitation (ChIP) assay. RAW 264.7 cell lysates were analyzed with a ChIP assay kit (Upstate Biotechnology), according to the manufacturer's instructions. Anti-p65 and anti–c-Jun antibodies were used to immunoprecipitate DNA protein complexes, and IgG alone was used as a negative control.

Determination of culture mineralization. Alizarin red staining and Von Kossa's staining were used to determine calcium deposition and calcium phosphate–containing nodules and indicate mineralization as previously described (33,37) (see Supplementary Methods, available on the *Arthritis & Rheumatology* web site at http://onlinelibrary.wiley.com/doi/10. 1002/art.40468/abstract).

Establishment of animal models. DBA/1 mice and BALB/c mice were purchased from Charles River. Modified collagen-induced arthritis (CIA) was induced as described in the Supplementary Methods. The CIA model used in the present study differed in 3 main features from the standard CIA model, which has been used extensively in studies of RA. First, only male DBA/1 mice were used for induction in the present study, while female mice have been found to be more susceptible to RA. Second, the observation period in the present study was not less than 30 weeks. Finally, we investigated not only peripheral joint remodeling but also spinal morphologic changes. The DBA/1 mouse model of spontaneous arthritis and proteoglycan-induced spondylitis (PGIS) were induced using previously described standard methods (12,21,22,38–40) (see Supplementary Methods for details). The Animal Ethics Committee of the First Affiliated Hospital of Sun Yat-sen University approved all animal experiments.

Micro–computed tomography (micro-CT) analysis and histologic analysis. Lumbar spine (spinal segment including intervertebral disc and adjacent end plates) and hind paw specimens were obtained from mice postmortem and fixed with 4% paraformaldehyde. For micro-CT scanning, specimens were fitted in a cylindrical sample holder and scanned using a Scanco μCT40 scanner set to 55 kVp and 70 μA. For visualization, the segmented data were imported and reconstructed as 3-dimensional images using MicroCT Ray V3.0 software (Scanco Medical). Kyphotic angles were measured using the Cobb angle as previously described (41–44) (see Supplementary Methods) with reliability analysis. Quantification of the Cobb angle was performed only in mice with pathologic kyphosis.

For histologic analysis, specimens were decalcified in 0.5*M* EDTA (Sigma-Aldrich) at 4°C. Paraffin-embedded sections were stained with hematoxylin and eosin (H&E) to evaluate general structures and with alizarin red to evaluate bone

formation. Immunohistochemical analysis of the specimens was conducted using specific antibodies. Tissue sections were quantitated according to the percentage of positive cells as previously described (45). The proportion of positive cells per visual field was calculated using the number of positive cells as the numerator and the number of total cells as the denominator.

Statistical analysis. Statistical significance was analyzed via one-way analysis of variance with Levene's test for homogeneity of variance, followed by the Bonferroni post hoc test or Dunnett's T3 post hoc test based on the comparison to be made and the statistical indication of each test. *P* values less than 0.05 were considered significant. Analyses were performed using SPSS software for Windows, version 16.0.

RESULTS

Expression of Wnt proteins in spinal ligaments and sera from patients with AS. To determine whether Wnt played a role in new bone formation in AS, we first examined the expression of Wnt proteins in spinal ligament tissue (ligamentum flavum, supraspinous ligament, and interspinous ligament) and serum samples (see Supplementary Figure 1, available on the *Arthritis & Rheumatology* web site at http://onlinelibrary.wiley.com/doi/10. 1002/art.40468/abstract) from patients with AS who underwent correction surgeries (Figure 1A). Wnt3a, Wnt4, Wnt5a, Wnt7b, and Wnt10b were found to be more highly expressed in spinal ligament tissue from patients with late-stage AS than patients with degenerative spine diseases (Figure 1B). Wnt3a, Wnt4, Wnt5a, Wnt7b, and Wnt10b were found to be expressed at significantly higher levels in sera from patients with early-stage AS with vertebral syndesmophytes, as well as patients with late-stage AS, than in healthy controls, patients with degenerative spine diseases, and patients with early-stage AS without vertebral syndesmophytes (Figure 1C). TNF was expressed at significantly higher levels in sera from both patients with early-stage AS and those with late-stage AS than in sera from healthy controls and patients with degenerative spine diseases (Figure 1C).

TNF induces Wnt expression in a dose- and time-dependent manner. In inflammatory bone diseases, monocytes are recruited and interact with cells of the osteogenic lineage by expressing anabolic and catabolic cytokines in both an autocrine and paracrine manner. To determine whether Wnt expression was induced by inflammatory stimulation, we stimulated a monocyte cell line, RAW 264.7, and human monocytes with TNF. Human monocytes were identified using previously described methods (36) (Supplementary Figure 2 and Supplementary Methods, available on the *Arthritis & Rheumatology* web site at http://onlinelibrary.wiley. com/doi/10.1002/art.40468/abstract). After conducting a cytotoxicity assay (Supplementary Figure 3, available
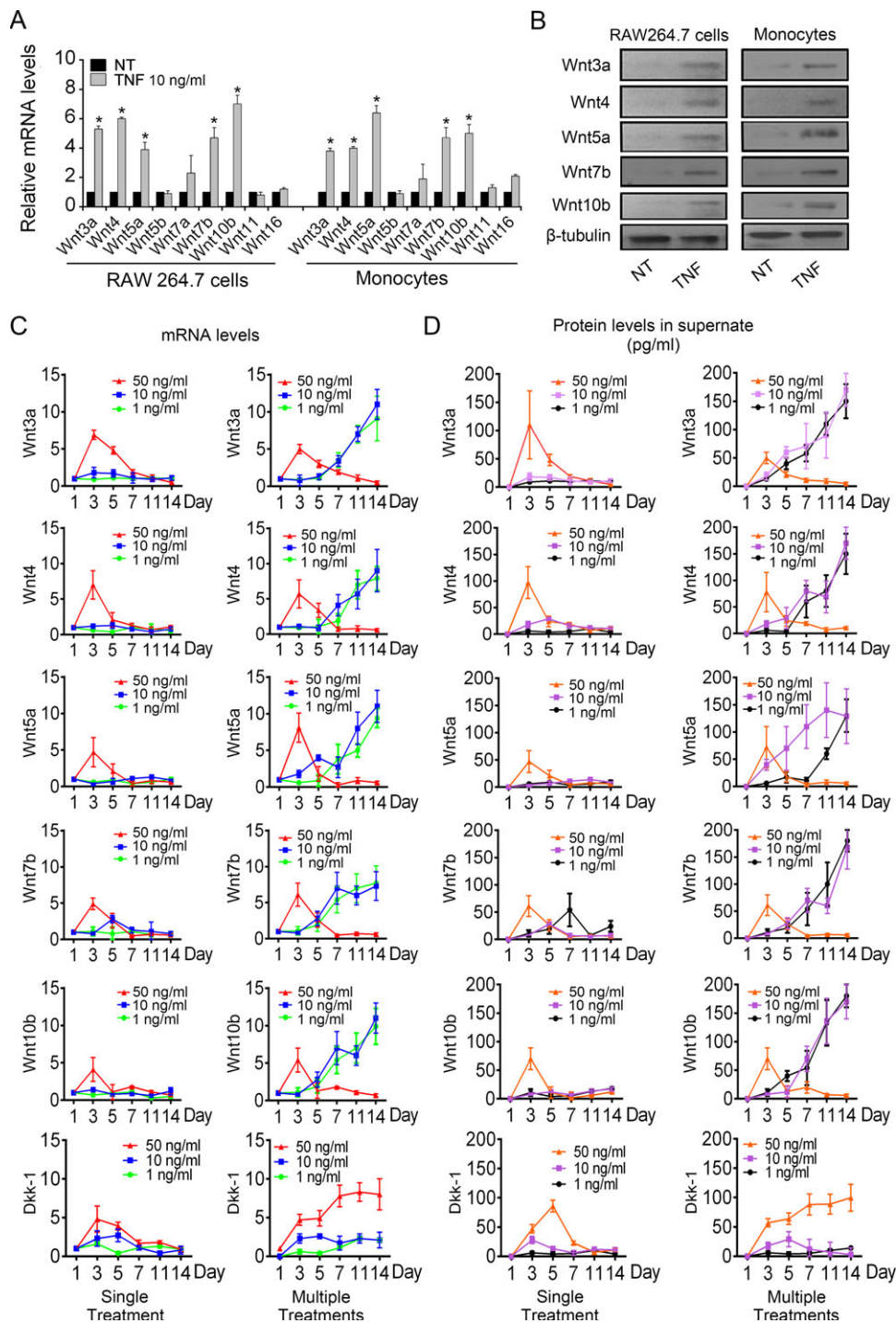
Figure 2. Induction of Wnt and Dkk-1 expression by tumor necrosis factor (TNF). TNF induced Wnt expression in a dose- and time-dependent manner. **A** and **B**, Quantitative reverse transcription–polymerase chain reaction (RT-PCR) (**A**) and Western blot analysis (**B**) of Wnt expression in RAW 264.7 cell and human monocyte cell cultures treated with TNF (10 ng/ml every 48 hours) or left untreated (not treated [NT]). $*$ = $P < 0.05$. **C** and **D**, Quantitative RT-PCR analysis (**C**) and enzyme-linked immunosorbent assay (**D**) of Wnt and Dkk-1 expression in RAW 264.7 cells stimulated with single treatments of TNF or multiple treatments of TNF (addition of fresh cytokine every 48 hours). Values are the mean ± SD from 1 representative experiment of 3 independent experiments each performed in triplicate. Color figure can be viewed in the online issue, which is available at http://onlinelibrary.wiley.com/doi/10.1002/art.40468/abstract.

on the *Arthritis & Rheumatology* web site at http://onlinelibrary.wiley.com/doi/10.1002/art.40468/abstract), we defined doses of 1 ng/ml and 10 ng/ml TNF as low-intensity inflammatory stimulation and a dose of 50 ng/ml TNF as high-intensity inflammatory stimulation.

TNF efficiently induced Wnt expression at both the mRNA and protein levels on day 7 (Figures 2A and B). Based on the results of a subsequent expression profile study, constitutive stimulation with a low-dose of TNF (1 ng/ml or 10 ng/ml, with multiple treatments every 48 hours) resulted in a persistent increase in Wnt expression but no increase in Dkk-1 expression at the mRNA level. In contrast, high-dose (50 ng/ml) or short-term (single treatment for 48 hours) stimulation with TNF resulted in increased Wnt expression in a pulsed manner or had no inductive effect. However, it increased the expression of Dkk-1, which is a well-known suppressor of bone formation (Figures 2C and D). Thus, only constitutive low-intensity inflammation induces persistent Wnt expression, while high-intensity inflammation induces expression of the Wnt antagonist Dkk-1.

Conditioned medium from cells constitutively stimulated with a low dose of TNF promotes bone formation in vitro. To clarify the correlation between inflammation and new bone formation, we established an in vitro cell culture system to mimic the inflammatory microenvironment of enthesitis, which contained the key elements of inflammatory bone-forming sites. The model included proinflammatory cells, osteoprogenitor cells, and the critical proinflammatory cytokine TNF. A similar in vitro cell culture system has been used to investigate the inflammatory microenvironment associated with tumorigenesis (46). We collected conditioned medium from RAW 264.7 cells treated with different doses of TNF for 14 days and then used it to stimulate different types of osteoprogenitors. Nodule formation by human bone mesenchymal stem cells, rat osteoblasts, and the MC3T3-E1 preosteoblast cell line was significantly increased following stimulation with conditioned medium from monocytes constitutively treated with a low dose of TNF. In contrast, conditioned medium from cells constitutively stimulated with a high dose of TNF or stimulated for a short duration did not significantly affect nodule formation (Figures 3A–F and Supplementary Figure 4). Similar inductive effects on the expression of osteogenic genes, including *RUNX2*, *Osx*, *ALP*, and *OCN*, were observed 24 hours after induction (Figures 3G–I). These results indicate that only constitutive low-intensity inflammation is osteoinductive.

Essential role of Wnt expression in bone formation induced by conditioned medium from cells stimulated with TNF. To explore whether Wnt proteins played a critical role in osteogenesis induced by TNF-stimulated conditioned medium, Wnt gene expression was knocked down with small interfering RNAs (siRNAs) targeting different Wnts (Supplementary Table 3, available on the *Arthritis & Rheumatology* web site at http://onlinelibrary.wiley.com/doi/10.1002/art.40468/abstract) and then bone formation was evaluated. Wnt expression was successfully silenced in RAW 264.7 cells (Supplementary Figure 5, available on the *Arthritis & Rheumatology* web site at http://onlinelibrary.wiley.com/doi/10.1002/art.40468/abstract), and nodule formation by MC3T3-E1 preosteoblasts was significantly decreased in the presence of conditioned medium from these RAW 264.7 cells stimulated with TNF compared to control conditioned medium (Figures 3J and K). Similar effects on the expression of osteogenic genes were observed 24 hours after induction (Figure 3L). These results suggest that the osteoinductive effect of conditioned medium from cells stimulated with TNF depends on Wnt proteins. We evaluated the osteoinductive capacity of each Wnt family member and provide the first comparative evidence showing that Wnt3a, Wnt4, Wnt5a, Wnt5b, Wnt7b, Wnt10b, Wnt11, and Wnt16b are osteoinductive proteins within an identical experimental system (Supplementary Figures 6 and 7, available on the *Arthritis & Rheumatology* web site at http://onlinelibrary.wiley.com/doi/10.1002/art.40468/abstract).

Both canonical and noncanonical Wnt signaling pathways are required for bone formation induced by conditioned medium from TNF-stimulated cells. To elucidate the involvement of Wnt pathways in bone formation induced by constitutive low-intensity inflammation, we examined the roles of 2 acknowledged osteogenic pathways, the Wnt/β-catenin and Wnt/PKCδ pathways, in osteogenesis using our TNF-stimulated conditioned medium–induced in vitro cell culture system of bone formation. The Wnt/β-catenin pathway inhibitor Dkk-1 and the Wnt/PKCδ pathway inhibitor Rottlerin significantly suppressed TNF-stimulated conditioned medium–induced nodule formation by different types of osteoprogenitors. Combined treatment with both inhibitors further decreased nodule formation (Figures 3M and N). Similarly, knockdown of β-catenin or PKCδ gene expression with siRNAs in osteoprogenitors (Supplementary Figure 5) significantly decreased nodule formation induced by conditioned medium from TNF-stimulated cells. Knockdown of both β-catenin and PKCδ resulted in further inhibition of nodule formation (Figures 3M and N). Similar inhibitory effects of inhibitors of these pathways on the expression of osteogenic genes were observed 24 hours after induction (Figure 3O). These results suggest that activation of both the canonical and noncanonical Wnt signaling pathways is required for inflammation-induced osteogenesis.
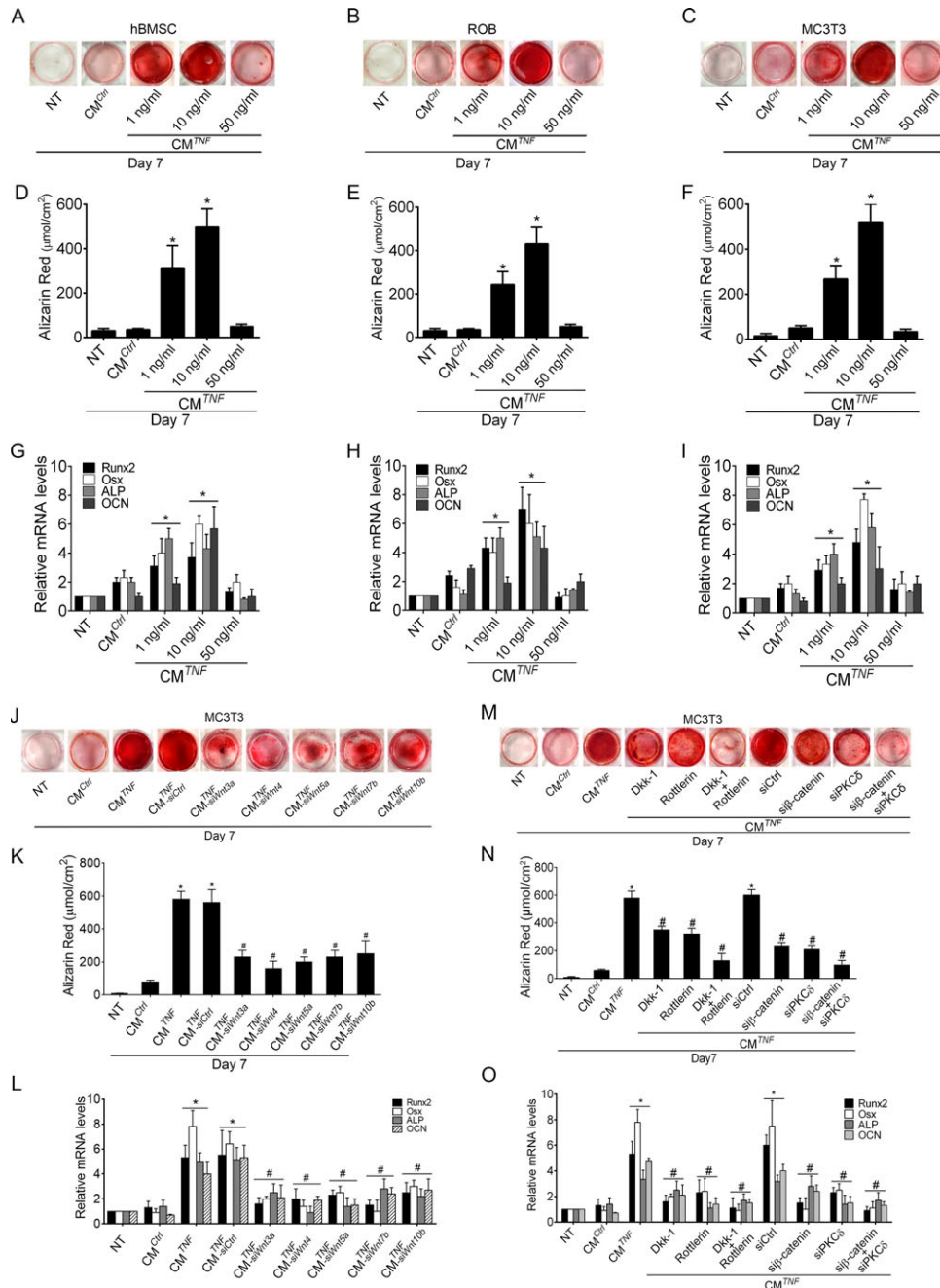
Figure 3. Essential role of Wnt signaling in bone formation induced by conditioned medium from cells stimulated with tumor necrosis factor (TNF) (CM^{TNF}). **A–C**, Alizarin red staining of human bone marrow stem cell (hBMSC) (**A**), rat osteoblast (ROB) (**B**), and MC3T3 (**C**) osteoprogenitor cells cultured in conditioned medium produced from RAW 264.7 cells stimulated with the indicated doses of TNF, cultured in control conditioned medium (CM^{Ctrl}), or left untreated (NT). **D–F**, Quantification of the results shown in **A–C** with absorbance at 450 nm (A$_{450\ nm}$). **G–I**, Quantitative reverse transcription–polymerase chain reaction (RT-PCR) analyses of osteogenesis markers. **J**, Alizarin red staining of MC3T3 cells stimulated with TNF-stimulated conditioned medium produced from RAW 264.7 cells transfected with individual Wnt small interfering RNAs (siRNAs) or the corresponding controls. **K**, Quantification of the results shown in **J** (A$_{450\ nm}$). **L**, Quantitative RT-PCR analyses of osteogenesis markers in MC3T3 cells treated with TNF-stimulated conditioned medium produced from RAW 264.7 cells transfected with individual Wnt siRNAs or the corresponding controls. **M**, Alizarin red staining of MC3T3 cells treated with β-catenin and protein kinase Cδ (PKCδ) inhibitors or transfected with β-catenin and PKCδ siRNAs and then treated with TNF-stimulated conditioned medium or the corresponding controls. **N**, Quantification of the results shown in **M** (A$_{450\ nm}$). **O**, Quantitative RT-PCR analyses of osteogenesis markers in MC3T3-E1 cells treated with β-catenin and PKCδ inhibitor or transfected with β-catenin and PKCδ siRNAs induced with TNF-stimulated conditioned medium or the corresponding controls. In **D–I** and **K–O**, bars show the mean ± SD from 1 representative experiment of 3 independent experiments each performed in triplicate. * = $P < 0.05$ versus untreated samples; # = $P < 0.05$, versus TNF-stimulated conditioned medium. Color figure can be viewed in the online issue, which is available at http://onlinelibrary. wiley.com/doi/10.1002/art.40468/abstract.
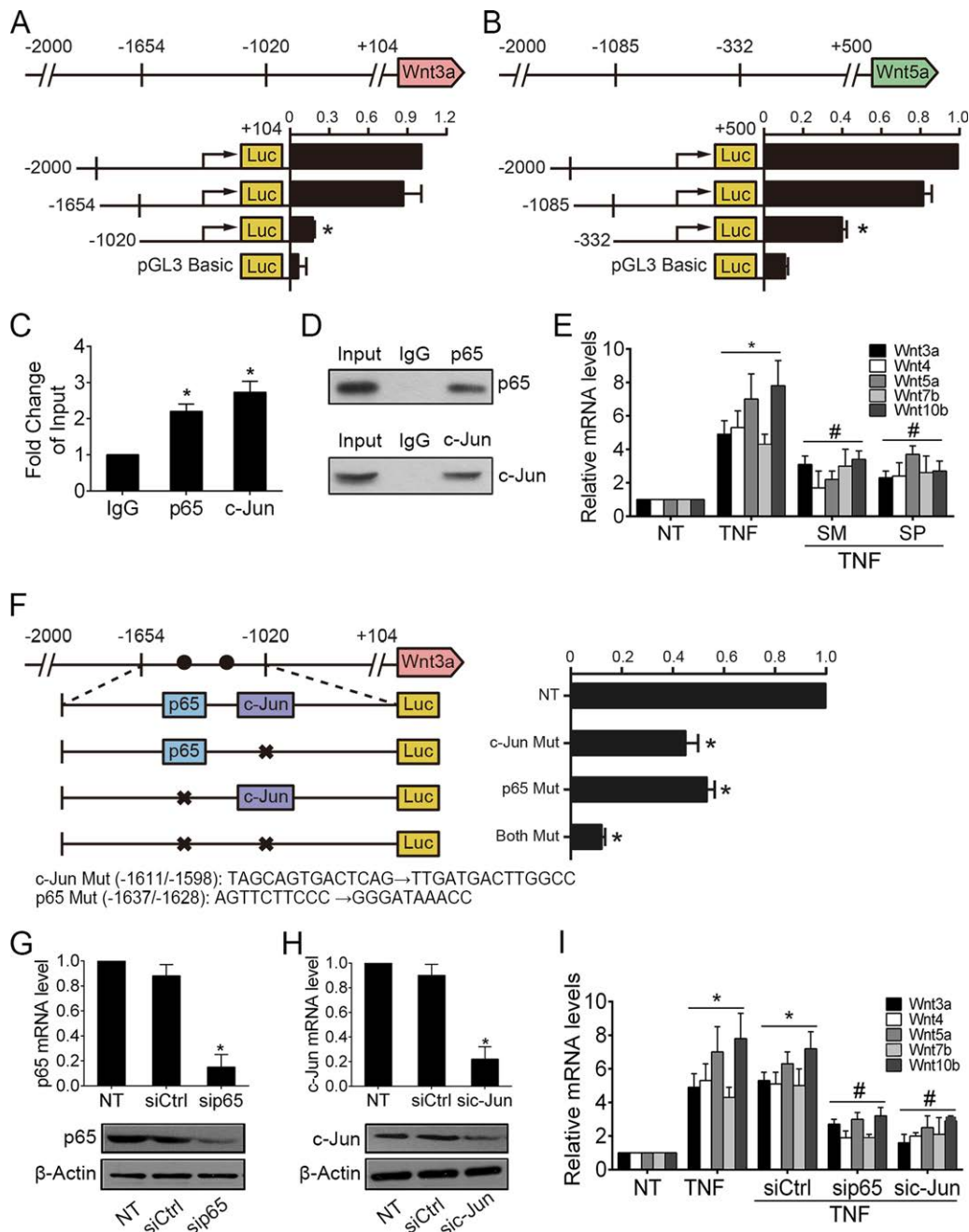
Figure 4. Tumor necrosis factor (TNF) regulates Wnt expression through NF-κB (p65) and JNK/activator protein 1 (AP-1) (c-Jun) signaling. **A** and **B**, Wnt3a (**A**) and Wnt5a (**B**) promoter deletion assays. **C**, Polymerase chain reaction (PCR) products from the input DNA and DNA precipitated with an anti-p65 or anti–c-Jun antibody using the same primers. Normal IgG was used as a negative control, and equal amounts of total genomic DNA were used as input. **D**, Western blot analysis of DNA–protein complexes immunoprecipitated with anti-p65 or anti–c-Jun antibody, showing that p65 and c-Jun were present in the precipitate. **E**, Quantitative reverse transcriptase–PCR (RT-PCR) analyses of Wnt mRNA levels in RAW 264.7 cells that were pretreated with an NF-κB inhibitor (SM7368 [SM]), a JNK inhibitor (SP600125 [SP]), or the corresponding controls and then stimulated with TNF (50 ng/ml) for 72 hours. **F**, Site-directed mutagenesis analysis of the Wnt3a promoter. **G** and **H**, Quantitative RT-PCR and Western blot analyses showing significant knockdown of p65 (**G**) and c-Jun (**H**) expression by small interfering RNA (siRNA). **I**, Quantitative RT-PCR analysis of Wnt mRNA levels in RAW 264.7 cells transfected with p65, c-Jun, or control siRNAs and stimulated with TNF (50 ng/ml) for 72 hours. In **A–C** and **E–I**, bars show the mean ± SD from 1 representative experiment of 3 independent experiments each performed in triplicate. * = $P < 0.05$ versus untreated (NT) samples; # = $P < 0.05$ versus TNF-treated samples. Color figure can be viewed in the online issue, which is available at http://onlinelibrary.wiley.com/doi/10.1002/art.40468/abstract.

TNF regulates Wnt expression through the NF-κB (p65) and JNK/activator protein 1 (AP-1) (c-Jun) pathways. Wnt expression is regulated by TNF in the setting of inflammation (47). However, the detailed molecular mechanism and regulatory pathway has not been identified. To further understanding of the molecular mechanism through which TNF regulates Wnt expression, we performed serial promoter analysis studies for the Wnt3a and Wnt5a genes and found p65 and c-Jun binding sites (Figures 4A and B). ChIP assay confirmed the actual binding of p65 and c-Jun to the promoter regions (Figures 4C and D). Site-directed mutagenesis significantly decreased TNF-induced promoter transactivity (Figure 4F). Inhibition of the NF-κB and JNK/AP-1 pathways with both pharmaceutical inhibitors and target-specific siRNA significantly attenuated the TNF-induced up-regulation of Wnt expression (Figures 4E and G–I). Further details are available in Supplementary Results, available on the *Arthritis & Rheumatology* web site at http://onlinelibrary.wiley.com/doi/10.1002/art.40468/abstract.

Activation of Wnt signaling is required for spinal ectopic new bone formation in vivo. To confirm the role of Wnt signaling in inflammation-related ankylosis, we established modified CIA and PGIS mouse models. We obtained the first evidence of whole-spine morphologic changes after collagen induction (Figure 5A). Micro-CT images showed significant spinal kyphosis in the mice with modified CIA 30 weeks after induction compared with controls. The Cobb angle at baseline was 37.46–40.88°. Thus, we defined a kyphotic phenotype with a Cobb angle of >45° as kyphosis. The mean ± SD incidence of kyphosis in these mice at 30 weeks was 35 ± 7%, and the mean ± SD angle of local kyphosis was 71.16 ± 6.23° (Figures 5B and C). This phenotype is similar to clinical observations of the spines of patients with AS (Figure 5D). Following treatment with Dkk-1 or Rottlerin, the mean ± SD incidences of kyphosis were significantly reduced to 23 ± 4% and 18 ± 4%, respectively. The mean ± SD kyphotic angles were reduced to 56.28 ± 4.65° and 59.97 ± 2.47°, respectively. Following treatment with both inhibitors, the incidence of kyphosis was further reduced to 13 ± 4%, and the kyphotic angle was reduced to 42.17 ± 1.63°, which were not significantly different from those in the controls (Figures 5B and C). Reliability testing showed that the measurement was reliable and reproducible (Supplementary Table 4, available on the *Arthritis & Rheumatology* web site at http://onlinelibrary.wiley.com/doi/10.1002/art.40468/abstract).

Furthermore, the occurrence of significant bony bridging between vertebrae (spinal ankylosis) was observed in a mean ± SD of 40 ± 7% of the mice with modified CIA (Figures 5E and F). Following treatment with Dkk-1 or Rottlerin, the mean ± SD incidences were reduced significantly, to 28 ± 4% and 23 ± 4%, respectively. Following treatment with both inhibitors, the incidence was further reduced to 8 ± 4% (Figure 5F). Similar osteogenic changes were observed in the hind paws (Figure 5E). New bone formed in the hind paws of a mean ± SD of 63 ± 4% of the mice with modified CIA 30 weeks after induction. Following treatment with Dkk-1 or Rottlerin, the mean ± SD incidence of osteophyte formation was significantly reduced to 43 ± 4% and 38 ± 4%, respectively. In the presence of both inhibitors, the incidence was further reduced to 18 ± 4% (Figure 5G).

H&E staining showed significant osteophyte formation and complete fusion between vertebrae 30 weeks after induction (Figure 6A). Positive immunohistochemical staining for Wnt3a, Wnt5a, and Wnt7b was detected at bone-forming sites from 16 to 30 weeks after induction (Figures 6B and C). Following treatment with Dkk-1 or Rottlerin, H&E and alizarin red staining revealed that the fusion was suppressed. Following treatment with both inhibitors, osteophyte formation and fusion were further inhibited (Figures 6A and D). In a comparative analysis, the arthritis severity score in the DBA/1 spontaneous arthritis model indicated a more rapidly progressive but self-limited pattern of inflammation, while the modified CIA model showed a relatively low-grade and long-lasting pattern of inflammation (Supplementary Figure 8, available on the *Arthritis & Rheumatology* web site at http://onlinelibrary.wiley.com/doi/10.1002/art.40468/abstract).

Similarly, in the PGIS model, bony bridging and fusion between vertebrae were observed with micro-CT, H&E staining, and alizarin red staining, and it was significantly reduced by treatment with Dkk-1 and Rottlerin (Supplementary Figures 9 and 10). Wnt protein expression in the bone-forming site was confirmed by immunohistochemical staining (Supplementary Figure 9). These results suggest that activation of Wnt signaling is required for ectopic new bone formation in vivo.

DISCUSSION

In an in vitro study, we made 3 key observations that provide new insights into the molecular mechanism of new bone formation in AS. First, we reported the novel observation of expression of Wnt proteins in the ligaments of patients with AS that were collected during correction surgeries (Figure 1). Second, using an in vitro cell culture system mimicking the inflammatory microenvironment of bone-forming sites, we found that conditioned medium from monocyte cultures that were
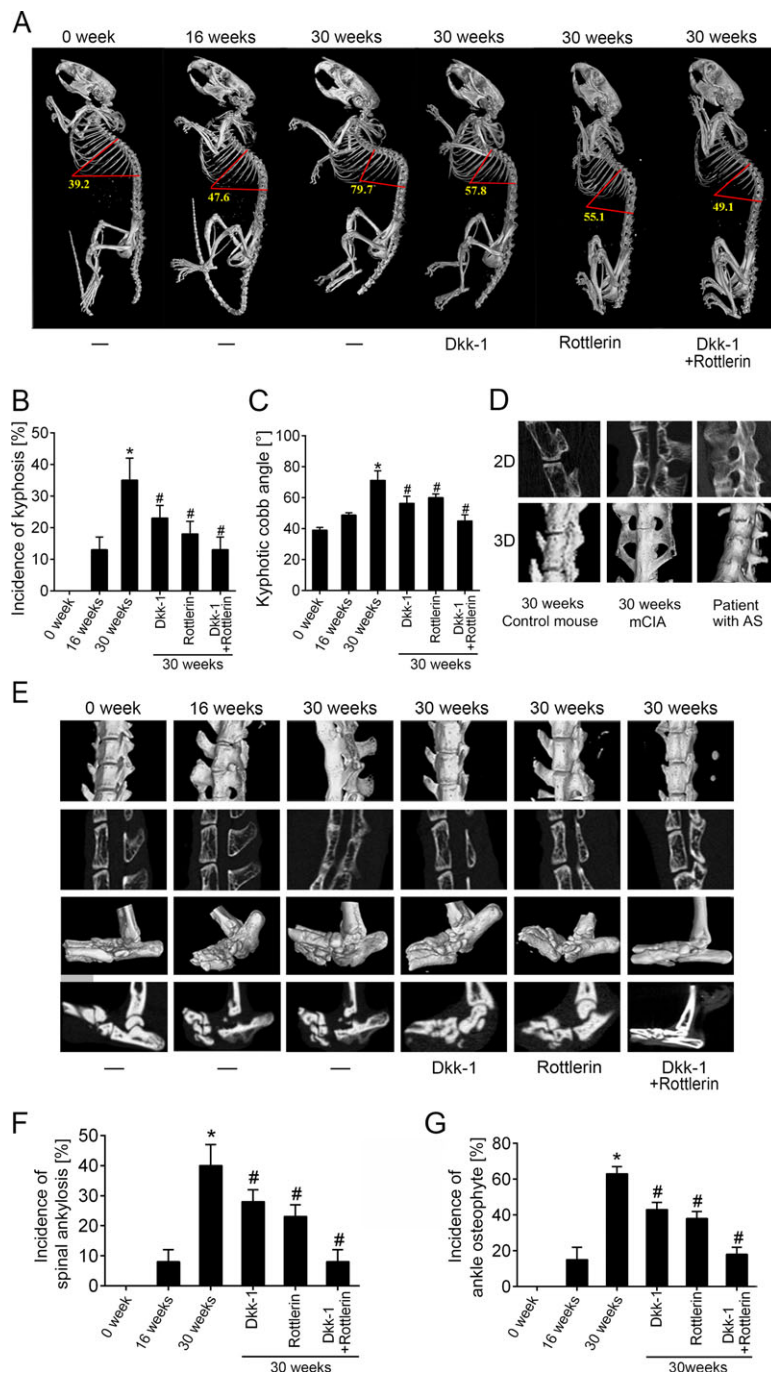
Figure 5. Activation of Wnt signaling is required for the ankylosis phenotype in vivo. **A**, Representative micro–computed tomography (micro-CT) images obtained at baseline (week 0 represents the time of last injection), 16 weeks, and 30 weeks after collagen induction showing the whole skeletons of untreated mice with modified collagen-induced arthritis (mCIA) and mice with modified CIA treated with Dkk-1, Rottlerin, or Dkk-1 plus Rottlerin. **B**, Incidence of kyphotic change in the spines of mice with modified CIA. **C**, Cobb angle of spinal kyphosis in mice with modified CIA. **D**, Comparison of micro-CT images of an untreated control mouse, a mouse with modified CIA at 30 weeks after induction, and the spinal segments of a patient with ankylosing spondylitis (AS) who had undergone correction surgery. **E**, Representative micro-CT images obtained at baseline, 16 weeks after induction, and 30 weeks after induction showing the spines and hind paws of untreated mice with modified CIA and mice with modified CIA treated with Dkk-1, Rottlerin, or Dkk-1 plus Rottlerin. **F**, Incidence of spinal ankylosis in mice with modified CIA. **G**, Incidence of osteophytes of the hind paws in mice with modified CIA (n = 20 per group). In **B**, **C**, **F**, and **G**, bars show the mean ± SD from 2 independent experiments. * = $P < 0.05$ versus baseline; # = $P < 0.05$ versus untreated mice at 30 weeks after induction. Color figure can be viewed in the online issue, which is available at http://onlinelibrary.wiley.com/doi/10.1002/art.40468/abstract.

constitutively stimulated with low-dose TNF, but not those stimulated with high-dose TNF or subjected to short-term stimulation with TNF, induced persistent Wnt expression through the NF-κB (p65) and JNK/AP-1 (c-Jun) pathways, followed by subsequent new bone formation (Figures 2–4). Third, we provided the first evidence that both the canonical Wnt/β-catenin and noncanonical Wnt/PKCδ signaling pathways are required for new bone formation (Figure 3).

Two main theories exist regarding the relationship between inflammation and ectopic new bone formation in AS (13). One theory postulates that inflammation triggered by unknown stimuli drives a bone catabolic process. Later, when inflammation fluctuates and is intermittently suppressed, the bone catabolic process is replaced by a bone anabolic response characterized by overreactive osteogenesis. The other theory suggests that inflammation and bone formation are uncoupled and that the same triggers independently activate inflammatory and stromal cells. The activation of stromal cells leads to bone formation. The suppression of inflammation might even promote bone formation (the TNF brake hypothesis).

Our in vitro cell culture system might provide a link between these theories by showing that TNF induces the expression of osteogenic Wnt proteins in the inflammatory microenvironment. Autoimmune responses cause inflammation in entheses. The inflammation level fluctuates in response to many factors, including autoantigen
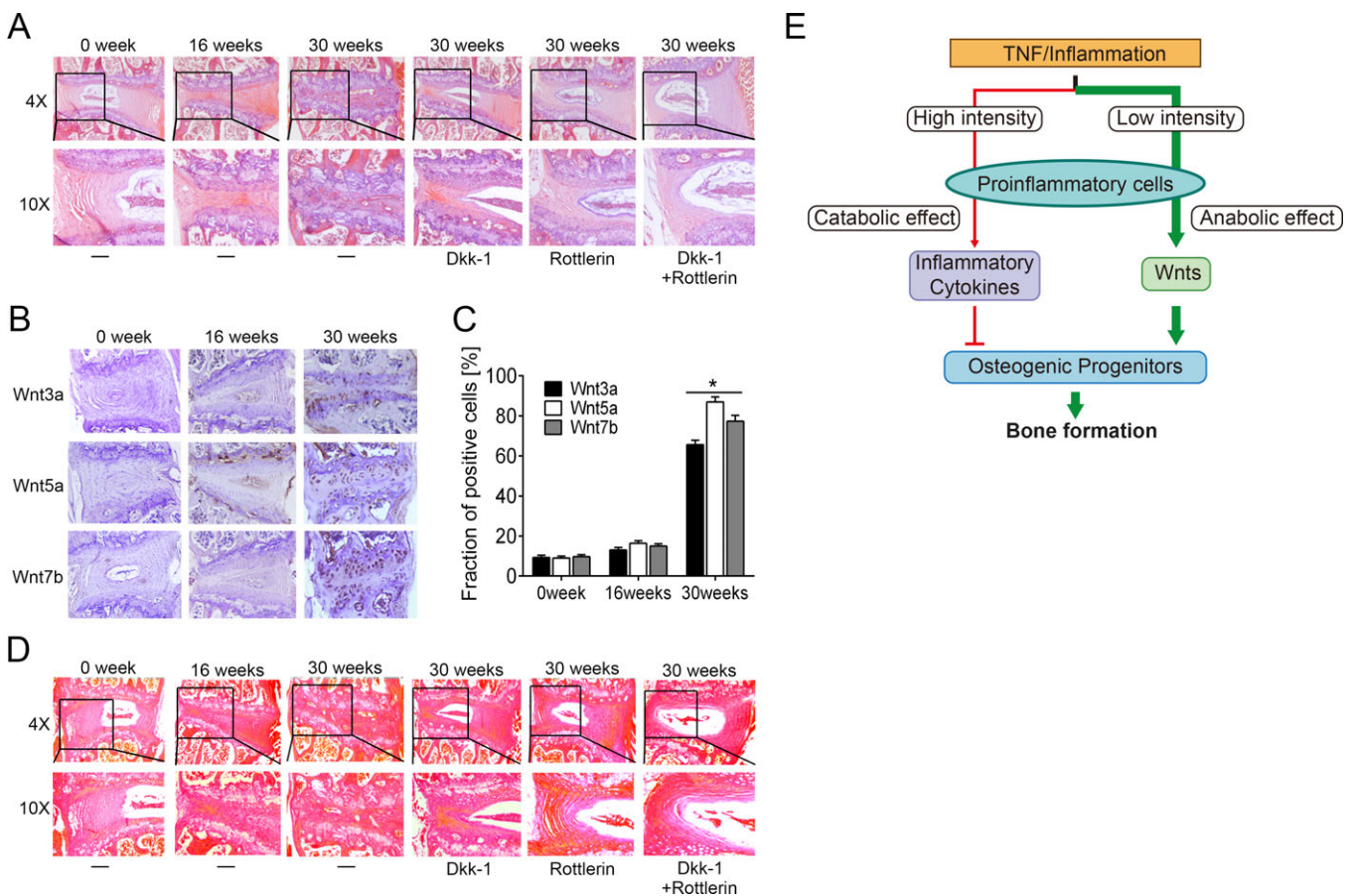
Figure 6. Activation of Wnt signaling is required for ectopic new bone formation in vivo. **A**, Hematoxylin and eosin staining of lumbar spine specimens from mice with modified collagen-induced arthritis (CIA) at baseline and 16 and 30 weeks after induction compared with mice with modified CIA treated with Dkk-1, Rottlerin, or Dkk-1 plus Rottlerin. The bottom row shows higher-magnification views of the boxed areas in the top row. **B**, Immunohistologic staining for Wnt3a, Wnt5a, and Wnt7b in lumbar spine specimens from mice with modified CIA at baseline and 16 and 30 weeks after induction. Brown indicates positive cells. Original magnification × 4. **C**, Quantification of the proportions of Wnt3a-, Wnt5a- and Wnt7b-positive cells in lumbar spine specimens. Bars show the mean ± SD (n = 20 mice per group). * = $P < 0.05$. **D**, Alizarin red staining of lumbar spine specimens from mice with modified CIA at baseline and 16 and 30 weeks after induction compared with mice with modified CIA treated with Dkk-1, Rottlerin, or Dkk-1 plus Rottlerin. The bottom row shows higher-magnification views of the boxed areas in the top row. **E**, Schematic diagram illustrating the theory presented in the current study. Fluctuations in the level of inflammation exert either a catabolic or an anabolic effect on bone formation. Inflammation intensity–dependent expression of osteoinductive Wnt proteins is a key link between inflammation and the ectopic formation of new bone in patients with ankylosing spondylitis. TNF = tumor necrosis factor. Color figure can be viewed in the online issue, which is available at http://onlinelibrary.wiley.com/doi/10.1002/art.40468/abstract.

exposure, immune cell responsiveness, and local blood supply. When the inflammation level is relatively low at a certain disease stage, low-intensity TNF stimulation induces strong and persistent expression of Wnt proteins at bone-forming sites. Subsequently, Wnt-induced osteogenesis occurs in an inflammation-independent manner. When the inflammation level becomes relatively high, elevated TNF levels induce the expression of numerous cytokines such as Dkk-1 (Figure 2C) with catabolic effects on bone structures, overcoming the anabolic effects of the osteogenic molecules. When the inflammation level again decreases, the bone-forming period resumes. Inflammation is an initiating factor and a restricting factor for new bone formation. The catabolic–anabolic cycle is driven by the intensity of inflammation. The osteogenic molecules induced by proinflammatory cytokines represent a key link between inflammation and new bone formation, whereas inflammation intensity is the bone formation switch.

The TNF brake hypothesis was proposed to explain the enhancement of new bone formation following TNF blockade in the clinical setting. Considering our findings, we speculate that the application of an effective anti-TNF treatment significantly decreases the TNF level, but it does not reach the baseline level observed in the normal population. This reduced TNF level no longer exerts an inhibitory effect on bone formation; rather, it increases the expression of osteogenic Wnt proteins and exerts an osteoinductive effect. This finding may explain the TNF brake hypothesis to some extent. However, if NSAIDs and TNF blockers are administered at a very early disease stage and are used for long periods, low-intensity inflammation may be further inhibited, and the inductive effect on osteogenic molecules might be sabotaged. This finding might explain the importance of the therapeutic time window and duration (14–16,48,49).

One of the complexities of Wnt signaling is that different Wnt proteins seem to have overlapping functions. The Wnt protein family currently comprises 19 members. Previous studies have shown that some members are osteogenic. However, results have varied among studies due to differences in experimental conditions, cell types, stimulation methods and durations, and osteogenesis measurements (27–29,50–52). We screened all family members in the current culture system using different osteoprogenitor cell types to compare the osteogenic abilities of the Wnt proteins. Wnt3a, Wnt4, Wnt5a, Wnt5b, Wnt7b, Wnt10b, Wnt11, and Wnt16b were found to be osteogenic (Supplementary Figure 6). To the best of our knowledge, this study provides the first comparison of the osteoinductive effect of different Wnt proteins in the same culture system.

To confirm the role of Wnt signaling in new bone formation, we further conducted an in vivo experiment. Wnt protein expression was observed at bone formation sites (Figures 6B and C and Supplementary Figure 9). Significant spinal ankylosis and obvious kyphosis were observed in mice with modified CIA, which are very similar to the morphologic changes observed in the spine of patients with AS (Figure 5D). Inhibition of Wnt signaling was found to significantly suppress new bone formation and kyphosis, indicating a critical role for Wnt signaling in the progression of ankylosis (Figures 5A–C). A PGIS model was also established, and the key role of Wnt in spinal ankylosis was confirmed in this model (Supplementary Figures 9 and 10).

An important and interesting finding of our in vivo experiment that has not been described previously was the spinal ankylosis and kyphosis observed during the late stage of the disease in the modified CIA model. Four non-transgenic models are most frequently used to study bone and joint pathology in rheumatic diseases: spontaneous arthritis in DBA/1 mice, CIA, collagen antibody–induced arthritis, and proteoglycan-induced arthritis/PGIS. In all of these models, bone remodeling and new bone formation were found to be closely correlated to the inflammation process (12,13,20–22,53–56). Of these models, osteophytes in the paws of DBA/1 mice and syndesmophytes leading to vertebral bony bridging in the PGIS model are most widely considered to be pathologic changes similar to new bone formation in the axial skeleton of patients with AS. Spinal syndesmophytes and fusion have only been shown to develop in the PGIS model in the existing literature (20,21,40,57–59).

Our novel finding of spinal fusion in mice with modified CIA might be due to 2 factors. First, low-intensity constitutive inflammation might be the important driving factor for osteogenesis. Previously, data from animals with CIA were obtained over periods of no longer than 70 days after the last induction; thus, potential subsequent changes in the spine have not been reported (60–64). In this study, we extended the observational period to 30 weeks and found that spinal changes began at week 16 and that 40% of the experimental animals had spinal ankylosis at week 30 after induction (Figures 5A–C). In our comparative analysis, in DBA/1 mice with spontaneous arthritis, which had no spinal involvement, the inflammation level reached a peak level more rapidly and decreased to almost the baseline level after 16–18 weeks. This finding is consistent with the major evidence showing that arthritis in this model is a self-limited process and ceases within 8–12 weeks after onset (65). In contrast, the mice with modified CIA more slowly reached a lower peak level of inflammation and then presented a relatively

persistent inflammation level for up to 30 weeks (Supplementary Figure 8). Although a direct comparison of inflammation severity may not be the most appropriate due to the great heterogeneity of the DBA/1 model (different time of onset, peak inflammation level, duration of the peak inflammation level, and duration of the whole disease process among different studies) (65–70), it at least supported the notion that spontaneous arthritis in DBA/1 mice presents a self-limited and unstable pattern of inflammation, whereas mice with CIA present with a relatively long-lasting and stable pattern of inflammation. These findings indicate that inflammation-induced osteogenesis depends on a certain intensity of constitutive inflammatory stimulation. Second, type II collagen in the intervertebral disc might be a key autoimmune target in the spine. Type II collagen is abundantly expressed in articular cartilage. However, in the spine, type II collagen is mainly expressed at high levels in the disc, which is basically an avascular tissue. Only blood vessel infiltration into a chronically inflamed and degenerative disc results in the exposure of type II collagen, which becomes a local autoantigen and autoimmune target that is reactivated by collagen or PG induction (40,59). The phenomenon of ankylosis and subsequent bone formation observed in the PGIS model and our long-term modified CIA model suggests that enthesitis and discs are important sites of inflammation-related ankylosis.

The present study has some limitations. First, the specific role of each Wnt protein in the ectopic formation of new bone is unclear. Further studies of the specific roles of these proteins would aid the treatment of patients with osteogenesis at different disease stages. Second, we have not clearly determined whether crosstalk occurs between Wnt signaling and other important osteogenic signaling pathways. Third, further investigations are required to determine whether other noncanonical Wnt pathways are also involved in this process. Moreover, whether our findings exist in transgenic mouse models with spinal syndesmophytes, especially HLA–B27–transgenic models (including B27/$h\beta_2$m-transgenic Lewis rats, B27/$h\beta_2$m-transgenic F344 rats, and B27/$h\beta_2$m-transgenic Lewis rats 21-3 × 283-2 F1), has not been verified in the present study. Further confirmation of our key findings in these models is important to conclude that our findings represent common phenomena in all mouse models with spinal ankylosis.

In summary, the novel findings of this study strongly suggest that inflammation intensity–dependent expression of osteoinductive Wnt proteins is a key link between inflammation and ectopic new bone formation in AS. Activation of both the canonical Wnt/β-catenin and noncanonical Wnt/PKCδ pathways is required for inflammation-induced new bone formation in AS. To translate our findings to therapeutic strategy, pathway complexity must be fully considered when targeting Wnt signaling pathways. The timing and duration of antiinflammatory treatments are of great importance for inhibiting the osteoinductive effect of low-intensity inflammation and preventing the onset and progression of ankylosis. Based on our findings, early, long-term, thorough antiinflammatory therapy is recommended.

AUTHOR CONTRIBUTIONS

All authors were involved in drafting the article or revising it critically for important intellectual content, and all authors approved the final version to be published. Dr. Liu had full access to all of the data in the study and takes responsibility for the integrity of the data and the accuracy of the data analysis.
Study conception and design. Liu.
Acquisition of data. X. Li, J. Wang, S. Li, K. Zhang, Pan, Z. Li, Liu.
Analysis and interpretation of data. X. Li, J. Wang, Zhan, Zheng, T. Wang, N. Zhang, Liu.

REFERENCES

1. Taurog JD, Chhabra A, Colbert RA. Ankylosing spondylitis and axial spondyloarthritis. N Engl J Med 2016;374:1302–3.
2. Tam LS, Gu J, Yu D. Pathogenesis of ankylosing spondylitis. Nat Rev Rheumatol 2010;6:399–405.
3. Pedersen SJ, Chiowchanwisawakit P, Lambert RG, Østergaard M, Maksymowych WP. Resolution of inflammation following treatment of ankylosing spondylitis is associated with new bone formation. J Rheumatol 2011;38:1349–54.
4. Maksymowych WP, Chiowchanwisawakit P, Clare T, Pedersen SJ, Østergaard M, Lambert RG. Inflammatory lesions of the spine on magnetic resonance imaging predict the development of new syndesmophytes in ankylosing spondylitis: evidence of a relationship between inflammation and new bone formation. Arthritis Rheum 2009;60:93–102.
5. Chiowchanwisawakit P, Lambert RG, Conner-Spady B, Maksymowych WP. Focal fat lesions at vertebral corners on magnetic resonance imaging predict the development of new syndesmophytes in ankylosing spondylitis. Arthritis Rheum 2011;63:2215–25.
6. Van der Heijde D, Machado P, Braun J, Hermann KG, Baraliakos X, Hsu B, et al. MRI inflammation at the vertebral unit only marginally predicts new syndesmophyte formation: a multilevel analysis in patients with ankylosing spondylitis. Ann Rheum Dis 2012;71:369–73.
7. Van der Heijde D, Salonen D, Weissman BN, Landewe R, Maksymowych WP, Kupper H, et al. Assessment of radiographic progression in the spines of patients with ankylosing spondylitis treated with adalimumab for up to 2 years. Arthritis Res Ther 2009;11:R127.
8. Baraliakos X, Listing J, Rudwaleit M, Brandt J, Sieper J, Braun J. Radiographic progression in patients with ankylosing spondylitis after 2 years of treatment with the tumour necrosis factor α antibody infliximab. Ann Rheum Dis 2005;64:1462–6.

9. Van der Heijde D, Landewé R, Baraliakos X, Houben H, van Tubergen A, Williamson P, et al. Radiographic findings following two years of infliximab therapy in patients with ankylosing spondylitis. Arthritis Rheum 2008;58:3063–70.

10. Van der Heijde D, Landewé R, Einstein S, Ory P, Vosse D, Ni L, et al. Radiographic progression of ankylosing spondylitis after up to two years of treatment with etanercept. Arthritis Rheum 2008;58:1324–31.

11. Baraliakos X, Listing J, Brandt J, Haibel H, Rudwaleit M, Sieper J, et al. Radiographic progression in patients with ankylosing spondylitis after 4 yrs of treatment with the anti-TNF-α antibody infliximab. Rheumatology (Oxford) 2007;46:1450–3.

12. Lories RJ, Derese I, De Bari C, Luyten FP. Evidence for uncoupling of inflammation and joint remodeling in a mouse model of spondylarthritis. Arthritis Rheum 2007;56:489–97.

13. Schett G, Stolina M, Dwyer D, Zack D, Uderhardt S, Krönke G, et al. Tumour necrosis factor α and RANKL blockade cannot halt bony spur formation in experimental inflammatory arthritis. Arthritis Rheum 2009;60:2644–54.

14. Baraliakos X, Haibel H, Listing J, Sieper J, Braun J. Continuous long-term anti-TNF therapy does not lead to an increase in the rate of new bone formation over 8 years in patients with ankylosing spondylitis. Ann Rheum Dis 2014;73:710–5.

15. Poddubnyy D, Rudwaleit M, Haibel H, Listing J, Marker-Hermann E, Zeidler H, et al. Effect of non-steroidal anti-inflammatory drugs on radiographic spinal progression in patients with axial spondyloarthritis: results from the German Spondyloarthritis Inception Cohort. Ann Rheum Dis 2012;71:1616–22.

16. Kroon F, Landewe R, Dougados M, van der Heijde D. Continuous NSAID use reverts the effects of inflammation on radiographic progression in patients with ankylosing spondylitis. Ann Rheum Dis 2012;71:1623–9.

17. Lories RJ, Dougados M. Inflammation and ankylosis: still an enigmatic relationship in spondyloarthritis. Ann Rheum Dis 2012;71:317–8.

18. González-Chávez SA, Quiñonez-Flores CM, Pacheco-Tena C. Molecular mechanisms of bone formation in spondyloarthritis. Joint Bone Spine 2016;83:394–400.

19. Ruiz-Heiland G, Horn A, Zerr P. Blockade of the hedgehog pathway inhibits osteophyte formation in arthritis. Ann Rheum Dis 2012;71:400–7.

20. Jacques P, Lambrecht S, Verheugen E, Pauwels E, Kollias G, Armaka M, et al. Proof of concept: enthesitis and new bone formation in spondyloarthritis are driven by mechanical strain and stromal cells. Ann Rheum Dis 2014;73:437–45.

21. Lories RJ, Derese I, Luyten FP. Modulation of bone morphogenetic protein signaling inhibits the onset and progression of ankylosing enthesitis. J Clin Invest 2005;115:1571–9.

22. Diarra D, Stolina M, Polzer K, Zwerina J, Ominsky MS, Dwyer D. Dickkopf-1 is a master regulator of joint remodeling. Nat Med 2007;13:156–63.

23. Appel H, Ruiz-Heiland G, Listing J, Zwerina J, Herrmann M, Mueller R, et al. Altered skeletal expression of sclerostin and its link to radiographic progression in ankylosing spondylitis. Arthritis Rheum 2009;60:3257–62.

24. Daoussis D, Liossis SN, Solomou EE, Tsanaktsi A, Bounia K, Karampetsou M, et al. Evidence that Dkk-1 is dysfunctional in ankylosing spondylitis. Arthritis Rheum 2010;62:150–8.

25. Thomas GP, Duan R, Pettit AR, Weedon H, Kaur S, Smith M, et al. Expression profiling in spondyloarthropathy synovial biopsies highlights changes in expression of inflammatory genes in conjunction with tissue remodeling genes. BMC Musculoskelet Disord 2013;14:354.

26. Corr M. Wnt signaling in ankylosing spondylitis. Clin Rheumatol 2014;33:759–62.

27. Maeda K, Kobayashi Y, Udagawa N, Uehara S, Ishihara A, Mizoguchi T, et al. Wnt5a-Ror2 signaling between osteoblast-lineage cells and osteoclast precursors enhances osteoclastogenesis. Nat Med 2012;18:405–12.

28. Yu B, Chang J, Liu Y, Li J, Kevork K, Al-Hezaimi K, et al. Wnt4 signaling prevents skeletal ageing and inflammation by inhibiting nuclear factor-κB. Nat Med 2014;20:1009–17.

29. Tu X, Joeng KS, Nakayama KI, Nakayama K, Raiaqopal J, Carroll TJ, et al. Noncanonical Wnt signaling through G protein-linked PKC δ activation promotes bone formation. Dev Cell 2007;12:113–27.

30. Van der Linden S, Valkenburg HA, Cats A. Evaluation of diagnostic criteria for ankylosing spondylitis: a proposal for modification of the New York criteria. Arthritis Rheum 1984;27:361–8.

31. Creemers MC, Franssen MJ, van 't Hof MA, Gribnau FW, van de Putte LB, van Riel PL. Assessment of outcome in ankylosing spondylitis: an extended radiographic scoring system. Ann Rheum Dis 2005;64:127–9.

32. Liu H, Bargouti M, Zughaier S, Zheng Z, Liu Y, Sangadala S, et al. Osteoinductive LIM mineralization protein-1 suppresses activation of NF-κB and selectively regulates MAPK pathways in pre-osteoclasts. Bone 2010;46:1328–35.

33. Liu H, Liu Y, Viggeswarapu M, Zheng Z, Titus L, Boden SD, et al. Activation of c-Jun NH(2)-terminal kinase 1 increases cellular responsiveness to BMP-2 and decreases binding of inhibitory Smad6 to the type 1 BMP receptor. J Bone Miner Res 2011;26:1122–32.

34. Colter DC, Class R, DiGirolamo CM, Prockop DJ. Rapid expansion of recycling stem cells in cultures of plastic-adherent cells from human bone marrow. Proc Natl Acad Sci USA 2000;97:3213–18.

35. Xie Z, Wang P, Li Y, Deng W, Zhang X, Su H, et al. Imbalance between bone morphogenetic protein 2 and noggin induces abnormal osteogenic differentiation of mesenchymal stem cells in ankylosing spondylitis. Arthritis Rheumatol 2016;68:430–40.

36. Ferrer DG, Jaldín-Fincati JR, Amigone JL, Capra RH, Collino CJ, Albertini RA, et al. Standardized flow cytometry assay for identification of human monocytic heterogeneity and LRP1expression in monocyte subpopulations: decreased expression of this receptor in nonclassical monocytes. Cytometry A 2014;85:601–10.

37. Pan H, Li X, Wang J, Zhang K, Yang H, Li Z, et al. LIM mineralization protein-1 enhances bone morphogenetic protein-2-mediated osteogenesis through activation of ERK1/2 MAPK pathway and upregulation of Runx2 transactivity. J Bone Miner Res 2015;30:1523–35.

38. Glant TT, Cs-Szabó G, Nagase H, Jacobs JJ, Mikecz K. Progressive polyarthritis induced in BALB/c mice by aggrecan from normal and osteoarthritic human cartilage. Arthritis Rheum 1998;41:1007–18.

39. Glant TT, Mikecz K. Proteoglycan aggrecan-induced arthritis: a murine autoimmune model of rheumatoid arthritis. Methods Mol Med 2004;102:313–38.

40. Bárdos T, Szabó Z, Czipri M, Vermes C, Tunyogi-Csapó M, Urban RM, et al. A longitudinal study on an autoimmune murine model of ankylosing spondylitis. Ann Rheum Dis 2005;64:981–7.

41. Wu T, Sun X, Zhu Z, Yan H, Guo J, Cheng JC, et al. Role of enhanced central leptin activity in a scoliosis model created in bipedal amputated mice. Spine (Phila Pa 1976) 2015;40:1041–5.

42. Smith RM, Dickson RA. Experimental structural scoliosis. J Bone Joint Surg Br 1987;69:576–81.

43. Langenskiold, Michelsson JE. Experimental progressive scoliosis in the rabbit. J Bone Joint Surg Br 1961;43:116–20.

44. Liu H, Li S, Zheng Z, Wang J, Wang H, Li X. Pelvic retroversion is the key protective mechanism of L4-5 degenerative spondylolisthesis. Eur Spine J 2015;24:1204–11.

45. Wang J, Markova D, Anderson D, Zheng Z, Shapiro IM, Risbud MV. TNF-α and IL-1β promote a disintegrin-like and metalloprotease with thrombospondin type I motif-5-mediated aggrecan degradation through syndecan-4 in intervertebral disc. J Biol Chem 2011;286:39738–49.

46. Oguma K, Oshima H, Aoki M, Uchio R, Naka K, Nakamura S, et al. Activated macrophages promote Wnt signaling through tumour necrosis factor-α in gastric tumour cells. EMBO J 2008;27:1671–81.

47. Briolay A, Lencel P, Bessueille L, Caverzasio J, Buchet R, Magne D. Autocrine stimulation of osteoblast activity by Wnt5a in response to

TNF-α in human mesenchymal stem cells. Biochem Biophys Res Commun 2013;430:1072–7.

48. Baraliakos X, Listing J, von der Recke A, Braun J. The natural course of radiographic progression in ankylosing spondylitis: evidence for major individual variations in a large proportion of patients. J Rheumatol 2009;36:997–1002.

49. Van Tubergen A, Ramiro S, van der Heijde D, Dougados M, Mielants H, Landewe R. Development of new syndesmophytes and bridges in ankylosing spondylitis and their predictors: a longitudinal study. Ann Rheum Dis 2012;71:518–23.

50. Chang J, Sonoyama W, Wang Z, Jin Q, Zhang C, Krebsbach PH, et al. Noncanonical Wnt-4 signaling enhances bone regeneration of mesenchymal stem cells in craniofacial defects through activation of p38 MAPK. J Biol Chem 2007;282:30938–48.

51. Takada I, Mihara M, Suzawa M, Ohtake F, Kobayashi S, Igarashi M, et al. A histone lysine methyltransferase activated by noncanonical Wnt signaling suppresses PPAR - γ transactivation. Nat Cell Biol 2007;9:1273–85.

52. Liu N, Shi S, Deng M, Tang L, Zhang G, Liu N, et al. High levels of β-catenin signaling reduce osteogenic differentiation of stem cells in inflammatory microenvironments through inhibition of the noncanonical Wnt pathway. J Bone Miner Res 2011;26:2082–95.

53. Hosoya T, Iwai H, Yamaguchi Y, Kawahata K, Miyasaka N, Kohsaka H. Cell cycle regulation therapy combined with cytokine blockade enhances antiarthritic effects without increasing immune suppression. Ann Rheum Dis 2016;75:253–9.

54. Tseng HW, Glant TT, Brown MA, Kenna TJ, Thomas GP, Pettit AR. Early anti-inflammatory intervention ameliorates axial disease in the proteoglycan-induced spondylitis mouse model of ankylosing spondylitis. BMC Musculoskelet Disord 2017;30:228.

55. Haynes KR, Tseng HW, Kneissel M, Glant TT, Brown MA, Thomas GP. Treatment of a mouse model of ankylosing spondylitis with exogenous sclerostin has no effect on disease progression. BMC Musculoskelet Disord 2015;26:368.

56. Haynes KR, Pettit AR, Duan R, Tseng HW, Glant TT, Brown MA, et al. Excessive bone formation in a mouse model of ankylosing spondylitis is associated with decreases in Wnt pathway inhibitors. Arthritis Res Ther 2012;22:R253.

57. Lories RJ. Animal models of spondyloarthritis. Curr Opin Rheumatol 2006;18:342–6.

58. Nandakumar KS, Holmdahl R. Efficient promotion of collagen antibody induced arthritis (CAIA) using four monoclonal antibodies specific for the major epitopes recognized in both collagen induced arthritis and rheumatoid arthritis. J Immunol Methods 2005;304:126–36.

59. Tseng HW, Pitt ME, Glant TT, McRae AF, Kenna TJ, Brown MA, et al. Inflammation-driven bone formation in a mouse model of ankylosing spondylitis: sequential not parallel processes. Arthritis Res Ther 2016;18:35.

60. O'Valle F, Peregrina M, Crespo-Lora V, Galindo-Moreno P, Roman M, Padial-Molina M, et al. Osteoarticular expression of musashi-1 in an experimental model of arthritis. Biomed Res Int 2015;2015:681456.

61. Kawamoto T, Abe Y, Ito J, Makino F, Kojima Y, Usui Y, et al. Anti-T cell immunoglobulin and mucin domain-2 monoclonal antibody exacerbates collagen-induced arthritis by stimulating B cells. Arthritis Res Ther 2011;13:R47.

62. Marchesan JT, Gerow EA, Schaff R, Taut AD, Shin SY, Sugai J, et al. Porphyromonas gingivalis oral infection exacerbates the development and severity of collagen-induced arthritis. Arthritis Res Ther 2013;15:R186.

63. Van Tok MN, Yeremenko NG, Teitsma CA, Kream BE, Knaup VL, Lories RJ, et al. Insulin-like growth factor I does not drive new bone formation in experimental arthritis. PLoS One 2016;11: e0163632.

64. Clement M, Fornasa G, Loyau S, Morvan M, Andreata F, Guedj K, et al. Upholding the T cell immune-regulatory function of CD31 inhibits the formation of T/B immunological synapses in vitro and attenuates the development of experimental autoimmune arthritis in vivo. J Autoimmun 2015;56:23–33.

65. Holmdahl R, Jansson L, Andersson M, Jonsson R. Genetic, hormonal and behavioural influence on spontaneously developing arthritis in normal mice. Clin Exp Immunol 1992;88:467–72.

66. Lories RJ, Matthys P, de Vlam K, Derese I, Luyten FP. Ankylosing enthesitis, dactylitis, and onychoperiostitis in male DBA/1 mice: a model of psoriatic arthritis. Ann Rheum Dis 2004;63:595–8.

67. Braem K, Carter S, Lories RJ. Spontaneous arthritis and ankylosis in male DBA/1 mice: further evidence for a role of behavioral factors in "stress-induced arthritis". Biol Proced Online 2012;14:10.

68. Lories RJ, Daans M, Derese I, Matthys P, Kasran A, Tylzanowski P, et al. Noggin haploinsufficiency differentially affects tissue responses in destructive and remodelling arthritis. Arthritis Rheum 2006;54: 1736–46.

69. Matthys P, Lories RJ, De Klerck B, Heremans H, Luyten FP, Billiau A. Dependence on interferon-γ for the spontaneous occurrence of arthritis in DBA/1 mice. Arthritis Rheum 2003;48: 2983–8.

70. Lories RJ, Derese I, Luyten FP. Inhibition of osteoclasts does not prevent joint ankylosis in a mouse model of spondyloarthritis. Rheumatology (Oxford) 2008;47:605–8.

BRIEF REPORT

A Randomized, Double-Blind, Parallel-Group, Placebo-Controlled, Multiple-Dose Study to Evaluate AMG 557 in Patients With Systemic Lupus Erythematosus and Active Lupus Arthritis

Laurence E. Cheng,[1] Zahir Amoura,[2] Benjamin Cheah,[3] Falk Hiepe,[4] Barbara A. Sullivan,[1] Lei Zhou,[1] Gregory E. Arnold,[1] Wayne H. Tsuji,[1] Joan T. Merrill,[5] and James B. Chung[1]

Objective. To evaluate the safety and potential efficacy of AMG 557, a fully human antibody directed against the inducible T cell costimulator ligand (ICOSL) in patients with systemic lupus erythematosus (SLE) with arthritis.

Methods. In this phase Ib, randomized, double-blind, placebo-controlled study, patients received AMG 557 210 mg (n = 10) or placebo (n = 10) weekly for 3 weeks, then every other week for 10 additional doses. The corticosteroid dosage was tapered to ≤7.5 mg/day by day 85, and immunosuppressants were discontinued by day 29. Primary end points on day 169 were safety, immunogenicity, the Lupus Arthritis Response Index (LARI; defined by a reduction in the tender and swollen joint counts), ≥1-letter improvement in the musculoskeletal domain of the British Isles Lupus Assessment Group (BILAG) index, and medication discontinuation. The secondary/exploratory end points were changes in the tender and swollen joint counts, BILAG index scores (musculoskeletal, global), and the Systemic Lupus Erythematosus Disease Activity Index (SLEDAI).

Results. The incidence of adverse events, most of which were mild, was similar between groups. LARI responses occurred in 3 of 10 patients receiving AMG 557 and 1 of 10 patients receiving placebo (*P* = 0.58). More patients in the AMG 557 group achieved a ≥4-point improvement in the SLEDAI score on day 169 (7 of 10 patients) compared with the placebo group (2 of 10 patients) (*P* = 0.07). Patients treated with AMG 557 (versus placebo) had greater improvements from baseline in the global BILAG index scores (–36.3% versus –24.7%) and the SLEDAI score (–47.8% versus –10.7%) and in tender (–22.8% versus –13.5%) and swollen (–62.1% versus –7.8%) joint counts on day 169.

Conclusion. AMG 557 showed safety and potential efficacy, supporting further evaluation of the clinical efficacy of ICOSL blockade in patients with SLE.

Systemic lupus erythematosus (SLE) is a complex autoimmune disease characterized by unpredictable flares of potentially destructive inflammation that can affect the skin, musculoskeletal, nervous, pulmonary, and renal systems (1). Joint involvement is a common manifestation of SLE; it has been estimated that 69–95% of patients have lupus arthritis (2). Currently available treatments are inadequate; hence, more effective therapies with fewer short-term and long-term toxicities are needed (1).

Deposits of autoantibody–antigen immune complexes are a hallmark of SLE and can be found in various organs, triggering complement and other inflammatory pathways (3). Autoantibodies are a key pathogenic marker of the disease and implicate immune dysregulation as a

driving force for disease pathogenesis (1,3). Production of antibodies from autoreactive B cells typically requires direct interaction with CD4+ T helper cells (4). Normal interactions between T cells and B cells are concentrated in specific anatomic areas of secondary lymphoid organs. A specialized CD4+ T helper cell subset, the follicular helper T (Tfh) cell, localizes there and is primarily responsible for promoting the B cell response leading to antibody production (5). Tfh cells express a specific pattern of cell surface receptors, including CXCR5, programmed cell death 1 (PD-1), and inducible T cell costimulator (ICOS) (5). ICOS is a member of the CD28 superfamily that is induced on T cells upon activation (6). ICOS has a sole ligand (ICOSL; also known as B7RP-1), which is a member of the immune system B7 family of costimulatory molecule ligands and is present primarily on the surface of antigen-presenting cells (6). Primary immunodeficiencies in patients lacking ICOS activity further support the requirements for these molecules in humoral immune responses in humans (7,8). Thus, inhibition of ICOS/ICOSL activity could interfere with Tfh cell–B cell interactions and modulate autoantibody production in autoimmune diseases such as SLE.

AMG 557 is a fully human IgG2 monoclonal antibody that binds with high specificity and affinity to human ICOSL to inhibit its function (9). Two phase I studies characterized the safety, tolerability, pharmacokinetics, immunogenicity, and pharmacodynamics of AMG 557 in patients with SLE after either single- or multiple-dose administration (9). Multiple-dose administration of AMG 557 was shown to selectively inhibit neoantigen-specific IgG production following keyhole limpet hemocyanin immunization (9).

The goal of the current study was to assess the safety and potential efficacy of ICOSL blockade in patients with active lupus arthritis. Historically, clinical studies in patients with SLE have been difficult to interpret because of the heterogeneity of immune pathology, clinical symptoms, and background medications (10). To overcome such difficulties, recent trials have used more discriminatory end points (11) and have enrolled large patient populations (12,13). For smaller studies, alternative approaches may be necessary, such as the use of lupus organ–specific end points and withdrawal/tapering of background medications (14). In the current study, using a small number of patients, a treatment withdrawal design and a focus on single-organ assessment (arthritis) were used to improve the detection of the clinical effects of AMG 557 relative to placebo.

PATIENTS AND METHODS

This was a phase Ib, randomized, double-blind, parallel-group, placebo-controlled, multiple-dose study in patients with active lupus arthritis. The study was performed at 8 centers in the US, Europe, and Malaysia. All patients provided written informed consent.

Key eligibility criteria. Patients were adults ages 18–65 years with a diagnosis of SLE for ≥6 months as defined by the American College of Rheumatology criteria (15,16), including positivity for antinuclear antibodies (ANAs) at screening or as previously documented. A positive ANA test was defined as a titer ≥1:80. Patients had inflammatory lupus arthritis with ≥4 tender joints and ≥4 swollen joints (28 joints assessed) and an SLE Disease Activity Index (SLEDAI) (17) score of ≥6 at screening. A requirement to be receiving immunosuppressants (methotrexate, azathioprine, or mycophenolate mofetil) for ≥12 weeks before study entry was subsequently removed to improve enrollment. Prednisone treatment was permitted if patients received a stable dosage of ≤20 mg/day (or comparable dose of another corticosteroid) for ≥4 weeks before screening. Antimalarial therapy was permitted, provided the dose had been stable for ≥4 weeks before the start of the trial.

Study design. Patients were randomized to receive 210 mg AMG 557 or equivalent placebo subcutaneously once weekly for 3 weeks, followed by 10 additional doses of AMG 557 or placebo every other week. The study initially required patients to be receiving an immunosuppressant agent at baseline, to be ≤55 years of age, and to have been immunized with H1N1 vaccine; the corticosteroid dosage permitted was ≤10 mg/day. Because of low enrollment, these criteria were later changed to remove the requirement for prestudy immunosuppressant treatment, increase the maximum age at enrollment to 65 years, require only relevant influenza vaccines during flu season, and increase the maximum corticosteroid dosage at entry to 20 mg/day. Withdrawal of immunosuppressants and corticosteroids was carried out according to a prespecified schedule (see Supplementary Figure 1, available on the *Arthritis & Rheumatology* web site at http://onlinelibrary.wiley.com/doi/10.1002/art.40479/abstract).

Immunosuppressant therapy was discontinued by day 29 in patients treated with an immunosuppressant agent at baseline. Prednisone at a dosage of ≤20 mg/day was permitted at the start of the trial, and the dosage was not to exceed 20 mg/day through day 29, not to exceed 15 mg/day through day 57, and not to exceed 7.5 mg/day by day 85. Patients received AMG 557 or placebo until the end of the study unless it was discontinued by the investigator because of adverse events (AEs), clinical laboratory abnormalities, physical examination findings, the inability to withdraw immunosuppressants by day 29, or the need to resume immunosuppressant treatment after day 29.

Assessments. The SLEDAI and British Isles Lupus Assessment Group (BILAG) index (18) were assessed at screening and on a monthly basis thereafter. Tender and swollen joint counts (68 joints and 66 joints, respectively) were assessed at screening and on days 1, 8, 15, and 29 and then monthly thereafter. Treatment response based on the Lupus Arthritis Responder Index (LARI) was used as a primary end point and was defined as follows: ≥50% decrease in the combined tender and swollen joint counts on day 169 compared with baseline, ≥1-letter improvement in the BILAG musculoskeletal system score on day 169 compared with baseline, and a reduction in and maintenance of the dosage of prednisone (or its equivalent) to ≤50% of baseline or ≤7.5 mg/day, whichever is lower, from day 85 to day 169 in patients not treated with immunosuppressants at baseline and ≤7.5 mg/day from day 85 to day 169 and discontinuation of immunosuppressants by day 29

in patients treated with immunosuppressants at baseline. AEs were monitored at each visit, graded according to the Common Terminology Criteria for Adverse Events (CTCAE), version 4.0, and coded using Medical Dictionary for Regulatory Activities version 19.0 (or a later version).

Biomarker analysis. Serum and whole blood samples were collected and sent to central (ICON plc) locations in the US, Ireland, and Singapore, for autoantibody, complement, and lymphocyte cell population measurements. Anti–AMG 557 antibodies were measured using a bridging assay that used AMG 557 to capture serum anti-drug antibodies. Any binding antibody–positive samples were subsequently tested for the presence of neutralizing antibodies (9). Lymphocyte populations were measured in whole blood, using a validated flow cytometry panel (see Supplementary Table 1, available on the *Arthritis & Rheumatology* web site at http://onlinelibrary.wiley.com/doi/10.1002/art.40479/abstract). Flow Cytometry Standard file data were analyzed centrally using a prespecified analysis template. All analytes were measured as a percentage of parent and as cells/μl (if TruCount) or as relative absolute counts (using the TBNK TruCount values as a denominator).

Statistical analysis. The primary end points were as follows: 1) safety, tolerability, and immunogenicity to day 309, and 2) response according to the LARI on day 169. Key secondary end points included the proportion of patients achieving a response according to the BILAG index musculoskeletal system score (≥1-letter improvement and a score of C or better) on day 169 and changes in tender and swollen joint counts on day 169. Exploratory end points included but were not limited to changes in the BILAG index score and the SLEDAI score by day 169 compared with placebo, proportion of patients achieving a ≥4-point decrease in the SLEDAI relative to baseline, and changes in biomarker end points including complement, autoantibodies, and lymphocyte subsets.

Descriptive statistics were reported for each end point, with no formal hypothesis testing. The LARI and other categorical end points were summarized using proportions and the associated 90% confidence intervals by treatment group. An analysis of covariance model was used to compare AMG 557 with placebo for joint counts, BILAG index, and SLEDAI on day 169 after adjusting for the baseline difference. A baseline-adjusted mixed-effects repeated measures regression model, with time and treatment as fixed factors, baseline as a covariate, patient as a random factor, and a time-by-treatment interaction term was used to compare AMG 557 with placebo for blood analyte levels. Values below the assay lower limit of quantitation (LoQ) were set to one-half the LoQ. *P* values were reported for descriptive purposes.

RESULTS

Patients. Twenty SLE patients with active lupus arthritis enrolled and received AMG 557 or placebo. The baseline demographics and disease characteristics of the enrolled patients are shown in Table 1. Most patients (95%) were women, the median age was 43 years in the AMG 557 group and 46 years in the placebo group, and the median duration of SLE was 7.8 years and 3.0 years, respectively. The mean baseline SLEDAI score was 10.4 in the AMG 557 group and 7.5 in the placebo group.

Baseline use of immunosuppressants and antimalarials was similar between the 2 groups. Four patients discontinued the investigational product: 2 because of AEs (both in the placebo group) and 2 because of increasing disease activity (1 each in the AMG 557 and placebo groups). Nineteen of 20 patients completed the study; 1 patient was lost to follow-up.

Safety. The most common events were headache and upper respiratory tract infection (see Supplementary Table 2, available on the *Arthritis & Rheumatology* web site at http://onlinelibrary.wiley.com/doi/10.1002/art.40479/abstract). The majority of AEs were CTCAE grade 1 or grade 2; 7 grade 3 events occurred in 4 patients. In the AMG 557 group, 3 grade 3 events occurred in 3 patients: depression, upper respiratory tract infection (neither considered treatment related), and myalgia (considered treatment related). In the placebo group, 1 patient experienced grade 3 headache, pyrexia, inflammation, and rash (not considered treatment related). No grade 4 events or deaths occurred during the study. Serious AEs were reported in 1 patient in the AMG 557 group (depression) and in 3 patients in the placebo group (lymphadenopathy, deafness, and pulmonary hypertension); none of these AEs was

Table 1. Baseline patient demographics and disease characteristics*

	Placebo (n = 10)	AMG 557 (n = 10)
Women	10 (100)	9 (90)
Race		
White	6 (60)	7 (70)
Asian	3 (30)	3 (30)
Black	1 (10)	0
Age, median years	46.0	43.0
SLE duration, mean years	3.0	7.8
ANA positive	10 (100)	8 (80)
Anti-dsDNA ≥30 IU/ml	4 (40)	6 (60)
BILAG global score, mean ± SD	5.3 ± 2.4	6.6 ± 3.9
SLEDAI score, mean ± SD	7.5 ± 2.0	10.4 ± 3.9
No. of tender joints (68 assessed), mean ± SD	22.9 ± 17.3	19.2 ± 12.5
No. of swollen joints (66 assessed), mean ± SD	15.5 ± 18.7	12.6 ± 13.1
Complement		
C3 <0.9 gm/liter	3 (30)	6 (60)
C4 <100 mg/liter	0	4 (40)
Treatment with prednisone >7.5 mg/day or equivalent	2 (20)	4 (40)
Immunosuppressant treatment	8 (80)	8 (80)
Methotrexate	6 (60)	7 (70)
Azathioprine	2 (20)	1 (10)
Etanercept†	0	1 (10)
Treatment with antimalarial agents	6 (60)	7 (70)

* Except where indicated otherwise, values are the number (%). ANA = antinuclear antibody; anti-dsDNA = anti–double-stranded DNA; BILAG = British Isles Lupus Assessment Group; SLEDAI = Systemic Lupus Erythematosus Disease Activity Index.
† One patient received azathioprine and etanercept; etanercept was started after AMG 557 therapy was completed, because of a disease flare.

**Table 2.** Efficacy and change from baseline in the SLEDAI, BILAG, and tender/swollen joint scores on day 169*

Variable	Treatment	
	Placebo	AMG 557
Efficacy end points		
LARI responders	1 (10) [2.3–34.8]	3 (30) [12.7–55.8]
Patients achieving a ≥4-point decrease in the SLEDAI	2 (20) [7.6–49.6]	7 (70) [44.2–87.3]
Index scores		
SLEDAI	−1.0 (−10.7)	−5.0 (−47.8)
BILAG global	−1.8 (−24.7)	−2.7 (−36.3)
No. of tender joints (28 assessed)	1.2 (−13.5)	−9.4 (−22.8)
No. of swollen joints (28 assessed)	2.0 (−7.8)	−8.9 (−62.1)

* Values for efficacy end points are the number (%) [90% confidence interval]. Values for index scores are the mean (% change from baseline). The mean change from baseline was calculated as the mean of individual changes from baseline. SLEDAI = Systemic Lupus Erythematosus Disease Activity Index; BILAG = British Isles Lupus Assessment Group; LARI = Lupus Arthritis Response Index.

considered treatment related. No anti–AMG 557 antibodies were detected at screening or at any time during the study.

Efficacy. The primary efficacy end point was the LARI, a composite measure incorporating improvements in the joint count and the musculoskeletal system component of the BILAG, discontinuation of immunosuppressants, when applicable, and the successful reduction of prednisone according to protocol. The numbers of LARI responders in both groups were relatively small. Three of 10 patients in the AMG 557 group met the criteria for a LARI response compared with 1 of 10 patients in the placebo group ($P = 0.58$) (Table 2).

Analysis of the impact of AMG 557 administration on the SLEDAI and BILAG index scores showed evidence of improvement. A greater number of patients in the AMG 557 group achieved a ≥4-point improvement in SLEDAI on day 169 (7 of 10 patients) compared with the placebo group (2 of 10 patients) ($P = 0.07$) (Table 2). The mean percent changes (improvement) in SLEDAI scores from baseline were –47.8% in patients in the AMG 557 group and –10.7% in the placebo group ($P = 0.14$). Global BILAG index scores improved by –36.3% and –24.7%, respectively, from baseline ($P = 0.89$) (Table 2). There was no discernible difference associated with AMG 557 treatment compared with placebo in the BILAG index musculoskeletal system score.
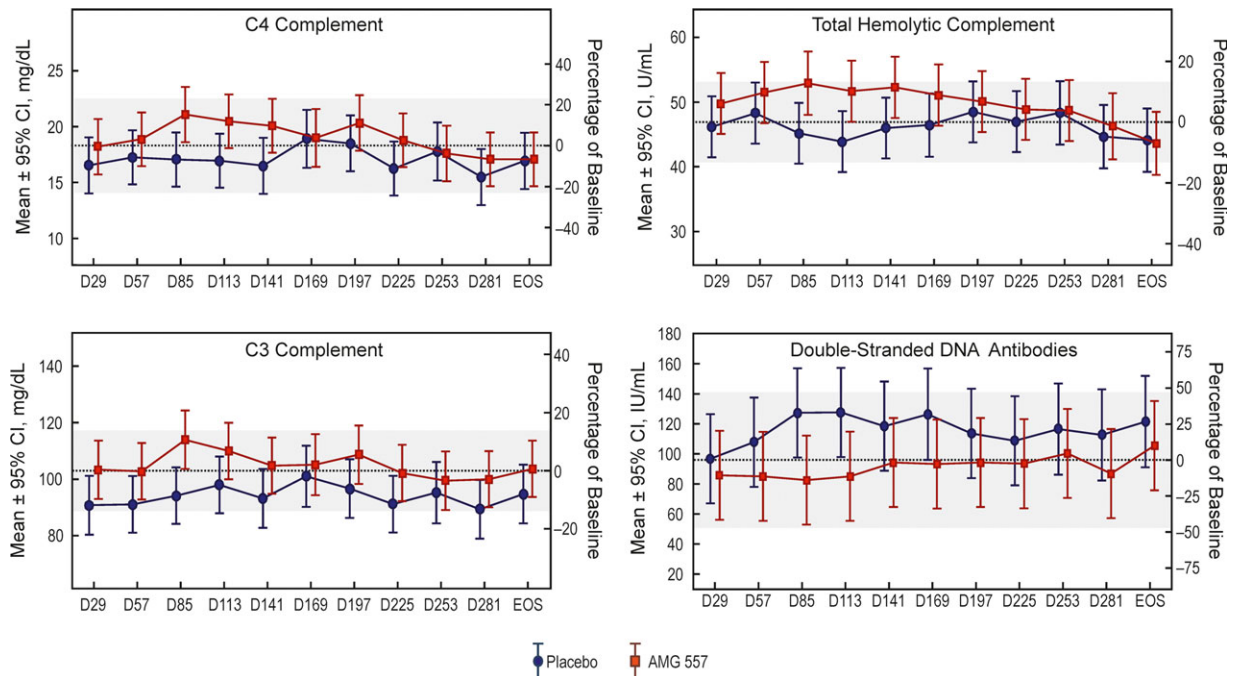
Figure 1. Biomarker analyses showing postdose changes in complement and double-stranded DNA. The dotted lines show the estimated pretreatment (baseline) mean analyte level in the study population (n = 20). The shaded bands represent the 95% confidence intervals (95% CIs) for the baseline means. The x-axis indicates the nominal time points in days. The y_1-axis (left) is the analyte level, and the y_2-axis (right) is the estimated study population mean analyte level as a percentage of baseline. All available clinical study samples were analyzed, typically resulting in 10 observations per time point per dose. For some time points, there are as few as 8 observations.

Evidence of improvement was observed with AMG 557 administration as reflected by changes in the tender and swollen joint counts from baseline (Table 2). The mean percent change in the tender joint count on day 169 was –22.8% in the AMG 557 group and –13.5% in the placebo group ($P = 0.11$), and the mean percent changes in the swollen joint count were –62.1% and –7.8%, respectively ($P = 0.03$).

Biomarkers. Although the current study was limited by a small sample size and high variability, there appeared to be differences between the treatment and placebo groups in the lupus-related biomarker end points C3, C4, total hemolytic complement, and anti-dsDNA antibodies (Figure 1), which is consistent with a beneficial treatment effect. Other autoantibodies were also measured at baseline and assessed over the course of treatment with AMG 557 or placebo (see Supplementary Figure 2, available on the *Arthritis & Rheumatology* web site at http://onlinelibrary. wiley.com/doi/10.1002/art.40479/abstract). No differences in the relative percentages of CD4+ T cells, Tfh cells, B cells, and plasma cells/plasmablasts were detected between day 29 and the end of the study.

DISCUSSION

The interaction between ICOS and ICOSL is important in T cell function, including cytokine production and differentiation to Tfh cells (6). Tfh cells play an integral role in selecting B cells for clonal expansion; hyperactivity of the ICOS pathway may lead to an imbalance in antibody-producing B cells (5). Dysregulation of T cells and B cells contributes to autoimmunity in SLE patients (3). The observed trends toward improvement in the levels of complement and anti-dsDNA in our study, and prior results demonstrating inhibition of antibody responses (9), support the hypothesis that AMG 557 blocks ICOSL and its biologic effects in an autoimmune setting.

Many biologics that target pathways supported by strong scientific rationale have failed to prove efficacy in SLE (10); trial design is suspected to play a role in these disappointing results. Because of the heterogeneous disease manifestations of lupus, multiple aggressive background medications have been allowed in trials that are suitable for patients with the most serious disease, which may yield high placebo response rates. This in turn results in the requirement for a large trial population to identify a significant treatment effect.

Here, two approaches were used to examine proof of concept in a small trial. Tender and swollen joint counts have been used successfully as an exploratory, organ-specific end point in smaller trials of SLE (19). In addition, withdrawal of background therapy has been performed safely in SLE populations with non–organ-threatening disease. This approach in a stable population has a number of advantages, as follows: supporting less-noisy immunologic profiling, exploring the pharmacodynamic effects of new agents, and lessening the high rates of placebo response to allow a small trial (14).

This study was designed as a pilot project to identify a clinical signal. The limited size of the patient population contributed to imbalances in demographics; therefore, limited conclusions can be made regarding the efficacy of AMG 557 in patients with SLE. However, changes in the LARI and SLEDAI, tender and swollen joint counts, and the proportion of responders who exhibited a 4-point drop in the SLEDAI score suggest that AMG 557 may be efficacious. Double-stranded DNA and complement measures also showed trends consistent with clinical benefit and the mechanism of action of AMG 557. AMG 557 was well tolerated, and no anti-drug antibodies were observed.

Previous phase I trials showed that AMG 557 inhibited the IgG anti–keyhole limpet hemocyanin response and had an acceptable safety profile in patients with mild, stable SLE (9). Our study extends these findings by examining patients with more significant disease over a longer period of time, providing additional data to suggest a promising safety profile as well as indicators of biologic activity and potential efficacy.

In conclusion, the safety, efficacy, and pharmacodynamic biomarker results from this small study support further evaluation of ICOSL blockade with AMG 557 as a potential therapeutic option for patients with SLE.

AUTHOR CONTRIBUTIONS

All authors were involved in drafting the article or revising it critically for important intellectual content, and all authors approved the final version to be published. Dr. Chung had full access to all of the data in the study and takes responsibility for the integrity of the data and the accuracy of the data analysis.
Study conception and design. Sullivan, Tsuji, Merrill, Chung.
Acquisition of data. Cheng, Amoura, Cheah, Hiepe, Sullivan, Tsuji, Merrill, Chung.
Analysis and interpretation of data. Cheng, Sullivan, Zhou, Arnold, Merrill, Chung.

ROLE OF THE STUDY SPONSOR

Amgen and AstraZeneca-MedImmune funded the study and were involved in the design, data collection, data analysis, and writing of the manuscript. They reviewed and approved the manuscript prior to submission. The authors independently interpreted the results and had the final approval and decision to submit the manuscript for

REFERENCES

1. Lisnevskaia L, Murphy G, Isenberg D. Systemic lupus erythematosus. Lancet 2014;384:1878–88.
2. Grossman JM. Lupus arthritis. Best Pract Res Clin Rheumatol 2009;23:495–506.
3. Kaul A, Gordon C, Crow MK, Touma Z, Urowitz MB, van Vollenhoven R, et al. Systemic lupus erythematosus. Nat Rev Dis Primers 2016;2:16039.
4. Craft JE. Follicular helper T cells in immunity and systemic autoimmunity. Nat Rev Rheumatol 2012;8:337–47.
5. Vinuesa CG, Linterman MA, Yu D, MacLennan IC. Follicular helper T cells. Annu Rev Immunol 2016;34:335–68.
6. Dong C, Nurieva RI. Regulation of immune and autoimmune responses by ICOS. J Autoimmun 2003;21:255–60.
7. Robertson N, Engelhardt KR, Morgan NV, Barge D, Cant AJ, Hughes SM, et al. Astute clinician report: a novel 10 bp frameshift deletion in exon 2 of ICOS causes a combined immunodeficiency associated with an enteritis and hepatitis. J Clin Immunol 2015; 35:598–603.
8. Grimbacher B, Hutloff A, Schlesier M, Glocker E, Warnatz K, Drager R, et al. Homozygous loss of ICOS is associated with adult-onset common variable immunodeficiency. Nat Immunol 2003;4: 261–8.
9. Sullivan BA, Tsuji W, Kivitz A, Peng J, Arnold GE, Boedigheimer MJ, et al. Inducible T cell co-stimulator ligand (ICOSL) blockade leads to selective inhibition of anti-KLH IgG responses in subjects with systemic lupus erythematosus. Lupus Sci Med 2016;3:e000146.
10. Gatto M, Saccon F, Zen M, Bettio S, Iaccarino L, Punzi L, et al. Success and failure of biological treatment in systemic lupus erythematosus: a critical analysis. J Autoimmun 2016;74:94–105.
11. Furie RA, Petri MA, Wallace DJ, Ginzler EM, Merrill JT, Stohl W, et al. Novel evidence-based systemic lupus erythematosus responder index. Arthritis Rheum 2009;61:1143–51.
12. Furie R, Petri M, Zamani O, Cervera R, Wallace DJ, Tegzová D, et al. A phase III, randomized, placebo-controlled study of belimumab, a monoclonal antibody that inhibits B lymphocyte stimulator, in patients with systemic lupus erythematosus. Arthritis Rheum 2011;63:3918–30.
13. Navarra SV, Guzman RM, Gallacher AE, Hall S, Levy RA, Jimenez RE, et al. Efficacy and safety of belimumab in patients with active systemic lupus erythematosus: a randomised, placebo-controlled, phase 3 trial. Lancet 2011;377:721–31.
14. Merrill JT, Immermann F, Whitley M, Zhou T, Hill A, O'Toole M, et al. The Biomarkers of Lupus Disease study: a bold approach may mitigate interference of background immunosuppressants in clinical trials. Arthritis Rheumatol 2017;69:1257–66.
15. Tan EM, Cohen AS, Fries JF, Masi AT, McShane DJ, Rothfield NF, et al. The 1982 revised criteria for the classification of systemic lupus erythematosus. Arthritis Rheum 1982;25:1271–7.
16. Hochberg MC, for the Diagnostic and Therapeutic Criteria Committee of the American College of Rheumatology. Updating the American College of Rheumatology revised criteria for the classification of systemic lupus erythematosus [letter]. Arthritis Rheum 1997;40:1725.
17. Bombardier C, Gladman DD, Urowitz MB, Caron D. Chang DH, and the Committee on Prognosis Studies in SLE. Derivation of the SLEDAI: a disease activity index for lupus patients. Arthritis Rheum 1992;35:630–40.
18. Yee CS, Farewell V, Isenberg DA, Prabu A, Sokoll K, Teh LS, et al. Revised British Isles Lupus Assessment Group 2004 index: a reliable tool for assessment of systemic lupus erythematosus activity. Arthritis Rheum 2006;54:3300–5.
19. Illei GG, Shirota Y, Yarboro CH, Daruwalla J, Tackey E, Takada K, et al. Tocilizumab in systemic lupus erythematosus: data on safety, preliminary efficacy, and impact on circulating plasma cells from an open-label phase I dosage-escalation study. Arthritis Rheum 2010;62:542–52.

Lupus Regulator Peptide P140 Represses B Cell Differentiation by Reducing HLA Class II Molecule Overexpression

Maud Wilhelm,[1] Fengjuan Wang,[2] Nicolas Schall,[2] Jean-François Kleinmann,[3] Michael Faludi,[4] Emil Pablo Nashi,[4] Jean Sibilia,[3] Thierry Martin,[5] Evelyne Schaeffer,[1] and Sylviane Muller[2]

Objective. Phosphopeptide P140 (Lupuzor) is an inhibitor of autophagy currently being evaluated in late-stage clinical trials for the treatment of lupus. This study was undertaken to investigate the effect of P140 ex vivo on human T and B cells.

Methods. Human B cells, T cells, and dendritic cells were analyzed by flow cytometry and cellular assays. The expression of autophagy markers was evaluated by immunoblotting and flow cytometry. The levels of B cell receptor (BCR) signaling markers and HLA molecules were assessed by flow cytometry. Toll-like receptor ligands were screened using an assay with transfected HEK 293 cells. P140 cell entry and trafficking were measured by immunofluorescence in the presence of various inhibitors of endosomal pathways.

Results. As was previously observed after intravenous injection of the peptide in a mouse model of lupus, P140 entered human B cells by a clathrin coat–dependent endocytosis process and homed into lysosomes. The peptide displayed no direct effect on BCR signaling of memory, naive mature, transitional, and B1 cells. However, it strongly reduced the overexpression of HLA class II molecules on lupus B cells that were acting as antigen-presenting cells, down-regulated the maturation and differentiation of B cells into plasma cells, and decreased IgG secretion.

Conclusion. These findings show that P140 down-regulates HLA class II overexpression in human lupus B cells, and also that P140 hampers the differentiation of B cells into autoantibody-secreting plasma cells, likely due to the resulting lack of T cell signaling and activation. This mechanism appears to switch off the downstream events leading to secretion of pathogenic autoantibodies, thus explaining the highly promising results obtained in clinical trials of P140 (Lupuzor) for the treatment of lupus.

A substantial body of evidence supports the notion that cell signaling dysfunction has a critical role in the pathogenesis and progression of systemic lupus erythematosus (SLE). In this prototypic autoimmune disease of intricate origin, immune system dysregulation seems generalized and can affect all of the compartments implicated in the innate and adaptive immune responses. Under the influence of genetic and epigenetic factors, as well as hormones and various cellular effectors, various subsets of T and B cells are generally shifted toward an overactivated state, resulting in the production of pathogenic factors, including autoantibodies, cytokines, and chemokines,

which, downstream, leads to widespread inflammation and tissue damage.

The phenotype of lupus lymphocytes is analytically complex, with some characteristics that appear to be opposite in function. As naive or anergic T cells, lupus T lymphocytes are less prone to produce cytokines such as interferon-γ and interleukin-2 (IL-2), whereas as activated and memory T cells, they show increased tyrosine phosphorylation of signaling intermediates, show a faster and stronger calcium flux response after T cell receptor (TCR) activation, and display higher levels of adhesion or costimulatory molecules such as CD44 and CD40L. The TCR composition is also profoundly altered in lupus. Compared to normal T cells, the levels of CD3 ζ-chain (CD3ζ) are lower in lupus T cells, and this component is replaced by the Fcε receptor common γ-chain (FcRγ), a component of the IgE receptor, which presents a structure similar to that of CD3ζ. This replacement is important because FcRγ signals through a different adaptor protein, known as Syk, rather than via the intracellular protein zeta-associated protein 70 kd (1).

In addition to these intrinsic structural disturbances that interfere with signal transduction between effector immune cells, the trafficking of these cells, as well as the secretion of mediators, can affect organelle homeostasis and cell metabolism in lupus (2). Significant alterations of the mitochondrial, endolysosomal, and autophagosomal compartments have been documented (2–6). These changes that modify the actual functioning of immune cells (e.g., ATP supply, life/death balance, impaired or excessive component elimination and recycling, and cell division, differentiation, and growth) are now known to occur in patients with SLE but are still far from being controlled appropriately by specific drugs.

As is generally the case in chronic, inflammatory autoimmune diseases, current pharmacologic treatments for SLE are largely palliative. Medications are focused on the dominant symptoms but do not address the defective pathways that are engaged in the lupus syndrome. In most patients, the drugs given for the treatment of SLE tend to result in nonspecific immunosuppression, which can be associated with disruption of innate and induced immunity, thereby aggravating the general health status of patients by generating significant adverse effects. Among the arsenal of medications that are under development, tools that target key components of the immune system, rather than those that globally reduce its hyperactivation, are still a rarity. Within this class of potent drugs, the phosphopeptide P140, which encompasses the sequence 131–151 of the U1-70K protein (7), is very promising for treating patients with SLE (8).

Following extensive studies in lupus-prone MRL/lpr mice, we discovered that P140 targets autophagy (9),

a finely orchestrated catabolic process involved in the regulation of inflammation and the biology of immune cells (10,11). P140 acts directly on a particular form of autophagy known as chaperone-mediated autophagy (CMA) (for more details, see ref. 12), which appears to be hyperactivated in MRL/lpr mouse B cells (9), and most likely acts indirectly on the macroautophagy process (12,13), which also shows higher activity in both T and B cells in lupus (9,13–17). Shortly after its intravenous administration into MRL/lpr mice, the P140 peptide, which we followed up in the splenic B cells of MRL/lpr mice, was endocytosed via a clathrin-mediated endocytosis (CME) pathway and was found to accumulate in the lysosomes of these B cells that were acting as antigen-presenting cells (APCs). Noticeably, MRL/lpr mouse splenic lysosomes were unexpectedly found to exhibit some intrinsic defects; they especially displayed, on average, a significantly higher lumenal pH (9,18).

Supported by in vitro and in vivo studies carried out in MRL/lpr mice (7,9,13,18–21), our current mechanistic view regarding the mode of action of P140 in MRL/lpr mice is as follows. The P140 peptide is known to readily interact with the constitutively expressed 70-kd heat-shock protein HSPA8 (22). Once the peptide is internalized into B cell lysosomes, it could compromise abnormally activated CMA by disrupting the lysosomal HSPA8 heterocomplexes containing HSP90AA1 (13). As a result, it is anticipated that cellular autoantigen loading to major histocompatibility complex (MHC) class II molecules in the late endosomal MHC class II compartments of B cell APCs would be altered, leading to a weaker priming of autoreactive T cells (19) and a probable reduction in the help signals to autoreactive B cells. These downstream events could contribute to the decrease in proliferation and differentiation of B cells into deleterious autoantibody-secreting plasma cells (ASPCs), resulting in a drop in autoantibody secretion (7) and a remarkable delay in mortality, as was found in P140-treated MRL/lpr mice compared to naive MRL/lpr mice that received saline only (7,20).

In a phase IIb multicenter, randomized, placebo-controlled clinical study of lupus, treatment with P140 (Lupuzor) was found to be safe and met its primary efficacy end points (8), thus confirming the validity of the preclinical data generated in lupus-prone mice (7,20). At the moment, however, although it was found in the MRL/lpr mouse model of lupus, the effective influence of the P140 peptide on the function of APCs and T cells in human patients has not yet been addressed. Moreover, the potential effect of P140 on B cell differentiation has not been documented, even in a mouse setting.

To address these significant evidence gaps, we deciphered the effects of P140 using peripheral blood

mononuclear cells (PBMCs) from healthy donors and patients with SLE. In addition, in some cases, when large numbers of B cells were required, we used the human Raji B cell line. In this study, we demonstrate that P140 down-regulates HLA class II overexpression on lupus B cells and hampers B cell differentiation into ASPCs. This mechanism potentially switches off the downstream events leading to pathogenic autoantibody secretion, thus explaining the highly promising results obtained in clinical trials of P140 (Lupuzor) for the treatment of lupus.

PATIENTS AND METHODS

Samples from patients and healthy donors. Blood samples were collected from 23 patients with SLE and 8 patients with systemic sclerosis (SSc). The characteristics of the SLE patients are listed in Supplementary Table 1 (available on the *Arthritis & Rheumatology* web site at http://onlinelibrary.wiley.com/doi/10.1002/art.40470/abstract). Fresh buffy coats containing most of the white blood cells and platelets from healthy donors were used as controls. Preparation of PBMCs and the methods used to investigate their reactivity are described in more detail in Supplementary Patients and Methods (on the *Arthritis & Rheumatology* web site at http://onlinelibrary.wiley.com/doi/10.1002/art.40470/abstract).

Peptides and peptide imaging. The phosphopeptides P140 (RIHMVYSKRpSGKPRGYAFIEY), truncated P140 desTyr[151] (RIHMVYSKRpSGKPRGYAFIE), and scrambled peptide ScP140 (YVSRYFGpSAIRHEPKMKIYRG), as well as the nonphosphorylated nominal peptide 131–151 (RIHM-VYSKRSGKPRGYAFIEY), were synthesized as described previously (7). Their homogeneity was checked by analytic high-performance liquid chromatography (HPLC) and their identity was assessed by mass spectrometry. For coupling purposes, peptides were also synthesized with a cysteine residue added at their N-terminus. Alexa Fluor 488–conjugated Cys peptides were prepared by reacting equimolar amounts of the maleimide derivatives (ThermoFisher Scientific) and peptides in dimethylformamide. The conjugates were purified by HPLC and lyophilized in the dark. Fluorescence imaging of the peptides accumulating into lysosomes is described in detail in Supplementary Patients and Methods (http://onlinelibrary.wiley.com/doi/10.1002/art.40470/abstract).

Commercial antibodies used. The full list of antibodies used for flow cytometry analysis of B and T cells, analyses of dendritic cells (DCs) and B cell receptor (BCR) signaling, and Western blotting experiments is included in Supplementary Patients and Methods (http://onlinelibrary.wiley.com/doi/10.1002/art.40470/abstract).

Isolation and culture of primary human B and T cells and Raji B cells, cellular assays, flow cytometry, and immunofluorescence experiments. Classic procedures were used for cell isolation and culture, cellular assays, flow cytometry analyses, and evaluation of the cells by immunofluorescence. The full experimental details are provided in Supplementary Patients and Methods (http://onlinelibrary.wiley.com/doi/10.1002/art.40470/abstract).

Evaluation of HLA molecule expression. Purified B cells (1×10^6 cells/ml) from healthy donors and SLE patients were incubated in complete culture medium. At 24 hours after incubation of the cells with peptides, expression of HLA molecules was evaluated by flow cytometry, using a fluorescein isothiocyanate–conjugated anti–HLA–DR/DP/DQ antibody.

Evaluation of macroautophagy and CMA levels by Western blotting and flow cytometry. The methods used to evaluate macroautophagy and the levels of CMA have been described recently (23). The full experimental details are provided in Supplementary Patients and Methods (http://onlinelibrary.wiley.com/doi/10.1002/art.40470/abstract).

Toll-like receptor (TLR) ligand screening. The TLR ligand screening assay (InvivoGen) was based on recombinant HEK 293 cells, which stably express the functional human TLRs 2, 3, 4, 5, 7, 8, and 9 and an NF-κB–inducible reporter gene. Cells incubated with TLR-specific ligands were used as a positive control.

Statistical analysis. Statistical analyses were performed using GraphPad Prism software version 5.0. Depending on the number of samples that were included in the analyses, statistical significance was assessed using the parametric Student's t-test or the nonparametric Mann-Whitney U test. P values less than 0.05 were considered significant.

RESULTS

Peptide characteristics. The 21-mer P140 peptide corresponds to sequence 131–151 of the spliceosomal small nuclear RNP U1-70K. It contains a phosphoserine residue at position 140, which was added chemically during its synthesis when we undertook our first investigations on its potent protective properties in mice with lupus (7). It subsequently emerged that this punctual modification corresponded to a natural, apoptosis-specific posttranslational modification of the protein (24). P140 alone (in saline or in mannitol) does not generate any antibody response in humans or in mice (21). Its stability (and that of the phosphoryl moiety) has been analyzed at different temperatures and pH levels in various salt conditions and in controlled medium (9,18). The structure of both phosphorylated and nonphosphorylated sequences in aqueous solution has been determined by ^{1}H-nuclear magnetic resonance spectrometry and calculation of molecular dynamics (22). P140, the sequence of which has been remarkably conserved over evolution, is a ligand of HSPA8; it interacts with the N-terminal nucleotide binding domain of the protein (9,18). It also promiscuously binds to murine and human MHC class II molecules in vitro and in vivo (7,25). In the present study, the first aspect that we explored in a human setting was to determine whether, as was observed in the context of lupus-prone MRL/lpr mice, P140 uses CME as a portal to enter B cells, and whether it affects the expression of HSPA8 and HLA class II molecules at the surface of those cells.

Entry of P140 into human B cells by a clathrin coat–dependent endocytosis process. In studies using markers of endocytosis and several cell-entry inhibitors that inhibit CME or caveolin-dependent endocytosis, we demonstrated

that Alexa Fluor 488–labeled P140 readily entered human Raji B cells by CME, whereas the Alexa Fluor 488–labeled unphosphorylated peptide 131–151 and the truncated Alexa Fluor 488–labeled analog of peptide P140 entered human Raji B cells to a much lesser extent or not at all via CME (Figures 1A–C and Supplementary Figure 1, available on the *Arthritis & Rheumatology* web site at http://onlinelibrary.wiley.com/doi/10.1002/art.40470/abstract). In addition, the phosphopeptide P140 homed to lysosomes (Figure 1D). The same lysosomal accumulation of P140 was observed using B cells from healthy donors (see Supplementary Figure 2, available on the *Arthritis & Rheumatology* web site at http://onlinelibrary.wiley.com/doi/10.1002/art.40470/abstract).

Collectively, our findings reveal the pathway used by the P140 peptide in human cells, and show the paramount importance of the phosphorylated moiety in this process. This set of experiments could not be performed using B cells from patients with SLE, due to the fact that only a low number of B cells could be purified from the PBMC fraction, as these patients are classically affected by lymphopenia.

Decreased overexpression of HLA class II molecules in the presence of P140 peptide. MHC class II molecules are overexpressed in MRL/lpr mouse splenic B cells, and we previously demonstrated that this overexpression was significantly diminished following daily

intraperitoneal injections of P140 into 12-week-old mice (13). Results from flow cytometry experiments confirmed that, as compared to healthy donor B cells, there was a significant increase in the levels of HLA–DR/DP/DQ molecules on SLE CD19+ B cells ($P = 0.0056$) but not on SSc CD19+ B cells (Figure 2A). Treatment with P140, but not the ScP140 control peptide, significantly decreased, in a dose-dependent manner, the overexpression of HLA class II molecules on total CD19+ B cells (Figure 2B), regardless of whether the B cells were activated or were not activated (mean ± SD decrease −9.07 ± 6.07% and −11.13 ± 10.23%, respectively, at a P140 peptide concentration of 30 μM; $P = 0.0004$) (Figures 2C and D). This effect, however, had no influence on the absolute number or relative number (percentage) of activated B cells in the total B cell population (results not shown). Moreover, it was not linked to a possible apoptotic effect of P140 that could have affected B cells (see Supplementary Figure 3, available on the *Arthritis & Rheumatology* web site at http://onlinelibrary.wiley.com/doi/10.1002/art.40470/abstract).

Of note, this abrogating effect of P140 on HLA–DR/DP/DQ overexpression was found to be related to individual scores on the SLE Disease Activity Index (SLEDAI) (26) in patients with SLE (Figure 2E). The higher the SLEDAI score in a patient, the stronger was
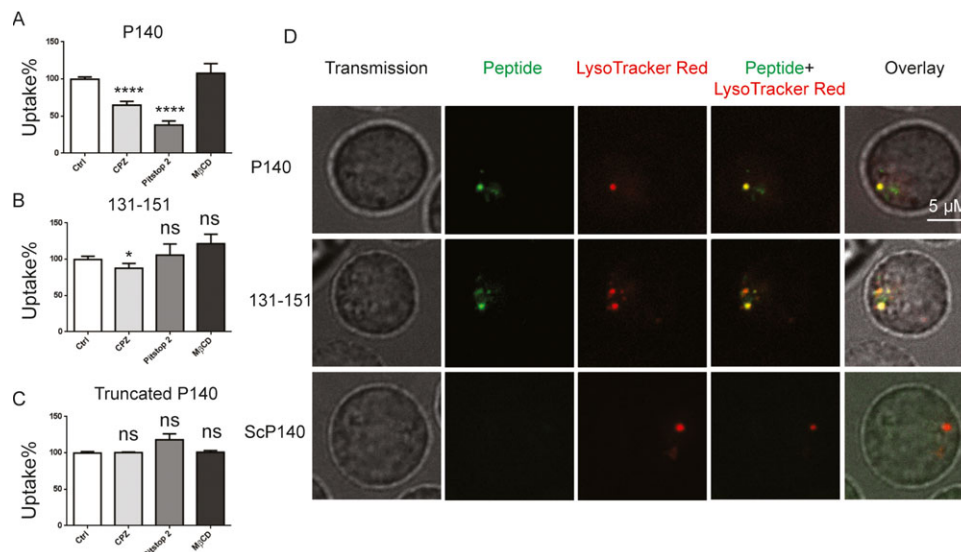
Figure 1. Entry of phosphopeptide P140 into human Raji B cells via a clathrin-mediated endocytosis pathway. **A–C,** Cellular uptake of Alexa Fluor 488–labeled P140 peptide **(A)**, 131–151 peptide **(B)**, and P140 desTyr[151] peptide **(C)** was quantified by flow cytometry in Raji cells that were left untreated (control [Ctrl]) or pretreated with various endocytosis inhibitors, namely chlorpromazine (CPZ) or Pitstop 2 for inhibition of clathrin-mediated endocytosis and methyl-β-cyclodextrin (MβCD) for inhibition of caveolin-mediated endocytosis. Mean fluorescence intensity values, normalized to those in untreated control cells, were used to calculate the percentage of uptake. Results are the mean ± SEM of triplicate experiments, from 3 independent experiments. **D,** B cell trafficking to lysosomes was evaluated using human Raji cells that were exposed to 10 μM Alexa Fluor 488–labeled peptides P140, 131–151, or ScP140 for 2 hours, followed by lysosomal staining with LysoTracker Red. Cells were washed and immediately imaged with a spinning disk microscope. Representative images from 2–3 independent experiments are shown. * = $P < 0.05$; **** = $P < 0.0001$ versus control, by Student's t-test. NS = not significant.
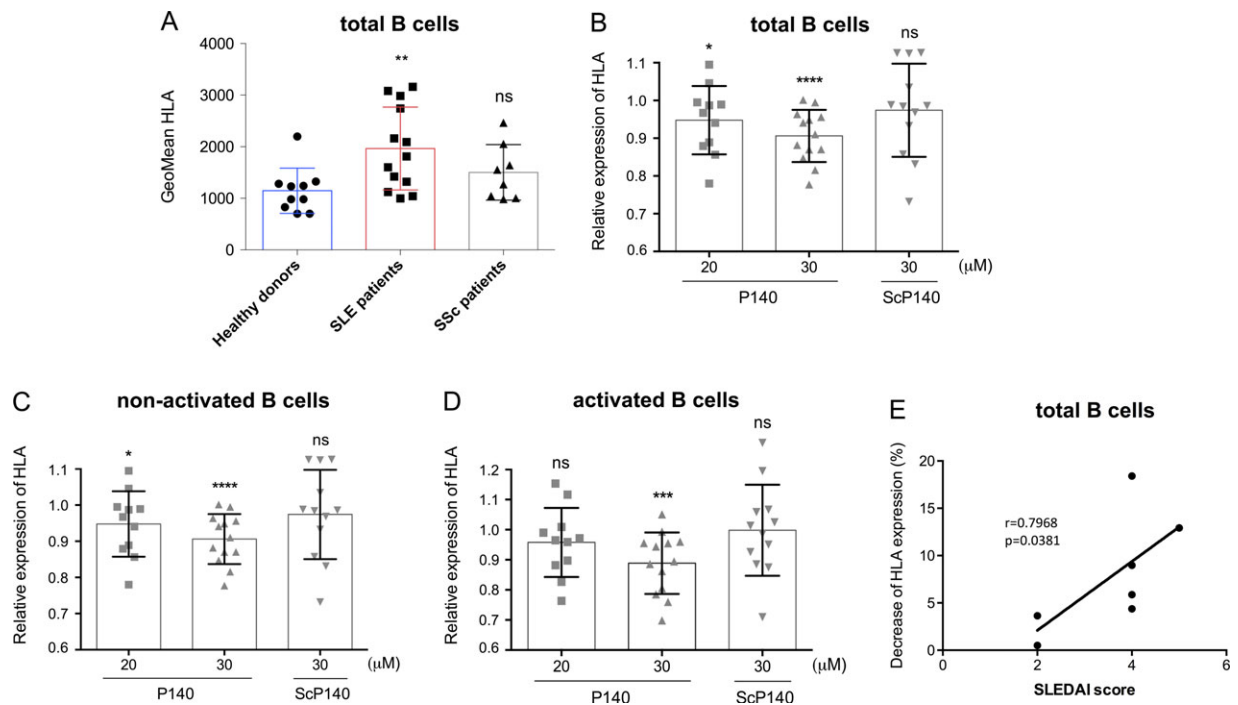
Figure 2. HLA class II expression on B cells from patients with systemic lupus erythematosus (SLE), and effect of peptide P140. **A,** HLA class II expression was compared in total CD19+ B cells from the peripheral blood mononuclear cells of healthy donors (n = 10), patients with SLE (n = 13), and patients with systemic sclerosis (SSc) (n = 8). ** = $P < 0.01$ versus healthy donors, by unpaired t-test. **B–D,** Expression of HLA–DR/DP/DQ was measured by flow cytometry in total CD19+ B cells (**B**), nonactivated CD19+CD86− B cells (**C**), and CD19+CD86+ activated B cells (**D**) after treatment with increasing concentrations of P140 or ScP140. Relative expression values were normalized to that of untreated cells. In **A–D**, each symbol represents an individual patient or healthy donor; bars show the mean ± SD. * = $P < 0.05$; *** = $P < 0.001$; **** = $P < 0.0001$, by unpaired t-test. **E,** Correlation between decreased HLA–DR/DP/DQ expression on nonactivated CD19+CD86− B cells and the SLE Disease Activity Index (SLEDAI) score in patients with SLE (effect measured at a P140 concentration of 30 µM). Following Spearman's correlation analysis, patients with a negative score were excluded from the study. NS = not significant. Color figure can be viewed in the online issue, which is available at http://onlinelibrary.wiley.com/doi/10.1002/art.40470/abstract.

the effect of P140 in terms of decreasing the expression of DR/DP/DQ molecules on the cell surface of CD19+ B cells. No direct relationship between the ex vivo effect of P140 and the levels of anti–double-stranded DNA (anti-dsDNA) antibodies was observed, thus indicating that the anti-dsDNA antibody is not a good marker of P140 efficacy.

It is also important to point out that treatment with P140 decreased, in a dose-dependent manner, the average expression of HLA class II molecules on B cells
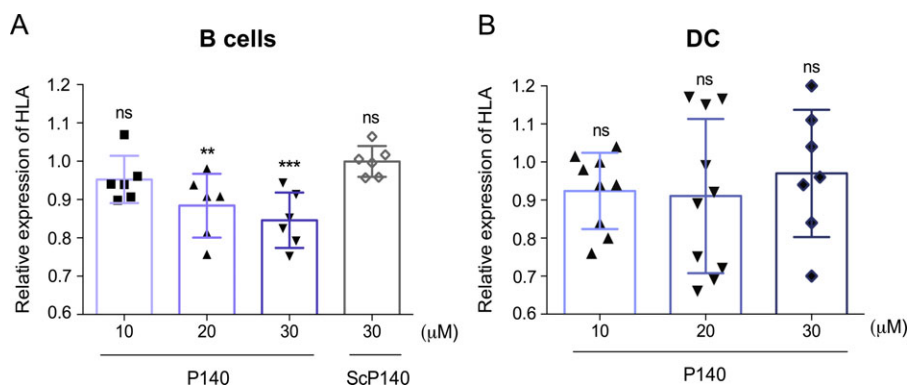
Figure 3. HLA class II expression on B cells and dendritic cells (DCs) from healthy donors, and effect of peptide P140. Expression of HLA–DR/DP/DQ was measured by flow cytometry in nonactivated CD19+CD86− B cells (**A**) or CD14^{low}CD1a^{high}DC-SIGN+ DCs (**B**) from 6–10 healthy donors. HLA class II expression in cells treated with increasing concentrations of either P140 or ScP140 was normalized to that of untreated cells. Each symbol represents an individual donor; bars show the mean ± SD. ** = $P < 0.01$; *** = $P < 0.001$, by unpaired t-test. NS = not significant. Color figure can be viewed in the online issue, which is available at http://onlinelibrary.wiley.com/doi/10.1002/art.40470/abstract.

from healthy donors (mean ± SD decrease −15.4 ± 7.23%) (Figure 3A). However, the peptide had only a minimal effect on the average expression of HLA class II molecules on DCs from healthy donors (mean ± SD decrease −3.0 ± 17%) (Figure 3B). Whether P140 had a noticeable effect on DCs was, however, highly dependent on the individual healthy donor cell source.

Autophagy in human B and T lymphocytes. Our earlier work showed that macroautophagy, the best-characterized type of autophagy, is abnormally enhanced in T lymphocytes from mice with lupus and patients with SLE (15). These results have been confirmed by others (16,27) and supported by a recently completed study in B cells from (NZB × NZW)F1 mice and patients with lupus (17). Furthermore, macroautophagy was shown to be required for differentiation of plasmablasts (28,29) and survival of memory B cells (30,31), thus indicating that this process seems to have a central role in humoral autoimmunity both in mice and in humans with lupus. In addition, our own studies demonstrated that CMA is also activated in MRL/lpr mouse B cells (9), and that this feature is associated with alteration of lysosomes, since the number and size, as well as average pH, of lysosomes were increased in our mouse model of lupus. In MRL/lpr mice that received P140 peptide intravenously, most of these alterations were no longer observed in B cells (9,18).

Consistent with our own observations made in MRL/lpr mouse B cells (15), no alteration of macroautophagy could be detected in human B cells in the present study (Figures 4A and B). This was measured by evaluating the intracellular expression of SQSTM1, which is selectively incorporated into autophagosomes and is degraded through macroautophagy (its cellular expression level negatively correlates with the activity of this process) (32). As expected in these conditions, no effect of P140 was noted.

With regard to the effects on T cells, when compared to cells from healthy donors, the levels of SQSTM1 expression were found to be lower in CD4+ and CD8+ T cells from patients with SLE (as exemplified by the findings in 1 SLE patient shown in Figures 4C and E, and as found in 4 of the 5 SLE patients tested [Figures 4D and F]). These results indicate that in contrast to B cells, T cells display higher macroautophagy activity.

Active autophagic flux (determined as the conversion from MAP1LC3-I to MAP1LC3-II) could also be measured in phorbol myristate acetate/ionomycin–stimulated T cell cultures that were treated with the protease inhibitors E64D and pepstatin A or left untreated. No significant differences were found between healthy donor and SLE T cells. In this cell type, no P140-dependent effect on the expression of MAP1LC3 or SQSTM1 could be observed (Figures 4A–F and Supplementary Figure 4,

available on the *Arthritis & Rheumatology* web site at http://onlinelibrary.wiley.com/doi/10.1002/art.40470/abstract).

CMA-associated markers were also studied in B and T cell subsets collected from the peripheral blood of healthy donors and patients with SLE; patients with SSc were used as controls. Both the expression of LAMP2A and expression of HSPA8 remained at the basal level in B cells and in resting or ex vivo–activated CD4+ and CD8+ T cells from all SLE blood donors examined (see Supplementary Figure 5, available on the *Arthritis & Rheumatology* web site at http://onlinelibrary.wiley.com/doi/10.1002/art.40470/abstract). As expected in the absence of any specific activation of CMA in lymphocytes from patients with SLE, P140 showed no effect in this setting.

Lack of effect of P140 on TLR activation. Functional interactions between autophagy and pattern-recognition receptors, such as TLRs, nucleotide-binding oligomerization domain–containing protein–like receptors, and retinoic acid–inducible gene 1–like receptors, have been described (33). Depending on the cell environment (e.g., cytokines/chemokines) or on the cell subtype, these interactions with innate immunity receptors can functionally exert either activation or down-regulation of the autophagic machinery. Thus, induction of autophagy by signaling through TLRs 2, 3, 4, 5, and 7 has been described (34,35). With the current knowledge regarding the key role played by some TLRs, such as TLRs 4, 7, and 9, in lupus (36,37) and the relationships that have been established between TLRs, autophagy, and lupus (35), we next determined whether P140 could interact with specific TLRs, particularly with endosomal TLRs 3, 7, 8, and 9. This possibility was tested using a screening assay based on recombinant HEK 293 cell lines expressing functional human TLRs, and an NF-κB–inducible reporter gene. P140 peptide was unable to activate any of the cell lines expressing human TLRs (see Supplementary Figure 6, available on the *Arthritis & Rheumatology* web site at http://onlinelibrary.wiley.com/doi/10.1002/art.40470/abstract), leading to the conclusion that, at least in the in vitro conditions used in the present study, P140 is not a TLR agonist.

To further consolidate these data, we studied the possible effect of P140 on the production of the proinflammatory cytokine tumor necrosis factor α (TNFα) by DCs collected from healthy donors. The antiinflammatory mannoside glycolipid conjugate 2U was used as an internal control (38). The results showed that, in contrast to the effects of the 2U compound, P140 did not inhibit lipopolysaccharide-induced production of TNFα (see Supplementary Figure 7, available on the *Arthritis & Rheumatology* web site at http://onlinelibrary.wiley.com/doi/10.1002/art.40470/abstract), thus further supporting the view that P140 has no effect on TLR-4 signaling.
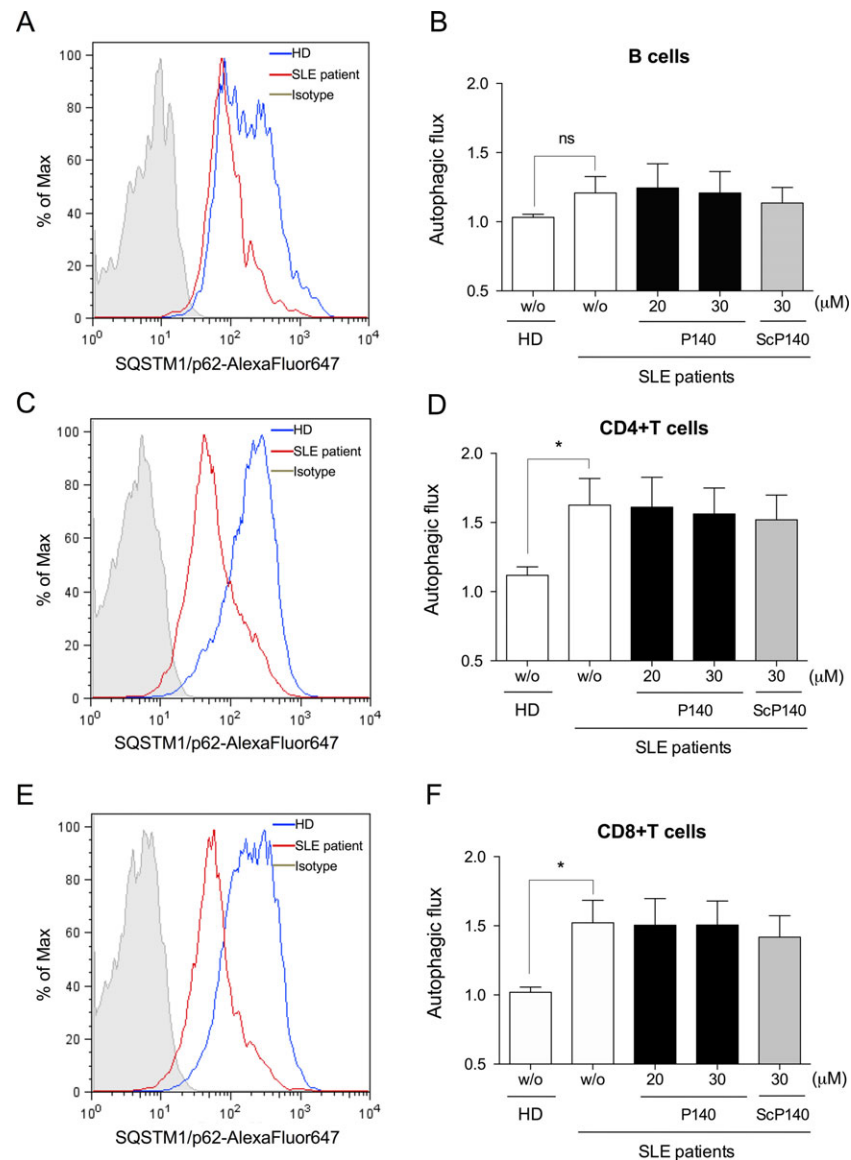
Figure 4. Expression of SQSTM1 in B and T cells from healthy donors (HDs) and patients with systemic lupus erythematosus (SLE). **A, C,** and **E,** Autophagic activity was measured by flow cytometry using intracellular staining of SQSTM1 in purified peripheral blood mononuclear cells (PBMCs) from SLE patients and healthy donors, with gating first on B cells and then on CD4+ and CD8+ T cells. Representative results from a single SLE patient and a single healthy donor are shown. **B, D,** and **F,** To visualize the accumulation of autophagic substrate SQSTM1, PBMCs were incubated in complete RPMI medium with or without 10 μg/ml of the protease inhibitors E64D and pepstatin A. Inhibitors were added 4 hours before the end of the cultures. The data reflect the ratio of SQSTM1 levels in the presence and absence of inhibitors. Autophagic flux in B cells **(B)**, CD4+ T cells **(D)**, and CD8+ T cells **(F)** was compared between healthy donors (n = 6) and SLE patients (n = 5), in cultures without (w/o) or with pretreatment with peptide P140. Results are the mean ± SEM. * = *P* < 0.05 by Mann-Whitney U test. NS = not significant.

Diminished proliferation of CD4+ T cells in the presence of P140-treated B cell APCs. We have demonstrated that P140 peptide readily reduces the expression of MHC class II molecules at the surface of B cells, both in human patients with SLE (Figure 2) and mice with lupus (13). We also showed previously in a lupus setting that P140 decreases the activity of self-reactive murine and human T cells (19,25). To determine whether these 2 functional events are directly linked, we developed a coculture system with B and T cells from distinct healthy donors, to induce an allogeneic response. B cells from healthy donor 1 were incubated with P140 at an optimal concentration of 30 μ*M* (or with ScP140 as a control) or left untreated (Figure 5A). At this concentration, P140 induced a 20% decrease in the levels of MHC class II expression (Figure 5B). After treatment with mitomycin
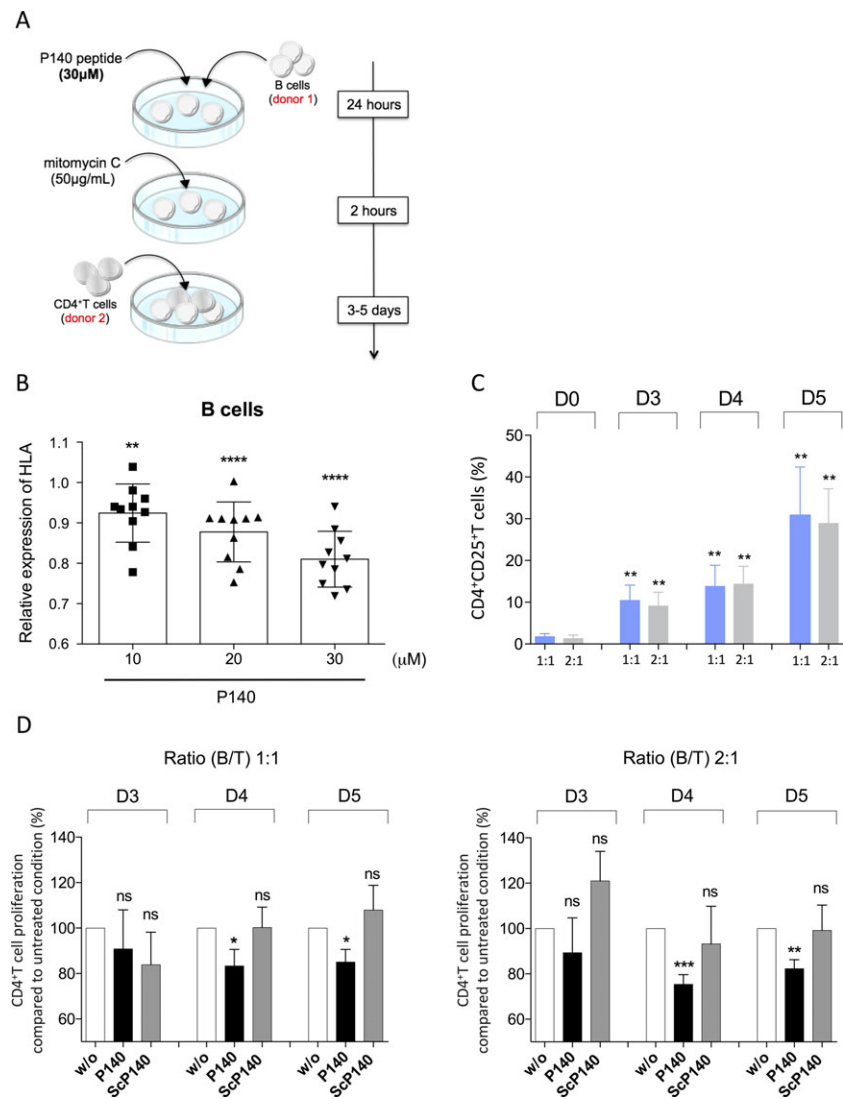
Figure 5. Effect of peptide P140 on the capacity of CD4+ T cells to proliferate. **A,** Study design. In order to induce an allogeneic reaction, B and T cells from 2 different healthy donors were mixed at different B cell:T cell ratios. **B,** The most effective concentration of P140 to induce a significant decrease in major histocompatibility complex class II expression was evaluated, demonstrating that 30 μM of P140 was the optimal concentration. Each symbol represents an individual donor; bars show the mean ± SD (n = 10). ** = $P < 0.01$; **** = $P < 0.0001$, by unpaired t-test. **C,** Purified B cells incubated with 30 μM P140 for 24 hours were treated with mitomycin C (50 μg/ml, for 2 hours at 37°C) and mixed at different ratios with CD4+ T cells from a second donor. The efficacy of the coculture system was validated by measuring the percentage of CD4+CD25+ T cells over several days (D0–D5) of coculture. Results are the mean ± SD (n = 6). ** = $P < 0.01$ versus day 0, by Mann-Whitney U test. **D,** Proliferation of CD4+ T cells (measured as tritiated thymidine incorporation) was evaluated at 2 different cell ratios over several days of coculture without (w/o) peptide or with peptide P140 or ScP140. Results are the mean ± SEM from 5 independent experiments. * = $P < 0.05$; ** = $P < 0.01$; *** = $P < 0.001$, by Mann-Whitney U test. NS = not significant. Color figure can be viewed in the online issue, which is available at http://onlinelibrary.wiley.com/doi/10.1002/art.40470/abstract.

C, B cells were incubated with CD4+ T cells from the second healthy donor, at B cell:T cell ratios of 1:1 and 2:1. In this experimental setting, if a decrease in MHC class II expression is induced by P140, less antigenic peptides should be presented to T cells and, consequently, their proliferation in vitro should be diminished.

As expected, in the absence of any peptide, a significant increase in the percentage of CD4+CD25+

T cells (mostly corresponding to activated T cells) was continuously observed over time in the cocultures (Figure 5C). In the presence of P140, however, CD4+ T cells proliferated significantly less actively (Figure 5D). Reductions in the proliferation levels were most effective on days +4 and +5 of the coculture and at a B cell:T cell ratio of 2:1, as compared to a B cell:T cell ratio of 1:1. It was specific to P140, as no effect

was noted when B cells introduced into the coculture were pretreated with ScP140. These findings strongly suggest that the decrease in CD4+ T cell proliferation is a direct consequence of the diminished expression of MHC class II molecules and reduction in antigen presentation induced by the P140 peptide.

Prevention of B cell maturation and differentiation and reduced secretion of IgG following P140 treatment. Our previous results (13,14,19,25) and the findings in the present study demonstrated that P140 induces a reduction in the level of expression of MHC class II molecules on B cell APCs and a lowering of T cell proliferation. We also showed previously, both in mice and in patients with lupus, that P140 in vivo administration leads to a reduction in the levels of blood circulating anti-dsDNA antibodies (7,39), which are markers of SLE. We therefore decided to conduct a set of experiments intended to determine a possible link between these 2 events, and in particular to examine whether, in conjunction with the effect of P140 on T cell activation, proliferation, and signaling ability, the drop in autoantibody secretion could be attributable to an altered capacity of B cells to differentiate into ASPCs. To
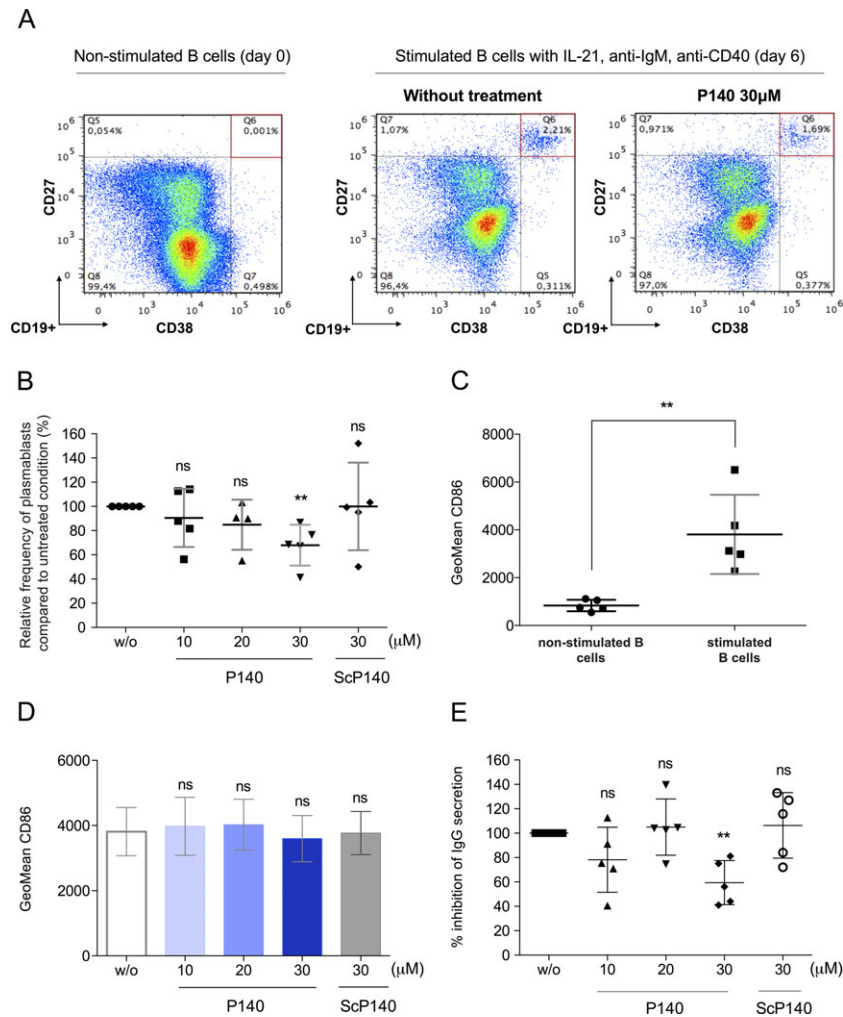
Figure 6. Effect of P140 on the capacity of B cells to differentiate into autoantibody-secreting plasma cells. Purified B cells from 5 healthy donors were allowed to differentiate in vitro in the presence of anti-CD40/anti-IgM antibodies and interleukin-21 (IL-21), without (w/o) or with increasing concentrations of P140 peptide. ScP140 was used as a control. Differentiation was assessed 6 days later by flow cytometry, by evaluating marker expression of CD19, CD27, and CD38. The fact that apoptosis did not occur until at least 6 days after addition of P140 to ScP140 to the cultures was also noted. **A,** Dot plots of the cells under each condition. Representative results of 5 independent experiments are shown. **B,** Changes in the percentage of plasmablasts (CD19+CD27^{high}CD38^{high} cells) as a function of P140 concentration. **C,** Activation status of B cells evaluated by measuring CD86 expression at the beginning and end of the culture. **D,** Effect of P140 on CD86 expression after 6 days of stimulation. **E,** Percentage of inhibition of IgG secretion as a function of P140 concentration. The supernatant was collected after 8 days of culture, and secretion of IgG was measured by enzyme-linked immunosorbent assay. Each symbol represents an individual healthy donor; bars show the mean ± SD (n = 5 independent experiments). ** = $P < 0.01$ by Mann-Whitney U test. NS = not significant.

check this ultimate property of P140, purified B cells from 5 healthy donors were allowed to differentiate in vitro with anti-CD40 antibodies, anti-IgM antibodies, and IL-21 (40) in the presence or absence of P140 peptide or control peptide ScP140. Six days later, B cell differentiation was assessed by flow cytometry to measure the expression of CD19, CD27, and CD38 (Figure 6A).

In a dose-dependent manner, P140, but not ScP140, decreased the percentage of CD19+CD27^{high}CD38^{high} plasma cells (Figure 6B). This finding was not linked to the apoptosis of B cells (results not shown), which can be a potential factor in 6-day cultures of B cells. Of note, the overall activation status of this depleted differentiated B cell population, as measured by CD86 marker expression, remained unchanged (Figures 6C and D). However, the levels of IgG secreted by differentiated B cells in the supernatant of 8-day cultures was significantly decreased in the presence of P140 (at a concentration of 30 μM), but not in the presence of the ScP140 control peptide (Figure 6E).

Lack of a direct effect of P140 on BCR signaling of memory, naive mature, transitional, and B1 cells. In our last series of experiments, which were important to elaborate our working assumptions of the P140 mechanism of action in humans, we wanted to check whether P140 could display a direct effect on BCR signaling. These experiments were undertaken using a validated flow cytometry–based assay designed to investigate the BCR signaling pathway (Faludi M, et al: unpublished observations), a pathway that is critical in the development and function of B cells. Studying different B cell subtypes under multiple conditions revealed no effect of P140 and ScP140 peptides on BCR signaling in IgM memory, IgG memory, naive mature, transitional, or B1 cells (see Supplementary Figure 8, available on the *Arthritis & Rheumatology* web site at http://onlinelibrary.wiley.com/doi/10.1002/art.40470/abstract).

Taken together, these whole series of data strongly support the view that P140 readily induces a drop in secretion of autoantibodies in patients with SLE via a mechanism involving the upstream step of T cell regulation (i.e., regulation of T cell activation, proliferation, and signaling ability) along with a strong downstream impact on B cell maturation and differentiation into ASPCs, but without directly acting on the maturation of B cells.

DISCUSSION

In the current study, which is the first to describe the molecular effect of therapeutic peptide P140 (Lupuzor) in human cells, we demonstrate that P140 has no direct effect on BCR signaling of memory, naive mature, or transitional B cells. This result suggests that P140 does not alter

B cell survival and maturation through a direct effect on these B cell subsets. However, we clearly show that P140 is highly efficient at modulating the APC functions of B cells (in lupus, B cells, rather than DCs, play a central role in antigen presentation [see refs. 41 and 42]). Ex vivo, P140 reduces the presentation of HLA class II molecules that are overexpressed on B cells from patients with SLE (but not patients with SSc). This P140-dependent decrease in HLA class II overexpression was directly related to the activity of lupus, as evaluated by the SLEDAI score. A similar effect was also visualized ex vivo on healthy donor B cells, but not on DCs collected from healthy volunteers.

The BCR studies required many experiments, and hence large numbers of B cells were needed for these studies. A sufficient number of B cells was not available from any lupus patient. If the BCR studies had been conducted on B cells from different lupus patients, the results would have been difficult to interpret, because the patients may have intrinsic differences in their BCR signaling. Therefore, these studies were carried out on B cells from a single patient without lupus. We are not aware of any therapy that affects BCR signaling exclusively in lupus patients.

In this study, we show that, as in MRL/lpr mice, P140 enters in human B cells by a clathrin coat–dependent endocytosis process and homes into lysosomes. Due to the lack of cell material, we were not able, in human SLE B cells, to demonstrate any alteration in macroautophagy or CMA processes with the use of classic markers of these pathways, nor were we able to raise any mechanistic conclusion regarding the possible effect of P140 on lysosome functioning in humans. However, using a combination of factors (anti-CD40 and anti-IgM antibodies in the presence of IL-21) to mimic T cell–driven B cell activation, expansion, and differentiation of normal B cells, we demonstrated very clearly that P140 down-regulates the maturation and differentiation of B cells into plasma cells and decreases IgG secretion by ASPCs.

Of important note, cells remaining after P140 treatment are fully active. If more cells from the peripheral blood of patients could become available, it would be interesting in this context to examine the capacity of P140 to interfere with activation, expansion, and differentiation of lupus B cells, with a particular emphasis on certain B cell subsets that are abnormally represented in patients with SLE, such as IgD−CD27+ post-switched memory B cells (43) and another class of memory B cells that are IgD−CD27− (44). The elevated frequency of the latter B cell subset in the peripheral blood of patients with SLE has been reported to correlate with the extent of disease activity, especially with renal disease, and the occurrence of autoantibodies such as anti–native DNA and anti-Sm/RNP antibodies (45,46). The fact that P140 is potent at down-

regulating the maturation and differentiation of human B cells into plasma cells is consistent with previous findings in mice with lupus, in which it was shown that the number of viable B220−CD138/syndecan 1+ plasma cells was decreased in the MRL/lpr mouse PBMC fraction after treatment with P140 peptide (22).

A few cellular studies have been performed to assess alterations in autophagy in lymphocytes from lupus patients. These studies are converging toward the conclusion that macroautophagy is altered in T and B cells (15–17,31). In the present study using peripheral blood cells, we found no disease-related defect responsible for altering macroautophagy in these cell types (when assessed as conversion of MAPLC3-I to MAPLC3-II on Western blotting or as expression of SQSTM1 by flow cytometry), with the only exception, however, being CD4+ and CD8+ T cells, which, on average, expressed lower levels of SQSTM1 compared to healthy donor T cells. This hyperactivity of macroautophagy in circulating CD4+ and CD8+ T cells was not rescued after ex vivo treatment with P140.

Future experiments with additional blood samples will clarify whether this observation reveals individual patient-related variations (due to their treatment or the stage, acute or quiescent, of the disease) or whether it could be attributed to a mechanistic feature with regard to, for example, specific cell subsets (including effector, memory, and regulatory T and B cells [see ref. 46]), localization of the cells (in the blood versus tissue), levels of activation or anergy (47) and stress in the cells, or eventual lysosomal defects in the cells. The medication taken by patients (such as hydroxy-chloroquine) may also greatly affect the results visualized ex vivo. To our knowledge, CMA, which has been shown to be enhanced in mice with lupus (9), has not been examined previously in patients with SLE. In the present study, no change could be highlighted by evaluating the expression of the CMA markers LAMP2A and HSPA8 in flow cytometry analyses. At this stage, the lack of availability of large numbers of cells from patients limits certain investigations and, consequently, an important question remains regarding the fine mechanism through which HLA class II molecules are destabilized and through which antigen presentation to T cells is repressed.

In the absence of macroautophagy and CMA dysregulation, notably in B cells acting as APCs, any possible effect of P140 was obviously not visualized. Future experiments will focus on precisely pointing out these yet unsolved aspects, particularly when samples from patients with SLE who are included in the ongoing phase III multicenter, placebo-controlled clinical trial become available (before and after treatment) for our authorized ancillary study.

Overall, our findings provide clear evidence that the P140 peptide down-regulates B cell maturation and differentiation through a mechanism that does not involve the BCR directly, but rather originates upstream, from a P140-induced defect of signaling by T cells, which are themselves anergized or rendered inactive via a lack of activation by the HLA–peptide complex. This lack of activation after P140 treatment likely occurs as a result of destabilization or a defect in presentation of HLA class II molecules in B cell APCs, a feature that seems specific to B cells but not to other professional APCs such as DCs.

AUTHOR CONTRIBUTIONS

All authors were involved in drafting the article or revising it critically for important intellectual content, and all authors approved the final version to be published. Dr. Muller had full access to all of the data in the study and takes responsibility for the integrity of the data and the accuracy of the data analysis.
Study conception and design. Wilhelm, Muller.
Acquisition of data. Wilhelm, Wang, Schall, Kleinmann, Faludi, Nashi, Sibilia, Martin, Schaeffer, Muller.
Analysis and interpretation of data. Wilhelm, Wang, Schall, Nashi, Sibilia, Martin, Schaeffer, Muller.

REFERENCES

1. Moulton VR, Tsokos GC. T cell signaling abnormalities contribute to aberrant immune cell function and autoimmunity. J Clin Invest 2015;125:2220–7.
2. Caza TN, Talaber G, Perl A. Metabolic regulation of organelle homeostasis in lupus T cells. Clin Immunol 2012;144:200–13.
3. Caza TN, Fernandez DR, Talaber G, Oaks Z, Haas M, Madaio MP, et al. HRES-1/Rab4-mediated depletion of Drp1 impairs mitochondrial homeostasis and represents a target for treatment in SLE. Ann Rheum Dis 2014;73:1888–97.
4. Gros F, Muller S. Pharmacological regulators of autophagy and their link with modulators of lupus disease. Br J Pharmacol 2014;171:4337–59.
5. Kobayashi T, Shimabukuro-Demoto S, Yoshida-Sugitani R, Furuyama-Tanaka K, Karyu H, Sugiura Y, et al. The histidine transporter SLC15A4 coordinates mTOR-dependent inflammatory responses and pathogenic antibody production. Immunity 2014;41:375–88.
6. Pierdominici M, Barbati C, Vomero M, Locatelli SL, Carlo-Stella C, Ortona E, et al. Autophagy as a pathogenic mechanism and drug target in lymphoproliferative disorders. FASEB J 2014;28:524–35.
7. Monneaux F, Lozano JM, Patarroyo ME, Briand JP, Muller S. T cell recognition and therapeutic effects of a phosphorylated synthetic peptide of the 70K snRNP protein administered in MRL/lpr lupus mice. Eur J Immunol 2003;33:287–96.

8. Zimmer R, Scherbarth HR, Rillo OL, Gomez-Reino J, Muller S. Lupuzor/P140 peptide in patients with systemic lupus erythematosus: a randomised, double-blind, placebo-controlled phase IIb clinical trial. Ann Rheum Dis 2013;72:1830–5.

9. Macri C, Wang F, Tasset I, Schall N, Page N, Briand JP, et al. Modulation of deregulated chaperone-mediated autophagy by a phosphopeptide. Autophagy 2015;11:472–86.

10. Mizushima N, Komatsu M. Autophagy: renovation of cells and tissues. Cell 2011;147:728–41.

11. Shibutani ST, Saitoh T, Nowag H, Münz C, Yoshimori T. Autophagy and autophagy-related proteins in the immune system. Nat Immunol 2015;16:1014–24.

12. Kaushik S, Cuervo AM. Chaperone-mediated autophagy: a unique way to enter the lysosome world. Trends Cell Biol 2012;22:407–17.

13. Page N, Gros F, Schall N, Décossas M, Bagnard D, Briand JP, et al. HSC70 blockade by the therapeutic peptide P140 affects autophagic processes and endogenous MHCII presentation in murine lupus. Ann Rheum Dis 2011;70:837–43.

14. Page N, Gros F, Schall N, Briand JP, Muller S. A therapeutic peptide in lupus alters autophagic processes and stability of MHCII molecules in MRL/lpr B cells. Autophagy 2011;7:539–40.

15. Gros F, Arnold J, Page N, Décossas M, Korganow AS, Martin T, et al. Macroautophagy is deregulated in murine and human lupus T lymphocytes. Autophagy 2012;8:1113–23.

16. Alessandri C, Barbati C, Vacirca D, Piscopo P, Confaloni A, Sanchez M, et al. T lymphocytes from patients with systemic lupus erythematosus are resistant to induction of autophagy. FASEB J 2012;26:4722–32.

17. Clarke AJ, Ellinghaus U, Cortini A, Stranks A, Simon AK, Botto M, et al. Autophagy is activated in systemic lupus erythematosus and required for plasmablast development. Ann Rheum Dis 2015;74:912–20.

18. Wang F, Muller S. Manipulating autophagic processes in autoimmune diseases: a special focus on modulating chaperone-mediated autophagy, an emerging therapeutic target. Front Immunol 2015;6:252.

19. Monneaux F, Parietti V, Briand JP, Muller S. Importance of spliceosomal RNP1 motif for intermolecular T-B cell spreading and tolerance restoration in lupus. Arthritis Res Ther 2007;9:R111.

20. Schall N, Page N, Macri M, Chaloin O, Briand JP, Muller S. Peptide-based approaches to treat lupus and other autoimmune diseases. J Autoimmunity 2012;39:143–53.

21. Schall N, Muller S. Resetting the autoreactive immune system with a therapeutic peptide in lupus. Lupus 2015;24:412–8.

22. Page N, Schall N, Strub JM, Quinternet M, Chaloin O, Décossas M, et al. The spliceosomal phosphopeptide P140 controls the lupus disease by interacting with the HSC70 protein and via a mechanism mediated by γδ T cells. PloS ONE 2009;4:e5273.

23. Wang F, Li B, Schall N, Wilhelm M, Muller S. Assessing autophagy in mouse models and patients with systemic autoimmune diseases. Cells 2017;6:16.

24. Dieker J, Cisterna B, Monneaux F, Décossas M, van der Vlag J, Biggiogera M, et al. Apoptosis changes the phosphorylation status and subcellular localization of the spliceosomal autoantigen U1-70K. Cell Death Diff 2008;15:793–804.

25. Monneaux F, Hoebeke J, Sordet C, Nonn C, Briand JP, Maillère B, et al. Selective modulation of CD4+ T cells from lupus patients by a promiscuous, protective peptide analog. J Immunol 2005;175:5839–47.

26. Bombardier C, Gladman DD, Urowitz MB, Caron D. Chang DH, and the Committee on Prognosis Studies in SLE. Derivation of the SLEDAI: a disease activity index for lupus patients. Arthritis Rheum 1992;35:630–40.

27. Pan Q, Gao C, Chen Y, Feng Y, Liu WJ, Liu HF. Update on the role of autophagy in systemic lupus erythematosus: a novel therapeutic target. Biomed Pharmacother 2015;71:190–3.

28. Pengo N, Scolari M, Oliva L, Milan E, Mainoldi F, Raimondi A, et al. Plasma cells require autophagy for sustainable immunoglobulin production. Nat Immunol 2013;14:298–305.

29. Conway KL, Kuballa P, Khor B, Zhang M, Shi HN, Virgin HW, et al. ATG5 regulates plasma cell differentiation. Autophagy 2013;9:528–37.

30. Chen M, Kodali S, Jang A, Kuai L, Wang J. Requirement for autophagy in the long-term persistence but not initial formation of memory B cells. J Immunol 2015;194:2607–15.

31. Arnold J, Murera D, Arbogast F, Fauny JD, Muller S, Gros F. Autophagy is dispensable for B cell development but essential for humoral autoimmune responses. Cell Death Diff 2016;23:853–64.

32. Klionsky DJ, Abdelmohsen K, Abe A, Abedin MJ, Abeliovich H, Acevedo Arozena A, et al. Guidelines for the use and interpretation of assays for monitoring autophagy. Autophagy 2016;12:1–222.

33. Into T, Inomata M, Takayama E, Takigawa T. Autophagy in regulation of Toll-like receptor signaling. Cell Signal 2012;24:1150–62.

34. Liu B, Yang Y, Dai J, Medzhitov R, Freudenberg MA, Zhang PL, et al. TLR4 up-regulation at protein or gene level is pathogenic for lupus-like autoimmune disease. J Immunology 2006;177:6880–8.

35. Marshak-Rothstein A. Toll-like receptors in systemic autoimmune disease. Nat Rev Immunol 2006;6:823–35.

36. Lartigue A, Colliou N, Calbo S, François A, Jacquot S, Arnoult C, et al. Critical role of TLR2 and TLR4 in autoantibody production and glomerulonephritis in lpr mutation-induced mouse lupus. J Immunology 2009;183:6207–16.

37. Weindel CG, Richey LJ, Bolland S, Mehta AJ, Kearney JF, Huber BT. B cell autophagy mediates TLR7-dependent autoimmunity and inflammation. Autophagy 2015;11:1010–24.

38. Flacher V, Neuberg P, Point F, Daubeuf F, Muller Q, Sigwalt D, et al. Mannoside glycolipid conjugates display anti-inflammatory activity by inhibition of Toll-like receptor-4 mediated cell activation. ACS Chem Biol 2015;10:2697–705.

39. Muller S, Monneaux F, Schall N, Rashkov RK, Oparanov BA, Wiesel P, et al. Spliceosomal peptide P140 for immunotherapy of systemic lupus erythematosus: results of an early phase II clinical trial. Arthritis Rheum 2008;58:3873–83.

40. Kuchen S, Robbins R, Sims GP, Sheng C, Phillips TM, Lipsky PE, et al. Essential role of IL-21 in B cell activation, expansion, and plasma cell generation during CD4+ T cell-B cell collaboration. J Immunol 2007;179:5886–96.

41. Yan J, Harvey BP, Gee RJ, Shlomchik MJ, Mamula MJ. B cells drive early T cell autoimmunity in vivo prior to dendritic cell-mediated autoantigen presentation. J Immunol 2006;177:4481–7.

42. Giles JR, Kashgarian M, Koni PA, Shlomchik MJ. B cell-specific MHC class II deletion reveals multiple nonredundant roles for B cell antigen presentation in murine lupus. J Immunol 2015;195:2571–9.

43. Odendahl M, Jacobi A, Hansen A, Feist E, Hiepe F, Burmester GR, et al. Disturbed peripheral B lymphocyte homeostasis in systemic lupus erythematosus. J Immunol 2000;165:5970–9.

44. Jacobi AM, Odendahl M, Reiter K, Bruns A, Burmester GR, Radbruch A, et al. Correlation between circulating CD27^{high} plasma cells and disease activity in patients with systemic lupus erythematosus. Arthritis Rheum 2003;48:1332–42.

45. Wei C, Anolik J, Cappione A, Zheng B, Pugh-Bernard A, Brooks J, et al. A new population of cells lacking expression of CD27 represents a notable component of the B cell memory compartment in systemic lupus erythematosus. J Immunol 2007;178:6624–33.

46. Tipton CM, Fucile CF, Darce J, Chida A, Ichikawa T, Gregoretti I, et al. Diversity, cellular origin and autoreactivity of antibody-secreting cell population expansions in acute systemic lupus erythematosus. Nat Immunol 2015;16:755–65.

47. Tretter T, Venigalla RK, Eckstein V, Saffrich R, Sertel S, Ho AD, et al. Induction of CD4+ T-cell anergy and apoptosis by activated human B cells. Blood 2008;112:4555–64.

Role of *Lgals9* Deficiency in Attenuating Nephritis and Arthritis in BALB/c Mice in a Pristane-Induced Lupus Model

Sonia Zeggar,[1] Katsue S. Watanabe,[1] Sanae Teshigawara,[1] Sumie Hiramatsu,[1]
Takayuki Katsuyama,[1] Eri Katsuyama,[1] Haruki Watanabe [1] Yoshinori Matsumoto,[1]
Tomoko Kawabata,[1] Ken-ei Sada,[1] Toshiro Niki,[2] Mitsuomi Hirashima,[2] and Jun Wada[1]

Objective. In systemic lupus erythematosus (SLE), an autoimmune disease associated with multiple organ involvement, the development of lupus nephritis determines prognosis, and arthritis impairs quality of life. Galectin 9 (Gal-9, *Lgals9*) is a β-galactoside–binding lectin that has been used for clinical application in autoimmune diseases, since recombinant Gal-9, as a ligand for T cell immunoglobulin and mucin domain–containing protein 3 (TIM-3), induces apoptosis of activated CD4+TIM-3+ Th1 cells. This study was undertaken to investigate whether deficiency of *Lgals9* has beneficial or deleterious effects on lupus in a murine model.

Methods. Gal-9$^{+/+}$ and Gal-9$^{-/-}$ female BALB/c mice were injected with pristane, and the severity of arthritis, proteinuria, and levels of autoantibody production were assessed at several time points immediately following injection. At 7 months after pristane injection, renal pathologic features, the severity of joint inflammation, and formation of lipogranulomas were evaluated. Subsets of inflammatory cells in the spleen and peritoneal lavage were characterized, and expression levels of cytokines from peritoneal macrophages were analyzed.

Results. *Lgals9* deficiency protected against the development of immune complex glomerulonephritis, arthritis, and peritoneal lipogranuloma formation in BALB/c mice in this murine model of pristane-induced lupus. The populations of T cell subsets and B cells in the spleen and peritoneum were not altered by *Lgals9* deficiency in pristane-injected BALB/c mice. Furthermore, *Lgals9* deficiency protected against pristane-induced lupus without altering the Toll-like receptor 7–type I interferon pathway.

Conclusion. Gal-9 is required for the induction and development of lupus nephritis and arthritis in this murine model of SLE. The results of the current investigation provide a potential new strategy in which antagonism of Gal-9 may be beneficial for the treatment of nephritis and arthritis in patients with SLE through targeting of activated macrophages.

Systemic lupus erythematosus (SLE) is a multiorgan autoimmune disease that is characterized by a wide array of clinical manifestations and multifactorial pathogenic pathways. The disease process of SLE involves genetic, epigenetic, hormonal, and environmental factors, all of which ultimately lead to a disturbance in the pathways of both innate and adaptive immunity. Despite notable progress in the understanding of this disease, its etiology remains unclear and is still to be unraveled. Kidney involvement in SLE is known to be associated with poor clinical outcomes, with 10–30% of young patients developing end-stage renal disease (ESRD) (1,2). Despite the wide availability of different regimens involving treatment with immunosuppressant agents, many of which have undoubtedly improved the prognosis and survival of patients with SLE, an increased risk of ESRD in SLE has been observed since the late 2000s (3).

In contrast to lupus nephritis, lupus arthritis is one of the frequently encountered manifestations in

SLE patients, and yet it may be overlooked behind the life-threatening conditions of lupus nephritis and neuropsychiatric SLE. Although few SLE patients develop full joint deformations, known as rhupus hands (4), lupus arthritis is a major cause of pain and discomfort and can impair the quality of life of patients (5).

Galectin 9 (Gal-9), a ubiquitously expressed β-galactoside–binding lectin (6,7), belongs to the tandem repeat subclass of the galectin superfamily, and is characterized by the presence of 2 distinct carbohydrate recognition domains joined by a link peptide (8). Among the 15 members of the galectin family, Gal-9 has been shown to function in both physiologic and pathologic conditions such as organogenesis, immune reactions, carcinogenesis, and metastasis (9). Gal-9 demonstrates bivalency and is able to cross link 2 glycoconjugates, and thus it is involved in the process of cell-to-cell and cell-to-matrix interactions. Results of recent investigations have suggested that the most dominant Gal-9 isoform, Gal-9Δ5, prevents metastasis by maintaining tissue integrity and inhibiting tumor migration and extravasation, while other Gal-9 isoforms facilitate metastasis (10). Gal-9 also modulates the processes of cell survival, such as apoptosis and cell cycle control, and induces apoptosis of various cell lines, such as the human melanoma cell line, T cell lines, and different types of leukemia cell lines (11,12).

In addition to the role of Gal-9 in cancer biology, it is involved actively at various stages of the immune response, and most of its effects are concentration dependent (13). Exogenous Gal-9 induces maturation of dendritic cells (DCs) associated with the up-regulation of costimulatory molecules such as CD40, CD54, CD80, CD83, and HLA–DR (14). The recombinant N-terminal Gal-9 is also effective in activating DCs by inducing a higher production of tumor necrosis factor (TNF) and interleukin-6 (IL-6), and greater phosphorylation of p38 and Akt (15). Through its divalent sugar-binding activity, Gal-9 forms Gal-9–glycan lattices with cell surface glycoproteins, which play major roles in the organization of cell membrane domains, regulation of thresholds of cell signaling, and receptor residency time on the cell surface (16). The local concentrations of Gal-9 and glycoconjugates determine the patterns of lattice formation and cellular response. At higher concentrations, Gal-9 induces apoptosis of CD4+ and CD8+ cells, while at lower concentrations, it increases cytokine production in activated T cells. T cell immunoglobulin and mucin domain–containing protein 3 (TIM-3), a glycoprotein with an N-glycan chain, is expressed on activated Th1 and Th17 cells. Gal-9 triggers calcium mobilization and activation of caspase 1, drives the apoptosis of Th1 and Th17 cells, and eliminates activated and exhausted T cells (11,17). In addition to Th1

cells, Gal-9 also induces apoptosis of B cells (B-lineage acute lymphoblastic leukemia 1 cells), monocytes (THP-1 cells), and myelocytes (HL-60 cells) (11). However, Gal-9 has not been found to exert apoptotic potential against Th2 and Treg cells lacking cell surface expression of TIM-3 (18,19).

The apoptotic potential of recombinant Gal-9 against immune-mediated cells prompted researchers to investigate the efficacy of recombinant Gal-9 in various disease models, such as experimental animal models of collagen-induced arthritis (CIA) (17,20,21), asthma (22), anti–glomerular basement membrane disease (23), lupus nephritis (24), diabetic nephropathy (25), and autoimmune encephalitis (17,26). In general, the apoptotic potential of Gal-9 is concentration dependent. A higher dose of recombinant Gal-9 induces apoptosis of Th1 and Th17 cells; however, a decline in its concentration by degradation may, inversely, stimulate CD4+ T cells, CD8+ T cells, and DCs to produce cytokines and chemokines.

Taking these findings into consideration, we investigated whether a total loss of Gal-9 would ameliorate or aggravate disease activity in a murine model of lupus, and determined whether blockade of Gal-9 and its signals might be beneficial in the treatment of SLE. To achieve this, we examined the effect of gene deletion of Lgals9 (a gene encoding Gal-9) in BALB/c mice with pristane-induced lupus (27). This lupus model is associated with intraperitoneal lipogranulomas, diffuse proliferative glomerulonephritis (28), production of autoantibodies (29), and an erosive arthritis resembling rheumatoid arthritis (30). We also investigated the effect of Lgals9 gene deficiency in a model of spontaneously induced SLE, using MRL/MpJ-Fas^lpr/J mice with a mutation in the gene encoding Fas. This model is associated with a defect in lymphocyte apoptosis and the impaired clearance of lymphocytes (31), high titers of autoantibodies, hypergammaglobulinemia, nephritis, vasculitis, and lymphadenopathy (32).

MATERIALS AND METHODS

Pristane-induced lupus model in BALB/c mice. BALB/c mice deficient in Gal-9 (Gal-9$^{-/-}$) were kindly provided by GalPharma (33,34). Using standard breeding techniques, Gal-9$^{-/-}$ BALB/c mice were crossed with BALB/cJ mice (The Jackson Laboratory) for 2 generations, and Gal-9$^{+/-}$ BALB/cJ mice were also bred, to obtain Gal-9$^{+/+}$ and Gal-9$^{-/-}$ littermates. Gal-9$^{-/-}$ female BALB/c mice (n = 12) and age- and sex-matched control Gal-9$^{+/+}$ mice (n = 12) were housed under specific pathogen–free conditions in a 12-hour light/dark cycle, with free access to water and standard rodent chow. The mice were injected intraperitoneally with 0.5 ml of pristane (chemical name 2,6,10,14-tetramethylpentadecane; Sigma-Aldrich) at age 7 weeks. Pristane-injected Gal-9$^{+/+}$ and Gal-9$^{-/-}$ BALB/c mice were designated as Gal-9$^{+/+}$ PI

and Gal-9$^{-/-}$ PI mice, respectively. During the course of the experiments, 1 of the Gal-9$^{+/+}$ PI mice accidentally died 4 months after pristane injection.

The severity of arthritis in the paws was evaluated every 2 weeks, and serum and urine samples were collected monthly. Peritoneal lavage, lipogranulomas in the peritoneal cavity, and spleen, kidney, and paw tissue were obtained at 7 months after pristane injection. For the characterization of Ly-6C^{high} monocytes and isolation of peritoneal macrophages, mice were euthanized at various time points: Gal-9$^{+/+}$ PI mice (n = 5) and Gal-9$^{-/-}$ PI mice (n = 5) at 24 hours after pristane injection, Gal-9$^{+/+}$ PI mice (n = 4) and Gal-9$^{-/-}$ PI mice (n = 4) at 15 days after pristane injection, and Gal-9$^{+/+}$ PI mice (n = 3) and Gal-9$^{-/-}$ PI mice (n = 3) at 4 weeks after pristane injection. For analysis of *Tnf* messenger RNA (mRNA) expression and quantification of TNF proteins, groups of Gal-9$^{+/+}$ PI mice (n = 4 per group) and Gal-9$^{-/-}$ PI mice (n = 4 per group) were euthanized at 4 hours, 24 hours, and 48 hours after pristane injection.

Generation of Gal-9$^{-/-}$ MRL/MpJ-Fas^{lpr}/J (MRL/lpr) mice. We generated Gal-9$^{-/-}$ MRL/lpr mice by mating Gal-9$^{-/-}$ female BALB/c mice with male MRL/lpr mice, to yield heterozygous F1 offspring. Gal-9$^{+/-}$ female F1 mice were further backcrossed with male MRL/lpr mice for 8 generations. Finally, Gal-9$^{+/-}$ F9 mice were intercrossed to obtain Gal-9$^{-/-}$ female MRL/lpr littermates (n = 15) and Gal-9$^{+/+}$ MRL/lpr littermates (n = 15). These mice were further monitored until age 16 weeks. Serum was collected at 8 and 16 weeks of age, while weight and proteinuria were assessed from 6 weeks of age and every 2 weeks thereafter. Tissue samples, including those from the spleen, lymph nodes, and kidneys, were obtained at the study end point.

All of the experimental procedures were approved by the Animal Care and Use Committee of the Department of Animal Resources, Advanced Science Research Center at Okayama University.

Determination of arthritis severity score. The mice were examined for the onset and severity of arthritis every 2 weeks after pristane injection. For scoring of arthritis severity, we used a previously published scoring system (35,36) with modification, as follows: score scale of 0–3, where 0 = normal, 1 = slight swelling or erythema of the wrist/ankle joint or footpad, 2 = moderate swelling and erythema of the wrist/ankle joint or footpad, and 3 = severe swelling and erythema of the paw. The scores for individual limbs were summed to obtain a total clinical arthritis severity score of 12 per animal. The incidence of arthritis was determined as the percentage of mice that had developed redness or swelling in at least 1 paw (representative images are shown in Supplementary Figure 1, available on the *Arthritis & Rheumatology* web site at http://onlinelibrary.wiley.com/doi/10.1002/art.40467/abstract).

Evaluation of histologic features and scoring of tissue samples. Samples of mouse kidney tissue were fixed in 10% formalin, and 4-μm paraffin-embedded sections were stained with hematoxylin and eosin (H&E), periodic acid–Schiff, periodic acid–methenamine silver, and Masson's trichrome stain. After H&E staining, glomerular hypercellularity was evaluated by counting the number of nuclei per glomerular cross-section (20 glomerular cross-sections per mouse), and tubulointerstitial nephritis was scored as previously described (37). For immunofluorescence analysis, the tissue samples were embedded in OCT compound (Sakura, Japan), and 4-μm cryostat sections were stained with fluorescein isothiocyanate

(FITC)–conjugated goat anti-mouse IgG or rabbit anti-mouse C3 (Cappel). For analysis of IgG subclasses, the sections were stained using FITC-conjugated goat anti-mouse IgG1, IgG2a, IgG2b, or IgG3 (Novus Biological). Staining of all sections was visualized with a fluorescence microscope (BZ-8000; Keyence) using a plan Apo 20x NA0.75 lens. Immunofluorescence intensity (measured as the number of pixels/μm^2) was quantified using BZ analyzer II image analysis software (version 1.31; Keyence). At least 10 glomeruli per section were analyzed.

The most severely affected hind paw of each mouse was removed and fixed in 10% formalin. After decalcification in 10% EDTA, the joints were embedded in paraffin, and 4-μm–thick sections were stained with H&E and toluidine blue as described previously (38). In brief, twenty 4-μm sagittal serial sections were cut, every fifth section was stained with H&E, and an adjacent section was stained with toluidine blue. Histopathologic scoring was performed using a semiquantitative score, as described previously (39). The final histopathologic arthritis score was evaluated in each mouse by calculating the sum values for inflammation: infiltration of leukocytes, synovial hyperplasia, and destruction of cartilage, including pannus formation and cartilage erosion.

Four-micrometer paraffin-embedded sections of lipogranulomas from the peritoneal cavity as well as sections from the spleen and lymph nodes were deparaffinized, rehydrated, subjected to inhibition of endogenous peroxidase, and incubated with Blocking One Histo (Nacalai Tesque). They were then incubated with a purified anti-mouse Gal-9 antibody (BioLegend) overnight at 4°C, followed by goat anti-rat IgG conjugated with horseradish peroxidase (Abcam) for 1 hour, and developed with diaminobenzidine (SK-4100; Vector) as the chromogen. Sections were counterstained with Mayer's hematoxylin.

Quantitative real-time reverse transcription–polymerase chain reaction (RT-PCR). Mice were euthanized at 7 months after pristane injection, and the paws were then cut under the furline, unskinned, and immediately flash frozen in liquid nitrogen. Individual lipogranulomas were picked from the peritoneal cavity of pristane-injected mice and pooled. Paws and lipogranulomas were disrupted and homogenized in TRIzol reagents with a TOMY Micro Smash MS-100R and 5.5-mm stainless steel beads. The homogenates were centrifuged for 10 minutes at 4°C at 14,000 revolutions per minute. Supernatants were transferred to 1.5-ml Eppendorf tubes, centrifuged for 10 minutes at 4°C at 14,000 rpm, and collected for RNA extraction.

Total RNA was extracted from the paws, lipogranulomas, and peritoneal macrophages using an RNeasy Mini kit (Qiagen). Complementary DNA (cDNA) was generated using a High-Capacity cDNA RT kit (Applied Biosystems). Quantitative real-time PCR was performed in a Step One Plus Real-Time PCR system (Applied Biosystems) with specific primers, Universal Master Mix II (Life Technologies), and TaqMan gene expression assays to evaluate the expression of *Tnf* (Mm00443258_m1), *Il1b* (Mm00434228_m1), *Il6* (Mm00446190_m1), *Lgals1* (Mm00839408_g1), *Lgals9* (Mm004 95295_m1), *Lgals3* (Mm00802901_m1), *Tlr3* (Mm01207404_m1), *Tlr4* (Mm00445273_m1), *Tlr7* (Mm00446590_m1), *Tlr9* (Mm004 46193_m1), *Ccl2* (Mm00441242_m1), *Ccl7* (Mm00443113_m1), *Ccl12* (Mm01617100_m1), *Mx1* (Mm00487796_m1), *Cxcl10* (Mm00445235_m1), and *Irf7* (Mm00516793_g1). The relative abundance of mRNAs was standardized against the levels of *Gapdh* mRNA (Mm99999915_g1) as the invariant control.

Flow cytometry analysis. The spleen, mesenteric, and axillary lymph nodes from MRL/lpr mice were finely minced and incubated in a fresh digestion medium containing 3 ml RPMI 1640 with 2 mg/ml collagenase D (Roche), 50 IU DNase (Takara), and 10% fetal calf serum (FCS) at 37°C for 30 minutes, with gentle shaking at 200 rpm on an orbital shaker. Single-cell suspensions were prepared from the spleens and peritoneal lavage of PI mice, and from the lymph nodes of MRL/lpr mice. Red blood cells were removed using a red cell lysing buffer (BD Pharm Lyse). The cells were first incubated at 4°C for 10 minutes with an Fc receptor (FcR) blocking reagent (Miltenyi Biotec) to reduce nonspecific binding of antibodies to FcRs. The cells (1×10^6) derived from the spleen, peritoneum, and lymph nodes were incubated at 4°C for 30 minutes in staining buffer (BioLegend) with the relevant optimized amount of fluorochrome-conjugated antibodies or the appropriate isotype controls: FITC-conjugated anti-CD4 (GK1.5), VioBlue-conjugated anti-CD4 (GK1.5), allophycocyanin (APC)–conjugated anti-CD8 (53-6.7), APC-conjugated anti-CD62L (MEL14-H2.100), phycoerythrin (PE)–conjugated anti-CD44 (IM7.8.1), APC-conjugated anti-CD19 (6D5), FITC-conjugated anti-CD45R (B220) (RA3-6B2), APC-conjugated anti–Ly-6C (1G7.G10), PE-conjugated anti-CD138 (clone REA104), and PE-conjugated anti–Ly-6G (clone 1G7.G10). All antibodies were purchased from Miltenyi Biotec except BV421-conjugated anti-CD3 (SK7), which was purchased from BD Biosciences, and eFluor 450–conjugated anti-CD11b (M1/70), which was purchased from eBioscience. Dead cells were excluded from the analysis using 7-aminoactinomycin D staining (BD PharMingen). All data were acquired with a FACSAria I flow cytometer (BD Biosciences) and analyzed using FlowJo software (TreeStar).

In vitro assays of peritoneal macrophages. Peritoneal macrophages were harvested 24 hours after the injection of either pristane or phosphate buffered saline (PBS) as a vehicle control. The cells were seeded at a concentration of 1×10^6/well in UpCell 24-well plates (CellSeed) in Dulbecco's modified Eagle's medium supplemented with 10% FCS and 100 IU/ml penicillin/streptomycin, and incubated for 2 hours at 37°C in an atmosphere of 5% CO_2. Nonadherent cells were removed by washing with warm medium, and then recounted to calculate the number of adherent cells in the wells by subtraction. The remaining adherent cells consisted of >95% macrophages, and adherent macrophages were then cultured in the presence or absence of Toll-like receptor (TLR) ligands as described previously (40), or underwent protein extraction using Cell Lytic M reagent (Sigma-Aldrich) following the manufacturer's instructions. All ligands were purchased from InvivoGen except for lipopolysaccharide (Sigma-Aldrich). The supernatants were collected after 24 hours, and RNA was extracted and stored at −80°C.

Enzyme-linked immunosorbent assays (ELISAs). Serum levels of total IgG (Abcam), anti–double-stranded DNA (anti-dsDNA) (Shibayagi, Japan), anti–nuclear RNP (anti-nRNP) (Alpha Diagnostic International), and TNF (R&D Systems) were measured using commercially available ELISA kits according to the manufacturer's instructions. The cutoff values of the assays were 7.8 ng/ml, 15.6 mU/ml, 50 units/ml, and 10.9 ng/ml, respectively.
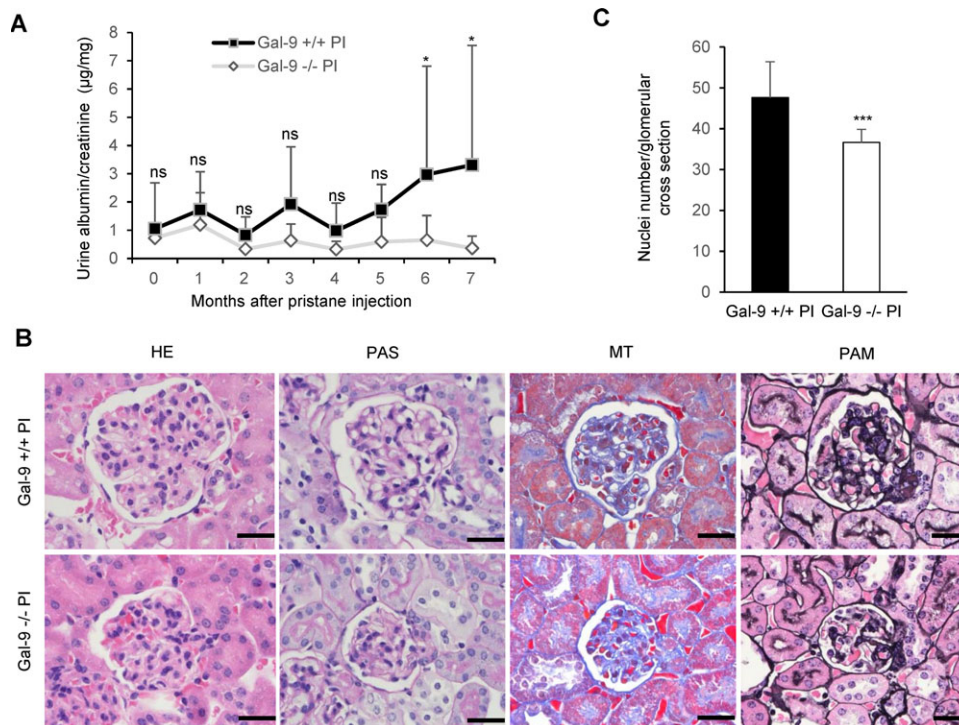
Figure 1. Attenuation of lupus nephritis in galectin 9–deficient (Gal-9$^{-/-}$) pristane-injected (PI) BALB/c mice. **A,** Levels of proteinuria in Gal-9$^{-/-}$ PI mice (n = 12) compared to Gal-9$^{+/+}$ PI mice (n = 11). **B,** Representative kidney sections from Gal-9$^{+/+}$ and Gal-9$^{-/-}$ PI mice, stained with hematoxylin and eosin (H&E), periodic acid–Schiff (PAS), Masson's trichrome (MT), and periodic acid–methenamine silver (PAM) for analysis of glomerular size and mesangial expansion. Bars = 30 μm. **C,** Numbers of glomerular nuclei in Gal-9$^{+/+}$ PI mice compared to Gal-9$^{-/-}$ PI mice (n = 10 per group). Results are the mean ± SD. * = $P < 0.05$; *** = $P < 0.001$, by Mann-Whitney U test in **A** and Student's t-test in **C**. NS = not significant.

Western blotting. For protein extraction, the tissue samples were homogenized in ice-cold radioimmunoprecipitation assay buffer. Total protein was quantified using the Pierce Protein Assay kit with Coomassie blue staining (Bradford) according to the manufacturer's instructions (ThermoFisher Scientific). A Mini-PROTEAN precast gel (Bio-Rad) was equally loaded with 8.5 μg of protein, and then electrophoresed and electrotransferred to a PVDF membrane. After blocking with 5% nonfat dry milk and TBS-T (0.05% Tween 20, 20 m*M* Tris HCl, and 150 m*M* NaCl [pH 7.6]), membranes were probed with a primary antibody rat anti-mouse Gal-9 clone (clone 108A2; BioLegend) or rabbit anti-mouse GAPDH (Cell Signaling Technology), and then incubated with anti-rat IgG conjugated with horseradish peroxidase (Abcam) or donkey anti-rabbit IgG conjugated with horseradish peroxidase (Santa Cruz Biotechnology), respectively. Blots were developed using a Pierce ECL Plus Western blotting substrate and visualized using an ImageQuant LAS 4000 Mini kit (GE Healthcare Life Sciences).

Statistical analysis. Data are expressed as the mean ± SD. Normal distribution of the data was assessed by Shapiro-Wilk test, and statistically significant differences between groups were determined using the Student's 2-tailed *t*-test or Mann-Whitney U test, as appropriate. The incidence of arthritis was analyzed using a Fisher's exact test. Data were analyzed using JMP 13 software (SAS). *P* values less than 0.05 were considered significant.

RESULTS

Attenuation of pristane-induced lupus nephritis in *Lgals9*-deficient mice. Pristane induces immune complex glomerulonephritis in BALB/c mice, a condition that is associated with the same autoantibodies typically observed in human SLE (28). Gal-9$^{-/-}$ PI mice (pristane-injected BALB/c mice) developed only modest proteinuria compared to Gal-9$^{+/+}$ PI mice (Figure 1A). Furthermore, light microscopic examination of the tissue sections demonstrated an attenuation of histologic damage in Gal-9$^{-/-}$ PI mice, as evidenced by a reduction in glomerular size, reduced cellularity, and suppression of mesangial expansion (Figures 1B and C).

We also assessed the effect of Gal-9 deficiency on glomerular immune complex formation/deposition. Kidney sections from Gal-9$^{-/-}$ and Gal-9$^{+/+}$ PI mice were stained for IgG and C3 at 7 months after pristane injection. As evident on the representative glomerular sections shown in Figure 2A, we found a significant reduction in the glomerular immune complex deposition of IgG, all of the IgG subclasses, and C3 in Gal-9$^{-/-}$ PI mice compared to their Gal-9$^{+/+}$ littermates.

In contrast, no differences with regard to kidney involvement between Gal-9$^{-/-}$ MRL/lpr mice and Gal-9$^{+/+}$ MRL/lpr mice were seen when measured as either albuminuria, glomerular hypercellularity, or tubulointerstitial disease (for results, see Supplementary Figures 2A–C, available on the *Arthritis & Rheumatology* web site at http://onlinelibrary.wiley.com/doi/10.1002/art.40467/abstract). Active pathologic features such as cellular crescents, wire loop formation, hyaline thrombi, and glomerular necrosis were similar between Gal-9$^{-/-}$ MRL/lpr mice and Gal-9$^{+/+}$ MRL/lpr mice (see Supplementary Figure 2D, http://onlinelibrary.wiley.com/doi/10.1002/art.40467/abstract).
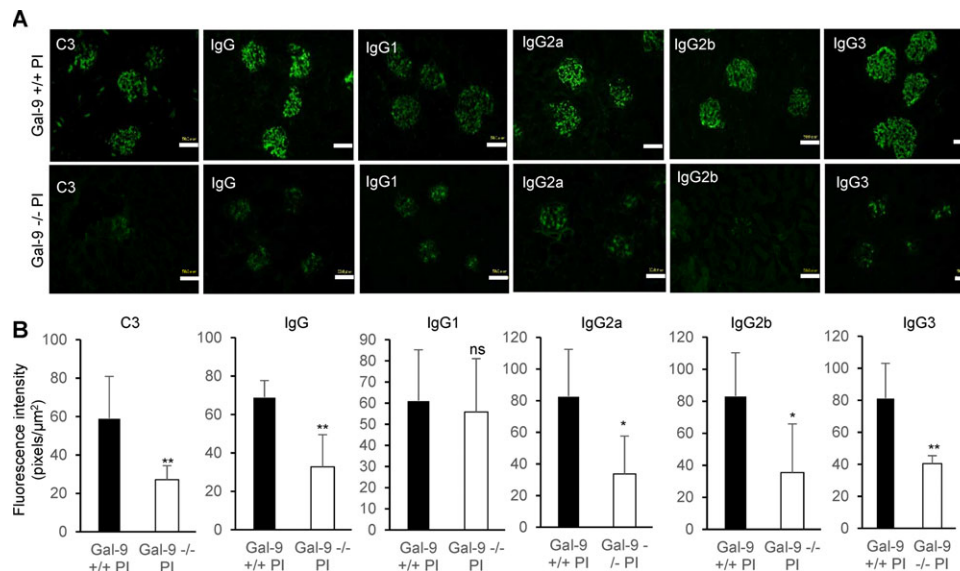
Figure 2. Reduced glomerular IgG deposition in Gal-9$^{-/-}$ PI mice. **A,** Deposition of C3, IgG, and IgG subclasses, as evaluated by direct immunofluorescence, in the kidneys from Gal-9$^{-/-}$ PI mice compared to Gal-9$^{+/+}$ PI mice. Images are representative of 5 mice per group. Bars = 50 μm. **B,** Immunofluorescence intensity of C3, IgG, and IgG-subclass deposits, as evaluated using computed image analysis software. The final fluorescence intensity score reflects the average of at least 10 glomeruli per mouse. Results are the mean ± SD. * = *P* < 0.05; ** = *P* < 0.01, by Student's *t*-test. See Figure 1 for definitions.

Furthermore, there were no alterations or reductions in immune complex deposition in Gal-9$^{-/-}$ MRL/lpr mice as compared to Gal-9$^{+/+}$ MRL/lpr littermates (see Supplementary Figures 2E and F, http://onlinelibrary.wiley.com/doi/10.1002/art.40467/abstract). These results suggest that Gal-9 deficiency is capable of suppressing the functional and pathologic damage to the kidneys induced by pristane injection, but it is not sufficient to prevent severe forms of kidney disease associated with impaired apoptosis/cell clearance in MRL/lpr mice.

Pristane-induced production of IgG and autoantibodies in Gal-9$^{-/-}$ BALB/c mice. Hypergammaglobulinemia and autoantibody production against a broad range of autoantigens are characteristic features of pristane-induced lupus in BALB/c mice (29,41,42). To evaluate the impact of *Lgals9* deficiency on pristane-induced hypergammaglobulinemia and autoantibody production, serum was collected at baseline and every month after pristane injection for 7 months. Serum levels of total IgG were significantly lower in Gal-9$^{-/-}$ PI mice compared to Gal-9$^{+/+}$ PI mice (Figure 3A). Body weight, spleen weight, and the total number of splenocytes were not altered in either Gal-9$^{-/-}$ or Gal-9$^{+/+}$ PI mice (for results, see Supplementary Figures 3A–C, available on the *Arthritis & Rheumatology* web site at http://onlinelibrary.wiley.com/doi/10.1002/art.40467/abstract). Flow cytometry analysis of the spleens and peritoneal lavage did not reveal any differences in the numbers of B cells and plasma cell subsets (Supplementary Figures 3D–F, http://onlinelibrary.wiley.com/doi/10.1002/art.40467/abstract).

We next investigated the titers of anti-nRNP and anti-dsDNA, both of which are hallmarks of SLE and have been previously found in 50–90% and 40% of pristane-treated BALB/c mice, respectively (29). The titers of anti-dsDNA and anti-nRNP antibodies were increased both in Gal-9$^{-/-}$ PI mice and in Gal-9$^{+/+}$ PI mice, but their titers were comparable between the 2 groups (Figures 3B and C). In Gal-9$^{-/-}$ and Gal-9$^{+/+}$ MRL/lpr mice, there were no statistically significant differences in the levels of anti-dsDNA antibodies (for results, see Supplementary Figure 2G, http://onlinelibrary.wiley.com/doi/10.1002/art.40467/abstract).

Body weights, spleen weights, lymph node weights, and total cell numbers in the spleen and lymph nodes were not altered in either Gal-9$^{-/-}$ or Gal-9$^{+/+}$ MRL/lpr mice (for results, see Supplementary Figures 4A–D, available on the *Arthritis & Rheumatology* web site at http://onlinelibrary.wiley.com/doi/10.1002/art.40467/abstract). Flow cytometry analysis of the spleen and lymph nodes did not reveal any differences in the numbers of B cells and T cell subsets, except that there was a reduction in the number of double-negative T cells in the spleens of Gal-9$^{-/-}$ MRL/lpr mice (see Supplementary Figures 4D–G, http://onlinelibrary.wiley.com/doi/10.1002/art.40467/abstract). Although deficiency of Gal-9 suppressed overall production of IgG in these mice, it did not diminish the production of pathogenic plasma cells producing antibodies against autoantigens.

Amelioration of arthritis in Gal-9$^{-/-}$ PI mice. A single injection of pristane into the peritoneal cavity induces an erosive arthritis in susceptible mouse strains such as BALB/cJ mice (30). In the present study, the incidence of arthritis increased over time and was higher in Gal-9$^{+/+}$ PI mice (72%) than in Gal-9$^{-/-}$ PI mice (33%) (Figure 4A). At 7 months after pristane injection, the mean clinical arthritis severity score was significantly reduced in Gal-9$^{-/-}$ PI mice compared to Gal-9$^{+/+}$ PI mice (Figure 4B). These results indicate that *Lgals9* deficiency fully protects against arthritis development in mice, and reduces the severity of arthritis in affected mice.

The extent of joint destruction and severity of inflammation were evaluated by H&E and toluidine blue staining of the joint sections. Synovial hyperplasia, severe leukocyte infiltration, pannus formation, and cartilage
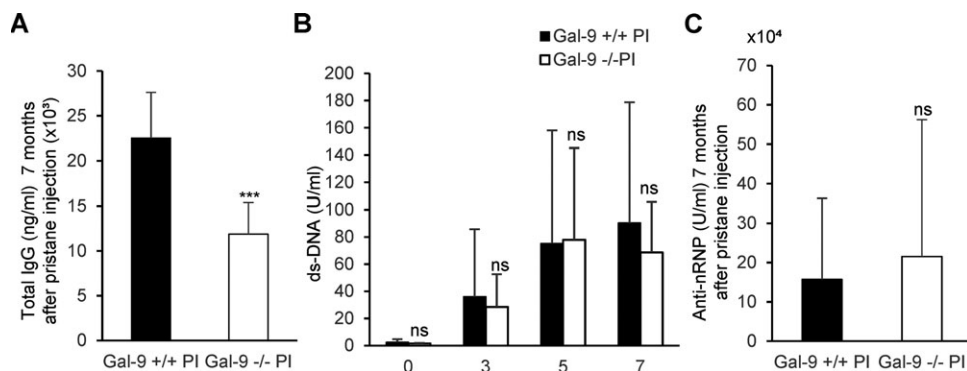
Figure 3. Hypergammaglobulinemia and autoantibody production in Gal-9$^{+/+}$ and Gal-9$^{-/-}$ PI mice. Serum levels of total IgG at 7 months following pristane injection (n = 8 mice per group) (**A**), double-stranded DNA (dsDNA) antibodies at 0, 3, 5, and 7 months postinjection (n = 6 mice per group) (**B**), and anti–nuclear RNP (anti-nRNP) antibodies at 7 months postinjection (n = 7 mice per group) (**C**) were measured by enzyme-linked immunosorbent assay in Gal-9$^{+/+}$ and Gal-9$^{-/-}$ PI mice. Results are the mean ± SEM in duplicate samples. *** = $P < 0.001$, by Student's *t*-test. See Figure 1 for other definitions.
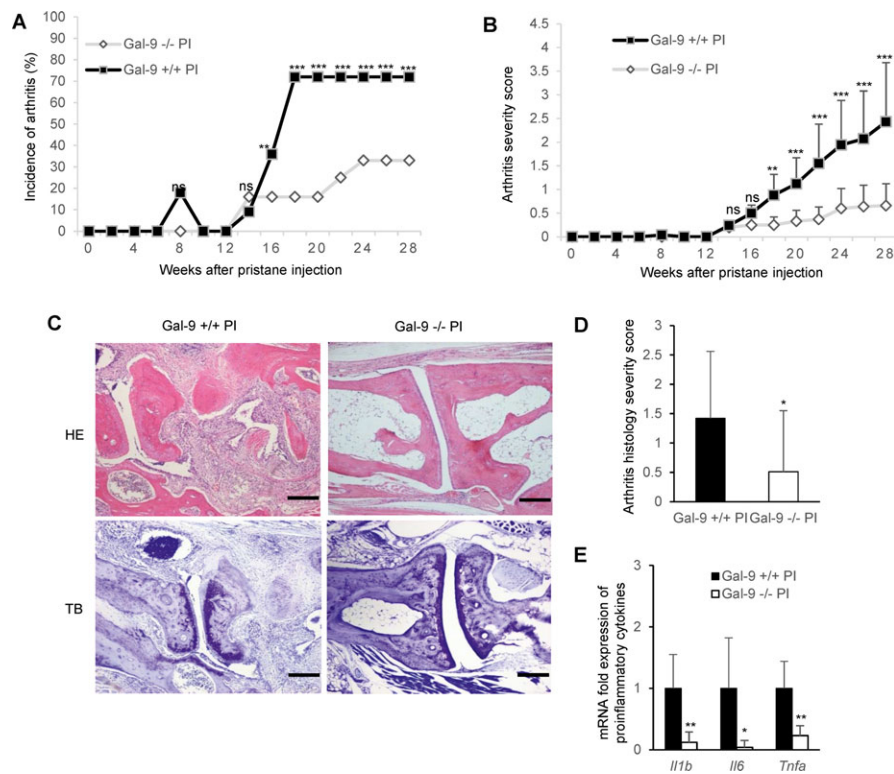
Figure 4. Incidence and severity of pristane-induced arthritis in Gal-9$^{-/-}$ and Gal-9$^{+/+}$ mice. **A,** Incidence of arthritis in Gal-9$^{-/-}$ PI mice (n = 12) compared to Gal-9$^{+/+}$ PI mice (n = 11), calculated as the percentage of mice that developed redness or swelling in at least 1 paw among all mice in each group. **B,** Mean clinical arthritis severity score in Gal-9$^{+/+}$ PI mice (n = 11) compared to Gal-9$^{-/-}$ PI mice (n = 12). The arthritis severity score (scale of 0–3) evaluated the severity of erythema/swelling in the wrist or ankle. **C,** Histopathologic evaluation of arthritis by staining of the joints with H&E and toluidine blue (TB). Representative histopathologic sections of the joints from Gal-9$^{+/+}$ and Gal-9$^{-/-}$ PI mice are shown. Bars = 30 μm. **D,** Semiquantitative histologic scoring of arthritis. Sections of the joints from Gal-9$^{-/-}$ PI and Gal-9$^{+/+}$ PI mice (n = 10 per group) were stained with H&E and TB and evaluated for the extent of inflammation and joint destruction. **E,** Determination of cytokine mRNA expression in the joints of Gal-9$^{+/+}$ PI mice compared to Gal-9$^{-/-}$ PI mice (n = 6 per group). Expression levels of *Il1b*, *Il6*, and *Tnfa* were assessed by reverse transcription–polymerase chain reaction. Results are the mean ± SD. * = $P < 0.05$; ** = $P < 0.01$; *** = $P < 0.001$, by Fisher's exact test in **A** and **B** and by Student's *t*-test in **D** and **E**. See Figure 1 for other definitions.

erosions were present in the joints of Gal-9$^{+/+}$ PI mice, whereas the joints of Gal-9$^{-/-}$ PI mice were largely spared, showing marked reductions in the extent of synovitis and severity of joint erosion (Figure 4C). The histopathologic arthritis severity scores were significantly lower in Gal-9$^{-/-}$ PI mice than in Gal-9$^{+/+}$ PI mice (Figure 4D). In addition, *Lgals9* deficiency reduced the expression of mRNA for several proinflammatory cytokines, including *Il1b*, *Il6*, and *Tnfa*, in Gal-9$^{-/-}$ PI mice compared to Gal-9$^{+/+}$ PI mice (Figure 4E).

Altered chronic peritoneal inflammatory response in Gal-9$^{-/-}$ PI mice. The pristane-induced lupus model is characterized by lipogranuloma formation, which is a chronic inflammatory response to the hydrocarbon oil and has morphologic and functional characteristics of secondary lymphoid tissue (43,44). At 7 months after pristane injection, numerous lipogranulomas were observed in the peritoneal cavity of Gal-9$^{+/+}$ PI mice, whereas lipogranulomas were markedly reduced in number and

size in Gal-9$^{-/-}$ PI mice (Figure 5A) and were completely absent in 2 of 12 Gal-9$^{-/-}$ PI mice (data not shown).

Intriguingly, H&E staining of the lipogranulomas demonstrated a smaller size, diminished cellularity, and absence of follicle-like structures in Gal-9$^{-/-}$ PI mice compared to Gal-9$^{+/+}$ PI mice (Figure 5A). The number of high endothelial venules (HEVs) was reduced in Gal-9$^{-/-}$ PI mice compared to Gal-9$^{+/+}$ PI mice (for results, see Supplementary Figure 5A, available on the *Arthritis & Rheumatology* web site at http://onlinelibrary.wiley.com/doi/10.1002/art.40467/abstract). The smaller oil droplets were surrounded by inflammatory cells and uniformly distributed in the lipogranulomas of Gal-9$^{+/+}$ PI mice, whereas larger oil droplets were eccentrically located and surrounded by fibrotic tissue (Figure 5A).

Moreover, Gal-9 was found to be distributed mainly in areas surrounding the follicle-like structure in lipogranulomas, the lymphoid follicle of the lymph nodes, and the marginal zone of the spleen (Figure 5B). RT-
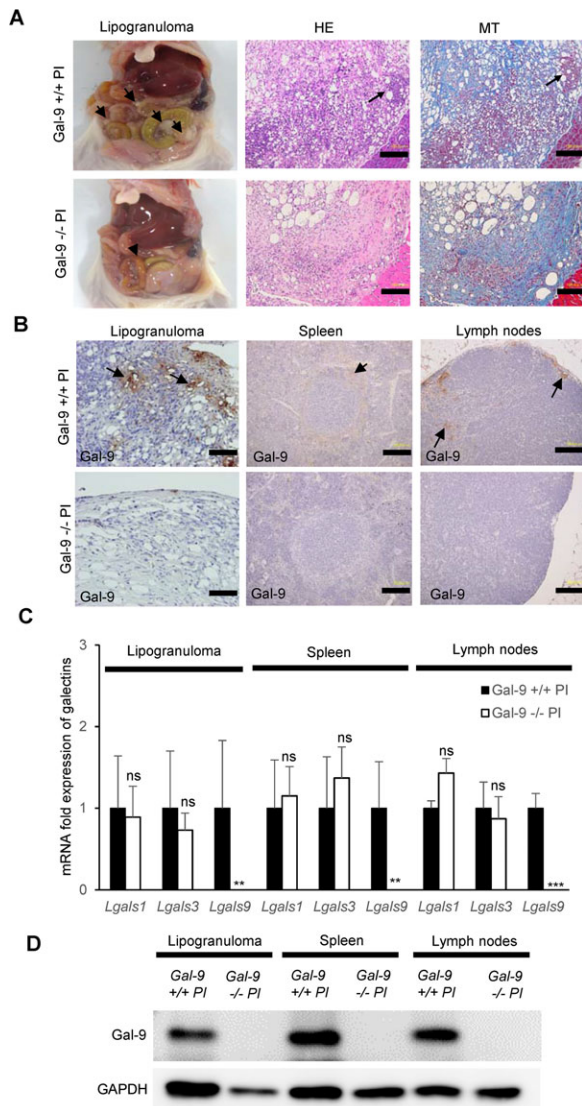
Figure 5. Reduction in the peritoneal inflammatory response in Gal-9$^{-/-}$ PI mice. **A,** Frequency of lipogranulomas in the peritoneal cavity of a Gal-9$^{-/-}$ PI mouse compared to a Gal-9$^{+/+}$ PI mouse. Left, Histopathologic sections were assessed for the presence of lipogranulomas. Differences between the 2 groups were characterized by differences in the size of the oil droplets, cells, and matrix distribution. Middle and Right, Sections of ectopic lymphoid tissue were stained with H&E and MT at 7 months after pristane injection. Bars = 20 μm. Representative samples are shown. **B,** Immunohistologic staining for the expression of Gal-9 in the lipogranulomas, spleen, and lymph nodes of a Gal-9$^{+/+}$ PI mouse compared to a Gal-9$^{-/-}$ PI mouse. Bars = 50 μm. In **A** and **B**, **arrows** indicate follicle-like structures. **C,** Expression levels of *Lgals* mRNA in the lipogranulomas, spleen, and lymph nodes of Gal-9$^{+/+}$ PI mice compared to a Gal-9$^{-/-}$ PI mice (n = 6 per group). Results are the mean ± SD. ** = $P < 0.01$; *** = $P < 0.001$, by Student's *t*-test. **D,** Representative Western blots of Gal-9 expression in the lipogranulomas, spleen, and lymph nodes of a Gal-9$^{+/+}$ PI mouse compared to a Gal-9$^{-/-}$ PI mouse; GAPDH was used as the invariant control. See Figure 1 for definitions.

PCR and Western blot analyses demonstrated that *Lgals9* mRNA was highly expressed in the lipogranulomas, spleens, and lymph nodes of Gal-9$^{+/+}$ PI mice and absent in Gal-9$^{-/-}$ PI mice (Figures 5C and D). There was no compensatory up-regulation of *Lgals1* and *Lgals3* mRNA in Gal-9$^{-/-}$ PI mice. These results suggest that Gal-9 is essentially required for the neogenesis of tertiary lymphoid tissue in response to pristane in vivo.

Effects of *Lgals9* deficiency on the innate immune response of peritoneal macrophages. Peritoneal macrophages are the foremost cells that sense and interact with pristane following its injection. As a result, they release a wide range of proinflammatory cytokines and chemokines in the peritoneal cavity, followed by accumulation of inflammatory Ly-6C^{high} monocytes, the main source of type I interferons (IFNs) in this model (45). We thus examined the effect of *Lgals9* deficiency on cellular composition in the spleen and peritoneal lavage cells at 15 days and 7 months after pristane injection. We observed no alterations in the frequency of T cells, B cells, effector/memory CD4+ T cells, and CD11b cells in Gal-9$^{-/-}$ PI mice compared to Gal-9$^{+/+}$ PI mice (results in Supplementary Figure 3D, http://onlinelibrary.wiley.com/doi/10.1002/art. 40467/abstract). At 15 days after pristane injection, the recruitment of CD11b+Ly-6C^{high} inflammatory monocytes into the peritoneal cavity was not impaired in Gal-9$^{-/-}$ PI mice (results in Supplementary Figure 3G, http://onlinelibrary. wiley.com/doi/10.1002/art.40467/abstract).

We then isolated peritoneal macrophages at 24 hours after pristane injection and cultured the cells for gene expression analyses. The peritoneal macrophages from Gal-9$^{-/-}$ PI mice demonstrated reduced *Tnfa* mRNA expression in response to pristane as compared to Gal-9$^{+/+}$ PI mice, and transcriptional activities of *Il1 and Il6* were not affected (Figure 6A). Moreover, *Lgals9* deficiency did not affect the expression of TLRs in peritoneal macrophages following pristane injection (Figure 6A). Such an effect appeared to be pristane-dependent, since the isolated and cultured peritoneal macrophages from PBS-injected Gal-9$^{-/-}$ mice did not show any significant up-regulation of *Il1b*, *Il6*, or *Tnfa* mRNA as compared to PBS-injected Gal-9$^{+/+}$ mice (Figure 6B). Although the expression of *Tnfa* mRNA was reduced in Gal-9$^{-/-}$ PI mice compared to their Gal-9$^{+/+}$ PI littermates, there were no significant differences in the TNF protein concentrations in the supernatants of cultured peritoneal macrophages from these mice (Figure 6C).

We also investigated time-course changes in *Tnfa* expression at 4, 24, and 48 hours after pristane injection, and TNF protein concentrations at 24 and 48 hours, in the isolated peritoneal macrophages without culture. Again, there were no significant differences in *Tnfa* mRNA expression between Gal-9$^{-/-}$ PI mice and Gal-9$^{+/+}$ PI mice (Figures 6D and E).
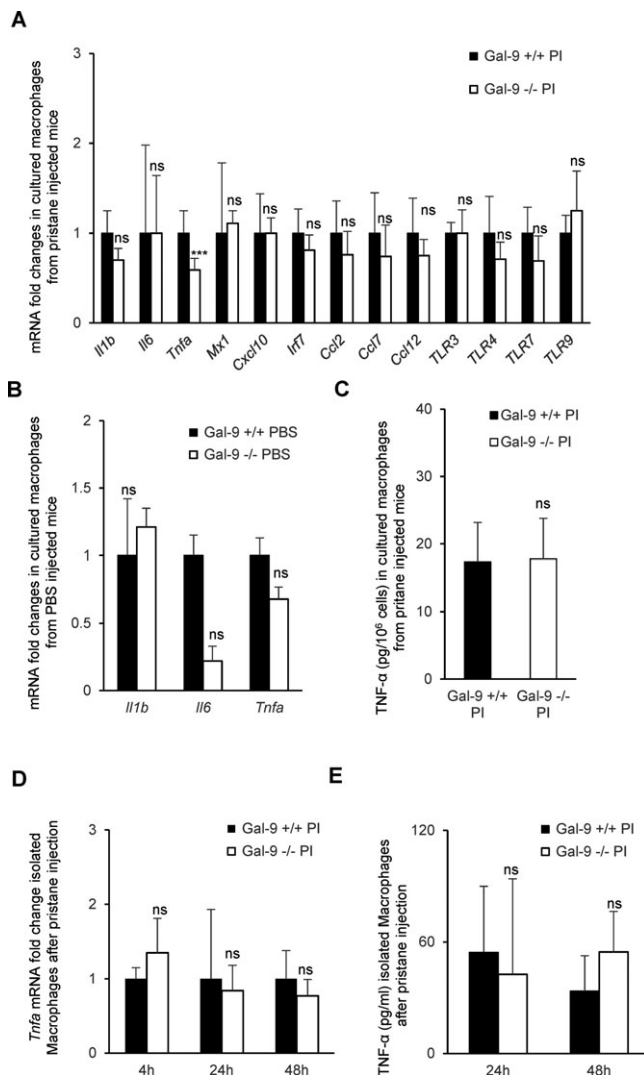
Figure 6. Expression of cytokines and Toll-like receptors (TLRs) in mouse peritoneal macrophages primed with pristane injection. **A,** Fold change in expression of mRNA for *Il1b, Il6, Tnfa,* interferon (IFN)–stimulated genes, type I IFN–induced chemokines, and TLRs was assessed by reverse transcription–polymerase chain reaction (RT-PCR) at 24 hours after pristane injection in peritoneal macrophages from Gal-9$^{-/-}$ PI mice compared to Gal-9$^{+/+}$ PI mice (n = 5 per group). **B,** Fold change in expression of mRNA for *Il1b, Il6,* and *Tnfa* was assessed in Gal-9$^{-/-}$ and Gal-9$^{+/+}$ mice (n = 3 per group) at 24 hours after phosphate buffered saline (PBS) injection. **C,** Production of tumor necrosis factor (TNF) was measured by enzyme-linked immunosorbent assay (ELISA) in culture supernatants of peritoneal macrophages from Gal-9$^{-/-}$ PI mice compared to Gal-9$^{+/+}$ PI mice (n = 5 per group) at 24 hours after pristane injection. **D,** Fold change in expression of mRNA for *Tnfa* was assessed by RT-PCR at 4 hours, 24 hours, and 48 hours after pristane injection in peritoneal macrophages from Gal-9$^{-/-}$ PI mice compared to Gal-9$^{+/+}$ PI mice (n = 4 per group). **E,** Production of TNF was measured by ELISA in cell lysates of peritoneal macrophages from Gal-9$^{-/-}$ PI mice compared to Gal-9$^{+/+}$ PI mice (n = 4 per group) at 24 hours and 48 hours after pristane injection. Results are the mean ± SD. *** = $P < 0.001$ by Student's *t*-test. See Figure 1 for other definitions.

We further analyzed the response of peritoneal macrophages to various TLR ligands. Unexpectedly, after stimulation of peritoneal macrophages with TLR ligands for 24 hours, positive effects of the TLR-3, TLR-4, and TLR-9 ligands on *Tnfa* gene expression were observed in the peritoneal macrophages from mice with *Lgals9* deficiency, with statistically significant differences compared to Gal-9$^{+/+}$ PI mice (for results, see Supplementary Figures 6A, B, and D, available on the *Arthritis & Rheumatology* web site at http://onlinelibrary.wiley.com/doi/10.1002/art.40467/abstract), whereas the TLR-7 ligand did not exert a stimulatory effect on *Tnfa* mRNA expression (see Supplementary Figure 6C, http://onlinelibrary.wiley.com/doi/10.1002/art.40467/abstract). Furthermore, stimulation with TLR ligands did not alter *Tnfa* mRNA expression, nor did it alter supernatant TNF concentrations, in cultured peritoneal macrophages from PBS-injected Gal-9$^{-/-}$ mice compared to PBS-injected Gal-9$^{+/+}$ mice (see Supplementary Figures 6E and F, http://onlinelibrary.wiley.com/doi/10.1002/art.40467/abstract). These results suggest that *Lgals9* deficiency does not alter the pristane-induced recruitment of inflammatory leukocytes into the peritoneal cavity, nor does it impair the sensitivities of cytokine production stimulated by TLR ligands.

Role of *Lgals9* deficiency in conferring protection against pristane-induced lupus in a manner independent of the TLR-7–type I IFN pathway. The activation of the TLR-7/myeloid differentiation factor 88 pathway triggers the subsequent secretion of type I IFN and the expression of IFN-stimulated genes (ISGs) and chemokines. Since TLR-7–type I IFN is the essential pathway for the development of pristane-induced lupus (46), we investigated whether *Lgals9* deficiency protected against the development of pristane-induced lupus via alterations in the TLR-7–type I IFN pathway in peritoneal macrophages. The expression levels of ISGs (*Mx1, Cxcl10,* and *Irf7*) and IFN-induced chemokines (*Ccl2, Ccl7,* and *Ccl12*) in the peritoneal macrophages were comparable between Gal-9$^{-/-}$ PI mice and Gal-9$^{+/+}$ PI mice (Figure 6A). In cultured peritoneal macrophages, there was no difference in the expression of ISGs and IFN-induced genes stimulated with various TLR ligands between Gal-9$^{-/-}$ PI mice and Gal-9$^{+/+}$ PI mice (see Supplementary Figures 5A–D, http://onlinelibrary.wiley.com/doi/10.1002/art.40467/abstract). These results suggest that *Lgals9* deficiency does not alter the TLR-7–type I IFN pathway in the peritoneal macrophages of mice with pristane-induced lupus.

DISCUSSION

It has been postulated that the application of exogenous Gal-9 may limit the pathogenic activities of T

cells, such as the activation of Th1 and Th17 cells (19). Indeed, the therapeutic effect of recombinant Gal-9 has been successfully demonstrated in several autoimmune disease models, including CIA (20,33), immune complex–induced arthritis (47), and spontaneous lupus in MRL/lpr mice (24). We initially hypothesized that *Lgals9* deficiency would exacerbate the clinical features of SLE in pristane-injected BALB/c mice and in the MRL/lpr mouse model of lupus. However, unexpectedly, *Lgals9* deficiency significantly ameliorated glomerulonephritis, arthritis, and lipogranuloma formation in pristane-injected BALB/c mice, whereas in MRL/lpr mice, glomerulonephritis and lymphadenopathy were not altered. Although many researchers have attempted to explore the clinical application of recombinant Gal-9 in autoimmune diseases, the development of antagonists to Gal-9 is also a new option in the treatment of autoimmune diseases. The small molecules that interfere with the binding between β-galactoside and Gal-9 may be such candidates for therapy. Human recombinant Gal-9 lacking a link peptide, designated hG9NC (null), is more resistant to proteolysis in the serum, limits lattice formation by reduced rotational freedom of carbohydrate binding domains (CRDs), and also works as an antagonist against the CRD-dependent effects of native Gal-9 (16).

Lgals9 deficiency did not alter the production of autoantibodies in either pristane-injected BALB/c mice or MRL/lpr mice, and anti-nRNP and anti-dsDNA antibodies were equally present in Gal-9$^{-/-}$ PI mice and Gal-9$^{+/+}$ PI mice. There was no impairment in the development of B cells and maturation to plasma cells, suggesting that Gal-9 is not required for autoantibody production, nor was B cell differentiation impaired in antibody-secreting cells. Although Gal-9 induces the differentiation of naive T cells to Treg cells and suppresses differentiation to Th1 and Th17 cells in in vitro experiments (20), we found no alterations of cell populations in lymphocytes from the spleen and peritoneal lavage between Gal-9$^{-/-}$ PI mice and Gal-9$^{+/+}$ PI mice. Double-negative T cells are known to expand and stimulate autoantibody production by secreting IL-17 and IFNγ (48), and reductions in the number of double-negative cells were observed in the spleens of Gal-9$^{-/-}$ MRL/lpr mice; however, we did not observe a reduction in autoantibody production.

In contrast to that seen in the spleen and lymph nodes, a significant reduction in lipogranuloma formation was observed in Gal-9$^{-/-}$ PI mice. Lipogranulomas induced by pristane injection consisted of B cells, CD4+ T cells, and DCs. Lipogranulomas are regarded as a form of ectopic lymphoid tissue, i.e., tertiary lymphoid tissue (44). The mechanism of lipogranuloma formation remains largely unknown, but presumably the recruitment of inflammatory cells in response to different chemokines and cytokines triggered by pristane injection plays a crucial role in the development of this unique structure. There was no impairment in leukocyte recruitment into the peritoneal cavity of Gal-9$^{-/-}$ PI mice; however, the formation and development of lipogranulomas was prominently diminished, and even completely absent, in some Gal-9$^{-/-}$ PI mice. Although the formation and development of lipogranulomas was not initially altered in Gal-9$^{-/-}$ PI mice, they might undergo resolution through the reduction in cellular maintenance and supply that occurs as result of the reduced number of HEVs, or through the reduction in pristane-induced cytokine production in the peritoneal cavity over time. The injection of pristane into the peritoneal cavity triggers an inflammatory local response characterized by the priming and activation of peritoneal macrophages (27), which results in the production of an array of inflammatory cytokines and chemokines, an enhanced stimulation by TLRs, and the recruitment, infiltration, and activation of inflammatory cells operating the innate and adaptive immune system in the peritoneal cavity.

We initially hypothesized that the ameliorated arthritis and glomerulonephritis in our model could be attributed to an impairment in the recruitment of inflammatory leukocytes into the peritoneal cavity, but Gal-9 deficiency did not affect the recruitment of inflammatory leukocytes into the peritoneal cavity. It is well-known that Gal-9 enhances TNF secretion in DCs (15,49) and microglial cells (50), belonging to the monocytic lineage. The interaction of TLRs and TLR ligands links to the common downstream signaling pathway, but their interaction produces different amounts or types of cytokines in the same cell, due in part to the quantitative and qualitative nature of the interaction between the TLRs and their ligand (51). Thus, we extensively investigated the basal and stimulated production of TNF protein by various TLR ligands, such as TLR-3, TLR-4, TLR-7, and TLR-9, in cultured peritoneal macrophages. In Gal-9$^{-/-}$ PI mice, the basal and TLR ligand–stimulated production of TNF protein from the peritoneal macrophages was not altered, although a certain degree of reduction in expression of *Tnfa* transcripts in the basal condition, and hyperresponsiveness in stimulated conditions, was observed. It is known that several cytokine genes, including *Tnfa*, undergo posttranscriptional regulation at the mRNA and protein translational levels (52), and the overall and final output of TNF in response to pristane was not influenced by *Lgals9* deficiency.

As demonstrated by several studies, the mouse model of pristane-induced lupus is known to be

dependent on the TLR-7–type I IFN pathway. Type I IFN is induced by the Ly-6C^{high} subset of immature monocytes, and the animal model is characterized by an increased expression of type I IFN–induced genes, the so-called IFN signature (45,46,53). The sustained production of anti-nRNP antibodies is dependent on TLR-7 ligand stimulation in the switched memory-like B cell subset (54). In the current investigation, we found no defects or reductions in the expression of several ISGs and IFN-induced chemokines, accumulation of Ly-6C^{high} inflammatory monocytes in the peritoneal cavity, or production of anti-nRNP. Thus, *Lgals9* deficiency appears to protect against pristane-induced lupus in mice in a manner independent of the TLR-7–type I IFN pathway in peritoneal macrophages.

Based on the findings in the current study, we can speculate as to why mice are protected against pristane-induced lupus in this model, while MRL/lpr mice are not. The single-cell response of basal and pristane-primed peritoneal macrophages to TLR ligands was not altered by *Lgals9* deficiency, as evidenced by the findings with regard to production of TNF, type I IFN, ISGs, and IFN-induced chemokines. However, Gal-9 is essentially required for the neogenesis of tertiary lymphoid tissue, which is characterized by lymphoid follicle–like structures and HEVs in response to pristane in vivo, although the formation of lymphoid tissues, such as lymph nodes and spleen, was not impaired in Gal-9$^{-/-}$ mice. The Gal-9Δ5 splice variant was found to be highly expressed in endothelial cells in different tumors, and it enhanced sprouting and migration of human umbilical vein endothelial cells toward a Gal-9Δ5 gradient (55). HEVs are the major entry port for immune cells in secondary lymphoid organs (56), and the reduced cellularity observed in Gal-9$^{-/-}$ PI mouse lipogranulomas suggests that inflammatory cells could be recruited via these newly formed vessels. Moreover, Gal-9 deficiency could have hampered their recruitment by inhibiting the formation of HEVs.

Another explanation for the protection against pristane-induced lupus in this model would be that Gal-9 is essential for lipogranuloma formation since it modulates cell adhesion and cell cluster formation (57). Lipogranulomas consist of immune cell clusters, and Gal-9 deficiency may impair cell adhesion, resulting in reduced cell aggregation and lipogranuloma formation. The formation of tertiary lymphoid-like structures also requires signals provided by the local environment, together with an appropriate stromal response, where Gal-9 is highly expressed.

In summary, the current investigation in Gal-9$^{-/-}$ PI mice suggests that the antagonism of Gal-9 is beneficial for the treatment of nephritis and arthritis in SLE. *Lgals9* deficiency did not affect the survival and apoptosis of T and B cells nor did it affect the production of cytokines from peritoneal macrophages; however, it notably caused a reduction in lipogranuloma formation. The apoptotic potential of the Gal-9 recombinant protein is dose-dependent, and a lower dose of Gal-9 or decline in the concentration of Gal-9 may cause enhanced cytokine production. The current therapy for SLE, which includes steroids and immunosuppressant agents, is associated with severe infections, a complication that impairs the quality of life in patients with SLE. A more robust and vigorous virus-specific immune response to acute and chronic viral infections is mounted in Gal-9–deficient mice, resulting in rapid viral clearance. Thus, antagonism of Gal-9 signaling may be beneficial for the prevention of various infections, including viral infection (58), in patients with SLE.

AUTHOR CONTRIBUTIONS

REFERENCES

1. Croca SC, Rodrigues T, Isenberg DA. Assessment of a lupus nephritis cohort over a 30-year period. Rheumatology (Oxford) 2011;50:1424–30.
2. Lateef A, Petri M. Unmet medical needs in systemic lupus erythematosus. Arthritis Res Ther 2012;14 Suppl 4:S4.
3. Tektonidou MG, Dasgupta A, Ward MM. Risk of end-stage renal disease in patients with lupus nephritis, 1971–2015: a systematic review and Bayesian meta-analysis. Arthritis Rheumatol 2016;68: 1432–41.
4. Van Vugt RM, Derksen RH, Kater L, Bijlsma JW. Deforming arthropathy or lupus and rhupus hands in systemic lupus erythematosus. Ann Rheum Dis 1998;57:540–4.
5. Bauernfeind B, Aringer M, Prodinger B, Kirchberger I, Machold K, Smolen J, et al. Identification of relevant concepts of functioning in daily life in people with systemic lupus erythematosus: a patient Delphi exercise. Arthritis Rheum 2009;61:21–8.
6. Wada J, Kanwar YS. Identification and characterization of galectin-9, a novel β-galactoside-binding mammalian lectin. J Biol Chem 1997;272:6078–86.
7. Wada J, Ota K, Kumar A, Wallner EI, Kanwar YS. Developmental regulation, expression, and apoptotic potential of galectin-9, a β-galactoside binding lectin. J Clin Invest 1997;99:2452–61.
8. Nio-Kobayashi J. Tissue- and cell-specific localization of galectins, β-galactose-binding animal lectins, and their potential functions in health and disease. Anat Sci Int 2017;92:25–36.
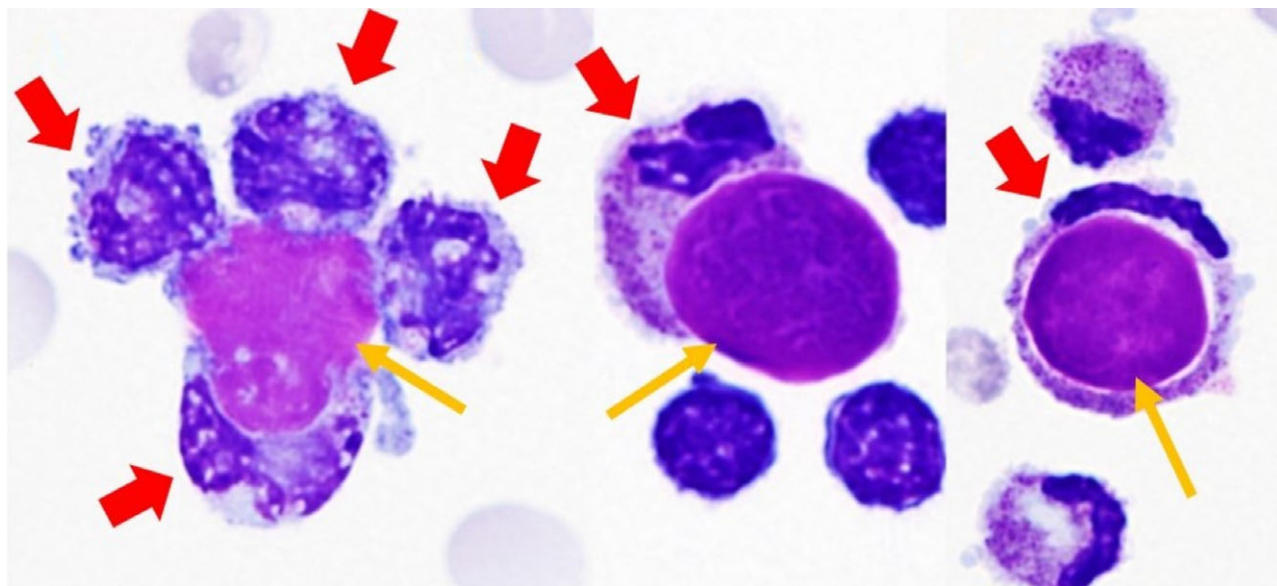
9. John S, Mishra R. Galectin-9: from cell biology to complex disease dynamics. J Biosci 2016;41:507–34.

10. Zhang ZY, Dong JH, Chen YW, Wang XQ, Li CH, Wang J, et al. Galectin-9 acts as a prognostic factor with antimetastatic potential in hepatocellular carcinoma. Asian Pac J Cancer Prev 2012;13:2503–9.

11. Kashio Y, Nakamura K, Abedin MJ, Seki M, Nishi N, Yoshida N, et al. Galectin-9 induces apoptosis through the calcium-calpain-caspase-1 pathway. J Immunol 2003;170:3631–6.

12. Lu LH, Nakagawa R, Kashio Y, Ito A, Shoji H, Nishi N, et al. Characterization of galectin-9-induced death of Jurkat T cells. J Biochem 2007;141:157–72.

13. Heusschen R, Griffioen AW, Thijssen VL. Galectin-9 in tumor biology: a jack of multiple trades. Biochim Biophys Acta 2013;1836:177–85.

14. Dai SY, Nakagawa R, Itoh A, Murakami H, Kashio Y, Abe H, et al. Galectin-9 induces maturation of human monocyte-derived dendritic cells. J Immunol 2005;175:2974–81.

15. Li Y, Feng J, Geng S, Geng S, Wei H, Chen G, et al. The N- and C-terminal carbohydrate recognition domains of galectin-9 contribute differently to its multiple functions in innate immunity and adaptive immunity. Mol Immunol 2011;48:670–7.

16. Fujita K, Iwama H, Oura K, Tadokoro T, Samukawa E, Sakamoto T, et al. Cancer therapy due to apoptosis: galectin-9. Int J Mol Sci 2017;18.

17. Zhu C, Anderson AC, Schubart A, Xiong H, Imitola J, Khoury SJ, et al. The Tim-3 ligand galectin-9 negatively regulates T helper type 1 immunity. Nat Immunol 2005;6:1245–52.

18. Gooden MJ, Wiersma VR, Samplonius DF, Gerssen J, van Ginkel RJ, Nijman HW, et al. Galectin-9 activates and expands human T-helper 1 cells. PLoS One 2013;8:e65616.

19. Wiersma VR, de Bruyn M, Helfrich W, Bremer E. Therapeutic potential of Galectin-9 in human disease. Med Res Rev 2013;33 Suppl 1:E102–26.

20. Seki M, Oomizu S, Sakata KM, Sakata A, Arikawa T, Watanabe K, et al. Galectin-9 suppresses the generation of Th17, promotes the induction of regulatory T cells, and regulates experimental autoimmune arthritis. Clin Immunol 2008;127:78–88.

21. Parker MH, Malone KH III, Trier AC, Striano TS. Evaluation of resistance form for prepared teeth. J Prosthet Dent 1991;66:730–3.

22. Katoh S, Ishii N, Nobumoto A, Takeshita K, Dai SY, Shinonaga R, et al. Galectin-9 inhibits CD44-hyaluronan interaction and suppresses a murine model of allergic asthma. Am J Respir Crit Care Med 2007;176:27–35.

23. Tsuchiyama Y, Wada J, Zhang H, Morita Y, Hiragushi K, Hida K, et al. Efficacy of galectins in the amelioration of nephrotoxic serum nephritis in Wistar Kyoto rats. Kidney Int 2000;58:1941–52.

24. Moritoki M, Kadowaki T, Niki T, Nakano D, Soma G, Mori H, et al. Galectin-9 ameliorates clinical severity of MRL/lpr lupus-prone mice by inducing plasma cell apoptosis independently of Tim-3. PLoS One 2013;8:e60807.

25. Baba M, Wada J, Eguchi J, Hashimoto I, Okada T, Yasuhara A, et al. Galectin-9 inhibits glomerular hypertrophy in db/db diabetic mice via cell-cycle-dependent mechanisms. J Am Soc Nephrol 2005;16:3222–34.

26. Oomizu S, Arikawa T, Niki T, Kadowaki T, Ueno M, Nishi N, et al. Galectin-9 suppresses Th17 cell development in an IL-2-dependent but Tim-3-independent manner. Clin Immunol 2012;143:51–8.

27. Satoh M, Reeves WH. Induction of lupus-associated autoantibodies in BALB/c mice by intraperitoneal injection of pristane. J Exp Med 1994;180:2341–6.

28. Satoh M, Kumar A, Kanwar YS, Reeves WH. Anti-nuclear antibody production and immune-complex glomerulonephritis in BALB/c mice treated with pristane. Proc Natl Acad Sci U S A 1995;92:10934–8.

29. Reeves WH, Lee PY, Weinstein JS, Satoh M, Lu L. Induction of autoimmunity by pristane and other naturally occurring hydrocarbons. Trends Immunol 2009;30:455–64.

30. Potter M, Wax JS. Genetics of susceptibility to pristane-induced plasmacytomas in BALB/cAn: reduced susceptibility in BALB/cJ with a brief description of pristane-induced arthritis. J Immunol 1981;127:1591–5.

31. Watanabe-Fukunaga R, Brannan CI, Copeland NG, Jenkins NA, Nagata S. Lymphoproliferation disorder in mice explained by defects in Fas antigen that mediates apoptosis. Nature 1992;356:314–7.

32. Adachi M, Suematsu S, Suda T, Watanabe D, Fukuyama H, Ogasawara J, et al. Enhanced and accelerated lymphoproliferation in Fas-null mice. Proc Natl Acad Sci U S A 1996;93:2131–6.

33. Seki M, Sakata KM, Oomizu S, Arikawa T, Sakata A, Ueno M, et al. Beneficial effect of galectin 9 on rheumatoid arthritis by induction of apoptosis of synovial fibroblasts. Arthritis Rheum 2007;56:3968–76.

34. Tsuboi Y, Abe H, Nakagawa R, Oomizu S, Watanabe K, Nishi N, et al. Galectin-9 protects mice from the Shwartzman reaction by attracting prostaglandin E2-producing polymorphonuclear leukocytes. Clin Immunol 2007;124:221–33.

35. Atkinson SM, Usher PA, Kvist PH, Markholst H, Haase C, Nansen A. Establishment and characterization of a sustained delayed-type hypersensitivity model with arthritic manifestations in C57BL/6J mice. Arthritis Res Ther 2012;14:R134.

36. Raatz Y, Ibrahim S, Feldmann M, Paleolog EM. Gene expression profiling and functional analysis of angiogenic markers in murine collagen-induced arthritis. Arthritis Res Ther 2012;14:R169.

37. Mannoor K, Matejuk A, Xu Y, Beardall M, Chen C. Expression of natural autoantibodies in MRL-lpr mice protects from lupus nephritis and improves survival. J Immunol 2012;188:3628–38.

38. Ji H, Pettit A, Ohmura K, Ortiz-Lopez A, Duchatelle V, Degott C, et al. Critical roles for interleukin 1 and tumor necrosis factor α in antibody-induced arthritis. J Exp Med 2002;196:77–85.

39. Simon J, Surber R, Kleinstauber G, Petrow PK, Henzgen S, Kinne RW, et al. Systemic macrophage activation in locally-induced experimental arthritis. J Autoimmun 2001;17:127–36.

40. Carlucci F, Ishaque A, Ling GS, Szajna M, Sandison A, Donatien P, et al. C1q modulates the response to TLR7 stimulation by pristane-primed macrophages: implications for pristane-induced lupus. J Immunol 2016;196:1488–94.

41. Satoh M, Richards HB, Shaheen VM, Yoshida H, Shaw M, Naim JO, et al. Widespread susceptibility among inbred mouse strains to the induction of lupus autoantibodies by pristane. Clin Exp Immunol 2000;121:399–405.

42. Hamilton KJ, Satoh M, Swartz J, Richards HB, Reeves WH. Influence of microbial stimulation on hypergammaglobulinemia and autoantibody production in pristane-induced lupus. Clin Immunol Immunopathol 1998;86:271–9.

43. Shaheen VM, Satoh M, Richards HB, Yoshida H, Shaw M, Jennette JC, et al. Immunopathogenesis of environmentally induced lupus in mice. Environ Health Perspect 1999;107 Suppl 5:723–7.

44. Nacionales DC, Kelly KM, Lee PY, Zhuang H, Li Y, Weinstein JS, et al. Type I interferon production by tertiary lymphoid tissue developing in response to 2,6,10,14-tetramethyl-pentadecane (pristane). Am J Pathol 2006;168:1227–40.

45. Lee PY, Weinstein JS, Nacionales DC, Scumpia PO, Li Y, Butfiloski E, et al. A novel type I IFN-producing cell subset in murine lupus. J Immunol 2008;180:5101–8.

46. Lee PY, Kumagai Y, Li Y, Takeuchi O, Yoshida H, Weinstein J, et al. TLR7-dependent and FcγR-independent production of type I interferon in experimental mouse lupus. J Exp Med 2008;205:2995–3006.

47. Arikawa T, Watanabe K, Seki M, Matsukawa A, Oomizu S, Sakata KM, et al. Galectin-9 ameliorates immune complex-induced arthritis by regulating FcγR expression on macrophages. Clin Immunol 2009;133:382–92.

48. Crispin JC, Oukka M, Bayliss G, Cohen RA, Van Beek CA, Stillman IE, et al. Expanded double negative T cells in patients

with systemic lupus erythematosus produce IL-17 and infiltrate the kidneys. J Immunol 2008;181:8761–6.

49. Kanzaki M, Wada J, Sugiyama K, Nakatsuka A, Teshigawara S, Murakami K, et al. Galectin-9 and T cell immunoglobulin mucin-3 pathway is a therapeutic target for type 1 diabetes. Endocrinology 2012;153:612–20.

50. Steelman AJ, Li J. Astrocyte galectin-9 potentiates microglial TNF secretion. J Neuroinflammation 2014;11:144.

51. Kanzler H, Barrat FJ, Hessel EM, Coffman RL. Therapeutic targeting of innate immunity with Toll-like receptor agonists and antagonists. Nat Med 2007;13:552–9.

52. Han J, Ulevitch RJ. Limiting inflammatory responses during activation of innate immunity. Nat Immunol 2005;6:1198–205.

53. Hagberg N, Ronnblom L. Systemic lupus erythematosus: a disease with a dysregulated type I interferon system. Scand J Immunol 2015;82:199–207.

54. Han S, Zhuang H, Xu Y, Lee P, Li Y, Wilson JC, et al. Maintenance of autoantibody production in pristane-induced murine lupus. Arthritis Res Ther 2015;17:384.

55. Heusschen R, Schulkens IA, van Beijnum J, Griffioen AW, Thijssen VL. Endothelial LGALS9 splice variant expression in endothelial cell biology and angiogenesis. Biochim Biophys Acta 2014;1842:284–92.

56. Ager A, May MJ. Understanding high endothelial venules: lessons for cancer immunology. Oncoimmunology 2015;4:e1008791.

57. Kageshita T, Kashio Y, Yamauchi A, Seki M, Abedin MJ, Nishi N, et al. Possible role of galectin-9 in cell aggregation and apoptosis of human melanoma cell lines and its clinical significance. Int J Cancer 2002;99:809–16.

58. Merani S, Chen W, Elahi S. The bitter side of sweet: the role of Galectin-9 in immunopathogenesis of viral infections. Rev Med Virol 2015;25:175–86.

Clinical Images: Lupus erythematosus cell

The patient, a 24-year-old woman with a history of systemic lupus erythematosus (SLE), presented with fever, polyarthralgia, and worsened neutropenia (0.5×10^9/liter). Results of a physical examination and routine laboratory evaluations were unremarkable. Examination of a peripheral blood smear showed neutrophils (**red arrows**) engulfing homogeneous, violaceus nuclear material (**yellow arrows**), confirming a suspected diagnosis of lupus flare. SLE-associated antinuclear antibodies opsonize nucleoproteins released from dying cells, with uptake by phagocytic cells, including polymorphonuclear leukocytes and macrophages: the so-called lupus erythematosus (LE) cells [1]. First described in 1948 in bone marrow preparations from patients with SLE [2], LE cells are rarely identified on peripheral blood smears but may be found during acute flares, as in our patient, and can help in making the correct diagnosis [3].

1. Snapper I, Nathan DJ. The mechanics of the L.E. cell phenomenon, studied with a simplified test. Blood 1955;10:718–29.
2. Hargraves MM, Richmond H, Morton R. Presentation of two bone marrow elements: the tart cell and the L.E. cell. Proc Staff Meet Mayo Clin 1948;23:25–8.
3. Aisenberg AC. Studies on the mechanism of the lupus erythematosus (L.E.) phenomenon. J Clin Invest 1959;38:325–33.

Armin Rashidi, MD, PhD
University of Minnesota
Minneapolis, MN
Stephen I. Fisher, MD
Eastern Virginia Medical School
Norfolk, VA

with systemic lupus erythematosus produce IL-17 and infiltrate the kidneys. J Immunol 2008;181:8761–6.

49. Kanzaki M, Wada J, Sugiyama K, Nakatsuka A, Teshigawara S, Murakami K, et al. Galectin-9 and T cell immunoglobulin mucin-3 pathway is a therapeutic target for type 1 diabetes. Endocrinology 2012;153:612–20.

50. Steelman AJ, Li J. Astrocyte galectin-9 potentiates microglial TNF secretion. J Neuroinflammation 2014;11:144.

51. Kanzler H, Barrat FJ, Hessel EM, Coffman RL. Therapeutic targeting of innate immunity with Toll-like receptor agonists and antagonists. Nat Med 2007;13:552–9.

52. Han J, Ulevitch RJ. Limiting inflammatory responses during activation of innate immunity. Nat Immunol 2005;6:1198–205.

53. Hagberg N, Ronnblom L. Systemic lupus erythematosus: a disease with a dysregulated type I interferon system. Scand J Immunol 2015;82:199–207.

54. Han S, Zhuang H, Xu Y, Lee P, Li Y, Wilson JC, et al. Maintenance of autoantibody production in pristane-induced murine lupus. Arthritis Res Ther 2015;17:384.

55. Heusschen R, Schulkens IA, van Beijnum J, Griffioen AW, Thijssen VL. Endothelial LGALS9 splice variant expression in endothelial cell biology and angiogenesis. Biochim Biophys Acta 2014;1842:284–92.

56. Ager A, May MJ. Understanding high endothelial venules: lessons for cancer immunology. Oncoimmunology 2015;4:e1008791.

57. Kageshita T, Kashio Y, Yamauchi A, Seki M, Abedin MJ, Nishi N, et al. Possible role of galectin-9 in cell aggregation and apoptosis of human melanoma cell lines and its clinical significance. Int J Cancer 2002;99:809–16.

58. Merani S, Chen W, Elahi S. The bitter side of sweet: the role of Galectin-9 in immunopathogenesis of viral infections. Rev Med Virol 2015;25:175–86.
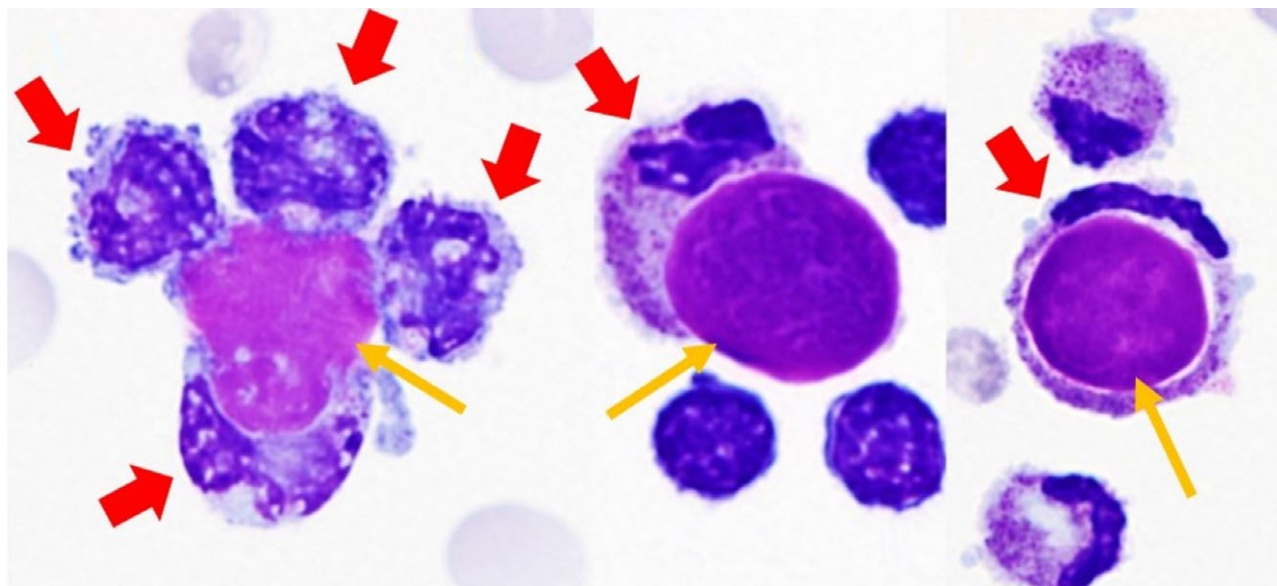
Clinical Images: Lupus erythematosus cell

The patient, a 24-year-old woman with a history of systemic lupus erythematosus (SLE), presented with fever, polyarthralgia, and worsened neutropenia (0.5×10^9/liter). Results of a physical examination and routine laboratory evaluations were unremarkable. Examination of a peripheral blood smear showed neutrophils (**red arrows**) engulfing homogeneous, violaceus nuclear material (**yellow arrows**), confirming a suspected diagnosis of lupus flare. SLE-associated antinuclear antibodies opsonize nucleoproteins released from dying cells, with uptake by phagocytic cells, including polymorphonuclear leukocytes and macrophages: the so-called lupus erythematosus (LE) cells (1). First described in 1948 in bone marrow preparations from patients with SLE (2), LE cells are rarely identified on peripheral blood smears but may be found during acute flares, as in our patient, and can help in making the correct diagnosis (3).

1. Snapper I, Nathan DJ. The mechanics of the L.E. cell phenomenon, studied with a simplified test. Blood 1955;10:718–29.

2. Hargraves MM, Richmond H, Morton R. Presentation of two bone marrow elements: the tart cell and the L.E. cell. Proc Staff Meet Mayo Clin 1948;23:25–8.

3. Aisenberg AC. Studies on the mechanism of the lupus erythematosus (L.E.) phenomenon. J Clin Invest 1959;38:325–33.

Armin Rashidi, MD, PhD
University of Minnesota
Minneapolis, MN
Stephen I. Fisher, MD
Eastern Virginia Medical School
Norfolk, VA

Evidence of Alternative Modes of B Cell Activation Involving Acquired Fab Regions of *N*-Glycosylation in Antibody-Secreting Cells Infiltrating the Labial Salivary Glands of Patients With Sjögren's Syndrome

Kristi A. Koelsch,[1] Joshua Cavett,[1] Kenneth Smith,[2] Jacen S. Moore,[1] Sylvain D. Lehoux,[3] Nan Jia,[3] Tim Mather,[2] Syed M. S. Quadri,[4] Astrid Rasmussen,[2] C. Erick Kaufman,[5] David M. Lewis,[6] Lida Radfar,[6] Teresa A. Scordino,[5] Christopher J. Lessard,[4] Biji T. Kurien,[1] Richard D. Cummings,[3] Judith A. James,[4] Kathy L. Sivils,[4] A. Darise Farris,[4] and R. Hal Scofield [1]

Objective. To better understand the role of B cells, the potential mechanisms responsible for their aberrant activation, and the production of autoantibodies in the pathogenesis of Sjögren's syndrome (SS), this study explored patterns of selection pressure and sites of *N*-glycosylation acquired by somatic mutation (ac*N*-glyc) in the IgG variable (V) regions of antibody-secreting cells (ASCs) isolated from the minor salivary glands of patients with SS and non-SS control patients with sicca symptoms.

Methods. A novel method to produce and characterize recombinant monoclonal antibodies (mAb) from single cell–sorted ASC infiltrates was applied to concurrently probe expressed genes (all heavy- and light-chain isotypes as well as any other gene of interest not related to immunoglobulin) in the labial salivary glands of patients with SS and non-SS controls. V regions were amplified by reverse transcription–polymerase chain reaction, sequenced, and analyzed for the incidence of *N*-glycosylation and selection pressure. For specificity

testing, the amplified regions were expressed as either the native mAb or mutant mAb lacking the ac*N*-glyc motif. Protein modeling was used to demonstrate how even an ac*N*-glyc site outside of the complementarity-determining region could participate in, or inhibit, antigen binding.

Results. V-region sequence analyses revealed clonal expansions and evidence of secondary light-chain editing and allelic inclusion, of which neither of the latter two have previously been reported in patients with SS. Increased frequencies of ac*N*-glyc were found in the sequences from patients with SS, and these ac*N*-glyc regions were associated with an increased number of replacement mutations and lowered selection pressure. A clonal set of polyreactive mAb with differential framework region 1 ac*N*-glyc motifs was also identified, and removal of the ac*N*-glyc could nearly abolish binding to autoantigens.

Conclusion. These findings support the notion of an alternative mechanism for the selection and pro-

liferation of some autoreactive B cells, involving V-region *N*-glycosylation, in patients with SS.

Sjögren's syndrome (SS) is a systemic, chronic autoimmune disease that is characterized by lymphocytic infiltration of the exocrine glands, inflammation, tissue damage, and secretory dysfunction. Typically, the lacrimal and salivary glands are affected, resulting in dry eyes (keratoconjuntivitis sicca) and dry mouth (xerosomia), but patients can also present with extraglandular complications or overlapping autoimmune diseases (1–5). In addition, patients with SS have an increased risk of progression to various non-Hodgkin's lymphomas (NHLs), resulting in significant morbidity (6).

There is evidence to indicate that chronic immune cell stimulation by bacteria is an active mechanism in the development of NHLs not associated with SS (7–9). It has been demonstrated that *Pseudomonas aeruginosa* and *Burkholderia cenocepacia* lectins bind to and activate B cells via B cell receptor variable (V)–region glycans (10). Similarly, in a patient with SS-associated NHL, evidence of a bacterial etiology was observed with the regression of a parotid mucosa-associated lymphoid tissue lymphoma after clearance of the patient's *Helicobacter pylori* infection (11).

It is known that dysregulation of both innate and adaptive immunity contributes to the etiology of SS and its complications; however, the pathophysiology of SS, as well as Sjögren's-associated lymphoma, is largely unknown. B cells play a role in the pathogenesis of SS, as evidenced by the presence of autoantigen-specific memory B cells (12,13) and the incidence of autoantibodies to Ro/SSA (Ro52 and Ro60) and La/SSB (14). An abundance of evidence has demonstrated that there is antigen-driven production of autoantibodies within the salivary glands of patients with SS (13,15,16). Ig V-region sequence analysis enables the identification of clonally expanded cells, serving as strong evidence of the antigen-driven activation and proliferation of B cells.

Antigen-driven activation can also be determined empirically by analyses of selection pressure in V-region sequences, in which the observed frequency of nonsynonymous (replacement) mutations is compared to their expected frequency in a state of no selection. When the frequency of replacement mutations is greater than expected, the Ig is considered to have undergone positive selection, and when the frequency is less than expected, negative selection is indicated. Typical antigen-driven activation results in positive selection in the complementarity-determining regions (CDRs), which directly interact with the antigen, and negative selection in the framework regions (FRs), which are important for structural integrity. Patterns of selective pressure contrary to this model indicate non-specific activation.

Somatic hypermutations (SHMs) leading to amino acid replacements can also give rise to posttranslational modifications by the introduction of *N*-linked glycosylation (*N*-glyc) motifs. This results in SHM-acquired *N*-glyc (ac*N*-glyc) of the antibody at these sites, and may have implications in immune responses or disease states. Ig V-region ac*N*-glyc motifs have been reported to be present in B cells from the parotid glands of patients with SS (17) and are strongly correlated with follicular lymphoma (18,19), a disease with a 4-fold increased incidence in patients with SS (20). Instances of single Ig V-region *N*-glycans introduced by SHM have been demonstrated to either strengthen (21), weaken, or abolish binding of self or foreign antigens (22). Conversely, bacterial or innate immune system lectins can bind V-region *N*-glycans, causing activation of B cells in an antigen-independent manner (10,23). Therefore, analyses of Ig V-region *N*-glycosylation may give clues with regard to the antibody–antigen interactions, tolerance mechanisms, and nonspecific modes of B cell activation that may drive proliferation of B cells in patients with SS.

In this study, we hypothesized that ac*N*-glyc in the V regions of IgG antibody-secreting cells (ASCs) isolated from the labial salivary glands of patients with SS and non-SS control patients with dry mouth and dry eye (sicca symptoms) may provide opportunities for antigen-independent proliferation of autoreactive B cells and antibody production in the salivary glands of patients with SS. Our findings support this hypothesis, suggesting an alternative means by which B cell selection and proliferation of some autoreactive B cells may occur in patients with SS.

PATIENTS AND METHODS

Collection of labial salivary gland samples and evaluation of human subjects. Studies were approved by the Oklahoma Medical Research Foundation (OMRF) and University of Oklahoma Health Sciences Center Institutional Review Boards. Samples and data were obtained from all subjects following their provision of written informed consent. Participants were evaluated in the OMRF Sjögren's Research Clinic (OSRC), as reported previously (24). Labial salivary glands were collected for single-cell sorting and production of monoclonal antibodies (mAb), as previously described (16). All 14 participants had symptoms of dry eyes and dry mouth, without a current diagnosis of, or history of, NHL. Of the 14 participants, 8 met the American–European Consensus Group classification criteria for primary SS (2), and 1 also met the American College of Rheumatology classification criteria for systemic lupus erythematosus (SLE) (25,26). Six subjects with sicca symptoms who did not meet the classification criteria for SS served as non-SS controls.

Hematoxylin and eosin (H&E)–stained salivary gland sections were obtained from the OSRC repository, and 2

independent evaluations of the tissue sections for the presence of ectopic germinal center structures were made both by an oral pathologist and by a hematopathologist (DML and TAS). The demographic characteristics of the participants, classification criteria met, clinical/extraglandular manifestations, and disease activity scores based on the EULAR Sjögren's Syndrome Disease Activity Index (ESSDAI) (with higher scores indicating a higher level of disease activity) (27) are summarized in Table 1. Patients with SS were evaluated for the predictive risk of developing NHL, as described in ref. 28 (risk factors are listed in Supplementary Table 1, available on the *Arthritis & Rheumatology* web site at http://onlinelibrary.wiley.com/doi/10.1002/art.40458/abstract).

Production of recombinant mAb. Single-cell suspensions were stained for fluorescence-activated cell sorting, as previously described (16). The recombinant mAb were produced from the labial salivary glands of 3 patients (1 patient with SS and SLE, and 2 patients with primary SS [patients pSS-1 and pSS-2 in Table 2]), using IgG and kappa gene primers, as previously described (29). For the remaining subjects, the protocol was modified as described herein (see Supplementary Materials and Methods, available on the *Arthritis & Rheumatology* web site at http://onlinelibrary.wiley.com/doi/10.1002/art.40458/abstract). Variable (V), diversity (D), and joining (J) domains, FRs, and CDRs, along with the germline sequences, were identified using the International Immunogenetics Information System (IMGT/V-Quest) database.

To make the mutant mAb clones used in this study, V-region genes cloned into expression vectors were subjected to site-directed mutagenesis using a Q5 site-directed mutagenesis kit (New England Biolabs), with nonoverlapping primers designed using the online tool NEBaseChanger (version 1.2.6; https://nebasechanger.neb.com). The mutated V genes were sequenced, amplified, and expressed in the same manner as described above.

Ig analyses for antigen-driven selection. The method known as BASELINe (i.e., Bayesian estimation of antigen-driven selection; http://clip.med.yale.edu/selection) can be used to detect and quantify antigen selection in individual or multiple sequences based on mutational patterns, normalized to germline sequences, and provides a visual representation of differences in selective pressure (30). Clonally related sequences were identified by manual examination of the V-region genes recognized by the IMGT/V-Quest system, with confirmation using the Clonal Relate program (http://www.cse.unsw.edu.au/~ihmmune/ClonalRelate) (31). To eliminate potential bias, we retained only the first randomly listed antibody in each of the clonal groups identified by ClonalRelate for the BASELINe analysis. The remaining productive heavy- and light-chain V-region sequences were then grouped (i.e., first by subject classification [SS or non-SS], and then by IgG allele [e.g., IGHV1-18*01, among others), and analyzed using BASELINe (version 1.3).

Ig heavy- and light-chain *N*-glycosylation motif analysis. Potential ac*N*-glyc sites in the heavy- and light-chain V-region amino acid sequences were identified using the Net-NGlyc web interface (http://www.cbs.dtu.dk/services/NetNGlyc/).

Table 1. Demographic characteristics, classification criteria met, and extraglandular/clinical manifestations in patients with SS and non-SS controls with sicca symptoms*

	Patients with SS (n = 8)	Non-SS sicca controls (n = 6)
Demographics		
Age, mean ± SD (range) years	44.23 ± 10.48 (30–58)	50 ± 11.97 (36–72)
Sex, no. female/no. male	8/0	5/1
Race, no.		
Black	1	1
White	5	4
White/Native American	2	1
Classification criteria		
van Bijsterveld ocular surface staining score for eye dryness/damage, no. positive	8	0
Schirmer's tear production test for dry eye, no. positive	3	0
Abnormal WUSF rate, no. positive†	3	2
Salivary gland biopsy interpretation, finding (no. positive)	FLS (8)	NSCS (5); FLS (1)
Focus score, mean ± SD (range)	4.41 ± 3.39 (1.8–12)	0.33 ± 0.82 (0–2)
Serum ANAs, no. positive	8	5
Serum anti-Ro/SSA, no. positive	6	1
Serum anti-La/SSB, no. positive	3	0
Clinical/extraglandular manifestations		
ESSDAI score, mean ± SD	1.625 ± 0.92	NA
Hyper-IgG, no. positive	5	1
Hypo-IgG, no. positive	0	1
Hyper-IgM, no. positive	1	0
Low C3, no. positive	0	0
Low C4, no. positive	1	0
Low CH50, no. positive	1	1
Salivary gland enlargement, current or past, no. positive	2	3
Arthritis/arthralgias, no. positive	2	2
Synovitis, no. positive	1	1
Raynaud's syndrome, no. positive	4	3

* SS = Sjögren's syndrome; FLS = focal lymphocytic sialadenitis; NSCS = nonspecific chronic sialadenitis; ANAs = antinuclear antibodies; ESSDAI = EULAR Sjögren's Syndrome Disease Activity Index; NA = not applicable.
† Representing the number of patients with a whole unstimulated salivary flow (WUSF) rate of ≤1.5 ml/15 minutes (the threshold for abnormal).

Table 2. Clonal expansions, light-chain editing, and allelic inclusion in the sequences from 3 patients with SS and 1 non-SS control

Subject*	Clone	Status	V_H gene	D_H gene	J_H gene	Light-chain V gene	Light-chain J gene
pSS-1	2-E04k	Clone 1†	4-59	4-23	4	$V_\kappa 1$-12	$J_\kappa 4$
pSS-1	3-C06k	Clone 1†	4-59	4-23	4	$V_\kappa 1$-12	$J_\kappa 4$
pSS-1	4-A01k	Clone 1†	4-59	4-23	4	$V_\kappa 1$-12	$J_\kappa 4$
pSS-1	4-B03k	Clone 1	4-59	4-23	4	$V_\kappa 1$-12	$J_\kappa 4$
pSS-1	4-G03k	Clone 1†	4-59	4-23	4	$V_\kappa 1$-12	$J_\kappa 4$
pSS-2	1-B03K	Clone 1	2-5	3-22	4	$V_\kappa 1$-39	$J_\kappa 2$
pSS-2	3-E04K	Clone 1	2-5	3-22	4	$V_\kappa 1$-39	$J_\kappa 2$
pSS-2	1-C01K	Clone 2	1-69	2-2	5	$V_\kappa 1$-39	$J_\kappa 2$
pSS-2	1-D03K	Clone 2	1-69	2-2	5	$V_\kappa 1$-39	$J_\kappa 2$
pSS-2	1-F01K	Clone 3	3-7	2-21	4	$V_\kappa 3$-11	$J_\kappa 5$
pSS-2	3-E01K	Clone 3	3-7	2-21	4	$V_\kappa 3$-11	$J_\kappa 5$
pSS-2	1-G02K	Clone 4 (light-chain replacement)	3-33	3-9	4	$V_\kappa 3$-20	$J_\kappa 4$
pSS-2	1-C06K	Clone 4 (light-chain replacement)	3-33	3-9	4	$V_\kappa 3$-15	$J_\kappa 2$
pSS-2	2-D06K	Clone 5 (light-chain replacement)	3-33	3-9	1	$V_\kappa 3$-15	$J_\kappa 3$
pSS-2	3-D06K	Clone 5 (light-chain replacement)	3-33	3-9	1	$V_\kappa 4$-1	$J_\kappa 1$
pSS-4	1-G01K	Clone 1	5-10-1	3-3	5	$V_\kappa 3$-20	$J_\kappa 5$
pSS-4	6-D06K	Clone 1	5-10-1	3-3	5	$V_\kappa 3$-20	$J_\kappa 5$
pSS-4	1-C02L	Clone 2 (light-chain replacement)	4-34	3-22	4	$V_\lambda 3$-25	$J_\lambda 2$
pSS-4	2-A06K	Clone 2 (light-chain replacement)	4-34	3-22	4	$V_\kappa 3$-20	$J_\kappa 1$
pSS-4	1-F03K	Clone 3 (light-chain replacement)	3-23	2-21	4	$V_\kappa 1$-5	$J_\kappa 1$
pSS-4	4-C03K	Clone 3 (light-chain replacement)	3-23	2-21	4	$V_\kappa 3$-15	$J_\kappa 2$
pSS-4	6-C06K	Clone 3 (light-chain replacement)	3-23	2-21	4	$V_\kappa 4$-1	$J_\kappa 5$
pSS-4	6-E01K	Allelic inclusion	3-21	6-19	6	$V_\kappa 1$-39	$J_\kappa 1$
pSS-4	6-E01L	Allelic inclusion	3-21	6-19	6	$V_\lambda 2$-11	$J_\lambda 2$
pSS-4	6-E04K	Allelic inclusion	3-53	6-13	5	$V_\kappa 1$-5	$J_\kappa 1$
pSS-4	6-E04L	Allelic inclusion	3-53	6-13	5	$V_\lambda 2$-14	$J_\lambda 2$
Non-SS control subject 2	1-F06K	Clone 1 (light-chain replacement)	3-15	6-19	4	$V_\kappa 1$-9	$J_\kappa 2$
Non-SS control subject 2	1-G04K	Clone 1 (light-chain replacement)	3-15	6-19	4	$V_\kappa 1$-12	$J_\kappa 1$

* Subject identifiers refer to 3 patients with primary Sjögren's syndrome (pSS) and 1 patient with sicca symptoms who did not meet the criteria for primary SS (non-SS control).
† Clone has heavy-chain N-glycosylation acquired by somatic mutation (ac$N$-glyc).

N-glycosylation motifs were defined as previously described (32). To confirm that all identified ac$N$-glyc sites were introduced by SHM, sequences were compared to their germline counterparts. The translated sequences of clonally related V regions were analyzed using the online Clustal Omega multiple sequence alignment program (http://www.ebi.ac.uk/Tools/msa/clustalo/) (33). Clonal sequences were not removed, because we found that each could yield unique glycosylation patterns. We excluded any possible N-glyc sites with a potential significance of association of ≤0.5, or jury agreement of <5 of 9 (34).

Glycoprotein and specificity analyses of mAb. For analyses of mAb, 1.5 μg of mAb or bovine IgG control (Equitech-Bio) were incubated at 37°C overnight with or without PNGase F (New England Biolabs), and then electrophoresed on a 4–12% sodium dodecyl sulfate–polyacrylamide gel electrophoresis (SDS-PAGE) gel (GenScript). For Coomassie blue staining, the gel was fixed in a destaining solution of 50% methanol and 10% acetic acid for 1 hour at room temperature, incubated for 1 hour with Coomassie brilliant blue (Bio-Rad), and then washed and destained with a destaining solution.

For analyses of lectin binding and immunoblotting of the mAb, samples were loaded onto a 4–12% SDS-PAGE gel (GenScript) and then electrophoresed, prior to transfer onto a cellulose membrane. For concanavalin A (Con A) staining, the membrane was blocked with a Tris buffered saline solution containing 0.05% Tween 20 (TBS-T) and 5% (weight/volume) bovine serum albumin (BSA) for 1 hour at room temperature, and then incubated with Con A–biotin (0.2 μg/ml) (Vector) in TBS-T with 1% BSA for 1 hour at room temperature, followed by incubation with streptavidin–horseradish peroxidase (HRP) (0.2 μg/ml) (Vector) in TBS-T containing 1% BSA for 1 hour at room temperature. For human IgG staining, the membrane was incubated with peroxidase-labeled goat anti-human IgG (Fc) antibody (KPL) at 0.2 μg/ml in TBS-T with 5% BSA for 1 hour at room temperature, and then washed with TBS-T. Signals were detected using an HRP chemiluminescence substrate (SuperSignal West Pico Chemiluminescent Substrate; Thermo Scientific).

Enzyme-linked immunosorbent assays (ELISAs) for screening of nuclear antigens were performed on all mAb in a manner as previously described (16).

Ig protein modeling. To visualize the location of the ac$N$-glyc sites in the clonal set of mAb, we utilized the crystal structure of the human IgG1 molecule (PDB accession number 3EYQ, 2.4 Å resolution) as a template for the HHPRED modeling server (https://toolkit.tuebingen.mpg.de/hhpred) (35). The individual somatic mutations from mAb clone 2-E04k were inserted where appropriate, and a representative Fab FR3 complex–type biantennary N-glycan, as identified in another published study (36), was modeled at the ac$N$-glyc site using MAIN software (37). The model graphics were created using PyMOL (PyMOL Molecular Graphics System, version 1.8.2; Schrödinger).

Statistical analysis. Fisher's exact tests were performed using GraphPad QuickCalcs (http://www.graphpad.com/quickcalcs/contingency1). GraphPad Prism software (version 7.0b) was used for the F test to compare variances, as well as for all parametric *t*-tests and nonparametric Mann-Whitney tests, which were each preceded by the D'Agostino and Pearson omnibus normality test.

RESULTS

Demographic and clinical characteristics of the participants. Evaluation of H&E-stained sections from the salivary gland biopsy tissue revealed that all patients with SS and non-SS controls had varying levels of chronic inflammation with lymphocytic infiltration (Table 1). In addition, 4 of the patients with SS (patients SS/SLE, pSS-1, pSS-2, and pSS-5 identified in Table 2 and Supplementary Table 1, http://onlinelibrary.wiley.com/doi/10.1002/art.40458/abstract]) had probable ectopic germinal center structures, including various associating cells such as plasma cells, follicular dendritic cells, and antigen-processing/presenting tingible body macrophages. We found no significant difference between patients with SS and non-SS controls with regard to the mean ± SD age (44 ± 10.48 years versus 50 ± 11.97 years, respectively; $P = 0.35$) or variance in age ($P = 0.72$). We found that 5 of the 8 patients with SS had an increased probability (39.9%) of future development of NHL (see Supplementary Table 1, http://onlinelibrary.wiley.com/doi/10.1002/art.40458/abstract), based on the presence of independent risk variables defined by a previously validated clinical tool (28).

Clonal expansions, secondary light-chain editing, and allelic inclusion, as revealed by Ig heavy- and light-chain sequence analyses. We cloned and sequenced a total of 122 productive IgG heavy-chain and kappa or lambda light-chain pairs from the ASCs of both groups. Of these, 100 pairs were from patients with SS (4 pairs from patient SS/SLE, 18 pairs from patient pSS-1, 23 pairs from patient pSS-2, 11 pairs from patient pSS-3, 36 pairs from patient pSS-4, 1 pair from patient pSS-5, 5 pairs from patient pSS-6, and 2 pairs from patient pSS-7), and 22 pairs were from non-SS controls (8 pairs from non-SS control subject 1, 6 pairs from non-SS control subject 2, 2 pairs from non-SS control subject 3, 1 pair from non-SS control subject 4, 4 pairs from non-SS control subject 5, and 1 pair from non-SS control subject 6). We identified several clonally related mAb. Of the patients with SS, patient pSS-1 had a single 5-member expansion, patient pSS-2 had a total of five 2-member expansions, and patient pSS-4 had a total of 5 expansions. There was 1 clonal pair identified in the sequences from non-SS control subject 2 (Table 2).

We found evidence of secondary light-chain editing in the sequences from patients pSS-2 and pSS-4 and non-SS control subject 2, indicated by the presence of

clonally related heavy chains with differential light-chain usage (clonal, with light-chain replacement) (Table 2). In addition, allelic inclusion, or 1 heavy chain with 2 distinct light chains within the same cell, was identified in 2 instances, in the ASCs from patient pSS-4 (clones 6-E01 and 6-E04) (Table 2). In each case, both a kappa light-chain sequence and a lambda light-chain sequence were amplified from the same cell.

Whether analyzed with clonal sequences or without clonal sequences, the length of the heavy-chain CDR3 was greater in patients with SS than in non-SS controls (with clonal sequences, 17 amino acids versus 15.5 amino acids in length, respectively [$P = 0.047$]; without clonal sequences, 17 amino acids versus 15 amino acids in length, respectively [$P = 0.048$]). There were no differences between patients and controls in the lengths of the light-chain CDR3s (11 amino acids in length, with or without clones, in both groups) or in the number of amino acid replacements in the heavy or light chains.

Differential acquisition of V-region *N*-glycoslyation motifs between patients with SS and non-SS controls. All of the *N*-glyc motifs identified in the heavy- and light-chain V regions of patients and controls were not germline encoded, and therefore had been acquired via SHM (ac*N*-glyc). We identified ac*N*-glyc motifs in sequences from 6 of 8 patients with SS (patients pSS/SLE, pSS-1, pSS-2, pSS-3, pSS-5, and pSS-6) and 2 of 6 non-SS controls (non-SS control subject 3 and non-SS control subject 5).

The acquisition of Fab *N*-glycosylation by SHM is a process that occurs in germinal centers. Therefore, we looked for correlations between the incidence of ac*N*-glyc and the presence of germinal centers in the salivary gland biopsy tissue. We found that in each of the 4 subjects identified with germinal center–like structures, all had V-region ac*N*-glyc motifs, but not all subjects with V-region ac*N*-glyc motifs had germinal center–like structures in the glands examined. The incidence of ac*N*-glyc in a heavy-chain/light-chain pair was more than doubled in sequences from patients with SS (29% [28 of 97]) as compared to non-SS controls (9% [2 of 22]); however, these differences only trended toward statistical significance ($P = 0.061$).

We found a trend toward an increased number of ac*N*-glyc sites in the FRs of sequences from patients with SS as compared to those from non-SS controls (22% [21 of 97] versus 5% [1 of 22], respectively; $P = 0.072$). In patients with SS, one-half (n = 11) of the FR ac*N*-glyc motifs were located in FR1 of the heavy and light chains. There were no FR1 ac*N*-glyc motifs in the non-SS control sequences. We found no instances of ac*N*-glyc motifs in the CDR3 regions of heavy or light chains, and no differences in the number of CDR1/CDR2 ac*N*-glyc motifs

between patients with SS and non-SS controls (11 of 97 versus 3 of 22, respectively; $P = 0.722$).

Association of ac*N*-glyc motifs with increased frequencies of SHM and amino acid replacements. We compared the heavy- and light-chain sequences that contained ac*N*-glyc (n = 31) to those without ac*N*-glyc (n = 91), without regard to disease classification (Figures 1A–C). Heavy chains with ac*N*-glyc motifs had significantly more SHMs than those without ac*N*-glyc motifs (mean ± SD number of SHMs 22.45 ± 1.047 versus 17.27 ± 0.8383; $P = 0.001$). The SHMs in heavy chains containing ac*N*-glyc sites also resulted in replacement mutations more often than in those without ac*N*-glyc sites (mean ± SD number of replacement mutations 16.65 ± 0.86 versus 12.88 ± 0.62; $P = 0.002$).

In the light chains, there was a trend toward more SHMs and replacement mutations in those containing ac*N*-glyc motifs than in those without ac*N*-glyc (mean number of SHMs 13 versus 10 [$P = 0.096$]; mean number of replacement mutations 9 versus 7 [$P = 0.146$]). Both heavy and light chains with ac*N*-glyc sites had significantly more amino acid replacements than did those without ac*N*-glyc sites (in heavy chains, mean ± SD 13.26 ± 0.599 versus 10.46 ± 0.462 [$P = 0.002$]; in light chains, 8.910 ± 0.843 versus 6.980 ± 0.416 [$P = 0.028$]).

Selection pressure patterns in the V regions of sequences from patients with SS compared to non-SS controls. We performed a BASELINe focused binomial test (30,38,39) on all of the unique sequences from patients with SS and non-SS controls, and found overall positive selection in the CDRs and negative selection in the FRs of the heavy chains from each group (for CDRs, $P = 0.009$ in patients with SS, $P = 0.05$ in non-SS controls; for FRs, $P = 2.99 \times 10^{-7}$ in patients with SS, $P = 0.02$ in non-SS controls). We found no significant selection pressure in the light-chain CDRs of sequences either in patients with SS or in non-SS controls ($P = 0.19$ and $P = 0.39$, respectively). However, both in the light-chain sequences from patients with SS and in the light-chain sequences from non-SS controls, negative selection in the FRs was observed ($P = 2.85 \times 10^{-14}$ and $P = 4.46 \times 10^{-8}$, respectively).

When we compared all of the SS sequences with all of the non-SS sequences, we found no significant differences in the selection pressures in either the heavy- or light-chain CDRs or FRs between the 2 groups (Figure 2A [for heavy chains] and Figure 2B [for light chains]).

Differential selection pressure patterns in Fab sequences with ac*N*-glyc motifs. Since we found an increased frequency of ac*N*-glyc motifs in the sequences from patients with SS, and since bacterial lectins have been reported to bind *N*-glycans and facilitate nonspecific B cell activation (10), we analyzed the effects of ac*N*-glyc on selection pressure. We compared heavy-chain sequences that contained ac*N*-glyc motifs to those without ac*N*-glyc motifs, without regard to disease classification. Results of the BASELINe focused binomial test indicated differential CDR selection between the 2 groups, in which there was no selection in the CDRs from heavy chains with ac*N*-glyc motifs ($P = 0.41$) but strong selection in the CDRs from heavy chains without ac*N*-glyc motifs ($P = 0.0007$). All sequences, both those with and those without ac*N*-glyc motifs, had negative selection in the FRs ($P = 3.91 \times 10^{-5}$ and $P = 5.6 \times 10^{-8}$, respectively).

When we compared the selection strengths of heavy chains with ac*N*-glyc motifs to those without ac*N*-glyc motifs, we found that heavy chains with ac*N*-glyc motifs showed a trend toward less positive selection in

Figure 1. Somatic hypermutations, replacement mutations, and amino acid (AA) changes in sequences in the presence or absence of regions of *N*-glycosylation acquired by somatic mutation (ac*N*-glyc). Sequence analyses of variable (V) regions were performed in the minor salivary gland antibody-secreting cells from patients with Sjögren's syndrome (SS) and non-SS control patients with sicca symptoms, in V regions with (n = 31) or without (n = 91) ac*N*-glyc motifs. **A,** Number of heavy- and light-chain V-region somatic hypermutations. **B,** Number of heavy- and light-chain replacement mutations. **C,** Number of heavy- and light-chain V-region amino acid changes. Results are the mean ± SD. * = $P < 0.05$; ** = $P < 0.01$. NS = not significant.

Figure 2. Comparison of selection pressure differences between groups using the Bayesian estimation of antigen-driven selection (BASELINe) method. The histograms provide a visualization of selection pressures for the complementarity-determining regions (CDRs) (red lines) and framework regions (FRs) (blue lines). Overlays of both, indicating the differences between groups, are shown in the lower left quadrants, with solid lines representing the column variable (e.g., in **A,** non–Sjögren's syndrome [SS] control patients with sicca symptoms) and broken lines representing the row variable (e.g., in **A,** patients with SS). Upper right quadrants show the statistically derived relative differences (determined with the binomial statistical test used by BASELINe) for each comparison, where the red boxes and positive numbers represent positive selection, and green boxes and negative numbers represent negative selection. Selection pressures in the heavy chains **(A)** and light chains **(B)** were compared between patients with SS and non-SS controls. Selection pressures in the heavy chains were also compared between those with N-glycosylation acquired by somatic mutation (ac$N$-glyc) and those without ac$N$-glyc **(C)**.

their CDRs ($P = 0.0679$) relative to the sequences without ac$N$-glyc motifs (Figure 2C).

Clonally related mAb with differential FR1 ac$N$-glyc motifs. Our analyses of ac$N$-glyc motifs also revealed a clonal set of differentially glycosylated Ig sequences

(patient pSS-1, clone 1 in Table 2). A multiple alignment of the heavy- and light-chain amino acid sequences (Figure 3A) revealed that 3 of the heavy-chain translated sequences in the clones were identical (for clones 2-E04k, 3-C06k, and 4-A01k). Clone 2-C06k and 4-A01k also
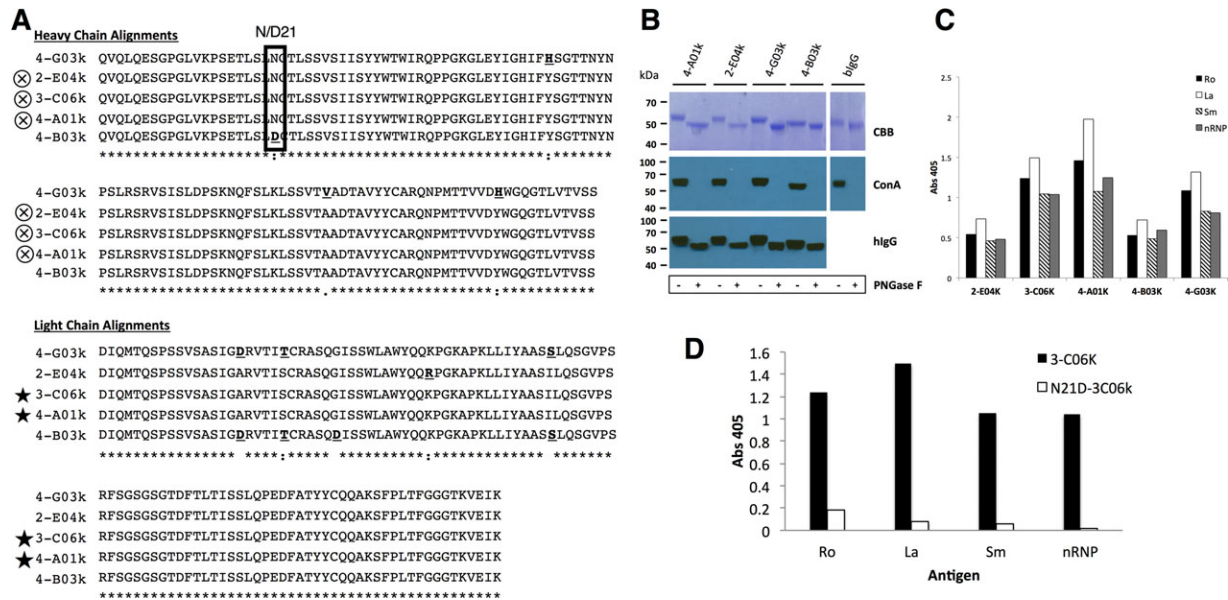
Figure 3. Clonal monoclonal antibody (mAb) *N*-glycosylation and antigen binding assessed by enzyme-linked immunosorbent assay (ELISA). **A,** Alignment of heavy- and light-chain amino acids from clonally related mAb derived from the antibody-secreting cells of a patient with primary Sjögren's syndrome (patient pSS-1) reveals differences that may affect antigen binding. Amino acids that are different from the consensus residues are indicated in boldface and underline. Boxed area indicates the site of an acquired *N*-glycosylation motif (ac*N*-glyc) (N-C-T, position 21) in 4 of the 5 clones. Circled X symbols indicate identical translated heavy-chain V-region sequences, while solid stars indicate identical translated light-chain V-region sequences. Asterisks indicate fully conserved residues, with the colon representing conservation between groups with strongly similar properties, and the period representing conservation between groups with weakly similar properties. **B,** The mAb heavy chains were assessed by mobility shift analysis. After digestion with PNGase F, followed by Coomassie blue (CBB) staining, a more modest shift could be seen in clone 4-B03k and bovine IgG (known to have 1 Fc-region *N*-glyc) as compared to clones 4-A01k, 2-E04k, and 4-G03k. Concanavalin A (Con A) staining indicates the complete removal of glycans by PNGase F. **C,** Binding of clonal mAb to Ro, La, Sm, and nuclear RNP (nRNP) was determined by ELISA. **D,** Antigen ELISA shows loss of antigen binding by mutant N21D-3C06k (lacking ac*N*-glyc) as compared to its glycosylated counterpart, 3-C06K. Results in **C** and **D** are expressed as the absorbance at 405 nm (Abs 405). Color figure can be viewed in the online issue, which is available at http://onlinelibrary.wiley.com/doi/10.1002/art.40458/abstract.

shared an identical light-chain sequence. Clone 4-B03k was the only 1 of the 5 clonal immunoglobulins that did not have an ac*N*-glyc at position 21 of the heavy chain (D21) in FR1.

To confirm that the FR1 (N21) *N*-glyc motifs in this clonal group could indeed be glycosylated at the protein level, the heavy- and light-chain V regions of the 5 pairs were cloned into expression vectors and expressed as mAb. Glycosylation studies were performed on mAb 4-A01k, 2-E04k, 4-G03k, and 4-B03k. Clone 3-C06k was not analyzed, as it was identical in amino acid sequence to clone 4-A01k (Figure 3A). After enzymatic removal of *N*-glycans with PNGase F and separation on an SDS-PAGE gel, staining with Coomassie brilliant blue showed that there was a motility shift in the heavy chain of the Ig molecules (Figure 3B), indicating that loss of *N*-glycans had occurred. The shift for clone 4-B03k, which lacked the FR1 *N*-glycan motif, was moderate compared to that for the other 3 clones, and comparable to that observed for bovine IgG, which was known to carry only 1 *N*-glycan per heavy chain. Staining with Con A, which binds mannose-containing *N*-glycans, confirmed the presence of

N-glycans in the untreated sample, and demonstrated that the *N*-glycans were quantitatively removed after treatment with PNGase F.

Effect of FR1 *N*-glycoslyation on mAb antigen binding. To determine whether these clones were autoreactive, the mAb were tested by ELISA for binding Ro, La, Sm, and nuclear RNP (nRNP) (Figure 3C). All 5 clones had some degree of binding to all antigens, with 3-C06k, 4-A01k, and 4-G03k having the highest levels of reactivity.

We next determined the effects of *N*-glycosylation in the FR1 on antigen binding. We removed the ac*N*-glyc motif from the FR1 of 3-C06k by replacing the asparagine (N) at position 21 with an aspartic acid (D) (N21D-3C06k). Conversely, we introduced an *N*-glyc motif to 4-B03k at the same position, converting the aspartic acid to an asparagine (D21N-4B03k). We expressed these mutant mAb and retested them for binding to Ro, La, Sm, and nRNP. We found that N21D-3C06k had almost completely lost all binding to all 4 antigens after removal of the FR1 *N*-glyc (Figure 3D). However, D21N-4B03k did not gain binding to any of the antigens after the addition of an *N*-glyc in FR1, but instead lost binding to La, Sm, and nRNP.

Potential mechanism for FR1 ac*N*-glyc participation in antigen binding via expansion of the antigen-binding site, as revealed by protein modeling. We used protein modeling of clone 2-E04k to visualize the location of the FR1 *N*-glyc in relation to the CDR antigen-binding pocket (Figures 4A and B). The heavy-chain FR1 ac*N*-glyc was oriented on the exterior of the molecule, very near the CDR binding site. We replaced the light chain in the model with the other light chains in the clonal group and found no appreciable difference in the orientation of the ac*N*-glyc (data not shown).

To visualize how an *N*-glyc might affect or participate in antigen binding, we added and remodeled an FR3

complex, biantennary *N*-glycan structure (4FQC), as was previously identified in another study (36), to our model (Figure 4C). We found that the binding surface could effectively be expanded by the close proximity of the branched carbohydrate structure (Figure 4D).

DISCUSSION

The non-SS controls used in this study were not healthy subjects, but unlike healthy controls, they had a sufficient number of ASCs for isolation by single-cell sorting, and therefore these subjects served as excellent sicca controls. Since the non-SS control subjects each had some
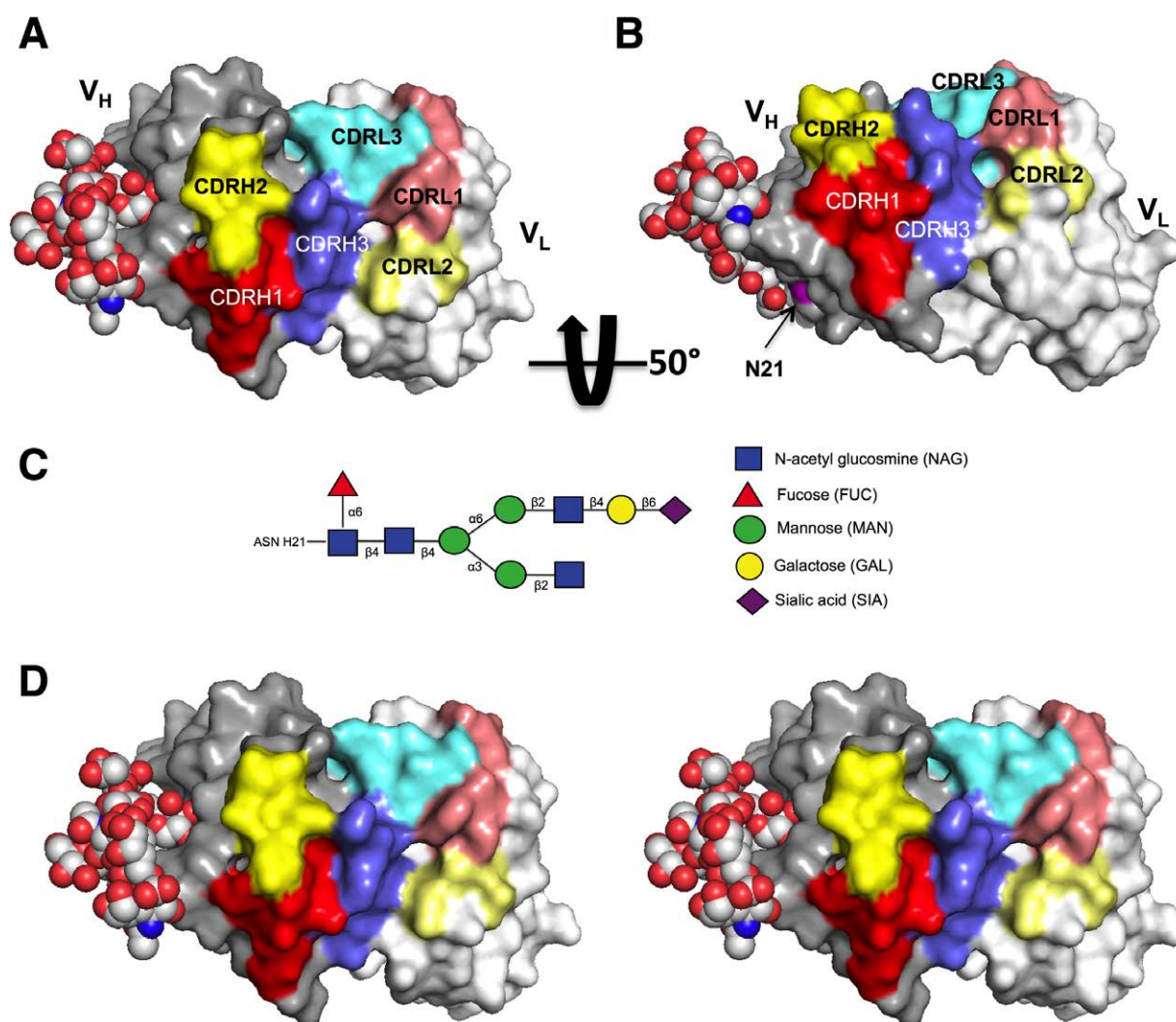
Figure 4. Protein model of 2-E04k monoclonal antibody variable (V) regions with complex-type framework region 1 *N*-glycan. **A,** The mono image shows the heavy-chain V region (V$_H$) oriented on the left, and light-chain V region (V$_L$) on the right. Heavy-chain complementarity-determining region (CDR) residues are indicated in red (CDR1), yellow (CDR2), and blue (CDR3). Light-chain CDR region residues are indicated in muted colors, pink (CDR1), light yellow (CDR2), and light blue (CDR3). **B,** The same model as in **A** is shown rotated upward ~50° about the horizontal axis, with the position of the heavy-chain acquired *N*-glycosylation (ac*N*-glyc) motif (N21) shown in magenta. **C,** The schematic diagram depicts the representative complex-type *N*-glycan utilized in the model. **D,** The stereo image depicts the same model as shown in **A**.

degree of glandular inflammation (see Table 1), the differences seen between patients with SS and non-SS controls in this study could not be attributed to an inflammatory milieu or the lack thereof. It will be interesting to follow up the non-SS controls longitudinally to determine if some progression to SS takes place over time, or if these subjects represent a distinct disease or subset not yet defined.

The ASCs from the first 3 subjects enrolled into this study were interrogated using a previously published reverse transcription–polymerase chain reaction (RT-PCR) protocol (29) that limited the probing of each single-sorted cell with multiplexed primers for only 1 heavy-chain and 1 light-chain isotype. The modification of our protocol for the remaining subjects to a 2-step RT-PCR method enabled probing for multiple heavy- and light-chain isotypes. The utility of this method could also extend to any other expressed gene of interest in single-sorted cells from any B cell population. Our efforts revealed what appear to be rare cases of allelic inclusion in 1 of the patients with primary SS (patient pSS-4), which would not have been identified with the previous method. We are uncertain whether both light chains are translated and expressed with heavy chains in these cells, or whether they remain as remnant messenger RNA from earlier selection events. B cells that express dual light chains on their surface have been described in healthy humans (40) and in various B cell lymphomas (41–43). The incidence of lymphoma is increased in SS, and it is possible that the dual light-chain ASCs that we identified are precursors to neoplastic lymphoblasts. Interestingly, patient pSS-4 was one of the patients who was also identified as having an increased probability of lymphoma development (28).

Secondary light-chain replacement, or receptor revision as it is called in the periphery, has been demonstrated in both mice and humans (44,45). Receptor revision has also been reported in patients with SLE (46) and in the cerebral spinal fluid infiltrating B cells from patients with multiple sclerosis (47,48), but to our knowledge, this process has not been previously reported in patients with SS. These findings are not likely to be the result of PCR contamination, as each light-chain replacement was a unique sequence, not found paired with any other heavy chain in the study. Whether the light-chain replacements identified represent a novel peripheral tolerance mechanism is unknown.

Our finding of somatically mutated, clonally related ASCs in 3 patients with SS and 1 non-SS control may represent evidence that antigen-driven B cell proliferation occurs within the labial salivary glands, and is consistent with findings from our previous study (16). The BASELINe analyses also supported this finding. A recent study by Hamza et al found no evidence for positive selection in SS parotid B cell heavy chains using the BASELINe method (17), but this may be easily explained by differences in study designs. The Hamza study involved bulk RNA from parotid tissue B cells, instead of single cell–sorted labial salivary gland ASCs as in our study. They also probed only the IgG V_H3-family genes, whereas we included primers for all V_H-family genes. Alternatively, there may be microenvironmental differences between the parotid gland and labial salivary gland tissue, or differences in B cell subsets, since memory B cells accumulate in the parotid tissue of patients with SS (49).

The increased incidence of ac$N$-glyc motifs, particularly those occurring in the FRs, was interesting. Hamza and colleagues also reported an increased frequency of FR ac$N$-glyc motifs in patients with SS. The increased rates of SHM in immunoglobulins with regions of ac$N$-glyc suggest that ac$N$-glyc motifs may drive SHM by facilitating increased activation signals via bacterial lectins, independent of antigen. This is supported by our finding that heavy chains with ac$N$-glyc motifs did not indicate selection of the CDR antigen-binding regions, suggesting that there is an antigen-independent mechanism for their origin. Alternatively, the likelihood of acquiring novel N-glycosylation motifs may increase as the rate of SHM increases. It was interesting that we found evidence of salivary gland germinal center structures in only 4 of the patients with ac$N$-glyc sites. This may be explained by the fact that these analyses were not performed in the same glands. Since the glands processed for single-cell sorting and mAb production/sequencing must be used in their entirety for the production of mAb, the germinal center analyses were performed on other glands biopsied at the same clinic visit.

Sequences with ac$N$-glyc motifs have at least 1 replacement mutation leading to the acquisition of the N-glyc, so it is possible that we have introduced bias to this analysis by parsing them into ac$N$-glyc–positive and ac$N$-glyc–negative groups. However, BASELINe analysis predicts selection pressures by identifying replacement mutations that occur at higher rates than would be expected in a scenario of "no selection," and therefore we would expect any bias of this nature to have resulted in increased positive selection, but we observed the opposite, which supports our data and reinforces the idea of a nonspecific activation of these cells. Since bacterial lectins have been demonstrated to bind Ig N-glycans and trigger nonspecific activation of the B cell (10), this is a possible mechanism for a break in tolerance leading to Ig autoreactivity, as well as a potential mechanism for the increased risk of lymphoma seen in patients with SS.

After removing the FR1 ac$N$-glyc from clone 3-C06k, binding to 4 common autoantigens was almost completely abolished, indicating that the acquisition of an

N-glycan via SHM can actually increase binding to the self antigens that are commonly bound by mAb produced from the labial salivary glands of patients with SS (16). Similar findings have been reported for a polyreactive mAb after removal of an FR3 *N*-glyc (50). The heavy chain is only partially responsible for antigen affinity, and between the 5 clones there were 4 light chains with unique mutations, which could explain the lowered binding by both D21N-4B03k and 2-E04k. Oligosaccharides are inherently flexible, and individual sugar linkages can exist in various conformations (51). The *N*-glycan conformation in our model is one possible, but hypothetical, conformation. In reality, the glycan at N21 probably freely explores the solvent space within its cone of rotation. In order for it to add surface area to the CDR3, it must be trapped in this conformation by stabilizing influences of the incoming antigen, or by antigen binding in those moments when the glycan stochastically occupies that space. Therefore, our model provides visual evidence of how glycan structures originating outside of the CDRs could affect antigen binding, depending on their placement, structure, and rotational conformations, by extending the surface of, or interfering with, the antigen-binding plane. This supports the possibility of either antigen-independent or codependent stimulation via lectin–glycan interactions, leading to B cell activation.

In summary, we have developed an improved method for the isolation and characterization of rare B cell populations and production of mAb from these cells, which provides data suggesting the possibility that peripheral tolerance mechanisms, which have not been previously reported, are active in the labial salivary gland ASCs of patients with SS. Overall, we found evidence of antigen-driven positive selection in these cells. However, our finding of reduced positive selection in ASCs harboring Ig ac*N*-glyc motifs suggests that in patients with SS, there may be potential alternative mechanisms for the selection and hyperactivation of B cells as well as the proliferation of some of the autoreactive cells frequently seen in this disease.

ACKNOWLEDGMENTS

AUTHOR CONTRIBUTIONS

All authors were involved in drafting the article or revising it critically for important intellectual content, and all authors approved the final version to be published. Drs. Koelsch and Scofield had full access to all of the data in the study and take responsibility for the integrity of the data and the accuracy of the data analysis.
Study conception and design. Koelsch, Scofield.
Acquisition of data. Koelsch, Cavett, Smith, Moore, Lehoux, Jia, Mather, Quadri, Rasmussen, Kaufman, Lewis, Radfar, Lessard, Kurien, Cummings, James, Sivils, Farris, Scofield.
Analysis and interpretation of data. Koelsch, Cavett, Mather, Scordino, Lewis, James, Scofield.

REFERENCES

1. Shiboski SC, Shiboski CH, Criswell LA, Baer AN, Challacombe S, Lanfranchi H, et al. American College of Rheumatology classification criteria for Sjögren's syndrome: a data-driven, expert consensus approach in the Sjögren's International Collaborative Clinical Alliance cohort. Arthritis Care Res (Hoboken) 2012;64:475–87.
2. Vitali C, Bombardieri S, Jonsson R, Moutsopoulos HM, Alexander EL, Carsons SE, et al. Classification criteria for Sjögren's syndrome: a revised version of the European criteria proposed by the American-European Consensus Group. Ann Rheum Dis 2002;61:554–8.
3. Ramos-Casals M, Brito-Zeron P, Font J. The overlap of Sjögren's syndrome with other systemic autoimmune diseases. Semin Arthritis Rheum 2007;36:246–55.
4. Garcia-Carrasco M, Ramos-Casals M, Rosas J, Pallares L, Calvo-Alen J, Cervera R, et al. Primary Sjögren syndrome: clinical and immunologic disease patterns in a cohort of 400 patients. Medicine (Baltimore) 2002;81:270–80.
5. Davidson BK, Kelly CA, Griffiths ID. Primary Sjögren's syndrome in the North East of England: a long-term follow-up study. Rheumatology (Oxford) 1999;38:245–53.
6. Voulgarelis M, Dafni UG, Isenberg DA, Moutsopoulos HM, and the members of the European Concerted Action On Sjögren's Syndrome. Malignant lymphoma in primary Sjögren's syndrome: a multicenter, retrospective, clinical study by the European Concerted Action on Sjögren's Syndrome. Arthritis Rheum 1999;42:1765–72.
7. Wotherspoon AC. Gastric MALT lymphoma and Helicobacter pylori. Yale J Biol Med 1996;69:61–8.
8. Schollkopf C, Melbye M, Munksgaard L, Smedby KE, Rostgaard K, Glimelius B, et al. Borrelia infection and risk of non-Hodgkin lymphoma. Blood 2008;111:5524–9.
9. Ponzoni M, Ferreri AJ, Guidoboni M, Lettini AA, Cangi MG, Pasini E, et al. Chlamydia infection and lymphomas: association beyond ocular adnexal lymphomas highlighted by multiple detection methods. Clin Cancer Res 2008;14:5794–800.
10. Schneider D, Duhren-von Minden M, Alkhatib A, Setz C, van Bergen CA, Benkisser-Petersen M, et al. Lectins from opportunistic bacteria interact with acquired variable-region glycans of surface immunoglobulin in follicular lymphoma. Blood 2015;125:3287–96.
11. Iwai H, Nakamichi N, Nakae K, Konishi M, Inaba M, Hoshino S, et al. Parotid mucosa-associated lymphoid tissue lymphoma regression after Helicobacter pylori eradication. Laryngoscope 2009;119:1491–4.
12. Le Pottier L, Devauchelle V, Fautrel A, Daridon C, Saraux A, Youinou P, et al. Ectopic germinal centers are rare in Sjögren's syndrome salivary glands and do not exclude autoreactive B cells. J Immunol 2009;182:3540–7.
13. Salomonsson S, Jonsson MV, Skarstein K, Brokstad KA, Hjelmström P, Wahren-Herlenius M, et al. Cellular basis of ectopic germinal center formation and autoantibody production in the target organ of patients with Sjögren's syndrome. Arthritis Rheum 2003;48:3187–201.
14. Ben-Chetrit E, Fischel R, Rubinow A. Anti-SSA/Ro and anti-SSB/La antibodies in serum and saliva of patients with Sjögren's syndrome. Clin Rheumatol 1993;12:471–4.
15. Jonsson MV, Skarstein K, Jonsson R, Brun JG. Serological implications of germinal center-like structures in primary Sjögren's syndrome. J Rheumatol 2007;34:2044–9.
16. Maier-Moore JS, Koelsch KA, Smith K, Lessard CJ, Radfar L, Lewis D, et al. Antibody-secreting cell specificity in labial salivary

glands reflects the clinical presentation and serology in patients with Sjögren's syndrome. Arthritis Rheumatol 2014;66:3445–56.

17. Hamza N, Hershberg U, Kallenberg CG, Vissink A, Spijkervet FK, Bootsma H, et al. Ig gene analysis reveals altered selective pressures on Ig-producing cells in parotid glands of primary Sjögren's syndrome patients. J Immunol 2015;194:514–21.

18. Zhu D, McCarthy H, Ottensmeier CH, Johnson P, Hamblin TJ, Stevenson FK. Acquisition of potential N-glycosylation sites in the immunoglobulin variable region by somatic mutation is a distinctive feature of follicular lymphoma. Blood 2002;99:2562–8.

19. Radcliffe CM, Arnold JN, Suter DM, Wormald MR, Harvey DJ, Royle L, et al. Human follicular lymphoma cells contain oligomannose glycans in the antigen-binding site of the B-cell receptor. J Biol Chem 2007;282:7405–15.

20. Ekstrom Smedby K, Vajdic CM, Falster M, Engels EA, Martinez-Maza O, Turner J, et al. Autoimmune disorders and risk of non-Hodgkin lymphoma subtypes: a pooled analysis within the InterLymph Consortium. Blood 2008;111:4029–38.

21. Wallick SC, Kabat EA, Morrison SL. Glycosylation of a VH residue of a monoclonal antibody against α(1—6) dextran increases its affinity for antigen. J Exp Med 1988;168:1099–109.

22. Sabouri Z, Schofield P, Horikawa K, Spierings E, Kipling D, Randall KL, et al. Redemption of autoantibodies on anergic B cells by variable-region glycosylation and mutation away from self-reactivity. Proc Natl Acad Sci U S A 2014;111:E2567–75.

23. Coelho V, Krysov S, Ghaemmaghami AM, Emara M, Potter KN, Johnson P, et al. Glycosylation of surface Ig creates a functional bridge between human follicular lymphoma and microenvironmental lectins. Proc Natl Acad Sci U S A 2010;107:18587–92.

24. Rasmussen A, Ice JA, Li H, Grundahl K, Kelly JA, Radfar L, et al. Comparison of the American-European Consensus Group Sjögren's syndrome classification criteria to newly proposed American College of Rheumatology criteria in a large, carefully characterised sicca cohort. Ann Rheum Dis 2014;73:31–8.

25. Tan EM, Cohen AS, Fries JF, Masi AT, McShane DJ, Rothfield NF, et al. The 1982 revised criteria for the classification of systemic lupus erythematosus. Arthritis Rheum 1982;25:1271–7.

26. Hochberg MC. Updating the American College of Rheumatology revised criteria for the classification of systemic lupus erythematosus. Arthritis Rheum 1997;40:1725.

27. Seror R, Ravaud P, Bowman SJ, Baron G, Tzioufas A, Theander E, et al, on behalf of the EULAR Sjögren's Task Force. EULAR Sjögren's Syndrome Disease Activity Index: development of a consensus systemic disease activity index for primary Sjögren's syndrome. Ann Rheum Dis 2010;69:1103–9.

28. Fragkioudaki S, Mavragani CP, Moutsopoulos HM. Predicting the risk for lymphoma development in Sjögren syndrome: an easy tool for clinical use. Medicine (Baltimore) 2016;95:e3766.

29. Smith K, Garman L, Wrammert J, Zheng NY, Capra JD, Ahmed R, et al. Rapid generation of fully human monoclonal antibodies specific to a vaccinating antigen. Nat Protoc 2009;4:372–84.

30. Uduman M, Yaari G, Hershberg U, Stern JA, Shlomchik MJ, Kleinstein SH. Detecting selection in immunoglobulin sequences. Nucleic Acids Res 2011;39(Web Server issue):W499–504.

31. Chen Z, Collins AM, Wang Y, Gaeta BA. Clustering-based identification of clonally-related immunoglobulin gene sequence sets. Immunome Res 2010;6 Suppl 1:S4.

32. Kasturi L, Chen H, Shakin-Eshleman SH. Regulation of N-linked core glycosylation: use of a site-directed mutagenesis approach to identify Asn-Xaa-Ser/Thr sequons that are poor oligosaccharide acceptors. Biochem J 1997;323:415–9.

33. Sievers F, Wilm A, Dineen D, Gibson TJ, Karplus K, Li W, et al. Fast, scalable generation of high-quality protein multiple sequence alignments using Clustal Omega. Mol Syst Biol 2011;7:539.

34. Balonova L, Hernychova L, Mann BF, Link M, Bilkova Z, Novotny MV, et al. Multimethodological approach to identification of glycoproteins from the proteome of Francisella tularensis, an intracellular microorganism. J Proteome Res 2010;9:1995–2005.

35. Soding J, Biegert A, Lupas AN. The HHpred interactive server for protein homology detection and structure prediction. Nucleic Acids Res 2005;33(Web Server issue):W244–8.

36. Mouquet H, Scharf L, Euler Z, Liu Y, Eden C, Scheid JF, et al. Complex-type N-glycan recognition by potent broadly neutralizing HIV antibodies. Proc Natl Acad Sci U S A 2012;109:E3268–77.

37. Turk D. MAIN software for density averaging, model building, structure refinement and validation. Acta Crystallogr D Biol Crystallogr 2013;69:1342–57.

38. Yaari G, Vander Heiden JA, Uduman M, Gadala-Maria D, Gupta N, Stern JN, et al. Models of somatic hypermutation targeting and substitution based on synonymous mutations from high-throughput immunoglobulin sequencing data. Front Immunol 2013;4:358.

39. Yaari G, Uduman M, Kleinstein SH. Quantifying selection in high-throughput Immunoglobulin sequencing data sets. Nucleic Acids Res 2012;40:e134.

40. Giachino C, Padovan E, Lanzavecchia A. κ+λ+ dual receptor B cells are present in the human peripheral repertoire. J Exp Med 1995;181:1245–50.

41. Del Senno L, Gandini D, Gambari R, Lanza F, Tomasi P, Castoldi G. Monoclonal origin of B cells producing k, λ and k λ immunoglobulin light chains in a patient with chronic lymphocytic leukemia. Leuk Res 1987;11:1093–8.

42. Matsuo Y, Nakamura S, Ariyasu T, Terao R, Imajyo K, Tsubota T, et al. Four subclones with distinct immunoglobulin light chain phenotypes. (κ+λ+, κ+, λ+ and κ-λ-) from acute leukemia. Leukemia 1996;10:700–6.

43. Peltomaki P, Bianchi NO, Knuutila S, Teerenhovi L, Elonen E, Leskinen R, et al. Immunoglobulin κ and λ light chain dual genotype rearrangement in a patient with κ-secreting B-CLL. Eur J Cancer Clin Oncol 1988;24:1233–8.

44. Wang YH, Diamond B. B cell receptor revision diminishes the autoreactive B cell response after antigen activation in mice. J Clin Invest 2008;118:2896–907.

45. De Wildt RM, Hoet RM, van Venrooij WJ, Tomlinson IM, Winter G. Analysis of heavy and light chain pairings indicates that receptor editing shapes the human antibody repertoire. J Mol Biol 1999;285:895–901.

46. Dorner T, Foster SJ, Farner NL, Lipsky PE. Immunoglobulin κ chain receptor editing in systemic lupus erythematosus. J Clin Invest 1998;102:688–94.

47. Lambrecht-Washington D, O'Connor KC, Cameron EM, Jowdry A, Ward ES, Frohman E, et al. Antigen specificity of clonally expanded and receptor edited cerebrospinal fluid B cells from patients with relapsing remitting MS. J Neuroimmunol 2007;186:164–76.

48. Monson NL, Brezinschek HP, Brezinschek RI, Mobley A, Vaughan GK, Frohman EM, et al. Receptor revision and atypical mutational characteristics in clonally expanded B cells from the cerebrospinal fluid of recently diagnosed multiple sclerosis patients. J Neuroimmunol 2005;158:170–81.

49. Hansen A, Odendahl M, Reiter K, Jacobi AM, Feist E, Scholze J, et al. Diminished peripheral blood memory B cells and accumulation of memory B cells in the salivary glands of patients with Sjögren's syndrome. Arthritis Rheum 2002;46:2160–71.

50. Leibiger H, Hansen A, Schoenherr G, Seifert M, Wustner D, Stigler R, et al. Glycosylation analysis of a polyreactive human monoclonal IgG antibody derived from a human-mouse heterohybridoma. Mol Immunol 1995;32:595–602.

51. Marino K, Bones J, Kattla JJ, Rudd PM. A systematic approach to protein glycosylation analysis: a path through the maze. Nat Chem Biol 2010;6:713–23.

BRIEF REPORT

Circulating Cytokine Profiles and Antineutrophil Cytoplasmic Antibody Specificity in Patients With Antineutrophil Cytoplasmic Antibody–Associated Vasculitis

Alvise Berti (iD),[1] Roscoe Warner,[2] Kent Johnson,[2] Divi Cornec,[3] Darrell Schroeder,[4] Brian Kabat,[4] Carol A. Langford,[5] Gary S. Hoffman,[5] Fernanado C. Fervenza,[4] Cees G. M. Kallenberg,[6] Philip Seo,[7] Robert Spiera,[8] E. William St.Clair,[9] Paul Brunetta,[10] John H. Stone,[11] Peter A. Merkel,[12] Ulrich Specks,[4] and Paul A. Monach,[13] for the RAVE-ITN Research Group

Objective. To evaluate circulating cytokine profiles in patients with antineutrophil cytoplasmic antibody–associated vasculitis (AAV), classified by antineutrophil cytoplasmic antibody (ANCA) specificity (proteinase 3 ANCA [PR3-ANCA] versus myeloperoxidase ANCA [MPO-ANCA]) or by clinical diagnosis (granulomatosis with polyangiitis [GPA] versus microscopic polyangiitis [MPA]).

Methods. A panel of 29 cytokines was tested in 186 patients with active AAV at inclusion into the Rituximab in AAV trial. Cytokine concentrations were compared between groups within each classification system. Multivariable analyses adjusted for age, sex, and renal insufficiency were performed, with each biomarker as a dependent variable and ANCA specificity and clinical diagnosis as explanatory variables of interest.

Results. Levels of 9 circulating cytokines (interleukin-6 [IL-6], granulocyte–macrophage colony-stimulating factor [GM-CSF], IL-15, IL-18, CXCL8/IL-8, CCL-17/thymus and activation–regulated chemokine [TARC], IL-18 binding protein [IL-18 BP], soluble IL-2 receptor α [sIL-2Rα], and nerve growth factor β [NGFβ]) were significantly higher in PR3-AAV than MPO-AAV, 4 cytokines (sIL6R, soluble tumor necrosis factor receptor type II [sTNFRII], neutrophil gelatinase–associated lipocalin [NGAL], and soluble intercellular adhesion molecule 1 [sICAM-1]) were higher in MPO-AAV than in PR3-AAV, 6 cytokines (IL-6, GM-CSF, IL-15, IL-18, sIL-2Rα, and NGFβ) were higher in GPA than in MPA, and 3 cytokines (osteopontin, sTNFRII, and NGAL) were higher in MPA than in GPA (all $P < 0.05$). For nearly all cytokines, the difference between PR3-AAV and MPO-AAV was larger than that between GPA and MPA. The multivariate analysis showed that 8 cytokines (IL-15, IL-8, IL-18 BP, NGF-β, sICAM-1, TARC, osteopontin, and kidney injury molecule 1

(P < 0.05) distinguished patients with AAV better (lower P values and larger effect sizes) when grouped by ANCA specificity than by clinical diagnosis.

Conclusion. **Distinct cytokine profiles were identified for PR3-AAV versus MPO-AAV and for GPA versus MPA. Differences in these circulating immune mediators are more strongly associated with ANCA specificity than with clinical diagnosis, suggesting that heterogeneity in the AAV subtypes extends beyond clinical phenotypes.**

Antineutrophil cytoplasmic antibodies (ANCAs) are the primary serologic markers of ANCA-associated vasculitis (AAV), a group of primary systemic necrotizing small vessel vasculitides that includes granulomatosis with polyangiitis (GPA) and microscopic polyangiitis (MPA) (1,2). GPA and MPA share many of the clinical features induced by capillaritis. Yet it remains a matter of debate whether they represent expression of the same disease spectrum or 2 distinct condition (1). GPA differs from MPA due to the presence of necrotizing granulomatous tissue inflammation, a different organ predilection, and association with different ANCA specificity (1).

Patients with GPA are more likely to have ANCAs directed against proteinase 3 (PR3), whereas patients with MPA more often have ANCAs against myeloperoxidase (MPO), but there is substantial overlap. Recent data suggest that ANCA specificity may have stronger associations with genetic predisposition (3), response to therapy (4), relapse risk (5,6), and long-term prognosis (7) than clinical diagnosis does, emphasizing the clinical utility of ANCA specificity in the classification of patients with AAV.

As in other autoimmune diseases, the role of cytokines in the pathogenesis of AAV is now emerging (8–11). The levels of some of these circulating immune mediators have been shown to be elevated in patients with severe active AAV and to decline after treatment, distinguishing active AAV from remission better than conventional markers such as the C-reactive protein level and erythrocyte sedimentation rate (9). Even though evidence supporting classification based on ANCA specificity is now accumulating, a specific characterization of circulating cytokine profiles associated with ANCA specificity or with clinical diagnosis has not yet been performed.

Therefore, we evaluated a panel of 29 circulating immune mediators associated with inflammation, proliferation, vascular injury, and tissue damage and repair in serum samples from patients with active AAV collected at the time of inclusion into a large, prospective clinical trial and determined their association with ANCA specificity (PR3-AAV versus MPO-AAV) and clinical diagnosis (GPA versus MPA).

PATIENTS AND METHODS

Patient classification and study design. The patients included in this study were enrolled in the Rituximab in AAV (RAVE) trial, a double-blind, double-dummy–controlled trial of 197 patients with active severe GPA or MPA randomized to receive either cyclophosphamide followed by azathioprine, or rituximab (12). A positive serum assay for PR3-ANCA or MPO-ANCA and a Birmingham Vasculitis Activity Score for Wegener's Granulomatosis (BVAS/WG) (13) of ≥3 were required for enrollment. Details of the trial design and the main study results have been published previously (12,14). Of the 197 patients included in the RAVE trial, 187 had baseline serum samples available for the purpose of this study. One patient was excluded from this analysis because a clinical diagnosis of GPA versus MPA was indeterminate. Thus, data for 186 patients were included. Patients were classified by their ANCA specificity (PR3-AAV or MPO-AAV) and by their clinical diagnosis (GPA or MPA), which were provided by the RAVE trial investigators at the time of enrollment (12).

The primary aim of this study was to compare the profiles of the selected serum biomarkers studied within each classification system. The secondary aim was to determine whether ANCA-based or clinical diagnosis–based classification showed more significant differences in these circulating immune mediators.

Baseline disease characteristics. Disease activity was assessed in all patients, using the BVAS/WG, and organ manifestations present at enrollment were recorded by the study investigators, all of whom were clinicians with expertise in vasculitis. We defined baseline phenotype categories (capillaritis, granulomatosis, renal involvement, and alveolar hemorrhage) based on the BVAS/WG items recorded at the time of enrollment, as previously described (6). Specific clinical features of classification grouping (ANCA specificity and clinical diagnosis) in the RAVE cohort were analyzed in a previous study (4).

Serum sample processing and cytokine assays. Serum was processed and stored at each study site and then shipped to a central repository and subsequently to the Johnson Laboratory at the University of Michigan. All samples remained frozen at −80°C until the day the assays were performed. A panel of 29 cytokines was originally compiled; these cytokines were selected for their possible role as markers of disease activity and classified roughly as molecules involved in inflammation or proliferation, chemokines, soluble receptors, markers of vascular injury, or markers of tissue damage and repair, as previously reported (9). Assays for all cytokines were performed using an antibody array (a set of miniaturized sandwich immunoassays) as previously described (9), except for BAFF, which was measured by enzyme-linked immunosorbent assay using monoclonal antibodies developed at Genentech.

Data processing and statistical analysis. Data were analyzed at the Mayo Clinic. Two classification systems, ANCA specificity and clinical diagnosis, defined groups for comparison. Continuous variables are summarized as the mean ± SD or the median and interquartile range (IQR), and nominal variables are summarized as frequencies and percentages. Baseline characteristics of the patients were compared between groups for each classification system using the Wilcoxon rank sum test for continuous variables and the chi-square test for nominal variables. The Wilcoxon rank sum test was used to compare values of each serum cytokine between groups within each classification

system. We also used parametric methods after a $\log_{10}$ transformation of values of each biomarker with resulting values standardized to have a mean of 0 and an SD of 1. We analyzed each cytokine individually, reporting individual P values and 95% confidence intervals. Then we evaluated the relative strength of association of biomarkers with groups defined using the 2 classification systems.

In order to address the question of whether ANCA specificity (PR3-ANCA versus MPO-ANCA) and clinical diagnosis (GPA versus MPA) predict the level of each cytokine, we conducted a multivariable linear regression analysis. We performed this analysis for each cytokine with the given cytokine as the dependent variable, ANCA specificity (PR3-ANCA versus MPO-ANCA), and clinical diagnosis (GPA versus MPA) as the explanatory variables of interest, and age, sex, and renal insufficiency (glomerular filtration rate <60 ml/minute/1.73 m^2) as covariates. Initial analyses were performed to verify the absence of ANCA-by-disease interaction effects. This model approach tries to explain the strength of the association of each biomarker with PR3-AAV or MPO-AAV and GPA or MPA. Results of the multivariable analyses were summarized by presenting the respective effect estimates (Z score) and corresponding 95% confidence intervals for ANCA specificity and clinical diagnosis.

P values less than 0.05 were considered significant. Multiple-comparisons correction methods were not applied in parametric, nonparametric, and multivariate analyses since each cytokine was analyzed separately and without considering a set of statistical inferences simultaneously. The 2-tailed P value for each analysis is presented in the Supplementary materials, available on the *Arthritis & Rheumatology* web site at http://onlinelibrary.wiley.com/doi/10.1002/art.40471/abstract. All analyses were performed using JMP and SAS software (SAS Institute).

RESULTS

Demographic and clinical features of the patients at enrollment. The 186 patients included 92 men and 94 women with a median age of 52 years (IQR 44–66, range 15–92), all of whom had severe disease, with a median BVAS/WG of 8 (IQR 5–10, range 3–23). Of these patients, 124 had PR3-ANCA and 62 had MPO-ANCA, whereas 140 were diagnosed as having GPA and 46 were diagnosed as having MPA. The baseline characteristics of the patients with PR3-ANCA versus those with MPO-ANCA and of the patients with GPA versus those with MPA are summarized in Table 1. There was substantial overlap in clinical disease manifestations between patients classified by ANCA specificity or clinical diagnosis. Yet within each classification group (ANCA specificity and clinical diagnosis), demographic characteristics, creatinine clearance, and all phenotype categories except alveolar hemorrhage were significantly different ($P < 0.05$ for all comparisons) (Table 1). BVAS/WG scores were not differently distributed across the subsets.

Comparison of blood cytokine profiles between disease categories. As previously reported, each of the cytokines tested at baseline was significantly increased in the RAVE cohort compared to healthy controls, except for RANTES, angiotensin-converting enzyme, basic fibroblast growth factor, and vascular cell adhesion molecule 1 (9). Circulating cytokine profiles differed significantly between

Table 1. Baseline characteristics of the 186 patients with AAV according to serologic and clinical classifications*

	ANCA specificity			AAV clinical diagnosis		
	PR3-AAV (n = 124)	MPO-AAV (n = 62)	P	GPA (n = 140)	MPA (n = 46)	P
Age at diagnosis, median (IQR) years	51 (40–60)	59 (47–71)	<0.001	51 (43–60)	66.5 (45–72.3)	<0.001
Men, no. (%)	70 (56.5)	22 (35.5)	0.004	76 (54.3)	16 (34.8)	0.027
Any capillaritis manifestation, no. (%)†	98 (79.0)	60 (96.8)	0.002	112 (80.0)	45 (97.8)	0.016
Any granulomatous manifestation, no. (%)‡	93 (75.0)	23 (37.1)	<0.001	106 (75.7)	10 (21.7)	<0.001
Alveolar hemorrhage, no. (%)§	32 (25.8)	13 (21.0)	0.413	34 (24.3)	11 (23.9)	0.849
Any renal involvement, no. (%)¶	71 (57.3)	50 (80.6)	0.003	83 (59.3)	38 (82.6)	0.007
Baseline creatinine clearance, median (IQR) ml/minute	92.1 (64.0–121.5)	50.26 (30.2–73.71)	<0.001	91.1 (58.7–121.4)	46.6 (29.9–71.6)	<0.001
Receiving steroids and/or immunosuppressive agents at screening, no. (%)	64 (51.6)	34 (54.8)	0.802	70 (50.0)	28 (60.9)	0.266
Baseline BVAS/WG score, median (IQR)	8 (5–10)	8 (6–10)	0.867	8 (5–10)	7 (5–9)	0.141

* AAV = antineutrophil cytoplasmic antibody–associated vasculitis; ANCA = antineutrophil cytoplasmic antibody; PR3 = proteinase 3; MPO = myeloperoxidase; GPA = granulomatosis with polyangiitis; MPA = microscopic polyangiitis; IQR = interquartile range.
† Defined as the presence of 1 or more of the following Birmingham Vasculitis Activity Score for Wegener's Granulomatosis (BVAS/WG) items: cutaneous purpura, scleritis, retinal hemorrhage or exudate, sensorineural deafness, hematuria, red blood cell casts on urinalysis or glomerulonephritis, increase in creatinine level, alveolar hemorrhage, mesenteric ischemia, sensory peripheral neuropathy, or motor mononeuritis multiplex.
‡ BVAS/WG items reflecting underlying necrotizing granulomatous inflammation included mouth ulcers, retroorbital mass/proptosis, bloody nasal discharge, sinus involvement, salivary gland enlargement, subglottic inflammation, conductive deafness, other major or minor ear, nose, and throat involvement, pulmonary nodule/cavity, endobronchial involvement, meningitis, and cord lesion.
§ A patient was categorized as having alveolar hemorrhage only if that item was scored on the BVAS/WG.
¶ Patients were considered to have renal disease if any renal item on the BVAS/WG (hematuria, red blood cell casts or glomerulonephritis, increase in creatinine level, or "other") was scored.
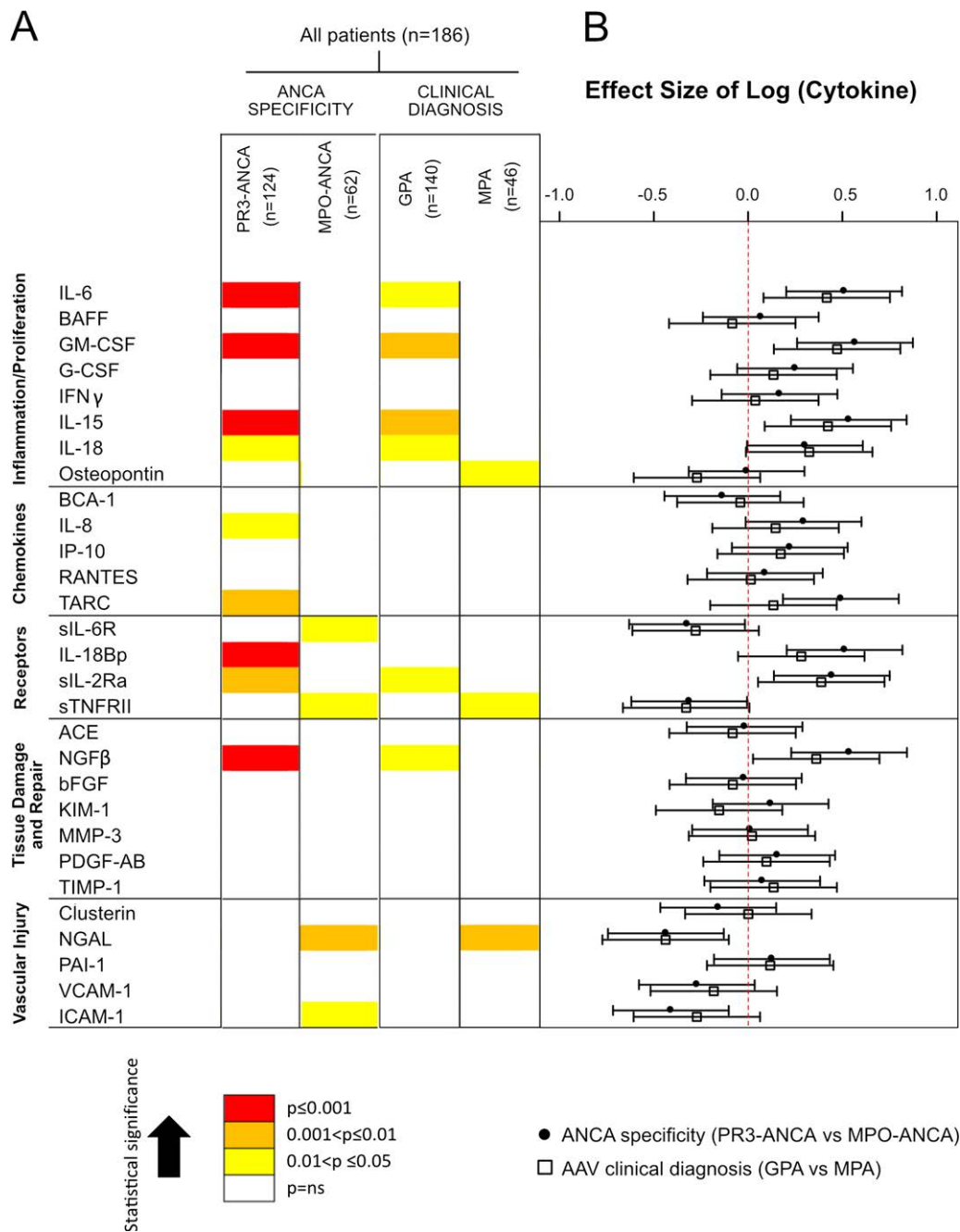
Figure 1. Association of circulating cytokines with antineutrophil cytoplasmic antibody (ANCA) type and ANCA-associated vasculitis (AAV) clinical diagnosis subgroups (ANCA against proteinase 3 [PR3-ANCA] versus ANCA against myeloperoxidase [MPO-ANCA] and granulomatosis with polyangiitis [GPA] versus microscopic polyangiitis [MPA]). **A**, Graphic representation of circulating cytokine profiles. Colors represent the strength of association in each classification system. **B**, Parametric analyses of the biomarkers (effect size) (see Patients and Methods for details). Values are the median (interquartile range). Broken line represents 0. IL-6 = interleukin-6; GM-CSF = granulocyte–macrophage colony-stimulating factor; G-CSF = granulocyte colony-stimulating factor; IFNγ = interferon-γ; BCA-1 = B cell–attracting chemokine 1; IP-10 = interferon-γ–inducible 10-kd protein; TARC = thymus and activation–regulated chemokine; sIL-6R = soluble IL-6 receptor; IL-18 BP = IL-18 binding protein; sTNFRII = soluble tumor necrosis factor receptor type II; ACE = angiotensin-converting enzyme; NGFβ = nerve growth factor β; bFGF = basic fibroblast growth factor; KIM-1 = kidney injury molecule 1; MMP-3 = matrix metalloproteinase 3; PDGF-AB = platelet-derived growth factor A and B; TIMP-1 = tissue inhibitor of metalloproteinases 1; NGAL = neutrophil gelatinase–associated lipocalin; PAI-1 = plasminogen activator inhibitor 1; VCAM-1 = vascular cell adhesion molecule 1; ICAM-1 = intercellular adhesion molecule 1; NS = not significant.

patients with PR3-AAV and those with MPO-AAV (Figure 1A and Supplementary Table 1, available on the *Arthritis & Rheumatology* web site at http://onlinelibrary.wiley.com/doi/10.1002/art.40471/abstract). Levels of 9 proteins were higher in patients with PR3-AAV than in patients with MPO-AAV (interleukin-6 [IL-6], granulocyte–macrophage colony-stimulating factor [GM-CSF], IL-15, IL-18, CXCL8/IL-8, CCL17/thymus and activation–regulated chemokine [TARC], IL-18 binding protein [IL-18 BP], soluble IL-2 receptor α [sIL-2Rα], and nerve growth factor β [NGFβ]), whereas 4 biomarkers were higher in patients with MPO-AAV than in patients with PR3-AAV (sIL-6R, soluble tumor necrosis factor receptor type II [sTNFRII], neutrophil gelatinase–associated lipocalin [NGAL], and soluble intercellular adhesion molecule 1 [sICAM-1]).

In contrast, the same biomarkers were less often associated with either GPA or MPA when patients were classified according to clinical diagnosis (Figure 1A and Supplementary Table 1). Serum levels of 6 markers were higher in patients with GPA than in those with MPA (IL-6, GM-CSF, IL-15, IL-18, sIL-2Rα, and NGFβ), and 3 were higher in patients with MPA than in patients with GPA (osteopontin, sTNFRII, and NGAL). Thus, more cytokines were associated with either PR3-AAV or MPO-AAV than with either GPA or MPA. The difference between biomarker concentrations was also greater for PR3-ANCA versus MPO-ANCA than for GPA versus MPA in 9 cases (Figures 1A and B). Patients with PR3-AAV had the highest number of significantly associated serum biomarkers, most of them with a stronger association when compared to other subsets (Figure 1).

We also compared cytokine levels among subgroups of patients with AAV by combining ANCA specificity and clinical phenotype, namely patients with GPA with PR3-ANCA (n = 121), patients with MPA with PR3-ANCA (n = 3), patients with GPA with MPO-ANCA (n = 19), and patients with MPA with MPO-ANCA (n = 43). The serum levels of 10 of 29 cytokines differed significantly between patients with GPA with PR3-ANCA and patients with GPA with MPO-ANCA, serum levels of 2 cytokines differed significantly between patients with GPA with MPO-ANCA and patients with MPA with MPO-ANCA (i.e., kidney injury molecule 1 [KIM-1] and osteopontin), and serum levels of 12 cytokines differed significantly between patients with GPA with PR3-ANCA and patients with MPA with MPO-ANCA (see Supplementary Table 2, available on the *Arthritis & Rheumatology* web site at http://onlinelibrary.wiley.com/doi/10.1002/art.40471/abstract).

Association of cytokines with ANCA specificity and clinical diagnosis. To evaluate how strongly each cytokine is associated with either ANCA specificity or clinical diagnosis, a multivariable analysis directly comparing each classification system was performed. From this analysis 8 biomarkers were found to have significant independent multivariable associations with ANCA specificity and/or clinical diagnosis (Figure 2A and Supplementary Table 3 and Supplementary Figure 1, available on the *Arthritis & Rheumatology* web site at http://onlinelibrary.wiley.com/doi/10.1002/art.40471/abstract). For 5 biomarkers there was an independent association with ANCA specificity only. IL-18 BP, NGF, IL-8, and IL-15 were associated with PR3-AAV, and sICAM-1 was associated with MPO-AAV. For 3 biomarkers there was a significant association with both ANCA specificity and clinical diagnosis. Osteopontin, KIM-1, and TARC were all associated with PR3-AAV and MPA. No biomarker was found to have a significant association with clinical diagnosis alone. Figure 2B illustrates the relative capacity of the 2 classification systems to simultaneously explain the values of all biomarkers tested.

DISCUSSION

The results of this exploratory analysis conducted in patients with severe active AAV suggest that circulating serum cytokines reflect ANCA specificity better than they reflect clinical diagnosis. Using a panel of 29 circulating cytokines that have already been shown to be individually associated with AAV disease activity or implicated in its pathogenesis (8,9), we demonstrated that these molecules are more strongly related to ANCA specificity (PR3-AAV versus MPO-AAV) than to clinical diagnosis (GPA versus MPA).

This study identified distinct cytokine profiles for PR3-AAV versus MPO-AAV and for GPA versus MPA, with a higher number of cytokines associated with and a larger effect size in favor of PR3-AAV than MPO-AAV, GPA, or MPA (Figure 1). These findings indirectly suggest that certain combinations of pathways might be more involved in PR3-AAV than in GPA, MPA, and MPO-AAV. For instance, signaling cascades critical for proliferation or survival of PR3-ANCA–producing B cells may drive or potentially be impacted by this cytokine network (11,15).

Since different subsets of patients showed distinctive cytokine profiles, our results suggest that different targeted treatment approaches could be evaluated separately in clinical trials for the different subsets of AAV, similar to other autoimmune diseases in which different cytokine profiles correspond to different disease activity and treatment responsiveness (16). Our study had low power to detect differences in subgroups defined by the combination of ANCA specificity and clinical phenotype, and we were unable to compare cytokine levels in the subgroup with
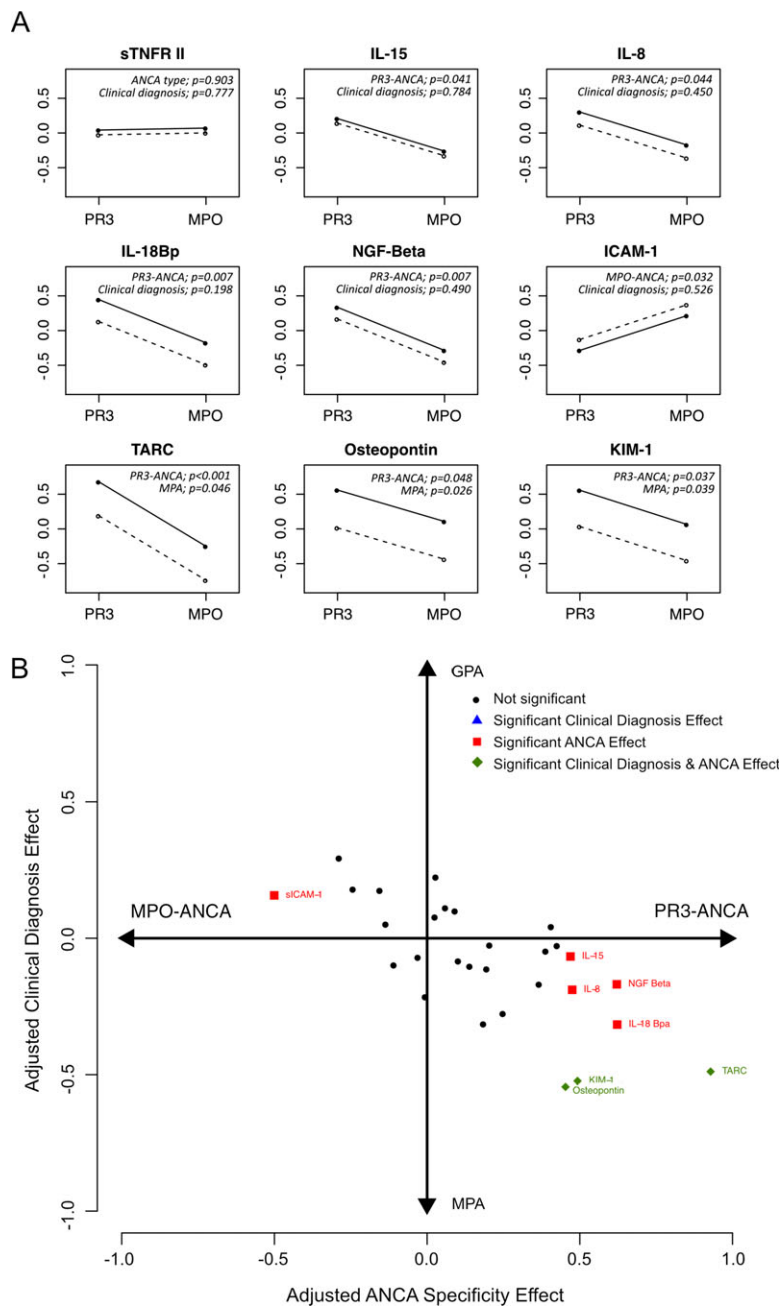
Figure 2. Multivariate analysis comparing the 2 classification systems (PR3-ANCA versus MPO-ANCA and GPA versus MPA) for each cytokine. **A**, Associations of each biomarker with ANCA specificity and clinical diagnosis. One example of a molecule not associated with either ANCA specificity or clinical diagnosis (sTNFRII) is shown. The other panels show the 8 soluble mediators with a significant association with ANCA type and/or clinical diagnosis. The magnitude of the difference between MPA (solid lines) and GPA (broken lines) is visually depicted by the distance between the 2 lines. The magnitude of the difference between PR3-ANCA and MPO-ANCA is visually represented by the slope of the lines. The statistical model forces them to be parallel. The direction and the grade of inclination represent the type and the strength of the association with ANCA type, respectively. **B**, Scatterplot comparing the effect of ANCA type and clinical diagnosis for all serum cytokines studied. The more a biomarker is skewed to the left or right, the more strongly it discriminates patients by ANCA type. The more a biomarker is skewed to the bottom or top, the more strongly it discriminates patients by clinical diagnosis. See Figure 1 for definitions. Color figure can be viewed in the online issue, which is available at http://onlinelibrary.wiley.com/doi/10.1002/art.40471/abstract.

PR3-ANCA and MPA because it comprised only 3 patients. Nevertheless, the differences observed between the PR3-ANCA and MPO-ANCA subgroups were also seen when patients with GPA with PR3-ANCA were compared to patients with GPA with MPO-ANCA, consistent with the main observation that cytokine profiles are more closely related to ANCA specificity than to disease phenotype. Further functional studies are needed to elucidate the interrelationships between these circulating molecules and the pathophysiologic or protective mechanisms in which they participate.

The multivariable analysis directly comparing each classification system identified 8 cytokines separating PR3-AAV from MPO-AAV. Three of them (KIM-1, TARC, and osteopontin) were also associated with clinical diagnosis and specifically with MPA. Intriguingly, no cytokines were associated with clinical diagnosis (either GPA or MPA) only, thus suggesting that these circulating immune mediators are better distinguished by ANCA specificity than by clinical diagnosis. In clinical practice, establishing an unequivocal diagnosis of GPA or MPA is often challenging for a variety of reasons, including incomplete disease manifestations at the time of the first diagnosis and disagreements between experts about the application of different definition schemes during the diagnostic evaluation of individual patients. In contrast, information on ANCA specificity is readily available and usually does not change during patient follow-up (1). Our findings provide a molecular basis supporting the concept of an ANCA-based classification of AAV, which has already been shown to convey useful information about clinical outcomes and prognoses (1,4,5).

The difference, if any exists, between PR3-ANCA–mediated inflammation and MPO-ANCA–mediated inflammation has not yet been entirely characterized, unlike for inflammation in GPA versus MPA. Histopathologic differences in inflammation between GPA and MPA are striking, and would have suggested that cytokines correlate with phenotype rather than ANCA specificity, since serum cytokines may be considered bona fide surrogates of the immunopathologic events occurring in AAV. Therefore, our findings represent the first formal demonstration of combinations of cytokine pathways differently activated in distinct AAV subsets, and particularly in ANCA-based subsets. This study has several strengths. First, the study cohort was recruited though a stringent clinical trial protocol at centers with expertise in the study of AAV. Second, the specimens were collected, handled, and studied using strict protocols, and the assays were performed in a single laboratory by personnel who were blinded with regard to group assignment.

This study also has limitations to be considered when interpreting the findings and implications of the work. First, we acknowledge that the absence of detailed data on recent glucocorticoid treatment is a limitation. The use of glucocorticoids as first treatment for active disease before blood sampling at the time of screening may thus have influenced our results in individual patients. However, recent treatment was not significantly different in each subgroup at the screening visit (Table 1). Moreover, we had previously shown that glucocorticoid treatment prior to obtaining the blood sample had no significant detectable effect on the levels of the majority of the cytokines (9), allowing us to conclude that the differences we observed in our study among distinct AAV subsets were not driven by the effects of glucocorticoids.

Second, patients with AAV without ANCA and those with non-severe disease activity were excluded from the RAVE trial, and our findings cannot therefore be generalized to all patients with GPA or MPA. However, recent evidence supports the notion that patients with AAV who are consistently ANCA-negative may represent different subsets of disease with different pathogenesis (1).

Third, the comparison of GPA to MPA had lower statistical power to detect differences than did the comparison of PR3-AAV to MPO-AAV, due to the greater imbalance in the number of patients in the clinical diagnosis groups. However, the comparison of PR3-AAV and MPO-AAV had not only lower P values, but also larger estimated effect sizes than the comparison by clinical diagnosis, highlighting the strength of our findings.

Finally, given the non-comprehensive and relatively limited number of cytokines studied, we were not able to comprehensively investigate possible mutual interactions or effects of the different cytokine pathways, thus not providing a pathophysiologic explanation of our results. The biomarkers tested were not specifically selected to represent pathophysiologic processes considered likely to differentiate subsets of AAV, and a replication of these results in an independent cohort of patients with AAV is recommended. The understanding of the reciprocal influence of these mediators is beyond the scope of our study.

In conclusion, this analysis supports the concept of an ANCA-based classification of AAV by showing that a set of selected serum biomarkers associates more strongly with either PR3-AAV or MPO-AAV than with GPA or MPA. Distinct cytokine profiles were identified for PR3-AAV versus MPO-AAV and for GPA versus MPA. Differences in these circulating immune mediators are more strongly associated with ANCA specificity than with clinical diagnosis, suggesting that heterogeneity in the AAV subtypes extends beyond the clinical phenotypes identified

by the conventional clinical classification (GPA versus MPA). Our results provide additional support for stratification of patients by ANCA specificity for treatment trials.

AUTHOR CONTRIBUTIONS

All authors were involved in drafting the article or revising it critically for important intellectual content, and all authors approved the final version to be published. Dr. Berti had full access to all of the data in the study and takes responsibility for the integrity of the data and the accuracy of the data analysis.

Study conception and design. Berti, Cornec, Merkel, Specks, Monach.

Acquisition of data. Berti, Cornec, Merkel, Specks, Monach.

Analysis and interpretation of data. Berti, Warner, Johnson, Cornec, Schroeder, Kabat, Langford, Hoffman, Fervenza, Kallenberg, Seo, Spiera, St.Clair, Brunetta, Stone, Merkel, Specks, Monach.

ADDITIONAL DISCLOSURES

Author Brunetta is an employee of Genentech.

REFERENCES

1. Cornec D, Cornec-Le Gall E, Fervenza FC, Specks U. ANCA-associated vasculitis: clinical utility of using ANCA specificity to classify patients. Nat Rev Rheumatol 2016;12:570–9.
2. Jennette JC, Falk RJ, Bacon PA, Basu N, Cid MC, Ferrario F, et al. 2012 revised International Chapel Hill Consensus Conference nomenclature of vasculitides. Arthritis Rheum 2013;65:1–11.
3. Lyons PA, Rayner TF, Trivedi S, Holle JU, Watts RA, Jayne DR, et al. Genetically distinct subsets within ANCA-associated vasculitis. N Engl J Med 2012;367:214–23.
4. Unizony S, Villarreal M, Miloslavsky EM, Lu N, Merkel PA, Spiera R, et al. Clinical outcomes of treatment of anti-neutrophil cytoplasmic antibody (ANCA)-associated vasculitis based on ANCA type. Ann Rheum Dis 2016;75:1166–9.
5. Hogan SL, Falk RJ, Chin H, Cai J, Jennette CE, Jennette JC, et al. Predictors of relapse and treatment resistance in antineutrophil cytoplasmic antibody-associated small-vessel vasculitis. Ann Int Med 2005;143:621–31.
6. Fussner LA, Hummel AM, Schroeder DR, Silva F, Cartin-Ceba R, Snyder MR, et al. Factors determining the clinical utility of serial measurements of antineutrophil cytoplasmic antibodies targeting proteinase 3. Arthritis Rheumatol 2016;68:1700–10.
7. Tanna A, Guarino L, Tam FW, Rodriquez-Cubillo B, Levy JB, Cairns TD, et al. Long-term outcome of anti-neutrophil cytoplasm antibody-associated glomerulonephritis: evaluation of the international histological classification and other prognostic factors. Nephrol Dial Transplant 2015;30:1185–92.
8. Monach PA, Tomasson G, Specks U, Stone JH, Cuthbertson D, Krischer J, et al. Circulating markers of vascular injury and angiogenesis in antineutrophil cytoplasmic antibody–associated vasculitis. Arthritis Rheum 2011;63:3988–97.
9. Monach PA, Warner RL, Tomasson G, Specks U, Stone JH, Ding L, et al. Serum proteins reflecting inflammation, injury and repair as biomarkers of disease activity in ANCA-associated vasculitis. Ann Rheum Dis 2013;72:1342–50.
10. Berti A, Cavalli G, Campochiaro C, Guglielmi B, Baldissera E, Cappio S, et al. Interleukin-6 in ANCA-associated vasculitis: rationale for successful treatment with tocilizumab. Semin Arthritis Rheum 2015;45:48–54.
11. Lepse N, Land J, Rutgers A, Kallenberg CG, Stegeman CA, Abdulahad WH, et al. Toll-like receptor 9 activation enhances B cell activating factor and interleukin-21 induced anti-proteinase 3 autoantibody production in vitro. Rheumatology (Oxford) 2016;55:162–72.
12. Stone JH, Merkel PA, Spiera R, Seo P, Langford CA, Hoffman GS, et al. Rituximab versus cyclophosphamide for ANCA-associated vasculitis. N Engl J Med 2010;363:221–32.
13. Stone JH, Hoffman GS, Merkel PA, Min YI, Uhlfelder ML, Hellmann DB, et al, for the International Network for the Study of the Systemic Vasculitides (INSSYS). A disease-specific activity index for Wegener's granulomatosis: modification of the Birmingham Vasculitis Activity Score. Arthritis Rheum 2001;44:912–20.
14. Specks U, Merkel PA, Seo P, Spiera R, Langford CA, Hoffman GS, et al. Efficacy of remission-induction regimens for ANCA-associated vasculitis. N Engl J Med 2013;369:417–27.
15. Cornec D, Berti A, Hummel A, Peikert T, Pers JO, Specks U. Identification and phenotyping of circulating autoreactive proteinase 3-specific B cells in patients with PR3-ANCA associated vasculitis and healthy controls. J Autoimmun 2017;84:122–31.
16. Ronnblom L, Eloranta ML. The interferon signature in autoimmune diseases. Curr Opin Rheumatol 2013;25:248–53.

U-Shaped Association Between Serum Uric Acid Level and Risk of Mortality

A Cohort Study

Sung Kweon Cho,[1] Yoosoo Chang,[2] Inah Kim,[3] and Seungho Ryu [iD][2]

Objective. In addition to the controversy regarding the association of hyperuricemia with cardiovascular disease (CVD) mortality, few studies have examined the impact of a low uric acid level on mortality. We undertook the present study to evaluate the relationship between both low and high uric acid levels and the risk of all-cause and cause-specific mortality in a large sample of Korean adults over a full range of uric acid levels.

Methods. A cohort study was performed in 375,163 South Korean men and women who underwent health check-ups from 2002 to 2012. Vital status and cause of death were ascertained from the national death records. Hazard ratios (HRs) and 95% confidence intervals (95% CIs) for mortality outcomes were estimated using Cox proportional hazards regression analysis.

Results. During a total of 2,060,721.9 person-years of follow-up, 2,020 participants died, with 287 CVD deaths and 963 cancer deaths. Low and high uric acid levels were associated with increased all-cause, CVD, and cancer mortality. The multivariable-adjusted HRs for all-cause mortality in the lowest uric acid categories (<3.5 mg/dl for men and <2.5 mg/dl for women) compared with the sex-specific reference category were 1.58 (95% CI 1.18–2.10) and 1.80 (95% CI 1.10–2.93), respectively. Corresponding HRs in the highest uric acid categories (≥9.5 mg/dl for men and ≥8.5 mg/dl for women) were 2.39 (95% CI 1.57–3.66) and 3.77 (95% CI 1.17–12.17), respectively.

Conclusion. In this large cohort study of men and women, both low and high uric acid levels were predictive of increased mortality, supporting a U-shaped association between serum uric acid levels and adverse health outcomes.

Uric acid is the final oxidation product of purine metabolism and is an established risk factor for gouty arthritis and kidney stones (1). A number of epidemiologic studies have shown that an elevated uric acid level is associated with a wide variety of adverse health outcomes, including hypertension, metabolic syndrome, kidney disease, cardiovascular disease (CVD), and cancer (2–6). However, the role of uric acid as an independent risk factor for CVD, cancer, and all-cause mortality remains a subject of controversy (7–11). Some studies demonstrated a positive association between hyperuricemia and cardiovascular mortality (12,13), while other studies did not (14,15). Furthermore, studies of the association between serum uric acid level and cancer mortality have provided conflicting results. Taghizadeh et al reported that a high level of uric acid was related to a lower risk of cancer mortality (16). In contrast, other cohort studies demonstrated that a high level of uric acid was associated with an increased risk of cancer-related mortality (17,18).

Most studies of the association between the uric acid level and mortality have focused on the role of hyperuricemia, but the influence of a low uric acid level on mortality has not been established. A cohort study in Japan demonstrated that low uric acid level (<4.6 mg/dl in men and <3.3 mg/dl in women) can increase CVD mortality (5).

Recently, several studies have shown that a low uric acid level was significantly associated with increased all-cause mortality in patients undergoing dialysis (19,20). The uric acid has an antioxidant effect (21), and it has been demonstrated that hypouricemia can injure the endothelium and induce oxidative stress–related disease such as hypertension, diabetes mellitus, and kidney disease (22,23). Few longitudinal studies have evaluated the risk of all-cause, cancer-specific, and CVD mortality across the full range of uric acid levels in the general population while considering both low and high uric acid levels. The purpose of this study was to evaluate the association of low and high uric acid levels with all-cause, CVD, and cancer-specific mortality in a large cohort of Korean adults who participated in a health screening examination program.

PATIENTS AND METHODS

Study population. The Kangbuk Samsung Health Study is a cohort study of Korean men and women who underwent comprehensive annual or biennial health examinations at the Kangbuk Samsung Hospital Total Healthcare Centers in Seoul and Suwon, South Korea (24,25). The current cohort included all men and women age ≥18 years who participated in a screening between January 1, 2002 and December 31, 2012 (n = 375,163). More than 80% of participants were employees of various companies and local government organizations and their spouses. In Korea, annual or biennial health screening examinations of employees are required by the Industrial Safety and Health Law.

We excluded 22,120 subjects who met one of the following exclusion criteria: unknown vital status (n = 2); missing data on uric acid level, glucose level, body mass index (BMI), or estimated glomerular filtration rate (GFR) (n = 320); a history of malignancy (n = 5,352); and/or a history of CVD (n = 16,643). Because some participants met more than one exclusion criterion, the total number of participants eligible for this study was 375,163. This study was approved by the institutional review board of Kangbuk Samsung Hospital. The requirement for informed consent was waived, because we used de-identified retrospective data routinely collected during the health screening process.

Data collection. All examinations were conducted at a Kangbuk Samsung Hospital Total Healthcare Center in Seoul or Suwon. Self-administered standardized questionnaires were used to identify medical history and medication use, smoking status, alcohol intake, and exercise frequency (24,25). CVD and malignancy were defined as physician-diagnosed heart disease or stroke and physician-diagnosed malignancy of any type, respectively. Smoking status was categorized as never, former, and current. Alcohol consumption was categorized as none, moderate (<20 gm/day), and high (≥20 gm/day). We also assessed the weekly frequency of moderate- or vigorous-intensity physical activity.

Sitting blood pressure (BP), height, and weight were measured by trained nurses. Body mass index (BMI) was calculated as the weight in kilograms divided by the height in meters squared. Obesity was defined as a BMI ≥25 kg/m^2, which is the proposed cutoff for Asian populations (26). Hypertension was defined as systolic BP ≥140 mm Hg, diastolic BP ≥90 mm Hg, or current use of antihypertensive medication.

Blood specimens were obtained from the antecubital vein after more than 10 hours of fasting. Serum levels of glucose, total cholesterol, low-density lipoprotein (LDL) cholesterol, high-density lipoprotein (HDL) cholesterol, triglycerides, creatinine, total bilirubin, and gamma glutamyl transferase (GGT) were measured at the Laboratory Medicine Department of Kangbuk Samsung Hospital as previously described (25). Serum uric acid levels were measured enzymatically using an automatic analyzer (either an Advia 1650 Auto analyzer [Bayer Diagnostics] or a Modular DP analyzer [Roche Diagnostics]). Insulin resistance was assessed with the homeostatic model assessment of insulin resistance (HOMA-IR) equation: fasting blood insulin (μU/ml) × fasting blood glucose (mmoles/liter)/22.5. Diabetes mellitus was defined as a fasting serum glucose level ≥126 mg/dl or current use of medication to treat diabetes mellitus.

We estimated GFR using the 4-variable Modification of Diet in Renal Disease study equation (27):

$$\text{GFR}\,(\text{ml/minute/1.73 m}^2\text{ body surface area})$$
$$= 186.3 \times (\text{serum creatinine})^{-1.154} \times \text{age}^{-0.203}$$
$$(\times\ 0.742\ \text{if female})$$

Chronic kidney disease was defined as an estimated GFR <60 ml/minute/1.73 m^2.

Mortality follow-up. The vital status of study subjects was identified through nationwide death certificate data from the Korea National Statistical Office through December 31, 2012. According to the registry for the Domestic Relations Act in Korea, all deaths of Koreans are reported to Statistics Korea, meaning that death certificate data among Korean adults can be considered 100% accurate. Concordance between the cause of death according to the death certificate and diagnosis based on medical utilization data (the death benefit record of the Korean Medical Insurance Corporation) was 72.2% for all-cause deaths and 94.9% for deaths from cancer of all sites, regardless of primary site (28).

CVD mortality was defined as International Statistical Classification of Diseases and Related Health Problems, Tenth Revision (ICD-10) codes I00 to I99. Cancer deaths were identified by ICD-10 codes C00–C97 as the underlying cause of death on the death certificates (29).

Statistical analysis. The chi-square test and one-way analysis of variance were used to compare the characteristics of the study participants at baseline regarding categories of uric acid level in men and women. There is no universally accepted definition of hypouricemia or hyperuricemia solely based on uric acid level, while sex differences regarding uric acid levels are well described in a previous report (30). Therefore, sex-specific values based on the uric acid distribution of our population were used in this study. Men were divided into 8 groups according to uric acid level in mg/dl (<3.5 [corresponding to approximately the 1.4th percentile in men], 3.5–4.4, 4.5–5.4, 5.5–6.4, 6.5–7.4, 7.5–8.4, 8.5–9.4, and ≥9.5). Women were also divided into 8 groups according to the uric acid level in mg/dl (<2.5 [corresponding to approximately the 1.7th percentile in women], 2.5–3.4, 3.5–4.4, 4.5–5.4, 5.5–6.4, 6.5–7.4, 7.5–8.4, and ≥8.5). The reference group was defined as the lowest mortality incidence group in both men and women (6.5–7.4 mg/dl in men and 3.5–4.4 mg/dl in women). Hazard ratios (HRs) with 95% confidence intervals (95% CIs) for mortality outcomes were estimated using Cox proportional hazards regression analysis. We used age as the time scale where subjects enter the analysis at their age at the time of their first health check-up examination (left

Table 1. Baseline characteristics of the study participants by uric acid level among men*

Characteristic	Uric acid level, mg/dl								P for quadratic trend
	<3.5	3.5–4.4	4.5–5.4	5.5–6.4	6.5–7.4	7.5–8.4	8.5–9.4	≥9.5	
Number	2,918	12,363	42,404	72,529	50,753	19,255	5,299	1,646	<0.001
Age, mean ± SD years	43.2 ± 11.3	42.6 ± 11.0	40.9 ± 10.2	39.2 ± 9.2	38.4 ± 8.7	38.2 ± 8.7	38.7 ± 9.3	39.0 ± 9.9	<0.001
BMI, mean ± SD kg/m²	23.5 ± 2.9	23.6 ± 2.9	23.6 ± 2.7	24.1 ± 2.7	24.9 ± 2.8	25.6 ± 2.9	26.2 ± 3.0	26.8 ± 3.3	<0.001
Obese, %	29.1	28.8	28.1	35.7	46.6	56.4	64.8	69.2	<0.001
Current smoker, %	44.2	45.1	44.9	45.2	44.9	45.1	42.7	41.9	0.111
Alcohol intake ≥20 gm/day, %	24.5	25.9	25.3	26.5	27.8	30.6	31.7	34.2	<0.001
Exercise ≥3 times/week, %	18.2	17.7	16.8	16.0	16.1	16.3	16.6	18.0	<0.001
College graduate or higher education level, %	70.5	72.1	76.7	80.5	82.1	82.8	82.6	80.4	<0.001
Diabetes mellitus, %	13.6	11.6	6.5	3.6	2.9	3.0	3.8	4.3	<0.001
Hypertension, %	18.1	19.5	17.6	17.8	20.5	24.6	31.3	39.8	0.008
Use of medication for dyslipidemia, %	1.7	1.5	1.1	0.9	1.1	1.2	2.0	2.1	<0.001
Systolic BP, mean ± SD mm Hg	116.7 ± 13.4	116.7 ± 13.3	116.2 ± 13.0	116.8 ± 12.8	118.0 ± 13.0	119.5 ± 13.4	121.1 ± 13.9	123.3 ± 14.4	<0.001
Diastolic BP, mean ± SD mm Hg	75.2 ± 9.2	75.4 ± 9.5	75.3 ± 9.4	75.9 ± 9.4	76.8 ± 9.5	77.9 ± 9.8	79.1 ± 10.1	80.8 ± 10.4	<0.001
Estimated GFR, mean ± SD ml/minute/1.73 m²	84.9 ± 12.6	83.7 ± 12.5	83.1 ± 11.7	81.5 ± 11.5	79.7 ± 11.3	77.9 ± 11.6	75.4 ± 12.2	71.6 ± 13.5	<0.001
Glucose, mean ± SD mg/dl	105.1 ± 35.7	102.6 ± 32.1	97.6 ± 21.5	95.6 ± 15.0	95.8 ± 13.0	96.4 ± 12.7	97.5 ± 13.1	97.7 ± 13.1	<0.001
Total cholesterol, mean ± SD mg/dl	193.0 ± 34.8	193.5 ± 34.5	193.4 ± 33.3	197.5 ± 33.9	202.8 ± 34.7	208.5 ± 35.8	213.2 ± 36.4	217.8 ± 38.4	<0.001
LDL cholesterol, mean ± SD mg/dl	114.8 ± 30.1	115.0 ± 29.5	115.2 ± 29.0	118.9 ± 29.5	122.9 ± 30.2	126.2 ± 31.0	128.9 ± 32.4	130.4 ± 33.7	<0.001
HDL cholesterol, mean ± SD mg/dl	54.1 ± 12.5	54.0 ± 12.3	53.7 ± 11.9	52.4 ± 11.4	51.1 ± 10.9	50.1 ± 10.6	49.5 ± 10.6	49.3 ± 10.9	<0.001
Triglycerides, median (IQR) mg/dl	108 (77–153)	107 (77–153)	108 (78–153)	118 (85–167)	134 (94–190)	152 (107–219)	167 (117–239)	185 (125–267)	<0.001
HOMA-IR value, median (IQR)	1.61 (1.12–2.28)	1.60 (1.11–2.24)	1.58 (1.10–2.17)	1.66 (1.17–2.25)	1.80 (1.27–2.43)	1.94 (1.36–2.63)	2.09 (1.46–2.86)	2.21 (1.56–3.01)	<0.001
hsCRP, median (IQR) mg/liter	0.5 (0.3–1.0)	0.5 (0.3–1.0)	0.5 (0.3–1.0)	0.5 (0.3–1.0)	0.6 (0.3–1.2)	0.7 (0.4–1.4)	0.9 (0.5–1.7)	1.2 (0.6–2.2)	<0.001
GGT, median (IQR) units/liter	25 (17–40)	25 (17–41)	25 (17–39)	27 (19–44)	32 (21–53)	38 (25–63)	44 (28–63)	49 (30–82)	<0.001
Total bilirubin, median (IQR) mg/dl	0.93 (0.73–1.20)	0.93 (0.75–1.20)	0.95 (0.76–1.20)	0.98 (0.78–1.21)	0.99 (0.79–1.22)	0.99 (0.79–1.24)	0.97 (0.78–1.20)	0.98 (0.78–1.20)	0.001
Homocysteine, median (IQR) μmoles/liter†	10.1 (8.5–12.2)	10.1 (8.6–12.1)	10.1 (8.6–12.0)	10.3 (8.7–12.2)	10.5 (8.9–12.5)	10.8 (9.1–12.8)	11.3 (9.5–13.5)	11.9 (10.1–14.6)	0.001

* BMI = body mass index; BP = blood pressure; GFR = glomerular filtration rate; LDL = low-density lipoprotein; HDL = high-density lipoprotein; IQR = interquartile range; HOMA-IR = homeostatic model assessment of insulin resistance; hsCRP = high-sensitivity C-reactive protein; GGT = gamma glutamyl transferase.
† Among 82,401 men with homocysteine measurements.

truncation) and exit at their age on the date of death or on December 31, 2012. This approach effectively controlled for age in the analysis. For analyses of cause-specific mortality, participants who died of other causes were censored at the date of death.

We used 2 models with progressively increased adjustments for confounding variables that could affect the association between uric acid level and mortality. We initially adjusted for study center (Seoul, Suwon), year of screening examination (1-year categories), education level (less than college education, college education or more, or unknown), alcohol intake (none, <20 gm/day, ≥20 gm/day, or unknown), smoking (never, past, current, or unknown), vigorous exercise (<3 times/week, ≥3 times/week, or unknown), and BMI (continuous). Next, we included history of hypertension (yes, no, or unknown), diabetes mellitus (yes, no, or unknown), medication for hyperlipidemia (yes, no, or unknown), medication for hypertension (yes, no, or unknown), and estimated GFR (continuous). We assessed the proportional hazards assumption by examining graphs of estimated log(−log) (survival). For tests of a quadratic trend, we squared the linear trend variable after centering it on the reference value in both men and women. To further explore the shape of the dose-response relationship between the uric acid level and the risk of all-cause, CVD, and cancer mortality, restricted cubic splines with knots were used at the 5th, 27.5th, 50th, 72.5th, and 95th percentiles of uric acid distribution.

Finally, we performed stratified analyses in the prespecified subgroups defined by smoking status (never or past smoker versus current smoker), alcohol intake (<20 gm/day versus ≥20 gm/day), obesity (BMI <25 kg/m^2 versus ≥25 kg/m^2), HOMA-IR value (<2.5 versus ≥2.5), chronic kidney disease (no versus yes), diabetes mellitus (no versus yes), and any comorbidities including hypertension, diabetes mellitus, and chronic kidney disease (no versus yes); interactions between subgroups were tested using likelihood ratio tests comparing models with and those without multiplicative interaction terms. All P values were 2-tailed, and P values less than 0.05 were considered significant. We used Stata software, version 14.0 (StataCorp) for data analysis.

RESULTS

Baseline characteristics of men and women are described in Tables 1 and 2, respectively. Serum uric acid levels were higher in men than in women. In men and women, an increase in serum uric acid level was positively associated with increased BMI, obesity, alcohol consumption, hypertension, elevated systolic and diastolic BP, total cholesterol, LDL cholesterol, triglycerides, HOMA-IR value, high-sensitivity C-reactive protein level, GGT level, and homocysteine level. An increase in the serum uric acid level was negatively associated with age and HDL cholesterol in men and with higher education level and HDL cholesterol in women. Serum uric acid levels increased with age in women but not in men.

The median follow-up duration was 5.7 years (interquartile range 2.3–8.7 years). There were 2,020 deaths documented during 2,060,721.9 person-years of follow-up (1,439 in men and 581 in women). Among the total deaths,

287 were ascribed to CVD (206 in men and 81 in women) and 963 to cancer (683 in men and 280 in women).

Table 3 shows the relationship between serum uric acid level and risks of all-cause, CVD, and cancer mortality in men. In a multivariable model adjusted for center, year of screening examination, education level, BMI, smoking status, alcohol intake, regular exercise, hypertension, diabetes mellitus, medication for hyperlipidemia, and estimated GFR, the lowest level of uric acid (<3.5 mg/dl) was associated with increased risk of all-cause, CVD, and cancer mortality in men. The corresponding HRs for all-cause, CVD, and cancer mortality comparing <3.5 mg/dl uric acid with 6.5–7.4 mg/dl uric acid were 1.58 (95% CI 1.18–2.10), 1.50 (95% CI 0.62–3.64), and 1.38 (95% CI 0.91–2.11), respectively. The highest level of uric acid (≥9.5 mg/dl) was also significantly associated with increased risk of all-cause, CVD, and cancer mortality in men. The multivariable-adjusted HRs for all-cause, CVD, and cancer mortality comparing ≥9.5 mg/dl uric acid with 6.5–7.4 mg/dl uric acid were 2.39 (95% CI 1.57–3.66), 3.76 (95% CI 1.54–9.20), and 2.67 (95% CI 1.47–4.87), respectively.

The lowest level of uric acid (<2.5 mg/dl) was associated with increased risk of all-cause, CVD, and cancer mortality in women (Table 4). The multivariable-adjusted HRs for all-cause, CVD, and cancer mortality comparing <2.5 mg/dl uric acid with 3.5–4.4 mg/dl uric acid were 1.80 (95% CI 1.10–2.93), 3.96 (95% CI 1.37–11.47), and 1.58 (95% CI 0.76–3.29), respectively. The highest level of uric acid (≥8.5 mg/dl) was associated with significantly increased risk of all-cause and CVD mortality, but a significant difference in cancer mortality was not observed. The multivariable-adjusted HRs for all-cause and CVD mortality comparing ≥8.5 mg/dl uric acid with 3.5–4.4 mg/dl uric acid were 377 (95% CI 1.17–12.17) and 11.44 (95% CI 2.74–47.68), respectively.

In multivariable-adjusted spline regression models for both men and women, a U-shaped association between uric acid and all-cause mortality was observed at ~7 mg/dl for men and ~4 mg/dl for women, as an inflection point (Figures 1 and 2). In prespecified subgroup analyses, associations between serum uric acid level and mortality were similar across subgroups of study participants with no significant interactions with regard to alcohol intake (<20 gm/day versus ≥20 gm/day), smoking status (never versus current), regular exercise (<3 times/week versus ≥3 times/week), BMI (<25 kg/m^2 versus ≥25 kg/m^2), HOMA-IR value (<2.5 versus ≥2.5), chronic kidney disease (no versus yes), diabetes mellitus (no versus yes), or comorbidities including hypertension, diabetes mellitus, and chronic kidney disease (no versus yes) (see Supplementary Tables 1 and 2, available on the *Arthritis & Rheumatology* web site at http://onlinelibrary. wiley.com/doi/10.1002/art.40472/abstract).

Table 2. Baseline characteristics of the study participants by uric acid level among women*

Characteristic	Uric acid level, mg/dl								P for quadratic trend
	<2.5	2.5–3.4	3.5–4.4	4.5–5.4	5.5–6.4	6.5–7.4	7.5–8.4	≥8.5	
Number	10,576	55,611	71,556	25,016	4,376	699	116	46	
Age, mean ± SD years	40.0 ± 9.8	39.6 ± 9.4	39.4 ± 9.6	40.0 ± 10.7	41.8 ± 12.2	45.0 ± 13.7	48.2 ± 14.8	49.1 ± 16.2	<0.001 <0.001
BMI, mean ± SD kg/m²	21.4 ± 2.6	21.5 ± 2.7	21.8 ± 2.8	22.6 ± 3.2	23.8 ± 3.7	25.4 ± 4.1	25.9 ± 4.3	24.9 ± 4.2	<0.001
Obese, %	8.5	9.8	12.4	20.5	34.2	51.5	56.8	46.2	<0.001
Current smoker, %	3.8	4.1	4.7	5.6	5.9	7.2	9.2	2.9	<0.001
Alcohol intake ≥20 gm/day, %	2.9	2.3	2.8	3.5	4.1	6.7	6.0	4.5	<0.001
Exercise ≥3 times/week, %	13.8	14.1	14.2	15.5	15.6	15.8	14.5	13.7	0.011
College graduate or higher education level, %	61.0	61.7	63.3	60.6	56.1	47.3	41.8	45.7	<0.001
Diabetes mellitus, %	3.0	2.5	2.0	2.5	4.1	8.3	12.3	14.1	<0.001
Hypertension, %	8.3	7.1	8.2	11.8	19.1	33.3	45.2	44.9	<0.001
Use of medication for dyslipidemia, %	1.1	0.8	0.8	1.2	1.6	3.4	4.0	5.2	<0.001
Systolic BP, mean ± SD mm Hg	107.4 ± 14.3	107.5 ± 13.6	107.9 ± 13.9	109.4 ± 14.8	112.4 ± 16.4	116.3 ± 17.9	120.7 ± 18.8	119.1 ± 19.9	<0.001
Diastolic BP, mean ± SD mm Hg	68.2 ± 9.4	68.3 ± 9.3	68.7 ± 9.4	69.8 ± 9.8	71.6 ± 10.5	74.0 ± 11.0	75.6 ± 11.0	75.2 ± 11.3	<0.001
Estimated GFR, mean ± SD ml/minute/1.73 m²	90.8 ± 19.1	88.7 ± 17.6	85.2 ± 15.7	81.9 ± 15.0	79.0 ± 15.8	74.6 ± 16.8	67.9 ± 19.2	62.0 ± 27.0	<0.001
Glucose, mean ± SD mg/dl	92.9 ± 19.9	91.9 ± 16.1	91.7 ± 13.2	92.4 ± 13.0	94.3 ± 15.7	97.7 ± 18.3	102.5 ± 23.8	100.4 ± 25.8	<0.001
Total cholesterol, mean ± SD mg/dl	182.4 ± 33.8	183.4 ± 32.8	186.4 ± 33.1	192.8 ± 34.9	202.0 ± 37.5	211.8 ± 41.2	216.1 ± 43.8	211.9 ± 52.7	<0.001
LDL cholesterol, mean ± SD mg/dl	101.3 ± 28.1	102.6 ± 27.4	105.4 ± 28.3	111.2 ± 30.5	119.2 ± 32.9	126.9 ± 36.2	129.2 ± 39.0	126.2 ± 41.3	<0.001
HDL cholesterol, mean ± SD mg/dl	63.0 ± 13.5	62.3 ± 13.4	61.7 ± 13.5	60.3 ± 13.6	58.6 ± 14.1	56.6 ± 14.6	56.1 ± 15.1	53.8 ± 13.9	<0.001
Triglycerides, median (IQR) mg/dl	72 (56–98)	74 (57–99)	76 (58–103)	83 (61–103)	98 (68–144)	119 (81–176)	137 (93–201)	119 (81–174)	<0.001
HOMA-IR value, median (IQR)	1.50 (1.03–2.06)	1.50 (1.03–2.02)	1.53 (1.05–2.07)	1.61 (1.11–2.22)	1.78 (1.20–2.52)	2.06 (1.36–2.98)	2.28 (1.63–3.33)	2.16 (1.37–3.05)	<0.001
hsCRP, median (IQR) mg/liter	0.3 (0.1–0.7)	0.3 (0.1–0.6)	0.3 (0.1–0.7)	0.4 (0.1–0.9)	0.6 (0.3–1.4)	1.0 (0.5–2.2)	1.3 (0.7–2.7)	1.2 (0.4–3.6)	<0.001
GGT, median (IQR) units/liter	11 (9–15)	11 (9–15)	12 (9–16)	13 (10–19)	16 (11–24)	20 (13–33)	24 (16–39)	24.5 (14–46)	<0.001
Total bilirubin, median (IQR) mg/dl	0.70 (0.55–0.90)	0.70 (0.57–0.90)	0.73 (0.60–0.92)	0.75 (0.60–0.93)	0.75 (0.60–0.93)	0.73 (0.59–0.92)	0.70 (0.57–0.90)	0.70 (0.53–0.91)	0.025
Homocysteine, median (IQR) μmoles/liter†	6.8 (5.9–8.2)	7.2 (6.0–8.6)	7.4 (6.3–8.8)	7.9 (6.7–9.3)	8.3 (7.1–9.9)	9.2 (7.5–10.9)	9.9 (8.9–11.5)	11.3 (10.0–12.7)	<0.001

* See Table 1 for definitions.
† Among 9,666 women with homocysteine measurements.

Table 3. All-cause, CVD, and cancer mortality by uric acid level among men*

Uric acid level, mg/dl	Person-years	No. of events	Mortality rate (per 100,000 person-years)	Adjusted HR (95% CI)†		
				Model 1	Model 2	Model 3
All-cause mortality						
<3.5	16,683.2	60	359.6	1.95 (1.47–2.58)	1.80 (1.35–2.39)	1.58 (1.18–2.10)
3.5–4.4	71,322.4	132	185.1	1.13 (0.91–1.40)	1.04 (0.84–1.29)	0.94 (0.75–1.16)
4.5–5.4	244,426.5	363	148.5	1.11 (0.95–1.30)	1.06 (0.90–1.24)	1.00 (0.85–1.17)
5.5–6.4	419,502.4	432	103.0	0.99 (0.85–1.15)	0.97 (0.83–1.13)	0.95 (0.81–1.10)
6.5–7.4	290,985.9	274	94.2	1.00 (reference)	1.00 (reference)	1.00 (reference)
7.5–8.4	108,976.8	122	112.0	1.20 (0.97–1.49)	1.21 (0.98–1.50)	1.23 (0.99–1.52)
8.5–9.4	29,359.2	32	109.0	0.98 (0.68–1.41)	1.01 (0.70–1.46)	1.04 (0.72–1.50)
≥9.5	8,907.3	24	269.4	2.13 (1.40–3.24)	2.25 (1.48–3.41)	2.39 (1.57–3.66)
P for quadratic trend				<0.001	<0.001	0.005
CVD mortality						
<3.5	16,683.2	6	36.0	1.53 (0.64–3.66)	1.51 (0.63–3.64)	1.50 (0.62–3.64)
3.5–4.4	71,322.4	12	16.8	0.83 (0.43–1.61)	0.80 (0.41–1.56)	0.79 (0.40–1.55)
4.5–5.4	244,426.5	52	21.3	1.26 (0.82–1.94)	1.26 (0.82–1.95)	1.25 (0.81–1.95)
5.5–6.4	419,502.4	68	16.2	1.22 (0.81–1.84)	1.24 (0.82–1.87)	1.25 (0.83–1.89)
6.5–7.4	290,985.9	35	12.0	1.00 (reference)	1.00 (reference)	1.00 (reference)
7.5–8.4	198,976.8	19	17.4	1.48 (0.85–2.59)	1.44 (0.83–2.53)	1.40 (0.80–2.45)
8.5–9.4	29,359.2	8	27.3	1.86 (0.86–4.02)	1.88 (1.87–4.07)	1.72 (0.79–3.77)
≥9.5	8,907.3	6	67.4	4.27 (1.79–10.20)	4.36 (1.82–10.44)	3.76 (1.54–9.20)
P for quadratic trend				0.490	0.528	0.551
Cancer mortality						
<3.5	16,683.2	28	167.8	1.74 (1.16–2.63)	1.62 (1.07–2.44)	1.38 (0.91–2.11)
3.5–4.4	71,322.4	61	85.5	1.00 (0.74–1.36)	0.94 (0.69–1.28)	0.83 (0.60–1.13)
4.5–5.4	244,426.5	182	74.5	1.09 (0.87–1.36)	1.05 (0.84–1.32)	0.97 (0.77–1.22)
5.5–6.4	419,502.4	201	47.9	0.93 (0.75–1.16)	0.92 (0.74–1.14)	0.88 (0.71–1.10)
6.5–7.4	290,985.9	133	45.7	1.00 (reference)	1.00 (reference)	1.00 (reference)
7.5–8.4	108,976.8	54	49.6	1.10 (0.80–1.51)	1.10 (0.80–1.52)	1.14 (0.83–1.57)
8.5–9.4	29,359.2	12	40.9	0.75 (0.42–1.36)	0.78 (0.43–1.41)	0.84 (0.46–1.52)
≥9.5	8,907.3	12	134.7	2.17 (1.20–3.92)	2.27 (1.26–4.12)	2.67 (1.47–4.87)
P for quadratic trend				0.008	0.029	0.172

* CVD = cardiovascular disease.
† Cox proportional hazards models using age as a time scale were used to estimate hazard ratios (HRs) and 95% confidence intervals (95% CIs). Model 1 was adjusted for age (time scale). Model 2 was further adjusted for center, year of screening examination, education level, body mass index, smoking status, alcohol intake, and regular exercise. Model 3 was further adjusted for hypertension, diabetes mellitus, use of medication for hyperlipidemia, use of medication for hypertension, and estimated glomerular filtration rate.

In a sensitivity analysis, we reanalyzed the association between uric acid and mortality in men and women after excluding those age >60 years. The results did not change qualitatively (see Supplementary Tables 3 and 4, http://onlinelibrary.wiley.com/doi/10.1002/art.40472/abstract).

DISCUSSION

In this large cohort study of young and middle-aged men and women, both low and high uric acid levels were significantly associated with increased mortality compared with the sex-specific reference group. This association remained statistically significant after further adjusting for potential confounders including estimated GFR. Our findings suggest a U-shaped, independent association between serum uric acid level and mortality in both men and women.

In contrast to our findings, a recent study showed no association between uric acid levels and all-cause or cardiovascular mortality (14). In that study, uric acid

was categorized according to quintiles (≤5.2, 5.3–5.8, 5.9–6.4, 6.5–7.1, and >7.1 mg/dl in men and ≤3.5, 3.6–4.0, 4.1–4.4, 4.5–5.0, and >5.0 mg/dl in women). While a quintile-based analytic approach is a commonly used method in epidemiologic research (31), by grouping uric acid levels according to quintiles, intracategory variation in mortality risk could not be examined, leading to the failure to detect the influence of very low and very high uric acid levels on mortality. The upper bound of the lowest uric acid quintile in that study was higher than that in our study, while the lower bound of the highest quintile was much lower than that in our study.

The Evidence for Cardiovascular Prevention from Observational Cohorts in Japan study of 36,313 subjects showed increased CVD mortality associated with low uric acid level in men but not in women, using a quintile-based approach (5); the lowest level of uric acid was defined as <4.6 mg/dl in men and <3.3 mg/dl in women. That study did not take into account several confounding factors such as glucose and creatinine levels, which were

Table 4. All-cause, CVD, and cancer mortality by uric acid level among women*

| Uric acid level, mg/dl	Person-years	No. of events	Mortality rate (per 100,000 person-years)	Adjusted HR (95% CI)†		
				Model 1	Model 2	Model 3
All-cause mortality						
<2.5	14,729.8	18	122.2	1.83 (1.12–2.98)	1.81 (1.11–2.95)	1.80 (1.10–2.93)
2.5–3.4	145,331.7	84	57.8	1.01 (0.79–1.30)	1.01 (0.78–1.30)	1.00 (0.78–1.29)
3.5–4.4	397,828.0	227	57.1	1.00 (reference)	1.00 (reference)	1.00 (reference)
4.5–5.4	246,319.4	162	65.8	1.00 (0.82–1.22)	0.99 (0.81–1.21)	0.99 (0.80–1.21)
5.5–6.4	55,964.8	60	107.2	1.22 (0.91–1.62)	1.21 (0.90–1.62)	1.19 (0.89–1.61)
6.5–7.4	8,566.2	19	221.8	1.53 (0.95–2.47)	1.47 (0.91–2.39)	1.43 (0.88–2.34)
7.5–8.4	1,450.3	8	551.6	2.55 (1.24–5.23)	2.61 (1.27–5.39)	2.36 (1.12–4.99)
≥8.5	368.0	3	81.5	3.60 (1.14–11.33)	3.99 (1.26–12.60)	3.77 (1.17–12.17)
P for quadratic trend				<0.001	<0.001	<0.001
CVD mortality						
<2.5	14,729.8	4	27.2	3.84 (1.33–11.04)	3.75 (1.30–10.82)	3.96 (1.37–11.47)
2.5–3.4	145,331.7	15	10.3	1.64 (0.87–3.12)	1.63 (0.86–3.10)	1.72 (0.90–3.29)
3.5–4.4	397,828.0	25	6.3	1.00 (reference)	1.00 (reference)	1.00 (reference)
4.5–5.4	246,319.4	20	8.1	1.06 (0.59–1.92)	1.04 (0.58–1.88)	0.93 (0.51–1.70)
5.5–6.4	55,964.8	9	16.1	1.44 (0.67–3.11)	1.40 (0.64–3.07)	1.08 (0.49–2.41)
6.5–7.4	8,566.2	2	23.4	1.19 (0.28–5.09)	1.13 (0.26–4.85)	0.75 (0.17–3.32)
7.5–8.4	1,450.3	3	206.9	6.00 (1.71–21.04)	6.00 (1.68–21.50)	2.29 (0.57–9.19)
≥8.5	368.0	3	815.1	23.01 (6.70–79.05)	28.69 (8.07–102.04)	11.44 (2.74–47.68)
P for quadratic trend				<0.001	<0.001	0.001
Cancer mortality						
<2.5	14,729.8	8	54.3	1.65 (0.80–3.44)	1.62 (0.78–3.37)	1.58 (0.76–3.29)
2.5–3.4	145,331.7	36	24.8	0.87 (0.60–1.26)	0.86 (0.59–1.26)	0.85 (0.58–1.24)
3.5–4.4	397,828.0	114	28.7	1.00 (reference)	1.00 (reference)	1.00 (reference)
4.5–5.4	246,319.4	88	35.7	1.08 (0.82–1.43)	1.07 (0.81–1.42)	1.10 (0.83–1.45)
5.5–6.4	55,964.8	23	41.1	0.95 (0.60–1.49)	0.93 (0.59–1.48)	0.96 (0.61–1.53)
6.5–7.4	8,566.2	8	93.4	1.43 (0.69–2.96)	1.39 (0.67–2.89)	1.47 (0.70–3.07)
7.5–8.4	1,450.3	3	206.9	2.28 (0.71–7.30)	2.27 (0.71–7.28)	2.55 (0.78–8.35)
≥8.5	368.0	0	0	–	–	–
P for quadratic trend				0.320	0.345	0.263

* CVD = cardiovascular disease.
† Cox proportional hazards models using age as a time scale were used to estimate hazard ratios (HRs) and 95% confidence intervals (95% CIs). Model 1 was adjusted for age (time scale). Model 2 was further adjusted for center, year of screening examination, education level, body mass index, smoking status, alcohol intake, and regular exercise. Model 3 was further adjusted for hypertension, diabetes mellitus, use of medication for hyperlipidemia, use of medication for hypertension, and estimated glomerular filtration rate.

unavailable. Approximately two-thirds of serum uric acid is excreted by the kidneys, and uric acid level is affected by renal function. It was difficult to determine whether the association between the uric acid level and mortality observed in previous studies was independent of decreased renal function as well as other confounders (32). Recently, a cohort study of 27,490 participants with normal kidney function demonstrated that a low uric acid level was an independent risk factor for all-cause mortality in men, while high uric acid levels were not (15); for women, there was no significant association between serum uric acid levels and mortality (15).

In our study, an association between low uric acid level (<3.5 mg/dl in men and <2.5 mg/dl in women) and all-cause mortality was found in both men and women and remained significant after adjustment for estimated GFR. A low uric acid level was also significantly associated with increased risk of cancer mortality in men (Table 3, models 1 and 2) and increased CVD mortality in women (Table 4, models 1–3), while a nonsignificant

increase in CVD mortality among men and in cancer mortality among women was observed. Our findings were consistent with those from earlier studies that showed U-shaped or J-shaped associations. A Taiwanese study showed U-shaped associations between uric acid levels and all-cause mortality and cardiovascular mortality in the general population (33). That study used the reference group of uric acid level (5–6 mg/dl) to evaluate low (<2.9 mg/dl) and high (>11.4 mg/dl) uric acid levels. However, that study was limited by the absence of important covariates such as smoking status, alcohol intake, and BMI. We found a U-shaped association after adjusting for these factors. Another small Taiwanese study showed a J-shaped association with all-cause mortality in patients receiving hemodialysis (34). Patients with low (<6.5 mg/dl) or high (>9.0 mg/dl) uric acid levels had a higher risk of mortality, with the highest risk at higher levels. A J-shaped association between serum uric acid level and poor renal survival was recently reported in patients with nephropathy (35).
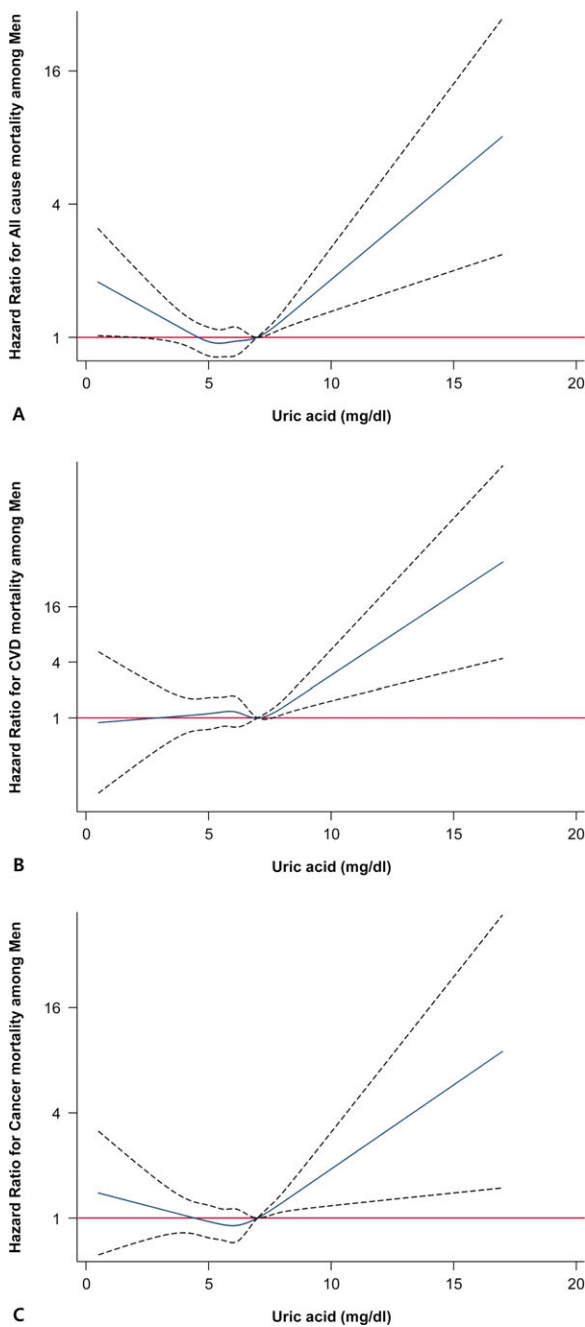
Figure 1. Multivariable-adjusted hazard ratios for all-cause (**A**), cardiovascular disease (CVD) (**B**), and cancer mortality (**C**) by uric acid level among men. Blue lines represent adjusted hazard ratios (with 95% confidence limits [dashed lines]) for all-cause, CVD, and cancer mortality based on restricted cubic splines with knots at the 5th, 27.5th, 50th, 72.5th, and 95th percentiles of uric acid distribution. Red lines represent references for hazard ratios. Models were adjusted for age (time scale), center, year of screening examination, smoking status, alcohol intake, physical activity, education level, body mass index, hypertension, diabetes mellitus, use of medication for hyperlipidemia, use of medication for hypertension, and estimated glomerular filtration rate.
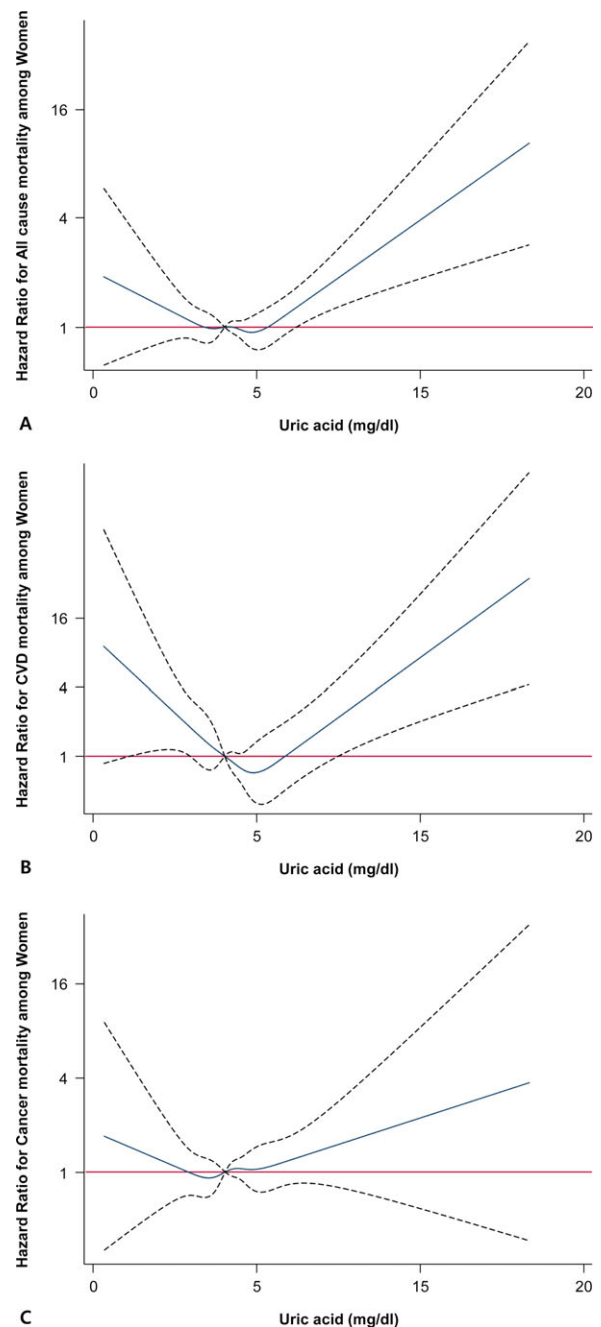
Figure 2. Multivariable-adjusted hazard ratios for all-cause (**A**), cardiovascular disease (CVD) (**B**), and cancer mortality (**C**) by uric acid level among women. Blue lines represent adjusted hazard ratios (with 95% confidence limits [dashed lines]) for all-cause, CVD, and cancer mortality based on restricted cubic splines with knots at the 5th, 27.5th, 50th, 72.5th, and 95th percentiles of uric acid distribution. Red lines represent references for hazard ratios. Models were adjusted for age (time scale), center, year of screening examination, smoking status, alcohol intake, physical activity, education level, body mass index, hypertension, diabetes mellitus, use of medication for hyperlipidemia, use of medication for hypertension, and estimated glomerular filtration rate.

Even though the mechanism underlying the increased risk of mortality related to a low uric acid level is not fully understood, there are some possible explanations. Low uric acid level can also be a marker of nutrition, possibly reflecting malnutrition (36). Unfortunately, the current study was not able to include nutritional information. Additionally, information about medication use that could affect uric acid levels was unavailable. However, our study population comprised young or middle-aged people with low levels of comorbid conditions including diabetes mellitus, hypertension, and renal diseases; thus, the observed association of low uric acid level and mortality might not be fully explained by unmeasured confounders. Indeed, uric acid acts as an antioxidant by increasing superoxide dismutation to hydrogen peroxide and decreasing the availability of superoxide and its harmful interaction with nitric oxide (37). Individuals with hypouricemia are hypothesized to develop increased risk of atherosclerotic diseases due to decreased antioxidant potential (38,39). The induction of cancer cell proliferation was observed in low uric acid conditions through reactive oxygen species (ROS) production in a mouse model (40). Further study is warranted to elucidate the mechanism underlying the role of low uric acid levels in adverse health outcomes.

A high uric acid level was associated with increased all-cause mortality and CVD mortality (3,12,41), while it was not associated with all-cause mortality in some previous studies (14,15). In our large cohort study, subjects in the groups with the highest uric acid levels ($\geq$9.5 mg/dl in men and $\geq$8.5 mg/dl in women) showed a significantly increased risk of all-cause and CVD mortality. The association was stronger in women, even though the absolute incidence of all-cause and CVD mortality was >2 times higher in men. Similarly, previous population-based studies found a stronger association between hyperuricemia and CVD mortality, more so among women than among men (12,13). The mechanism behind hyperuricemia-related all-cause and CVD mortality can be explained by inflammasome and oxidative stress. Hyperuricemia can activate the NLRP3 inflammasome and induce the production of interleukin-1β (42). These events stimulate the inflammatory cascade reaction. Intracellular hyperuricemia also generates inflammatory stress from ROS/reactive nitrogen species (RNS) generation and cyclooxygenase 2 (COX-2) activation. Oxidative stress with activation of the renin–angiotensin system in human vascular endothelial cells is the main mechanism of uric acid–induced endothelial dysfunction (43). Genetic variants related to serum uric acid level were reported previously by the Global Urate Genetics Consortium (44). Using Mendelian randomization with reported genetic variants,

Kleber et al demonstrated that a high uric acid level is causally related to adverse cardiovascular outcomes (45). As their study focused on subjects with European ancestry, analysis of related health outcomes with a genetic variant in an Asian population is needed.

Additionally, in our study, increased risk of cancer mortality was observed only in men with the highest uric acid levels and not in women; however, this inconclusive result for women might be explained by the small number of outcome events, which could lead to imprecise estimates. Elevated serum uric acid levels have been reported to be associated with excess cancer occurrence, recurrence, and cancer mortality in several studies (17,46,47). High uric acid levels contribute to tumorigenesis by promoting both transformation and tumor cell proliferation mediating progression from early stage cancer to highly aggressive cancer (48). This effect is thought to generate inflammatory stress arising from ROS/RNS generation and COX-2 activation. Hyperuricemia is also regarded as a consequence of high tumor cell proliferation rate and accelerated purine breakdown (48,49). The observed positive association between high uric acid level and cancer mortality may be due to the aggressive cancer status (50,51). Future studies are needed to assess the role of uric acid in cancer development, its progression, and related mortality while considering both low and high uric acid levels.

This study has several limitations. First, we did not adjust for dietary factors and drug histories. Data on urate-lowering medications were not available. The target uric acid level is <6 mg/dl during urate-lowering therapy according to the 2012 American College of Rheumatology guidelines for management of gout (52). The mean uric acid–lowering effect is 2.7 mg/dl in hyperuricemic patients (53). Furthermore, a very low level of uric acid (such as <3 mg/dl) is not recommended for gout management (54). Therefore, a uric acid level below 3.5 mg/dl in men and 2.5 mg/dl in women, which were the lowest in our study, might not be affected by treatment. Second, repeated serum uric acid measurement data were not used. We used a single assessment of uric acid levels at baseline and did not incorporate changes in uric acid levels or other changes in lifestyle factors and covariates during follow-up. Third, information on smoking, alcohol use, physical activity, and medical history was obtained via a self-administered structured questionnaire used in health check-up programs in Korea as part of the National Health Insurance Program, and measurement error in these variables could have resulted in some degree of residual confounding.

Fourth, the significant findings are primarily driven by extreme categories of uric acid with a small number of

events, as shown in Tables 3 and 4. Fluctuations in uric acid levels are multifactorial: BMI, waist circumference, BP, insulin resistance, renal disease, diet, medication use, and genetic factors are all known to contribute to the variability of uric acid levels (55). Although we cannot exclude the possibility of unmeasured or residual confounding factors, our results were derived from a young Asian population and thus might have been less likely to be affected by comorbidities. Another possibility is that low extreme and high extreme levels of uric acid could be explained by genetic factors (56–58). The prevalence of hypouricemia was reported to be 1.39% in Korea, which is higher than that reported in Western countries (59). Finally, the subjects included in this study were young and middle-aged Korean men and women who regularly attended health screening examinations, most often as part of work-related health check-up programs; thus, generalization of these results to other age or race/ethnicity groups should be undertaken with caution.

Despite these limitations, the considerable strengths of this study included its large sample size and the use of carefully standardized clinical, imaging, and laboratory procedures. These strengths enabled researchers to examine the relationship between uric acid and cause-specific mortality across a full range of uric acid levels independently of possible confounders.

In conclusion, our study demonstrated that low uric acid levels were independently associated with increased risk of all-cause mortality in men and women, increased risk of CVD mortality in women, and increased risk of cancer mortality in men. Our study supports a J- or U-shaped association between serum uric acid levels and all-cause mortality, CVD mortality, and cancer mortality.

AUTHOR CONTRIBUTIONS

All authors were involved in drafting the article or revising it critically for important intellectual content, and all authors approved the final version to be published. Drs. Chang and Ryu had full access to all of the data in the study and take responsibility for the integrity of the data and the accuracy of the data analysis.
Study conception and design. Cho, Chang, Ryu.
Acquisition of data. Cho, Chang, Kim, Ryu.
Analysis and interpretation of data. Cho, Chang, Ryu.

REFERENCES

1. Wu XW, Muzny DM, Lee CC, Caskey CT. Two independent mutational events in the loss of urate oxidase during hominoid evolution. J Mol Evol 1992;34:78–84.
2. Feig DI, Kang DH, Johnson RJ. Uric acid and cardiovascular risk. N Engl J Med 2008;359:1811–21.
3. Fang J, Alderman MH. Serum uric acid and cardiovascular mortality the NHANES I epidemiologic follow-up study, 1971-1992. National Health and Nutrition Examination Survey. JAMA 2000; 283:2404–10.
4. Lehto S, Niskanen L, Rönnemaa T, Laakso M. Serum uric acid is a strong predictor of stroke in patients with non-insulin-dependent diabetes mellitus. Stroke 1998;29:635–9.
5. Zhang W, Iso H, Murakami Y, Miura K, Nagai M, Sugiyama D, et al. Serum uric acid and mortality form cardiovascular disease: EPOCH-JAPAN study. J Atheroscler Thromb 2016;23:692–703.
6. Liese AD, Hense HW, Löwel H, Döring A, Tietze M, Keil U. Association of serum uric acid with all-cause and cardiovascular disease mortality and incident myocardial infarction in the MONICA Augsburg cohort. World Health Organization monitoring trends and determinants in cardiovascular diseases. Epidemiology 1999;10:391–7.
7. Norvik JV, Schirmer H, Ytrehus K, Storhaug HM, Jenssen TG, Eriksen BO, et al. Uric acid predicts mortality and ischaemic stroke in subjects with diastolic dysfunction: the Tromso Study 1994–2013. ESC Heart Fail 2017;4:154–61.
8. Lamacchia O, Fontana A, Pacilli A, Copetti M, Fariello S, Garofolo M, et al. On the non-linear association between serum uric acid levels and all-cause mortality rate in patients with type 2 diabetes mellitus. Atherosclerosis 2017;260:20–6.
9. Yang J, Wang Y, Zhao Q, Zhang X, Wang X, Qin X, et al. Association of serum uric acid with increased risk of cancer among hypertensive Chinese. Int J Cancer 2017;141:112–20.
10. Deng Z, Gu Y, Hou X, Zhang L, Bao Y, Hu C, et al. Association between uric acid, cancer incidence and mortality in patients with type 2 diabetes: Shanghai diabetes registry study. Diabetes Metab Res Rev 2016;32:325–32.
11. Yan S, Zhang P, Xu W, Liu Y, Wang B, Jiang T, et al. Serum uric acid increases risk of cancer incidence and mortality: a systematic review and meta-analysis. Mediators Inflamm 2015;2015:764250.
12. Chen JH, Chuang SY, Chen HJ, Yeh WT, Pan WH. Serum uric acid level as an independent risk factor for all-cause, cardiovascular, and ischemic stroke mortality: a Chinese cohort study. Arthritis Rheum 2009;61:225–32.
13. Zuo T, Liu X, Jiang L, Mao S, Yin X, Guo L. Hyperuricemia and coronary heart disease mortality: a meta-analysis of prospective cohort studies. BMC Cardiovasc Disord 2016;16:207.
14. Cheong E, Ryu S, Lee JY, Lee SH, Sung JW, Cho DS, et al. Association between serum uric acid and cardiovascular mortality and all-cause mortality: a cohort study. J Hypertens 2017;35 Suppl 1: S3–9.
15. Kang E, Hwang S, Kim DK, Oh K, Joo KW, Kim YS, et al. Sex-specific relationship of serum uric acid with all-cause mortality in adults with normal kidney function: an observational study. J Rheumatol 2017;44:380–7.
16. Taghizadeh N, Vonk JM, Boezen HM. Serum uric acid levels and cancer mortality risk among males in a large general population-based cohort study. Cancer Causes Control 2014;25:1075–80.
17. Strasak AM, Rapp K, Hilbe W, Oberaigner W, Ruttmann E, Concin H, et al. Serum uric acid and risk of cancer mortality in a large prospective male cohort. Cancer Causes Control 2007;18:1021–9.
18. Juraschek SP, Tunstall Pedoe H, Woodward M. Serum uric acid and the risk of mortality during 23 years follow-up in the Scottish Heart Health Extended Cohort Study. Atherosclerosis 2014;233: 623–9.
19. Bae E, Cho H, Shin N, Kim SM, Yang SH, Kim DK, et al. Lower serum uric acid level predicts mortality in dialysis patients. Medicine (Baltimore) 2016;95:e3701.
20. Park C, Obi Y, Streja E, Rhee CM, Catabay CJ, Vaziri ND, et al. Serum uric acid, protein intake and mortality in hemodialysis patients. Nephrol Dial Transplant 2017;32:1750–7.
21. Cutler RG. Urate and ascorbate: their possible roles as antioxidants in determining longevity of mammalian species. Arch Gerontol Geriatr 1984;3:321–48.
22. Stiburkova B, Stekrova J, Nakamura M, Ichida K. Hereditary renal hypouricemia type 1 and autosomal dominant polycystic kidney disease. Am J Med Sci 2015;350:268–71.
23. Wakasugi M, Kazama JJ, Narita I, Konta T, Fujimoto S, Iseki K, et al. Association between hypouricemia and reduced kidney

24. Ryu S, Chang Y, Yun KE, Jung HS, Shin JH, Shin H. Gallstones and the risk of gallbladder cancer mortality: a cohort study. Am J Gastroenterol 2016;111:1476–87.

25. Chang Y, Ryu S, Choi Y, Zhang Y, Cho J, Kwon MJ, et al. Metabolically healthy obesity and development of chronic kidney disease: a cohort study. Ann Intern Med 2016;164:305–12.

26. Wen CP, Cheng TY, Tsai SP, Chan HT, Hsu HL, Hsu CC, et al. Are Asians at greater mortality risks for being overweight than Caucasians? Redefining obesity for Asians. Public Health Nutr 2009;12:497–506.

27. Manjunath G, Sarnak MJ, Levey AS. Prediction equations to estimate glomerular filtration rate: an update. Curr Opin Nephrol Hypertens 2001;10:785–92.

28. Song YM, Sung J. Body mass index and mortality: a twelve-year prospective study in Korea. Epidemiology 2001;12:173–9.

29. Pavillon G, Maguin P. The 10th revision of the International Classification of Diseases. Rev Epidemiol Sante Publique 1993;41:253–5. In French.

30. Chen J, Yeh W, Chuang S, Wu Y, Pan W. Gender-specific risk factors for incident gout: a prospective cohort study. Clin Rheumatol 2012;31:239–45.

31. Bennette C, Vickers A. Against quantiles: categorization of continuous variables in epidemiologic research, and its discontents. BMC Med Res Methodol 2012;12:21.

32. Suliman ME, Johnson RJ, Garcia-Lopez E, Qureshi AR, Molinaei H, Carrero JJ, et al. J-shaped mortality relationship for uric acid in CKD. Am J Kidney Dis 2006;48:761–71.

33. Kuo CF, See LC, Yu KH, Chou IJ, Chiou MJ, Luo SF. Significance of serum uric acid levels on the risk of all-cause and cardiovascular mortality. Rheumatology (Oxford) 2013;52:127–34.

34. Hsu SP, Pai MF, Peng YS, Chiang CK, Ho TI, Hung KY. Serum uric acid levels show a 'J-shaped' association with all-cause mortality in haemodialysis patients. Nephrol Dial Transplant 2004;19: 457–62.

35. Matsukuma Y, Masutani K, Tanaka S, Tsuchimoto A, Fujisaki K, Torisu K, et al. A J-shaped association between serum uric acid levels and poor renal survival in female patients with IgA nephropathy. Hypertens Res 2017;40:291–7.

36. Beberashvili I, Sinuani I, Azar A, Shapiro G, Feldman L, Stav K, et al. Serum uric acid as a clinically useful nutritional marker and predictor of outcome in maintenance hemodialysis patients. Nutrition 2015;31:138–47.

37. Davies KJ, Sevanian A, Muakkassah-Kelly SF, Hochstein P. Uric acid-iron ion complexes: a new aspect of the antioxidant functions of uric acid. Biochem J 1986;235:747–54.

38. Johnson RJ, Kang D, Feig D, Kivlighn S, Kanellis J, Watanabe S, et al. Is there a pathogenetic role for uric acid in hypertension and cardiovascular and renal disease? Hypertension 2003;41: 1183–90.

39. Ames BN, Cathcart R, Schwiers E, Hochstein P. Uric acid provides an antioxidant defense in humans against oxidant- and radical-caused aging and cancer: a hypothesis. Proc Natl Acad Sci U S A 1981;78: 6858–62.

40. Itahana Y, Han R, Barbier S, Lei Z, Rozen S, Itahana K. The uric acid transporter SLC2A9 is a direct target gene of the tumor suppressor p53 contributing to antioxidant defense. Oncogene 2015;34:1799–810.

41. Sumino H, Ichikawa S, Kanda T, Nakamura T, Sakamaki T. Reduction of serum uric acid by hormone replacement therapy in post-menopausal women with hyperuricaemia. Lancet 1999;354:650.

42. Braga TT, Forni MF, Correa-Costa M, Ramos RN, Barbuto JA, Branco P, et al. Soluble uric acid activates the NLRP3 inflammasome. Sci Rep 2017;7:39884.

43. Yu MA, Sánchez-Lozada LG, Johnson RJ, Kang DH. Oxidative stress with an activation of the renin-angiotensin system in human vascular endothelial cells as a novel mechanism of uric acid-induced endothelial dysfunction. J Hypertens 2010;28:1234–42.

44. Köttgen A, Albrecht E, Teumer A, Vitart V, Krumsiek J, Hundertmark C, et al. Genome-wide association analyses identify 18 new loci associated with serum urate concentrations. Nat Genet 2013;45:145–54.

45. Kleber ME, Delgado G, Grammer TB, Silbernagel G, Huang J, Krämer BK, et al. Uric acid and cardiovascular events: a Mendelian randomization study. J Am Soc Nephrol 2015;26:2831–8.

46. Kolonel LN, Yoshizawa C, Nomura AM, Stemmermann GN. Relationship of serum uric acid to cancer occurrence in a prospective male cohort. Cancer Epidemiol Biomarkers Prev 1994;3:225–8.

47. Levine W, Dyer AR, Shekelle RB, Schoenberger JA, Stamler J. Serum uric acid and 11.5-year mortality of middle-aged women: findings of the Chicago Heart Association Detection Project in Industry. J Clin Epidemiol 1989;42:257–67.

48. Fini MA, Elias A, Johnson RJ, Wright RM. Contribution of uric acid to cancer risk, recurrence, and mortality. Clin Transl Med 2012;1:16.

49. Criscuolo M, Fianchi L, Dragonetti G, Pagano L. Tumor lysis syndrome: review of pathogenesis, risk factors and management of a medical emergency. Expert Rev Hematol 2016;9:197–208.

50. Yuan C, Xu X, Wang X, Xu L, Chen Z, Li Y. Relationship between serum uric acid and metastatic and nonmetastatic rectal cancer patients with undergoing no chemotherapy. Medicine (Baltimore) 2016;95:e5463.

51. Arthur FK, Owusu L, Yeboah FA, Rettig T, Osei-Akoto A. Prognostic significance of biochemical markers in African Burkitt's lymphoma. Clin Transl Oncol 2011;13:731–6.

52. Khanna D, FitzGerald JD, Khanna PP, Bae S, Singh MK, Neogi T. 2012 American College of Rheumatology guidelines for management of gout. Part 1: Systematic nonpharmacologic and pharmacologic therapeutic approaches to hyperuricemia. Arthritis Care Res (Hoboken) 2012;64:1431–46.

53. Tausche AK, Reuss-Borst M, Koch U. Urate lowering therapy with febuxostat in daily practice-a multicentre, open-label, prospective observational study. Int J Rheumatol 2014;2014:123105.

54. Richette P, Doherty M, Pascual E, Barskova V, Becce F, Castaneda-Sanabria J, et al. 2016 updated EULAR evidence-based recommendations for the management of gout. Ann Rheum Dis 2017;76:29–42.

55. Nath SD, Voruganti VS, Arar NH, Thameem F, Lopez-Alvarenga JC, Bauer R, et al. Genome scan for determinants of serum uric acid variability. J Am Soc Nephrol 2007;18:3156–63.

56. Lee JH, Choi HJ, Lee BH, Kang HK, Chin HJ, Yoon HJ, et al. Prevalence of hypouricaemia and SLC22A12 mutations in healthy Korean subjects. Nephrology (Carlton) 2008;13:661–6.

57. Enomoto A, Kimura H, Chairoungdua A, Shigeta Y, Jutabha P, Cha SH, et al. Molecular identification of a renal urate anion exchanger that regulates blood urate levels. Nature 2002;417:447–52.

58. Cho SK, Kim S, Chung J, Jee SH. Discovery of URAT1 SNPs and association between serum uric acid levels and URAT1. BMJ Open 2015;5:e009360.

59. Son CN, Kim JM, Kim SH, Cho SK, Choi CB, Sung YK, et al. Prevalence and possible causes of hypouricemia at a tertiary care hospital. Korean J Intern Med 2016;31:971–6.

A CD8α− Subset of CD4+SLAMF7+ Cytotoxic T Cells Is Expanded in Patients With IgG4-Related Disease and Decreases Following Glucocorticoid Treatment

Emanuel Della-Torre,[1] Emanuele Bozzalla-Cassione,[2] Clara Sciorati,[3] Eliana Ruggiero,[3] Marco Lanzillotta,[2] Silvia Bonfiglio,[3] Hamid Mattoo,[4] Cory A. Perugino,[4] Enrica Bozzolo,[2] Lucrezia Rovati,[2] Paolo Giorgio Arcidiacono,[3] Gianpaolo Balzano,[3] Dejan Lazarevic,[3] Chiara Bonini,[3] Massimo Falconi,[3] John H. Stone,[4] Lorenzo Dagna,[2] Shiv Pillai,[4] and Angelo A. Manfredi[2]

Objective. An unconventional population of CD4+ signaling lymphocytic activation molecule family member 7–positive (SLAMF7+) cytotoxic effector memory T (T_{EM}) cells (CD4+ cytotoxic T lymphocytes [CTLs]) has been linked causally to IgG4-related disease (IgG4-RD). Glucocorticoids represent the first-line therapeutic approach in patients with IgG4-RD, but their mechanism of action in this specific condition remains unknown. We undertook this study to determine the impact of glucocorticoids on CD4+ CTLs in IgG4-RD.

Methods. Expression of CD8α, granzyme A, perforin, and SLAMF7 within the effector memory compartment of CD45RO+ (T_{EM}) and CD45RA+ effector memory T (T_{EMRA}) CD4+ cells was quantified by flow cytometry in 18 patients with active IgG4-RD, both at baseline and after 6 months of glucocorticoid treatment. Eighteen healthy subjects were studied as controls. Next-generation sequencing of the T cell receptor α- and β-chain gene was performed on circulating CD4+ CTLs from patients with IgG4-RD before and after treatment and in affected tissues.

Results. Circulating CD4+ T_{EM} and T_{EMRA} cells were not expanded in IgG4-RD patients compared to healthy controls. CD4+SLAMF7+ T_{EM} cells (but not T_{EMRA} cells) were significantly increased among IgG4-RD patients. Within CD4+SLAMF7+ T_{EM} cells, CD8α− cells but not CD8α^{low} cells were elevated in IgG4-RD patients. The same dominant clones of CD8α−CD4+SLAMF7+ T_{EM} cells found in peripheral blood were also identified in affected tissue. CD8α− and CD8α^{low}CD4+SLAMF7+ T_{EM} cells both expressed cytolytic molecules. Clonally expanded CD8α− but not CD8α^{low}CD4+SLAMF7+ T_{EM} cells decreased following glucocorticoid-induced disease remission.

Conclusion. A subset of CD8α−CD4+SLAMF7+ cytotoxic T_{EM} cells is oligoclonally expanded in patients with active IgG4-RD. This T_{EM} cell population contracts following glucocorticoid-induced remission. Further characterization of this cell population may provide prognostic information and targets for therapeutic intervention.

IgG4-related disease (IgG4-RD) is an increasingly recognized immune-mediated condition that includes a

variety of clinical manifestations previously regarded as unique, single-organ disorders unrelated to each other. The clinical manifestations of IgG4-RD include autoimmune pancreatitis, retroperitoneal fibrosis, chronic sialadenitis, and hypertrophic pachymeningitis, among others (1,2). IgG4-RD is also commonly referred to as a fibroinflammatory disorder characterized by tumefactive lesions, frequent elevation of serum IgG4 levels, and tissue fibrosis (1). Glucocorticoids represent the treatment of choice to induce IgG4-RD remission, but their effect on the cells orchestrating the disease remains unknown (1). Likewise, the profibrotic mechanisms driving IgG4-RD remain poorly elucidated.

Recently, the accepted view of IgG4-RD as a Th2-mediated disorder has been questioned by the identification of an unusual population of clonally expanded CD4+ cytotoxic T lymphocytes (CTLs) that accumulate within affected tissues (3–5). In contrast to the lack of correlation with Th2 lymphocytes, CD4+ CTLs appear linked to IgG4-RD activity because they are increased in the peripheral blood of subjects with active disease and decrease following rituximab-induced remission despite their lack of CD20 expression (3–8). They express CD8α/α homodimers in addition to CD4 and share several features with CD8+ CTLs (which express CD8α/β heterodimers as well as CD8α/α homodimers), including the production of cytolytic molecules (4,9). Moreover, CD4+ CTLs in patients with IgG4-RD secrete profibrotic cytokines (such as interleukin-1β, interferon-γ, and transforming growth factor β) and express signaling lymphocytic activation molecule family member 7 (SLAMF7), a surface antigen implicated in homotypic interactions with activated B cells and disease immunopathogenesis (4,10). Thus, because CD4+ CTLs have the potential both to stimulate fibroblast activation and to interact with antigen-presenting B cells, these cells may play a central role in the pathogenesis of IgG4-RD (1).

To better clarify the mechanisms of action of glucocorticoids in IgG4-RD and the pathogenic relevance of CD4+ CTLs, we aim to describe the effects of corticosteroid treatment on CD4+ CTLs. Glucocorticoids offer a unique vantage point for observing variations of putatively pathogenic T lymphocytes, because it has been shown that they do not drastically perturb B and T cell counts in the peripheral blood (11,12). On the other hand, rituximab reduces the circulating levels of activated CD4+ T lymphocytes in a global manner by abrogating the survival and differentiation signals provided by naive B cells (13,14). In the present work, we also identify a population of CD8α−CD4+SLAMF7+ effector memory T (T_{EM}) cells—corresponding to a subset of CD4+ CTLs—that are oligoclonally expanded in the peripheral blood of patients with active IgG4-RD and whose numbers contract with disease remission.

PATIENTS AND METHODS

Patients. Eighteen consecutive patients with active, untreated IgG4-RD who had been referred to the San Raffaele Scientific Institute were included in this observational prospective study (15). IgG4-RD was diagnosed according to the consensus statement on the pathology of IgG4-RD and the comprehensive diagnostic criteria for IgG4-RD (16,17). Patients with isolated pancreatic involvement who did not undergo pancreatic biopsy were diagnosed as having definite IgG4-RD according to the international consensus diagnostic criteria for autoimmune pancreatitis (18). All patients were initially treated with prednisone (0.6–1 mg/kg) for 1 month; prednisone was gradually tapered and withdrawn after 6 months in accordance with international guidelines (12). Blood for serologic and immunologic studies and clinical correlations was obtained at baseline and 6 months after the institution of glucocorticoid treatment. Eighteen healthy age- and sex-matched subjects served as controls. All patients gave written informed consent for the analyses performed. The study was conducted according to the Declaration of Helsinki and approved by the Ethics Committee of the San Raffaele Scientific Institute.

Disease activity. IgG4-RD activity was assessed by means of the IgG4-RD responder index (RI). Active disease was defined by an IgG4-RD RI ≥3. Disease remission was defined by an IgG4-RD RI <3. A reduction in the IgG4-RD RI of ≥2 points still with a total score ≥3 was considered a partial response to glucocorticoid treatment (19).

Flow cytometry. Peripheral blood mononuclear cells were isolated from patients with IgG4-RD and healthy controls by Ficoll density-gradient centrifugation (GE Healthcare), resuspended in fetal bovine serum (FBS) containing 10% DMSO, and cryopreserved. For T cell surface staining, cells were stained at 4°C for 30 minutes in staining buffer containing optimized concentrations of the following fluorochrome-conjugated anti-human antibodies (purchased from BioLegend unless otherwise specified): phycoerythrin (PE)–conjugated anti-CD4 (clone RPA-T4; BD Biosciences), PE–Cy7–conjugated anti-CD4 (clone OKT4), fluorescein isothiocyanate (FITC)–conjugated anti-CD8α (clone HIT8a; BD Biosciences), PE-conjugated anti-CD8α (clone SK1), allophycocyanin (APC)–Cy7–conjugated anti-CD27 (clone 0323), BV510-conjugated anti-CD27 (clone MT271), Pacific Blue (PB)–conjugated anti-CD45RO (clone UCHLa), BV605-conjugated anti-CD45RA (clone HI100; BD Biosciences), PE–Cy7–conjugated anti-CD62L (clone DREG-56), APC-conjugated anti-CD319/SLAMF7 (clone 162.1), and Alexa Fluor 647–conjugated anti-CD319/SLAMF7 (clone 235614; BD Biosciences).

Viable cells were identified among those negative for 7-aminoactinomycin D Viability Staining Solution (BioLegend). For intracellular staining of granzyme A and perforin on T cells using PE-conjugated anti–granzyme A (clone CB9d) and FITC-conjugated antiperforin (clone dG9), cells were fixed and permeabilized with a BD Cytofix/Cytoperm kit according to the instructions of the manufacturer (BD Biosciences) and then stained in permeabilization buffer at 4°C for 30 minutes. CD45RO+ T_{EM} cells were defined as CD4+CD45RO+ $CD27^{low}CD62L^{low}$ cells. CD45RA+ effector memory T (T_{EMRA})

cells were identified as CD4+CD45RA+CD27^{low}CD62L^{low} cells (see Supplementary Figure 1, available on the *Arthritis & Rheumatology* web site at http://onlinelibrary.wiley.com/doi/10.1002/art.40469/abstract). To identify CD4+ CTLs, we assessed granzyme A and perforin expression among SLAMF7+ cells within the T$_{EM}$ and T$_{EMRA}$ cell compartments. Flow cytometry was performed on a BD LSRII flow cytometer (BD Biosciences), and the Flow Cytometry Standard files were analyzed using FlowJo software, version 10 (Tree Star).

For plasmablast staining, 10-color flow cytometry (Navios cytometer; Beckman Coulter) was readily performed on EDTA-treated fresh whole blood samples using a lyse-no-wash technique (ammonium chloride) and the following panel of directly conjugated antibodies: FITC-conjugated anti-CD3, PE-conjugated anti-CD56, energy-coupled dye–conjugated anti-CD4, PC5.5-conjugated anti-CD138, PC7-conjugated anti-CD27, APC-conjugated anti-CD20, Alexa Fluor 700–conjugated anti-CD19, Alexa Fluor 750–conjugated anti-CD38, PB-conjugated anti-CD8, and Krome Orange–conjugated anti-CD45 (all from Beckman Coulter). Plasmablasts were identified within the lymphocyte gate as CD19+ CD20−CD27+CD38$^{+/bright}$ cells.

Cell sorting and immunofluorescence. Using a Beckman Coulter MoFlo XDP instrument, CD4+CD45RO+CD27^{low} CD62L^{low}CD319/SLAMF7+CD8− cells were sorted from 2 patients with IgG4-RD at the time of diagnosis (patients 1 and 5) and from 1 patient after 6 months of glucocorticoids (patient 1). Cells were cultured overnight in Dulbecco's modified Eagle's medium/10% FBS, L-glutamine, and antibiotics on Lab-Tek Chamber Slides (Thermo Fisher) previously coated with poly-L-lysine (Sigma-Aldrich). Cells were fixed in 4% paraformaldehyde for 10 minutes at room temperature followed by incubation for 1 hour with phosphate buffered saline (PBS) containing 0.1% Triton X-100, 10% serum, and 3% bovine serum albumin (BSA) (blocking solution). For granzyme staining, cells were incubated with mouse anti-human granzyme A monoclonal antibody (Chemicon) overnight at 4°C in PBS/10% BSA followed by an Alexa Fluor 488–conjugated goat anti-mouse secondary antibody (Invitrogen) and Hoechst 33342 Solution (Thermo Fisher) (for nuclear staining). Unrelated mouse IgG antibody was used in parallel as isotype control. Images were captured using a PerkinElmer Ultraview ESR Laser Scanning Confocal microscope. Linear adjustments of the images were done using Adobe Photoshop CS4.

Next-generation sequencing. Total RNA was extracted from formalin-fixed paraffin-embedded (FFPE) tissues from patient 1 (pancreas) and patient 5 (lacrimal gland and lungs) (Pathology Unit of San Raffaele Institute) using a Maxwell 16 LEV RNA FFPE kit according to the protocol of the manufacturer (Promega). RNA extraction from sorted CD8α−CD4+ SLAMF7+ CTLs was performed with a PicoPure RNA Isolation Kit (Thermo Fisher). RNA concentration was assessed with a Qubit 2.0 Fluorometer (Thermo Fisher) using a Qubit RNA Assay kit (Thermo Fisher). RNA integrity (the RNA integrity number) was evaluated on an Agilent 2100 Bioanalyzer with an RNA 6000 Nano kit (Agilent).

High-throughput sequencing of the T cell receptor (TCR) α- and β-chain repertoire was performed by using a modified rapid amplification of complementary DNA (cDNA) ends polymerase chain reaction (PCR) protocol (20,21). TCR-specific cDNA was reverse transcribed using the SmartScribe enzyme (Takara Bio) in the presence of biotinylated primers specific for the constant α- and β-chain genes and in the presence of a barcoded (5-bp) template switching primer. Enrichment of the TCR-specific biotinylated cDNA molecules was obtained using streptavidin magnetic beads (Dynabeads; Life Technologies). Upon magnetic capture, TCR-specific cDNA was washed and resuspended in 10 μl water. One microliter of cDNA and 1 μl of the first PCR product were used as input material for the first and second exponential PCRs, respectively. In the first exponential PCR, primers specific for the constant α- and β-chain gene and for the template switching sequence were used. In the second exponential PCR, fusion primers harboring Illumina MiSeq sequencing adaptors were added. In particular, a barcoded (10-bp) fusion primer specific for the constant TCR genes was used to tag each individual sample. PCR amplicons were purified using AmPure beads (Beckman Coulter).

Library quantification was performed with a Qubit 2.0 Fluorometer using a Qubit double-stranded DNA HS kit (Thermo Fisher), and the fragment length distribution was assessed on an Agilent 2100 Bioanalyzer with a High Sensitivity DNA kit (Agilent). Libraries were sequenced in paired-end mode (300 bp read 1 plus 150 bp read 2) on a MiSeq platform using MiSeq version 3 600-cycle reagents (Illumina). After demultiplexing of the sequencing results, analysis of the third complementarity-determining region (CDR3) clonotypes was carried out using MiTCR software (22,23).

Statistical analysis. Statistical analysis was performed with GraphPad Prism software, version 6.0. The population distributions were analyzed for normality with the D'Agostino-Pearson normality test. Comparisons between the different populations were performed with paired and unpaired Mann-Whitney and Wilcoxon correction tests. Correlation studies were performed with Pearson or Spearman correlation tests. Linear regression analyses were performed, and their results are expressed as *P* values. Results are presented as the median and range unless otherwise specified. *P* values less than 0.05 were considered significant.

RESULTS

Clinical, serologic, and immunologic features in the cohort of patients with IgG4-RD. Eighteen patients (11 men and 7 women) with a mean age of 64 years (range 47–83 years) were included in the study (Table 1). All patients had definite IgG4-RD based on the 2012 consensus statement on the pathology of IgG4-RD (16). The pancreas was the most commonly affected organ (10 cases), followed by lymph nodes (6 cases), the biliary tree (3 cases), the aorta (3 cases), and the lacrimal glands (2 cases). The parotid glands, lung, and submandibular glands were involved in 1 case each. Eight patients (44%) had ≥2 organs involved by IgG4-RD. All patients had active IgG4-RD as defined by a mean IgG4-RD RI of 8 (range 6–15; normal <3). The mean levels of serum IgG4 and circulating plasmablasts were 423 mg/dl (range 156–1,360 mg/dl; normal <135 mg/dl) and 5,781 cells/ml (range 140–40,840 cells/ml; normal 0–653 cells/ml), respectively. Serum IgG4 levels were elevated in all patients. Circulating plasmablasts were elevated in 16 patients (89%).

CD4+ T_{EM} and T_{EMRA} cells are not expanded in treatment-naive patients with newly diagnosed, active IgG4-RD. In patients with IgG4-RD, CD4+ CTLs have been identified following the observation of expanded circulating CD4+CD45RO+CD27^{low}CD62L^{low} T_{EM} cells during active disease (4). Therefore, to study CD4+ CTLs, we first performed flow cytometry analysis on CD27^{low} CD62L^{low} cells within the CD4+CD45RO+ memory T cell compartment. Circulating CD4+ T_{EM} cells were not increased in our cohort of patients with active, untreated IgG4-RD compared to age- and sex-matched healthy individuals. In particular, the absolute counts of circulating CD4+ T_{EM} cells in IgG4-RD patients and healthy subjects were a median of 85,830 cells/ml (range 18,462–239,643 cells/ml) and 82,385 cells/ml (range 32,832–194,000 cells/ml), respectively ($P > 0.05$). CD4+ T_{EM} cells in IgG4-RD patients and controls represented a median of 20% (range 10.4–64.7%) and 18% (range 10.8–46.2%), respectively, of total CD4+CD45RO+ memory T cells ($P > 0.05$) (Figures 1A and B). Absolute counts of CD4+ T_{EM} cells did not correlate with the number of organs involved by IgG4-RD, the IgG4-RD RI, serum IgG4 levels, or numbers of circulating plasmablasts (data not shown).

CD4+ CTLs were described originally in the setting of chronic viral infections as CD27^{low}CD62L^{low}CD4+ CD45RA+ effector memory T (T_{EMRA}) cells that acquire a cytolytic gene program after down-regulation of the transcription factor Th-inducing POZ/Kruppel-like factor and up-regulation of eomesodermin and RUNX-3 (24,25).

Therefore, we also examined the expansion of CD27^{low} CD62L^{low} cells within the CD4+CD45RA+ (T_{EMRA}) cell compartment by flow cytometry, but we did not identify significant differences between IgG4-RD patients and healthy subjects ($P > 0.05$) (Figures 1C and D).

Expansion of CD8α−CD4+SLAMF7+ T_{EM} cells in peripheral blood of patients with active, untreated IgG4-RD. CD4+ CTLs in IgG4-RD have been described as SLAMF7-expressing cells within the CD4+ T_{EM} cell compartment (4). To assess the frequency of circulating CD4+ CTLs in patients with active, untreated IgG4-RD, we analyzed T_{EM} cells for the expression of SLAMF7. The fraction of total T_{EM} cells that were circulating CD4+SLAMF7+ T_{EM} cells in IgG4-RD patients was significantly increased compared to that in healthy individuals (median of 54.1% [range 35.9–83.4%] and 40.5% [range 20.7–66.8%], respectively; $P < 0.01$) (Figures 2A and C). Absolute counts of circulating CD4+SLAMF7+ T_{EM} cells in IgG4-RD patients were increased compared to those in healthy individuals, but not to a significant extent (median of 51,893 cells/ml [range 9,430–188,840 cells/ml] and 26,570 cells/ml [range 9,740–53,670 cells/ml], respectively; $P = 0.07$) (data not shown).

Because CD4+ CTLs have also been shown to express CD8α, we further assessed circulating CD4+SLAMF7+ T_{EM} cells for the expression of this surface marker (24,25). CD8α− but not CD8α^{low}CD4+ SLAMF7+ T_{EM} cells were significantly expanded in patients with active IgG4-RD compared to healthy

**Table 1.** Clinical, serologic, and immunologic features of the patients*

Patient/age/sex	T_{EM} cells/ml	SLAMF7+ T_{EM} cells/ml	CD8α−SLAMF7+ T_{EM} cells/ml	Plasmablasts/ml†	Serum IgG4 level, mg/dl‡	Organ involvement	IgG4-RD RI§
1/83/F	226,389	188,840	146,877	9,000	1,360	Pancreas, biliary tree	12
2/66/M	40,299	17,071	14,459	7,140	485	Biliary tree, parotid glands, lymph nodes	15
3/67/M	25,778	14,595	13,962	940	720	Pancreas	6
4/70/M	25,037	9,430	9,176	5,400	343	Pancreas, lymph nodes	9
5/72/M	46,035	31,540	29,221	250	368	Lacrimal glands, lungs	6
6/70/M	239,643	131,204	129,987	3,560	221	Pancreas, lymph nodes	9
7/47/F	90,251	45,535	44,635	140	177	Pancreas, lacrimal glands	9
8/73/F	30,749	15,619	15,558	7,000	534	Pancreas, lymph nodes	12
9/53/M	141,512	72,899	68,959	9,300	973	Lymph nodes	6
10/63/M	101,729	48,667	45,213	810	156	Submandibular glands	6
11/65/M	48,234	24,250	23,819	4,000	308	Pancreas	6
12/71/F	84,439	46,744	37,063	1,000	420	Aorta	6
13/51/F	45,877	26,225	23,796	6,000	178	Aorta	6
14/53/F	38,232	16,677	15,891	1,030	173	Aorta	6
15/66/M	48,115	26,576	26,040	1,760	362	Pancreas	6
16/75/M	93,084	47,096	38,084	2,150	314	Biliary tree	6
17/51/F	18,462	9,974	9,688	40,840	253	Pancreas	15
18/71/M	201,073	161,133	156,111	3,740	282	Pancreas, lymph nodes	6

* T_{EM} cells = effector memory T cells; SLAMF7+ = signaling lymphocytic activation molecule family member 7 positive; IgG4-RD RI = IgG4-related disease responder index.
† Normal 0–653 cells/ml (see ref. 7).
‡ Normal <135 mg/dl.
§ Normal <3.
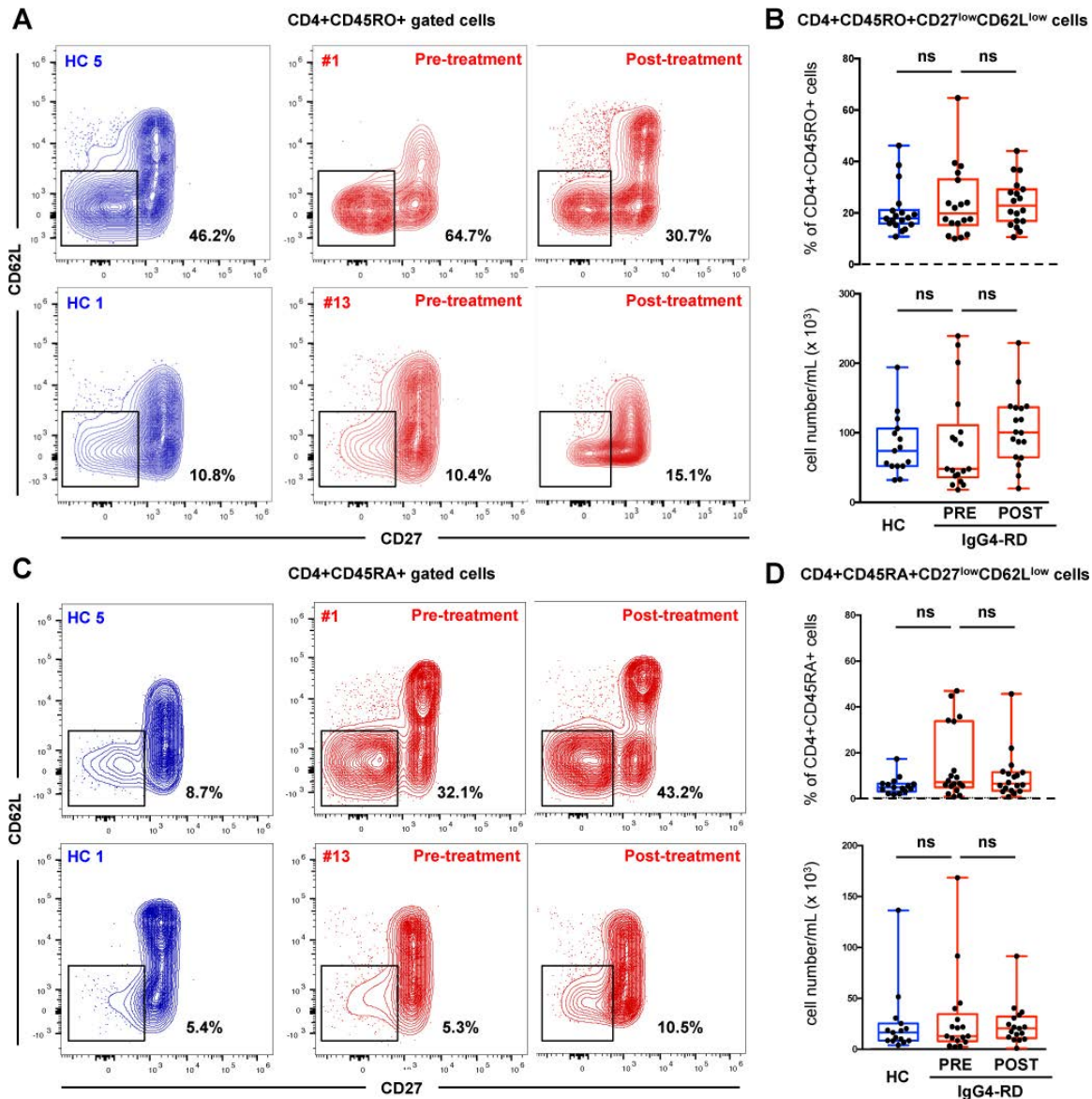
Figure 1. CD4+CD45RO+ effector memory T (T_{EM}) cells and CD4+CD45RA+ effector memory T (T_{EMRA}) cells are not expanded in patients with active, untreated IgG4-related disease (IgG4-RD). **A** and **C,** Contour plots showing different frequencies of CD4+CD45RO+CD27^{low}CD62L^{low} T_{EM} cells (**A**) and CD4+CD45RA+CD27^{low}CD62L^{low} T_{EMRA} cells (**C**) in peripheral blood from 2 representative healthy controls (HC) and 2 representative patients with IgG4-RD (patients 1 and 13) before and after glucocorticoid treatment. **B** and **D,** Percentages and numbers of CD4+CD45RO+CD27^{low}CD62L^{low} T_{EM} cells (**B**) and CD4+CD45RA+CD27^{low}CD62L^{low} T_{EMRA} cells (**D**) in peripheral blood from healthy controls and patients with IgG4-RD before and after glucocorticoid treatment. Symbols represent individual subjects. Data are shown as box plots. Each box represents the 25th to 75th percentiles. Lines inside the boxes represent the median. Lines outside the boxes represent minimum and maximum values. NS = not significant. Color figure can be viewed in the online issue, which is available at http://onlinelibrary.wiley.com/doi/10.1002/art.40469/abstract.

controls, both in absolute numbers and in percentage of T_{EM} cells. In particular, the median number of circulating CD8α−CD4+SLAMF7+ T_{EM} cells in patients with active IgG4-RD and healthy subjects was 47,141 cells/ml (range 9,176–146,877 cells/ml) and 23,872 cells/ml (range 9,430–42,420 cells/ml), respectively (P =

0.05). The median fraction of circulating T_{EM} cells that had a CD8α−CD4+SLAMF7+ phenotype was 51.8% (range 37.6–77.6%) in patients with active IgG4-RD and 37.1% (range 21.0–53.7%) in healthy controls (P = 0.0008). The median number of circulating CD8α^{low} CD4+SLAMF7+ T_{EM} cells in patients with active
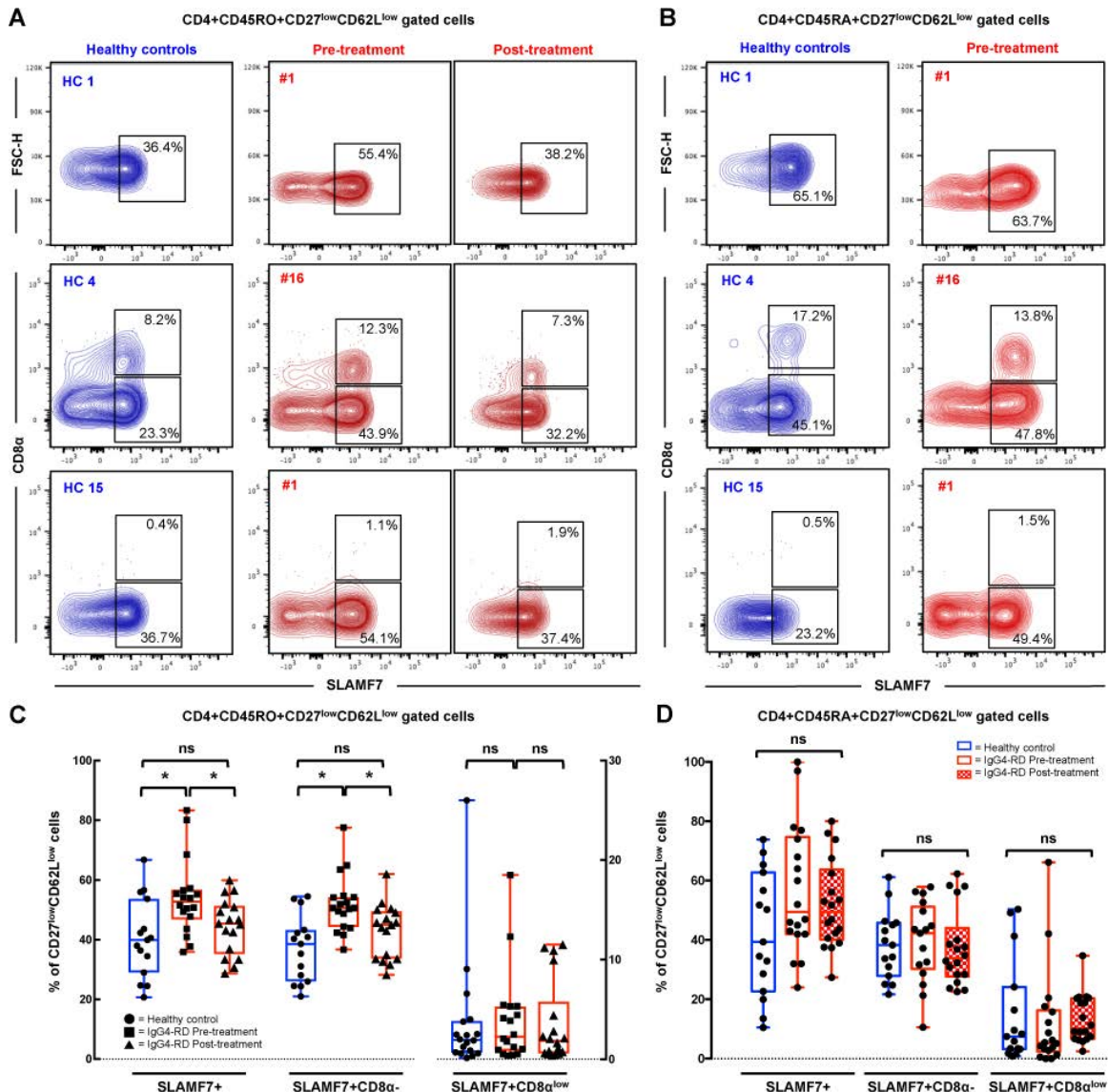
Figure 2. CD4+CD8α− signaling lymphocytic activation molecule family member 7–positive (SLAMF7+) T_{EM} cells are expanded in patients with active, untreated IgG4-RD and decrease following glucocorticoid treatment. **A** and **B,** Contour plots showing different frequencies of CD8α^{low} and CD8α−SLAMF7+CD4+ T_{EM} cells (**A**) and T_{EMRA} cells (**B**) in peripheral blood from representative healthy controls and patients with IgG4-RD (patients 1 and 16) before (**A** and **B**) and after (**A**) glucocorticoid treatment. **C** and **D,** Percentages of CD8α^{low} and CD8α−SLAMF7+CD4+ T_{EM} cells (**C**) and T_{EMRA} cells (**D**) in peripheral blood from healthy controls and patients with IgG4-RD before and after glucocorticoid treatment. Symbols represent individual subjects. Data are shown as box plots. Each box represents the 25th to 75th percentiles. Lines inside the boxes represent the median. Lines outside the boxes represent minimum and maximum values. * = $P < 0.05$ by Mann-Whitney test. See Figure 1 for other definitions. Color figure can be viewed in the online issue, which is available at http://onlinelibrary.wiley.com/doi/10.1002/art.40469/abstract.

IgG4-RD and healthy subjects was 4,478 cells/ml (range 200–41,960 cells/ml) and 2,989 cells/ml (range 160–20,890 cells/ml), respectively ($P > 0.05$). Circulating CD8α^{low}CD4+SLAMF7+ T_{EM} cells in patients with active IgG4-RD and healthy subjects represented a median of 3.9% (range 0.4–18.5%) and 3.7% (range 0.1–26%) of T_{EM} cells, respectively ($P > 0.05$) (Figures 2A and C).

Great variability in the frequency of circulating CD8α^{low}CD4+SLAMF7+ T_{EM} cells was observed both in IgG4-RD patients and in healthy individuals. Indeed, while circulating CD8α−CD4+SLAMF7+ T_{EM} cells were uniformly expanded in IgG4-RD patients compared to controls, circulating CD8α^{low}CD4+SLAMF7+ T_{EM} cells were present both in 10 of 18 IgG4-RD patients and in 10 of 18 healthy subjects (56% of each group). Absolute numbers

of total CD4+SLAMF7+ T_{EM} cells and CD8α−CD4+ SLAMF7+ T_{EM} cells did not correlate with the number of organs involved by IgG4-RD, the IgG4-RD RI, serum IgG4 levels, or numbers of circulating plasmablasts (data not shown). In addition, the absolute number (data not shown) as well as the percentage (Figures 2B and D) of

SLAMF7+ cells within the T_{EMRA} cell compartment were increased compared to controls, but not to a significant extent. Percentages of CD8α^{low} and CD8α−CD4+-SLAMF7+ T_{EMRA} cells did not differ between IgG4-RD patients and healthy subjects (Figures 2B and D). Of note, CD8α^{low}CD4+SLAMF7+ T_{EMRA} cells were absent in the
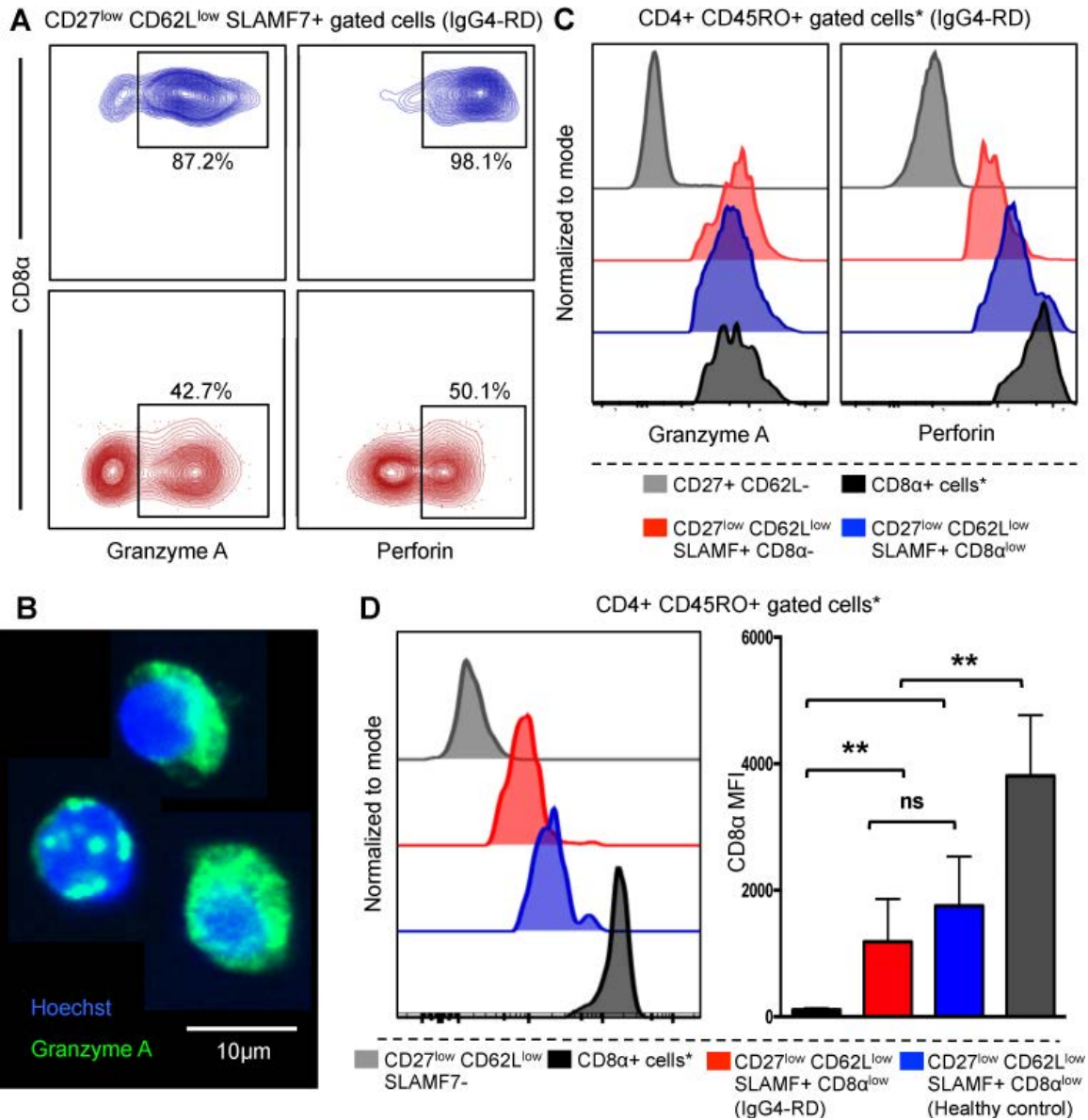
Figure 3. Expression of cytolytic molecules on CD8α− and CD8α^{low} CD4+ signaling lymphocytic activation molecule family member 7–positive (SLAMF7+) T_{EM} cells. A, Contour plots showing different frequencies of perforin- and granzyme A–positive CD8α− and CD8α^{low} CD4+ T_{EM} SLAMF7+ cytotoxic T lymphocytes (CTLs) from a patient with IgG4-RD. Results are representative of 10 independent experiments. B, Immunofluorescence analysis of bulk-sorted CD8α− CD4+ T_{EM} SLAMF7+ CTLs showing granzyme A production. C, Histograms showing expression of granzyme A and perforin on CD8α− and CD8α^{low} CD4+ T_{EM} SLAMF7+ CTLs from a patient with IgG4-RD. Results are representative of 10 independent experiments. D, Expression of CD8α on CD8α^{low}CD4+SLAMF7+ CTLs from a representative patient with IgG4-RD and from a representative healthy control (histograms; left) and in the study cohort presented as the mean ± SD median fluorescence intensity (MFI) (right). ** = P < 0.01. Asterisks in C and D indicate gated on CD8+ T lymphocytes. See Figure 1 for other definitions.

same IgG4-RD patients and healthy controls lacking CD8α−CD4+SLAMF7+ T_{EM} cells.

CD8α−CD4+SLAMF7+ T_{EM} cells in IgG4-RD are oligoclonally expanded and bear a cytolytic phenotype, and the same clones found in the blood also infiltrate affected organs. To compare the cytotoxic phenotype of the expanded CD8α−CD4+SLAMF7+ T_{EM} cells and of CD8α^{low}CD4+SLAMF7+ T_{EM} cells in patients with IgG4-RD, we used flow cytometry to assess the expression of granzyme A and perforin on both cell populations. Coexpression of the 2 cytolytic molecules was detected on half of the CD8α−CD4+SLAMF7+ T_{EM} cells (average 51.7%, range 37.1–62.0%) and on almost all

CD8α^{low}CD4+SLAMF7+ T_{EM} cells (Figure 3A). Granzyme A expression on sorted CD8α−CD4+SLAMF7+ T_{EM} cells was also confirmed by immunofluorescence (Figure 3B). Of note, the expression levels of granzyme A and perforin both on CD8α^{low} and on CD8α−CD4+SLAMF7+ T_{EM} cells were comparable to those on professional cytotoxic CD8+ T cells (Figure 3C). Conversely, the expression of CD8α on CD8α^{low}CD4+SLAMF7+ T_{EM} cells was comparable in IgG4-RD patients and healthy individuals, but significantly lower than that on professional CD8+ T cells (Figure 3D).

To gain clues about the involvement of CD8α−CD4+ CTLs in IgG4-RD pathogenesis, we profiled the
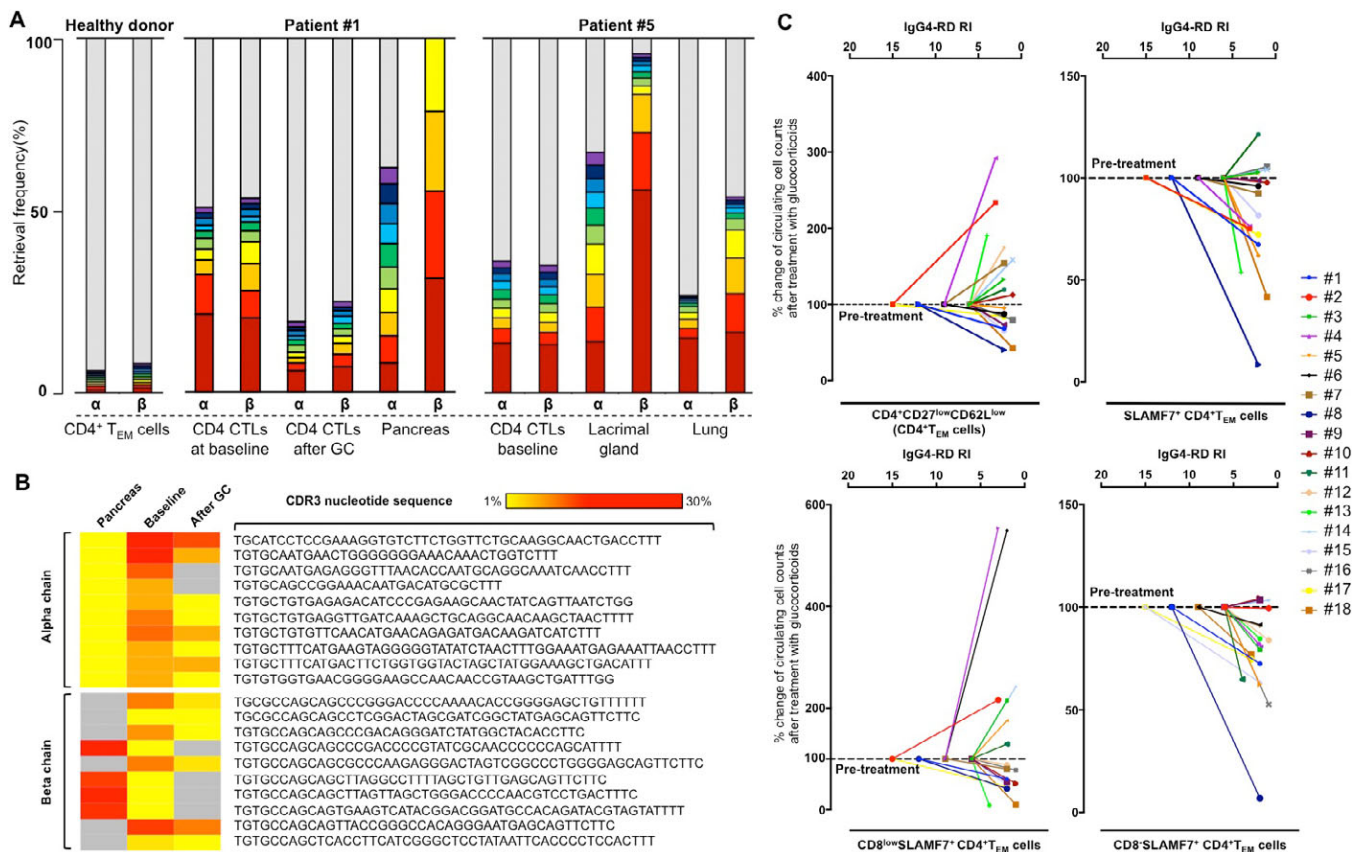
Figure 4. Clinical improvement induced by glucocorticoid (GC) treatment correlates with contraction of clonally expanded circulating CD8α−CD4+ signaling lymphocytic activation molecule family member 7–positive (SLAMF7+) T_{EM} cells. **A,** Retrieval frequency of third complementarity-determining region (CDR3) amino acid sequences of T cell receptor (TCR) α- and β-chains from circulating CD8α−CD4+SLAMF7+ T_{EM} cells before and after treatment and in the pancreas of patient 1 and in the blood, lacrimal gland, and lung tissues of patient 5, showing an oligoclonal pattern on next-generation sequencing analysis. Circulating CD4+ T_{EM} cells from a healthy donor are polyclonal. Red bars indicate the most frequently encountered sequences; violet bars represent the 10th most frequently encountered sequences; gray bars represent overall remaining CDR3 sequences. The higher is the gray bar, the more polyclonal is the sample. Patient 1 also shows an increased polyclonality of the TCR α- and β-chain repertoire after treatment. **B,** Ten CDR3 nucleotide sequences of the TCR α- and β-chains most frequently shared between circulating CD8α−CD4+SLAMF7+ T_{EM} cells and pancreatic tissue of patient 1. The frequency of clones expanded at baseline decreases after glucocorticoid treatment, together with clinical improvement. Gray panels indicate missing nucleotide sequences. **C,** Percentage decrease of circulating CD4+ T_{EM} cells, total SLAMF7+CD4+ cytotoxic T lymphocytes (CTLs), CD8α^{low}SLAMF7+CD4+ CTLs, and CD8α−SLAMF7+CD4+ CTLs in all 18 study patients after 6 months of glucocorticoid treatment (normalized to pretreatment levels), plotted against the IgG4-RD responder index (RI). See Figure 1 for other definitions. Color figure can be viewed in the online issue, which is available at http://onlinelibrary.wiley.com/doi/10.1002/art.40469/abstract.

TCR α- and β-chain repertoire in peripheral blood from patients 1 and 5 and looked for shared clones in tissue biopsy samples obtained before treatment at the time of diagnosis. Comprehensive analysis of the TCR α- and β-chain nucleotide sequences showed an oligoclonal TCRα/β repertoire of circulating CD8α−CD4+SLAMF7+ T_{EM} cells and CDR3 clonotypes that were identical to those sequenced within the tissue from each patient (Figures 4A and B).

Contraction of clonally expanded CD8α−CD4+ SLAMF7+ T_{EM} cells following glucocorticoid-induced disease remission. Six months after institution of glucocorticoid treatment, we performed a second flow cytometry analysis to assess the effects of glucocorticoids on CD4+ T_{EM} cells and CD4+SLAMF7+ T_{EM} cells. At that time point, the mean IgG4-RD RI value was 2 (range 1–4), consistent with a clinical improvement in all patients. Fifteen patients had disease in remission, and 3 had achieved a partial response.

The median number of circulating CD4+ T_{EM} cells was 105,672 cells/ml (range 38,501–229,949 cells/ml), representing a median of 23.9% of total CD4+CD45RO+ memory T cells (range 10.6–44.1%), and did not differ from pretreatment level (paired $P > 0.05$) (Figures 1A and B). Following clinical improvement, the number of circulating CD4+SLAMF7+ T_{EM} cells decreased to a median of 46,585 cells/ml (range 2,304–104,390 cells/ml), and the frequency of these cells decreased to a median of 45.5% of total CD4+ T_{EM} cells (range 28.7–59.9%) (paired $P < 0.05$ compared to baseline values) (Figure 2C). The mean percentage decline of circulating SLAMF7-expressing CD4+ T_{EM} cells from pretreatment level was 19%.

Among CD4+SLAMF7+ T_{EM} cells, the counts of CD8α− lymphocytes decreased selectively and reached levels comparable to those in healthy individuals following clinical improvement (Figure 3C). In particular, circulating CD8α−CD4+SLAMF7+ CTLs decreased to a median of 42.8% of total CD4+ T_{EM} cells (range 28.2–50.4%) (paired $P = 0.001$ compared to baseline value) (Figure 2C). The mean percentage decline of circulating CD8α−CD4+ SLAMF7+ CTLs compared to pretreatment level was 28%. CD8α^{low}CD4+SLAMF7+ T_{EM} cells were not affected by glucocorticoid treatment (Figure 2C). Therefore, the reduction of CD4+SLAMF7+ T_{EM} cells after glucocorticoid treatment was mainly due to the selective decrease of the CD8α− subset of CD4+SLAMF7+ T_{EM} cells (Figure 4C). In a single patient in whom the analysis was performed, the TCRα/β chain repertoire of CD8α−CD4+SLAMF7+ CTLs showed a decrease in the frequency of the initially expanded clones, corresponding to an increase in the repertoire diversity (Figure 4A). No

significant effect of glucocorticoids was observed on the T_{EMRA} cell compartment.

DISCUSSION

The concept of cytotoxicity associated with CD4+ Th lymphocytes has steadily emerged in recent years, in contrast with the traditional view of CTLs originating only from major histocompatibility complex (MHC) class I–restricted CD8+ T lymphocytes. CD4+ CTLs, which represent uncommon subsets of highly differentiated CD4+ T_{EM} and CD4+ T_{EMRA} lymphocytes that retain the ability to kill target cells in an MHC class II–dependent manner, arise in response to repeated antigen stimulation (24,25). In particular, CD4+ CTLs have been extensively characterized in the setting of chronic viral infections such as cytomegalovirus, dengue, HIV, and hepatitis B and hepatitis C viruses, where they likely complement CD8+ and natural killer T cell immune responses (26–28). These cells appear to be of particular importance and superior to CD8+ cytotoxic T cells in maintaining viral latency (29). CD4+ CTLs have also been identified in autoimmune diseases such as rheumatoid arthritis, inflammatory bowel disease, and systemic sclerosis, indicating that they might contribute to chronic inflammation and fibrosis as well (24,25,30).

More recently, we contributed to the identification of CD4+ CTLs in the increasingly recognized fibroinflammatory condition IgG4-RD, and we further characterized them as SLAMF7-expressing cells within the CD4+ T_{EM} cell compartment (4). Indeed, SLAMF7+CD4+ T_{EM} cells exhibited distinctive features of CD8+ CTLs, such as 1) expression of the surface antigen CD8α, 2) expression of the transcription factors eomesodermin and RUNX-3, 3) secretion of the cytolytic molecules granzyme A and perforin, and 4) in vitro cytotoxic activity (4).

Herein we describe for the first time the effects of glucocorticoids on CD4+ CTLs, and we demonstrate that the expression of CD8α identifies at least 2 distinct subsets of CD4+SLAMF7+ CTLs within the T_{EM} and T_{EMRA} cell compartments of patients with IgG4-RD. CD8α− but not CD8α^{low}CD4+SLAMF7+ T_{EM} CTLs correlate with IgG4-RD activity, since the former, in contrast to the latter, are increased in the peripheral blood of patients with active, untreated disease, express TCR clones also found in affected lesions, and appear to be selectively modulated with disease remission after glucocorticoid treatment. Indeed, the finding of common CDR3 sequences expressed by dominant circulating CD8α−CD4+SLAMF7+ CTL clones and tissue-infiltrating lymphocytes strongly supports a pathophysiologic relevance of these cells in IgG4-RD, because it indicates that antigen-specific cytotoxic T cells activated in secondary lymphoid organs are

directly present at the site of active disease. In this sense, CD8α−CD4+SLAMF7+ CTLs might represent the intralesional SLAMF7+CD4+ granzyme A–positive T cells that have been previously shown to infiltrate tissues in patients with IgG4-RD, although further studies are warranted to address this issue (5). Definitive confirmation of this finding would require TCR repertoire analysis on CD8α−CD4+SLAMF7+ CTLs sorted directly from fresh IgG4-RD biopsy samples.

The response of CD8α−CD4+SLAMF7+ T_{EM} cells to glucocorticoids also represents an important finding above and beyond the previously reported effect of rituximab on CD4+SLAMF7+ CTLs in patients with IgG4-RD (4). By depleting CD20+ naive B cells, rituximab is presumed to deprive activated CD4+ T lymphocytes of B cell–derived survival signals, thus limiting the expansion of both pathogenic and bystander T cell clones (11,12). Accordingly, the decreased CD4+SLAMF7+ CTL counts that we previously observed in IgG4-RD patients treated with rituximab might have been a general consequence of B cell depletion on activated CD4+ T cells. Conversely, glucocorticoids have minimal long-term effects on circulating CD19+ and CD20+ B cells in IgG4-RD patients, which offers a different perspective for identifying alterations of putatively pathogenic cells eventually associated with disease remission (Lanzillotta M, et al: unpublished observations). Therefore, the selective decrease of CD8α−CD4+SLAMF7+ CTLs but not of CD8α^{low}CD4+SLAMF7+ CTLs induced by glucocorticoid treatment further strengthens the pathogenic link between CD8α−CD4+SLAMF7+ CTLs and IgG4-RD and unveils a potentially relevant mechanism behind the efficacy of glucocorticoids in patients with this condition. The reduced frequency of expanded CD8α−CD4+SLAMF7+ T cell clones that we observed in a single patient after glucocorticoid treatment also supports the hypothesis of a contraction of antigen-specific T lymphocytes but deserves additional confirmation in a larger number of patients.

On the other hand, CD8α^{low}CD4+ CTLs represented a minor population within the expanded CD4+ SLAMF7+ T_{EM} cell pool in IgG4-RD patients, and these could also be found in healthy individuals, which is inconsistent with a causal role in IgG4-RD inflammation and fibrosis. In particular, while circulating CD8α−CD4+ SLAMF7+ T_{EM} cells appeared to be uniformly expanded only in patients with active IgG4-RD, CD8α^{low}CD4+ SLAMF7+ T cells were detectable in 50–60% of both patients and controls. Therefore, these results suggest that CD8α^{low}CD4+ CTLs may not be linked to active IgG4-RD per se but may reflect an underlying chronic disease or preexisting immune responses to common chronic viral infections (e.g., cytomegalovirus and hepatitis B or hepatitis C viruses), as occurs in otherwise healthy subjects. Activation assays with viral peptides would be necessary to confirm this hypothesis and to address the antigen specificity of CD8α^{low} compared to CD8α−CD4+ SLAMF7+ T_{EM} cells.

In conclusion, we report for the first time that glucocorticoid-induced remission in patients with IgG4-RD is associated with a decrease of circulating CD4+ CTLs, a recently identified potentially pathogenic population of T lymphocytes. Moreover, we identify a CD8α− subpopulation of CD4+SLAMF7+ CTLs that has a stronger association with IgG4-RD, as it is selectively depleted by glucocorticoids. Additional studies are needed to address the biologic relationship between CD8α−CD4+SLAMF7+ T_{EM} and T_{EMRA} cells in IgG4-RD, to functionally characterize them, and to understand the pathogenic relevance of concomitant chronic viral infections in patients with IgG4-RD.

AUTHOR CONTRIBUTIONS

All authors were involved in drafting the article or revising it critically for important intellectual content, and all authors approved the final version to be published. Dr. Della-Torre had full access to all of the data in the study and takes responsibility for the integrity of the data and the accuracy of the data analysis.

Study conception and design. Della-Torre, Bozzalla-Cassione, Pillai, Manfredi.
Acquisition of data. Della-Torre, Bozzalla-Cassione, Sciorati, Ruggiero, Lanzillotta, Bonfiglio, Bozzolo, Rovati, Arcidiacono, Balzano, Lazarevic, Falconi, Pillai, Manfredi.
Analysis and interpretation of data. Della-Torre, Bozzalla-Cassione, Sciorati, Ruggiero, Lanzillotta, Bonfiglio, Mattoo, Perugino, Bozzolo, Rovati, Lazarevic, Bonini, Stone, Dagna, Pillai, Manfredi.

REFERENCES

1. Della-Torre E, Lanzillotta M, Doglioni C. Immunology of IgG4-related disease. Clin Exp Immunol 2015;181:191–206.
2. Lu LX, Della-Torre E, Stone JH, Clark SW. IgG4-related hypertrophic pachymeningitis: clinical features, diagnostic criteria, and treatment. JAMA Neurol 2014;71:785–93.
3. Mattoo H, Della-Torre E, Mahajan VS, Stone JH, Pillai S. Circulating Th2 memory cells in IgG4-related disease are restricted to a defined subset of subjects with atopy. Allergy 2014;69:399–402.
4. Mattoo H, Mahajan VS, Maehara T, Deshpande V, Della-Torre E, Wallace ZS, et al. Clonal expansion of CD4+ cytotoxic T

lymphocytes in patients with IgG4-related disease. J Allergy Clin Immunol 2016;138:825–38.

5. Maehara T, Mattoo H, Ohta M, Mahajan VS, Moriyama M, Yamauchi M, et al. Lesional CD4^{+} IFN-γ^{+} cytotoxic T lymphocytes in IgG4-related dacryoadenitis and sialoadenitis. Ann Rheum Dis 2017;76:377–85.

6. Della-Torre E, Feeney E, Deshpande V, Mattoo H, Mahajan V, Kulikova M, et al. B-cell depletion attenuates serological biomarkers of fibrosis and myofibroblast activation in IgG4-related disease. Ann Rheum Dis 2015;74:2236–43.

7. Wallace ZS, Mattoo H, Carruthers M, Mahajan VS, Della Torre E, Lee H, et al. Plasmablasts as a biomarker for IgG4-related disease, independent of serum IgG4 concentrations. Ann Rheum Dis 2015;74:190–5.

8. Mattoo H, Mahajan VS, Della-Torre E, Sekigami Y, Carruthers M, Wallace ZS, et al. De novo oligoclonal expansions of circulating plasmablasts in active and relapsing IgG4-related disease. J Allergy Clin Immunol 2014;134:69–87.

9. Detre C, Keszei M, Romero X, Tsokos GC, Terhorst C. SLAM family receptors and the SLAM-associated protein (SAP) modulate T cell functions. Semin Immunopathol 2010;32:157–71.

10. Lee JK, Mathew SO, Vaidya SV, Kumaresan PR, Mathew PA. CS1 (CRACC, CD319) induces proliferation and autocrine cytokine expression on human B lymphocytes. J Immunol 2007;179: 4672–8.

11. Olnes MJ, Kotliarov Y, Biancotto A, Cheung F, Chen J, Shi R, et al, and the CHI Consortium. Effects of systemically administered hydrocortisone on the human immunome. Sci Rep 2016;6:23002.

12. Khosroshahi A, Wallace ZS, Crowe JL, Akamizu T, Azumi A, Carruthers MN, et al. International Consensus Guidance statement on the management and treatment of IgG4-related disease. Arthritis Rheumatol 2015;67:1688–99.

13. Lavielle M, Mulleman D, Goupille P, Bahuaud C, Sung HC, Watier H, et al. Repeated decrease of CD4+ T-cell counts in patients with rheumatoid arthritis over multiple cycles of rituximab treatment. Arthritis Res Ther 2016;18:253.

14. Crawford A, Macleod M, Schumacher T, Corlett L, Gray D. Primary T cell expansion and differentiation in vivo requires antigen presentation by B cells. J Immunol 2006;176:3498–506.

15. Campochiaro C, Ramirez GA, Bozzolo EP, Lanzillotta M, Berti A, Baldissera E, et al. IgG4-related disease in Italy: clinical features and outcomes of a large cohort of patients. Scand J Rheumatol 2016;45:135–45.

16. Deshpande V, Zen Y, Chan JK, Yi EE, Sato Y, Yoshino T, et al. Consensus statement on the pathology of IgG4-related disease. Mod Pathol 2012;25:1181–92.

17. Umehara H, Okazaki K, Masaki Y, Kawano M, Yamamoto M, Saeki T, et al. Comprehensive diagnostic criteria for IgG4-related disease (IgG4-RD), 2011. Mod Rheumatol 2012;22:21–30.

18. Shimosegawa T, Chari ST, Frulloni L, Kamisawa T, Kawa S, Mino-Kenudson M, et al. International consensus diagnostic criteria for autoimmune pancreatitis: guidelines of the International Association of Pancreatology. Pancreas 2011;40:352–8.

19. Carruthers MN, Stone JH, Deshpande V, Khosroshahi A. Development of an IgG4-RD Responder Index. Int J Rheumatol 2012;2012:259408.

20. Bolotin DA, Mamedov IZ, Britanova OV, Zvyagin IV, Shagin D, Ustyugova SV, et al. Next generation sequencing for TCR repertoire profiling: platform-specific features and correction algorithms. Eur J Immunol 2012;42:3073–83.

21. Ruggiero E, Nicolay JP, Fronza R, Arens A, Paruzynski A, Nowrouzi A, et al. High-resolution analysis of the human T-cell receptor repertoire. Nat Commun 2015;6:8081.

22. Bolotin DA, Shugay M, Mamedov IZ, Putintseva EV, Turchaninova MA, Zvyagin IV, et al. MiTCR: software for T-cell receptor sequencing data analysis. Nat Methods 2013;10:813–4.

23. Shannon CE. The mathematical theory of communication. 1963. MD Comput 1997;14:306–17.

24. Tian Y, Sette A, Weiskopf D. Cytotoxic CD4 T cells: differentiation, function, and application to dengue virus infection. Front Immunol 2016;7:531.

25. Oja AE, Vieira Braga FA, Remmerswaal EB, Kragten NA, Hertoghs KM, Zuo J, et al. The transcription factor Hobit identifies human cytotoxic CD4^{+} T cells. Front Immunol 2017;8:325.

26. Zloza A, Schenkel JM, Tenorio AR, Martinson JA, Jeziorczak PM, Al-Harthi L. Potent HIV-specific responses are enriched in a unique subset of CD8^{+} T cells that coexpresses CD4 on its surface. Blood 2009;114:3841–53.

27. Nascimbeni M, Pol S, Saunier B. Distinct CD4^{+} CD8^{+} double-positive T cells in the blood and liver of patients during chronic hepatitis B and C. PLoS One 2011;6:e20145.

28. Nascimbeni M, Shin EC, Chiriboga L, Kleiner DE, Rehermann B. Peripheral CD4^{+}CD8^{+} T cells are differentiated effector memory cells with antiviral functions. Blood 2004;104:478–86.

29. Mason G, Jackson S, Okecha G, Poole E, Sissons JG, Sinclair J, et al. Human cytomegalovirus latency-associated proteins elicit immune-suppressive IL-10 producing CD4^{+} T cells. PLoS Pathog 2013;9:e1003635.

30. Parel Y, Aurrand-Lions M, Scheja A, Dayer JM, Roosnek E, Chizzolini C. Presence of CD4+CD8+ double-positive T cells with very high interleukin-4 production potential in lesional skin of patients with systemic sclerosis. Arthritis Rheum 2007;56:3459–67.

Subcutaneous Abatacept in Patients With Polyarticular-Course Juvenile Idiopathic Arthritis

Results From a Phase III Open-Label Study

Hermine I. Brunner,[1] Nikolay Tzaribachev,[2] Gabriel Vega-Cornejo,[3] Ingrid Louw,[4] Alberto Berman,[5] Inmaculada Calvo Penadés,[6] Jordi Antón,[7] Francisco Ávila-Zapata,[8] Rubén Cuttica,[9] Gerd Horneff,[10] Ivan Foeldvari,[11] Vladimir Keltsev,[12] Daniel J. Kingsbury,[13] Diego Oscar Viola,[14] Rik Joos,[15] Bernard Lauwerys,[16] Maria Eliana Paz Gastañaga,[17] Maria Elena Rama,[18] Carine Wouters,[19] John Bohnsack,[20] Johannes Breedt,[21] Michel Fischbach,[22] Thomas Lutz,[23] Kirsten Minden,[24] Tatiana Miraval,[25] Mahmood M. T. M. Ally,[26] Nadina Rubio-Pérez,[27] Elisabeth Solau Gervais,[28] Riana van Zyl,[29] Xiaohui Li,[30] Marleen Nys,[31] Robert Wong,[30] Subhashis Banerjee,[30] Daniel J. Lovell,[1] Alberto Martini,[32] and Nicolino Ruperto,[32] for the Paediatric Rheumatology International Trials Organisation (PRINTO) and the Pediatric Rheumatology Collaborative Study Group (PRCSG)

Objective. To investigate the pharmacokinetics, effectiveness, and safety of subcutaneous (SC) abatacept treatment over 24 months in patients with polyarticular-course juvenile idiopathic arthritis (JIA).

Methods. In this phase III, open-label, international, multicenter, single-arm study, patients with polyarticular JIA (cohort 1, ages 6–17 years and cohort 2, ages 2–5 years) in whom treatment with ≥1 disease-modifying antirheumatic drug was unsuccessful received weight-tiered SC abatacept weekly: 10 to <25 kg (50 mg), 25 to <50 kg (87.5 mg), ≥50 kg (125 mg). Patients who had met the JIA–American College of Rheumatology 30% improvement criteria (achieved a JIA-ACR 30 response) at month 4 were given the option to continue SC abatacept to month 24.

The primary end point was the abatacept steady-state serum trough concentration (C_{minss}) in cohort 1 at month 4. Other outcome measures included JIA-ACR 30, 50, 70, 90, 100, and inactive disease status, the median Juvenile Arthritis Disease Activity Score in 71 joints using the C-reactive protein level (JADAS-71–CRP) over time, safety, and immunogenicity.

Results. **The median abatacept C_{minss} at month 4 (primary end point) and at month 24 was above the target therapeutic exposure (10 μg/ml) in both cohorts. The percentage of patients who had achieved JIA-ACR 30, 50, 70, 90, or 100 responses or had inactive disease responses at month 4 (intent-to-treat population) was 83.2%, 72.8%, 52.6%, 28.3%, 14.5%, and 30.1%, respectively, in cohort 1 (n = 173) and 89.1%, 84.8%, 73.9%, 58.7%, 41.3%, and 50.0%, respectively, in cohort 2 (n = 46); the responses were maintained to month 24. The median (interquartile range) JADAS-71–CRP improved from baseline to month 4: cohort 1, from 21.0 (13.5, 30.3) to 4.6 (2.1, 9.4); cohort 2, from 18.1 (14.0, 23.1) to 2.1 (0.3, 4.4). Improvements were sustained to month 24, at which time 27 of 173 patients (cohort 1) and 11 of 22 patients (cohort 2) had achieved JADAS-71–CRP remission. No unexpected adverse events were reported; 4 of 172 patients (2.3%) in cohort 1 and 4 of 46 (8.7%) in cohort 2 developed anti-abatacept antibodies, with no clinical effects.**

Conclusion. **Weight-stratified SC abatacept yielded target therapeutic exposures across age and weight groups, was well tolerated, and improved polyarticular JIA symptoms over 24 months.**

Juvenile idiopathic arthritis (JIA) is a rheumatic disease presenting in children <16 years of age (1–3). For polyarticular-course JIA (JIA of any category with ≥5 affected joints [1,4,5]), methotrexate (MTX) is the recommended first-line disease-modifying antirheumatic drug (DMARD) therapy (3). If disease activity remains moderate or high after 3 months of MTX treatment, a biologic agent is frequently initiated and a tumor necrosis factor inhibitor (TNFi) is most commonly employed, followed by an anti–interleukin-6 agent or abatacept (6). However, it is important to have multiple treatment options in this pediatric population, particularly for patients who are intolerant of or do not respond to MTX or TNFi (2,7–15) or who live in a tuberculosis-endemic country.

Abatacept, which selectively modulates the CD80/CD86:CD28 costimulatory signal required for full T cell activation, has a distinct mechanism of action upstream of that of other currently available treatments for rheumatic diseases (13,16–18). In adults with rheumatoid arthritis (RA), intravenous (IV) abatacept inhibits structural damage, reduces disease progression, and improves function and health-related quality of life, with good safety and tolerability (16,19,20). IV-administered abatacept has been proven effective and well tolerated in polyarticular JIA clinical trials and real-world settings (21), with benefits of treatment sustained up to 7 years in patients ages 6–17 years (2,9,13). A subcutaneous (SC) abatacept formulation is also available, allowing for administration at home, thus providing greater flexibility (22).

The exposure–response relationship established in RA and JIA has demonstrated that abatacept steady-state serum trough concentration (C_{minss}) is a good predictor of efficacy (23,24). A C_{minss} of 10 μg/ml has been shown to correlate with near-maximal efficacy, based on response as assessed by the Disease Activity Score in 28 joints (24) in RA and the JIA–American College of Rheumatology 30% improvement criteria (JIA-ACR 30) (21,23,25) in JIA. In adults with RA, a weight-tiered 10 mg/kg monthly IV dose and 125 mg weekly SC fixed dose of abatacept have shown equivalent efficacy and comparable safety (22), but the effectiveness and safety of SC abatacept in polyarticular JIA have yet to be demonstrated in a clinical trial.

The aim of this study was to investigate the pharmacokinetics (PK), effectiveness, safety, and immunogenicity of weekly weight-tiered treatment with SC abatacept in patients with active polyarticular JIA, including those ≥2 years of age, over a period of 24 months.

PATIENTS AND METHODS

Study design. This 24-month, single-arm, open-label, international, multicenter, 2-part, phase III study (26) was initiated in August 2013 and conducted across 48 centers worldwide by members of the Paediatric Rheumatology International Trials Organisation (PRINTO) (27) and the Pediatric Rheumatology Collaborative Study Group (PRCSG) (see Appendix A for investigators who participated in this study). The study included 2 age cohorts (cohort 1, ages 6–17 years and cohort 2, ages 2–5 years). During the first 4 months (part 1), patients received open-label SC abatacept weekly, based on body-weight tier at each study visit (10 to <25 kg [50 mg], 25 to <50 kg [87.5 mg], and ≥50 kg [125 mg]) (see Supplementary Materials, available on the *Arthritis & Rheumatology* web site at http://onlinelibrary.wiley.com/doi/10.1002/art.40466/abstract for rationale for the dosing regimen).

At month 4, JIA-ACR 30 responders (28) were given the opportunity to participate in a 20-month extension (part 2 of the study) and continue open-label abatacept treatment according to the previous dosing regimen; part 1 and part 2 formed the 24-month cumulative period. Also at month 4, JIA-ACR 30 nonresponders were given the option to continue SC abatacept for an additional 3 months and to discontinue treatment if a JIA-ACR 30 response was not achieved by month 7. After part 2, long-term follow-up began, in which patients who completed both parts of the study entered a post-study drug access program. The study was conducted in accordance with the Declaration of Helsinki (29), the International Conference on Harmonisation Guidelines for Good Clinical Practice, and local regulations. At each site, an institutional review board or independent ethics committee approved the protocol, consent forms, and any other written information provided to patients or their legal representatives.

Patients. Enrolled patients met the International League of Associations for Rheumatology criteria for JIA (4) in 1 of the following categories: extended oligoarticular JIA, polyarticular JIA rheumatoid factor (RF) positive, polyarticular JIA RF negative, enthesitis-related arthritis, psoriatic arthritis, or systemic JIA (with systemic features absent for ≥6 months prior to enrollment). Patients also had a history of ≥5 joints with active disease and active articular disease at baseline, defined as ≥2 active joints and ≥2 joints with limitation of motion.

In addition, patients were naive to treatment with abatacept but may have had an inadequate response or prior intolerance to ≥1 nonbiologic or biologic DMARD, including TNFi. Patients with systemic JIA at onset were restricted to ≤10% of the study population, and those with a prior inadequate response to TNFi or other biologic DMARDs were restricted to ≤30% of the study population (see Supplementary Materials, available at http://onlinelibrary.wiley.com/doi/10.1002/art.40466/abstract). All patients or their legal representatives provided written informed consent prior to study entry.

Study end points. The primary end point was abatacept C_{minss} in cohort 1 (ages 6–17 years) at month 4 of the study (end of part 1). Secondary end points included the proportion of patients in cohort 1 achieving JIA-ACR 30 response by the end of part 1 and the proportion of patients with serious adverse events (SAEs), AEs, AEs leading to discontinuation, death, marked laboratory abnormalities, and positive immunogenic responses (defined as the presence of antibodies reactive with abatacept in serum) (30) in both cohorts over parts 1 and 2. Abatacept C_{minss} to month 24 (end of part 2) was an exploratory end point for both cohorts.

Prespecified exploratory efficacy end points for both cohorts included the proportions of patients achieving JIA-ACR 30, 50, 70, 90, 100 responses or inactive disease (modified criteria), defined as absence of active joints, physician's global assessment of disease severity ≤10 mm, and C-reactive protein (CRP) level ≤0.6 mg/dl (based on the normal range for CRP as defined by the central analysis site) (31) over time to the end of part 2. JIA-ACR response rates were not corrected for MTX or corticosteroid use; however, if patients received an intraarticular corticosteroid injection, the treated joint was designated as active for the following 3 months. Other prespecified exploratory end points for cohort 1 included median post-baseline values of the 6 JIA-ACR core set variables: number of active joints, number of joints with limitation of motion, physician's global assessment, parent's global assessment of patient overall well-being, cross-culturally adapted and validated version of the Childhood Health Assessment Questionnaire disability index (C-HAQ DI) (32), and laboratory marker of acute inflammation (CRP level). Post hoc analyses in both cohorts were conducted to determine the median Juvenile Arthritis Disease Activity Score in 71 joints using the CRP level (JADAS-71–CRP) (33,34) over time, and the proportion of patients achieving low disease activity according to the JADAS-71–CRP (cutoff value in polyarthritis ≤3.8) and remission (defined as a JADAS-71–CRP value of ≤1 for ≥6 months) (33,35). In addition, post hoc subgroup analyses of JIA-ACR response rates and proportions of patients achieving JADAS-71–CRP low disease activity and remission in cohort 1 were performed using baseline concomitant MTX treatment, prior biologic treatment, and JIA category as subgroups (see Supplementary Materials, available at http://onlinelibrary.wiley.com/doi/10.1002/art.40466/abstract).

Analysis populations. In both cohorts, the PK analysis population for month 4 (end of part 1) comprised treated patients for whom PK measurements were collected in the 4–10-day window after the most recent SC dose; these patients also had 7 consecutive weekly SC abatacept injections at the same dosage prior to month 4. The PK analysis population at the time points other than month 4 also comprised those patients with PK measurements collected in the 4–10-day window after the most recent SC dose.

Effectiveness analyses were conducted on the intent-to-treat (ITT) population (defined as all treated patients) for both cohorts in part 1, as prespecified. For part 2, an "as-observed" analysis was planned for both cohorts. However, in cohort 1 (ages 6–17 years), ITT analyses were also performed for the evaluation of effectiveness (sensitivity analysis), except for median post-baseline values for JADAS-71–CRP and the 6 JIA-ACR core set variables over the cumulative period. In cohort 2 (ages 2–5 years), only as-observed analyses were performed for part 2, as not all patients had completed treatment at the time of database locking.

Safety analyses were performed on the ITT population in both cohorts, taking into consideration all events during parts 1 and 2. Marked laboratory abnormalities criteria were prespecified (see Supplementary Materials, available at http://onlinelibrary.wiley.com/doi/10.1002/art.40466/abstract). Immunogenicity was assessed in patients in the ITT population for whom ≥1 post-baseline immunogenicity result was collected.

Statistical analysis, sample size, and power calculation. As the aim of this study was to assess the PK of SC abatacept treatment, it was not powered for statistical hypothesis testing. A sample size of ~160 patients for cohort 1 (ages 6–17 years) was

planned to allow for assessment of PK, effectiveness, safety, and immunogenicity, resembling the sample size of the 4-month lead-in phase of the IV abatacept JIA study (13). Enrollment of ~160 patients into the 3 body-weight tiers was predicted to ensure that the half-width of the 90% confidence interval (90% CI) for C_{minss} would be within 18% of the true population mean for each body-weight tier group, calculated based on a log-transformed standard deviation for C_{minss} of 0.49. For JIA-ACR 30 response, a sample of 160 patients would yield a precision of 7.4% for the half-width of the 95% CI, assuming an underlying true responder rate of 64%, as seen with IV abatacept in JIA (13). For cohort 2 (ages 2–5 years), a sample size of ≥30 patients permitted initial descriptive assessment of PK, effectiveness, safety, and immunogenicity.

All effectiveness, safety, and PK analyses were descriptive, with no formal statistical testing. For effectiveness analyses using the ITT population, patients with missing data were imputed as nonresponders. CIs for proportions were computed using normal approximation, provided that the actual number of events was ≥5; otherwise, computed CIs were calculated using an exact method. In order to investigate the impact of immunogenicity on effectiveness, safety, and PK, a clinical review of the data on effectiveness, safety, and PK for patients who had positive immunogenic responses was performed.

RESULTS

Patient disposition and baseline characteristics. A total of 219 patients entered part 1 of the study; 173 were ages 6–17 years (cohort 1) and 46 were ages 2–5 years (cohort 2). As shown in Figure 1, 132 patients (76.3%) in cohort 1 and 24 (52.2%) in cohort 2 completed both parts 1 and 2. In both cohorts, the discontinuation rate was low across both parts of the trial; overall, the main reasons for discontinuation were lack of efficacy, withdrawal of

consent, and AEs. Treatment in the cumulative period was ongoing for 15 patients (32.6%) in cohort 2 at the time of database locking. Baseline demographic and disease characteristics for cohorts 1 and 2 are shown in Table 1. Whereas 41.0% of patients (71 of 173) in cohort 1 had a disease duration of ≥2 years, most patients (91.3% [42 of 46]) in cohort 2—which included patients as young as 2 years of age—had a disease duration of <2 years (median 0.5 years). At baseline, 78.6% of patients in cohort 1 and 80.4% in cohort 2 were receiving concomitant MTX. A protocol violation occurred in cohort 1, due to inclusion of 5 patients from noneligible JIA categories in the analysis. The median exposure to abatacept during the cumulative period was 24.3 months (range 1.9–28.0) in cohort 1 and 24.1 months (range 4.0–26.2) in cohort 2.

Pharmacokinetics. The median abatacept C_{minss} values at months 4 and 24 in cohort 1 were 40.5 μg/ml (range 9.3–97.0; n = 135) and 43.0 μg/ml (range 0.0–105.2; n = 79), respectively, and were 51.2 (20.1–122.1; n = 30) and 58.7 (26.5–103.7; n = 19) in cohort 2, respectively (Figure 2). Across all weight groups in cohort 1 and overall in cohort 2, the median C_{minss} values were consistent and above the target therapeutic exposure of 10 μg/ml. After the effect of body weight was taken into account, there was no independent age effect on C_{minss} (see Supplementary Materials, available at http://onlinelibrary.wiley.com/doi/10.1002/art.40466/abstract). The results of this study do not indicate that C_{minss} values >10 μg/ml were associated with either greater effectiveness or an increase in rates of AEs (including infections) at the month 4 time point (data not shown).
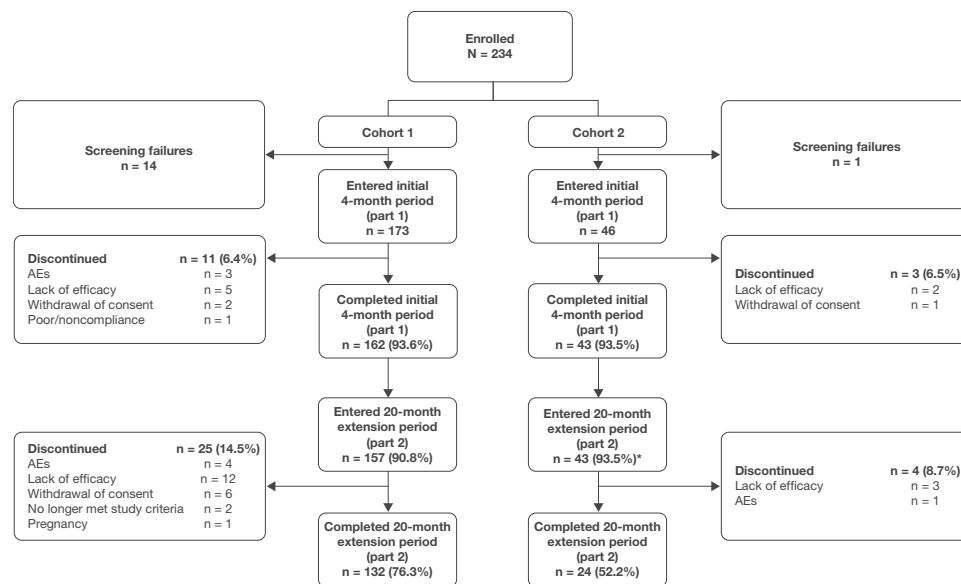
Figure 1. Patient disposition. * = treatment ongoing at time of analysis in 15 patients (32.6%). AEs = adverse events.

Table 1. Summary of baseline demographics and clinical characteristics of the JIA patients*

Characteristic	Cohort 1 (n = 173)	Cohort 2 (n = 46)
Age, median (IQR) years	13.0 (10.0–15.0)	4.0 (3.0–5.0)
Female sex	136 (78.6)	28 (60.9)
Weight, median (IQR) kg	45.0 (31.5–57.0)	18.0 (15.0–21.1)
Weight category		
<25 kg	18 (10.4)	43 (93.5)
25 to <50 kg	74 (42.8)	3 (6.5)
≥50 kg	81 (46.8)	0
Ethnicity		
White	144 (83.2)	44 (95.7)
African American	14 (8.1)	1 (2.2)
Other	15 (8.7)	1 (2.2)
Disease duration, median (IQR)	2.0 (0.0–4.0)	0.5 (0.0–1.0)
<2 years	102 (59.0)	42 (91.3)
2 to <5 years	37 (21.4)	4 (8.7)
5 to ≤10 years	30 (17.3)	0
>10 years	4 (2.3)	0
JIA category		
Polyarthritis RF negative	94 (54.3)	29 (63.0)
Polyarthritis RF positive	46 (26.6)	3 (6.5)
Extended oligoarthritis	19 (11.0)	10 (21.7)
Systemic arthritis	5 (2.9)	0
Psoriatic arthritis	0	4 (8.7)
Enthesitis-related arthritis	4 (2.3)	0
Undifferentiated or persistent oligoarthritis†	5 (2.9)	0
JIA-ACR core set variable, median (IQR)		
No. of active joints	10.0 (6.0–19.0)	7.0 (6.0–12.0)
No. of joints with limitation of motion	8.0 (4.0–15.0)	8.0 (4.0–11.0)
Physician global assessment	48.0 (31.0–67.0)	50.0 (35.0–60.0)
Parent's global assessment‡	47.8 (24.1–68.0)	42.1 (17.9–54.7)
C-HAQ DI‡	0.9 (0.4–1.5)	1.2 (0.8–1.6)
CRP, mg/dl§	0.2 (0.1–0.9)	0.1 (0.1–1.4)
JADAS-71–CRP, median (IQR)¶	21.0 (13.5–30.3)	18.1 (14.0–23.1)
MTX use at baseline	136 (78.6)	37 (80.4)
MTX dose at baseline, median (IQR) mg/m^2/week	11.6 (9.7–14.4)	13.3 (10.9–15.3)
Route of MTX administration		
Oral	76 (43.9)	18 (39.1)
Parenteral#	60 (34.7)	19 (41.3)
Oral corticosteroid use at baseline**	56 (32.4)	9 (19.6)
Oral prednisone (or equivalent) dose at baseline, median (IQR) mg/kg/day††	0.1 (0.1–0.2)	0.2 (0.2–0.4)
Prior biologic use‡‡	46 (26.6)	10 (21.7)

* Except where indicated otherwise, values are the number (%) of patients. Cohort 1 consisted of patients ages 6–17 years, and cohort 2 consisted of patients ages 2–5 years. JIA = juvenile idiopathic arthritis; IQR = interquartile range; RF = rheumatoid factor; JIA-ACR = JIA–American College of Rheumatology criteria for improvement; C-HAQ DI = Childhood Health Assessment Questionnaire disability index; JADAS-71–CRP = Juvenile Arthritis Disease Activity Score in 71 joints using the C-reactive protein level; MTX = methotrexate.
† Protocol violation.
‡ In cohort 1, n = 172.
§ Normal ≤0.6 mg/dl.
¶ In cohort 1, n = 171.
\# Includes subcutaneous and intramuscular administration.
** Prednisone or prednisolone.
†† In cohort 1, n = 52; in cohort 2, n = 8.
‡‡ Adalimumab, etanercept, or tocilizumab.

Effectiveness. In both cohorts, robust JIA-ACR responses were observed as early as month 1 (Figures 3A and B) (for "as observed" analysis, see Supplementary Materials). At month 4, JIA-ACR 30 response rates were 83% and 89% in cohorts 1 (n = 173) and 2 (n = 46), respectively. JIA-ACR 30 response rates in cohorts 1 and 2, respectively, were 75% and 96% at month 21, and 58% and 100% at month 24. Higher-level JIA-ACR response rates increased steadily to month 21 (see Figures 3A and B, and Supplementary Materials, available at http://online library.wiley.com/doi/10.1002/art.40466/abstract). Inactive disease status was achieved at month 4 by 30% and 50% of patients in cohorts 1 and 2, respectively. JIA-ACR responses were in line with JADAS-71–CRP scores, per the "as-observed" analysis, reflecting low disease activity in 42.8% and 90.9% of patients in cohorts 1 and 2,
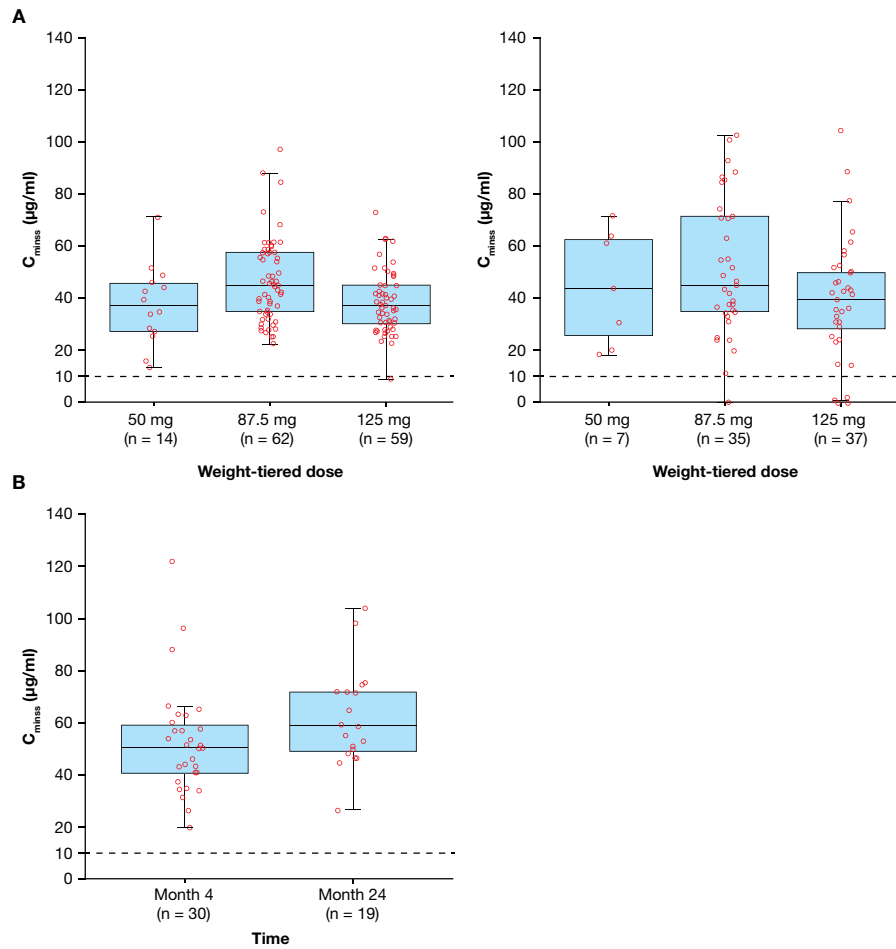
Figure 2. Abatacept steady-state trough concentration (C_{minss}) in patients ages 6–17 years (cohort 1) by weight group (**A**) at month 4 (left) and month 24 (right), and patients ages 2–5 years (cohort 2) at months 4 and 24 (**B**). C_{minss} was summarized for treated patients (≥1 dose of study medication) with evaluable pharmacokinetic measurements at each time point. Data are shown as box plots. Each symbol represents a single subject. Boxes represent the upper and lower interquartile range. Lines inside the boxes represent the median. Whiskers represent the 5th and 95th percentiles. Dashed lines indicate the target therapeutic concentration.

respectively, at month 24. The median JADAS-71–CRP values were below the cutoff value for low disease activity in polyarthritis by month 7 in cohort 1 and by month 3 in cohort 2; these values reached the lowest level of 1.3 at month 24 in cohort 1, and of 0.5 at month 19 in cohort 2 (Figures 4A and B). In cohort 1, all 6 JIA-ACR core set variables, including C-HAQ DI and parent's global assessment of patient overall well-being, improved over time and these values were maintained until the end of the study (see Supplementary Materials, available on the *Arthritis & Rheumatology* web site at http://onlinelibrary.wiley.com/doi/10.1002/art.40466/abstract). Additional results of JIA category analyses (cohort 1) can also be found in the Supplementary Materials.

Safety and immunogenicity. In total, 309.8 and 71.0 patient-years of follow-up were available from the

safety populations in cohorts 1 and 2, respectively. As shown in Table 2, abatacept was well tolerated in both cohorts throughout the study. AEs occurred in 152 patients (87.9%) in cohort 1 and in 43 patients (93.5%) in cohort 2. SAEs occurred in 14 patients (8.1%) in cohort 1 and 3 (6.5%) in cohort 2. In cohort 1, the incidence rates of AEs and SAEs per 100 patient-years of exposure were 173.0 (95% CI 147.6–202.8) and 4.7 (95% CI 2.8–7.9), respectively. Two SAEs were considered related to the study drug: sepsis (n = 1; severe intensity) in cohort 1 and overdose (n = 1; mild intensity) in cohort 2, in a patient in whom a higher abatacept dose was administered due to misclassification of weight tier. One malignancy, stage III ovarian germ cell teratoma (severe intensity) was reported in cohort 1 on study day 99, but was considered by the investigator to

A

JIA-ACR 30	0	59.5	73.4	80.9	83.2	79.2	80.3	78.6	77.5	73.4	74.6	58.4
JIA-ACR 50	0	43.4	59.5	71.1	72.8	76.9	77.5	75.1	74.6	72.8	72.3	56.1
JIA-ACR 70	0	16.2	37.0	54.3	52.6	61.3	69.9	67.6	67.1	65.3	63.0	52.6
JIA-ACR 90	0	6.4	15.0	22.5	28.3	34.7	46.2	51.4	55.5	52.6	48.0	41.0
Inactive disease	0	5.8	17.3	24.9	30.1	34.1	43.4	43.9	46.2	46.2	46.2	35.8
Patients evaluated, n	173	173	173	173	173	173	173	173	173	173	173	173

B

JIA-ACR 30	0	62.5	84.8	89.1	89.1	95.3	94.9	96.8	92.6	96.3	96.2	100
JIA-ACR 50	0	52.2	80.4	87.0	84.8	95.3	94.9	96.8	92.6	96.3	96.2	100
JIA-ACR 70	0	32.6	67.4	73.9	73.9	83.7	92.3	93.5	88.9	96.3	96.2	100
JIA-ACR 90	0	15.2	39.1	50.0	58.7	72.1	87.2	80.6	81.5	88.9	88.5	90.9
Inactive disease	0	23.9	43.5	41.3	50.0	65.1	65.8	66.7	70.4	73.1	73.1	77.3
Patients evaluated, n												
JIA-ACR	46	46	46	46	46	43	39	31	27	27	26	22
Inactive disease	46	46	46	46	46	43	38	30	27	26	26	22

Figure 3. Juvenile Idiopathic Arthritis–American College of Rheumatology (JIA-ACR) 30, 50, 70, 90 improvement criteria response rates over time for patients ages 6–17 years (cohort 1; intent-to-treat [ITT] population analysis) (**A**) and patients ages 2–5 years (cohort 2; ITT population analysis to month 4 [study part 1], "as-observed" population analysis thereafter to month 24 [study part 2]) (**B**). Bars show the 95% confidence intervals. The apparent decrease in response rates at month 24 in cohort 1 reflects a decreased number of patients with available data at this time point and the associated increased proportion of patients imputed as nonresponders due to missing values.

be unrelated to the study drug. Three autoimmune disorders (none of which were considered related to the study drug) were reported in cohort 1: pediatric autoimmune neuropsychiatric disorder associated with streptococcal infection (mild intensity) on study day 71, psoriasis (mild intensity) on study day 327, and Takayasu arteritis (moderate intensity) on study day

416. There were no reported cases of malignancies or autoimmune disorders in cohort 2.

Local injection site reactions were of mild or moderate intensity and occurred in 12 patients (6.9%) in cohort 1 and 2 (4.3%) in cohort 2 (none of which led to discontinuation). Seven local injection site reactions of moderate intensity occurred in 3 patients in cohort 1, and

1 patient required treatment. The overall rates of patients with infections in cohorts 1 and 2, respectively, were 68.2% and 78.3%. All marked laboratory abnormalities were mild or moderate, and no deaths occurred during the study (for further details, see Supplementary Materials, available on the *Arthritis & Rheumatology* web site at http://onlinelibrary.wiley.com/doi/10.1002/art.40466/abstract).

Overall, 4 of 172 patients (2.3%) in cohort 1, and 4 of 46 (8.7%) in cohort 2 developed antibodies reactive with abatacept while receiving treatment during the cumulative period, but antibody positivity did not persist. The presence of these antibodies had no apparent effect on PK, effectiveness, or safety (see Supplementary Materials, available at http://onlinelibrary.wiley.com/doi/10.1002/art.40466/abstract).
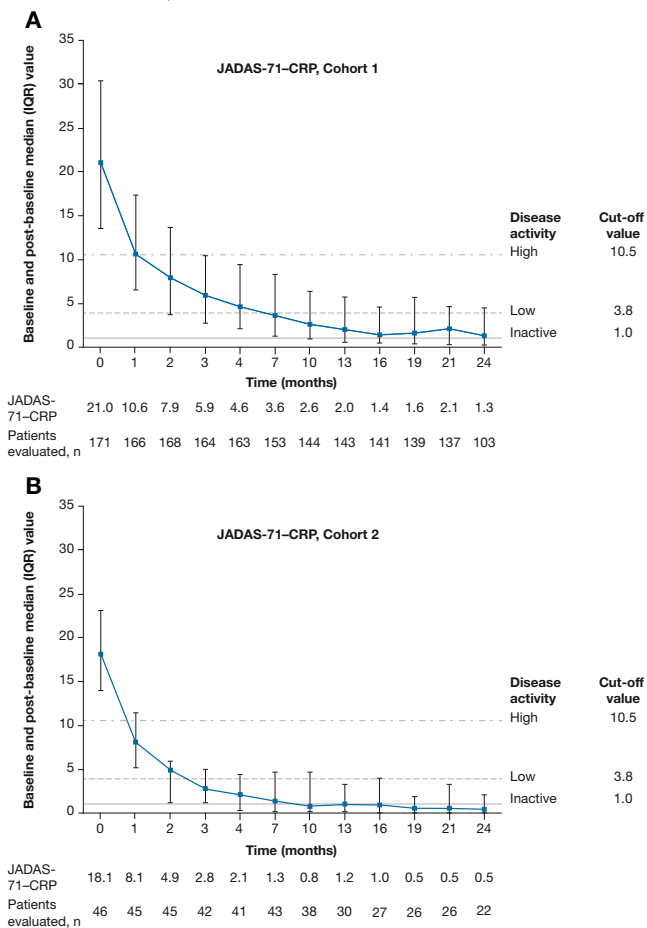
Figure 4. Baseline and post-baseline Juvenile Arthritis Disease Activity Score in 71 joints using the C-reactive protein level (JADAS-71–CRP) in cohort 1 (**A**) and cohort 2 (**B**). Values are the median and interquartile range. JADAS-71–CRP variables included number of active joints, physician's global assessment of disease activity, parent's global assessment of patient well-being, and laboratory measurement of inflammation, as measured by CRP. Dashed lines show the JADAS-71–CRP cutoff values for inactive disease, low disease activity, and high disease activity (1, 3.8, and 10.5, respectively) (33,35).

Table 2. Adverse events over the 24-month cumulative period (all treated patients)*

Event	Cohort 1 (n = 173)	Cohort 2 (n = 46)
Exposure, patient-years	309.8	71.0
Deaths	0	0
SAEs†	14 (8.1)	3 (6.5)
Treatment-related SAEs‡	1 (0.6)	1 (2.2)
Discontinuations due to SAEs	4 (2.3)§	0
Incidence rate, per 100 patient-years	4.68	4.41
AEs (including SAEs)	152 (87.9)	43 (93.5)
Treatment-related AEs	54 (31.2)	27 (58.7)
Discontinuations due to AEs¶	7 (4.0)	1 (2.2)
Incidence rate, per 100 patient-years	173.03	426.44
AEs of special interest#		
Malignancies	1 (0.6)	0
Autoimmune disorders	3 (1.7)	0
Local injection-site reactions/pain	12 (6.9)	2 (4.3)
Infections	118 (68.2)	36 (78.3)

* Except where indicated otherwise, values are the number (%) of patients.
† In cohort 1, serious adverse events (SAEs) included sepsis, abdominal pain, and upper respiratory tract infection (all 3 of which occurred in 1 patient), hypomagnesemia and stage III ovarian germ cell teratoma (both occurred in 1 patient), appendicitis, pneumonia, pyelonephritis, concussion, radius fracture, urinary calculus, nephrolithiasis, anemia, vertigo, chest pain, synovitis, and autonomic nervous system imbalance; in cohort 2, SAEs included overdose, tendon disorder, and febrile convulsion (each in 1 patient).
‡ Treatment-related SAEs included sepsis of severe intensity in cohort 1 and an overdose of mild intensity (administration of a higher abatacept dose due to misclassification by weight tier) in cohort 2.
§ Includes discontinuations due to the following SAEs: sepsis, vertigo, stage III ovarian germ cell teratoma, and autonomic nervous system imbalance.
¶ Discontinuations due to sepsis, vertigo, stage III ovarian germ cell teratoma, autonomic nervous system imbalance, exanthema, fatigue, and aphthous ulcer in cohort 1; and pyrexia, rhinitis, and cough (all in 1 patient) in cohort 2.
# No opportunistic infections (including extrapulmonary tuberculosis and herpes zoster) related to study drug occurred in either cohort during the study. In cohort 1, stage III ovarian germ cell teratoma was the only malignancy; autoimmune disorders included pediatric autoimmune neuropsychiatric disorders associated with streptococcal infections, psoriasis, and Takayasu arteritis.

DISCUSSION

In this phase III study of weekly weight-tiered SC abatacept in patients with polyarticular JIA, the primary end point of abatacept C_{minss} at month 4 in patients ages 6–17 years was shown to be consistently above the planned minimal target therapeutic exposure of C_{minss} 10 µg/ml, without compromising patient safety. The target therapeutic exposure was achieved at month 4 across all weight groups in cohort 1, and overall in cohort 2. SC abatacept was effective and improved function and patient well-being over the 24-month cumulative treatment period in both cohorts, with a low rate of discontinuation due to AEs.

The PK data confirm the feasibility of a weekly weight-tiered SC abatacept treatment regimen for

polyarticular JIA in patients ages 2–17 years old (see Supplementary Materials, http://onlinelibrary.wiley.com/doi/10.1002/art.40466/abstract). The observed C_{minss} values were within the ranges of exposure previously found for IV abatacept (10 mg/kg) in patients with JIA (23) and in adults with RA receiving IV or SC abatacept treatment (36) (also see Supplementary Materials). Abatacept C_{minss} values at months 4 and 24 were comparable, demonstrating that the target therapeutic exposure is maintained with continued treatment.

The robust JIA-ACR response rates and improvements in JADAS-71–CRP scores to month 24 demonstrated in our study support the use of weekly weight-tiered SC abatacept therapy in patients with polyarticular JIA. In both cohorts, an early onset of treatment response was observed, with responses maintained throughout the study. In cohort 1, analysis of the 6 JIA-ACR core variables revealed a beneficial effect of SC abatacept on function (C-HAQ DI) and well-being (parent's global assessment of patient overall well-being).

SC abatacept was well tolerated in both cohorts, with no new safety concerns observed. Safety and immunogenicity profiles were similar in cohorts 1 and 2. Although the rate of infections was higher than that observed in a study of adult patients with RA who were treated with abatacept (16), this finding was somewhat expected due to a known greater susceptibility of children to infections as compared with adults. Notably, there were no reported opportunistic infections related to abatacept treatment in patients with polyarticular JIA, even in countries with a high burden of tuberculosis, which is consistent with observations in adults with RA who receive abatacept treatment (37). In addition, there were no malignancies or autoimmune disorders in cohort 2, and the rate of these events was minimal in cohort 1. The safety of SC abatacept was largely consistent with that of IV abatacept in polyarticular JIA (2,9,13).

Tolerability of SC injections is of special concern in pediatric patients. In this study, SC abatacept treatment yielded an overall low rate of local injection site reactions, most of which were mild—only a few moderate and no severe reactions were reported. Notably, no local injection site reactions led to treatment discontinuation. Fewer patients developed anti-abatacept antibodies while receiving SC abatacept treatment compared with IV abatacept treatment (2); this was somewhat expected given that similar trends were observed in a study of adult patients with RA who received SC or IV abatacept plus MTX and had inadequate responses to MTX (22). This finding was also possibly related to the concomitant use of MTX in ≥75% of patients in the current study and differences in study designs.

The effectiveness of SC abatacept treatment demonstrated in the current study constitutes a conservative interpretation of the data. Despite the observational character of the study, an ITT analysis was performed for the cumulative period in cohort 1 and up to month 4 in cohort 2, in which patients discontinuing the study prior to month 24 or not having data available at this time point were imputed as nonresponders.

Abatacept is seldom used to treat polyarticular JIA early in the disease course. The results from cohort 2 in this study, in which abatacept treatment was initiated in patients with a median disease duration of only 0.5 years, provide valuable data regarding the early introduction of abatacept therapy; notably, JIA-ACR response rates were consistently higher in cohort 2 than in cohort 1.

The study has some limitations, including the open-label design and a protocol violation, in which a few patients with undifferentiated and persistent oligoarthritis entered the trial despite not meeting the eligibility criteria. Additionally, the use of concomitant medications such as MTX and corticosteroids, as well as prior use of biologic DMARDs (including TNFi) in some patients, may have had confounding effects. However, the sample sizes of the corresponding subgroups were too small to analyze.

In conclusion, weight-tiered weekly SC abatacept was effective in patients with polyarticular JIA, with no new safety concerns identified. These data suggest that SC abatacept provides an effective and well-tolerated treatment option for patients with polyarticular JIA, with the additional benefit of the convenience associated with self or parent/caregiver administration of the treatment.

ACKNOWLEDGMENTS

AUTHOR CONTRIBUTIONS

All authors were involved in drafting the article or revising it critically for important intellectual content, and all authors approved the final version to be published.

Dr. Brunner had full access to all of the data in the study and takes responsibility for the integrity of the data and the accuracy of the data analysis.

Study conception and design. Brunner, Lovell, Martini, Ruperto, Wong.
Acquisition of data. Brunner, Tzaribachev, Vega-Cornejo, Louw, Berman, Calvo Penadés, Antón, Ávila-Zapata, Cuttica, Horneff, Foeldvari, Keltsev, Kingsbury, Viola, Joos, Lauwerys, Paz Gastañaga, Rama, Wouters, Bohnsack, Breedt, Fischbach, Lutz, Minden, Miraval, Ally, Rubio-Pérez, Solau Gervais, van Zyl, Lovell, Ruperto.

Analysis and interpretation of data. Brunner, Tzaribachev, Vega-Cornejo, Louw, Berman, Calvo Penadés, Antón, Ávila-Zapata, Cuttica, Horneff, Foeldvari, Keltsev, Kingsbury, Viola, Joos, Lauwerys, Paz Gastañaga, Rama, Wouters, Bohnsack, Breedt, Fischbach, Lutz, Minden, Miraval, Ally, Rubio-Pérez, Solau Gervais, van Zyl, Li, Nys, Wong, Banerjee, Lovell, Martini, Ruperto.

ROLE OF THE STUDY SPONSOR

The study was designed jointly by academic authors and Bristol-Myers Squibb, with data collected by PRINTO/PRCSG investigators. The first and subsequent versions of the manuscript were written, edited, and revised critically by academic authors. Bristol-Myers Squibb facilitated the study design and reviewed and approved the manuscript prior to submission. All authors independently collected the data, interpreted the results, had the final decision to submit the manuscript for publication, and had the right to accept or reject comments or suggestions. Writing assistance was funded by Bristol-Myers Squibb. Publication of this article was not contingent upon approval by Bristol-Myers Squibb.

REFERENCES

1. Ravelli A, Martini A. Juvenile idiopathic arthritis. Lancet 2007;369:767–78.
2. Ruperto N, Lovell DJ, Quartier P, Paz E, Rubio-Pérez N, Silva CA, et al. Long-term safety and efficacy of abatacept in children with juvenile idiopathic arthritis. Arthritis Rheum 2010;62:1792–802.
3. Webb K, Wedderburn LR. Advances in the treatment of poly-articular juvenile idiopathic arthritis. Curr Opin Rheumatol 2015;27:505–10.
4. Petty RE, Southwood TR, Manners P, Baum J, Glass DN, Goldenberg J, et al. International League of Associations for Rheumatology classification of juvenile idiopathic arthritis: second revision, Edmonton, 2001. J Rheumatol 2004;31:390–2.
5. Rosenberg AM, Oen KG. Polyarticular juvenile idiopathic arthritis. In: Petty RE, Laxer RM, Lindsley CB, Wedderburn LR, editors. Textbook of pediatric rheumatology. 7th ed. Philadelphia: Elsevier Health Sciences; 2015. p. 217.
6. Beukelman T, Patkar NM, Saag KG, Tolleson-Rinehart S, Cron RQ, DeWitt EM, et al. 2011 American College of Rheumatology recommendations for the treatment of juvenile idiopathic arthritis: initiation and safety monitoring of therapeutic agents for the treatment of arthritis and systemic features. Arthritis Care Res (Hoboken) 2011;63:465–82.
7. Brunner HI, Ruperto N, Zuber Z, Keane C, Harari O, Kenwright A, et al. Efficacy and safety of tocilizumab in patients with poly-articular-course juvenile idiopathic arthritis: results from a phase 3, randomised, double-blind withdrawal trial. Ann Rheum Dis 2015;74:1110–7.
8. Brunner HI, Ruperto N, Tzaribachev N, Horneff G, Chasnyk VG, Panaviene V, et al. Subcutaneous golimumab for children with active polyarticular-course juvenile idiopathic arthritis: results of a multicentre, double-blind, randomised-withdrawal trial. Ann Rheum Dis 2018;77:21–9.
9. Lovell D, Ruperto N, Mouy R, Paz E, Rubio-Pérez N, Silva CA, et al. Long-term safety, efficacy, and quality of life in patients with juvenile idiopathic arthritis treated with intravenous abatacept for up to seven years. Arthritis Rheumatol 2015;67:2759–70.
10. Lovell DJ, Giannini EH, Reiff A, Cawkwell GD, Silverman ED, Nocton JJ, et al, for the Pediatric Rheumatology Collaborative Study Group. Etanercept in children with polyarticular juvenile rheumatoid arthritis. N Engl J Med 2000;342:763–9.
11. Lovell DJ, Ruperto N, Goodman S, Reiff A, Jung L, Jarosova K, et al. Adalimumab with or without methotrexate in juvenile rheumatoid arthritis. N Engl J Med 2008;359:810–20.
12. Ruperto N, Lovell DJ, Cuttica R, Wilkinson N, Woo P, Espada G, et al. A randomized, placebo-controlled trial of infliximab plus methotrexate for the treatment of polyarticular-course juvenile rheumatoid arthritis. Arthritis Rheum 2007;56:3096–106.
13. Ruperto N, Lovell DJ, Quartier P, Paz E, Rubio-Perez N, Silva CA, et al. Abatacept in children with juvenile idiopathic arthritis: a randomised, double-blind, placebo-controlled withdrawal trial. Lancet 2008;372:383–91.
14. Silverman E, Spiegel L, Hawkins D, Petty R, Goldsmith D, Schanberg L, et al. Long-term open-label preliminary study of the safety and efficacy of leflunomide in patients with polyarticular-course juvenile rheumatoid arthritis. Arthritis Rheum 2005;52:554–62.
15. Silverman E, Mouy R, Spiegel L, Jung LK, Saurenmann RK, Lahdenne P, et al. Leflunomide or methotrexate for juvenile rheumatoid arthritis. N Engl J Med 2005;352:1655–66.
16. Genovese MC, Schiff M, Luggen M, Becker JC, Aranda R, Teng J, et al. Efficacy and safety of the selective co-stimulation modulator abatacept following 2 years of treatment in patients with rheumatoid arthritis and an inadequate response to anti-tumour necrosis factor therapy. Ann Rheum Dis 2008;67:547–54.
17. Orencia (abatacept) prescribing information. Princeton (NJ): Bristol-Myers Squibb; 2017. URL: http://packageinserts.bms.com/pi/pi_orencia.pdf.
18. Mease PJ, Gottlieb AB, van der Heijde D, FitzGerald O, Johnsen A, Nys M, et al. Efficacy and safety of abatacept, a T-cell modulator, in a randomised, double-blind, placebo-controlled, phase III study in psoriatic arthritis. Ann Rheum Dis 2017;76:1550–8.
19. Kremer JM, Genant HK, Moreland LW, Russell AS, Emery P, Abud-Mendoza C, et al. Results of a two-year follow up study of patients with rheumatoid arthritis who received a combination of abatacept and methotrexate. Arthritis Rheum 2008;58:953–63.
20. Westhovens R, Kremer JM, Moreland LW, Emery P, Russell AS, Li T, et al. Safety and efficacy of the selective costimulation modulator abatacept in patients with rheumatoid arthritis receiving background methotrexate: a 5-year extended phase IIB study. J Rheumatol 2009;36:736–42.
21. Lovell D, Ruperto N, Tzaribachev N, Zeft A, Cimaz R, Stanevica V, et al. Long-term effectiveness and safety of abatacept in juvenile idiopathic arthritis: interim results from the abatacept in JIA registry [abstract]. Arthritis Rheumatol 2016;68 Suppl 10. URL: http://acrabstracts.org/abstract/long-term-effectiveness-and-safety-of-abatacept-in-juvenile-idiopathic-arthritis-interim-results-from-the-abatacept-in-jia-registry-2/.
22. Genovese MC, Covarrubias A, Leon G, Mysler E, Keiserman M, Valente R, et al. Subcutaneous abatacept versus intravenous abatacept: a phase IIIb noninferiority study in patients with an inadequate response to methotrexate. Arthritis Rheum 2011;63:2854–64.
23. Li X, Passarell JA, Lin K, Roy A, Murthy B, Girgis IG. Population pharmacokinetics and exposure-response analyses for abatacept in juvenile idiopathic arthritis [poster]. Presented at the American Conference on Pharmacometrics (ACoP8); 2017 October 15–18; Fort Lauderdale, FL.
24. Zhou Z, Roy A, Murthy B, Gao L, Teng J, Kaul S, et al. Relationship between systemic exposure and the efficacy and safety of abatacept administered subcutaneously and intravenously in adult rheumatoid arthritis patients [poster]. Presented at the American Association of Pharmaceutical Scientists National Biotechnology Conference; 2011 May 16–18; San Francisco, CA.
25. Ruperto N, Lovell DJ, Tzaribachez N, Vega-Cornejo G, Louw I, Berman A, et al. Subcutaneous abatacept in patients with polyarticular juvenile idiopathic arthritis and inadequate response to biologic or non-biologic disease-modifying antirheumatic drugs: pharmacokinetics, efficacy and safety. Ann Rheum Dis 2016;75:138.
26. Bristol-Myers Squibb, sponsor. A phase 3 multi-center, open-label study to evaluate pharmacokinetics, efficacy and safety of abatacept administered subcutaneously (SC) in children and adolescents with active polyarticular juvenile idiopathic arthritis (pJIA) and inadequate response (IR) to biologic or non biologic disease modifying anti-rheumatic drugs (DMARDs). ClinicalTrials.gov identifier: NCT01844518; 2013.

27. Ruperto N, Martini A. Networking in paediatrics: the example of the Paediatric Rheumatology International Trials Organisation (PRINTO). Arch Dis Child 2011;96:596–601.

28. Giannini EH, Ruperto N, Ravelli A, Lovell DJ, Felson DT, Martini A. Preliminary definition of improvement in juvenile arthritis. Arthritis Rheum 1997;40:1202–9.

29. World Medical Association Declaration of Helsinki (1964). Recommendations guiding physicians in biomedical research involving human subjects. BMJ 1996;313:1448.

30. Haggerty HG, Abbott MA, Reilly TP, DeVona DA, Gleason CR, Tay L, et al. Evaluation of immunogenicity of the T cell costimulation modulator abatacept in patients treated for rheumatoid arthritis. J Rheumatol 2007;34:2365–73.

31. Wallace CA, Giannini EH, Huang B, Itert L, Ruperto N, for the Childhood Arthritis and Rheumatology Research Alliance (CARRA), the Pediatric Rheumatology Collaborative Study Group (PRCSG), and the Paediatric Rheumatology International Trials Organisation (PRINTO). American College of Rheumatology provisional criteria for defining clinical inactive disease in select categories of juvenile idiopathic arthritis. Arthritis Care Res (Hoboken) 2011;63:929–36.

32. Ruperto N, Ravelli A, Pistorio A, Malattia C, Cavuto S, Gado-West L, et al. Cross-cultural adaptation and psychometric evaluation of the Childhood Health Assessment Questionnaire (CHAQ) and the Child Health Questionnaire (CHQ) in 32 countries: review of the general methodology. Clin Exp Rheumatol 2001;19:S1–S9.

33. Nordal EB, Zak M, Aalto K, Berntson L, Fasth A, Herlin T, et al. Validity and predictive ability of the juvenile arthritis disease activity score based on CRP versus ESR in a Nordic population-based setting. Ann Rheum Dis 2012;71:1122–7.

34. Consolaro A, Ruperto N, Bazso A, Pistorio A, Magni-Manzoni S, Filocamo G, et al. Development and validation of a composite disease activity score for juvenile idiopathic arthritis. Arthritis Rheum 2009;61:658–66.

35. Consolaro A, Bracciolini G, Ruperto N, Pistorio A, Magni-Manzoni S, Malattia C, et al. Remission, minimal disease activity, and acceptable symptom state in juvenile idiopathic arthritis: defining criteria based on the juvenile arthritis disease activity score. Arthritis Rheum 2012;64:2366–74.

36. Iwahashi M, Inoue H, Matsubara T, Tanaka T, Amano K, Kanamono T, et al. Efficacy, safety, pharmacokinetics, and immunogenicity of abatacept administered subcutaneously or intravenously in Japanese patients with rheumatoid arthritis and

37. Louw I, Ally M, Janse van Rensburg DC, van Duuren E, Nel D, Miller-Janson H, et al. Retention of use and safety of subcutaneous abatacept in rheumatoid arthritis: a patient record assessment in a compassionate use programme in South Africa, a tuberculosis endemic country [abstract]. Arthritis Rheumatol 2016;68 Suppl 10. URL: http://acrabstracts.org/abstract/retention-of-use-and-safety-of-subcutaneous-abatacept-in-rheumatoid-arthritis-a-patient-record-assessment-in-a-compassionate-use-programme-in-south-africa-a-tuberculosis-endemic-country/.

inadequate response to methotrexate: a Phase II/III, randomized study. Mod Rheumatol 2014;24:885–91.

APPENDIX A: STUDY INVESTIGATORS

The following investigators participated in the study: Mara L Becker (The Children's Mercy Hospital and Clinics, Kansas City, MO), Norman T Ilowite (Montefiore Medical Center, Bronx, NY), Jason A Dare (Arkansas Children's Hospital, Little Rock), Paula K Morris (Arkansas Children's Hospital, Little Rock), Timothy G Beukelman (The Children's Hospital of Alabama, Birmingham), Linda Wagner-Weiner (The University of Chicago, Chicago, Illinois), Lawrence Zemel (Connecticut Children's Medical Center, Hartford), Pierre Quartier (Groupe Hospitalier Necker-Enfants Malades, Paris, France), Isabelle Kone-Paut (CHU de Bicêtre Service de pédiatrie, Kremlin-Bicêtre Cedex, France), Alexandre Belot (Hôpital Femme Mère Enfant, Lyon, France), Valeria Gerloni (Istituto Ortopedico Gaetano Pini, Milan, Italy), Manuel Ferrandiz (Instituto Nacional de Salúd del Niño, Breña, Peru), Dina Janse Van Rensburg (Emmed Research, Eloffsdal, South Africa), Iloite Maria Scheibel (Hospital Nossa Senhora De Conceição, Porto Alegre, Brazil), Claudia Goldstein-Schainberg (Hospital das Clínicas da Faculdade de Medicina da USP, São Paulo, Brazil), Clovis Silva (Hospital das Clínicas da Faculdade de Medicina da USP, São Paulo, Brazil), Maria Teresa Sande e Lemos Ascensao Terreri (UNIFESP-Universidade Federal de São Paulo, São Paulo, Brazil), Maria Gamir (Hospital Universitario Ramón y Cajal, Madrid, Spain), Ruben Burgos Vargas (Hospital General de México, Mexico City, Mexico), Enrique Faugier Fuentes (Hospital Infantil de México Federico Gómez, Mexico City, Mexico), Rolando Cimaz (Ospedale Pediatrico Anna Meyer, Florence, Italy), Maria Alessio (Università degli Studi di Napoli Federico II, Naples, Italy) and Graciela Espada (Hospital de Niños Dr Ricardo Gutiérrez, Buenos Aires, Argentina).

Identification of an Amino Acid Motif in HLA–DRβ1 That Distinguishes Uveitis in Patients With Juvenile Idiopathic Arthritis

Anne-Mieke J. W. Haasnoot,[1] Marco W. Schilham,[2] Sylvia Kamphuis,[3] Petra C. E. Hissink Muller,[2] Arnd Heiligenhaus,[4] Dirk Foell,[5] Kirsten Minden,[6] Roel A. Ophoff,[7] Timothy R. D. J. Radstake,[1] Anneke I. Den Hollander,[8] Tjitske H. C. M. Reinards,[2] Sanne Hiddingh,[1] Nicoline E. Schalij-Delfos,[2] Esther P. A. H. Hoppenreijs,[8] Marion A. J. van Rossum,[9] Carine Wouters,[10] Rotraud K. Saurenmann,[11] J. Merlijn van den Berg,[12] Nico M. Wulffraat,[1] ICON-JIA Study Group, Rebecca ten Cate,[2] Joke H. de Boer,[1] Sara L. Pulit,[13] and Jonas J. W. Kuiper[1]

Objective. Uveitis is a visually debilitating disorder that affects up to 30% of children with the most common forms of juvenile idiopathic arthritis (JIA). The disease mechanisms predisposing only a subgroup of children to uveitis are unknown. This study was undertaken to identify genetic susceptibility loci for uveitis in JIA, using a genome-wide association study in 522 children with JIA.

Methods. Two cohorts of JIA patients with ophthalmologic follow-up data were genotyped. Data were then imputed using a genome-wide imputation reference panel, and an HLA-specific reference panel was used for imputing amino acids and HLA types in the major histocompatibility complex (MHC). After imputation, genome-wide and MHC-specific analyses were performed, and a reverse immunology approach was utilized to model antigen presentation at 13 common HLA–DRβ1 alleles.

Results. Presence of the amino acid serine at position 11 (serine 11) in *HLA–DRβ1* was associated with an increased risk of uveitis in JIA patients (odds ratio [OR] 2.60, $P = 5.43 \times 10^{-10}$) and was specific to girls ($P_{females} = 7.61 \times 10^{-10}$ versus $P_{males} = 0.18$). Serine 11 resides in the YST motif in the peptide-binding groove of HLA–DRβ1; all 3 amino acids in this motif are in perfect linkage disequilibrium and show identical association with disease. Quantitative prediction of binding affinity revealed that HLA–DRβ1 alleles with the YST motif could be distinguished on the basis of discernable peptide-binding preferences.

[1]Anne-Mieke J. W. Haasnoot, MD, Timothy R. D. J. Radstake, MD, PhD, Sanne Hiddingh, Nico M. Wulffraat, MD, PhD, Joke H. de Boer, MD, PhD, Jonas J. W. Kuiper, PhD: University Medical Center Utrecht, Utrecht University, Utrecht, The Netherlands; [2]Marco W. Schilham, PhD, Petra C. E. Hissink Muller, PhD, Tjitske H. C. M. Reinards, MD, Nicoline E. Schalij-Delfos, MD, PhD, Rebecca ten Cate, MD, PhD: Leiden University Medical Center, Leiden, The Netherlands; [3]Sylvia Kamphuis, MD, PhD: Sophia Children's Hospital, Erasmus University Medical Center, Rotterdam, The Netherlands; [4]Arnd Heiligenhaus, MD, PhD: St. Franziskus-Hospital, Muenster, Germany, and University of Duisburg, Essen, Germany; [5]Dirk Foell, MD: University of Muenster, Muenster, Germany; [6]Kirsten Minden, MD, PhD: German Rheumatism Research Center Berlin-Leibniz Institute and Charite University Medicine, Berlin, Germany; [7]Roel A. Ophoff, PhD: University Medical Center Utrecht, Utrecht, The Netherlands, and University of California, Los Angeles; [8]Anneke I. Den Hollander, PhD, Esther P. A. H. Hoppenreijs, MD: Radboud University Medical Center, Nijmegen, The Netherlands; [9]Marion A. J. van Rossum, MD, PhD: Emma Children's Hospital AMC and Amsterdam Rheumatology and Immunology Center Reade, Amsterdam, The Netherlands; [10]Carine Wouters, MD, PhD: University of Leuven and University Hospitals Leuven, Leuven, Belgium; [11]Rotraud K. Saurenmann, MD, PhD: University Children's Hospital, Zurich, Switzerland; [12]J. Merlijn van den Berg, MD, PhD: Emma Children's Hospital AMC and University of Amsterdam, Amsterdam, The Netherlands; [13]Sara L. Pulit, PhD: University Medical Center Utrecht, Utrecht, The Netherlands, and Oxford University, Oxford, UK.

Drs. de Boer, Pulit, and Kuiper contributed equally to this work.

Conclusion. **These findings highlight a genetically distinct, sexually dimorphic feature of JIA with uveitis as compared to JIA without uveitis. The association could be indicative of the potential involvement of antigen presentation by HLA–DRβ1 in the development of uveitis in JIA. The results of this study may advance our progress toward improved treatments for, and possible prevention of, the sight-threatening complications of uveitis in children with JIA.**

Juvenile idiopathic arthritis (JIA) is the most common chronic rheumatic disease in childhood, affecting ~16–150 per 100,000 individuals (1). As many as 1 in 3 children diagnosed as having one of the most common categories of JIA, either oligoarticular JIA or rheumatoid factor (RF)–negative polyarticular JIA, develop chronic anterior uveitis. Uveitis in JIA specifically is a chronic inflammatory eye disease, and is the most frequent extraarticular manifestation of JIA (2). Uveitis threatens the sight of those affected, and can result in complications, including band keratopathy, cataracts, glaucoma, macular edema, and, in severe cases, hypotony (2). Because it typically afflicts children younger than age 7 years, uveitis can dramatically impact the quality of life of children and can continue to impact patients into adulthood (2,3).

Early detection and adequate ophthalmologic management of JIA-associated uveitis are critical to prevent sight-threatening complications (4,5). Despite its severity, chronic anterior uveitis is typically insidious in onset and often becomes symptomatic only after irreversible damage has occurred. Consequently, rigorous ophthalmologic screening of all JIA patients is required for early detection and prompt treatment of uveitis associated with JIA (6). Despite screening, severe ocular complications may already be present at the time of the uveitis diagnosis.

JIA and uveitis are complex, multifactorial autoimmune disorders with both genetic and environmental risk factors (2,3,7). Genome-wide association studies (GWAS) in JIA (regardless of uveitis status) have revealed a number of loci associated with the disease (8–10), which, collectively, can explain ~20% of the phenotypic variation (8). A number of HLA alleles have also been identified as factors that increase the risk of JIA-associated uveitis compared to an unaffected control group (11). However, genome-wide genetic markers that distinguish JIA without uveitis from JIA with uveitis remain elusive. Furthermore, whereas girls comprise the majority of JIA patients (female-to-male ratio ~2:1) (12), the extent to which the biologic risk of developing uveitis in JIA is sexually dimorphic is unknown (12).

In the present study, we performed genotyping and imputation of the major histocompatibility complex (MHC) in 192 patients with JIA-associated uveitis and 330 JIA patients without uveitis (hereafter referred to as non-uveitis JIA controls), with the aim of identifying those genetic variants that segregate more commonly in JIA patients with uveitis compared to those without uveitis.

PATIENTS AND METHODS

Data collection. We performed data collection, quality control, and statistical analyses in 2 phases, and then jointly analyzed the data from both phases to improve the power of locus discovery (Table 1; see also Supplementary Methods, available on the *Arthritis & Rheumatology* web site at http://onlinelibrary. wiley.com/doi/10.1002/art.40484/abstract) (13). Analysis code, supporting data files, and links to summary-level data can be found at https://github.com/saralpulit/UveitisJIA_MHC-fineMapping. Samples for genotyping were collected from 2 cohorts: 1) a Dutch cohort, comprising 137 patients with JIA-associated uveitis and 247 non-uveitis JIA control patients (phase 1), and 2) a cohort of samples collected in Germany, Belgium, and Switzerland, comprising 77 patients with JIA-associated uveitis and 115 non-uveitis JIA controls (phase 2).

Table 1. Samples included in phase 1 and phase 2 of the analysis*

	All patients with JIA	Patients with JIA-associated uveitis	Patients with JIA without uveitis
Samples, pre-QC			
Phase 1	384	137 (64)	247 (68)
Phase 2	192	77 (36)	115 (32)
Total	576	214	362
Samples, post-QC			
Phase 1	357	126 (66)	231 (70)
Phase 2	165	66 (34)	99 (30)
Total	522	192	330
ANA status			
ANA+	304	150 (78)	154 (47)
ANA−	182	32 (17)	150 (46)
Data unavailable	36	10 (5)	26 (8)
Sex			
Female	364	136 (71)	228 (69)
Male	158	56 (29)	102 (31)
JIA category†			
Oligoarticular (persistent)	214	101 (53)	113 (34)
Oligoarticular (extended)	98	36 (19)	62 (19)
Polyarticular RF-negative	169	46 (24)	123 (37)
Other‡	41	9 (4)	32 (10)

* Sample numbers (%) are shown both pre– and post–quality control (QC) for all patients with juvenile idiopathic arthritis (JIA), patients with JIA-associated uveitis, and JIA patients without uveitis. The presence or absence of antinuclear antibodies (ANAs), sex distribution, and JIA categories are also shown.
† An extended description of sex and ANA status within the JIA categories can be found in Supplementary Table 6 (http://onlinelibrary. wiley.com/doi/10.1002/art.40484/abstract).
‡ Includes rheumatoid factor (RF)–positive polyarthritis (n = 4), psoriatic arthritis (n = 6), enthesitis-related arthritis (n = 15), systemic arthritis (n = 3), other arthritis (n = 10), and unknown (n = 3).

Patients were diagnosed as having JIA according to the criteria of the International League of Associations for Rheumatology or the European League Against Rheumatism (14,15). Ophthalmologists screened all patients according to the Academy of Pediatrics guidelines (6), and patients with no clinical signs of uveitis at the time of screening were followed up for at least 4 years after the onset of JIA. Patients in whom trace cells or more abundant cells were found in the anterior chamber and who were treated with at least topical steroids during the ophthalmologic examinations were diagnosed as having JIA-associated (anterior) uveitis.

DNA material from all JIA patients in phase 1 were collected at the University Medical Center Utrecht, University Medical Center Leiden, Erasmus Medical Center Rotterdam, Academic Medical Center Amsterdam, and Radboud University Medical Center Nijmegen (all in The Netherlands). Phase 2 samples were collected from the Inception Cohort of Newly Diagnosed Patients with Juvenile Idiopathic Arthritis (ICON-JIA) Study Group and provided by the ICON Biobank at the Westfälische Wilhelms-Universität Münster in Germany, the University Hospitals Leuven in Belgium, and the University Children's Hospital in Zurich, Switzerland.

Genotype data from 398 unrelated and unaffected Dutch subjects were used as population-level controls. These subjects had previously been genotyped using the same platform as used in the present study (16).

This study was approved by the local Institutional Review Boards and is in compliance with the principles of the Declaration of Helsinki. Informed consent was obtained from all participating patients if they were age 18 years or older, from both parents and patients if they were age 12–18 years, and from only parents if they were younger than age 12 years.

Prephasing and imputation. We genotyped all samples on the Infinium HumanOmniExpress-24 array (version 1.1). In each phase, we performed sample- and variant-level quality control, prephasing, and imputation. We prephased the phase 1 and phase 2 data separately using the ShapeIt2 program (17). As the sample size was >100 samples, we ran prephasing without a reference panel, in accordance with the ShapeIt2 recommendations. Following prephasing, we imputed the prephased samples using Impute2 software (18), and an imputation reference panel was constructed using the 2,504 samples that were whole-genome sequenced in the 1000 Genomes Project (phase 3) (19).

To impute amino acids and HLA alleles in the MHC, we used the SNP2HLA pipeline (20). This panel includes single-nucleotide polymorphisms (SNPs) and amino acids in the MHC, as well as HLA class I and class II types. HLA types are imputed to 2- and 4-digit resolution. The SNP2HLA pipeline uses the Beagle program (21) to phase and impute the data. Full details on prephasing and imputation can be found in Supplementary Methods (http://onlinelibrary.wiley.com/doi/10.1002/art.40484/abstract).

Genome-wide association testing. Our data enabled 3 comparisons: 1) all JIA cases versus population-level controls, 2) JIA-associated uveitis cases versus population-level controls, and 3) JIA-associated uveitis cases versus non-uveitis JIA controls. As we sought to compare the genetic architecture of JIA and uveitis, and because far larger GWAS of JIA and population-level controls have already been completed (22), we performed the first 2 comparisons for the purposes of quality control and to look up known associations (22,23) (for more details, see Supplementary Figures 1 and 2 and Supplementary Table 1, available on the *Arthritis & Rheumatology* web site at http://onlinelibrary.wiley.

com/doi/10.1002/art.40484/abstract). We accounted for these comparisons when considering multiple testing. Herein we focused on the comparison between JIA-associated uveitis cases and non-uveitis JIA controls.

Within each study phase, we performed a GWAS, using Plink software version 1.9 (24), in an additive logistic regression model, with corrections for sex and the first 2 principal components (PCs; to account for sample ancestry) (see Supplementary Methods and Supplementary Figures 3 and 4, available on the *Arthritis & Rheumatology* web site at http://onlinelibrary.wiley.com/doi/10.1002/art.40484/abstract). We meta-analyzed the results using the METAL program (25) for a combined analysis of 192 patients with JIA-associated uveitis and 330 non-uveitis JIA controls (Table 1). To ensure that we were analyzing SNPs with high-quality imputation, we only analyzed common SNPs (i.e., those with a minor allele frequency of >1%) with an imputation quality (info) score of >0.7. The single signal identified as achieving genome-wide significance ($P < 2 \times 10^{-8}$, accounting for 3 phenotype comparisons) resided in the MHC (see Supplementary Figures 3 and 4, http://onlinelibrary.wiley.com/doi/10.1002/art.40484/abstract).

Association testing and fine-mapping in the MHC. To identify the amino acids or HLA types driving the genome-wide association signal, we imputed the MHC region on chromosome 6 using an MHC-specific imputation panel (20). We merged the imputation dosages from phase 1 and phase 2 to perform a mega-analysis, running a logistic regression across the merged data, with corrections for the top 5 PCs, sex, and analysis phase (i.e., phase 1 or phase 2). To ensure that this mega-analysis approach was appropriate, we additionally performed an inverse variance–weighted meta-analysis (26,27) of the 2 phases. We found that the results were highly concordant (r = 0.95 for Pearson's correlation of genome-wide β values; see Supplementary Methods and Supplementary Figure 5, available on the *Arthritis & Rheumatology* web site at http://onlinelibrary.wiley.com/doi/10.1002/art.40484/abstract). Our mega-analysis approach has the additional advantages of allowing for interaction testing and conditional analysis. To identify independent signals within the MHC, we performed conditional analyses (results shown in Figure 1).

In silico prediction of peptide binding to *HLA–DRβ1*. We used proteome data from human iris tissue (2,959 nonredundant proteins) as a representative source of proteins present in iris tissue (28). Patients with JIA-associated uveitis commonly have antinuclear antibodies (ANAs) and antibodies directed to iris tissue, and therefore we focused on nuclear iris proteins to generate a potentially disease-relevant data set. We selected 147 proteins that fulfilled these criteria (see Supplementary Table 2, available on the *Arthritis & Rheumatology* web site at http://onlinelibrary.wiley.com/doi/10.1002/art.40484/abstract), and their full-length amino acid sequences were fed into the neural network of the *netMHCIIpan3.1* server.

We next tested the predicted affinities of all 83,686 overlapping 15-mer peptides from the selected 147 proteins in *netMHCIIpan3.1* for binding to representative 4-digit alleles of *HLA–DRB1*. The affinity data were log-transformed to a value between 0 and 1 using the calculation $1 - \log(IC_{50\,nM})/\log(50{,}000)$ (29), where $IC_{50\,nM}$ represents the half maximal inhibitory concentration.

To categorize *HLA–DRB1* allotypes with similar predicted binding preferences, we performed unsupervised hierarchical clustering and generated heatmaps based on the Euclidean distance measure and the Ward's linkage method, using the MetaboAnalyst server (30). We computed the ratio of
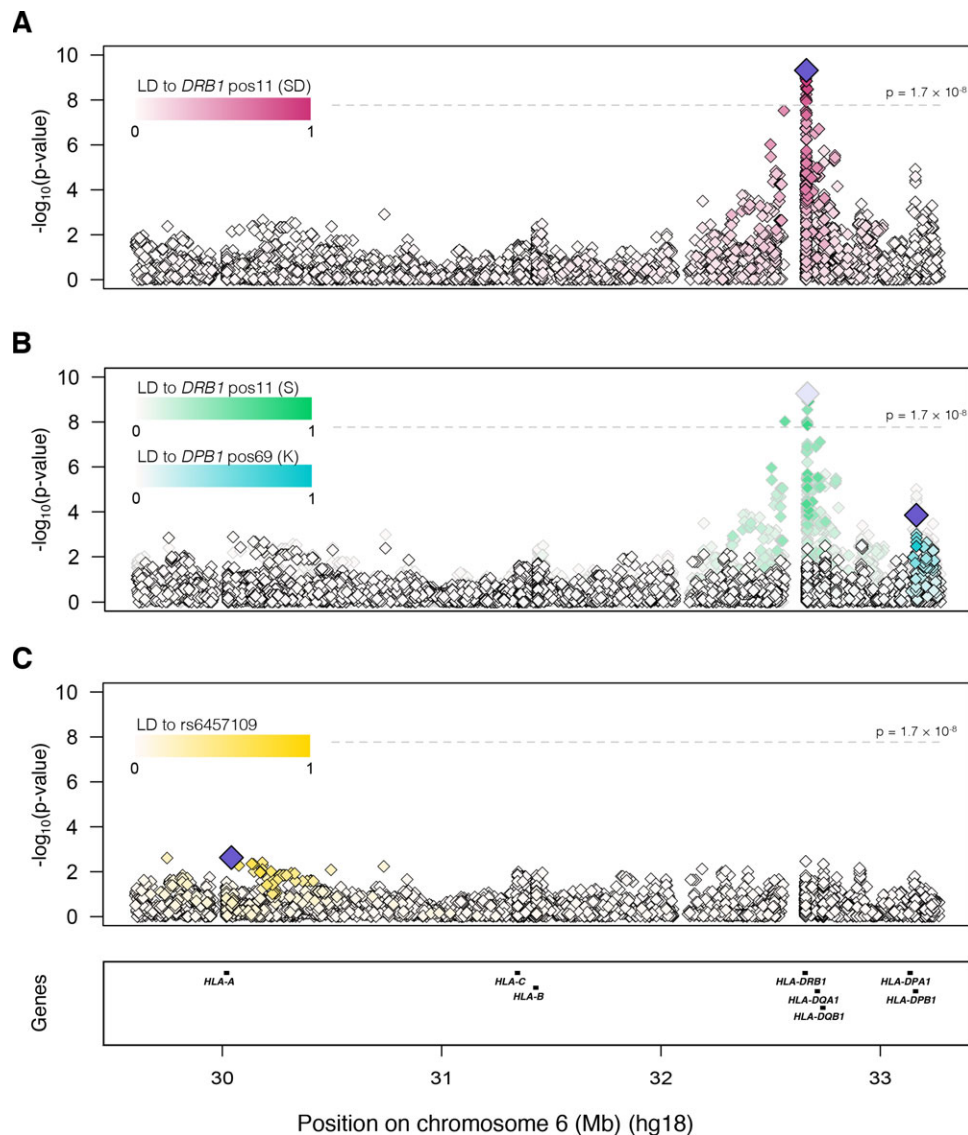
Figure 1. Association and conditional testing in *HLA–DRB1*. **A,** Initial association testing in the major histocompatibility complex (MHC) revealed a genome-wide significant signal at *HLA–DRB1* position 11 (presence of serine [S] or aspartic acid [D]; purple diamond). **B,** Conditioning on the presence of aspartic acid at position 11 (green and white diamonds, gray outline) left the association signal essentially unchanged, while presence of serine (pale purple diamond) remained the strongest association. Conditioning on the presence of serine at position 11 (aquamarine and white diamonds, black outline) dramatically mitigated the association signal, indicating that the presence of serine explains the bulk of the association at *DRB1* position 11. Presence of lysine (K) at position 69 in *HLA–DPB1* (dark purple diamond) remained modestly associated. **C,** Conditioning on lysine at position 69 in *HLA–DPB1* (rs6457109, dark purple diamond) removed the remainder of the signal ($P = 0.0024$). LD = linkage disequilibrium.

the average binding affinity of HLA–DRβ1 molecules that contain serine 11 in the peptide-binding groove to the average binding affinity of HLA–DRβ1 proteins that have other amino acids at this position, as a measure of the overall difference in predicted binding affinity for each peptide.

RESULTS

Of the SNPs, amino acids, and classic alleles tested in the MHC for an association with uveitis in JIA

(see Supplementary Table 3, available on the *Arthritis & Rheumatology* web site at http://onlinelibrary.wiley.com/doi/10.1002/art.40484/abstract), we observed the strongest association with the presence of either serine or aspartic acid at position 11 in *HLA–DRB1* (odds ratio [OR] 2.59, 95% confidence interval [95% CI] 1.92–3.50; $P = 4.80 \times 10^{-10}$) (Figure 1A and Table 2).

To identify which of the possible residues at position 11 explained the signal, we first performed an

Table 2. Association analyses of amino acids in *HLA–DRB1* in relation to risk of JIA-associated uveitis*

Model, population, *DRβ1* position, amino acid residue	Classic HLA alleles	Mega-analysis		
		Frequency (cases/controls)	OR (95% CI)	*P*
Initial association testing				
All JIA				
Position 11				
Ser or Asp	*03, *08, *09, *11, *12, *13, *14	0.79/0.59	2.59 (1.92–3.50)	4.80×10^{-10}
Ser	*03, *08, *11, *12, *13, *14	0.77/0.57	2.47 (1.84–3.32)	1.44×10^{-9}
Conditioning on Asp at position 11				
All JIA				
Position 11				
Ser or Asp	*03, *08, *09, *11, *12, *13, *14	0.79/0.59	2.60 (1.92–3.52)	5.43×10^{-10}
Ser	*03, *08, *11, *12, *13, *14	0.77/0.57	2.60 (1.92–3.52)	5.46×10^{-10}
Conditioning on Ser at position 11				
All JIA				
Position 11				
Ser or Asp	*03, *08, *09, *11, *12, *13, *14	0.79/0.59	2.36 (0.93–5.98)	0.069
Sex-specific association testing				
Female				
Position 233				
Thr	*01, *04, *07, *08, *09, *10, *15, *16	0.18/0.44	0.30 (0.20–0.43)	3.50×10^{-10}
Male				
Position 233				
Thr	*01, *04, *07, *08, *09, *10, *15, *16	0.37/0.46	0.73 (0.44–1.20)	0.210
Female				
Position 11				
Ser or Asp	*03, *08, *09, *11, *12, *13, *14	0.84/0.59	3.48 (2.35–5.16)	4.92×10^{-10}
Male				
Position 11				
Ser or Asp	*03, *08, *09, *11, *12, *13, *14	0.67/0.56	1.52 (0.92–2.51)	0.100
Female				
Position 11				
Ser	*03, *08, *11, *12, *13, *14	0.82/0.57	3.30 (2.26–4.83)	7.61×10^{-10}
Male				
Position 11				
Ser	*03, *08, *11, *12, *13, *14	0.64/0.55	1.41 (0.86–2.31)	0.177
Conditioning on Thr at position 233				
Female				
Position 11				
Ser or Asp	*03, *08, *09, *11, *12, *13, *14	0.84/0.59	1.98 (0.73–5.32)	0.178
Male				
Position 11				
Ser or Asp	*03, *08, *09, *11, *12, *13, *14	0.67/0.56	3.14 (0.70–14.15)	0.136
Female				
Position 11				
Ser	*03, *08, *11, *12, *13, *14	0.82/0.57	0.84 (0.10–6.94)	0.878
Male				
Position 11				
Ser	*03, *08, *11, *12, *13, *14	0.64/0.55	2.83 (0.16–51.47)	0.482
Sex interaction association				
All JIA				
Position 11	*03, *08, *11, *12, *13, *14	–/–	2.25 (1.22–4.15)	0.0096

* These are the top results from the mega-analysis of *HLA–DRB1* in samples from patients with juvenile idiopathic arthritis (JIA)–associated uveitis (cases) versus JIA patients without uveitis (controls). All reported results correspond to the presence of the given amino acid residues. Presence of serine (Ser) or aspartic acid (Asp) at position 11 in *HLA–DRB1* (imputation info score 1.11) was the top hit after initial association testing. Conditioning on either aspartic acid or serine revealed that the amino acids at positions 10–13, all well-imputed (imputation info score 1.08) and in perfect linkage disequilibrium, explain the bulk of the initial signal. Association statistics for tyrosine (position 10), threonine (Thr) (position 12), and serine or glycine (position 13) are identical to the association statistics reported for serine (position 11) due to linkage disequilibrium. OR = odds ratio; 95% CI = 95% confidence interval.

omnibus test of all but 1 of the 6 alleles present at *HLA–DRB1* position 11 as compared to a null model. We found that the goodness-of-fit of the omnibus test far exceeded that of the null model (which included only the variables of sex, PCs, and study phase) (likelihood ratio test $P = 1.5 \times 10^{-9}$).

Next, to test whether a single *HLA–DRB1* position 11 allele was driving the top association signal (as

opposed to all possible alleles together, as modeled by the omnibus test), we performed conditional testing of the top association signal by first including the imputation dosages for serine, and then separately including aspartic acid at position 11 as an additional covariate in the logistic regression model (Figure 1B and Table 2). After conditioning on serine 11, the association signal dropped substantially ($P = 0.069$), whereas conditioning on aspartic acid at position 11 left the signal essentially unchanged (OR 2.60, 95% CI 1.92–3.52; $P = 5.43 \times 10^{-10}$), indicating that the presence of serine explains the bulk of the signal.

The association with the presence of serine at position 11 in *HLA–DRB1* was consistent both in the phase 1 cohort (OR 2.15, 95% CI 1.52–3.05; $P = 1.59 \times 10^{-5}$) and in the phase 2 cohort (OR 3.34, 95% CI 1.92–5.83; $P = 2.11 \times 10^{-5}$), indicating that both study phases contributed to the signal identified as showing genome-wide significance in the overall mega-analysis (13). In separate subset analyses of samples from patients with oligoarticular (extended or persistent) JIA or RF–negative polyarticular JIA, which represent the phenotypes in which typical chronic anterior uveitis most commonly occurs, the association results were not affected (for serine 11, OR 2.42, $P = 1.72 \times 10^{-8}$) (see Supplementary Results, http://onlinelibrary.wiley.com/doi/10.1002/art.40484/abstract).

HLA–DRB1 serine 11 is positioned in the middle of what is known as the YST motif (31,32). The motif is composed of tyrosine (Y) at position 10, serine (S) at position 11, and threonine (T) at position 12. All 3 amino acids are in perfect linkage disequilibrium (LD) with one another (i.e., $r^2 = 1$ between all residue pairs). Additionally, the residues in the YST motif are in near-perfect LD ($r^2 = 0.9999994$) with a fourth residue, the presence of serine or glycine at position 13 (OR 2.47, 95% CI 1.84–3.32; $P = 1.44 \times 10^{-9}$). Thus, all 4 amino acid configurations show identical, statistically significant associations with JIA-associated uveitis (Table 2).

To further decipher the specific residues across positions 10–13 driving the association in uveitis, we performed a series of likelihood ratio tests. Briefly, a likelihood ratio test compares the fit of 2 models to the observed data and indicates if either model best fits that data. First, as expected, we found that a model containing serine 11 (or tyrosine 10 or threonine 12) best fit the data ($P = 1.48 \times 10^{-10}$, compared to a model containing only PCs and sex as variables), a finding that is consistent with the results from our initial association testing.

We next combined the serine or glycine residue at position 13 with the YST motif in a single model, and compared that model to 1 containing the PCs, sex, and serine 11. The model including serine/glycine 13 only modestly improved the model fit (likelihood ratio test

$P = 0.043$); neither serine 13 nor glycine 13 alone improved the model ($P = 0.70$ for both tests).

We then wanted to test whether the uveitis-associated serine 11 signal was independent of associations previously observed in all patients with JIA (including uveitis cases) found at *HLA–DRB1* serine 13 and glycine 13 (22) and replicated in our own data (for results, see Supplementary Table 4, available on the *Arthritis & Rheumatology* web site at http://onlinelibrary.wiley.com/doi/10.1002/art.40484/abstract). We observed a modest LD between serine 11 and serine 13 ($r^2 = 0.621$) and between serine 11 and glycine 13 ($r^2 = 0.104$). Conditioning serine 11 on serine 13 in our comparison of patients with JIA-associated uveitis and non-uveitis JIA patients, we found that the serine 11 signal was modestly affected (OR 2.61, 95% CI 1.74–3.93; $P = 3.83 \times 10^{-6}$). Similarly, conditioning on glycine 13 revealed a modest signal change (OR 2.41, 95% CI 1.75–3.32; $P = 6.49 \times 10^{-8}$). These results indicate that the association signal at serine 11 primarily represents an effect that is independent of that of serine 13 and glycine 13 in all patients with JIA.

Sexual dimorphism in JIA-associated uveitis. As uveitis is epidemiologically known to be more prevalent in female patients with oligoarticular JIA (33), we wanted to formally test whether the genetic association signal in uveitis was sexually dimorphic. In analyzing female patients only (136 samples from girls with JIA and uveitis versus 228 samples from girls with JIA without uveitis), we found a genome-wide significant signal at serine 11 in *HLA–DRB1* (OR 3.30, 95% CI 2.26–4.83; $P = 7.61 \times 10^{-10}$). We found no evidence of association with serine 11 in male patients (56 boys with JIA and uveitis versus 102 boys with JIA without uveitis) (OR 1.41, 95% CI 0.86–2.31; $P = 0.177$) (Table 2 and Supplementary Figure 6, available on the *Arthritis & Rheumatology* web site at http://onlinelibrary.wiley.com/doi/10.1002/art.40484/abstract). Although the most significant association with uveitis in girls was mapped to amino acid position 233 in the cytoplasmic domain of *HLA–DRB1* (for the presence of threonine, OR 0.30, 95% CI 0.20–0.43; $P = 3.50 \times 10^{-10}$) (Table 2), this position is in near-perfect LD ($r^2 = 0.98$) with the residues in the YST motif (positions 10–12), as well as with the presence of serine or glycine at position 13 (results in Supplementary Figure 7, available on the *Arthritis & Rheumatology* web site at http://onlinelibrary.wiley.com/doi/10.1002/art.40484/abstract), and consequently yields a nearly identical association to that at serine 11 (Table 2).

To further explore the potential for a sex-specific effect, we ran the association test at serine 11 across all samples and included an interaction term between sex and the imputed dosage for presence of serine 11. We found a significant effect of the interaction term (OR 2.25, 95% CI

1.22–4.15; $P = 0.0096$), indicating that the *HLA–DRB1* serine 11 signal was indeed sex specific. When we reduced our analysis to the subsets of patients with oligoarticular (extended or persistent) JIA and those with RF-negative polyarticular JIA, the interaction results remained unchanged ($P = 0.0121$) (see Supplementary Results, available on the *Arthritis & Rheumatology* web site at http://onlinelibrary.wiley.com/doi/10.1002/art.40484/abstract).

In silico peptide binding to HLA–DRβ1. Polymorphisms in the HLA–DRB1 β-chain specify the peptide-binding preference of HLA–DR. The YST motif containing serine 11 is located in the bottom of the antigen-binding groove of the HLA–DR protein (Figure 2), suggesting that different peptide-binding preferences of HLA–DRB1 may confer a risk of uveitis. To explore whether the presence of serine 11 affects peptide–MHC class II interactions, we compared the predicted binding affinity for 13 common *HLA–DRB1* allotypes (representing 79% of the *DRB1* alleles in JIA cases) using a panel of >80,000 peptides based on proteome data from human iris tissue (see

Supplementary Results and Supplementary Table 2, available on the *Arthritis & Rheumatology* web site at http://onlinelibrary.wiley.com/doi/10.1002/art.40484/abstract) implemented in the *NetMHCIIpan* server (29). The neural network–based *NetMHCIIpan* algorithm is capable of reliably detecting differences between peptide-binding repertoires of highly similar MHC class II molecules (29).

To compare predicted binding preferences, we performed unsupervised hierarchical clustering on the binding profiles of all *DRB1* alleles; clustering discerned 2 major clusters of classic alleles strikingly similar to the distribution of serine at position 11 (results in Supplementary Figure 8, available on the *Arthritis & Rheumatology* web site at http://onlinelibrary.wiley.com/doi/10.1002/art.40484/abstract). We observed that the average binding affinity of the peptide panel was higher for the *HLA–DRB1* alleles that encode serine at position 11 than for the alleles that have other amino acids at this position ($P = 3.44 \times 10^{-136}$, by Wilcoxon signed rank test) (results in Supplementary Table 5, available on the *Arthritis &*
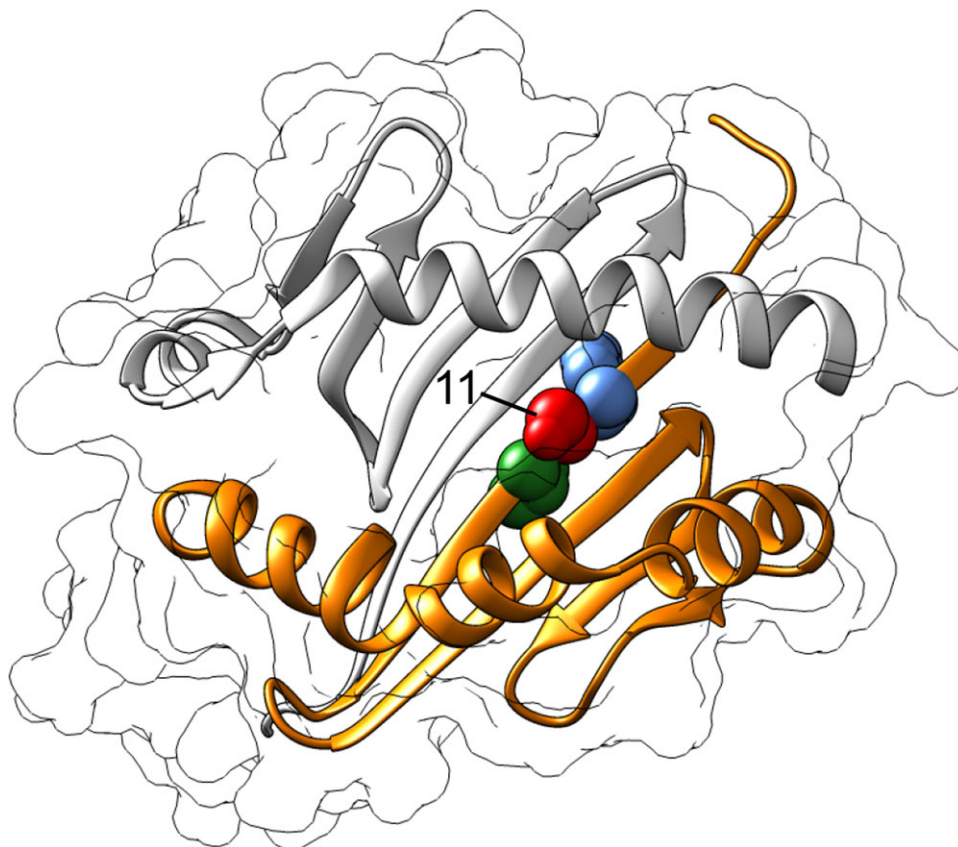
Figure 2. Three-dimensional ribbon model for HLA–DR (Protein Data Bank entry: 3pdo). The molecule is positioned to provide a view from the top of the peptide-binding groove. The β-chain (DRβ) is highlighted in orange. Amino acid serine at position 11 (red) is located in the bottom center of the peptide-binding groove of HLA–DRβ1. Adjacent amino acid tyrosine at position 10 (green) and threonine at position 12 (blue) and serine at position 11 are displayed as spheres. The 3-dimensional structure was produced using the UCSF Chimera system (see ref. 30). Color figure can be viewed in the online issue, which is available at http://onlinelibrary.wiley.com/doi/10.1002/art.40484/abstract.

Rheumatology web site at http://onlinelibrary.wiley.com/doi/10.1002/art.40484/abstract).

To compare these 2 clusters, we computed the ratio of the average binding affinity of the 6 *HLA–DRB1* allotypes that contain serine 11 and the average binding affinity of the 7 allotypes that have other amino acids at this position (see Supplementary Table 5, http://onlinelibrary.wiley.com/doi/10.1002/art.40484/abstract). Since MHC class II molecules at the cell surface present repertoires that are skewed in favor of high-affinity binders (29), we selected for those peptides that had an affinity (IC$_{50}$ $_{\text{n}M}$) of <500 nM (an affinity of <500 nM is routinely used as a threshold for potential immunogenicity) or <50 nM (strong binding peptides) for *HLA–DRB1* allotypes with serine 11 (see Supplementary Methods, http://onlinelibrary.wiley.com/doi/10.1002/art.40484/abstract). The data indicated that peptides with an intermediate or high affinity for allotypes containing serine 11 had less affinity to allotypes that contained other amino acids at position 11 (for results, see Supplementary Table 5, http://onlinelibrary.wiley.com/doi/10.1002/art.40484/abstract).

DISCUSSION

Through interrogation of imputed HLA types and amino acids, we have identified the amino acid serine at position 11 in the *HLA–DRB1* gene as being strongly associated with an increased risk of uveitis in female JIA patients. The perfect LD observed across the YST motif (positions 10–12) makes it impossible to disentangle the 3 amino acids in a statistical framework; a subset of the amino acids, all 3 (i.e., the complete YST motif), or a more complex interaction of these variants with others in the region may all be key to disease onset. Interrogation of larger sample collections and extensive functional work in this region will be necessary to fully understand the mechanism(s) driving the association. Nevertheless, our findings indicate that, although JIA with uveitis and JIA without uveitis share clinical features and HLA-specific genetic risk factors (23), there appear to be genetic signals that are specific to JIA with uveitis.

Further analyses revealed that the serine 11 signal is sexually dimorphic and unique to female patients with JIA. The reduced number of male patients with JIA-associated uveitis (Table 1) and resulting reduced power in the male-only analysis may explain the absence of association signal. However, we had 98.5% power to detect an association ($P < 0.05$) at serine 11 in the male-only analysis, assuming that the OR in male patients was the same as in female patients (OR 3.30). Assuming a more modest effect in male patients (OR 2.00), we still had 75.2% power to detect a signal at $P < 0.05$. To detect more subtle effects in male patients or other lower-penetrance,

sexually dimorphic effects in either sex, larger case collections will be necessary.

Although JIA-associated uveitis is known to occur more frequently in girls (33), more detailed sex-specific epidemiologic data in JIA-associated uveitis are sparse. The genotype-by-sex interaction informs an exciting field of future research aimed at elucidating potential sex-specific uveitis risk mechanisms (e.g., hormone regulation) underlying the *HLA–DRB1* signal. The sexually dimorphic serine 11 association (or the complete YST motif) may also help explain the previously reported evidence of sexually dimorphic severity or course of the disease in children with JIA-associated uveitis (34). Moreover, the findings indicate that sex stratification may be beneficial for future clinical trials, as some therapeutic agents may be more efficacious in female patients only or in male patients only (35).

Although all 3 YST-motif residues reside at the bottom of the HLA–DRB1 peptide-binding groove, only serine 11 is positioned toward, and thus most likely interacting with, binding peptide epitopes (Figure 2). Previous work has identified serine 11 as the strongest risk factor in seronegative rheumatoid arthritis (RA) (36). Some JIA patients with uveitis might be categorized as having seronegative RA by the time that they reach adulthood, and seronegative RA is considered to genetically mirror the uveitis-prone JIA categories (22). In contrast, serine 11 is highly protective against seropositive RA, a biologically distinct form of RA in which uveitis is not common (<1% of cases) (37).

HLA–DRβ1 is essential to immunity and orchestrates the downstream immune response by presenting a dynamic cargo of thousands of different peptides for scrutiny by T helper cells (38); both JIA and uveitis are thought to be mediated by T helper cell subsets (2). A potential explanation for the strong association of an amino acid motif (tagged by serine 11) in *HLA–DRB1* is that predetermined peptide preferences may affect T helper cell regulation. Although the large panel of putative antigens that we tested (see Supplementary Table 2, http://onlinelibrary.wiley.com/doi/10.1002/art.40484/abstract) was by no means exhaustive, the experiment demonstrated that the presence of serine 11 in *HLA–DRB1* is accompanied by changes in binding affinity in the resulting protein (see Supplementary Table 5 and Supplementary Figure 8, available on the *Arthritis & Rheumatology* web site at http://onlinelibrary.wiley.com/doi/10.1002/art.40484/abstract), suggesting that antigen presentation by the HLA–DRβ1 protein may (partially) underpin the susceptibility to uveitis. *HLA–DRB1* risk alleles that encode serine 11 (Supplementary Table 3, http://onlinelibrary.wiley.com/doi/10.1002/art.40484/abstract) may communicate distinct peptidomes that influence T helper cells and increase the likelihood of downstream immune responses (e.g., generation of ANAs) to the eye; ANA positivity was

modestly correlated with the presence of serine 11 in the cases studied herein (Pearson's r = 0.21, $P = 1.0 \times 10^{-6}$). Functional studies using HLA-proteomic approaches will be necessary to experimentally validate and systematically dissect the complex downstream effects of serine 11 on tissue-specific antigen presentation by HLA–DRβ1 in uveitis.

The relatively high frequency of serine 11 in the JIA patients who did not develop uveitis (Table 2) indicates the likely involvement of additional (epi)genetic and environmental factors in uveitis. Only a handful of candidate gene studies (2,39), HLA-specific analyses (23), and a recent GWAS (40) have investigated uveitis as a phenotype separate from JIA overall, with the latter study identifying *HLA–DRB1*1501* as a uveitis risk factor. Genes outside the MHC have also been implicated in JIA-associated uveitis, including a polymorphism in *VTCN1* (41) and variants near the immune genes *TRAF1* and *C5* (42). Other studies have implicated a role for infiltrated plasma cells (43), T helper cells (2), and changes in the ocular fluid microenvironment (44–46). Although our study was well powered to detect common (frequency >10%) and highly penetrant (OR >3 [Supplementary Figure 9]) genetic variations that were associated with increased uveitis risk, the study was underpowered to identify common (frequency 1–10%), modestly penetrant variants (ORs 1.05–1.5), which are the hallmark genetic feature of complex phenotypes (47,48). Future studies will need to interrogate much larger samples from an array of global populations (49) in order to identify additional genetic signals that influence disease risk.

A number of risk factors, including young age and presence of ANAs (assumed to reflect aberrant immune activation [50]), are used to regularly screen (~4 times/year) JIA patients for early detection of uveitis. However, a considerable number of uveitis cases are diagnosed after sight-threatening complications have already occurred (6). A biomarker test, such as a test for the presence of serine 11, would significantly simplify the diagnosis and prevent unnecessary ophthalmologic screening in JIA patients who have a low susceptibility to uveitis (4). Deeper examination of our phenotypic data showed that 99% of female JIA patients with uveitis carried at least one copy of the variant coding for serine 11. The only female JIA patient with uveitis who lacked serine 11 in *HLA–DRB1* appeared to have ANA-negative oligoarthritis with mild vitritis and peripheral multifocal choroiditis in the absence of anterior segment inflammation. This ocular finding is atypical for JIA, and thus, according to our inclusion criteria, this sample was likely improperly included at cohort collection. Prospective studies in larger populations, including detailed clinical evaluation of development of uveitis and secondary

uveitis phenotypes, will be necessary to dissect the potential of serine 11 or other genotypes to serve as biomarkers for disease risk. Regardless, the current study justifies further genetic analysis.

The results of our study represent a key step in understanding the pathogenesis of uveitis in JIA, helping to discern biologically shared and distinct features of JIA-associated uveitis and JIA without uveitis. Future work will allow us to further disentangle the 2 phenotypes, evaluate shared and distinct disease etiology, identify disease pathways, and evaluate the efficacy of serine 11 or other genetic markers as potentially efficient clinical decision-making tools. By pinpointing and understanding the molecular mechanisms of uveitis, we can identify biomarkers that stratify patients for disease risk, catalyze future lines of research in precision medicine, and make advancements toward improving the treatment and prevention of sight-threatening complications of uveitis in children with JIA.

ACKNOWLEDGMENTS

AUTHOR CONTRIBUTIONS

All authors were involved in drafting the article or revising it critically for important intellectual content, and all authors approved the final version to be published. Drs. Haasnoot and Kuiper had full access to all of the data in the study and take responsibility for the integrity of the data and the accuracy of the data analysis.
Study conception and design. Haasnoot, Schilham, Radstake, Den Hollander, Saurenmann, ten Cate, de Boer, Pulit, Kuiper.
Acquisition of data. Haasnoot, Schilham, Kamphuis, Muller, Heiligenhaus, Foell, Minden, Ophoff, Reinards, Hiddingh, Schalij-Delfos, Hoppenreijs, van Rossum, Wouters, Saurenmann, van den Berg, Wulffraat, ten Cate, de Boer, Pulit, Kuiper.
Analysis and interpretation of data. Haasnoot, Foell, Radstake, ten Cate, de Boer, Pulit, Kuiper.

REFERENCES

1. Ravelli A, Martini A. Juvenile idiopathic arthritis. Lancet 2007; 369:767–78.
2. Sen ES, Dick AD, Ramanan AV. Uveitis associated with juvenile idiopathic arthritis. Nat Rev Rheumatol 2015;11:338–48.
3. Haasnoot AJ, Vernie LA, Rothova A, Doe PV, Los LI, Schalij-Delfos NE, et al. Impact of juvenile idiopathic arthritis
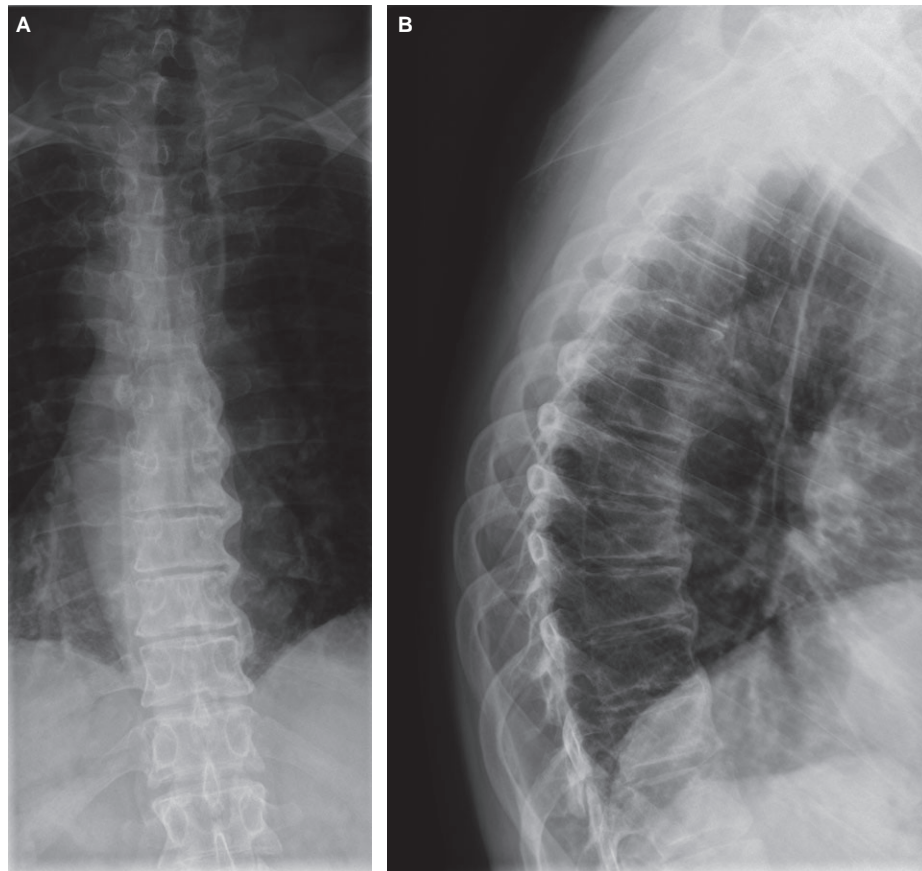
associated uveitis in early adulthood. PLoS One 2016;11: e0164312.

4. Gregory AC II, Kempen JH, Daniel E, Kaçmaz RO, Foster CS, Jabs DA, et al. Risk factors for loss of visual acuity among patients with uveitis associated with juvenile idiopathic arthritis: the Systemic Immunosuppressive Therapy for Eye Diseases study. Ophthalmology 2013;120:186–92.

5. De Boer J, Wulffraat N, Rothova A. Visual loss in uveitis of childhood. Br J Ophthalmol 2003;87:879–84.

6. Cassidy J, Kivlin J, Lindsley C, Nocton J. Section on Rheumatology, Section on Ophthalmology. Ophthalmologic examinations in children with juvenile rheumatoid arthritis. Pediatrics 2006;117:1843–5.

7. Kalinina Ayuso V, Makhotkina N, van Tent-Hoeve M, de Groot-Mijnes JD, Wulffraat NM, Rothova A, et al. Pathogenesis of juvenile idiopathic arthritis associated uveitis: the known and unknown. Surv Ophthalmol 2014;59:517–31.

8. Hinks A, Cobb J, Marion MC, Prahalad S, Sudman M, Bowes J, et al. Dense genotyping of immune-related disease regions identifies 14 new susceptibility loci for juvenile idiopathic arthritis. Nat Genet 2013;45:664–9.

9. Thompson SD, Marion MC, Sudman M, Ryan M, Tsoras M, Howard TD, et al. Genome-wide association analysis of juvenile idiopathic arthritis identifies a new susceptibility locus at chromosomal region 3q13. Arthritis Rheum 2012;64:2781–91.

10. Hinks A, Barton A, Shephard N, Eyre S, Bowes J, Cargill M, et al. Identification of a novel susceptibility locus for juvenile idiopathic arthritis by genome-wide association analysis. Arthritis Rheum 2009;60:258–63.

11. Angeles-Han ST, Yeh S, Vogler LB. Updates on the risk markers and outcomes of severe juvenile idiopathic arthritis-associated uveitis. Int J Clin Rheumtol 2013;8.

12. Heiligenhaus A, Heinz C, Edelsten C, Kotaniemi K, Minden K. Review for disease of the year: epidemiology of juvenile idiopathic arthritis and its associated uveitis: the probable risk factors. Ocul Immunol Inflamm 2013;21:180–91.

13. Skol AD, Scott LJ, Abecasis GR, Boehnke M. Joint analysis is more efficient than replication-based analysis for two-stage genome-wide association studies. Nat Genet 2006;38:209–13.

14. Petty RE, Southwood TR, Manners P, Baum J, Glass DN, Goldenberg J, et al. International League of Associations for Rheumatology classification of juvenile idiopathic arthritis: second revision, Edmonton, 2001. J Rheumatol 2004;31:390–2.

15. Berntson L, Fasth A, Andersson-Gäre B, Kristinsson J, Lahdenne P, Marhaug G, et al. Construct validity of ILAR and EULAR criteria in juvenile idiopathic arthritis: a population based incidence study from the Nordic countries. J Rheumatol 2001;28:2737–43.

16. Kuiper JJ, van Setten J, Ripke S, van 'T Slot R, Mulder F, Missotten T, et al. A genome-wide association study identifies a functional ERAP2 haplotype associated with birdshot chorioretinopathy. Hum Mol Genet 2014;23:6081–7.

17. Delaneau O, Marchini J, Zagury JF. A linear complexity phasing method for thousands of genomes. Nat Methods 2011;9:179–81.

18. Howie B, Marchini J, Stephens M, Chakravarti A. Genotype imputation with thousands of genomes. G3 (Bethesda) 2011;1:457–70.

19. Auton A, Abecasis GR, Altshuler DM, Durbin RM, Bentley DR, Chakravarti A, et al. A global reference for human genetic variation. Nature 2015;526:68–74.

20. Jia X, Han B, Onengut-Gumuscu S, Chen WM, Concannon PJ, Rich SS, et al. Imputing amino acid polymorphisms in human leukocyte antigens. PLoS One 2013;8:e64683.

21. Browning BL, Browning SR. A unified approach to genotype imputation and haplotype-phase inference for large data sets of trios and unrelated individuals. Am J Hum Genet 2009;84:210–23.

22. Hinks A, Bowes J, Cobb J, Ainsworth HC, Marion MC, Comeau ME, et al. Fine-mapping the MHC locus in juvenile idiopathic arthritis (JIA) reveals genetic heterogeneity corresponding to distinct adult inflammatory arthritic diseases. Ann Rheum Dis 2017;76:765–72.

23. Angeles-Han ST, McCracken C, Yeh S, Jang SR, Jenkins K, Cope S, et al. HLA associations in a cohort of children with juvenile idiopathic arthritis with and without uveitis. Invest Ophthalmol Vis Sci 2015;56:6043–8.

24. Chang CC, Chow CC, Tellier LC, Vattikuti S, Purcell SM, Lee JJ. Second-generation PLINK: rising to the challenge of larger and richer datasets. Gigascience 2015;4:1–16.

25. Willer CJ, Li Y, Abecasis GR. METAL: fast and efficient meta-analysis of genomewide association scans. Bioinformatics 2010;26:2190–1.

26. Lin DY, Zeng D. Meta-analysis of genome-wide association studies: no efficiency gain in using individual participant data. Genet Epidemiol 2010;34:60–6.

27. Schizophrenia Psychiatric Genome-Wide Association Study (GWAS) Consortium. Genome-wide association study identifies five new schizophrenia loci. Nat Genet 2011;43:969–76.

28. Zhang P, Kirby D, Dufresne C, Chen Y, Turner R, Ferri S, et al. Defining the proteome of human iris, ciliary body, retinal pigment epithelium, and choroid. Proteomics 2016;16:1146–53.

29. Andreatta M, Karosiene E, Rasmussen M, Stryhn A, Buus S, Nielsen M. Accurate pan-specific prediction of peptide-MHC class II binding affinity with improved binding core identification. Immunogenetics 2015;67:641–50.

30. Pettersen EF, Goddard TD, Huang CC, Couch GS, Greenblatt DM, Meng EC, et al. UCSF Chimera: a visualization system for exploratory research and analysis. J Comput Chem 2004;25:1605–12.

31. Bengtsson M, Jansson IE, Danielsson F, Henrysson H, Källsten K. Identification of a novel HLA DRB1 exon 2 sequence, DRB1*1345. Tissue Antigens 2002;59:159–61.

32. Kriener K, O'hUigin C, Tichy H, Klein J. Convergent evolution of major histocompatibility complex molecules in humans and New World monkeys. Immunogenetics 2000;51:169–78.

33. Moradi A, Amin RM, Thorne JE. The role of gender in juvenile idiopathic arthritis-associated uveitis. J Ophthalmol 2014;2014:461078.

34. Kalinina Ayuso V, Ten Cate HA, van der Does P, Rothova A, de Boer JH. Male gender as a risk factor for complications in uveitis associated with juvenile idiopathic arthritis. Am J Ophthalmol 2010;149:994–9.e5.

35. Whitley H, Lindsey W. Sex-based differences in drug activity. Am Fam Physician 2009;80:1254–8.

36. Han B, Diogo D, Eyre S, Kallberg H, Zhernakova A, Bowes J, et al. Fine mapping seronegative and seropositive rheumatoid arthritis to shared and distinct HLA alleles by adjusting for the effects of heterogeneity. Am J Hum Genet 2014;94:522–32.

37. Vignesh AP, Srinivasan R. Ocular manifestations of rheumatoid arthritis and their correlation with anti-cyclic citrullinated peptide antibodies. Clin Ophthalmol 2015;9:393–7.

38. Gutierrez-Arcelus M, Rich SS, Raychaudhuri S. Autoimmune diseases: connecting risk alleles with molecular traits of the immune system. Nat Rev Genet 2016;17:160–74.

39. Giannini EH, Malagon CN, van Kerckhove C, Taylor J, Lovell DJ, Levinson JE, et al. Longitudinal analysis of HLA associated risks for iridocyclitis in juvenile rheumatoid arthritis. J Rheumatol 1991;18:1394–7.

40. Márquez A, Cordero-Coma M, Martín-Villa JM, Gorroño-Echebarría MB, Blanco R, Díaz Valle D, et al. New insights into the genetic component of non-infectious uveitis through an Immunochip strategy. J Med Genet 2017;54:38–46.

41. Alberdi-Saugstrup M, Enevold C, Zak M, Nielsen S, Nordal E, Berntson L, et al. Non-HLA gene polymorphisms in juvenile idiopathic arthritis: associations with disease outcome. Scand J Rheumatol 2017;46:369–76.

42. Pers YM, Le Blay P, Ludwig C, Rittore C, Tejedor G, Foliwe R, et al. Association of TRAF1-C5 with risk of uveitis in juvenile idiopathic arthritis. Joint Bone Spine 2017;84:305–8.

43. Kalinina Ayuso V, van Dijk MR, de Boer JH. Infiltration of plasma cells in the iris of children with ANA-positive anterior uveitis. Invest Ophthalmol Vis Sci 2015;56:6770–8.

44. Haasnoot AJ, Kuiper JJ, Hiddingh S, Schellekens PA, de Jager W, Imhof SM, et al. Ocular fluid analysis in children reveals interleukin-29/interferon-λ1 as a biomarker for juvenile idiopathic arthritis-associated uveitis. Arthritis Rheumatol 2016;68:1769–79.

45. Sijssens KM, Rijkers GT, Rothova A, Stilma JS, Schellekens PA, de Boer JH. Cytokines, chemokines and soluble adhesion molecules in aqueous humor of children with uveitis. Exp Eye Res 2007;85:443–9.
46. Kalinina Ayuso V, de Boer JH, Byers HL, Coulton GR, Dekkers J, de Visser L, et al. Intraocular biomarker identification in uveitis associated with juvenile idiopathic arthritis. Invest Ophthalmol Vis Sci 2013;54:3709–20.
47. Manolio TA. Bringing genome-wide association findings into clinical use. Nat Rev Genet 2013;14:549–58.
48. Visscher PM, Brown MA, McCarthy MI, Yang J. Five years of GWAS discovery. Am J Hum Genet 2012;90:7–24.
49. Pulit SL, Voight BF, de Bakker PI. Multiethnic genetic association studies improve power for locus discovery. PLoS One 2010; 5:e12600.
50. Saurenmann RK, Levin AV, Feldman BM, Rose JB, Laxer RM, Schneider R, et al. Prevalence, risk factors, and outcome of uveitis in juvenile idiopathic arthritis: a long-term followup study. Arthritis Rheum 2007;56:647–57.

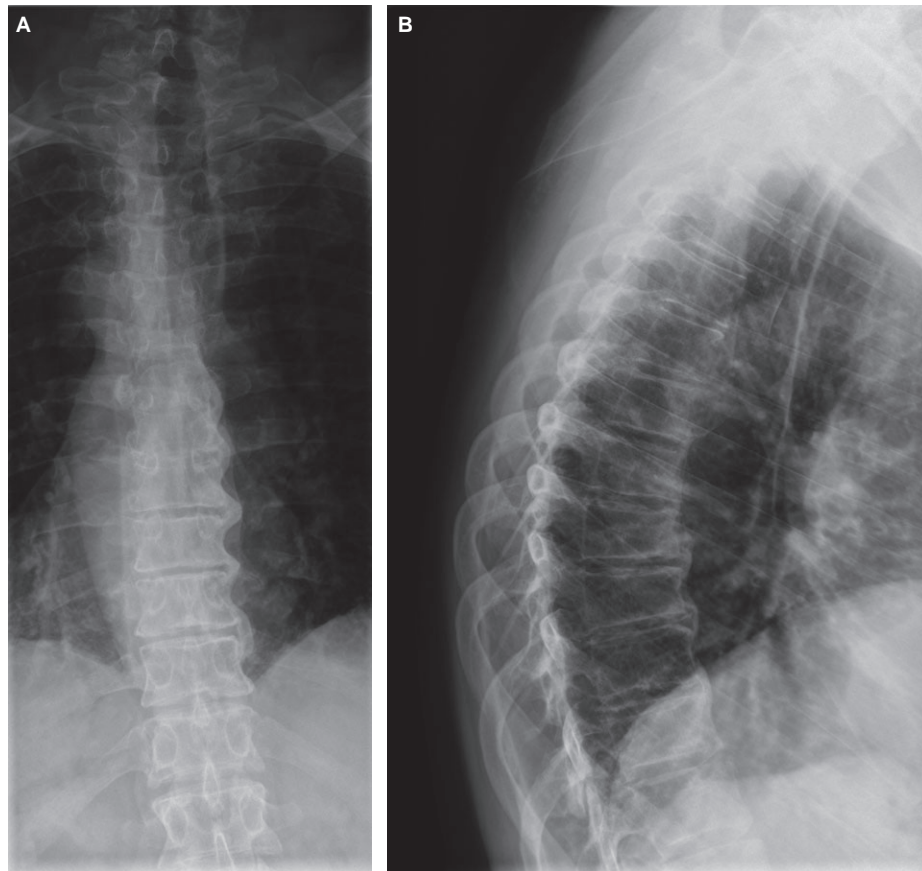*Clinical Images: Diffuse idiopathic skeletal hyperostosis—on the wrong side?*

The patient, a 58-year-old man, was referred to our rheumatology department because of arthralgia and generalized stiffness. He had already been diagnosed as having Kartagener syndrome with situs inversus. Physical examination revealed multiple painful entheses and stiffness of the thoracic spine. There were no signs of arthritis. Diffuse idiopathic skeletal hyperostosis (DISH) was suspected. Radiography of the thoracic spine revealed continuous ossification between 5 contiguous vertebral bodies (**A**). The lateral view showed extensive ossification of the anterior longitudinal ligament (**B**). DISH was diagnosed. In DISH, the ossification is normally localized on the right side of the spine. It is hypothesized that the descending aorta inhibits ossification on the left side. In our patient, however, the ossification occurred on the left side. We concluded that along with the situs inversus due to Kartagener syndrome the pathologic features of DISH had also "moved" to the contralateral side. This feature has rarely been reported in patients with DISH.

Henk A. Martens, MD, PhD
Simone S. Boks, MD, PhD
Sint Maartenskliniek
Nijmegen, The Netherlands

45. Sijssens KM, Rijkers GT, Rothova A, Stilma JS, Schellekens PA, de Boer JH. Cytokines, chemokines and soluble adhesion molecules in aqueous humor of children with uveitis. Exp Eye Res 2007;85:443–9.

46. Kalinina Ayuso V, de Boer JH, Byers HL, Coulton GR, Dekkers J, de Visser L, et al. Intraocular biomarker identification in uveitis associated with juvenile idiopathic arthritis. Invest Ophthalmol Vis Sci 2013;54:3709–20.

47. Manolio TA. Bringing genome-wide association findings into clinical use. Nat Rev Genet 2013;14:549–58.

48. Visscher PM, Brown MA, McCarthy MI, Yang J. Five years of GWAS discovery. Am J Hum Genet 2012;90:7–24.

49. Pulit SL, Voight BF, de Bakker PI. Multiethnic genetic association studies improve power for locus discovery. PLoS One 2010; 5:e12600.

50. Saurenmann RK, Levin AV, Feldman BM, Rose JB, Laxer RM, Schneider R, et al. Prevalence, risk factors, and outcome of uveitis in juvenile idiopathic arthritis: a long-term followup study. Arthritis Rheum 2007;56:647–57.

Clinical Images: Diffuse idiopathic skeletal hyperostosis—on the wrong side?

The patient, a 58-year-old man, was referred to our rheumatology department because of arthralgia and generalized stiffness. He had already been diagnosed as having Kartagener syndrome with situs inversus. Physical examination revealed multiple painful entheses and stiffness of the thoracic spine. There were no signs of arthritis. Diffuse idiopathic skeletal hyperostosis (DISH) was suspected. Radiography of the thoracic spine revealed continuous ossification between 5 contiguous vertebral bodies (**A**). The lateral view showed extensive ossification of the anterior longitudinal ligament (**B**). DISH was diagnosed. In DISH, the ossification is normally localized on the right side of the spine. It is hypothesized that the descending aorta inhibits ossification on the left side. In our patient, however, the ossification occurred on the left side. We concluded that along with the situs inversus due to Kartagener syndrome the pathologic features of DISH had also "moved" to the contralateral side. This feature has rarely been reported in patients with DISH.

Henk A. Martens, MD, PhD
Simone S. Boks, MD, PhD
Sint Maartenskliniek
Nijmegen, The Netherlands

LETTERS

Ultrasonography and power Doppler studies in chikungunya disease: comment on the article by Chang et al

To the Editor:

We read with interest the recent article by Chang et al regarding the frequency of chronic joint pain following chikungunya infection (1). We would like to congratulate the authors for their excellent study, a pioneer in the American continents, in such a large cohort (500 patients) and over a lengthy period of time.

Our group recently performed studies in 50 patients with a confirmed diagnosis of chikungunya fever (2,3). The study was performed between 2016 and 2017 in Rio de Janeiro, Brazil. In our study, ultrasonography was used to examine lesions on the wrists, hands, and ankles. As in the study by Chang et al, there was a predominance of female patients. However, parameters such as educational level and absenteeism from work were not positively correlated with disease severity (4). Based on our observations about the data that were collected and partially analyzed, the use of power Doppler studies could have relevance for predicting cases with a worse prognosis or cases that do not respond adequately to steroids or immunosuppressive drugs or cases that may progress to other forms of arthritis such as rheumatoid arthritis (RA) or psoriatic arthritis (PsA).

In the Chang article, the definition of the initial period of infection is unclear. Classically, there are 3 phases of disease: acute (first 10 days), subacute (between 10 and 90 days), and chronic (after 90 days). In our studies (2,3,5), ultrasonography was performed, on average, during the subacute stage of the disease. We believe that this period is the most appropriate for identifying, with ultrasonography and power Doppler studies, cases with the potential to evolve poorly. In their study in a cohort of 500 patients, the authors did not cite any case that has evolved into other forms of arthritis. In our smaller series, 2 cases of arthritis (RA and PsA, respectively) were identified after chikungunya infection. Was the exclusion of patients with RA or PsA deliberate? Patients with the chronic form of chikungunya fever may have mild, moderate, or severe presentations, and it can be estimated by the number of compromised joints and the presence of neurologic symptoms (for example, carpal tunnel syndrome). Thus, some patients may have only mild pain in 1 joint and others may present with a severe polyarticular form that prevents them from working or may progress to RA. It would have been interesting if the authors discriminated the degree of impairment in patients in whom chronic pain developed.

Roberto Mogami, MD, PhD
Flavio Sztajnbock, MD, PhD
Ana C. B. Koifman, MD, PhD
André de A. Vieira, MD
Rodrigo S. Torezan, MD
State University of Rio de Janeiro
Mirhelen M. De Abreu, MD, PhD
Yêdda de F. B. Chagas, MD
João L. P. Vaz, MD, PhD
Federal University of Rio de Janeiro
Rio de Janeiro, Brazil

1. Chang AY, Encinales L, Porras A, Pacheco N, Reid SP, Martins KA, et al. Frequency of chronic joint pain following chikungunya infection: a Colombian cohort study. Arthritis Rheumatol 2018;70:578–84.
2. Mogami R, Vaz JL, Chagas YF, Torezani RS, Vieira AA, Koifman AC, et al. Ultrasound of ankles in the diagnosis of complications of chikungunya fever. Radiol Bras 2017;50:71–5.
3. Mogami R, Vaz JL, Chagas YF, De Abreu MM, Torezani RS, Vieira AA, et al. Ultrasonography of hands and wrists in the diagnosis of complications of chikungunya fever. J Ultrasound Med 2018;37:511–20.
4. Mogami R, Torezani RS, Vaz JL, Chagas YF, Vieira AA, Junqueira Filho EA, et al. A proposal for ultrasound staging of musculoskeletal complications of chicungunya fever. Presented at the Jornada Paulista de Radiologia; 2017 May 4–7; Sao Paulo, Brazil.
5. Mogami R, de Almeida Vieira A, Junqueira Filho EA, Lopes A. Chikungunya fever outbreak in Rio de Janeiro, Brazil: ultrasonographic aspects of musculoskeletal complications. J Clin Ultrasound 2017;45:43–4.

Reply

To the Editor:

We would like to thank Dr. Mogami and colleagues for sharing their experience with chikungunya virus in Brazil and especially for highlighting the possible utility of ultrasonography during the subacute disease phase to identify severe or evolving cases of arthritis. Indeed, Doppler ultrasonography may be an effective approach to identifying patients who might benefit from treatment with disease-modifying agents such as methotrexate during the subacute phase. However, additional peer-reviewed research is needed to define the role of ultrasound in the selection of patients for aggressive treatment.

Table 1 in our article shows prior comorbidities in the patients, including any type of arthritis, gout, and osteoarthritis. None of these patients were excluded from the analysis. There were no significant differences in the percentage of prior comorbidities between patients with and those without persistent joint pain. The evolution of diagnosed RA or PsA following a confirmed episode of chikungunya fever was not assessed. This is an astute observation by Mogami et al and has been included in our 3-year follow-up study.

To clarify, the definition of the initial period of infection, shown in Table 2 as the "initial chikungunya virus symptom duration," represents the patient-reported duration of systemic illness on days that are associated with chikungunya viral infection characterized by muscle pain, weakness, joint pain, rash, and fever. The median initial chikungunya virus symptom duration was 4 days (interquartile range 3–8) among all patients with confirmed chikungunya infection.

Joint pain severity and disability among patients with persistent joint pain attributed to the chikungunya infection are shown in Table 3, with 27% of patients reporting symptoms impacting their ability to continue normal activities of daily living. Furthermore, those patients had a significantly greater number of swollen joints (mean ± SD 0.5 ± 1.0) and tender joints (2.9 ± 2.3) compared with those without persistent joint pain (0.06 ± 0.3 and 0.2 ± 0.8, respectively). Interestingly, the global pain score in the last week (range 0–100) was not significantly different between patients with and those without persistent joint pain attributed to chikungunya infection, which indicated a high

prevalence of generalized pain among all patients with serologically confirmed chikungunya infection regardless of arthralgia status. Further evaluation for depression and other types of arthritis in patients with chikungunya infection compared with controls is needed (Suhrbier A, Jaffar-Bandjee M, Gasque P. Arthritogenic alphaviruses: an overview. Nat Rev Rheumatol 2012;8:420–9).

Aileen Y. Chang, MD, MSPH (iD)
Jeffrey M. Bethony, PhD
Gary L. Simon, MD, PhD
George Washington University
Washington, DC
Liliana Encinales, MD
Allied Research Society
Barranquilla, Colombia

Familial Mediterranean fever: new insights into cancer immunoprevention? Comment on the article by Brenner et al

To the Editor:

We read with interest the report by Brenner et al describing their study which showed that familial Mediterranean fever (FMF), which is prevalent in our country of Turkey as well as in Israel where their study was conducted, was associated with lower risk of cancer (1). We have some comments and suggestions.

FMF is a chronic autoinflammatory disorder caused by mutations in the *MEFV* gene, which encodes pyrin. In FMF, *MEFV* has either gain-of-function or loss-of-function mutations, resulting in activation of caspase 1 and increased levels of interleukin-1β (IL-1β). IL-1β is the key molecule in activation of the innate immune system, mainly macrophages and granulocytes. Beyond being the first-line defense against infections by other microorganisms, innate immunity exerts tumoricidal activity via several different mechanisms. Natural killer (NK) cells can recognize cell surface stress ligands and tumor-derived glycolipids, macrophages can kill tumor cells with nitric oxide products, and eosinophils can destroy tumor cells via major basic protein and granzyme A molecules (2). Monoclonal antibodies have been commonly used in cancer treatment for a decade, and these antibodies activate antibody-dependent cellular cytotoxicity by NK cells, neutrophils, and macrophages (3,4).

Overactivation of innate immunity in FMF may lead to better tumor immunosurveillance and clearance of tumor cells in the early phases of carcinogenesis. This might explain the lower risk of cancer in patients with FMF and can be a model for therapies that modulate the innate immune system both to fight against, and more importantly to prevent, cancer. Many preclinical studies and early clinical trials have shown that antitumor immunity may be enhanced by combination immunotherapies that activate both innate and adaptive immunity, as reviewed recently by Moynihan and Irvine (2). Selected patients with high cancer risk (e.g., familial cancer syndromes, high-grade dysplasia, chronic inflammatory diseases) may derive benefit from such therapies in terms of cancer immunoprevention (2).

On the other hand, recent studies have shown that inflammasomes, which are the major component of the innate

immune system that function to induce maturation of inflammatory cytokines such as IL-1β and IL-18, might also have roles in tumor progression, depending on the tumor type and stage of tumor progression, as shown in breast and skin tumor models (2). Thus, innate immunity seems to function as a "double-edged sword" for cancer development: prevention in early phases but, once immunoediting, evasion, and escape occur in tumor cells, it may further augment cancer progression. Therefore, the course of cancer in patients with FMF might be more aggressive. This issue was not addressed in the study by Brenner et al, and might be assessed in follow-up investigations.

Finally, the type and duration of biologic treatment, if received by any of the patients included in the study by Brenner and colleagues, might be an important consideration as there are concerns that these therapies may increase the risk of some cancers.

Emre Bilgin, MD
Abdulsamet Erden, MD
Ömer Dizdar, MD, PhD
Hacettepe University School of Medicine
Ankara, Turkey

1. Brenner R, Ben-Zvi I, Shinar Y, Liphshitz I, Silverman B, Peled N, et al. Familial Mediterranean fever and incidence of cancer: an analysis of 8,534 Israeli patients with 258,803 person-years. Arthritis Rheumatol 2018;70:127–33.
2. Moynihan KD, Irvine DJ. Roles for innate immunity in combination immunotherapies [review]. Cancer Res 2017;77:5215–21.
3. Siders WM, Shields J, Garron C, Hu Y, Boutin P, Shankara S, et al. Involvement of neutrophils and natural killer cells in the anti-tumor activity of alemtuzumab in xenograft tumor models. Leuk Lymphoma 2010;51:1293–304.
4. Albanesi M, Mancardi DA, Jönsson F, Iannascoli B, Fiette L, Di Santo JP, et al. Neutrophils mediate antibody-induced antitumor effects in mice. Blood 2013;122:3160–4.

Reply

To the Editor:

We thank Dr. Bilgin and colleagues for their enlightening comments regarding our recent report in *Arthritis and Rheumatology*. We completely agree with their notion that the innate immune system may be a double-edged sword with regard to cancer; we noted this in the Discussion section of the article. Although the innate immune response likely prevents earlier, and enhances later, phases of cancer, this could not be addressed in our study, which investigated the rate, but not the course, of cancer in FMF. As FMF is a disease with prominent innate immune activation, it may serve as a model to test such ideas, but this will require a separate investigation. Biologic treatments, mainly canakinumab and anakinra, are being used to treat our patients with colchicine-resistant FMF, but this has begun only recently. Because the proportion of these patients in our cohort is negligible, no conclusions on the role of IL-1 blockade in cancer could be drawn based on our study. Interestingly, canakinumab was found to reduce the aggressiveness and prevalence of lung cancer in a post hoc analysis of the Canakinumab Anti-inflammatory Thrombosis Outcomes Study (Ridker PM, MacFadyen JG, Thuren T, Everett BM, Libby P, Glynn RJ, CANTOS Trial Group. Effect of interleukin-1β inhibition with canakinumab on incident lung cancer in patients with atherosclerosis: exploratory results from a randomised, double-blind, placebo-controlled trial. Lancet

2017;390:1833–42). Interpretation of this finding entails the same dilemmas we had regarding the roles of IL-1 and anti–IL-1 in cancer in patients with FMF.

Ronen Brenner, MD
Wolfson Medical Center
Holon, Israel
Ilan Ben-Zvi, MD
Yael Shinar, PhD
Avi Livneh, MD
Sheba Medical Center
Tel Hashomer, Israel
Irena Liphshitz, MSc
Barbara Silverman, MD, MPH

Israel Ministry of Health
Jerusalem, Israel
Nir Peled, MD, PhD
Rabin Medical Center
Petah Tikvah, Israel
Carmit Levy, PhD
Tel Aviv University
Tel Aviv, Israel
Eldad Ben-Chetrit, MD
Hadassah–Hebrew University Medical Center
Jerusalem, Israel
Shaye Kivity, MD
Sheba Medical Center
Tel Hashomer, Israel

Clinical Images: Osteomalacia due to drug-induced Fanconi syndrome
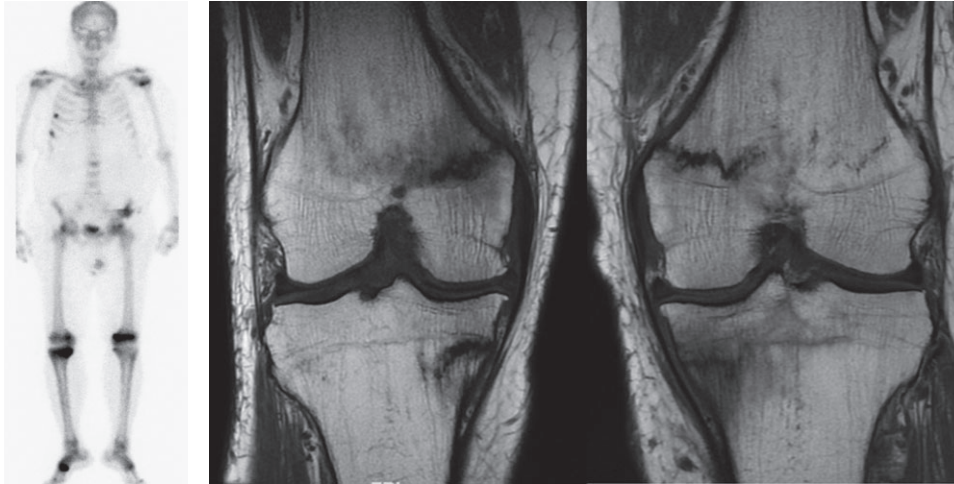
The patient, a 70-year-old man, presented with a 1-year history of bilateral deep knee pain and myalgia. For the last 10 years he had been taking adefovir (10 mg/day) for hepatitis B. He was also taking metformin for diabetes mellitus. Examination revealed mild bilateral patellofemoral crepitus and proximal myopathy. Laboratory investigations showed an increased level of alkaline phosphatase (449 units/liter [normal 40–130]) and hypophosphatemia (1.5 mg/dl [normal 2.6–4.5]). Renal function and corrected calcium, 25-hydroxyvitamin D, and creatine kinase levels were normal, as were thyroid function, serum protein electrophoresis results, and levels of parathyroid hormone, testosterone, and serum free light chain. Knee radiography showed only mild degenerative changes. However, bone scanning with isotope labeling revealed multiple foci of increased tracer uptake at the right fifth and seventh ribs, L2 vertebra, proximal humeri, left distal femur, and right proximal tibia (left). Coronal T1-weighted magnetic resonance imaging of the knees showed bilateral symmetric pseudofractures in the medial tibia and femur metaphysis perpendicular to the long axis of the bones, characteristic of Looser zones (1) (right). Further investigation revealed reduced tubular phosphate reabsorption (0.17 mmoles/liter, calculated using the ratio of urine fractional excretion of phosphate to the glomerular filtration rate [2] [normal 0.80–1.35]), metabolic acidosis with positive urine anion gap, hypouricemia, and normoglycemic glycosuria. Levels of 1,25-hydroxyvitamin D and fibroblast growth factor 23 were normal. We diagnosed osteomalacia due to adefovir-induced Fanconi syndrome with multiple pseudofractures. Fanconi syndrome is a proximal tubular defect in which reabsorption of phosphate is reduced, resulting in hypophosphatemia and consequent osteomalacia, along with other biochemical abnormalities. In cases of adult-onset osteomalacia in which vitamin D deficiency has been ruled out, drug causes must be considered. Other drugs known to cause Fanconi syndrome include chemotherapy agents, antiepileptic agents, and antibiotics (3). It is postulated that these drugs directly damage mitochondria in the proximal tubules. In our patient, we substituted entecavir for the adefovir and initiated treatment with phosphate replacement and calcitriol. His symptoms resolved within 4 months.

1. Chang CY, Rosenthal DI, Mitchell DM, Handa A, Kattapuram SV, Huang AJ. Imaging findings of metabolic bone disease. Radiographics 2016;36:1871–87.
2. Payne RB. Renal tubular reabsorption of phosphate (TmP/GFR): indications and interpretation. Ann Clin Biochem 1995;35:201–6.
3. Hall AM, Bass P, Unwin RJ. Drug-induced renal Fanconi syndrome [review]. Q J Med 2014;107:261–9.

Jiacai Cho, MBBS, MMed, MRCP iD
Peter P. Cheung, MBBS, FRACP, PhD
National University Hospital
and Yong Loo Lin School of Medicine
Singapore, Singapore

ACR ANNOUNCEMENTS

ACR Meetings

Annual Meetings
   October 19–24, 2018, Chicago
   November 8–13, 2019, Atlanta

For additional information, contact the ACR office.

Join Us in Chicago for the 2018 ACR/ARHP Annual Meeting, October 19–24

High-impact learning starts with our pre-meeting courses. Pre-meeting courses offer attendees unique learning opportunities in specific topic areas. They will be held October 19–20 at McCormick Place Convention Center. Whatever your area of research or practice, you're sure to find something just for you!

- ACR Basic Research Conference: Epigenetics in Immune-Mediated Disease (October 19–20)
- ACR Clinical Research Conference: Applications of Mobile Health Technologies (October 19–20)
- Musculoskeletal Ultrasound Course for Rheumatologists—Fundamentals (October 19–20)
- Coding: Unlock the Mysteries of Advanced Coding for Rheumatology (October 19)
- ACR Review Course (October 20)
- ACR/ARHP Immunology Breakthroughs: Impact on Diagnosis and Therapy (October 20)
- Musculoskeletal Ultrasound Course for Rheumatologists—Advanced (October 20)
- Practice Management: Putting the Pieces Together—Winning Strategies for Rheumatology Practices (October 20)

2018 Opening Lecture: Saturday, October 20. What factors can predict survival in times of great adversity? Surely the most important is resilience. In this year's unique, compelling Opening Lecture, a Hollywood mogul shares his story of resilience in surviving an acute, life-threatening medical crisis and his arduous road to recovery with physical rehabilitation and therapy. Veteran film and television producer Jonathan Koch, President and CCO of Asylum Entertainment, LLC, will focus on the patient's journey, highlighting how a team of dedicated, skilled, and resilient health care professionals can work with the patient as partners to triumph over a challenging rare illness. A few years ago, Mr. Koch, a busy executive and dad, rapidly developed a serious illness that led quickly to hospitalization in an intensive care unit. It was a puzzling and rare diagnosis: acute hemophagocytic lymphohistiocytosis. He faced losing not just his successful career in the entertainment industry, but his life, and the life yet to be lived with his loved ones. While Mr. Koch's initial therapy saved his life, he awoke from a medically induced coma with severe necrosis in his extremities, necessitating amputation of his hands and feet. In this lecture, he will describe the physical and emotional trauma he endured, and share his experiences working with his health care team to restore his independence and mobility so he could return to his career, dance with his daughter, and even play tennis. This heartbreaking and heartwarming talk will illuminate the patient's perspective on care, the pain and grief associated with illness, and the power of resilience to fuel recovery and restored independence. Mr. Koch's inspiring story will also spotlight how health care providers can emphasize resilience in the care setting, not just for their patients struggling to overcome illness, but for themselves.

ARHP Keynote Address: Sunday, October 21. The ARHP Keynote Address, 2030: A Rheumatology Odyssey, will be a discussion of the history and future of rheumatoid arthritis diagnosis, treatment, and ongoing maintenance as told through the science, research, and the interprofessional team of providers it takes to care for these patients. Using an engaging, TED-style presentation format, Iain McInness, PhD, FRCP, FRSE from the University of Glasgow and member of the EULAR Executive Committee, and Ben Smith, PA-C, DFAAPA from Florida State University will lead the audience on a journey through the history of RA, arriving in the future. As innovative therapies have evolved, so has the team of experts treating RA. Along with rehabilitation specialists, nurses, and researchers, the team of the present includes NPs, PAs, pharmacists, and highly educated office staff. What will be the role of artificial intelligence, social media, telemedicine, and precision medicine in the future of RA care? The work force shortage will be addressed through unique strategies expected to bridge the gaps and advance access to rheumatologic care for RA patients all over the world.

Register now. The deadline for advance registration for the 2018 Annual Meeting is October 3. Go to rheumatology.org/Annual-Meeting/Registration to register or obtain more information on all Annual Meeting sessions.

Education Programs

4th Annual Conference of the Emirates Society for Rheumatology. October 10–12, 2018, Dubai, UAE. Conference sessions will cover recent updates in the management of specific rheumatic diseases. An accredited musculoskeletal ultrasound course will be offered, and there will be meet-the-expert sessions and workshops, as well as educational activities for nurses and patients in addition to the numerous sessions geared toward physicians. The deadline for submission of abstracts is July 31, 2018. The official language will be English. The registration fee is $200 through July 3, 2018, and $300 thereafter. For additional information, e-mail infomed@infomedweb.com or Nathalie@infomedweb.com.